frontiers | Research Topics

New perspectives on osteoclasts in health and disease

Edited by
Stefania Mariggiò, Maria-Bernadette Madel, Enrico Iaccino and Claudine Blin-Wakkach

Published in
Frontiers in Cell and Developmental Biology
Frontiers in Molecular Biosciences

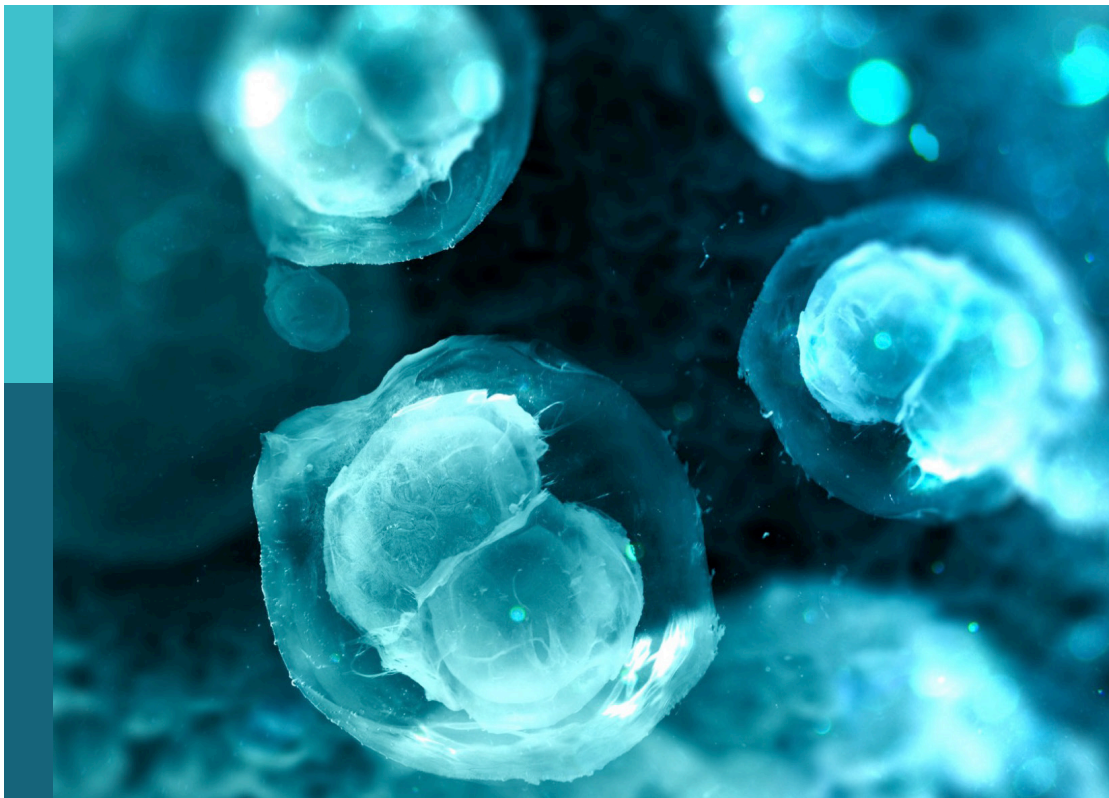

ISSN 1664-8714
ISBN 978-2-83251-005-6
DOI 10.3389/978-2-83251-005-6

About Frontiers

Frontiers is more than just an open access publisher of scholarly articles: it is a pioneering approach to the world of academia, radically improving the way scholarly research is managed. The grand vision of Frontiers is a world where all people have an equal opportunity to seek, share and generate knowledge. Frontiers provides immediate and permanent online open access to all its publications, but this alone is not enough to realize our grand goals.

Frontiers journal series

The Frontiers journal series is a multi-tier and interdisciplinary set of open-access, online journals, promising a paradigm shift from the current review, selection and dissemination processes in academic publishing. All Frontiers journals are driven by researchers for researchers; therefore, they constitute a service to the scholarly community. At the same time, the *Frontiers journal series* operates on a revolutionary invention, the tiered publishing system, initially addressing specific communities of scholars, and gradually climbing up to broader public understanding, thus serving the interests of the lay society, too.

Dedication to quality

Each Frontiers article is a landmark of the highest quality, thanks to genuinely collaborative interactions between authors and review editors, who include some of the world's best academicians. Research must be certified by peers before entering a stream of knowledge that may eventually reach the public - and shape society; therefore, Frontiers only applies the most rigorous and unbiased reviews. Frontiers revolutionizes research publishing by freely delivering the most outstanding research, evaluated with no bias from both the academic and social point of view. By applying the most advanced information technologies, Frontiers is catapulting scholarly publishing into a new generation.

What are Frontiers Research Topics?

Frontiers Research Topics are very popular trademarks of the *Frontiers journals series*: they are collections of at least ten articles, all centered on a particular subject. With their unique mix of varied contributions from Original Research to Review Articles, Frontiers Research Topics unify the most influential researchers, the latest key findings and historical advances in a hot research area.

Find out more on how to host your own Frontiers Research Topic or contribute to one as an author by contacting the Frontiers editorial office: frontiersin.org/about/contact

New perspectives on osteoclasts in health and disease

Topic editors

Stefania Mariggiò — Institute of Biochemistry and Cell Biology, Department of Biomedical Sciences, National Research Council (CNR), Italy

Maria-Bernadette Madel — Baylor College of Medicine, United States

Enrico Iaccino — Magna Græcia University of Catanzaro, Italy

Claudine Blin-Wakkach — UMR7370 Laboratoire de Physio Médecine Moléculaire (LP2M), France

Citation

Mariggiò, S., Madel, M.-B., Iaccino, E., Blin-Wakkach, C., eds. (2022). *New perspectives on osteoclasts in health and disease*. Lausanne: Frontiers Media SA. doi: 10.3389/978-2-83251-005-6

Table of contents

frontiers | Frontiers in Cell and Developmental Biology

TYPE Editorial
PUBLISHED 25 November 2022
DOI 10.3389/fcell.2022.1093394

OPEN ACCESS

EDITED AND REVIEWED BY
Cecilia Giulivi,
University of California, Davis,
United States

*CORRESPONDENCE
Stefania Mariggiò,
stefania.mariggio@ibbc.cnr.it

†These authors share last authorship

SPECIALTY SECTION
This article was submitted to Cellular Biochemistry,
a section of the journal
Frontiers in Cell and Developmental Biology

RECEIVED 09 November 2022
ACCEPTED 10 November 2022
PUBLISHED 25 November 2022

CITATION
Madel M-B, Iaccino E, Blin-Wakkach C and Mariggiò S (2022), Editorial: New perspectives on osteoclasts in health and disease.
Front. Cell Dev. Biol. 10:1093394.
doi: 10.3389/fcell.2022.1093394

Editorial: New perspectives on osteoclasts in health and disease

Maria-Bernadette Madel[1], Enrico Iaccino[2], Claudine Blin-Wakkach[3†] and Stefania Mariggiò[4*†]

[1]Department of Orthopedic Surgery, Baylor College of Medicine, Houston, TX, United States, [2]Department of Experimental and Clinical Medicine, University Magna Graecia of Catanzaro, Catanzaro, Italy, [3]Université Côte d'Azur, CNRS, LP2M, Nice, France, [4]Department of Biomedical Sciences, Institute of Biochemistry and Cell Biology, CNR, Naples, Italy

KEYWORDS

osteoclast differentiation, multinucleated cells, bone resorption, bone signaling pathways, bone tumors, osteoimmunology

Editorial on the Research Topic
New perspectives on osteoclasts in health and disease

Introduction

Since their discovery 150 years ago, osteoclasts have been the subject of an increasing number of studies. Osteoclasts are indeed very particular because they are among the very few physiologically multinucleated cells, they are the only ones capable of resorbing bone matrix and, although they play a key role in bone remodeling, they belong to the monocyte lineage. Their functions extend far beyond bone resorption, and they are involved in many biological and pathological processes, including osteoporosis, bone tumor and metastasis, rare diseases, and chronic inflammatory diseases. As a result, they remain the subject of intense research, and the number of publications on osteoclasts continues to grow exponentially.

The 13 articles in this Research Topic, including 8 Original Research and 1 Method papers plus 3 Reviews and 1 Minireview, to which 97 authors and 28 reviewers from all over the world contributed, reflect the continuing high level of interest in osteoclasts. They bring new data or review recent advances in the regulation of osteoclast differentiation and function, their role in the pathological context and their interest as therapeutic targets, as well as new tools for measuring osteoclast activity and number in *in-vitro* assays (Figure 1).

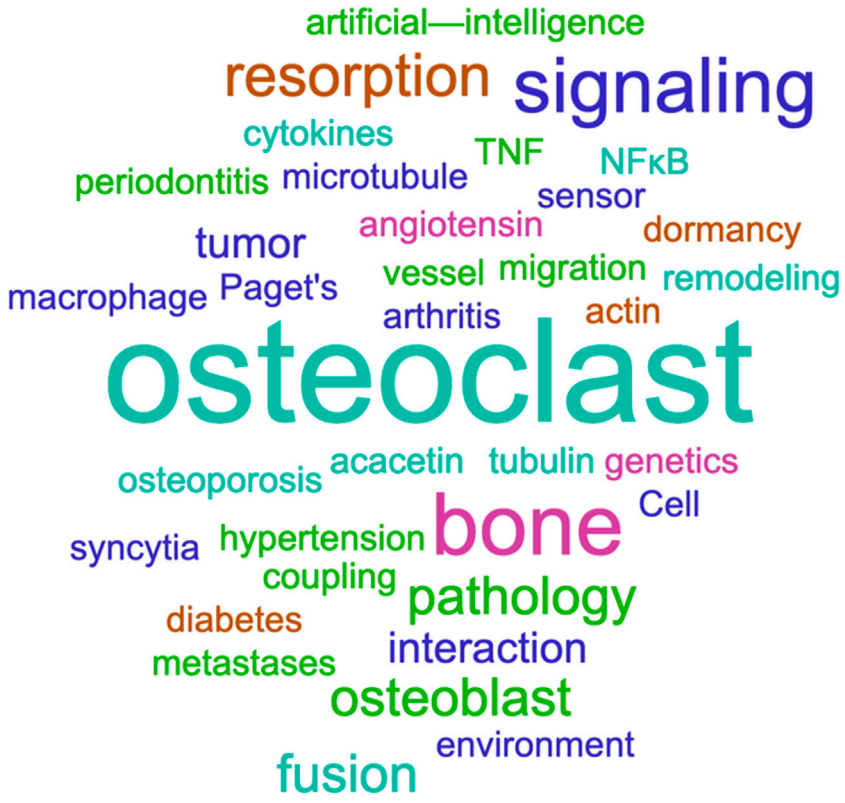

FIGURE 1
Areas covered by the Research Topic "*New perspectives on osteoclasts in health and disease*". The word cloud is based on the main keywords and topics of the 13 papers included in this Research Topic. It was built using Word It Out (https://worditout.com/). The word size is proportional to the weight of the word. Colors are random.

Overview

Cell signaling and molecular regulation of osteoclast differentiation, fusion, and function

At the molecular and cellular level, this topic has contributed to refine membrane receptors and cell signaling in osteoclast physiology and dysfunction, and addressed molecular aspects of osteoclast differentiation, fusion, and function. Bae et al. provided new insights into mTORC1-mediated regulation of osteoclastogenesis and bone resorption, revealing the interplay between MYC and mTORC1 signaling pathways in the regulation of osteoclast resorption. Furthermore, they demonstrated for the first time that the MYC-GADD34 axis is an upstream regulator of mTORC1 activation in osteoclast differentiation, suggesting that this axis is a potential therapeutic target for mTORC1 regulation and pathological bone resorption.

Osteoclast fusion is a tightly regulated process involving cell adhesion and actin reorganization (Dufrancais et al., 2021). Ahmadzadeh et al. summarized recent insights into osteoclast biogenesis, focusing on syncytial cell formation. Osteoclasts are considered the physiological counterpart of the less well-characterized Langhans and foreign body giant cells (Anderson, 2000), formed upon macrophage fusion under pathological conditions (e.g., granuloma or foreign material exposure). Osteoclasts retain several immunomodulatory functions of macrophages, such as phagocytic activity to resorb bone. These observations, together with the osteoclast contribution to bone promotion and angiogenesis, further crushes the image of osteoclasts as specialized cells dedicated exclusively to bone resorption. Two original research articles further explored the mechanisms of cell fusion in osteoclastogenesis. Mangini et al. demonstrated evidence for multimodal regulation of osteoclast differentiation and activity by group IIA secreted phospholipase A_2 ($sPLA_2$-IIA). Using different approaches (KO mice, siRNAs, recombinant proteins, and inhibitors), they reported the involvement of $sPLA_2$-IIA in the control of osteoclast differentiation, syncytium formation, and resorption activity in a both catalytically dependent and independent manner. Maurin

et al. shed new light on the control of microtubule dynamics in osteoclasts using an osteoclast KO model for TUBB6, a β-tubulin isotype responsible for cytoskeleton organization. The authors showed that TUBB6 is essential in regulating microtubule and actin cytoskeleton dynamics in osteoclasts. Furthermore, this study developed a proteomic approach and identified proteins whose association with microtubules was affected by TUBB6.

Osteoclast activity and differentiation are controlled by their interaction with the osteoblastic lineage, a process termed coupling. Borggaard et al. investigated the spatial organization of several putative secreted and membrane-bound coupling factors and their receptors in human cortical bone remodeling processes. They identified coupling factors such as LIF, SEMA4D and PDGFB in human bone-resorbing osteoclasts and their respective receptors LIFR, PLXNB1, PDGFRA, and PDGFRB in neighboring reversal cells and osteoblasts. These findings support previous functional studies and highlight the critical role of these coupling factors in the osteoclast-osteoblast coupling in human bone remodeling. In their review, Russo et al. introduces the osteoclastogenesis process illustrating the reciprocal regulation of osteoclasts and other bone resident cells. To date multiple osteoclast precursor subsets and initiation of differentiation sites have been identified, contributing to osteoclast diversity.

Perspectives in pharmacological targeting of osteoclasts for diagnosis and treatment of bone pathologies

The crosstalk of osteoclasts with other cell types not only contributes to bone homeostasis maintenance but can also exacerbate several pathological conditions leading to bone destruction. This is particularly the case in many chronic inflammatory diseases and in cancer.

As an example, Tao et al. emphasize the common pathways shared in diabetes and periodontitis by exploring the effect of the antidiabetic drug metformin on osteoblast and osteoclast formation and function *in vitro*. While metformin does not affect periodontal ligament-driven osteoblastogenesis, it effectively inhibits osteoclast formation by acting on the production of RANKL and M-CSF by fibroblasts and altering the differentiation of potential osteoclast progenitors. The link between chronic diseases and osteoclastogenesis was also demonstrated by Pramusita et al. in a murine model of salt-sensitive hypertension. This model is characterized by increased osteoclast formation and bone loss associated to a high TNF-α production and angiotensin II type 1 receptor upregulation in osteoblasts, which may contribute to increased RANKL levels. Another example of the importance of the interplay between osteoclasts and neighboring cells is provided by Lin et al. who explored the protective effect of the anti-inflammatory flavonoid acacetin in the context of osteoporosis. They showed that acacetin decreases osteoclast formation by interfering with RANK signaling pathway and stimulates the capacity of bone-marrow derived macrophages to promote angiogenesis, both *in vivo* and *in vitro*, limiting bone loss in osteoporotic mice. Ruocco et al. provide detailed information on the role of the complement C5a-C5aR1 axis in bone pathogenesis of the most common inflammatory bone diseases such as rheumatoid arthritis, as well as in osteoporosis and cancer. The authors discuss available C5aR1-based therapeutic approaches along with the importance of the C5a-C5aR1 axis in the interaction between the skeletal and immune system and its potential use as a new therapeutic target for the treatment of inflammatory bone diseases.

In their review, Russo et al. focused on osteoclast involvement in skeletal tumor progression. Osteoclasts can increase the aggressiveness of primary bone tumors or reinforce the bone metastatic process and reactivate dormant cancer cells in bone marrow niches. The authors discussed current therapies targeting bone resorption and osteoclastogenesis. Excessive bone turnover is typical of Paget's disease and is associated with an increase in size and number of resorbing osteoclasts (Paget, 1877). Gennari et al. realized a comprehensive review on recent advances related to the pathogenesis of this disease. Although the mechanisms underlying the development of this disorder remain largely unknown, concomitant factors other than genetic susceptibility, such as viral infections and/or environmental factors, have been suggested as possible etiologies. The efforts toward a deeper understanding of this disease are driven by the lack of a resolutive cure, with current treatment being bisphosphonates (Lipton, 2005) and symptomatic medications for pain relief.

Development in technology

In recent decades, significant advances have been made in the characterization of osteoclast physiopathology despite technology limitations. Even today, evaluation of osteoclast number, size and activity is greatly time consuming and exhibits operator-related bias despite having trained personnel, making continuous monitoring of osteoclast function difficult. Harnessing the potential of electric cell-substrate impedance sensing (ECIS), Jansen et al. developed an impedimetric bioassay for real-time resorption quantification. This allowed the monitoring of IL-1β-induced resorptive activity during osteoclast culturing, highlighting how this inflammatory factor accelerates resorption in the initial phase of stimulation, although final total resorption (generally quantified by classical methods) was unaffected. In addition, Kohtala et al. developed an automated method for the quantification of osteoclast number and dimension using machine learning-based object detection. All steps are executed by a specific software that performs single-

cell analysis after pixel translation. The application of machine learning can partially overcome the user's subjectivity in osteoclast evaluation. These highlighted contributions are only examples of the collective efforts in the direction of the standardization of reliable methods to quantify osteoclast number, size, and biological activities over time, not only *in vitro*, but also using non-invasive *in-vivo* approaches.

Concluding remarks

This Research Topic prospects the central role of the osteoclasts in bone pathophysiology, collecting recent evidence from in-depth analysis of the mechanisms regulating osteoclast formation and activity, as well as their communication with the surrounding system. It provides a better understanding of the role of osteoclasts in chronic diseases and cancer associated with bone loss. In addition, this Research Topic confirms that osteoclast research continues to provide new data and concepts, as well as new perspectives, both at the fundamental level and in terms of new therapeutic opportunities.

Author contributions

M-BM, EI, CB-W, and SM designed the project and contributed equally to the writing of the manuscript.

Conflict of interest

The authors declare that the research was conducted in the absence of any commercial or financial relationships that could be construed as a potential conflict of interest.

Publisher's note

References

Anderson, J. M. (2000). Multinucleated giant cells. *Curr. Opin. Hematol.* 7 (1), 40–47. doi:10.1097/00062752-200001000-00008

Dufrancais, O., Mascarau, R., Poincloux, R., Maridonneau-Parini, I., Raynaud-Messina, B., and Verollet, C. (2021). Cellular and molecular actors of myeloid cell fusion: Podosomes and tunneling nanotubes call the tune. *Cell Mol. Life Sci.* 78 (17-18), 6087–6104. doi:10.1007/s00018-021-03875-x

Lipton, A. (2005). New therapeutic agents for the treatment of bone diseases. *Expert Opin. Biol. Ther.* 5 (6), 817–832. doi:10.1517/14712598.5.6.817

Paget, J. (1877). On a form of chronic inflammation of bones (Osteitis Deformans). *Med. Chir. Trans.* 60, 37–64. doi:10.1177/095952877706000105

frontiers in Cell and Developmental Biology

ORIGINAL RESEARCH
published: 18 November 2021
doi: 10.3389/fcell.2021.778887

The Beta-Tubulin Isotype TUBB6 Controls Microtubule and Actin Dynamics in Osteoclasts

Justine Maurin[1], Anne Morel[1], David Guérit[1], Julien Cau[2], Serge Urbach[3], Anne Blangy[1†] and Guillaume Bompard[1*†]*

[1] Centre de Recherche de Biologie Cellulaire de Montpellier, CNRS, Montpellier University, Montpellier, France, [2] BioCampus Montpellier, CNRS, INSERM, Montpellier University, Montpellier, France, [3] Institute of Functional Genomics, CNRS, INSERM, Montpellier University, Montpellier, France

OPEN ACCESS

Edited by:
Enrico Iaccino,
Magna Graecia University of Catanzaro, Italy

Reviewed by:
Lavinia Raimondi,
Rizzoli Orthopedic Institute, Scientific Institute for Research, Hospitalization and Healthcare (IRCCS), Italy
Erika Cione,
University of Calabria, Italy
Antonella Zannetti,
Institute of Biostructure and Bioimaging, Consiglio Nazionale delle Ricerche (CNR), Italy

***Correspondence:**
Anne Blangy
anne.blangy@crbm.cnrs.fr
Guillaume Bompard
guillaume.bompard@crbm.cnrs.fr

[†] These authors share senior authorship

Specialty section:
This article was submitted to Cellular Biochemistry, a section of the journal Frontiers in Cell and Developmental Biology

Received: 17 September 2021
Accepted: 11 October 2021
Published: 18 November 2021

Citation:
Maurin J, Morel A, Guérit D, Cau J, Urbach S, Blangy A and Bompard G (2021) The Beta-Tubulin Isotype TUBB6 Controls Microtubule and Actin Dynamics in Osteoclasts. Front. Cell Dev. Biol. 9:778887. doi: 10.3389/fcell.2021.778887

Osteoclasts are bone resorbing cells that participate in the maintenance of bone health. Pathological increase in osteoclast activity causes bone loss, eventually resulting in osteoporosis. Actin cytoskeleton of osteoclasts organizes into a belt of podosomes, which sustains the bone resorption apparatus and is maintained by microtubules. Better understanding of the molecular mechanisms regulating osteoclast cytoskeleton is key to understand the mechanisms of bone resorption, in particular to propose new strategies against osteoporosis. We reported recently that β-tubulin isotype TUBB6 is key for cytoskeleton organization in osteoclasts and for bone resorption. Here, using an osteoclast model CRISPR/Cas9 KO for Tubb6, we show that TUBB6 controls both microtubule and actin dynamics in osteoclasts. Osteoclasts KO for Tubb6 have reduced microtubule growth speed with longer growth life time, higher levels of acetylation, and smaller EB1-caps. On the other hand, lack of TUBB6 increases podosome life time while the belt of podosomes is destabilized. Finally, we performed proteomic analyses of osteoclast microtubule-associated protein enriched fractions. This highlighted ARHGAP10 as a new microtubule-associated protein, which binding to microtubules appears to be negatively regulated by TUBB6. ARHGAP10 is a negative regulator of CDC42 activity, which participates in actin organization in osteoclasts. Our results suggest that TUBB6 plays a key role in the control of microtubule and actin cytoskeleton dynamics in osteoclasts. Moreover, by controlling ARHGAP10 association with microtubules, TUBB6 may participate in the local control of CDC42 activity to ensure efficient bone resorption.

Keywords: osteoclast, tubulin isotype, microtubule, actin, bone resorption, GRAF2, PS-GAP

INTRODUCTION

Osteoclasts are giant multinucleated cells involved in bone resorption. Their counterparts, osteoblasts, participate in new bone formation. Both cell types are thus crucial for bone homeostasis which is highly dynamic despite bone stiffness. Furthermore, whereas an equilibrium between the activities of osteoclasts and osteoblasts is crucial for bone renewal, a pathological excess in osteoclast

activity results in bone loss and may lead to osteoporosis; this is the case in number of physio-pathological situations such as from age-related sexual hormone decay, chronic inflammation, and cancer (Khosla and Hofbauer, 2017). Bone resorption by osteoclasts relies on their ability to organize a specific adhesive structure called the sealing zone or podosome belt, composed of actin rich αvβ3 integrin-containing adhesive structures called podosomes (Blangy et al., 2020). The sealing zone surrounds a highly convoluted plasma membrane domain: the ruffled border, which is specifically involved in bone resorption being the siege of acid and protease secretions respectively dissolving mineral matrix and digesting bone proteins. The dynamic of this podosomal structure allows osteoclast sliding and generates series of resorption pits at the bone surface (Søe and Delaissé, 2017).

Various approaches to regulate osteoclast activity have been developed, mostly focused on pathways regulating differentiation, but targeting the sealing zone formation also appears an interesting alternative for the treatment of osteoporosis (Blangy et al., 2020; Mounier et al., 2020). Combining transcriptomic and proteomic approaches, we recently highlighted the β-tubulin isotype TUBB6 as important for the establishment and/or the maintenance of the podosome belt and for osteoclast activity (Guérit et al., 2020). Microtubules are dynamic polymers of α- and β- tubulin heterodimers, which oscillate between growing and shrinking phases, a process known as dynamic instability. The specific regulation of MT dynamics and organization allows their adaptation to diverse cellular functions, such as cell division, motility, shape, and intracellular transport. Tubulin isotypes and post-translational modifications generate a so-called "tubulin code" translated into a given function through the recruitment of specific microtubule-associated proteins (Janke and Magiera, 2020). Indeed, the nature of β-tubulin isotypes was shown to affect microtubule dynamics *in vitro* (Vemu et al., 2017; Ti et al., 2018). TUBB6 was found to exert a microtubule-destabilizing effect in cycling cells (Bhattacharya and Cabral, 2009; Bhattacharya et al., 2011). Moreover, TUBB6 is expressed at low levels in most tissues (Leandro-García et al., 2010), and high expression of TUBB6 is characteristic of osteoclasts (Guérit et al., 2020). Microtubules and the actin cytoskeleton are physically and functionally intimately connected (Dogterom and Koenderink, 2019). In particular in osteoclasts, both actin cytoskeleton and microtubules are key for the formation of the podosome belt and for bone resorption (Okumura et al., 2006), but their regulatory crosstalk remains poorly understood in osteoclast (Blangy et al., 2020).

We reported recently that TUBB6 plays a key role in actin organization in osteoclasts and their resorption activity (Guérit et al., 2020). In the present study, we investigated further how TUBB6 regulates actin cytoskeleton in osteoclast, through the development of a cellular model knocked out for Tubb6 gene. We found that actin organization and bone resorption defects of Tubb6 KO osteoclasts are correlated not only with changes in microtubule but also actin dynamics. Furthermore, we developed a proteomic approach and identified proteins whose association with microtubules is affected by TUBB6.

MATERIALS AND METHODS

Mice, Cell Lines, and Lentivirus Production

Four-week-old C57Bl/6J mice were purchased from Harlan France and maintained in the animal facilities of the CNRS in Montpellier, France. Procedures involving mice were performed in compliance with local animal welfare laws, guidelines, and policies, according to the rules of the regional ethical committee. RAW264.7 cells were a gift from Kevin P McHugh (Gainesville, FL, United States). Lentiviral particles were produced at the Plateforme de Vectorologie de Montpellier (Montpellier, France).

Osteoclast Differentiation and Activity

For osteoclast differentiation, RAW264.7 cells between passages 5 and 12 were cultured in a humidified incubator at 37°C and 5% CO_2, in α-MEM supplemented with 10% heat inactivated fetal calf serum (Biowest), Penicillin-Streptomycin (Life Technologies), 2 mM glutamine (Lonza), and 50 ng/mL RANKL (Peprotech). Medium was changed every other day until osteoclast differentiation at day 4 or 5. When appropriated, at day 2 of differentiation, siRNAs were transfected with siImporter (Millipore) in OptiMEM medium (Life Technologies) containing 50 ng/mL RANKL, as described previously (Touaitahuata et al., 2016), using 100 nM of the siRNAs described previously: luciferase control and Tubb6 siRNAs si1077 and si1373 (Guérit et al., 2020). Primary osteoclasts were obtained from mouse bone marrow as described previously (Vives et al., 2011; Touaitahuata et al., 2016). Briefly, non-adherent bone marrow cells from long bones of 6- to 8-week-old C57BL/6J mice were grown for 48 h in α-MEM containing 10% heat-inactivated fetal calf serum, 2 mM glutamine, and 30 ng/mL macrophage colony-stimulating factor (M-CSF; Miltenyi) to obtain bone marrow macrophages (BMMs); BMMs were then grown in the same medium complemented with 50 ng/mL RANKL for 5 days to obtain osteoclasts. Differentiation was performed on glass or on Apatite Collagen Complex (ACC)-coated coverslips, prepared as reported previously (Maurin et al., 2018).

To measure their activity, osteoclasts were detached from the culture plate by scrapping at day 3 of differentiation and seeded for 3 more days onto inorganic crystalline calcium phosphate (CaP)-coated multiwells (Osteo Assay Surface, Corning), eight wells per condition. For each condition, 4 wells were then stained for tartrate resistant acid phosphatase (TRAP) activity to measure osteoclast surface and 4 wells stained with von Kossa to measure CaP dissolution as described previously (Brazier et al., 2009). Wells were imaged with a Nikon SMZ1000 stereomicroscope equipped with a Nikon DXM 1200F CCD camera and the quantifications were carried out with ImageJ 1.53c software. In each experiment, osteoclast specific activity was expressed as the average area resorbed in the four wells stained with von Kossa normalized by the osteoclast surface in the four wells stained with TRAP.

Generation of Tubb6 Knock-Out RAW264.7 Cells

A guide RNA (gRNA) targeting the second exon of mouse Tubb6 gene (5′-CGACCAGGCCGGAGGCTACG-3′) was designed and cloned in lentiCRISPRv2 vector, which also provides the expression of the *Streptococcus pyogenes* Cas9 and puromycin resistance, a gift from Feng Zhang (Addgene plasmid # 52961; http://n2t.net/addgene:52961; RRID:Addgene_52961) (Sanjana et al., 2014). Empty and Tubb6 gRNA-containing lentiCRISPRv2 were used to produce lentiviruses and generate respectively control (WT) and Tubb6 KO RAW264.7 cells. For this, growing RAW264.7 cells were infected with lentiviral particles and selected with 3 μg/ml puromycin 48 h later. Puromycin-resistant WT and Tubb6 KO RAW264.7 clones were individually picked, expanded, and TUBB6 expression was monitored by immunoblot analysis using home-made polyclonal antibodies against the C-terminal end of mouse TUBB6, generated in rabbit at Eurogentec by injection of peptide GGGEINE as described (Spano and Frankfurter, 2010). Selected clones of RAW264.7 cells were used to differentiate WT and Tubb6 KO osteoclasts.

Quantitative Polymerase Chain Reaction

DNaseI-treated total RNA was prepared using the RNeasy Minikit (Qiagen); RNA was primed with 10-mer random primers and reverse transcription was catalyzed using Superscript II reverse transcriptase (Invitrogen) to generate cDNAs. Quantitative Polymerase Chain Reaction (Q-PCR) was performed an Mx3000p PCR system (Stratagene) using the Platinium Taq DNA polymerase (Invitrogen) and SYBR Green I (Bio Wittaker) as described (Maurin et al., 2018). Primers used were 5′-ACAGTCCATGCCATCACTGCC-3′ and 5′-GCCTGCTTCACCACCTTCTT-3′ for Gapdh and 5′-GAACTATGTGCACCGGGACC-3′ and 5′-GAGCTCGCTC AGCAGAATCC-3′ for Src and 5′-TGGAGGCCTCTCTTG GTGTC-3′ and CCACAAGATTCTGGGGACTC-3′ for Cathepsin K. The threshold cycle (Ct) of each amplification curve was calculated by Roche Diagnostics LightCycler 480 software using the second derivative maximum method. The relative amount of a given mRNA was calculated using the ΔCt method (Livak and Schmittgen, 2001).

Immunoblot

Osteoclast lysates were prepared in lysis buffer (50 mM Tris pH7.4, 150 mM NaCl, 1% IGEPAL CA-630, 2 mM EDTA, 50 mM NaF, 10% glycerol, protease inhibitor cocktail). Culture supernatants were collected to assess the secretion of Cathepsin K. Protein concentrations were determined with Bradford. After resolution by SDS-PAGE, proteins were transferred to PVDF-FL membranes (Immobilon-FL Transfer Membrane) and analyzed by immunoblot. Primary antibodies were: TUBB6 (1:1000), ARHGAP10 (ProteinTech S5136AP, 1:1000), GAPDH (CellSignaling #2118, 1:5000), Sigma antibodies EB1 (E3406, 1:2500), K40-acetylated tubulin (T6793, 1:1000) and actin (A2103, 1:1000), Abcam antibodies Vinculin (ab108620, 1:5000), CLASP1 (ab108620, 1:5000) and Histone H3 (ab1791, 1:1000), total β tubulin (Developmental Studies Hybridoma Bank E7, 1:1000), Santa Cruz Biotechnologies antibodies TUBB5 (SAO.4G5, sc-58884, 1:5000) and Cathepsin K (E-7, sc-48353, 1:500). Secondary antibodies were: Goat-anti-mouse Dylight680 (Invitrogen, 35518), Goat-anti-mouse Dylight800 (Invitrogen, SA535521), Goat-anti-rabbit Dylight680 (Invitrogen, 35568), Goat-anti-rabbit Dylight800 (Invitrogen, SA535571). Signals were acquired using the Odyssey Infrared Imaging System (LI-COR Biosciences, United States).

Immunofluorescence

All imaging was performed at Montpellier Ressources Imagerie (MRI) in Montpellier. For immunofluorescence, osteoclasts were differentiated on glass coverslips. Alternatively, osteoclasts at day 3 of differentiation were detached by scrapping and seeded for 2 more days on ACC as described previously (Maurin et al., 2018). Cells were fixed for 5 min in methanol at −20°C followed by 10 min permeabilization in 0.1% Triton X-100 in PBS in the case of endogenous EB1 labeling. Alternatively, cells were fixed for 20 min at room temperature in 3.2% paraformaldehyde and 10 μM Paclitaxel (Sigma) in PHEM (60 mM PIPES, 25 mM HEPES, 10 mM EGTA, 4 mM $MgSO_4$, pH 6.9) and cells were then permeabilized with 0.1% Triton X-100 in PBS for 1 min. After blocking for 1 h with 2% BSA in PBS, cells were processed for immunofluorescence. Primary antibodies used were: TUBB6 (1:1000), α-tubulin (1:2000, Sigma T5168) or α-tubulin (1:200, YOL3/4 Santa Cruz Biotechnologies sc53030), ARHGAP10 (1:200), EB1 (BD 610534, 1:500) in 2% BSA in PBS. Secondary antibodies used were from Invitrogen: donkey anti-mouse Alexa fluor 488 (Invitrogen A21202), donkey anti-rabbit Alexa fluor 546 (Invitrogen, A10040), goat anti-rat Alexa fluor 633 (Invitrogen, A21094), all used 1:1000. When appropriate, F-actin was labeled with Phalloidin Alexa fluor 647 (1:1000, Invitrogen A22287) or Phalloidin rhodamine (Sigma P1951, 1:10,000). Coverslips were mounted in Citifluor MWL4-88-25 (CliniSciences), imaged with Leica SP5 SMD confocal microscope equipped with oil objective 63X HCX Plan Apo CS oil 1.4NA under Metamorph 7.7.6.

Image Quantification and Live Imaging

Actin organization was evaluated visually after F-actin staining in fixed osteoclasts; a podosome belt was classified abnormal when F-actin staining was fragmented, weak, or absent in more than half of the osteoclast periphery, as described previously (Maurin et al., 2018).

For live imaging, osteoclasts were differentiated from WT and Tubb6 KO RAW264.7 cells expressing either LifeAct-mCherry to follow actin dynamics or EB1-GFP to follow microtubule dynamics. LifeAct-mCherry was subcloned into pMXs-Puro, retroviral particles were produced as described (Guimbal et al., 2019), and RAW264.7 cells were infected for 24 h in 8 μg/ml polybrene (Sigma). Alternatively, RAW264.7 were infected with lentiviral particles obtained from EB1-GFP lentiviral vector, a gift from Ken-Ichi Takemaru (Addgene plasmid # 118084; RRID:Addgene_118084)[1] for 5 h in 8 μg/ml polybrene (Sigma).

[1]http://n2t.net/addgene:118084

For microtubule regrowth assays, osteoclasts were treated with 10 μM nocodazole on ice for 2.5 h to depolymerize microtubules. Medium was then replaced by nocodazole-free medium at 37°C. At desired time points, cells were rinsed in PHEM containing 0.1% saponin, 0.25 nM nocodazole, and 0.25 nM paclitaxel, and fixed with methanol at –20°C for 5 min. After 1-h saturation in 2% BSA in PBS, cells were processed for immunofluorescence to label microtubules with α tubulin antibody (1:2000) and donkey anti-mouse Alexa488 secondary antibody (1:1000). Images were acquired as described in the Immunofluorescence section above. Aster areas were measured using Segmented Line function in ImageJ 1.53c.

For microtubule dynamics, EB1-GFP-expressing osteoclasts were imaged at 37°C with inverted spinning disk Nikon Ti Andor CSU-X1 equipped with EMCCD iXon897 Andor camera, one image per second for 2 min, with oil objective 100x Plan Apo lambda 1.45 NA. EBI-GFP comet mean growth speed, mean length, and mean lifetime were determined using u-track (V2.0) software. Comet detection settings were 2 and 4 pixels respectively for low-pass and high-pass Gaussian standard deviation. For tracking the maximum gap to close was set to 4 frames while the minimum length of track segment from first step was set to 10 frames. The remaining settings used for tracking were the u-track default ones. Images were also analyzed in ImageJ 1.53c with MTrackJ function microtubule growth speed, as described (Guimbal et al., 2019).

Endogenous EB1 and EB1-GFP comet length were measured with the Straight-Line function of ImageJ 1.53c.

For podosome belt dynamics, LifeAct-mCherry-expressing osteoclasts were imaged at 37°C with Dragonfly spinning disk microscope equipped with an EMCCD iXon888 Life Andor camera (Andor Technology), two images per minute, with 40X plan fluor 1,3 NA DT 0.2 μm objective. The overlap of actin ring position between different time points was determined with the function Measure in ImageJ 1.53c.

For individual podosome dynamics, LifeAct-mCherry-expressing osteoclasts were imaged at 37°C with CSU-X1 spinning disk microscope as above, one image per second was acquired for 10 min, with 100X plan Apo lambda 1.45 NA objective. Podosome life time was determined by tracking manually on the videos the interval between the appearance and disappearance of individual podosomes.

Preparation of Osteoclast Microtubule-Associated Protein Enriched Fractions

Osteoclasts were lysed in Tub/MT microtubule stabilizing buffer (80 mM MES, 1 mM EGTA, 4M glycerol, 2 mM $MgCl_2$, 1 mM Na_3VO_4, pH 6.8) supplemented with 0.1% Triton X-100 and protease inhibitory cocktail for 4 min at room temperature. Lysates were centrifuged for 10 min at room temperature at 16,000 × *g*. Pellets were resuspended in Tub/MT supplemented with 20 μM paclitaxel, 0.1 μM GTP, 350 mM NaCl and protease inhibitory cocktail and centrifuged at 21,500 × *g* for 10 min. The resulting supernatant S2, enriched in microtubule binding proteins, was further analyzed by proteomics.

Microtubule Co-sedimentation Assay

Human embryonic kidney 293T (HEK293T) cells were transfected with either pRK5 HA-GST (Bompard et al., 2018) or pRK5 HA-GST ARHGAP10, PCR-cloned into pRK5 HA-GST using pEGFP-N3 ARHGAP10 as template, a generous gift from Dr. Daisuke Mori (Sekiguchi et al., 2020), using jetPEI (Polyplus transfection) following manufacturer instructions. Twenty-four hours post transfection, cells were harvested, washed twice in ice cold 1X PBS, and lysed in 1X BRB80 (80 mM PIPES, 1 mM EGTA, 1 mM MgCl2, pH 6.8) supplemented with 1 mM DTT, protease inhibitor cocktail, and 0.1% IGEPAL CA-630 for 20 min on ice. Cell lysates were clarified at 100,000 × *g*. for 30 min at 4°C. 100 μg of clarified lysates were supplemented with 2 mM GTP, incubated 5 min on ice followed by 10 min at 37°C. A total of 20 μM paclitaxel was added and the reaction incubated at 37°C for 10 more min. Reaction was loaded on a 40% glycerol cushion made in 1X BRB80 supplemented with 20 μM paclitaxel and centrifuged at 100,000 × *g* for 15 min at 30°C. Pellet was rinsed once with 1X BRB80 supplemented with 20 μM paclitaxel and resuspended in the same volume as supernatant. For control experiments, all steps were performed at 4°C in the absence of GTP and Paclitaxel. Samples were then analyzed by immunoblot.

Proteomics

After reduction (DTT 1M, 30 min at 60°C) an alkylation (IAA 0.5M, 30 min RT) microtubule-associated protein enriched fractions were digested using trypsin (Gold, Promega, 1 μg/sample, overnight at 30°C). Peptide clean-up was done using OMIX C18 (Agilent) according to manufacturer protocol. For LC MSMS analysis, samples were loaded onto a 25 cm reversed-phase column (75 mm inner diameter; Acclaim PepMap 100 C18; Thermo Fisher Scientific) and separated with an UltiMate 3000 RSLC system (Thermo Fisher Scientific) coupled to a QExactive HFX system (Thermo Fisher Scientific). Tandem mass spectrometry analyses were performed in a data-dependent mode. Full scans (350–1,500 m/z) were acquired in the Orbitrap mass analyzer with a resolution of 120,000 at 200 m/z. For MS scans, 3e6 ions were accumulated within a maximum injection time of 60 ms. The 20 most intense ions with charge states $\geq$ 2 were sequentially isolated (1e5) with a maximum injection time of 50 ms and fragmented by higher-energy collisional dissociation (normalized collision energy of 28) and detected in the Orbitrap analyzer at a resolution of 30,000. Raw spectra were processed with MaxQuant v 1.6.10.43 (Cox and Mann, 2008) using standard parameters with LFQ and match between runs option. Spectra were matched against the UniProt reference proteome of *Mus musculus* (UP000000589, release 2020_04[2]) and 250 frequently observed contaminants, as well as reversed sequences of all entries. The maximum false discovery rate for peptides and proteins was set to 0.01. Representative protein ID in each protein group was automatically selected using the in-house developed Leading tool v 3.4 (Raynaud et al., 2018). Statistical analysis (*t*-test) were done using Perseus v 1.6.10.43 (Tyanova et al., 2016). Briefly, after reverse and contaminants entries removal, LFQ data were log2 transformed. Imputation

[2]http://www.uniprot.org

was performed using "Replace missing values from normal distribution" with standard parameters. Difference between the two groups was then assessed using a standard *t*-test.

GO term enrichment analyses were performed using Panther 16.0 software[3] (GO Ontology database DOI: 10.5281/zenodo.5080993 Released 2021-07-02). UniProtIDs were employed as input type IDs and the total list of *Mus musculus* genes was used as reference. GO cellular component, molecular function, and cellular component terms with $P < 0.05$ with Fisher's Exact were considered significantly enriched.

Statistical Analyses

Statistical significance was assessed either with parametric statistical test after normality assessment or with non-parametric tests. All analyses were done with GraphPad Prism 9.2.0 (GraphPad Software, Inc.), with $p < 0.05$ considered statistically significant.

RESULTS

TUBB6 Impacts Microtubule Dynamics in Osteoclasts

To understand how TUBB6 controls actin organization and bone resorption, we generated RAW264.7 cells KO for Tubb6 by CRISPR/Cas9 from which we derived osteoclasts (**Figures 1A,B** and **Supplementary Figure 1A**). Similar to what we described in primary osteoclasts treated with Tubb6 siRNAs (Guérit et al., 2020), we found that osteoclasts derived from RAW264.7 Tubb6 KO cells presented several defects when plated on glass: increase of abnormal podosome belts and podosome rings, which are immature podosome belts (**Figures 1C,D** and **Supplementary Figure 1B**). Consistently, Tubb6 KO led to osteoclasts with less sealing zones on mineralized substrates and more rings, which are immature sealing zones (**Figures 1E,F** and **Supplementary Figure 1C**), as well as reduced resorption activity (**Figure 1G**). The induction of the expression of osteoclastic markers Src and CtsK was not affected during Tubb6 KO osteoclast differentiation, as assessed by Q-PCR (**Supplementary Figures 1D,E**). Tartrate-resistant acid protease (TRAP) staining of WT and Tubb6 KO osteoclasts was comparable (**Supplementary Figure 1F**), as well as Cathepsin K intracellular content and secretion (**Supplementary Figure 1G**). Finally, the global expression of β tubulin (**Figure 1A**) and the expression of β tubulin isotype TUBB5 were also unchanged (**Supplementary Figure 1H**). Altogether, this shows that RAW264.7 osteoclasts KO for Tubb6 recapitulate the features of primary osteoclasts treated with Tubb6 siRNAs.

To assess the impact of TUBB6 on osteoclast microtubule dynamics, we first performed microtubule regrowth assay consisting in studying microtubule polymerization after cold and nocodazole treatment followed by nocodazole washout. We found that microtubule regrowth was slower in Tubb6 KO osteoclasts (**Figures 2A,B**). To confirm this, we used Tubb6 siRNAs to lower TUBB6 expression (Guérit et al., 2020). Again, we found that Tubb6 siRNAs reduced the speed of microtubule regrowth (**Supplementary Figure 2**). To get additional information regarding this defect, we performed live imaging of osteoclasts expressing the microtubule plus tip-binding protein EB1 fused to GFP (**Figure 3A**). Using time lapse microscopy and u-track software, we tracked EB1-GFP comets on individual microtubule (**Figure 3B** and **Supplementary Videos 1, 2**) and measured microtubule dynamic parameters. Thereby, we found a significant decrease of microtubule growth speed in Tubb6 KO osteoclasts from a mean value of 16 μm/min in the wild type (WT) down to 12.9 μm/min in the KO (**Figure 3C** and **Supplementary Figure 3A**). Similar results were found by manual tracking using the MTrack plugin in ImageJ (**Supplementary Figures 3B–D**). Conversely, we found an increase in microtubule growth time from 18.1 s in the WT to 20.3 s in the KO, but no significant change in microtubule growth length (**Figure 3C** and **Supplementary Figure 3A**). We also observed that the level of tubulin acetylation, a marker of microtubule stability, was higher in Tubb6 KO osteoclasts (**Figures 3D,E**), potentially consistent with longer microtubule growth time. Finally, we measured the size of endogenous EB1 staining at microtubule ends, as indicative of the length of the microtubule GTP cap that is known to be proportional to growth speed. We found that the length of EB1 staining was reduced form 1.393 μm in WT down to 1.089 μm in Tubb6 KO osteoclasts (**Figure 3F**), consistent with their lower microtubule growth speed (Vemu et al., 2017). The length of the EB1-GFP staining at the end of microtubules was similarly reduced in Tubb6 KO osteoclasts (**Supplementary Figures 3E–G**).

These results show that TUBB6 has an impact on the parameters of microtubule dynamics, increasing microtubule growth speed while decreasing microtubule lifetime.

TUBB6 Impacts on Actin Dynamics in Osteoclasts

Actin cytoskeleton and microtubules are intimately linked and Tubb6 KO osteoclasts show abnormal actin cytoskeleton organization. Thus, we further examined the impact of TUBB6 on actin dynamics, by performing live imaging of osteoclasts expressing LifeAct-mCherry to visualize actin cytoskeleton (**Figure 4A**, **Supplementary Figure 4**, and **Supplementary Videos 3, 4**). Major differences in podosome belt dynamics were observed and we thus assessed the stability of the podosome belt by comparing the position of LifeAct-mCherry labeling between time points. In control osteoclasts, the median overlap of LifeAct-mCherry staining between time 0 and time 1 = 3 min was 69.56%, whereas this overlap was significantly reduced to 55.79% in Tubb6 KO osteoclasts (**Figures 4A,B**). Similar observations were made at time 2 = 6.5 min (**Supplementary Figure 4**). Finally, we measured the life span of isolated podosomes and found that Tubb6 KO increased to 3.31 min, instead of 2.5 min in the WT (**Figure 4C** and **Supplementary Videos 5, 6**).

This suggests that, on top of microtubules, TUBB6 also impacts on actin dynamics in osteoclasts: TUBB6 tends to reduce podosome life span whereas it increases the stability of the podosome belt. Altogether, the data show that TUBB6, which is required for correct podosome patterning and bone resorption, influences both actin and microtubule dynamics in osteoclasts.

[3] pantherdb.org/

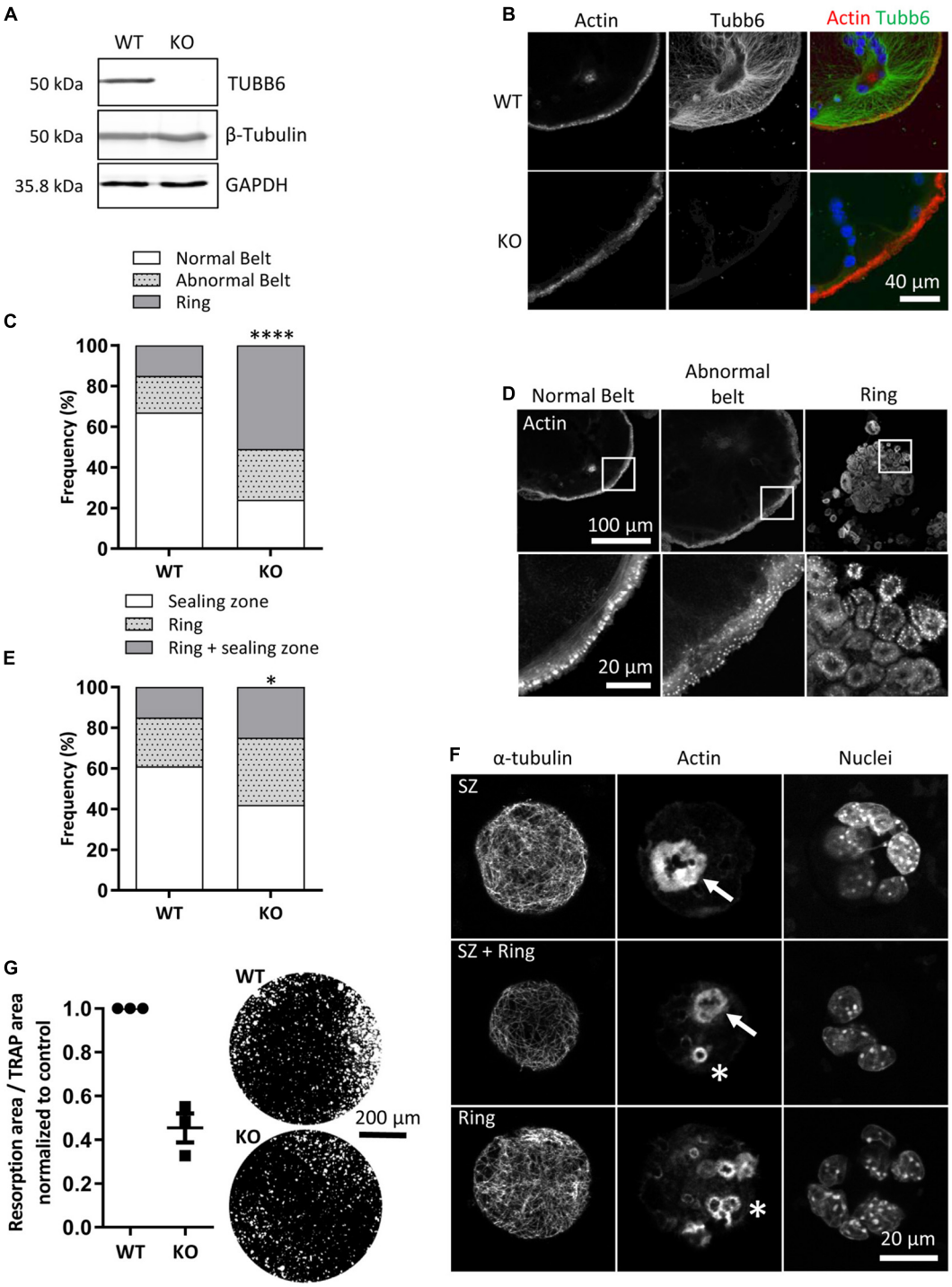

FIGURE 1 | Tubb6 gene knockout alters osteoclast actin cytoskeleton and activity. **(A)** Representative immunoblot analyses of lysates from wild type (WT) and Tubb6 KO (KO) osteoclasts. GAPDH control shows that total β-tubulin levels are not affected in osteoclasts that do not express TUBB6. **(B)** Representative maximum intensity projection (MIP) confocal images of WT and KO osteoclasts seeded on glass and stained for endogenous F-actin and TUBB6. **(C)** Bar graph showing the frequency of WT and KO osteoclasts seeded on glass and presenting podosome rings, a normal or an abnormal podosome belt, counting more than 200 WT and KO osteoclasts in four independent experiments, $\chi 2$ contingency test, $^{****}p < 0.0001$. **(D)** Representative MIP images illustrating the different categories of actin organization considered in **(C)**. **(E)** Bar graph showing the frequency of WT and KO osteoclasts seeded on mineral matrix and presenting either sealing zones (SZ), or rings or both, counting more than 150 WT and KO osteoclasts in three independent experiments, $\chi 2$ contingency test, $^{*}p < 0.05$. **(F)** Representative MIP images illustrating the different categories of actin organization considered in **(E)**, with SZ and rings respectively indicated with arrows and stars respectively. **(G)** Graph showing the average and SEM specific resorption activity of KO osteoclasts normalized to the activity of WT osteoclasts in three independent experiments, 4 wells per experiments. Representative image of von Kossa staining of the resorption wells are presented on the right.

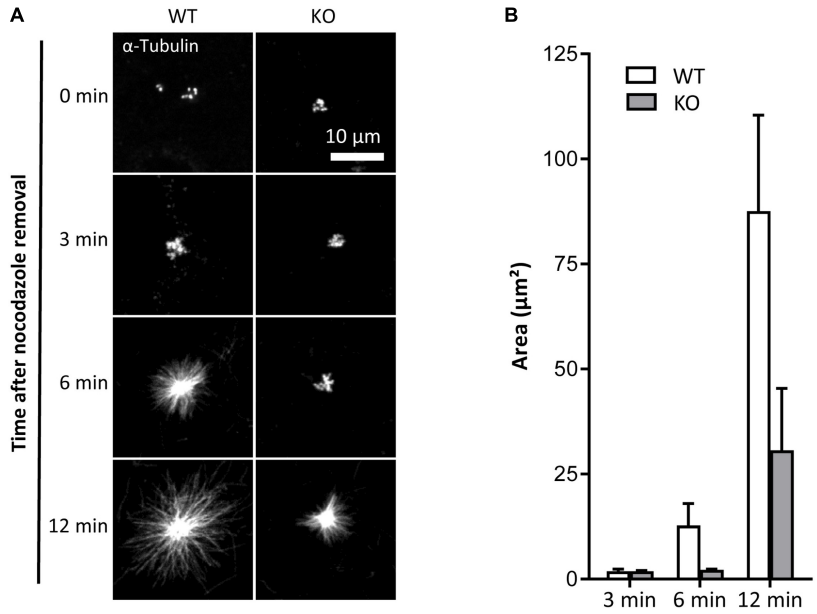

FIGURE 2 | TUBB6 depletion affects MT polymerization. **(A)** Representative MIP images of WT and KO osteoclasts stained for α-tubulin, after release from nocodazole and cold treatment for indicated times. **(B)** Bar graph showing mean and SEM of α-tubulin aster area in WT and KO osteoclasts treated as in **(A)**, 80 WT and KO asters in four independent experiments.

TUBB6 Moderately Affects Protein Binding to Osteoclast Microtubules

To understand the impact of TUBB6 on osteoclast cytoskeleton, we examined whether Tubb6 KO could affect protein binding to osteoclast microtubules. For this, we thought to prepare osteoclast fractions enriched in microtubule-associated proteins (**Figure 5A**). Osteoclasts lysates were prepared at room temperature, in a paclitaxel-free microtubule-preserving hypotonic buffer. Lysates were centrifuged to separate the supernatant (S1) from the pellet. The pellet was then washed with the same buffer supplemented with 350 mM NaCl, GTP and paclitaxel, to detach microtubule-bound proteins (S2) from microtubules while preserving the latter, which were finally pelleted (P) (**Figure 5A**). Immunoblot analysis of the different fractions showed the expected marker distribution: total tubulin equally distributed in S1 and P whereas acetylated tubulin fell predominantly in P, which contains microtubules; the microtubule-associated protein CLASP1 was found in S2 whereas vinculin was predominantly in S1 (**Figure 5B**). Of note, all fractions contained similar amounts of actin, indicative of partial F-actin depolymerization in 350 mM NaCl (**Figure 5B**). Finally, histone H3 was found in the pellet, in agreement with the presence of nuclei in this fraction; small amounts of histone H3 were also found in S2, likely due to nuclear protein leaking out of the nucleus upon high salt incubation after hypotonic lysis of osteoclasts (**Figure 5B**).

We performed label-free proteomics to compare protein content in the S2 fractions of WT and Tubb6 KO osteoclasts, in four independent experiments. We identified 2799 protein groups, considering two peptides for adequate protein identification, among which 2778 corresponded unambiguously to a single Uniprot identifier and to a unique protein (**Supplementary Table 1**). To examine whether S2 fraction was enriched in cytoskeleton regulatory proteins, we used Panther 16.0 to perform gene ontology analyses of the 2773 proteins (5 Uniprot identifiers could not be mapped in Panther), as compared to the total mouse genome (**Supplementary Table 2**). Using actin, tubulin, microtubule, and cytoskeleton as keywords, we found that all Gene Ontology (GO) terms associated with the cytoskeleton in molecular functions, cellular components, and biological process showed a significant enrichment in the S2 fraction (**Supplementary Table 2**). Cytoskeleton-related proteins associated with these GO terms encompassed 601 of the 2773 proteins we analyzed in Panther (**Supplementary Table 3**). Thus, S2 contains a great proportion of proteins related to microtubules and actin cytoskeleton.

Applying a twofold change cutoff with a p-value below 10^{-2}, we found only seven proteins showing significant changes in the S2 of Tubb6 KO osteoclasts as compared to WT (**Figure 5C** and **Table 1**). Among these, only two were part of the 601 proteins associated with cytoskeleton-related GO terms: the podosome-associated protein LSP1 (lymphocyte specific 1) and the Rho-family GTPase regulating protein ARHGAP10 (also known as GRAF2 or PS-GAP) (**Figure 5C** and **Table 1**).

These results show that TUBB6 has little effect on the content of the osteoclast S2 fraction, which is enriched in microtubule-associated protein. In particular, among the 601 proteins present in S2 and associated with a cytoskeleton-related GO term, only LSP1 and ARHGAP10 showed significant changes. This suggests that TUBB6 can affect the interaction of LSP1 and ARHGAP10 with F-actin and/or microtubules.

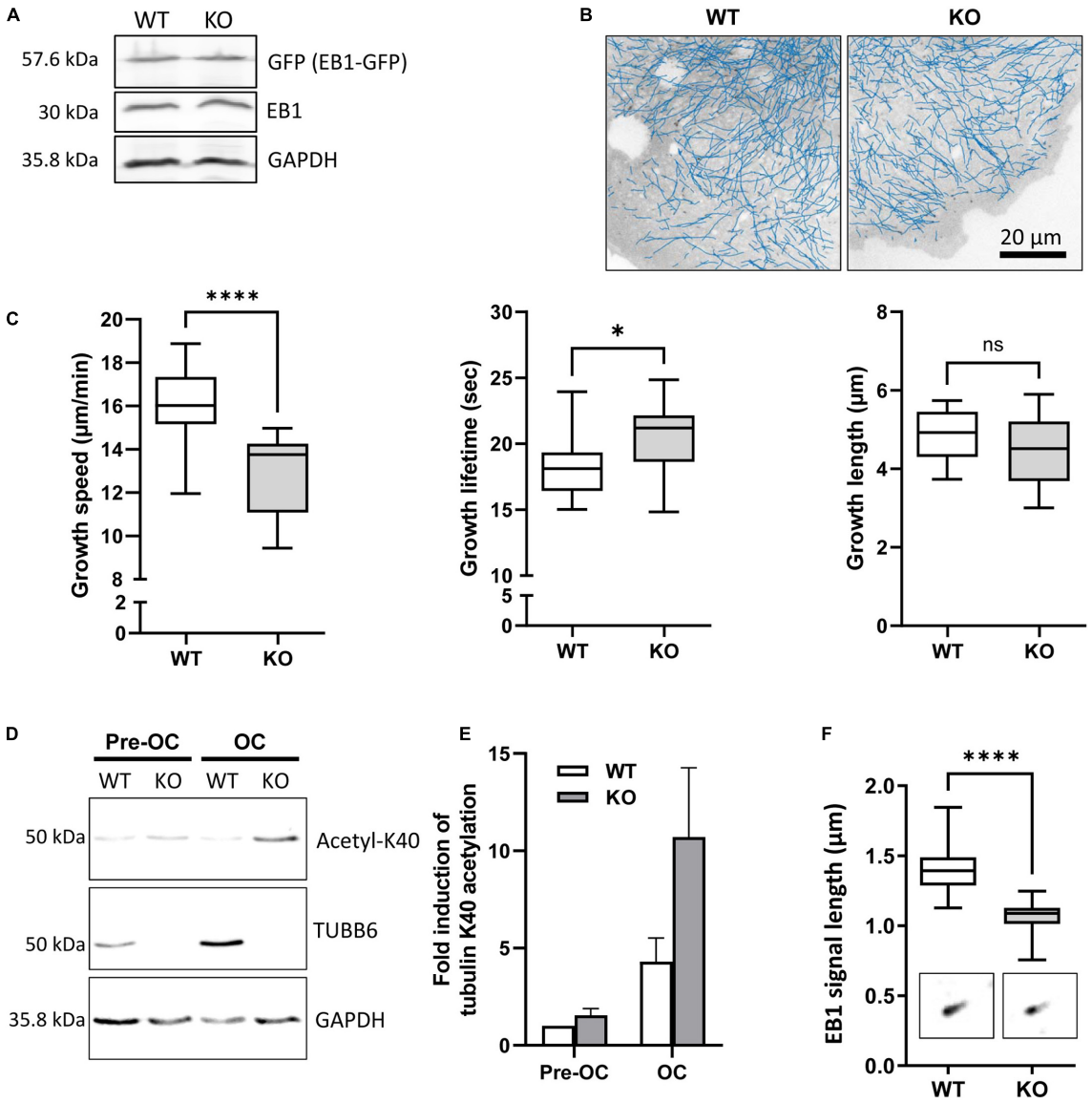

FIGURE 3 | TUBB6 regulates MT dynamics. **(A)** Representative immunoblot analysis of protein lysates from WT and KO osteoclasts expressing EB1-GFP (GFP); note that the expression levels of EB1-GFP and endogenous EB1 are similar in WT and KO osteoclasts. **(B)** Blue lines show representative EB1-GFP comet tracking using u-track software in WT and KO osteoclasts from confocal images over a period of 2 min with 1 s increment between frames (see section "Materials and Methods" for detailed settings). **(C)** Minimum to maximum boxplots with median and interquartile range (25–75%) showing the distribution of growth speed (left), lifetime (middle) and length (right) of EB1-GFP tracked comets per single WT and KO osteoclast, 18 WT and 14 KO osteoclasts from 3 independent experiments; Mann Whitney test: $^{****}p < 0.0001$ and $^{*}p < 0.05$. For details see table in **Supplementary Figure 3A**. **(D)** Representative immunoblot analysis of protein lysates from WT or KO RAW264.7 cells (Pre-OC) and derived osteoclasts (OC), showing TUBB6, acetylated K40 α-tubulin (acetyl-K40), and GAPDH expression. **(E)** Bar graph shows mean and SEM levels of acetylated K40 α-tubulin in WT and KO pre-OC and OC, normalized to 1 in WT pre-osteoclasts, from four independent experiments. **(F)** Minimum to maximum boxplot showing endogenous EB1 cap length in WT and KO osteoclasts, measuring 25 comets in each osteoclast to determine the average cap length per osteoclast, in 27 WT and 27 KO osteoclasts from three different experiments; Mann–Whitney test: $^{****}p < 0.0001$.

ARHGAP10 Associates With Both Actin and Microtubules in Osteoclasts

ARHGAP10 was shown to be a negative regulator of the activity of the GTPases CDC42, in a PYK2-kinase dependent fashion (Ren et al., 2001; Koeppel et al., 2004); ARHGAP10 can also regulate negatively the activity of GTPase RHOA (Ren et al., 2001). It was reported in RAW264.7-derived osteoclasts that Arhgap10 siRNAs led to smaller sealing zones, without affecting the proportion of osteoclasts with a sealing zone (Steenblock et al., 2014). Interestingly, we also observed smaller sealing zones upon Tubb6 KO (**Figure 1** and **Supplementary Figure 1**), as well as with Tubb6 siRNAs in primary mouse and human osteoclasts (Guérit et al., 2020). We found that ARHGAP10 expression was strongly induced during both WT

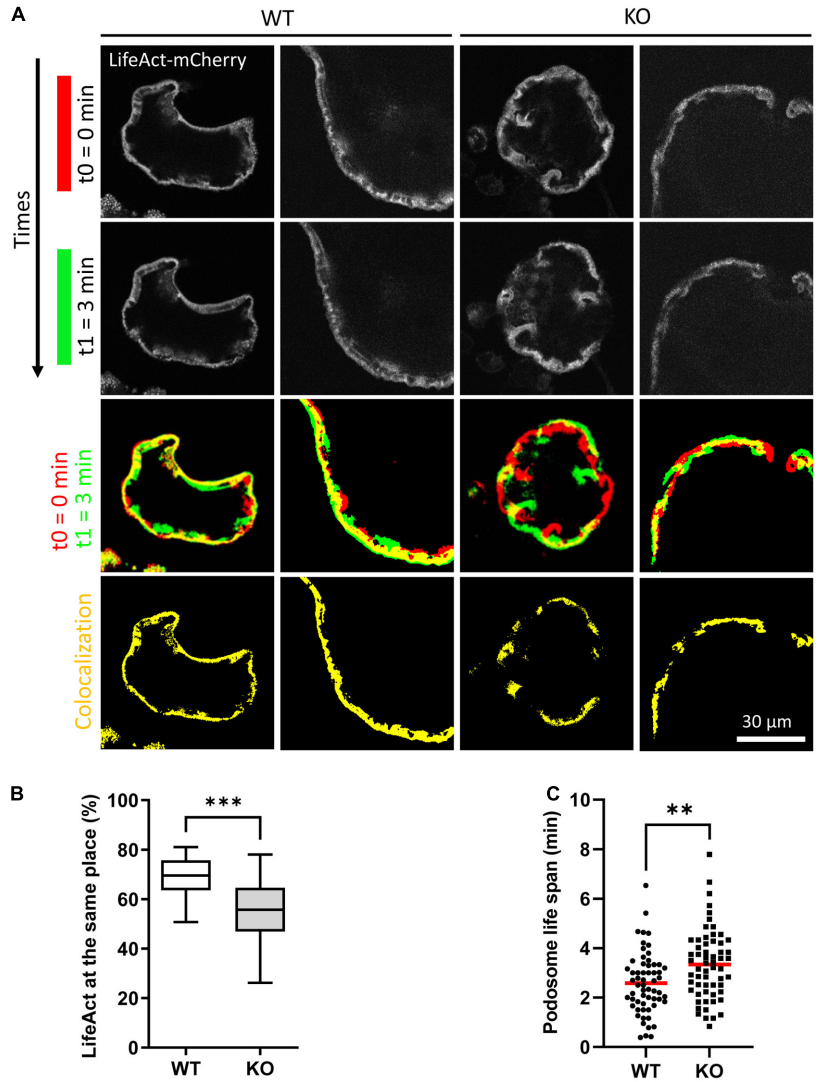

FIGURE 4 | TUBB6 depletion affects podosome belt dynamics. **(A)** Representative live confocal images of osteoclasts derived from WT or Tubb6 KO osteoclasts expressing LifeAct-mCherry and sitting on glass, showing the localization of LifeAct-mCherry signal at t0 = 0 min (red) and t1 = 3 min (green), with the overlapping areas in yellow. **(B)** Minimum to maximum boxplot showing the percentage of LifeAct-mCherry signal at t0 that persists at the same position at t3 in WT or Tubb6 KO osteoclasts; in a total of 22 WT and 21 KO osteoclasts from 4 different experiments. Mann–Whitney test: $***p < 0.0002$. See also **Supplementary Figure 4** and **Supplementary Videos 3, 4**. **(C)** Dot plot showing the life span with mean of individual podosomes in WT or Tubb6 KO osteoclasts. Total of 60 podosomes in six different wild type and KO osteoclasts, from three independent experiments. Student's *t*-test: $**p < 0.002$. See also **Supplementary Videos 5, 6**.

and Tubb6 KO osteoclasts (**Figure 5D**). Endogenous ARHGAP10 colocalized with the podosome belt in RAW264.7-derived and primary osteoclasts, as well as with the sealing zone of osteoclasts plated on ACC (**Figures 6A,B**). Interestingly, we also observed endogenous ARHGAP10 colocalization with osteoclast microtubules (**Figures 6C,D**). To confirm that ARHGAP10 can interact with microtubules, we overexpressed ARHGAP10 fused to a HA-GST tag in HEK293T cells, which do not express endogenous ARHGAP10 (Koeppel et al., 2004), or HA-GST as a control. After lysis in a buffer compatible with microtubule polymerization and clarification by high-speed centrifugation, lysates were either incubated at 4°C or 37°C in the presence of GTP and paclitaxel to induce microtubule polymerization. Finally, the fraction of HA-GST fused proteins co-sedimenting with microtubules were analyzed by immunoblot after a final high-speed centrifugation. Tubulin was found only in the 37°C-pellet, indicating that no microtubule polymerized at 4°C. As expected, HA-GST was only retrieved in supernatants regardless the temperatures (**Figure 6E**). Interestingly, at 37°C, HA-GST ARHGAP10 almost exclusively co-sedimented with microtubules whereas it was retained in the supernatant when the experiment was performed at 4°C to prevent microtubule polymerization (**Figure 6F**). Of note, very little actin was retrieved in the osteoclast lysate and no actin could be detected in the pellets that contained ARHGAP10 (**Figure 6F**). These data show that ARHGAP10 is indeed a microtubule-associated protein.

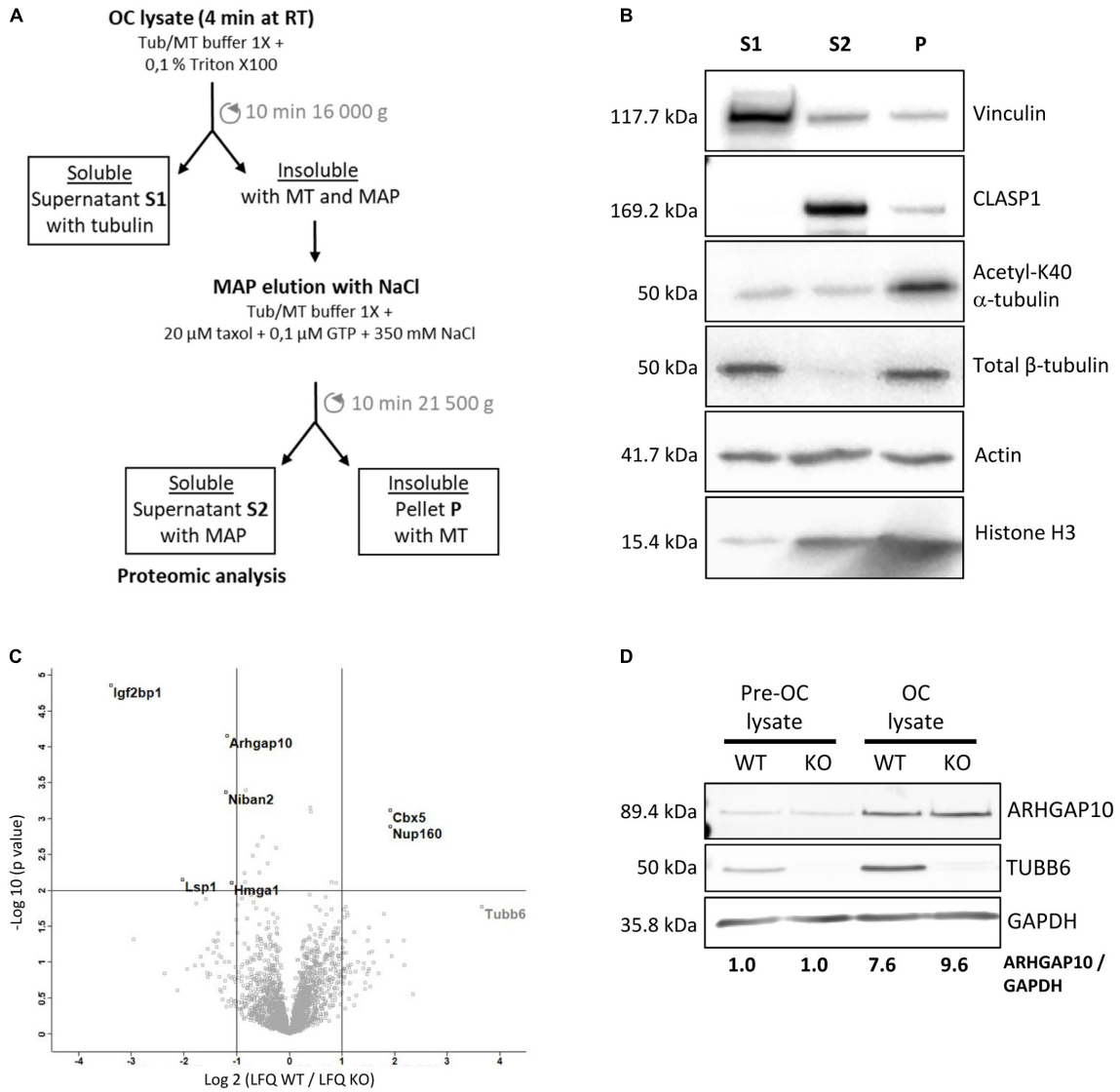

FIGURE 5 | Characterization of the microtubule-associated protein fraction of WT and Tubb6 KO osteoclasts. **(A)** Schematic representation of the osteoclast fractionation strategy in microtubule-stabilizing Tub/MT buffer to obtain soluble proteins (S1), a fraction enriched in microtubule-binding protein (S2) and an insoluble fraction containing microtubules (P). **(B)** Representative immunoblot analysis of selected protein distribution between the different fractions: Vinculin, CLASP1, acetylated K40 α-tubulin, β-tubulin, actin, and Histone H3. **(C)** Volcano plot of Label Free Quantitation (LFQ) results from four independent mass spectrometry experiments, showing proteins that are significantly more abundant in S2 from KO (top left) and WT (top right) osteoclast, with vertical lines indicating twofold change cut off and horizontal line $p = 0.01$ cut off, with x axis in $\log_2$(LFQ WT/LFQ KO) and y axis in $-\log_{10}$(p-value). **(D)** Representative immunoblot analysis of ARHGAP10, TUBB6 and GAPDH expressions in WT or Tubb6 KO RAW264.7 cells (Pre-OC) and in the osteoclasts (OC) derived from these cells.

Altogether, our data suggest that TUBB6 can control the amount of ARHGAP10 associated with microtubules in osteoclasts. This may contribute to control the size of sealing zones, which was shown to involve both TUBB6 (Guérit et al., 2020) and ARHGAP10 (Steenblock et al., 2014).

DISCUSSION

The cytoskeleton plays a key role in bone resorption by osteoclasts. F-actin organizes as a belt of podosomes required for adhesion and as backbone of the ruffled border, which is the actual bone resorption apparatus. Microtubules are also instrumental for podosome organization in osteoclasts and bone resorption, but the coordination mechanisms between the actin and tubulin cytoskeletons remain poorly characterized.

We identified previously TUBB6 as a β-tubulin isotype essential in osteoclasts for podosome belt integrity and for resorption (Guérit et al., 2020). To study the implications of TUBB6 in cytoskeleton dynamic parameters, we developed a model of osteoclasts KO for Tubb6 using the RAW264.7 pre-osteoclast cell line, which recapitulates the phenotype we

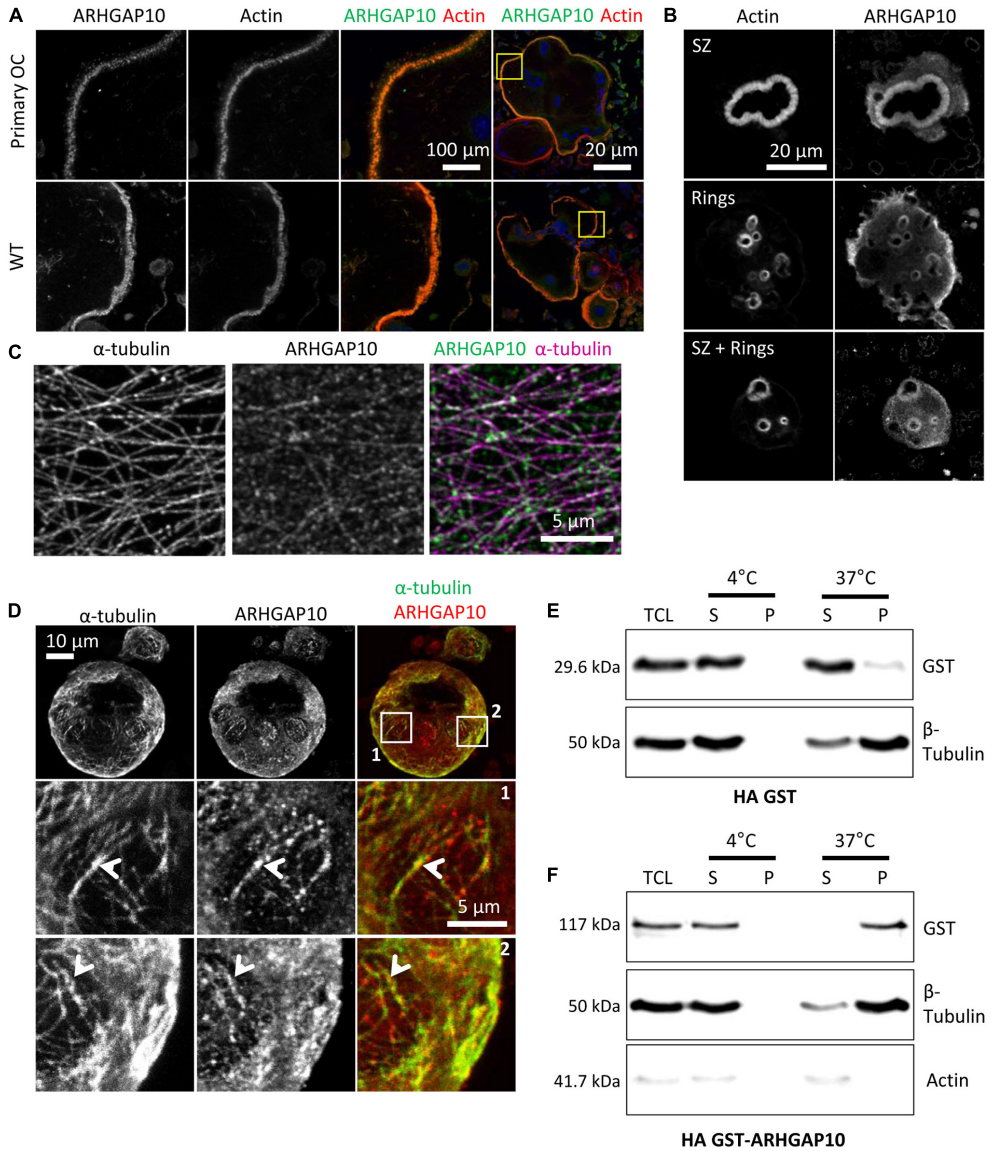

FIGURE 6 | ARHGAP10 is associated with both actin and microtubules. **(A)** Representative MIP images of RAW264.7 derived or primary (primary OC) osteoclasts seeded on glass and stained for ARHGAP10, actin, and DNA. Left images show enlargement of boxed areas in the images on the right. **(B)** Representative MIP images showing ARHGAP10 and actin localization in WT and Tubb6 KO osteoclasts sitting on ACC. **(C)** Representative single plan confocal image of a WT osteoclast stained for ARHGAP10 (green) and α-tubulin (pink). **(D)** Representative MIP images of a WT osteoclast sitting on ACC and stained for ARHGAP10 and α-tubulin. Boxed areas in top images are enlarged below, to show ARHGAP10 colocalization with microtubules (arrowheads). **(E,F)** Immunoblot analysis of lysates from HEK293T cells expressing HA-GST **(E)** or HA-GST-ARHGAP10 **(F)**, and subjected to microtubule pelleting assays at 4°C or 37°C. ARHGAP10 co-sediments at 37°C with microtubules in the pellet, which contains β tubulin but is devoid of actin.

reported recently for primary osteoclasts treated with Tubb6 siRNAs (Guérit et al., 2020). On top of the expected abnormal actin organization and reduced resorption activity, we found that the lack of TUBB6 also effected microtubule dynamics in osteoclasts: the speed of microtubule repolymerization after nocodazole treatment was reduced as well as individual microtubule growth speed, whereas their lifetime was increased, accompanied by an increase in tubulin acetylation. This suggests that TUBB6 has a microtubule-destabilizing effect in osteoclasts. Interestingly, overexpression of TUBB6 was reported previously to disrupt microtubule organization in various cycling cell types (Bhattacharya and Cabral, 2004) and to induce paclitaxel resistance, with serine 239 being essential for TUBB6 microtubule-destabilizing activity (Bhattacharya and Cabral, 2009). Serine 239 is located within the core of β-tubulin and it is conserved in TUBB1 and TUBB3. Interestingly, similarly to TUBB6, high expression of TUBB3 is suspected to participate in paclitaxel resistance (Kato et al., 2018). Furthermore, TUBB3 has been shown to significantly decrease microtubule growth rates (Pamula et al., 2016; Vemu et al., 2016), similar to what we

TABLE 1 | Protein changes in fractions S2.

Uniprot ID	Protein name	Gene name	Peptide counts	Coverage%	LFQ fold change KO/WT	*P*-value
More abundant in Tubb6 KO osteoclast S2						
O88477	Insulin-like growth factor 2 mRNA-binding protein 1	Igf2bp1	9	20.1	10.44	1.39E-05
P19973	Lymphocyte-specific protein 1	Lsp1	5	27.9	4.06	7.16E-03
Q8R1F1	Protein Niban 2	Niban2	23	42.3	2.30	4.27E-04
Q6Y5D8	Rho GTPase-activating protein 10	Arhgap10	24	36.1	2.27	7.00E-05
P17095	High mobility group protein HMG-I/HMG-Y	Hmga1	7	48.6	2.14	7.90E-03
More abundant in WT osteoclast S2						
Q9Z0W3	Nuclear pore complex protein Nup160	Nup160	6	6.9	0.26	1.30E-03
Q61686	Chromobox protein homolog 5	Cbx5	6	40.3	0.26	7.61E-04

found here for TUBB6. Furthermore, this intrinsic property on microtubule dynamics does not require residues located within the carboxy-terminal tail of TUBB3 leaving the possibility of serine 239 involvement (Pamula et al., 2016). Based on these data, it is very likely that TUBB6 intrinsically alters the dynamics of microtubules, similar to TUBB3.

We noticed an increase of K40-acetylation of α-tubulin upon KO of Tubb6 in osteoclasts, as also observed in CHO cells expressing Tubb6 shRNAs (Bhattacharya et al., 2011). K40-acetylation of α-tubulin is a well described marker of stable MT (Janke and Magiera, 2020). The increase of K40-acetylation we observed in Tubb6 KO osteoclasts may thus be a consequence of the increase of MT lifetime that we measured. K40-acetylation has been shown to play a crucial role in podosome belt establishment and/or stability in osteoclasts (Destaing et al., 2005). Lower K40-acetylation levels were also associated with various genetic defects leading to the alteration of podosome patterning in osteoclasts, such as the KO of Pyk2, myosin IXB, or cofilin 1 (Gil-Henn et al., 2007; McMichael et al., 2014; Zalli et al., 2016). In the case of Tubb6 gene disruption, we found conversely an increase of K40-acetylation associated with an abnormal organization of podosomes. Microtubule acetylation was shown to enhance their flexibility (Portran et al., 2017) and actually microtubules are heavily buckled in the podosome belt area of primary osteoclasts treated with Tubb6 siRNAs as compared to control (Guérit et al., 2020). Thus, an optimal level of microtubule acetylation appears essential for osteoclast function, potentially to provide microtubules with appropriate flexibility and mechanical resistance (Portran et al., 2017; Xu et al., 2017). Such optimal balance is known for other PTMs in general and for microtubule PTMs in particular. For instance, increasing and decreasing the level of microtubule glutamylation equally impair ciliary function in the nematode (O'Hagan et al., 2017). K40-acetylation could also participate in the changes in podosome dynamics we observed in Tubb6 KO osteoclasts. Indeed, dynamic microtubules were shown to regulate podosome fate in macrophages: podosome contact by plus-end MT mostly induces their dissolution or fission (Kopp et al., 2006) and increasing K40-acetylation of microtubules diminishes microtubule plus ends targeting of podosomes (Bhuwania et al., 2014). In Tubb6 KO osteoclasts, we observe increased podosome life span correlated with increased microtubule acetylation, which may result from a reduction in contacts between microtubules and podosomes.

Apart from directly impacting on the dynamics of microtubules, tubulin isotypes influence the recruitment of proteins on microtubules, which can also modulate their dynamics as well as cargo transport (Janke and Magiera, 2020). Our proteomic analyses of osteoclast S2 fractions, enriched in microtubule-associated proteins, did not reveal major changes whether osteoclasts expressed TUBB6 or not. Still, we found two cytoskeleton-related proteins: ARHAP10 and LSP1, which were increased in S2 in the absence of TUBB6. Similar to what was reported with Arhgap10 siRNAs (Steenblock et al., 2014), we found that the osteoclast KO of Tubb6 have small sealing zones that often remain immature. ARHGAP10 is a GAP that negatively regulates the activity of CDC42 (Ren et al., 2001). It was shown in osteoclasts to participate in a complex with the CDC42 exchange factor FGD6, all three proteins localizing at the sealing zone (Steenblock et al., 2014). Our data show that ARHGAP10 also colocalizes with osteoclast microtubules and that ARHGAP10 associates very efficiently with microtubules in an actin-independent fashion, suggesting that ARHGAP10 can associate with both microtubules and actin cytoskeleton in osteoclasts. CDC42 is essential for the correct dynamics of actin rings in osteoclasts and for bone resorption *in vitro* and *in vivo* in the mouse; conversely, excessive activity of CDC42 causes osteoclast hyperactivity and osteoporosis (Ito et al., 2010). The global level of CDC42 activity was not affected in osteoclasts KO for Tubb6 as compared to WT (data not shown), suggesting that by controlling ARHGAP10 association with the cytoskeleton, TUBB6 could contribute to the fine tuning of local CDC42 activity to ensure an optimal level of resorption. LSP1 is an actin-regulating protein, which was recently shown to associate with the cap of podosomes in macrophages (Cervero et al., 2018). LSP1 regulates macrophage podosome properties: the levels of LSP1 control the frequency and amplitude of podosome oscillations, and interfering with LSP1 expression reduces podosome life span and the protruding forces they exert on the extracellular matrix (Cervero et al., 2018). Moreover, lack of LSP1 was recently shown to affect the microtubule network in macrophages (Schäringer et al., 2021). Here we found that in the absence of TUBB6, podosome have longer life-span and we found increased amounts of LSP1 in the S2 fraction of Tubb6 KO osteoclasts, suggesting that LSP1 may participate in the control of actin-dynamics in osteoclasts in a TUBB6-dependent

fashion. The function of LSP1 in osteoclasts would deserve further investigations.

To conclude, our data highlight the crucial role of microtubule dynamics in podosome belt integrity in general and the involvement of TUBB6 in particular. We provide new insights into the control of microtubule dynamics in osteoclasts and position β-tubulin isotype TUBB6 as a key regulator of the crosstalk between actin and microtubules in osteoclast. Our results uncover novel regulatory mechanisms of osteoclast cytoskeleton and contribute to the better knowledge of the molecular processes controlling bone resorption. Our data could be valuable also in the context of osteolytic bone diseases and pave the way for novel solutions against osteoporosis by targeting osteoclast cytoskeleton.

DATA AVAILABILITY STATEMENT

Proteomic data from Max Quant treated with Perseus are in **Supplementary Table 1**.

AUTHOR CONTRIBUTIONS

AB and GB: conceptualization and supervision. AB, GB, JM, AM, DG, JC, and SU: methodology. GB, JM, AM, DG, JC, and SU: validation. AB, GB, JM, AM, DG, and SU: formal analyses. GB, JM, AM, DG, and SU: investigation. AB, GB, JM, and SU: writing – original draft. AB: project administration and funding acquisition. All authors contributed to the article and approved the submitted version.

FUNDING

This study was supported by the Centre National de la Recherche Scientifique (CNRS) and by the Universiteì de Montpellier, and by grants from the Fondation pour la Recherche Meìdicale (DEQ20160334933 to AB), the Fondation ARC pour la Recherche sur le Cancer (PJA 20191209321 to AB), and the Ligue Contre le Cancer Comité de l'Hérault (Grant LNCC HERAULT LS 199545 2020 to AB).

ACKNOWLEDGMENTS

We acknowledge the imaging facility Montpellier Ressources Imagerie (MRI), a member of the national infrastructure France-BioImaging supported by the French National Research Agency (ANR-10-INBS-04, 'Investments for the future'). Mass spectrometry experiments were carried out using the facilities of the Montpellier Proteomics Platform (PPM, BioCampus Montpellier). We are very grateful to Ariane Abrieu, Leslie Bancel-Vallée, Daniel Bouvard, Juliette van Dijk, Nathalie Morin, Didier Portran, and Amélie Viel (CRBM Montpellier, France) to for technical assistance, helpful advice and discussions. We also thank Daisuke Mori (Nagoya University, Japan) for the generous gift of ARHGAP10 expression vector.

SUPPLEMENTARY MATERIAL

The Supplementary Material for this article can be found online at: https://www.frontiersin.org/articles/10.3389/fcell.2021.778887/full#supplementary-material

Supplementary Figure 1 | (A) Representative immunoblot showing TUBB6 and GAPDH expression in WT and Tubb6 KO RAW264.7 clones. Note in overexposed panel in the middle that clones 2 and 4 retain traces of TUBB6. **(B)** Bar graph showing the frequency of WT and KO osteoclasts seeded on glass and presenting podosome rings, normal or abnormal podosome belt, counting a total of 200 WT and KO osteoclasts in two independent experiments. **(C)** Bar graph showing the frequency of WT and KO osteoclasts seeded on ACC and presenting sealing zone and/or rings counting over 50 osteoclasts per clone. **(D,E)** Bar graphs showing the level of osteoclast characteristic Cathepsin K **(D)** and Src **(E)** mRNAs relative to Gapdh as determined by Q-PCR in WT or Tubb6 KO RAW264.7 cells (Pre-OC) or osteoclasts (OC). **(F)** Representative images showing TRAP staining in WT and Tubb6 KO osteoclasts. **(G)** Representative immunoblot blot showing intracellular content of alpha-tubulin, Cathepsin K proenzyme, and its mature form in total cell lysates of WT and Tubb6 KO osteoclasts, and the secretion of mature Cathepsin K in the culture medium of the same cells. **(H)** Representative immunoblot blot showing TUBB5, TUBB6 and GAPDH expression in primary bone marrow macrophages (Pre-OC) and osteoclasts (OC) and in WT or Tubb6 KO RAW264.7 cells (pre-OC) or osteoclasts (OC).

Supplementary Figure 2 | Bar graph showing mean and SEM α-tubulin aster area after nocodazole washout in osteoclasts transfected with luciferase control siRNA or Tubb6 siRNAs si1077 and si1373, measuring at least 20 asters per group were measured in four independent experiments.

Supplementary Figure 3 | (A) Table showing the details of microtubule dynamics parameters from u-track analysis **(B)** Minimum to maximum boxplot showing microtubule growth speed determined in ImageJ 1.53c with MTrackJ in 15 WT and Tubb6 KO osteoclasts expressing EB1-GFP from three independent experiments and measuring 10–11 comets per osteoclasts; Mann–Whitney test: $^{***}p < 0.0002$. **(C,D)** Representative EB1-GFP comets tracks in WT **(C)** and Tubb6 KO **(D)** analyzed in **(B)**. **(E)** Minimum to maximum boxplot showing the length of the EB1-GFP signal in 18 WT and Tubb6 KO osteoclasts per condition from three independent experiments and measuring 25 comets in each osteoclast to determine the average comet length per osteoclast; Mann–Whitney test: $^{****}p < 0.0001$. **(F,G)** Representative images of the EB1-GFP signal at the tip of microtubules in WT **(F)** and KO **(G)** osteoclasts analyzed in **(E)**.

Supplementary Figure 4 | (A) Representative live confocal images of osteoclasts derived from WT or Tubb6 KO osteoclasts expressing LifeAct-mCherry and sitting on glass, showing the localization of LifeAct-mCherry signal at t0 = 0 min (red) and t2 = 6.5 min (green), with the overlapping areas in yellow. **(B)** Minimum to maximum boxplot showing the percentage of LifeAct-mCherry signal at t0 that persists at the same position at t2 in WT or Tubb6 KO osteoclasts; in a total of 22 WT and 21 KO osteoclasts from four different experiments. Mann–Whitney test: $^{**}p < 0.01$.

Supplementary Table 1 | Proteomic data from Max Quant treated with Perseus.

Supplementary Table 2 | Gene Onthology analysis of the proteins in the S2 fraction.

Supplementary Table 3 | List of the 601 proteins of the S2 fraction associated with a cytoskeleton-related Gene Ontology term.

Supplementary Videos 1, 2 | Detection and tracking of EB1-GFP expressing osteoclasts WT **(video 1)** or KO **(video 2)** using u-track software and settings described in Materials and Methods. Time is indicated as min:sec and frame is 68 μm.

Supplementary Videos 3, 4 | Live imaging of LifeAct-mCherry expressing WT **(video 3)** or KO **(video 4)** osteoclasts. Time is indicated as min:sec and frame is 90.5 μm.

Supplementary Videos 5, 6 | Live imaging of LifeAct-mCherry expressing WT **(video 5)** or KO **(video 6)** osteoclasts. Time is indicated as min:sec and frame is 16 μm.

REFERENCES

Bhattacharya, R., and Cabral, F. (2004). A ubiquitous beta-tubulin disrupts microtubule assembly and inhibits cell proliferation. *Mol. Biol. Cell* 15, 3123–3131. doi: 10.1091/mbc.E04-01-0060

Bhattacharya, R., and Cabral, F. (2009). Molecular basis for class V beta-tubulin effects on microtubule assembly and paclitaxel resistance. *J. Biol. Chem.* 284, 13023–13032. doi: 10.1074/jbc.M900167200

Bhattacharya, R., Yang, H., and Cabral, F. (2011). Class V β-tubulin alters dynamic instability and stimulates microtubule detachment from centrosomes. *Mol. Biol. Cell* 22, 1025–1034. doi: 10.1091/mbc.E10-10-0822

Bhuwania, R., Castro-Castro, A., and Linder, S. (2014). Microtubule acetylation regulates dynamics of KIF1C-powered vesicles and contact of microtubule plus ends with podosomes. *Eur. J. Cell Biol.* 93, 424–437. doi: 10.1016/j.ejcb.2014.07.006

Blangy, A., Bompard, G., Guerit, D., Marie, P., Maurin, J., Morel, A., et al. (2020). The osteoclast cytoskeleton - current understanding and therapeutic perspectives for osteoporosis. *J. Cell Sci.* 133:jcs244798. doi: 10.1242/jcs.244798

Bompard, G., van Dijk, J., Cau, J., Lannay, Y., Marcellin, G., Lawera, A., et al. (2018). CSAP acts as a regulator of TTLL-mediated microtubule glutamylation. *Cell Rep.* 25, 2866–2877. doi: 10.1016/j.celrep.2018.10.095

Brazier, H., Pawlak, G., Vives, V., and Blangy, A. (2009). The Rho GTPase Wrch1 regulates osteoclast precursor adhesion and migration. *Int. J. Biochem. Cell Biol.* 41, 1391–1401. doi: 10.1016/j.biocel.2008.12.007

Cervero, P., Wiesner, C., Bouissou, A., Poincloux, R., and Linder, S. (2018). Lymphocyte-specific protein 1 regulates mechanosensory oscillation of podosomes and actin isoform-based actomyosin symmetry breaking. *Nat. Commun.* 9:515. doi: 10.1038/s41467-018-02904-x

Cox, J., and Mann, M. (2008). MaxQuant enables high peptide identification rates, individualized p.p.b.-range mass accuracies and proteome-wide protein quantification. *Nat. Biotechnol.* 26, 1367–1372. doi: 10.1038/nbt.1511

Destaing, O., Saltel, F., Gilquin, B., Chabadel, A., Khochbin, S., Ory, S., et al. (2005). A novel Rho-mDia2-HDAC6 pathway controls podosome patterning through microtubule acetylation in osteoclasts. *J. Cell Sci.* 118, 2901–2911. doi: 10.1242/jcs.02425

Dogterom, M., and Koenderink, G. H. (2019). Actin-microtubule crosstalk in cell biology. *Nat. Rev. Mol. Cell Biol.* 20, 38–54. doi: 10.1038/s41580-018-0067-1

Gil-Henn, H., Destaing, O., Sims, N. A., Aoki, K., Alles, N., Neff, L., et al. (2007). Defective microtubule-dependent podosome organization in osteoclasts leads to increased bone density in Pyk2(-/-) mice. *J. Cell Biol.* 178, 1053–1064.

Guérit, D., Marie, P., Morel, A., Maurin, J., Verollet, C., Raynaud-Messina, B., et al. (2020). Primary myeloid cell proteomics and transcriptomics: importance of β-tubulin isotypes for osteoclast function. *J. Cell Sci.* 133:jcs239772. doi: 10.1242/jcs.239772

Guimbal, S., Morel, A., Guérit, D., Chardon, M., Blangy, A., and Vives, V. (2019). Dock5 is a new regulator of microtubule dynamic instability in osteoclasts. *Biol. Cell* 111:21. doi: 10.1111/boc.201900014

Ito, Y., Teitelbaum, S. L., Zou, W., Zheng, Y., Johnson, J. F., Chappel, J., et al. (2010). Cdc42 regulates bone modeling and remodeling in mice by modulating RANKL/M-CSF signaling and osteoclast polarization. *J. Clin. Invest.* 120, 1981–1993. doi: 10.1172/JCI39650

Janke, C., and Magiera, M. M. (2020). The tubulin code and its role in controlling microtubule properties and functions. *Nat. Rev. Mol. Cell Biol.* 21, 307–326. doi: 10.1038/s41580-020-0214-3

Kato, A., Naiki-Ito, A., Naitoh, I., Hayashi, K., Nakazawa, T., Shimizu, S., et al. (2018). The absence of class III β-tubulin is predictive of a favorable response to nab-paclitaxel and gemcitabine in patients with unresectable pancreatic ductal adenocarcinoma. *Hum. Pathol.* 74, 92–98. doi: 10.1016/j.humpath.2018.01.009

Khosla, S., and Hofbauer, L. C. (2017). Osteoporosis treatment: recent developments and ongoing challenges. *Lancet Diabetes Endocrinol.* 5, 898–907. doi: 10.1016/S2213-8587(17)30188-2

Koeppel, M. A., McCarthy, C. C., Moertl, E., and Jakobi, R. (2004). Identification and Characterization of PS-GAP as a novel regulator of caspase-activated PAK-2. *J. Biol. Chem.* 279, 53653–53664. doi: 10.1074/jbc.M410530200

Kopp, P., Lammers, R., Aepfelbacher, M., Woehlke, G., Rudel, T., Machuy, N., et al. (2006). The kinesin KIF1C and microtubule plus ends regulate podosome dynamics in macrophages. *Mol. Biol. Cell* 17, 2811–2823.

Leandro-García, L. J., Leskelä, S., Landa, I., Montero-Conde, C., ópez-Jiménez, E. L., Letón, R., et al. (2010). Tumoral and tissue-specific expression of the major human beta-tubulin isotypes. *Cytoskeleton* 67, 214–223. doi: 10.1002/cm.20436

Livak, K. J., and Schmittgen, T. D. (2001). Analysis of relative gene expression data using real-time quantitative PCR and the 2(-Delta Delta C(T)) Method. *Methods* 25, 402–408. doi: 10.1006/meth.2001.1262

Maurin, J., Morel, A., Hassen-Khodja, C., Vives, V., Jurdic, P., Machuca-Gayet, I., et al. (2018). Combined strategy of siRNA and osteoclast actin cytoskeleton automated imaging to identify novel regulators of bone resorption shows a non-mitotic function for anillin. *Eur. J. Cell Biol.* 97, 568–579. doi: 10.1016/j.ejcb.2018.10.002

McMichael, B. K., Scherer, K. F., Franklin, N. C., and Lee, B. S. (2014). The RhoGAP activity of myosin IXB is critical for osteoclast podosome patterning, motility, and resorptive capacity. *PLoS One* 9:e87402. doi: 10.1371/journal.pone.0087402

Mounier, L., Morel, A., Ferrandez, Y., Morko, J., Vääräniemi, J., Gilardone, M., et al. (2020). Novel 2,7-diazaspiro[4,4]nonane derivatives to inhibit mouse and human osteoclast activities and prevent bone loss in ovariectomized mice without affecting bone formation. *J. Med. Chem.* 63, 13680–13694. doi: 10.1021/acs.jmedchem.0c01201

O'Hagan, R., Silva, M., Nguyen, K. C. Q., Zhang, W., Bellotti, S., Ramadan, Y. H., et al. (2017). Glutamylation regulates transport, specializes function, and sculpts the structure of cilia. *Curr. Biol.* 27, 3430–3441. doi: 10.1016/j.cub.2017.09.066

Okumura, S., Mizoguchi, T., Sato, N., Yamaki, M., Kobayashi, Y., Yamauchi, H., et al. (2006). Coordination of microtubules and the actin cytoskeleton is important in osteoclast function, but calcitonin disrupts sealing zones without affecting microtubule networks. *Bone* 39, 684–693. doi: 10.1016/j.bone.2006.04.010

Pamula, M. C., Ti, S.-C., and Kapoor, T. M. (2016). The structured core of human β tubulin confers isotype-specific polymerization properties. *J. Cell Biol.* 213, 425–433. doi: 10.1083/jcb.201603050

Portran, D., Schaedel, L., Xu, Z., Théry, M., and Nachury, M. V. (2017). Tubulin acetylation protects long-lived microtubules against mechanical ageing. *Nat. Cell Biol.* 19, 391–398. doi: 10.1038/ncb3481

Raynaud, F., Homburger, V., Seveno, M., Vigy, O., Moutin, E., Fagni, L., et al. (2018). SNAP23–Kif5 complex controls mGlu1 receptor trafficking. *J. Mol. Cell Biol.* 10, 423–436. doi: 10.1093/jmcb/mjy031

Ren, X.-R., Du, Q.-S., Huang, Y.-Z., Ao, S.-Z., Mei, L., and Xiong, W.-C. (2001). Regulation of Cdc42 gtpase by proline-rich tyrosine kinase 2 interacting with Psgap, a novel pleckstrin homology and src homology 3 domain containing rhogap protein. *J. Cell Biol.* 152, 971–984. doi: 10.1083/jcb.152.5.971

Sanjana, N. E., Shalem, O., and Zhang, F. (2014). Improved vectors and genome-wide libraries for CRISPR screening. *Nat. Methods.* 11, 783–784. doi: 10.1038/nmeth.3047

Schäringer, K., Maxeiner, S., Schalla, C., Rütten, S., Zenke, M., and Sechi, A. (2021). LSP1-myosin1e bimolecular complex regulates focal adhesion dynamics and cell migration. *FASEB J* 35:e21268. doi: 10.1096/fj.202000740RR

Sekiguchi, M., Sobue, A., Kushima, I., Wang, C., Arioka, Y., Kato, H., et al. (2020). ARHGAP10, which encodes Rho GTPase-activating protein 10, is a novel gene for schizophrenia risk. *Transl. Psychiatry* 10:247. doi: 10.1038/s41398-020-00917-z

Søe, K., and Delaissé, J.-M. (2017). Time-lapse reveals that osteoclasts can move across the bone surface while resorbing. *J. Cell. Sci.* 130, 2026–2035. doi: 10.1242/jcs.202036

Spano, A. J., and Frankfurter, A. (2010). Characterization of anti-beta-tubulin antibodies. *Methods Cell Biol.* 95, 33–46. doi: 10.1016/S0091-679X(10)95003-6

Steenblock, C., Heckel, T., Czupalla, C., Espírito Santo, A. I., Niehage, C., Sztacho, M., et al. (2014). The Cdc42 guanine nucleotide exchange factor FGD6 coordinates cell polarity and endosomal membrane recycling in osteoclasts. *J. Biol. Chem.* 289, 18347–18359. doi: 10.1074/jbc.M113.504894

Ti, S.-C., Alushin, G. M., and Kapoor, T. M. (2018). Human β-tubulin isotypes can regulate microtubule protofilament number and stability. *Dev. Cell* 47, 175–190. doi: 10.1016/j.devcel.2018.08.014

Touaitahuata, H., Morel, A., Urbach, S., Mateos-Langerak, J., de Rossi, S., and Blangy, A. (2016). Tensin 3 is a new partner of Dock5 that controls osteoclast podosome organization and activity. *J. Cell Sci.* 129, 3449–3461. doi: 10.1242/jcs.184622

Tyanova, S., Temu, T., Sinitcyn, P., Carlson, A., Hein, M. Y., Geiger, T., et al. (2016). The perseus computational platform for comprehensive analysis of (prote)omics data. *Nat. Methods* 13, 731–740. doi: 10.1038/nmeth.3901

Vemu, A., Atherton, J., Spector, J. O., Moores, C. A., and Roll-Mecak, A. (2017). Tubulin isoform composition tunes microtubule dynamics. *Mol. Biol. Cell* 28, 3564–3572. doi: 10.1091/mbc.E17-02-0124

Vemu, A., Atherton, J., Spector, J. O., Szyk, A., Moores, C. A., and Roll-Mecak, A. (2016). Structure and dynamics of single-isoform recombinant neuronal human tubulin. *J. Biol. Chem.* 291, 12907–12915. doi: 10.1074/jbc.C116.731133

Vives, V., Laurin, M., Cres, G., Larrousse, P., Morichaud, Z., Noel, D., et al. (2011). The Rac1 exchange factor Dock5 is essential for bone resorption by osteoclasts. *J. Bone Miner. Res.* 26, 1099–1110. doi: 10.1002/jbmr.282

Xu, Z., Schaedel, L., Portran, D., Aguilar, A., Gaillard, J., Marinkovich, M. P., et al. (2017). Microtubules acquire resistance from mechanical breakage through intralumenal acetylation. *Science* 356, 328–332. doi: 10.1126/science.aai8764

Zalli, D., Neff, L., Nagano, K., Shin, N. Y., Witke, W., Gori, F., et al. (2016). The actin-binding protein cofilin and its interaction with cortactin are required for podosome patterning in osteoclasts and bone resorption in vivo and in vitro. *J. Bone Miner. Res.* 31, 1701–1712. doi: 10.1002/jbmr.2851

Conflict of Interest: The authors declare that the research was conducted in the absence of any commercial or financial relationships that could be construed as a potential conflict of interest.

Publisher's Note: All claims expressed in this article are solely those of the authors and do not necessarily represent those of their affiliated organizations, or those of the publisher, the editors and the reviewers. Any product that may be evaluated in this article, or claim that may be made by its manufacturer, is not guaranteed or endorsed by the publisher.

frontiers in Cell and Developmental Biology

ORIGINAL RESEARCH
published: 13 January 2022
doi: 10.3389/fcell.2021.777450

Diabetes Medication Metformin Inhibits Osteoclast Formation and Activity in *In Vitro* Models for Periodontitis

*Lucy Y. Tao[1,2†], Katarzyna B. Łagosz-Ćwik[3†], Jolanda M.A. Hogervorst[4], Ton Schoenmaker[1], Aleksander M. Grabiec[3], Tim Forouzanfar[5], Fridus A. van der Weijden[1] and Teun J. de Vries[1]**

[1]Department of Periodontology, Academic Centre for Dentistry Amsterdam, University of Amsterdam and Vrije University Amsterdam, Amsterdam, Netherlands, [2]Amsterdam University College, University of Amsterdam and Vrije University Amsterdam, Amsterdam, Netherlands, [3]Department of Microbiology, Faculty of Biochemistry, Biophysics and Biotechnology, Jagiellonian University, Kraków, Poland, [4]Department of Oral Cell Biology, Academic Centre for Dentistry Amsterdam, University of Amsterdam and Vrije University Amsterdam, Amsterdam, Netherlands, [5]Department of Oral and Maxillofacial Surgery and Oral Pathology, Amsterdam UMC, Amsterdam, Netherlands

OPEN ACCESS

Edited by:
Stefania Mariggiò,
National Research Council (CNR), Italy

Reviewed by:
Martina Rauner,
Technical University Dresden, Germany
Rupesh K. Srivastava,
All India Institute of Medical Sciences, India

***Correspondence:**
Teun J. de Vries
teun.devries@acta.nl

†These authors have contributed equally to this work

Specialty section:
This article was submitted to Cellular Biochemistry, a section of the journal Frontiers in Cell and Developmental Biology

Received: 15 September 2021
Accepted: 13 December 2021
Published: 13 January 2022

Citation:
Tao LY, Łagosz-Ćwik KB, Hogervorst JMA, Schoenmaker T, Grabiec AM, Forouzanfar T, van der Weijden FA and de Vries TJ (2022) Diabetes Medication Metformin Inhibits Osteoclast Formation and Activity in In Vitro Models for Periodontitis. Front. Cell Dev. Biol. 9:777450. doi: 10.3389/fcell.2021.777450

Diabetes and periodontitis are comorbidities and may share common pathways. Several reports indicate that diabetes medication metformin may be beneficial for the periodontal status of periodontitis patients. Further research using appropriate cell systems of the periodontium, the tissue that surrounds teeth may reveal the possible mechanism. Periodontal ligament fibroblasts anchor teeth in bone and play a role in the onset of both alveolar bone formation and degradation, the latter by inducing osteoclast formation from adherent precursor cells. Therefore, a cell model including this type of cells is ideal to study the influence of metformin on both processes. We hypothesize that metformin will enhance bone formation, as described for osteoblasts, whereas the effects of metformin on osteoclast formation is yet undetermined. Periodontal ligament fibroblasts were cultured in the presence of osteogenic medium and 0.2 or 1 mM metformin. The influence of metformin on osteoclast formation was first studied in PDLF cultures supplemented with peripheral blood leukocytes, containing osteoclast precursors. Finally, the effect of metformin on osteoclast precursors was studied in cultures of $CD14^+$ monocytes that were stimulated with M-CSF and receptor activator of Nf-κB ligand (RANKL). No effects of metformin were observed on osteogenesis: not on alkaline phosphatase activity, Alizarin red deposition, nor on the expression of osteogenic markers RUNX-2, Collagen I and Osteonectin. Metformin inhibited osteoclast formation and accordingly downregulated the genes involved in osteoclastogenesis: RANKL, macrophage colony stimulating factor (M-CSF) and osteoclast fusion gene DC-STAMP. Osteoclast formation on both plastic and bone as well as bone resorption was inhibited by metformin in M-CSF and RANKL stimulated monocyte cultures, probably by reduction of RANK expression. The present study unraveling the positive effect of metformin in periodontitis patients at the cellular level, indicates that metformin inhibits osteoclast formation and activity, both when orchestrated by periodontal ligament fibroblasts and in cytokine driven osteoclast formation assays. The results indicate that

metformin could have a systemic beneficiary effect on bone by inhibiting osteoclast formation and activity.

Keywords: periodontitis, osteoclasts, diabetes, metformin, peridontal ligament

INTRODUCTION

There are indications that diabetes patients have an increased risk of developing periodontitis ((Nascimento et al., 2018; Verhulst et al., 2019). Therefore, common pathogenesis pathways may exist. Periodontitis is the inflammation-related disease. It is characterized by degradation of alveolar bone that surrounds teeth, a process activated by recruited multinucleated osteoclasts. From a pharmacological point of view one could argue that medication that is used for diabetes may also benefit periodontitis patients. Metformin could be such a pleiotropic drug, showing positive effects not only in diabetes, but also in osteoporosis and periodontitis (Ursini et al., 2018). Its principal mode of action is as insulin sensitizer. It lowers the blood sugar level, which makes it a suitable drug for treating diabetes type II patients. It is a biguanid that has been used as an insulin sensitizer for more than 50 years (Halimi, 2006). The last 10 years have shown that metformin could be beneficial in various bone diseases as well, including periodontitis (Chandran, 2017).

Diabetes adversely affects a variety of organ systems in the body, including bones. It diminishes bone-mineral density and therefore weakens bone strength (Bak et al., 2010). When blood glucose levels increase, cartilage quality and quantity decrease (Mannucci and Dicembrini 2015). Diabetes patients have lower bone quality, and metformin may reverse these effects on bone, as shown in preclinical animal studies and clinical applications (Bahrambeigi 2019). It is therefore hypothesized that insulin stimulates osteoblast differentiation and bone matrix synthesis.

A beneficiary effect of metformin on bone has also been studied in periodontitis models (Bak et al., 2010; Araújo et al., 2017; Sun et al., 2017). Bak et al. investigated the effects of metformin on the progression of periodontitis in rats with ligature-induced periodontitis. Metformin reduced inflammatory cell infiltration and alveolar bone loss in periodontal tissues (Bak et al., 2010). This and other findings (Araújo et al., 2017) suggest that low doses of metformin reduce bone loss. Sun et al. found a higher number of osteoclasts in diabetic rats compared to non-diabetic rats (Sun et al., 2017). In the same study, it was shown that metformin decreased the number of osteoclasts compared to untreated diabetic rats (Sun et al., 2017). Gingival fibroblasts, when exposed to lipopolysaccharide (LPS) from periodontopathic bacterium *Porphyromonas gingivalis*, respond to metformin by severely lowering the expression of inflammatory cytokines IL-6, IL-1β and TNF-α, demonstrating an anti-inflammatory function of metformin (Kang et al., 2017). Calcium phosphate scaffolds with incorporated metformin showed increased osteogenic activity by periodontal ligament fibroblasts, which holds promise for use of metformin in bone regeneration (Zhao et al., 2019). These mouse studies urge extrapolating research using human cell systems on both the bone formation and bone degradation site, hereby elucidating the beneficiary effect of metformin in the human context.

Clinically, metformin has been applied in experimental treatments of periodontitis patients. Metformin was applied in gels at the site of alveolar bone loss. Patients were treated with a gel consisting of 0.5, 1 or 1.5% metformin locally at the site of bone loss. 10 μL of gel was injected into the periodontal pockets, and during the trial time of 6 months, gingival crevicular fluid was collected for analysis (Pradeep et al., 2013). Comparing all metformin test groups to the control, periodontal parameters significantly improved (Pradeep et al., 2013). Rao et al. treated smokers with chronic periodontitis using 1% metformin gel in a clinical trial (Rao et al., 2013) and showed similar improvements. Subsequent follow-up studies with slight modifications resulted in similar results (Pradeep et al., 2015; Pradeep et al., 2016).

These promising results with metformin in animal studies as well as in clinical studies urge mechanistic insight using a relevant cell system. Periodontal ligament fibroblasts anchor teeth in bone and also play a crucial role in both osteogenesis and osteoclastogenesis, processes that can be elegantly mimicked *in vitro* (De Vries et al., 2017; Ruppeka-Rupeika et al., 2018; De Vries et al., 2019; Karlis et al., 2020; Loo-Kirana R.; Gilijamse M.; Hogervorst J., 2021). Support for the relevance of periodontal ligament fibroblasts comes from an animal study where periodontal ligament fibroblasts were shown to play a key role in alveolar bone regeneration (Ren et al., 2015).

In the present study, we assessed whether metformin has an alleged positive effect on osteogenesis by culturing periodontal ligament fibroblasts in the presence of osteogenic medium and metformin. The effect of metformin on mineralization was assessed by quantifying alkaline phosphatase activity, by staining deposited mineral with Alizarin red staining and by gene expression of osteogenic transcription factor RUNX-2, matrix protein collagen type I and bone matrix protein Osteonectin. The effect of metformin on osteoclastogenesis was assessed in co-cultures of periodontal ligament fibroblasts and peripheral blood mononuclear cells (PBMCs) containing osteoclast precursors. Here, the formation of multinucleated cells was assessed after staining osteoclast characteristic tartrate resistant acid phosphatase (TRAcP) and by counting the nuclei. Since osteoclast-like cells that are formed in these cocultures do not resorb bone (De Vries et al., 2006; Sokos et al., 2015), we further assessed the effect of metformin on osteoclast activity by culturing $CD14^+$ monocytes in the presence of M-CSF and RANKL, a cocktail yielding osteoclasts.

MATERIALS AND METHODS

Cell Cultures

The periodontal ligament fibroblasts were isolated from nine different donors who had their wisdom teeth extracted for medical reasons. Sampling from the donors was conducted at

Amsterdam University Hospital, location VU University Hospital under supervision of TF. The studies involving human participants were reviewed and approved by the Medische Etische Toetsingscommissie VU Medisch Centrum, Amsterdam, the Netherlands. The teeth containing periodontal ligament fibroblasts were surgical waste control material for osteogenic differentiation of adipose tissue derived stem cells.

All the individuals were informed that the cells retrieved from the surgical waste material was used for research on bone formation and bone degradation. A signed informed consent and samples were coded to guarantee the anonymity of the donors as required by Dutch law. The use of buffy coats from the blood bank (Sanquin, Amsterdam) was under ethical committee number NVT230.01. Researchers handling the fibroblasts (LT, KL-C, TJdV) could not in any way trace back the identity of the donors. Cells were scraped off the middle one third of the root and were propagated until passage three and subsequently frozen in liquid nitrogen. Cells from passage five were used in all experiments.

Osteogenesis and Osteoclastogenesis Assays Using Periodontal Ligament Fibroblasts

Confluent flasks at passage four were trypsinized and cells were seeded at day -1 in 48 wells plates at $1.5{\cdot}10^4$ cells per well for osteoclastogenesis assays or $3{\cdot}10^4$ cells per well for osteogenesis assays. At day 0, the start of the experiment, the culture medium was removed from the 48-well plates. For the osteogenesis-assay plates, 0.4 ml mineralisation medium - composed of DMEM, 10% FCI, 1% PSF, 50 µg/ml ascorbic acid (Sigma), 10 nM β-Glycerophosphate (Sigma), and different metformin concentrations (or the solvent volume of sterile water, in the case of 0 mM metformin) were added to the wells. For osteoclastogenesis assays, peripheral blood mononuclear cells (PBMCs) derived from a buffy coat (Sanquin, Amsterdam) were added as source containing osteoclast precursors. ACTA has an agreement with bloodbank Sanquin to use buffy coats for research purposes. Metformin (Sigma Aldrich, D150959) was dissolved in demineralized water and added to cultures in a range between 0 and 1.0 mM, according to concentrations used in the literature.

For the osteoclastogenesis-assay plates, 0.2 ml containing $5{\cdot}10^5$ PBMCs in culture medium were added to the wells as well as 0.2 ml of metformin-consisting medium. During the 21 days duration of the experiment, culture- and mineralization-medium with the appropriate concentration of metformin was replenished twice a week.

DNA Concentration and Alkaline Phosphatase Activity

Cells were harvested at day 0 and day 14 of culturing. In order not to sample dead cells, the adherent cells were washed twice with PBS. Next, they were lysed in 150 µl MilliQ per well and stored in −20°C. Prior to analysis, the plates underwent three cycles of freeze-thawing. Alkaline phosphatase (ALP) activity was measured using 4-nitrophenyl phosphate disodium salt (Merck, Darmstadt, Germany) at pH 10.3 as a substrate for ALP according to the method described by Bastidas-Coral (Bastidas-Coral et al., 2016). After incubation of 60 min at 37°C, the reaction was stopped with sodium hydroxide. Absorbance was measured with 405 nm with a Synergy HT spectrophotometer (BioTek Instruments Inc., Winooski, VT). DNA concentration (ng/ml) was measured using CyQuant Cell Proliferation Assay Kit (Molecular Probes, Leiden, Netherlands) mixed with lysis buffer. Fluorescence was measured at 485 nm excitation and 528 nm emission with a Synergy HT spectrophotometer (BioTek Instruments Inc., Winooski, VT, United States). ALP activity was expressed as ALP per DNA (nMol/ng).

Alizarin Red Staining

Alizarin red staining was performed after 14 or 21 days to analyze the mineral deposition. 2% Alizarin red S at pH 4.3 (Sigma-Aldrich) was used for staining. Cells were fixed for 10 min in 4% formaldehyde and rinsed with deionized water before adding 300 µl of 2% Alizarin solution per well. After incubation of 15 min at room temperature, the cells were washed with deionized water and air-dried. Mineral deposition was visualized as red nodules.

Quantitative Polymerase Chain Reaction

Quantitative polymerase chain reaction (qPCR) analysis was performed for osteogenesis and osteoclastogenesis at day 0 and 14 or 21. At these time points the culture medium was removed and 200 µl RNA lysis buffer (Qiagen, Hilden, Germany) was added per well. Subsequently, the 48-well plates were stored at −80°C until further use. RNA isolation was performed with Qiagen RNeasy Mini kit according to the manufacturer's instructions. The RNA concentration and quality was determined using absorption read at 260 and 280 nm with Synergy HT spectrophotometer (BioTek Instruments Inc., Winooski, VT). RNA was reverse transcribed to cDNA with the MBI Fermentas cDNA synthesis Kit (Vilnius, Lithuania). Oligo(dT) 18 and D(N)6 were used as primers. Real time primers were designed for several genes. PCR was performed on the LC480 light cycler (Roche, Basel, Switzerland). Beta-2-microglobulin (β2M) was used as a housekeeping gene for the osteogenesis markers, while hypoxanthine phosphoribosyltransferase 1 (HPRT1) was used as housekeeping gene for the osteoclastogenesis and osteoclast makers. Gene expression was normalized for β2M or HPRT1 expression following the comparative threshold (Ct) method. ΔC ($Ct_{\text{gene of interest}} - Ct_{\text{housekeeping gene}}$) was calculated and relative expression of the genes was determined as $2^{-\Delta Ct}$. The primer sequences are listed in **Table 1**.

TRAcP Staining and Osteoclast Counts

Plates for detecting tartrate resistant acid phosphatase (TRAcP) activity staining were harvested in duplicate on t = 21. Cells were washed with PBS and fixed with 4% PBS buffered formaldehyde for 10 min before being stored with PBS at 4°C. After washing the cells with water at 37°C, TRAcP staining solution was made consisting of Fast Garnet GBC base, sodium nitrate, acetate, naphthol AS-BI and tartrate in AD on 37°C, using the leukocyte acid phosphate kit (Sigma) following the

TABLE 1 | primers used.

Genes	Primer sequence 5′-3′	Amplicon length (bp)	ENSEMBL gene ID
Housekeeping gene			
HPRT	Fw TgACCTTgATTTATTTgCATACC	101	ENSG00000165704
	Rv CGAgCAAgACgTTCAgTCCT		
B2M	Fw CgACggCCgCTgTCA	100	ENSG00000160255
	Rv TgTTgTTTTCAgCCAgCTTgTg		
Osteogenesis			
RUNX2	Fw CCAgAAggCACAgACAgAAgCT	156	ENSG00000124813
	Rv AggAATgCgCCCTAAATCACT		
Collagen I	Fw TCCAACgAgATCgAgATCC	190	ENSG00000108821
	Rv AAgCCgAATTCCTggTCT		
Osteonectin	Fw TACATCgggCCTTgCAAATAC	100	ENSG00000231061
	Rv AgggTgACCAggACgTTCTTg		
Osteoclastogenesis		67	ENSG00000141655
RANK	Fw CCTggACCAACTgTACCTTCCT		
	Rv ACCgCATCggATTTCTCTgT	60	ENSG00000120659
RANKL	Fw CATCCCATCTggTTCCCATAA		
	Rv gCCCAACCCCgATCATg	100	ENSG00000164761
OPG	Fw CTgCgCgCTCgTgTTTC		
	Rv ACAgCTgATgAgAggTTTCTTCgT	100	ENSG00000184371
M-CSF	Fw CCgAggAggTgTCggAgTAC		
	Rv AATTTggCACgAggTCTCCAT		
DC-STAMP	Fw ATTTTCTCAgTgAgCAAgCAgTTTC	101	ENSG00000164935
	Rv gAATCATggATAATATCTTgAgTTCCTT		
TRAcP	Fw CACAATCTgCAgTACCTgCAAggAT	128	ENSG00000102575
	Rv CCCATAGTggAAgCgCAgATA		
CD14	Fw ggTTCggAAgACTTATCgACCAT	109	ENSG00000170458
	Rv TCATCgTCCAgCTCACAAggT		
Cathepsin K	Fw CCATATgTgggACAggAAgAgAgTT	149	ENSG00000143387
	Rv TgCATCAATggCCACAgAgA		
Nfatc1	Fw AgCAgAgCACggACAgCTATC	143	ENSG00000131196
	Rv ggTCAgTTTTCgCTTCCATCTC		
Cox1	5′ AgTACAgCTACgAgCAgTT 3′	100	ENSG00000229899
	5′ gAgACTCCCTgATgACATCC 3′		
Cox2	5′ gCATTCTTTgCCCAgCACTT 3′	100	ENSG00000267084
	5′ AgACCAggCACCAgACCAAAgA 3′		

manufacturer's instructions. The cells were counterstained with DAPI (diamidino-2phenylindole dihydrochloride). A distinction was made between cells with 3-5 nuclei, and cells with ≤6 nuclei. For analyses, the average of the number counted in the duplicate wells per patient was used.

Blood Cell Isolation

Buffy coats (Sanquin, Amsterdam, Netherlands) of healthy donors were diluted 1:1 in 1% PBS-citrate (pH 7.4). Thereafter, 25 ml of diluted blood was carefully layered on 15 ml Lymphoprep (Axisshield Po CAS, Oslo, Norway) and centrifuged for 30 min at 800 x G without brake. The interphase containing the PBMCs was collected and washed three times in 1% PBS-citrate by spinning down the cells at 400 g with full brakes and by decanting the supernatant. Finally, the cells were recovered in culture medium.

Monocyte Isolation

$CD14^+$ monocytes retrieved from peripheral blood were used in experiments where osteoclasts were grown using M-CSF and RANKL instead of fibroblasts and PBMCs. Here, $CD14^+$ cells were isolated using $CD14^+$ microbeads (Miltenyi, Bergisch Gladbach, Germany) according to a previously described method (Ten Harkel et al., 2015). $CD14^+$ monocytes were cultured for 3 days in M-CSF (25 ng/ml), followed by 10 ng/mL M-CSF and 10 ng/ml RANKL until 21 days.

Bone Resorption

Bone resorption was analyzed in cultures on bone after a culture period of 21 days. After this period, the cells present on the bovine cortical bone slices were removed with 0.25 M NH_4OH followed by sonication in ice water for 30 min. The slices were washed in distilled water, incubated in a saturated alum solution, washed in distilled water, and stained with Coomassie Brilliant blue. The surface areas of individual resorption pits were measured using Image-Pro Plus software (Media Cybernetics, Silver Spring, MD).

Statistical Analysis

The effects on the cells between different metformin concentrations over time were compared using one way ANOVA followed by the non-parametric Friedman test, using GraphPad Prism software. Dunn's multiple comparison test was done as a post-test. A p value of $^*p \leq 0.05$ was chosen to determine the level of significance.

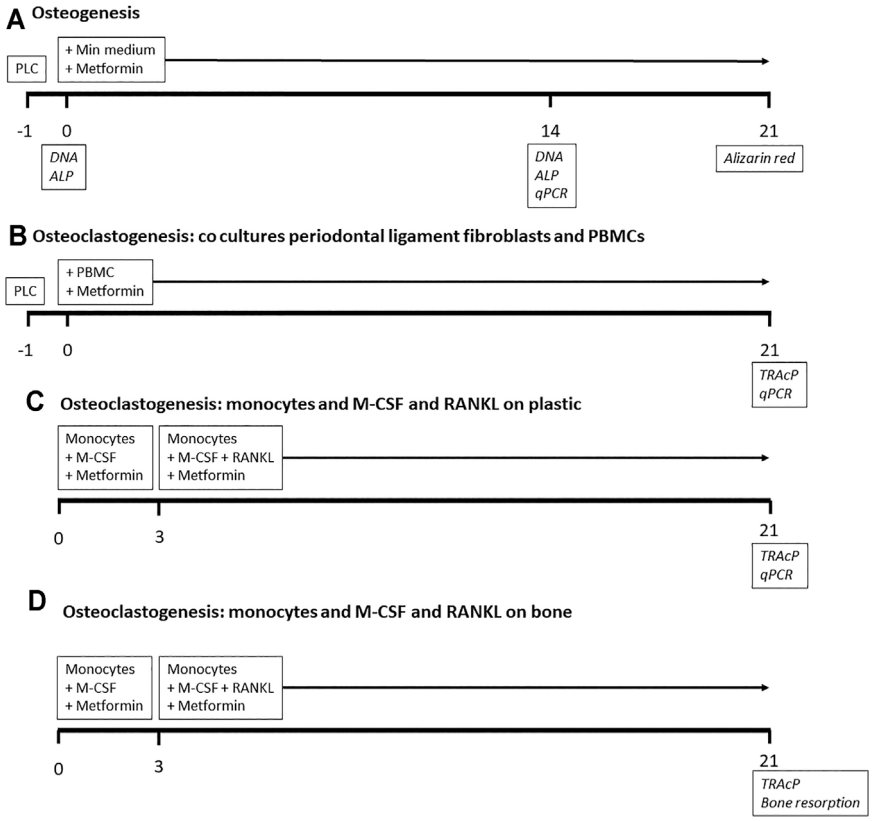

FIGURE 1 | Outline of experiments. Timeline in days. For osteogenesis and osteoclastogenesis co culture experiments, periodontal ligament cells (PLC) were cultured 1 day before the start of the experiment. Metformin was added throughout all experiments. Analyses in italics at the days of sampling. PBMCs: peripheral blood mononuclear cells.

RESULTS

Metformin Titration in Periodontal Ligament Mediated Osteogenesis

In order to establish whether metformin plays a role in periodontal ligament driven osteogenesis, we added 5-fold dilutions (0.008–1 mM) of metformin in mineralization assays (n = 3 donors). As first measurement, we assessed whether metformin could influence proliferation, measure of how metformin could influence metabolic activity such as proliferation. Metformin had no effect on proliferation (**Supplementary Figure S1A**), nor on the alkaline phosphatase activity per cell (**Supplementary Figure S1B**). Alizarin red staining showed donor variability at 14 days, which vanished at 21 days (**Supplementary Figure S1C**). At higher magnification, the alizarin red staining appeared in nodule-like structures (**Supplementary Figure S1D**). No clear effect of metformin on mineralization was observed.

Metformin Does Not Affect Periodontal Ligament Mediated Osteogenesis

The above titration experiment showed that metformin was tolerated at high concentrations and seemed not to affect osteogenesis. All subsequent osteogenesis and osteoclastogenesis experiments were performed using a higher number periodontal ligament donors (n = 6) with 0.2 and 1.0 mM metformin. Compared to day 0, ALP enzyme was significantly higher at day 14, with no differences between normal medium, mineralization medium without or with metformin (**Figure 2A**). Alizarin red staining demonstrated greater variability compared to the donors of **Figure 1**, but again with no clear metformin effect (**Figure 2B**). qPCRs for early osteogenic marker RUNX 2 (**Figure 2C**), Collagen type I (**Figure 2D**) and late osteogenic marker Osteonectin (**Figure 2E**) showed an increase in expression over time (t = 0 vs. t = 14) for all genes. Only osteonectin expression differed between normal medium and mineralization medium at t = 14 days. Metformin had no effect on osteogenic gene expression. These experiments together showed that metformin did not affect osteogenic differentiation of periodontal ligament fibroblasts.

Effect of Metformin in Periodontal Ligament- PBMC Co Cultures

As previously shown (De Vries et al., 2017; Ruppeka-Rupeika et al., 2018; Loo-Kirana R.; Gilijamse M.; Hogervorst J., 2021), the periodontal ligament plays a role in both osteogenesis and osteoclastogenesis. We next assessed whether metformin could

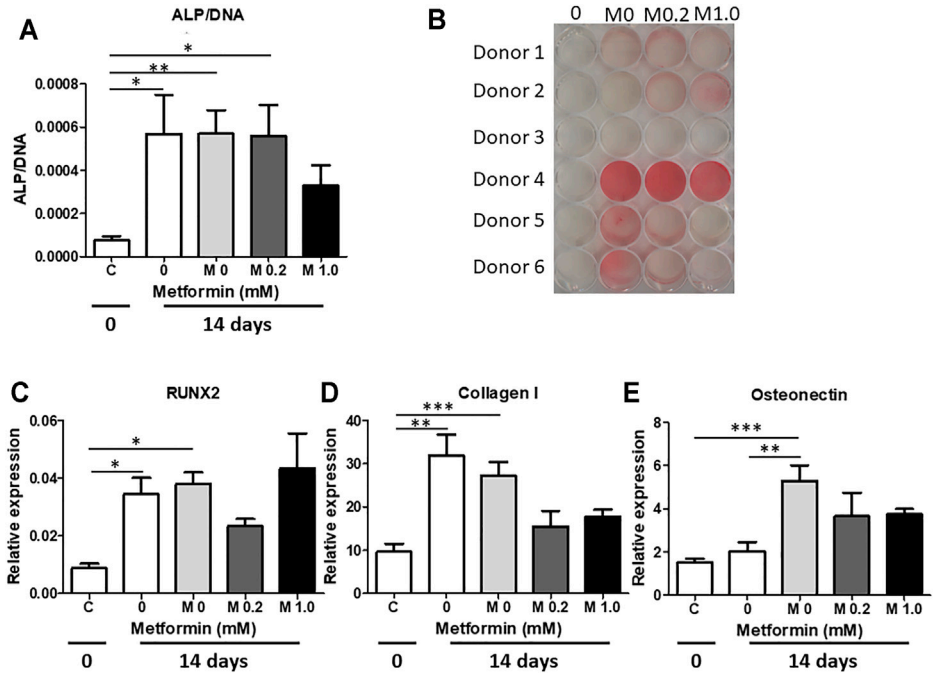

FIGURE 2 | Metformin does not increase mineralization by periodontal ligament fibroblast cultures. Metformin was used in two concentrations (0.2 and 1.0 mM) in mineralization assays. **(A)** Alkaline phosphatase enzyme activity per cell at 0 **(C)** and 14 days (0 – normal medium without metformin; M0, M0.2 and M1.0 0, 0.2 and 1.0 mM Metformin in Mineralization medium). **(B)** Alizarin red staining at 21 days, **(C–E)**: genes expression of RUNX2 **(C)**, Collagen I **(D)** and Osteocalcin **(E)** at 0 days **(C)** and at 14 days (0 – normal medium without Metformin; M0, M0.2 and M1.0 0, 0.2 and 1.0 mM Metformin in Mineralization medium). *: $p < 0.05$; **: $p < 0.01$; ***: $p < 0.001$. All data are from n = 6 donors.

inhibit osteoclast formation by making use of periodontal ligament fibroblasts-PBMC co-cultures. To determine the number of osteoclasts, cells were stained with TRAcPand counterstained with DAPI to visualize nuclei. Cells containing ≥3 nuclei are considered as osteoclasts. Metformin was used in concentrations that did not affect osteogenesis: 0.2 and 1.0 mM. A decrease in osteoclast formation was observed with both concentrations (**Figures 3A–C**), affecting total number of cells containing more than two nuclei (**Figure 3D**), the smaller ones containing 3–5 nuclei (**Figure 3E**) as well as the larger ones with six and more nuclei (**Figure 3F**). Expression of genes associated with osteoclast formation such as RANKL (**Figure 3G**), OPG (**Figure 3H**), M-CSF (**Figure 3J**), and osteoclast genes TRAcP (**Figure 3K**) and DC-STAMP (**Figure 3L**) displayed a similar pattern of decreased expression in the presence of 0.2 or 1.0 mM metformin. RANKL was not detetable by qPCR in monocyte cultures stimulated with M-CSF and RANKL. OPG was detected with high Ct values, with an unreliable relative expression between 0.0002 and 0.001. These results confirm what we have previously seen (De Vries et al., 2006; Bloemen et al., 2010), showing that OPG and RANKL were solely expressed by periodontal ligament fibroblasts in co culture. Monocyte marker CD14 was elevated at 0.2 mM of metformin (**Figure 3M**), suggesting that the inhibitory effect of metformin was due to a decrease in osteoclast differentiation rather than loss of precursor cells.

Metformin Inhibits M-CSF and RANKL Mediated Osteoclast Formation and Bone Resorption

Although periodontal ligament fibroblasts contribute to osteoclast formation, M-CSF and RANKL are required for the generation of bone resorbing osteoclasts (De Vries et al., 2006). In order to study the effect of metformin on M-CSF and RANKL mediated osteoclast formation and bone resorption, $CD14^+$ cells were seeded on plastic or bone for assessing the impact of metformin on osteoclastogenesis. In a separate seeding on bone, the effect on bone resorption was assessed.

As in the co-cultures, metformin inhibited osteoclast formation in a dose dependent manner on plastic (**Figures 4A–C**) as well as on bone (**Figures 4D–F**). Note that monocytes remained mononuclear at 1.0 mM metformin (**Figures 4B,E**). In parallel to decreased osteoclast formation on bone slices, bone resorption was abolished at 1.0 mM metformin (**Figure 4H**).

Gene expression of osteoclast genes RANK and CathK was inhibited at high dose of metformin (**Figure 5**). Peculiarly, the reverse was true for TRAcP expression (**Figure 5**), where higher expression was observed when cultured with 1.0 mM metformin. Expression of DC-STAMP, Nfatc1 and CD14 was not altered by metformin.

Gene expression of mitochondrial markers COX1 and COX2 tended to be lower at 1.0 mM metformin (**Supplementary Figure S2** (non-significant).

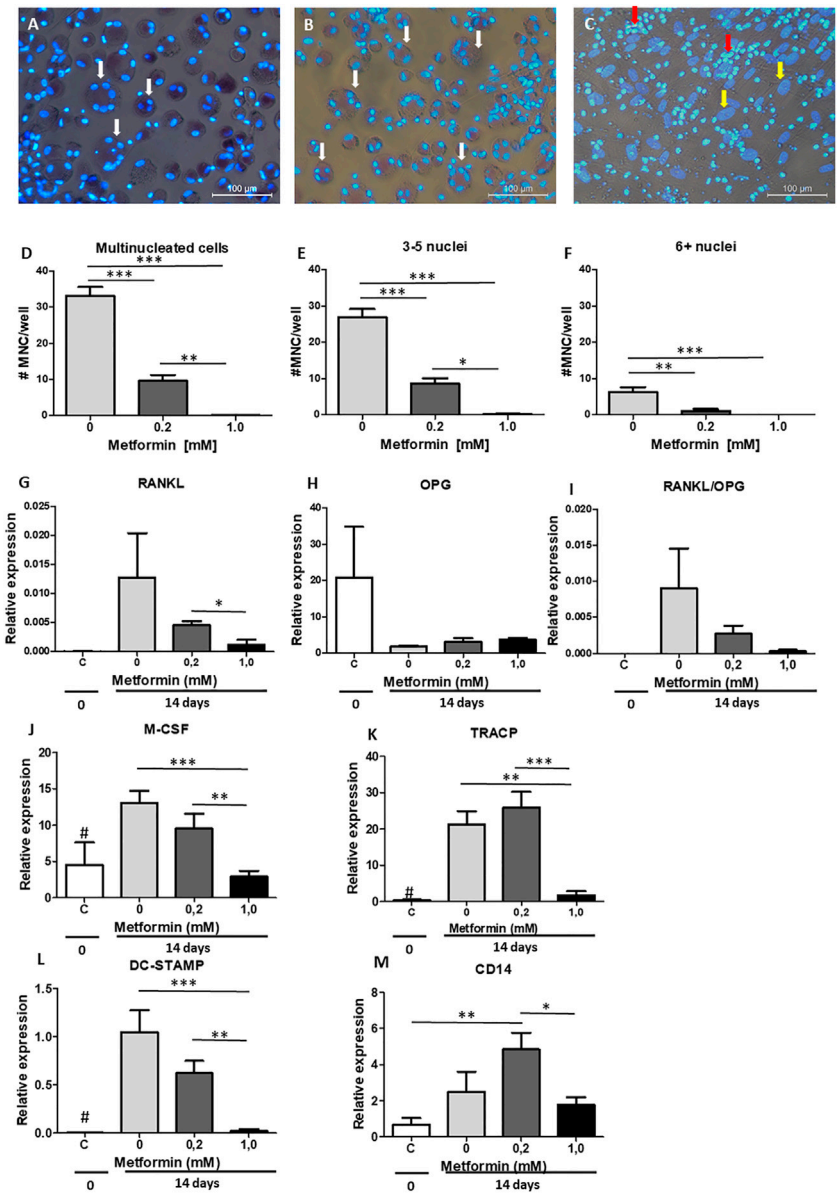

FIGURE 3 | Metformin inhibits periodontal ligament fibroblasts mediated osteoclast formation. PBMC were cultured on periodontal ligament fibroblasts and osteoclast formation was assessed at 21 days after TRAcP staining **(A–C)**. **(A)** Control, without metformin, **(B)** 0.2 mM metformin and **(C)** 1.0 mM metformin. **(D–F)**: Inhibition of numbers of multinucleated cells (MNC) formed, both when assessing all multinucleated cells **(D**, >2 nuclei**)**, small multinucleated cells with 3-5 nuclei **(E)**, or larger multinucleated cells **(F**, 6+ nuclei**)**. **(G–M)**: Gene expression at 0 days **(C**, periodontal ligament fibroblasts without PBMCs**)** or 21 days (co-cultures periodontal ligament fibroblasts 0, 0.2 and 1.0 mM metformin) of RANKL **(G)**, OPG **(H)**, the ratio RANKL/OPG **(I)**, M-CSF **(J)**, TRACP **(K)**, DC-STAMP **(L)**, and CD14 **(M)** is inhibited by metformin. All results are from n = 6 periodontal ligament fibroblast donors. White arrow in **A** and **B**: multinucleated cells, Yellow arrow in **C**: fibroblast nucleus, Red arrow in **C**: PBMCs that are not fused and TRACP negative. # in **G–I**: Control significantly lower ($p < 0.05$) expression than 0 and 0.2 mM metformin in co-cultures. *: $p < 0.05$; **: $p < 0.01$; ***: $p < 0.001$. All data are from n = 6 donors. Osteoclast assay **(A–F)** was performed twice, obtaining similar results, with two groups of six different donors (by LT and KL), results from one experiment are shown.

DISCUSSION

Various animal (Bak et al., 2010; Araújo et al., 2017) and clinical studies (Pradeep et al., 2013; Pradeep et al., 2015; Pradeep et al., 2016; Pradeep et al., 2017; Kurian et al., 2018) have pointed out a beneficiary effect of metformin in down modulating the severity of periodontitis, when induced or when used as a clinical adjuvant improving bone health and periodontal status. The present study contributes to an understanding at the cellular level using the appropriate model of periodontal ligament fibroblasts. Using two confirmatory assays, results unequivocally point out a role for metformin by inhibiting osteoclast formation and activity.

Our original hypothesis that metformin would have a positive effect on osteogenesis, has to be partially rejected and modified.

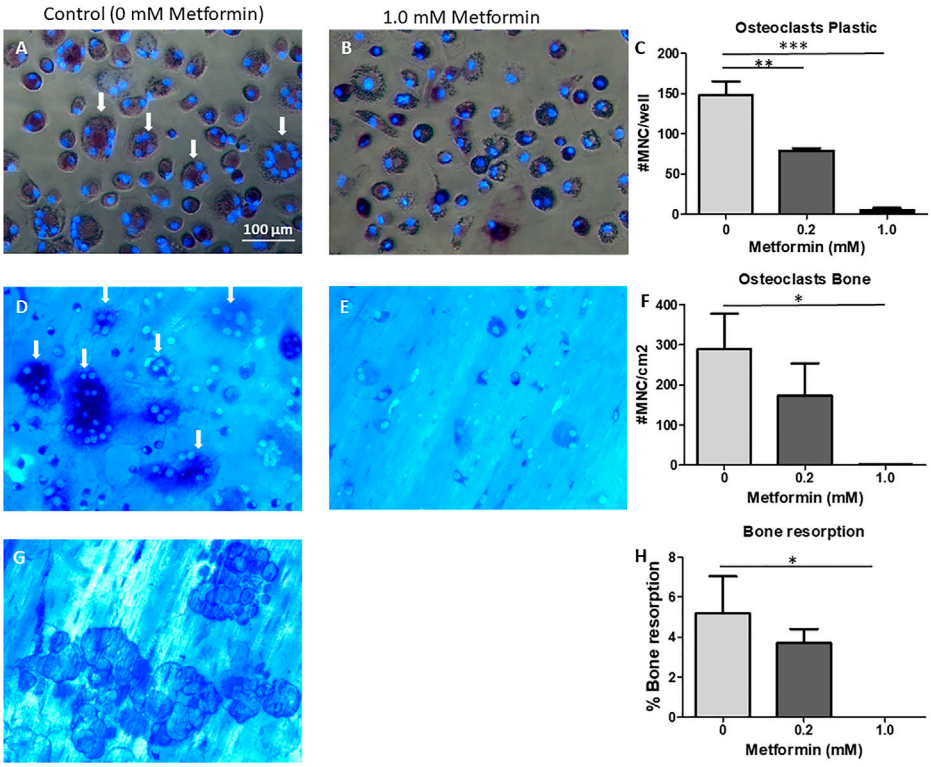

FIGURE 4 | Metformin inhibits M-CSF and RANKL driven osteoclast formation. $CD14^+$ cells as source of osteoclast precursors were seeded on plastic **(A–C)**, or on bone **(D–H)** and cultured with M-CSF and RANKL, without or with 0.2 or 1.0 mM Metformin. Micrographs of cells on plastic **(A,B)** or on cortical bone slices **(D,E)** or bone resorption pits **(G)**. Quantification of cell counts on plastic **(C)**, bone **(F)**. **(H)**: Quantification of bone resorption. Quantitative data were from quadruplicate seeding. *: $p < 0.05$; **: $p < 0.01$; ***: $p < 0.001$. Scale bar in **A** applies to all micrographs. Arrows point to TRAcP multinucleated cells/ osteoclasts.

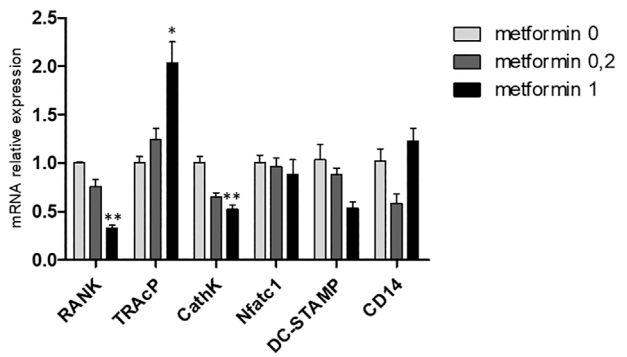

FIGURE 5 | Metformin affects gene expression in M-CSF and RANKL driven osteoclast cultures. Gene expression of RANK, TRAcP, Cathepsin K, NFATc1, DC-STAMP and CD14 at 21 days. Expression of the control, metformin 0, was set at 1.0. Decreased expression of RANK and Cathepsin K was observed and increased expression of TRAcP. *:$p < 0.05$, **:$p < 0.01$.

Based on our results, metformin treatment did not induce alkaline phosphatase activity nor did it increase Alizarin Red staining. This is in line with a recent publication on the effect of metformin on periodontal ligament fibroblasts (Jia et al., 2020). In contrast to Jia et al., we did not observe a positive effect on osteogenic markers such as RUNX-2. Differences in periodontal ligament fibroblast heterogeneity, such as seen for Alizarin Red staining in **Figure 2B** could account for this difference, but also methodological differences, such as use of dexamethasone and a different concentration of ascorbic acid and glycerophosphate could give rise to such discrepancies. Concentrations that were used in our study did not affect proliferation, since no differences in DNA content were observed in the titration experiment (Suppl. **Figure 1A**). As in previous studies from our group (Karlis et al., 2020; Loo-Kirana et al., 2021), the observed Alizarin Red staining was due to so-called nodules or hot-spots of mineralization that formed on top of the fibroblasts (**Figure 1D**). Interestingly, mineralization medium only induced osteopontin expression when compared to normal medium, whereas RUNX-2, Collagen-I expression and the activity of Alkaline phosphatase was not influenced, not by mineralization medium nor by metformin. Clearly, most of the expression data revealed a time effect (t = 0 vs. 14 days), which possibly can be explained by a more confluent layer of cells, whichmay ignite these expressions. By nature, periodontal ligament fibroblasts express alkaline phosphatase abundantly (Groeneveld et al., 1995), which may explain why mineralization medium did not alter the expression.

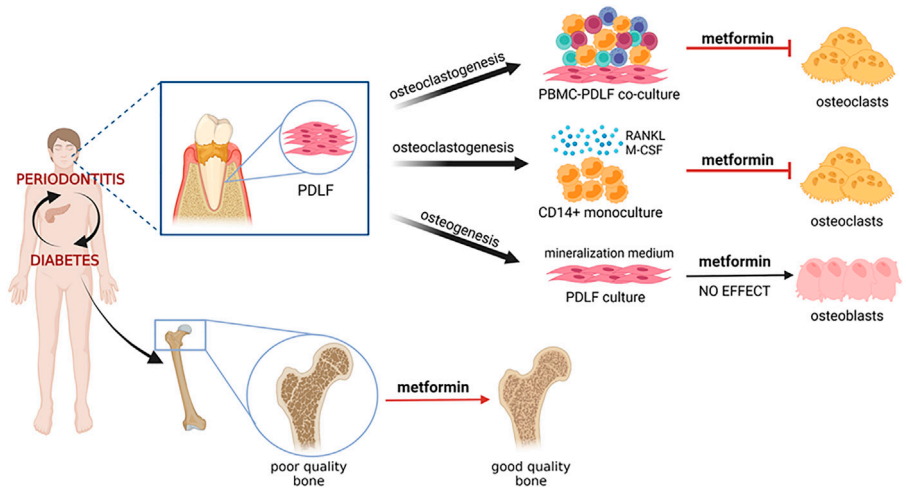

FIGURE 6 | Graphical abstract. Diabetes and periodontitis are clinically associated.Mouse experimental periodontitis modelas and preliminary clinical studies show that diabetes drug metformin has beneficial effects on the periodontium, the tooth associated tissues including bone. This study has analyzed the effect of metformin on clinically relevant cell models: periodontal ligament derived fibroblasts (PDLF) that were either steered into osteogenesis pathways or into osteoclastogenesis pathways, together with peripheral blood monocnuclear cells (PBMCs) under continual exposure to metformin. The effect of metformin on osteoclast formation was further assessed with $CD14^+$ monocytes that were subjected to osteoclast differentiation with osteoclastogenesis driving cytokines M-CSF and RANKL. Our results all indicate an inhibitory effect on osteoclast formation, which could, in a broader sense, be the mechanism that explains clinically observed bone improvement in metformin users.

Metformin inhibited osteoclast formation or osteoclastogenesis in the periodontal ligament-PBMC co cultures. Downregulation of typical osteoclastogenesis genes, such as RANKL and M-CSF, that are expressed by periodontal ligament fibroblasts as well as the downregulation of osteoclast gene DC-STAMP shows that metformin affects both the fibroblast side that orchestrate osteoclast formation (RANKL and M-CSF), as well as precursor cells (DC-STAMP). Downregulation of DC-STAMP most likely resulted in a lack of fusion (**Figure 3C**), where only mononuclear cells were seen in conjunction with fibroblasts. Concerning mechanistic insight, pleotropic effects of metformin beyond facilitating insulin's glucose lowering effects should be considered (Ursini et al., 2018). It has been described in a cell culture using gingiva fibroblasts that metformin reduces the expression of inflammatory factors IL-1β, TNF-α and IL-6 (Wu et al., 2015; Kang et al., 2017). Recently, we showed that co-cultures of gingiva fibroblasts with leukocytes induces IL-1β and TNF-α (Moonen et al., 2018), but also periodontal ligament fibroblasts induce M-CSF, IL-1β and TNF-α early during osteoclast formation (Bloemen et al., 2010). These factors are adjuvant cytokines for osteoclast formation, since osteoclast formation can be inhibited by anti-TNF (De Vries et al., 2016; Zamri and De Vries, 2020) and stimulated by TNF-α (Cao et al., 2017) and IL-1β (Cao et al., 2016). *In vivo* evidence for metformin anti-inflammatory mode of action was obtained in a mouse model of rheumatoid arthritis (Fan et al., 2020) where it primarily affected IL-1β. Together with the downregulated crucial osteoclastogenesis factor RANKL (Kong et al., 1999) (**Figure 3G**), it seems likely that also other inflammatory osteoclastogenesis genes could be affected. Downregulation of RANKL was also seen in ovariectomized rats that were treated with metformin (Mai et al., 2011), who also showed that this brought down the number of osteoclasts *in vivo*. Co. cultures in the present study were performed with unsorted PBMCs, which makes it likely that also Th17 T-cells were present in the culture. These cells may contribute to osteoclast formation by interacting with osteoclast precursors (Moonen et al., 2018), producing the osteoclastogenesis activating cytokine IL-17 (Sprangers et al., 2016). Interestingly, it was shown that metformin lowers the Th17/Treg ratio (Son et al., 2014). Whether metformin affects this T-cell subset and thus contribute to the inhibitory effect remains to be investigated.

Metformin likewise inhibited monocytes in the absence of periodontal ligament fibroblasts to differentiate into osteoclasts, both on plastic and on bovine bone slices. Here, no resorptive activity was observed when the highest concentration of metformin was used. qPCR revealed cathepsin K and RANK to be downregulated by metformin, mRNAs that could not be identified as osteoclast precursor specific in the cocultures with periodontal ligament fibroblasts, since these molecules are also detectable in monocultures of periodontal ligament fibroblasts. These results indicate that metformin inhibits genes important for early differentiation events (RANK) as well as genes involved in differentiated osteoclasts, such as cathepsin K. One of the mechanistically interesting aspects that could explain the observed reduced osteoclast formation and function, is metformin's mildly inhibitory effect on mitochondrial function (Apostolova et al., 2020). Recent studies interfering with osteoclast presence (Weivoda et al., 2020) could correlate osteoclast activity to a general energetic state. Abundance of mitochondria is a hallmark of osteoclasts, and interference with

mitochondrial function interferes with osteoclast formation (Park-Min, 2019; Weivoda et al., 2020). Preliminary results indicate that 1.0 mM could have a downregulatory effect on the expression of mitochondrial markers COX1 and COX2 (**Figure 5B**). Contra intuitively, TRAcP was upregulated by metformin, which was also seen with 0.2 mM in the cocultures. This could indicate that metformin diversely affects the transcription of osteoclast genes: DC-STAMP and Cathepsin K were downregulated whereas TRAcP was upregulated, which is different from our previous work on mouse osteoclasts, where upregulation of all osteoclast genes was similar (De Vries et al., 2009). TRAcP is also expressed by the osteoclast's mononuclear family members, macrophages and dendritic cells. Here, TRAcP may be of importance in bacterial clearance and general functionality of macrophages and dendritic cells (Haymon 2008). It is therefore feasible that metformin shifts the differentiation of monocytes towards macrophages and dendritic cells.

Concerning the balance of strong and weaker points of this study, we show with two assays that osteoclast formation and osteoclast activity are inhibited by metformin. 1) Metformin inhibited cell-cell mediated osteoclastogenesis, with the identification of various PDL related genes that are downregulated (M-CSF, RANKL). 2) In assays using only osteoclast CD14 precursors, it was shown that also in this "pure" system, osteoclast formation and activity is inhibited, concomitant with down regulation of RANK and Cathepsin K. A weak point in our study is that, although metformin did not interfere with cell numbers of periodontal ligament fibroblasts, it is not clear whether metformin may also induce secreted osteoclastogenesis inhibitory molecules. Also, the possible effects of metformin on the energy metabolism, such as in osteoclasts, needs further investigation.

Anti-aging has recently been added to the long list of metformin's pleotropic effects (Hu et al., 2021; Mohammed et al., 2021). Increase in osteoclasts and osteoclastic activity can be seen as a result of aging, especially as a result of menopause. The present study therefore could add anti-osteoclast formation as one of the aspects of anti-aging. Metformin influence both the orchestrator of osteoclastogenesis, the periodontal ligament fibroblast, as well as the monocyte osteoclast precursor. Our results, summarized in **Figure 6**, illustrate that the alleged bone sparing mechanism of metformin could be due to inhibiting osteoclasts, rather than, or in parallel with increased osteogenesis.

DATA AVAILABILITY STATEMENT

The raw data supporting the conclusions of this article will be made available by the authors, without undue reservation.

ETHICS STATEMENT

All the individuals were informed that the cells retrieved from the surgical waste material was used for research on bone formation and bone degradation. A signed informed consent and samples were coded to guarantee the anonymity of the donors as required by Dutch law. The use of buffy coats from the blood bank, (Sanquin, Amsterdam) was under ethical committee number NVT230.01.

AUTHOR CONTRIBUTIONS

LT, KŁ performed the experiments under guidance of TJdeV. Osteogenesis assays were assisted by JH, qPCR by TS. TF organized the collection of peridoontal ligament fibroblasts. Original idea for the study by FvdW and TJdV, AG assisted with writing. TJdV initiated writing, all authors contributed to the final manuscript.

SUPPLEMENTARY MATERIAL

The Supplementary Material for this article can be found online at: https://www.frontiersin.org/articles/10.3389/fcell.2021.777450/full#supplementary-material

Supplementary Figure S1 | Titration of metformin in a mineralization assay. Periodontal ligament fibroblasts were subjected to increasing concentrations of metformin (five-fold dilutions from 1- 0.008 mM in mineralization medium. **A.** Effect of metformin on proliferation. DNA was measured at t=0, (C) and 0-1.0 in mineralization medium at t=14 days. #: t=0 Significantly different from all t=14 conditions, no differences between the metformin treated donor cells. **B.** Alkaline phosphatase per cell, metformin did not affect alkaline phosphatase activity per cell. **C.** Alizarin red staining was assessed for 3 donors after 14 and 21 days of culture. Heterogeneous staining between donors at 14 days, whereas all donors were positive at 21 days. No effects of metformin were observed. **D.** Micrograph of alizarin red staining, showing red, circular structures, reminiscent of nodules.

Supplementary Figure S2 | Effect of metformin on COX1 and COX2 expression. Gene expression of mitochondrial enzymes COX1 and COX2, with tendency of downregulation (n.s.)

REFERENCES

Apostolova, N., Iannantuoni, F., Gruevska, A., Muntane, J., Rocha, M., and Victor, V. M. (2020). Mechanisms of Action of Metformin in Type 2 Diabetes: Effects on Mitochondria and Leukocyte-Endothelium Interactions. *Redox Biol.* 34, 101517. doi:10.1016/j.redox.2020.101517

Araújo, A. A., Pereira, A. S. B. F., Medeiros, C. A. C. X., Brito, G. A. C., Leitão, R. F. C., Araújo, L. S., et al. (2017). Effects of Metformin on Inflammation, Oxidative Stress, and Bone Loss in a Rat Model of Periodontitis. *PLoS One* 12, e0183506. doi:10.1371/journal.pone.0183506

Bak, E. J., Park, H. G., Kim, M., Kim, S. W., Kim, S., Choi, S.-H., et al. (2010). The Effect of Metformin on Alveolar Bone in Ligature-Induced Periodontitis in Rats: a Pilot Study. *J. Periodontol.* 81, 412–419. doi:10.1902/jop.2009.090414

Bastidas-Coral, A. P., Bakker, A. D., Zandieh-Doulabi, B., Kleverlaan, C. J., Bravenboer, N., Forouzanfar, T., et al. (2016). Cytokines TNF-α, IL-6, IL-17F, and IL-4 Differentially Affect Osteogenic Differentiation of Human Adipose Stem Cells. *Stem Cell Int* 2016, 1318256. doi:10.1155/2016/1318256

Bloemen, V., Schoenmaker, T., De Vries, T. J., and Everts, V. (2010). Direct Cell-Cell Contact between Periodontal Ligament Fibroblasts and Osteoclast Precursors Synergistically Increases the Experession Ofgenes Related to Osteoclastogenesis. *J. Cel Physiol.* 222, 565–573. doi:10.1002/jcp.21971

Cao, Y., Jansen, I. D. C., Sprangers, S., De Vries, T. J., and Everts, V. (2017). TNF-α Has Both Stimulatory and Inhibitory Effects on Mouse Monocyte-Derived Osteoclastogenesis. *J. Cel Physiol.* 232, 3273–3285. doi:10.1002/jcp.26024

Cao, Y., Jansen, I. D., Sprangers, S., Stap, J., Leenen, P. J., Everts, V., et al. (2016). IL-1beta Differently Stimulates Proliferation and Multinucleation of Distinct Mouse Bone Marrow Osteoclast Precursor Subsets. *J. Leukoc. Biol.* 100, 513–523. doi:10.1189/jlb.1A1215-543R

Chandran, M. (2017). Diabetes Drug Effects on the Skeleton. *Calcif Tissue Int.* 100, 133–149. doi:10.1007/s00223-016-0203-x

De Vries, T. J., Schoenmaker, T., Hooibrink, B., Leenen, P. J. M., and Everts, V. (2009). Myeloid Blasts Are the Mouse Bone Marrow Cells Prone to Differentiate into Osteoclasts. *J. Leukoc. Biol.* 85, 919–927. doi:10.1189/jlb.0708402

De Vries, T. J., Schoenmaker, T., Micha, D., Hogervorst, J., Bouskla, S., Forouzanfar, T., et al. (2017). Periodontal Ligament Fibroblasts as a Cell Model to Study Osteogenesis and Osteoclastogenesis in Fibrodysplasia Ossificans Progressiva. *Bone* 109, 168–177. doi:10.1016/j.bone.2017.07.007

De Vries, T. J., Schoenmaker, T., Van Veen, H. A., Hogervorst, J., Krawczyk, P. M., Moonen, C. G. J., et al. (2019). The Challenge of Teaching Essential Immunology Laboratory Skills to Undergraduates in One Month-Experience of an Osteoimmunology Course on TLR Activation. *Front. Immunol.* 10, 1822. doi:10.3389/fimmu.2019.01822

De Vries, T. J., Schoenmaker, T., Wattanaroonwong, N., van den Hoonaard, M., Beertsen, W., and Everts, V. (2006). Gingival Fibroblasts Are Better at Inhibiting Osteoclast Formation Than Periodontal Ligament Fibroblasts. *J. Cel. Biochem.* 98, 370–382. doi:10.1002/jcb.20795

De Vries, T. J., Yousovich, J., Schoenmaker, T., Scheres, N., and Everts, V. (2016). Tumor Necrosis Factor-α Antagonist Infliximab Inhibits Osteoclast Formation of Peripheral Blood Mononuclear Cells but Does Not Affect Periodontal Ligament Fibroblast-Mediated Osteoclast Formation. *J. Periodont Res.* 51, 186–195. doi:10.1111/jre.12297

Fan, K.-J., Wu, J., Wang, Q.-S., Xu, B.-X., Zhao, F.-T., and Wang, T.-Y. (2020). Metformin Inhibits Inflammation and Bone Destruction in Collagen-Induced Arthritis in Rats. *Ann. Transl Med.* 8, 1565. doi:10.21037/atm-20-3042

Groeneveld, M. C., Everts, V., and Beertsen, W. (1995). Alkaline Phosphatase Activity in the Periodontal Ligament and Gingiva of the Rat Molar: its Relation to Cementum Formation. *J. Dent. Res.* 74, 1374–1381. doi:10.1177/00220345950740070901

Halimi, S. (2006). Metformin: 50 Years Old, Fit as a Fiddle, and Indispensable for its Pivotal Role in Type 2 Diabetes Management. *Diabetes Metab.* 32, 555–556. doi:10.1016/s1262-3636(07)70309-9

Haymon, A. R. (2008). Tartrate-acid Phosphatase (TRAP) and the Osteoclast/immune Cell Dichotomy. *Autoimmunity* 41, 218–223. doi:10.1080/08916930701694667

Hu, D., Xie, F., Xiao, Y., Lu, C., Zhong, J., Huang, D., et al. (2021). Metformin: A Potential Candidate for Targeting Aging Mechanisms. *Aging Dis.* 12, 480–493. doi:10.14336/ad.2020.0702

Jia, L., Xiong, Y., Zhang, W., Ma, X., and Xu, X. (2020). Metformin Promotes Osteogenic Differentiation and Protects against Oxidative Stress-Induced Damage in Periodontal Ligament Stem Cells via Activation of the Akt/Nrf2 Signaling Pathway. *Exp. Cel Res.* 386, 111717. doi:10.1016/j.yexcr.2019.111717

Kang, W., Wang, T., Hu, Z., Liu, F., Sun, Y., and Ge, S. (2017). Metformin Inhibits Porphyromonas Gingivalis Lipopolysaccharide-Influenced Inflammatory Response in Human Gingival Fibroblasts via Regulating Activating Transcription Factor-3 Expression. *J. Periodontol.* 88, e169–e178. doi:10.1902/jop.2017.170168

Karlis, G. D., Schöningh, E., Jansen, I. D. C., Schoenmaker, T., Hogervorst, J. M. A., Van Veen, H. A., et al. (2020). Chronic Exposure of Gingival Fibroblasts to TLR2 or TLR4 Agonist Inhibits Osteoclastogenesis but Does Not Affect Osteogenesis. *Front. Immunol.* 11, 1693. doi:10.3389/fimmu.2020.01693

Kong, Y. Y., Boyle, W. J., and Penninger, J. M. (1999). Osteoprotegerin Ligand: a Common Link between Osteoclastogenesis, Lymph Node Formation and Lymphocyte Development. *Immunol. Cel Biol* 77, 188–193. doi:10.1046/j.1440-1711.1999.00815.x

Kurian, I. G., Dileep, P., Ipshita, S., and Pradeep, A. R. (2018). Comparative Evaluation of Subgingivally-Delivered 1% Metformin and Aloe Vera Gel in the Treatment of Intrabony Defects in Chronic Periodontitis Patients: A Randomized, Controlled Clinical Trial. *J. Investig. Clin. Dent* 9, e12324. doi:10.1111/jicd.12324

Loo-Kirana, R., Gilijamse, M., Hogervorst, J., Schoenmaker, T., and De Vries, T. J. (2021). Although Anatomically Micrometers Apart: Human Periodontal Ligament Cells Are Slightly More Active in Bone Remodeling Than Alveolar Bone Derived Cells. *Front. Cel Develop. Biol.* 9, 709408. doi:10.3389/fcell.2021.709408

Mai, Q.-G., Zhang, Z.-M., Xu, S., Lu, M., Zhou, R.-P., Zhao, L., et al. (2011). Metformin Stimulates Osteoprotegerin and Reduces RANKL Expression in Osteoblasts and Ovariectomized Rats. *J. Cel. Biochem.* 112, 2902–2909. doi:10.1002/jcb.23206

Mohammed, I., Hollenberg, M. D., Ding, H., and Triggle, C. R. (2021). A Critical Review of the Evidence that Metformin Is a Putative Anti-aging Drug that Enhances Healthspan and Extends Lifespan. *Front. Endocrinol.* 12, 718942. doi:10.3389/fendo.2021.718942

Moonen, C. G. J., Alders, S. T., Bontkes, H. J., Schoenmaker, T., Nicu, E. A., Loos, B. G., et al. (2018). Survival, Retention, and Selective Proliferation of Lymphocytes Is Mediated by Gingival Fibroblasts. *Front. Immunol.* 9, 1725. doi:10.3389/fimmu.2018.01725

Nascimento, G. G., Leite, F. R. M., Vestergaard, P., Scheutz, F., and López, R. (2018). Does Diabetes Increase the Risk of Periodontitis? A Systematic Review and Meta-Regression Analysis of Longitudinal Prospective Studies. *Acta Diabetol.* 55, 653–667. doi:10.1007/s00592-018-1120-4

Park-Min, K.-H. (2019). Metabolic Reprogramming in Osteoclasts. *Semin. Immunopathol* 41, 565–572. doi:10.1007/s00281-019-00757-0

Pradeep, A. R., Nagpal, K., Karvekar, S., Patnaik, K., Naik, S. B., and Guruprasad, C. N. (2015). Platelet-rich Fibrin with 1% Metformin for the Treatment of Intrabony Defects in Chronic Periodontitis: a Randomized Controlled Clinical Trial. *J. Periodontol.* 86, 729–737. doi:10.1902/jop.2015.140646

Pradeep, A. R., Patnaik, K., Nagpal, K., Karvekar, S., Guruprasad, C. N., and Kumaraswamy, K. M. (2017). Efficacy of 1% Metformin Gel in Patients with Moderate and Severe Chronic Periodontitis: A Randomized Controlled Clinical Trial. *J. Periodontol.* 88, 1023–1029. doi:10.1902/jop.2017.150096

Pradeep, A. R., Patnaik, K., Nagpal, K., Karvekar, S., Ramamurthy, B. L., Naik, S. B., et al. (2016). Efficacy of Locally-Delivered 1% Metformin Gel in the Treatment of Intrabony Defects in Patients with Chronic Periodontitis: a Randomized, Controlled Clinical Trial. *J. Investig. Clin. Dent* 7, 239–245. doi:10.1111/jicd.12150

Pradeep, A. R., Rao, N. S., Naik, S. B., and Kumari, M. (2013). Efficacy of Varying Concentrations of Subgingivally Delivered Metformin in the Treatment of Chronic Periodontitis: a Randomized Controlled Clinical Trial. *J. Periodontol.* 84, 212–220. doi:10.1902/jop.2012.120025

Rao, N. S., Pradeep, A. R., Kumari, M., and Naik, S. B. (2013). Locally Delivered 1% Metformin Gel in the Treatment of Smokers with Chronic Periodontitis: a Randomized Controlled Clinical Trial. *J. Periodontol.* 84, 1165–1171. doi:10.1902/jop.2012.120298

Ren, Y., Han, X., Ho, S. P., Harris, S. E., Cao, Z., Economides, A. N., et al. (2015). Removal of SOST or Blocking its Product Sclerostin Rescues Defects in the Periodontitis Mouse Model. *FASEB J.* 29, 2702–2711. doi:10.1096/fj.14-265496

Ruppeka-Rupeika, E., Hogervorst, J., Wouters, F., Schoenmaker, T., Forouzanfar, T., and De Vries, T. J. (2018). Osteogenic and Osteoclastogenic Potential of Jaw Bone-Derived Cells-A Case Study. *J. Cel Biochem* 119, 5391–5401. doi:10.1002/jcb.26690

Sokos, D., Everts, V., and De Vries, T. J. (2015). Role of Periodontal Ligament Fibroblasts in Osteoclastogenesis: a Review. *J. Periodont Res.* 50, 152–159. doi:10.1111/jre.12197

Son, H. J., Lee, J., Lee, S. Y., Kim, E. K., Park, M. J., Kim, K. W., et al. (2014). Metformin Attenuates Experimental Autoimmune Arthritis through Reciprocal Regulation of Th17/Treg Balance and Osteoclastogenesis. *Mediators Inflamm.* 2014, 973986. doi:10.1155/2014/973986

Sprangers, S., Schoenmaker, T., Cao, Y., Everts, V., and De Vries, T. J. (2016). Different Blood-Borne Human Osteoclast Precursors Respond in Distinct Ways to IL-17A. *J. Cel. Physiol* 231, 1249–1260. doi:10.1002/jcp.25220

Sun, J., Du, J., Feng, W., Lu, B., Liu, H., Guo, J., et al. (2017). Histological Evidence that Metformin Reverses the Adverse Effects of Diabetes on Orthodontic Tooth Movement in Rats. *J. Mol. Hist.* 48, 73–81. doi:10.1007/s10735-016-9707-y

Ten Harkel, B., Schoenmaker, T., Picavet, D. I., Davison, N. L., De Vries, T. J., and Everts, V. (2015). The Foreign Body Giant Cell Cannot Resorb Bone, but Dissolves Hydroxyapatite like Osteoclasts. *Plos. ONE* 10, e0139564. doi:10.1371/journal.pone.0139564

Ursini, F., Russo, E., Pellino, G., D'Angelo, S., Chiaravalloti, A., De Sarro, G., et al. (2018). Metformin and Autoimmunity: A "New Deal" of an Old Drug. *Front. Immunol.* 9, 1236. doi:10.3389/fimmu.2018.01236

Verhulst, M. J. L., Loos, B. G., Gerdes, V. E. A., and Teeuw, W. J. (2019). Evaluating All Potential Oral Complications of Diabetes Mellitus. *Front. Endocrinol.* 10, 56. doi:10.3389/fendo.2019.00056

Weivoda, M. M., Chew, C. K., Monroe, D. G., Farr, J. N., Atkinson, E. J., Geske, J. R., et al. (2020). Identification of Osteoclast-Osteoblast Coupling Factors in Humans Reveals Links between Bone and Energy Metabolism. *Nat. Commun.* 11, 87. doi:10.1038/s41467-019-14003-6

Wu, Y.-Y., Xiao, E., and Graves, D. T. (2015). Diabetes Mellitus Related Bone Metabolism and Periodontal Disease. *Int. J. Oral Sci.* 7, 63–72. doi:10.1038/ijos.2015.2

Zamri, F., and De Vries, T. J. (2020). Use of TNF Inhibitors in Rheumatoid Arthritis and Implications for the Periodontal Status: For the Benefit of Both. *Front. Immunol.* 11, 591365. doi:10.3389/fimmu.2020.591365

Zhao, Z., Liu, J., Schneider, A., Gao, X., Ren, K., Weir, M. D., et al. (2019). Human Periodontal Ligament Stem Cell Seeding on Calcium Phosphate Cement Scaffold Delivering Metformin for Bone Tissue Engineering. *J. Dentistry* 91, 103220. doi:10.1016/j.jdent.2019.103220

Conflict of Interest: The authors declare that the research was conducted in the absence of any commercial or financial relationships that could be construed as a potential conflict of interest.

Publisher's Note: All claims expressed in this article are solely those of the authors and do not necessarily represent those of their affiliated organizations, or those of the publisher, the editors and the reviewers. Any product that may be evaluated in this article, or claim that may be made by its manufacturer, is not guaranteed or endorsed by the publisher.

frontiers | Frontiers in Cell and Developmental Biology

ORIGINAL RESEARCH
published: 04 April 2022
doi: 10.3389/fcell.2022.816764

Salt-Sensitive Hypertension Induces Osteoclastogenesis and Bone Resorption *via* Upregulation of Angiotensin II Type 1 Receptor Expression in Osteoblasts

Adya Pramusita[1], Hideki Kitaura[1], Fumitoshi Ohori[1], Takahiro Noguchi[1], Aseel Marahleh[1], Yasuhiko Nara[1], Ria Kinjo[1], Jinghan Ma[1], Kayoko Kanou[1], Yukinori Tanaka[2] and Itaru Mizoguchi[1]*

[1]*Division of Orthodontics and Dentofacial Orthopedics, Tohoku University Graduate School of Dentistry, Sendai, Japan,* [2]*Division of Dento-Oral Anesthesiology, Tohoku University Graduate School of Dentistry, Sendai, Japan*

OPEN ACCESS

Edited by:
Enrico Iaccino, Magna Græcia University of Catanzaro, Italy

Reviewed by:
Ling-Qing Yuan, Central South University, China
Yi Zhou, Zhejiang University, China

***Correspondence:**
Hideki Kitaura
hideki.kitaura.b4@tohoku.ac.jp

Specialty section:
This article was submitted to Cellular Biochemistry, a section of the journal Frontiers in Cell and Developmental Biology

Received: *17 November 2021*
Accepted: *07 February 2022*
Published: *04 April 2022*

Citation:
Pramusita A, Kitaura H, Ohori F, Noguchi T, Marahleh A, Nara Y, Kinjo R, Ma J, Kanou K, Tanaka Y and Mizoguchi I (2022) Salt-Sensitive Hypertension Induces Osteoclastogenesis and Bone Resorption via Upregulation of Angiotensin II Type 1 Receptor Expression in Osteoblasts. Front. Cell Dev. Biol. 10:816764. doi: 10.3389/fcell.2022.816764

Hypertension is a chronic-low grade inflammatory disease, which is known to be associated with increased bone loss. Excessive activity of the local renin–angiotensin system (RAS) in bone leads to increased bone resorption. As inflammatory cytokines may activate RAS components, we hypothesized that the elevated proinflammatory cytokine levels in hypertension activate bone RAS and thus lead to increased bone resorption. To investigate whether salt-sensitive hypertension (SSHTN) induces osteoclastogenesis and bone resorption, we generated a model of SSHTN in C57BL/6J mice by post-N^{ω}-nitro-L-arginine methyl ester hydrochloride (L-NAME) high-salt challenge. SSHTN led to the reduction of distal femur trabecular number and bone volume fraction, while trabecular separation of femoral bone showed a significant increase, with no change in cortical thickness. Histomorphometric examination showed a significant reduction in trabecular bone volume fraction with an increased number of multinucleated tartrate-resistant acid phosphatase (TRAP)-positive cells and increased osteoclast surface fraction in the trabecular distal femur of hypertensive mice. Furthermore, analysis of gene expression in bone tissue revealed that TRAP and RANKL/OPG mRNA were highly expressed in hypertensive mice. TNF-α and angiotensin II type 1 receptor (AGTR1) mRNA and protein expression were also upregulated in SSHTN mice. These observations suggested that TNF-α may have an effect on AGTR1 expression leading to osteoclast activation. However, TNF-α stimulation did not promote AGTR1 mRNA expression in osteoclast precursors in culture, while TNF-α increased AGTR1 mRNA expression in osteoblast culture by activation of downstream p38. Angiotensin II was also shown to increase TNF-α-induced RANKL/OPG mRNA expression in primary osteoblast culture and osteoclastogenesis in a TNF-α-primed osteoblast and osteoclast precursor co-culture system. In addition, local injection of lipopolysaccharide into the supracalvariae of SSHTN mice markedly promoted osteoclast and bone resorption. In conclusion, mice with SSHTN show increased osteoclastogenesis and bone resorption due mainly to increased TNF-α and partly to the upregulation of AGTR1 in osteoblasts.

Keywords: angiotensin II type 1 receptor, mouse, osteoblast, osteoclast, salt-sensitive hypertension, TNF-α

1 INTRODUCTION

Hypertension is a major global health problem due to its high prevalence and because it is one of the most important risk factors for cardiovascular, cerebrovascular, and chronic kidney diseases, which are the leading causes of death worldwide (Ettehad et al., 2016; Li et al., 2016; Xie et al., 2016; Arvanitakis et al., 2018). The number of adults with hypertension is increasing, with worldwide estimated prevalence rates of 26.4% (corresponding to 972 million adults) in 2000 and 31.1% (corresponding to 1.39 billion adults) in 2010 (Kearney et al., 2005; Mills et al., 2016). Moreover, the global burden of hypertension is expected to increase by 60% reaching approximately 1.56 billion adults by 2025 (Kearney et al., 2005).

The systemic renin–angiotensin system (RAS) has been widely investigated because of its roles in the regulation of blood pressure, electrolyte homeostasis, and the development of hypertension (Ahn et al., 2017; Han et al., 2017). Several human studies suggested that hypertension is associated with low bone mineral density and increased risk of fracture (Li et al., 2017; Lian et al., 2017; Ye et al., 2017). In addition to systemic RAS, many tissues, including bone, have a local RAS the excessive activity of which leads to increased bone resorption and decreased bone formation (Shimizu et al., 2008; Asaba et al., 2009; Zhou et al., 2017). In a previous study, RAS components were expressed in the femora of both sham and ovariectomized (OVX) rats, and the levels of angiotensin II, angiotensin II type 1 receptor (AGTR1), and angiotensin converting enzyme (ACE) protein expression were shown to be upregulated in the OVX group, while OVX-induced bone loss was ameliorated by 6 weeks of oral losartan treatment, an inhibitor of AGTR1 (Abuohashish et al., 2017c).

Inflammation is known to be closely related to hypertension. Recent animal studies have shown that hypertension is associated with elevated plasma levels of proinflammatory cytokines, such as C-reactive protein (CRP), interleukin (IL)-6, IL-1β, and tumor necrosis factor (TNF)-α (Lu et al., 2016; Liu et al., 2019; Dai et al., 2020). Consistent with the results of animal studies, a number of clinical studies have also shown that patients with hypertension commonly have elevated plasma concentrations of proinflammatory cytokines compared to normotensive patients (Jiménez et al., 2016; Pouvreau et al., 2018; Chen et al., 2019; Jayedi et al., 2019). In addition, there is emerging evidence that proinflammatory cytokines activate RAS components. Both IL-1β and TNF-α were shown to induce AGTR1 expression in cultured cardiac fibroblasts and chondrocytes (Peng et al., 2002; Gurantz et al., 2005; Tsukamoto et al., 2014). Moreover, the osteoclastogenic cytokine, TNF-α, is a potent stimulator of osteoclast activity, and plays pivotal roles in bone metabolism and under pathological conditions in bone diseases. TNF-α was shown to directly promote the differentiation of osteoclast precursors into multinucleated tartrate-resistant acid phosphatase (TRAP)-positive osteoclasts in the presence of monocyte colony-stimulating factor (M-CSF) and in the absence of receptor activator of nuclear factor-κB ligand (RANKL) (Kishikawa et al., 2019; Noguchi et al., 2020; Ohori et al., 2020). On the other hand, TNF-α has also been shown to stimulate the production of M-CSF and RANKL in osteoblast-like cells (Xiong et al., 2014).

Lipopolysaccharide (LPS), a major cell-surface antigen of gram-negative bacteria, acts as a potent stimulator of inflammation and osteolytic bone loss (Abu-Amer et al., 1997; Sakuma et al., 2000). LPS has been shown to induce the release of several proinflammatory cytokines and factors, including TNF-α, IL-1, prostaglandin E2 (PGE2), and RANKL, from fibroblasts, macrophages, osteoblasts, and other cell types at inflammatory sites. Daily subcutaneous supracalvarial injection of LPS was also reported to induce osteoclastogenesis and bone resorption due to increases in levels of RANKL and TNF-α (Shen et al., 2018; Shima et al., 2018; Kishikawa et al., 2019). However, there have been no previous studies regarding the effects of salt-sensitive hypertension (SSHTN) on inflammation-induced osteoclastogenesis and bone resorption.

Based on the observations outlined above, we hypothesized that elevated level of the proinflammatory cytokine, TNF-α, under conditions of hypertension may promote bone RAS activation, resulting in the induction of osteoclastogenesis and bone resorption. To test this hypothesis, we generated a mouse model of SSHTN by post-N^{ω}-nitro-L-arginine methyl ester hydrochloride (L-NAME) high-salt challenge. Here, we found that SSHTN mice exhibited marked increases in osteoclast number and bone resorption area due mainly to increased TNF-α and partly to the upregulation of AGTR1 in osteoblasts.

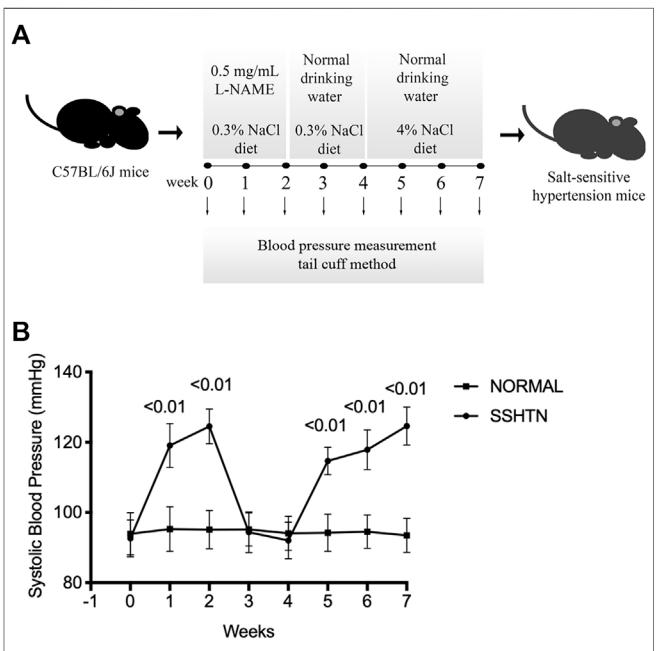

FIGURE 1 | Systolic blood pressure. **(A)** The experimental protocol to generate SSHTN mouse model consisted of three consecutive periods: a 2-weeks nitric oxide synthesis inhibition period with L-NAME, followed by a 2-weeks washout period, and subsequent high-salt diet for 3 weeks. **(B)** SBP was measured in normal control mice and SSHTN mice (n = 4).

2 MATERIALS AND METHODS

2.1 SSHTN Mouse Model and Reagents

Male C57BL/6J mice, 7–10 weeks old, were purchased from CLEA Japan (Tokyo, Japan). To generate the SSHTN model, mice were administered L-NAME (0.5 mg/mL; Sigma-Aldrich, St. Louis, MO, United States) in their drinking water for 2 weeks to inhibit nitric oxide synthesis, followed by a 2-weeks washout period, and a 3-weeks exposure to a high-salt diet (CE-2 containing 4% NaCl; CLEA Japan) (Lopez Gelston et al., 2018) (**Figure 1A**). Normal control mice received tap water and standard diet for 7 weeks. All diets and water were provided ad libitum. Systolic blood pressure (SBP) was monitored weekly by tail-cuff plethysmography using a blood pressure monitor (MK-1030; Muromachi Kikai Co., Tokyo, Japan) in previously trained mice. All animal care and experiments were approved by Tohoku University of Science Animal Care and Use Committee. LPS from *Escherichia coli*, angiotensin II, and olmesartan (angiotensin II type 1 receptor blocker) were purchased from Sigma-Aldrich. Recombinant murine TNF-α was prepared in our laboratory as described previously (Kitaura et al., 2004).

2.2 Histological Analysis

The femora of normal control and SSHTN mice were resected immediately after sacrifice, fixed in 4% formaldehyde in phosphate-buffered saline (PBS), and then demineralized in 14% ethylenediaminetetraacetic acid (EDTA) for 5 weeks. After dehydration through a graded ethanol series, they were embedded in paraffin and cut into sections 5 μm thick. Hematoxylin and eosin (H&E) and tartrate-resistant acid phosphatase (TRAP) staining were performed as described previously (Nara et al., 2020) to evaluate trabecular bone volume fraction (BV/TV, %), osteoclast surface fraction (Oc.S/BS, %), and the number of TRAP-positive cells (i.e., osteoclasts) per bone perimeter (N.Oc/B.Pm, 1/mm) using ImageJ software (NIH, Bethesda, MD, United States). TRAP-positive cells containing three or more nuclei were considered to be osteoclasts. The regions of interest (ROIs; 250 μm × 250 μm) were limited to trabecular bone and extended 250 μm proximal to the distal growth plate to exclude primary spongiosa, new bone growth, and cortical bone.

In addition, osteoclastogenesis was induced by subcutaneous supracalvarial injection of LPS at a dose of 100 μg/day for 5 days as described previously (Ishida et al., 2019). All animals were randomly divided into five groups as follows: normal controls with daily subcutaneous injection of PBS, 10 μg/day LPS, or 100 μg/day LPS; SSHTN mice with daily subcutaneous injection of PBS or 10 μg/day LPS. Calvariae were resected on day 6, decalcified in 14% EDTA for 3 days, embedded in paraffin, and cut into sections 5 μm thick perpendicular to the sagittal suture. TRAP and hematoxylin counterstaining were performed as described previously (Ishida et al., 2019). The number of osteoclasts located in the mesenchyme of the sagittal suture was counted in all slides as described previously (Ishida et al., 2019). All sections were observed and photographed using a light microscope (Olympus DP72; Olympus Co., Ltd., Tokyo, Japan).

2.3 Cell Culture

Osteoclast precursors were obtained as described previously (Marahleh et al., 2019). Briefly, bone marrow cells were flushed from the femora and tibiae of male C57BL/6J mice into sterile 6-cm culture dishes with α-modified minimal essential medium (α-MEM; Wako, Osaka, Japan) using a 30-gauge needle. The bone marrow was then filtered through a 40-μm nylon cell strainer (Falcon, Corning, NY, United States) and centrifuged. The harvested cells were incubated in α-MEM containing 10% fetal bovine serum (FBS) (Biowest, Nuaillé, France), 100 IU/ml penicillin G, 100 μg/ml streptomycin (Wako), and M-CSF for 3 days. Non-adherent cells were removed by washing with PBS and adherent cells were harvested using trypsin-EDTA solution (Gibco; Thermo Fisher Scientific, Inc., Waltham, MA, USA). These cells were used as osteoclast precursors in this study.

Primary osteoblasts were isolated from the calvariae of neonatal C57BL/6J mice as described previously (Shima et al., 2018). Briefly, calvariae were incubated with 0.2% (w/v) collagenase in isolation buffer (70 mM NaCl, 10 mM $NaHCO_3$, 60 mM sorbitol, 3 mM K_2HPO_4, 1 mM $CaCl_2$, 0.1% (w/v) BSA, 0.5% (w/v) glucose, and 25 mM HEPES) for 20 min at 37°C with agitation at 300 rpm (fraction 1), followed by digestion with 5 mM EDTA (Wako) in PBS containing 0.1% BSA (Sigma-Aldrich) for 15 min at 37°C with agitation at 300 rpm (fraction 2), then incubated in collagenase for 20 min twice to obtain fraction 3 and fraction 4. Cells from fraction 2–4 were collected as the osteoblast-rich fraction (Ohori et al., 2019; Asano et al., 2021).

To investigate the effects of angiotensin II on priming of osteoblasts by TNF-α, osteoblasts (1×10^4 cells) were cultured in the presence or absence of TNF-α for 24 h, and then washed three times with PBS to remove TNF-α. Osteoclast precursors (5×10^4 cells) were then added on top of the osteoblasts in 96-well plates and cultured in α-MEM with 10^{-8} M $1.25(OH)_2D_3$ + 10^{-6} M PGE_2 (both from Sigma-Aldrich), 10^{-8} M $1.25(OH)_2D_3$ + 10^{-6} M PGE_2 + 10^{-6} M angiotensin II, 10^{-8} M $1.25(OH)_2D_3$ + 10^{-6} M PGE_2 + 10^{-6} M angiotensin II + 10^{-5} M angiotensin II type 1 receptor blocker or without additional agents as controls for 3 days. Cells were fixed with 4% formaldehyde and incubated with TRAP solution consisting of acetate buffer (pH 5.0), naphthol AS-MX phosphate, fast red violet LB salt, and 50 mM sodium tartrate at 37°C for 30 min. TRAP-positive multinucleated osteoclasts ≥150 μm in diameter with three or more nuclei were visualized and counted manually under a light microscope as described previously (Nara et al., 2020).

2.4 Real-Time RT-PCR Analysis

For real-time RT-PCR analysis, tibiae were crushed using a cell disrupter (Micro Smash MS-100R; Tomy Seiko, Tokyo, Japan) in 800 μL of TRIzol reagent (Invitrogen, Carlsbad, CA, United States). For *in vitro* experiments, osteoclast precursors and osteoblasts were cultured in serum-free medium overnight, followed by incubation in culture medium supplemented with TNF-α (100 ng/mL) or PBS as controls for 24 h. Moreover, to examine whether an increase in AGTR1 mRNA expression level in TNF-α-primed osteoblast affected the levels of RANKL and OPG mRNA expression, primary osteoblasts were cultured in

culture medium supplemented with PBS or TNF-α (100 ng/mL) for 24 h followed by changing the medium to remove TNF-α. Osteoblasts were then exposed to 10^{-6} M angiotensin II for 24 h. Total RNA was extracted from cells and tissue samples using a RNeasy Mini Kit (Qiagen, Hilden, Germany). cDNA was synthesized using Superscript IV reverse transcriptase (Invitrogen) with the same amount of total RNA. The levels of TNF-α, IL-1β, AGTR1, ACE, TRAP, RANKL, OPG, and glyceraldehyde 3-phosphate dehydrogenase (GAPDH) gene expression were measured using TB Green Premix Ex Taq II (Takara, Shiga, Japan) and a thermal cycler (Dice Real Time System; Takara) under the following conditions: initial denaturation at 95°C for 30 s followed by 50 cycles of denaturation at 95°C for 5 s and annealing at 60°C for 30 s, and final dissociation stage. Relative expression levels of target mRNAs were calculated by normalization relative to GAPDH mRNA. The primer sequences were as follows: 5′-GGTGGAGCC AAAAGGGTCA-3′ and 5′-GGGGGCTAAGCAGTTGGT-3′ for GAPDH; 5′-CTGTAGCCCACGTCGTAGC-3′ and 5′-TTGAGA TCCATGCCGTTG-3′ for TNF-α; 5′-CTCAACTGTGAAATG CCACC-3′ and 5′-TGTCCTCATCCTGGAAGGT-3′ for IL-1β; 5′-AGTCGCACTCAAGCCTGTCT-3′ and 5′-ACTGGTCCT TTGGTCGTGAG-3′ for AGTR1; 5′-CCACTATGGGTCCGA GTACATCAA-3′ and 5′-AGGGCGCCACCAAATCATAG-3′ for ACE; 5′-AACTTGCGACCATTGTTA-3′ and 5′-GGGGAC CTTTCGTTGATGT-3′ for TRAP; 5′-CCTGAGGCCCAGCCA TTT-3′ and 5′-CTTGGCCCAGCCTCGAT-3′ for RANKL; and 5′ -ATCAGAGCCTCATCACCTT-3′ and 5′ -CTTAGGTCC AACTACAGAGGAAC- 3′ for OPG.

2.5 Western Blotting Analysis

To investigate the effects of TNF-α on ERK1/2, p38, JNK mitogen-activated protein kinases (MAPKs), and IκBα phosphorylation in osteoblasts, primary osteoblasts were cultured in 60-mm cell culture dishes (Corning) in serum-free medium for 3 h. TNF-α (100 ng/mL) was then added to the dishes for specific periods (0, 5, 15, 30, 60 min). To examine the effects of MAPKs and nuclear factor (NF)-κB in the regulation of AGTR1 protein expression, TNF-α-pretreated osteoblasts were preincubated with 10 μM p38 MAPK inhibitor (InSolution™ SB 203580; EMD Millipore, Billerica, MA, United States), 10 μM ERK1/2 inhibitor (InSolution™ U0126; EMD Millipore), 10 μM JNK inhibitor (InSolution™ JNK Inhibitor II; EMD Millipore), and 10 μM NF-κB inhibitor (BAY11-7082; Sigma-Aldrich), and then exposed to TNF-α (100 ng/mL) for 24 h. The distal femur and cells were extracted using radioimmunoprecipitation assay (RIPA) lysis buffer (Millipore, Burlington, MA, United States) containing 1% protease and phosphatase inhibitor (Thermo Fisher Scientific). Total protein concentrations were quantified using a Pierce BCA protein assay kit (Thermo Fisher Scientific). Protein was treated with β-mercaptoethanol (Bio-Rad, Hercules, CA, United States) and Laemmli sample buffer (Bio-Rad) and denatured at 95°C for 5 min prior to SDS-PAGE. Equal amounts of protein were loaded onto 4–15% Mini-PROTEAN TGX Precast Gels (Bio-Rad) and transferred to a PVDF Trans-Blot Turbo Transfer System (Bio-Rad). The membranes were blocked in Block-Ace (DS Pharma Biomedical, Osaka, Japan) for 1 h at room temperature and incubated with antibodies against phospho-p38 MAPK (Thr180/Tyr182) (D3F9) XP, phospho-SAPK/JNK (Thr183/Tyr185) (98F2), phospho-p44/42MAPK (ERK1/2) (Thr202/Tyr204), phospho-IκBα (Ser32) (14D4) (monoclonal rabbit IgG, 1:1,000; Cell Signaling Technology, Danvers, MA, United States), AGTR1 (polyclonal rabbit IgG, 1:1,000; Proteintech Group, Inc., Chicago, IL, United States), TNF-α (polyclonal rabbit IgG, 1:500; GTX110520, Funakoshi, Japan), and β-actin (monoclonal mouse IgG, 1:1,000; Sigma-Aldrich) overnight at 4°C. The membranes were washed in Tris-buffered saline with Triton X-100 (TBS-T) and Tris-buffered saline (TBS), and then incubated with HRP-conjugated anti-rabbit IgG antibody (1:1,000–1:5,000; Cell Signaling Technology) or anti-mouse antibody (1:3,000–1:10,000; GE Healthcare, Chicago, IL, United States) for 1 h at room temperature. Bound antibodies were detected with SuperSignalWest Femto Maximum Sensitivity Substrate (Thermo Fisher Scientific) and a FUSION-FX7. EDGE Chemiluminescence Imaging System (Vilber Lourmat, Collégien, France).

2.6 Micro-Computed Tomography

Micro-computed tomography (CT) was performed using ScanXmate-E090 (Comscan, Kanagawa, Japan). Formalin-fixed femora were scanned with isotropic voxel size of 20 μm, x-ray tube voltage of 90 kV, x-ray tube current of 91 μA, with acquisition of 600 projections over 360° rotation, and reconstructed with 1,024 × 1008-pixels matrices. The calvariae were scanned under the same conditions as femora except using a voxel size of 60 μm, x-ray tube voltage of 60 kV, and x-ray tube current of 85 μA, and were reconstructed with 512 × 504-pixels matrices. After image acquisition, three-dimensional images were reconstructed to measure the morphometric parameters using TRI/3D-BONE64 software (RATOC System Engineering, Tokyo, Japan). To analyze the trabecular bone microarchitecture, the ROI for the distal femur began 1 mm proximal to the growth plate and extended 0.5 mm proximally. For cortical bone analysis, 0.5 × 4 mm region was selected in the midshaft centered at 50% of the total femoral length. The standard trabecular morphometric parameters determined were trabecular BV/TV (%), trabecular thickness (Tb.Th, μm), trabecular number (Tb.N, 1/mm), trabecular separation (Tb.Sp, μm), and bone surface area to volume ratio (BS/BV, 1/mm). The cortical morphometric parameter calculated was cortical thickness (Ct.Th, μm). Moreover, a rectangular region of 50 × 70 pixels cantered at the frontal suture was selected to quantify area of destruction in the calvariae using ImageJ (NIH) (Ishida et al., 2019).

2.7 ELISA Assay for TNF-α

Serum samples were obtained from normal control and SSHTN mice. TNF-α concentration was measured using ELISA MAX Standard Set Mouse TNF-α (Biolegend, United States) according to the manufacturer's protocols. 96-well ELISA plates (Biolegend) were precoated with monoclonal hamster antibody in carbonate buffer and incubated overnight at 4°C. To block non-specific binding and reduce background, the plates were incubated for 1 h at room temperature with the addition of 1% bovine serum

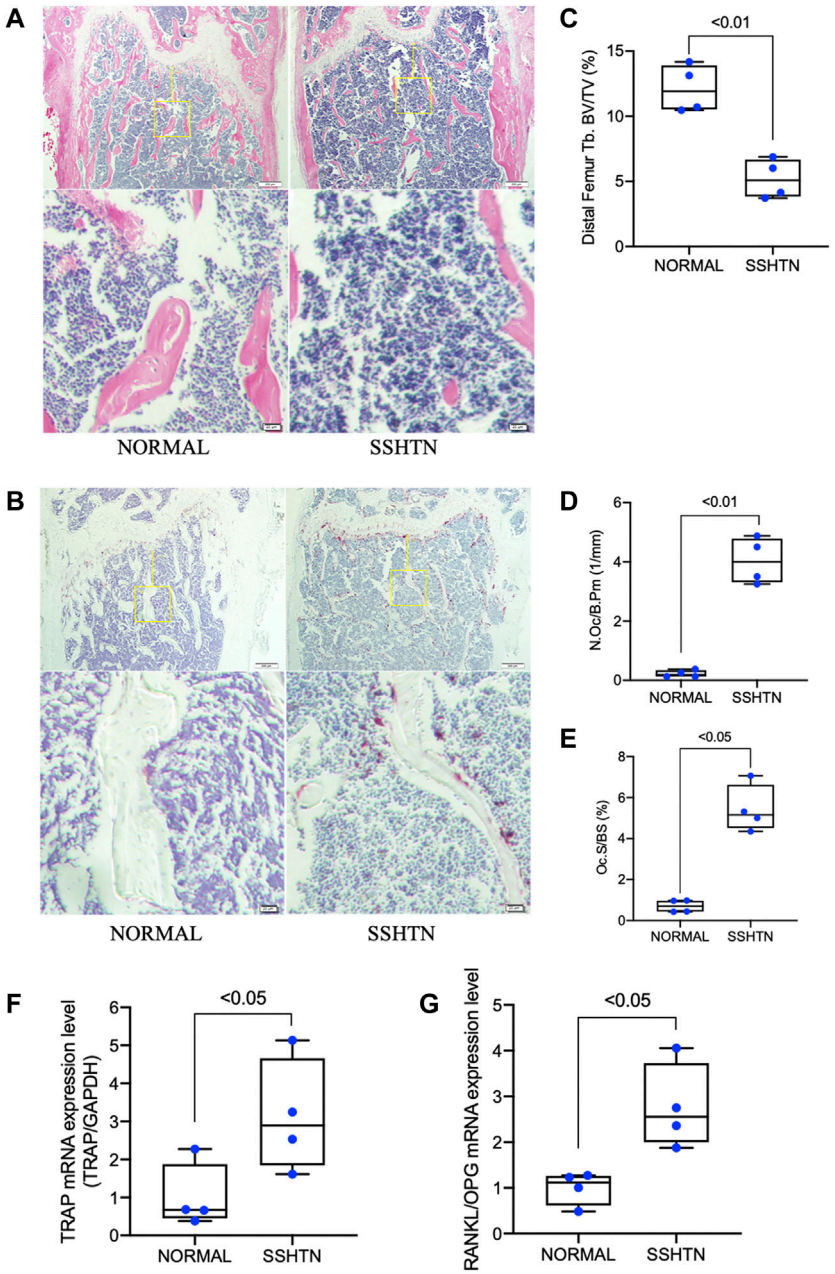

FIGURE 2 | SSHTN was associated with increased bone loss and elevated osteoclastogenesis as determined by histological analysis. Histological sections of decalcified femora from normal control mice or SSHTN mice (n = 4) stained with H&E **(A)** and TRAP **(B)**. Scale bar = 200 μm (20 μm in the enlarged picture). **(C)** Quantitative measurement of bone volume fraction (BV/TV). Quantitative measurement of the ratio of **(D)** osteoclast number/bone perimeter (N.Oc/B.Pm) and **(E)** osteoclast surface fraction (Oc.S/BS). **(F)** TRAP mRNA expression level and **(G)** RANKL/OPG mRNA expression level in the tibiae of normal control and SSHTN mice. TRAP, RANKL, and OPG mRNA expression levels were determined by real-time RT-PCR and were normalized relative to GAPDH (n = 4).

albumin (BSA; Sigma-Aldrich) in PBS. Diluted mouse TNF-α standard and serum samples were added to the wells and incubated for 2 h at room temperature. Biotinylated goat polyclonal anti-mouse TNF-α detection antibody was added to the wells with 1 h incubation at room temperature. The bound IgG was detected by incubation with HRP-conjugated avidin, followed by colorimetric detection with TMB substrate solution (Biolegend). The reaction was stopped with 2 N H_2SO_4 after 30 min, and the absorbance was measured at 450 nm using a microplate reader (Remote Sunrise, Tecan, Japan). Absorbance value at 595 nm was used as a reference.

2.8 Statistical Analysis

All results are shown in box plots with the median, interquartile range (IQR), and individual data points. Data were analyzed using GraphPad Prism 9.0 (GraphPad Software, Inc. La Jolla, CA,

United States). The distribution of variables was evaluated using the Shapiro–Wilk test. Student's *t* test or the Mann–Whitney test was used to compare means between two groups, while differences between all groups were examined by one-way analysis of variance (ANOVA) and Tukey's multiple comparison test or Kruskal–Wallis and Dunn's multiple comparison test. In all analyses, $p < 0.05$ was taken to indicate statistical significance.

3 RESULTS

3.1 Post L-NAME High-Salt Challenge Resulted in Increased Systolic Blood Pressure

To induce salt sensitivity, mice were administered L-NAME in their drinking water for 2 weeks, followed by a 2-weeks washout period, and then 3 weeks of exposure to high-salt diet (**Figure 1A**). Consistent with a previous study (Lopez Gelston et al., 2018), after 2 weeks of L-NAME administration, SBP in L-NAME-treated mice increased to 125 ± 5 mmHg compared to non-treated mice (95 ± 6 mmHg, $p < 0.01$). The SBP of L-NAME-treated mice returned to normal after the 2-weeks washout period (92 ± 5 mmHg). After 3 weeks of salt loading, L-NAME-treated mice showed salt-induced hypertension (125 ± 5 mmHg vs. 93 ± 5 mmHg, $p < 0.01$; **Figure 1B**).

3.2 SSHTN Increased Bone Loss and Osteoclastogenesis

The effects of SSHTN on osteoclastogenesis and bone loss were analyzed by histomorphometric analyses (**Figures 2A,B**). H&E staining showed that trabecular bone volume was significantly reduced in SSHTN mice (**Figure 2C**). In addition, TRAP staining was performed to evaluate several bone parameters to elucidate the effects of SSHTN on osteoclastogenesis *in vivo*. The trabecular distal femur of SSHTN mice showed an increased number of multinucleated TRAP-positive cells (**Figure 2D**). Consistent with these observations, quantitative histomorphometric analysis showed that Oc.S/BS was elevated in SSHTN mice compared to normal controls (5.43 vs. 0.7%, respectively, $p < 0.05$; **Figure 2E**). As expected, the mRNA expression level of TRAP, a primary osteoclast marker, was elevated in the tibiae of SSHTN mice compared with normal controls (**Figure 2F**). RANKL/OPG mRNA expression, important factor for determining osteoclast activation, was also upregulated by hypertension condition (**Figure 2G**). These results showed that SSHTN resulted in high levels of osteoclastogenesis and increased bone loss.

3.3 SSHTN Significantly Increased Bone Resorption Detected on Micro-CT

To examine the effects of SSHTN on bone resorption, we examined the morphometric parameters of femoral bone from normal control and SSHTN mice by micro-CT analysis (**Figure 3A**). Compared to that of the normal control mice, SSHTN mice showed reductions of 29 and 35% in trabecular number and BV/TV, respectively, while Tb.Sp showed a significant increase by 56% (**Figures 3B–D**). On the other hand, SSHTN did not have any impact on trabecular thickness, BS/BV, or cortical thickness (**Figures 3E–G**). These observations confirmed that SSHTN significantly elevated bone resorption, although trabecular and cortical thickness were not altered in these animals.

3.4 SSHTN Increased TNF-α and Activated Bone RAS *In Vivo*

As hypertension is considered to be a low-grade inflammatory condition related to the elevation of proinflammatory cytokines, we further examined the effects of SSHTN on proinflammatory cytokine mRNA expression in the tibia in comparison to normal controls. SSHTN stimulated the expression of TNF-α but had no impact on IL-1β mRNA expression (**Figures 4A,B**). Furthermore, to determine whether the increases in osteoclastogenesis and bone resorption in SSHTN mice could be explained by excessive activation of RAS within the bone, we also investigated AGTR1 and ACE mRNA expression. The results showed that AGTR1 mRNA expression was increased in the tibiae of SSHTN mice, while ACE mRNA expression was similar between normal control and SSHTN mice (**Figures 4C,D**). Since TNF-α and AGTR1 mRNA expression was increased in SSHTN mice, we also determined the protein expression of TNF-α and AGTR1. As expected, SSHTN upregulated TNF-α and AGTR1 protein expression (**Figures 4E,F**). In addition, TNF-α serum level was increased in SSHTN mice compare to normal control mice (**Figure 4G**).

3.5 TNF-α Priming Did Not Affect AGTR1 mRNA Expression in Osteoclast Precursors, but Increased AGTR1 mRNA Expression in Osteoblasts Through p38 Activation

The increased levels of both TNF-α and AGTR1 in SSHTN mice suggested that TNF-α may have an effect on AGTR1 expression in bone cells leading to the activation of osteoclasts. Therefore, we examined the effects of TNF-α on osteoclast precursors. Unexpectedly, treatment with TNF-α did not upregulate AGTR1 mRNA expression in osteoclast precursors (**Figure 5A**). However, stimulation of osteoblasts with TNF-α led to an increase in AGTR1 mRNA expression as determined by real-time RT-PCR (**Figure 5B**). We further clarified the cellular signaling of TNF-α responsible for upregulation of AGTR1 in osteoblasts. Treatment with TNF-α rapidly increased phosphorylation of ERK1/2, p38, JNK MAPKs, and IκBα in osteoblasts (**Figure 5C**). Pretreatment with the p38 MAPK inhibitor, SB 203580, attenuated TNF-α-induced upregulation of AGTR1 protein expression in osteoblasts, whereas the MEK1/2 inhibitor, U0126, JNK Inhibitor II, and NF-κB inhibitor, BAY11-0782, showed no such effect (**Figures 5D,E**). These results suggested a role of the p38 pathway in TNF-α-induced upregulation of AGTR1 protein expression in osteoblasts.

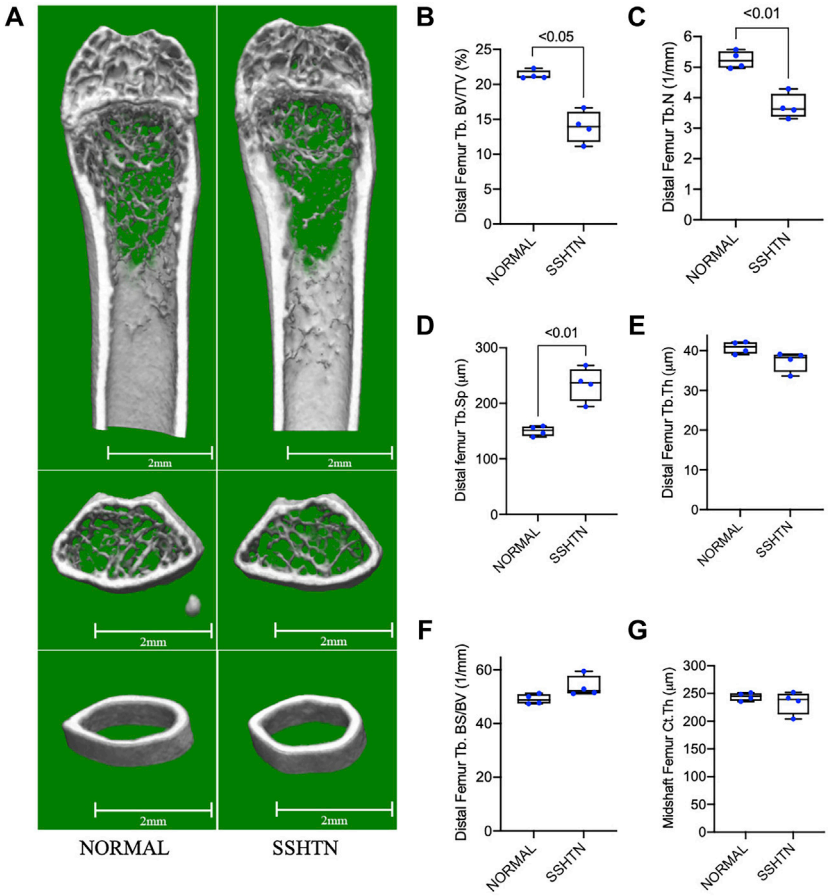

FIGURE 3 | SSHTN mice showed significant elevation of bone resorption determined by micro-CT. **(A)** Micro-CT reconstruction of the trabecular region below the distal femur growth plate and the cortical region of femoral midshaft of normal control or SSHTN mice ($n = 4$). Scale bar = 2 mm. **(B–G)** Quantitative measurement of bone morphometric-related parameters; **(B)** trabecular bone volume fraction (BV/TV), **(C)** trabecular number (Tb.N), **(D)** trabecular separation (Tb.Sp), **(E)** trabecular thickness (Tb.Th), **(F)** trabecular bone surface (BS/BV), and **(G)** cortical thickness (Ct.Th) of normal control and SSHTN mice ($n = 4$).

3.6 Angiotensin II Increased RANKL/OPG Ratio in TNF-α-Primed Osteoblasts and Enhanced Osteoclastogenesis in TNF-α-Primed Osteoblast/Osteoclast Precursor Co-Culture

As TNF-α did not induce upregulation of AGTR1 mRNA expression in osteoclast precursors, we further examined whether the increase in AGTR1 mRNA expression level in TNF-α-primed osteoblasts affected the mRNA expression of the osteoclast-related cytokines, RANKL and OPG, resulting in an increase in osteoclast number. Stimulation of TNF-α-primed osteoblasts with 10^{-6} M angiotensin II led to an increase in RANKL mRNA expression (**Figure 6A**) without significant effect in OPG mRNA expression, as determined by real-time RT-PCR (**Figure 6B**), resulting in an increase in the RANKL/OPG ratio (**Figure 6C**). Further analyses using an osteoblast/osteoclast precursor co-culture system showed that angiotensin II enhanced osteoclastogenesis in TNF-α-primed osteoblasts compared to unprimed osteoblasts, whereas cotreatment with an angiotensin II type 1 receptor blocker, olmesartan, completely abolished these effect (**Figures 6D,E**). Taken together, these results showed that angiotensin II stimulation and increased AGTR1 expression by TNF-α priming increased the RANKL/OPG ratio in osteoblasts leading to osteoclast activation.

3.7 SSHTN Exacerbated LPS-Induced Osteoclastogenesis *In Vivo*

To further examine whether SSHTN enhances LPS-induced osteoclastogenesis, mouse calvariae were subcutaneously injected with PBS or LPS daily for 5 days. Histological sections of calvariae from both normal control and SSHTN mice were stained for TRAP to identify osteoclasts (**Figure 7A**). The results showed that injection of 100 μg/day LPS in normal control mice resulted in numerous multinucleated TRAP-positive osteoclasts. There were no significant changes in osteoclast number when 10 μg/day LPS was injected into the calvariae of normal control mice and PBS was injected into the calvariae of SSHTN mice. In contrast, 10 μg/day LPS injection in SSHTN mice led to a marked

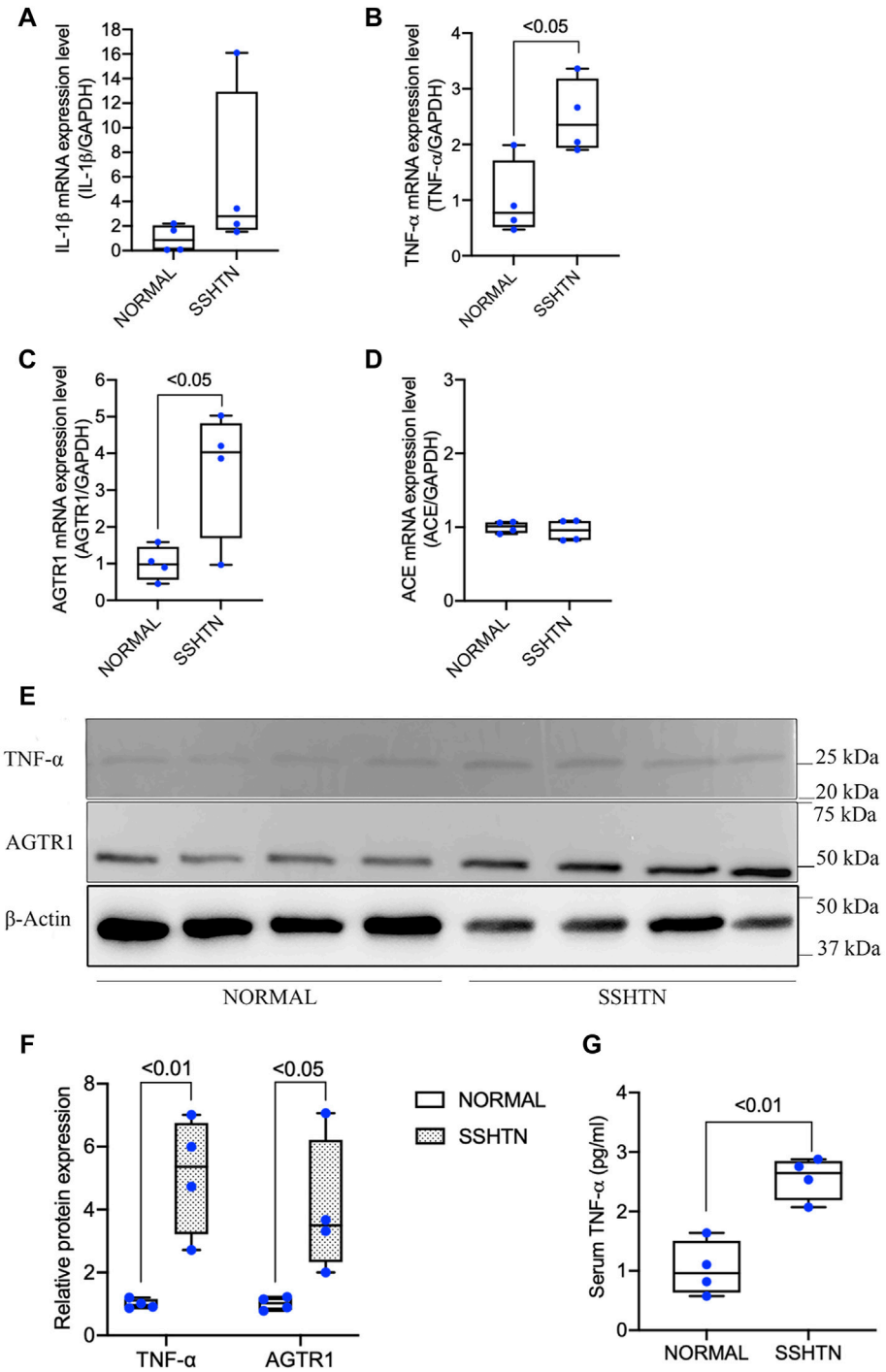

FIGURE 4 | SSHTN mice showed increased TNF-α and activation of bone RAS *in vivo*. **(A)** IL-1β mRNA expression levels in normal control and SSHTN mice. **(B)** TNF-α mRNA expression levels in normal control and SSHTN mice. **(C)** AGTR1 mRNA expression levels in normal control and SSHTN mice. **(D)** ACE mRNA expression levels in normal control and SSHTN mice. IL-1β, TNF-α, AGTR1, and ACE mRNA levels were measured by real-time RT-PCR. Total RNA was isolated from the tibiae of normal control and SSHTN mice. Expression levels of IL-1β, TNF-α, AGTR1, and ACE mRNA were normalized relative to GAPDH ($n = 4$). **(E)** Western blot analysis bands showing the expressions of TNF-α and AGTR1 protein in the distal femur of normal control and SSHTN mice. **(F)** Relative protein expression of TNF-α and AGTR1 were measured using ImageJ software ($n = 4$). β-Actin was used as a loading control. **(G)** Serum levels of TNF-α was determined using ELISA MAX Standard Set Mouse TNF-α. Serum samples were collected from normal control and SSHTN mice ($n = 4$).

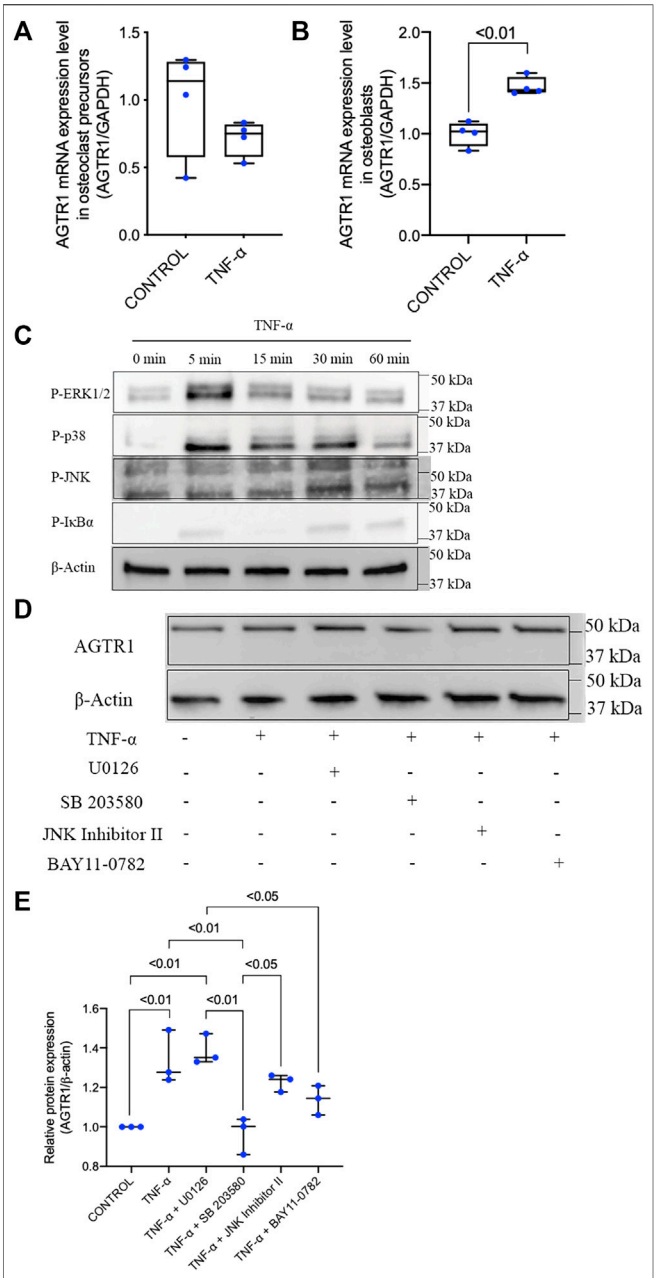

FIGURE 5 | TNF-α had no effect on AGTR1 mRNA expression in osteoclast precursors but increased AGTR1 mRNA expression in osteoblasts through p38 activation. **(A)** AGTR1 mRNA expression level in TNF-α pretreated osteoclast precursors and **(B)** osteoblasts for 24 h. AGTR1 mRNA expression level was determined by real-time RT-PCR. The levels of AGTR1 mRNA expression were normalized relative to GAPDH (n = 4). **(C)** Osteoblasts were incubated with TNF-α for 0, 5, 15, 30, or 60 min. Cells were lysed and analyzed by Western blotting using antibodies to phospho-ERK1/2, phospho-p38, phospho-JNK, and phospho-IκBα. β-Actin was used as a loading control. **(D)** Inhibition of p38 signaling prevented induction of AGTR1 protein expression by TNF-α *in vitro*. Osteoblasts were preincubated with or without MAPK and NF-κB inhibitors and then treated with TNF-α for 24 h. Cells were lysed and analyzed by Western blotting using an antibody to AGTR1. **(E)** Relative protein expression of AGTR1 were measured using ImageJ software (n = 3). β-Actin was used as a loading control.

increase in number of multinucleated TRAP-positive osteoclasts (**Figure 7B**). These observations indicated that the combination of LPS injection and SSHTN led to a further increase in osteoclastogenesis.

3.8 SSHTN Exacerbated LPS-Induced Bone Resorption *In Vivo*

To determine bone resorption area, the mouse calvariae were examined by micro-CT. **Figure 8A** shows micro-CT images of the calvariae from normal control and SSHTN mice. As shown in **Figure 8B**, 100 μg/day LPS injection in normal control mice resulted in a significant increase in bone resorption area by 7.1%, while 10 μg/day LPS injection in normal control mice and PBS injection in SSHTN mice did not have any impact on bone resorption area. However, SSHTN mice injected with 10 μg/day LPS showed a marked increase in bone resorption area by 6.9%, suggesting that LPS and SSHTN had a synergistic effect on bone resorption.

4 DISCUSSION

It has been difficult to assess the impact of high blood pressure on bone health and bone quality, leading to conflicting reports on hypertension-related bone loss (Tsuda et al., 2001; Javed et al., 2012). In this study, we used post-L-NAME high-salt challenge to generate a mouse model of hypertension to investigate its effects on bone. Our results showed that high blood pressure upregulates osteoclastogenesis, bone resorption, and exacerbates LPS-induced osteoclastogenesis and bone resorption. The distal femora of SSHTN mice showed increased osteoclast number and osteoclast surface fraction, but decreased trabecular bone fraction, which is primarily associated with reduced trabecular number and increased trabecular separation. Consistent with our results, a previous study showed that high blood pressure in spontaneously hypertensive rats (SHR) was associated with significantly reduced bone mineral density and increased risk of fracture with upregulation of markers of bone resorption (Tiyasatkulkovit et al., 2019). Moreover, Dahl salt-sensitive rats also showed osteopenia after chronic salt loading with sodium retention and calcium loss (Titze et al., 2004). Furthermore, recent epidemiological studies demonstrated an association between osteoporosis and high blood pressure. Individuals with higher blood pressure were shown to have increased osteoporotic fracture risk (Li et al., 2017). In addition, a meta-analysis showed that hypertensive women and men have increased bone mineral loss in the lumbar spine, femoral neck, Ward's triangle, femoral intertrochanteric region, calcaneus, and distal forearm (Ye et al., 2017). Moreover, elevated blood pressure was shown to be associated with decreased bone mineral density (Tiyasatkulkovit et al., 2019; Uchikawa et al., 2019).

To elucidate the mechanisms by which hypertension induces bone resorption, we examined the mRNA expression levels of proinflammatory cytokines and factors and found that SSHTN

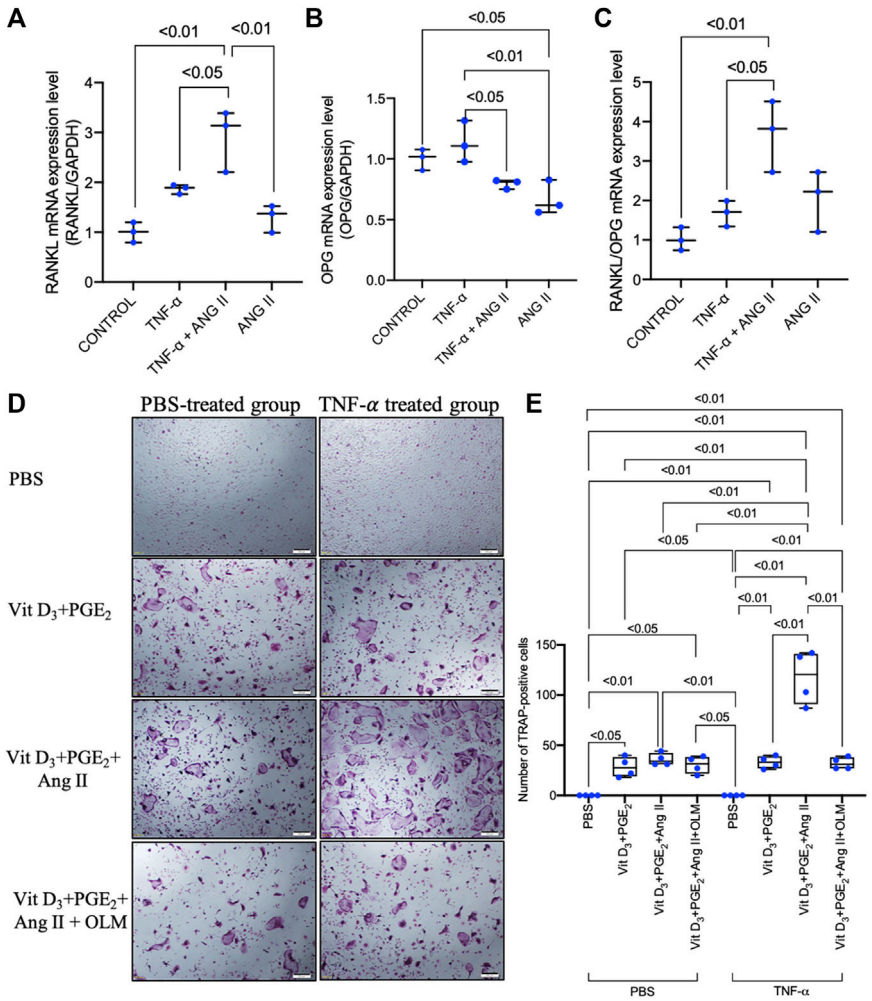

FIGURE 6 | Angiotensin II enhanced the TNF-α-induced increase in RANKL/OPG ratio in osteoblasts and enhanced osteoclastogenesis in TNF-α-primed osteoblast and osteoclast precursor co-culture. **(A)** RANKL mRNA expression level in osteoblasts. **(B)** OPG mRNA expression level in osteoblasts. **(C)** RANKL/OPG mRNA expression levels in osteoblasts. RANKL and OPG mRNA expression levels were determined by real-time RT-PCR and were normalized relative to GAPDH ($n = 3$). **(D)** Micrographs and **(E)** number of large TRAP-positive cells in co-cultures of TNF-α-primed or non-primed osteoblasts and osteoclast precursors treated with PBS, $1.25(OH)_2D_3$ + PGE_2, $1.25(OH)_2D_3$ + PGE_2 + angiotensin II, and $1.25(OH)_2D_3$ + PGE_2 + angiotensin II + angiotensin II type 1 receptor blocker. Scale bar = 200 μm ($n = 4$).

mice had elevated TNF-α mRNA, protein expression, and serum level in comparison to normal controls. Hypertension is known to be associated with inflammation. Increased serum levels of proinflammatory plasma cytokines, such as CRP, IL-6, IL-1β, and TNF-α, were observed in hypertensive rodent models (Lu et al., 2016; Liu et al., 2019; Dai et al., 2020). In addition, human subjects with high blood pressure were reported to show elevation of circulating proinflammatory cytokine and CRP levels (Jiménez et al., 2016; Pouvreau et al., 2018; Chen et al., 2019; Jayedi et al., 2019). High-salt diet was reported to induce elevation of TNF-α mRNA expression in the paraventricular nucleus and aorta in Dahl salt-sensitive rats, but not in normal controls (Yu et al., 2012; Jiang et al., 2018). Moreover, elevation of proinflammatory cytokines during chronic inflammation has been reported to have a significant effect on bone metabolism, leading to increased risk of bone loss (Baum and Gravallese, 2014; Amarasekara et al., 2015). TNF-α is an effective inducer of osteoclast activity, and has been shown to play important roles in bone metabolism and pathological bone diseases (Kishikawa et al., 2019; Ohori et al., 2020). Therefore, the findings outlined above suggest that TNF-α may have important roles in the processes of bone loss and bone resorption in this SSHTN mouse model.

The systemic RAS is an endocrine system with important roles in regulating blood pressure and electrolyte homeostasis (Ahn et al., 2017; Han et al., 2017). Various organs and tissues, including bone, have also been shown to have local tissue-specific RAS. Moreover, bone RAS overactivation can induce metabolic bone disorders and cause deterioration of bone microcirculation (Shimizu et al., 2008; Asaba et al., 2009; Zhou et al., 2017). ACE and AGTR1 were shown to be highly expressed in the femoral head in an ovariectomized rat model of

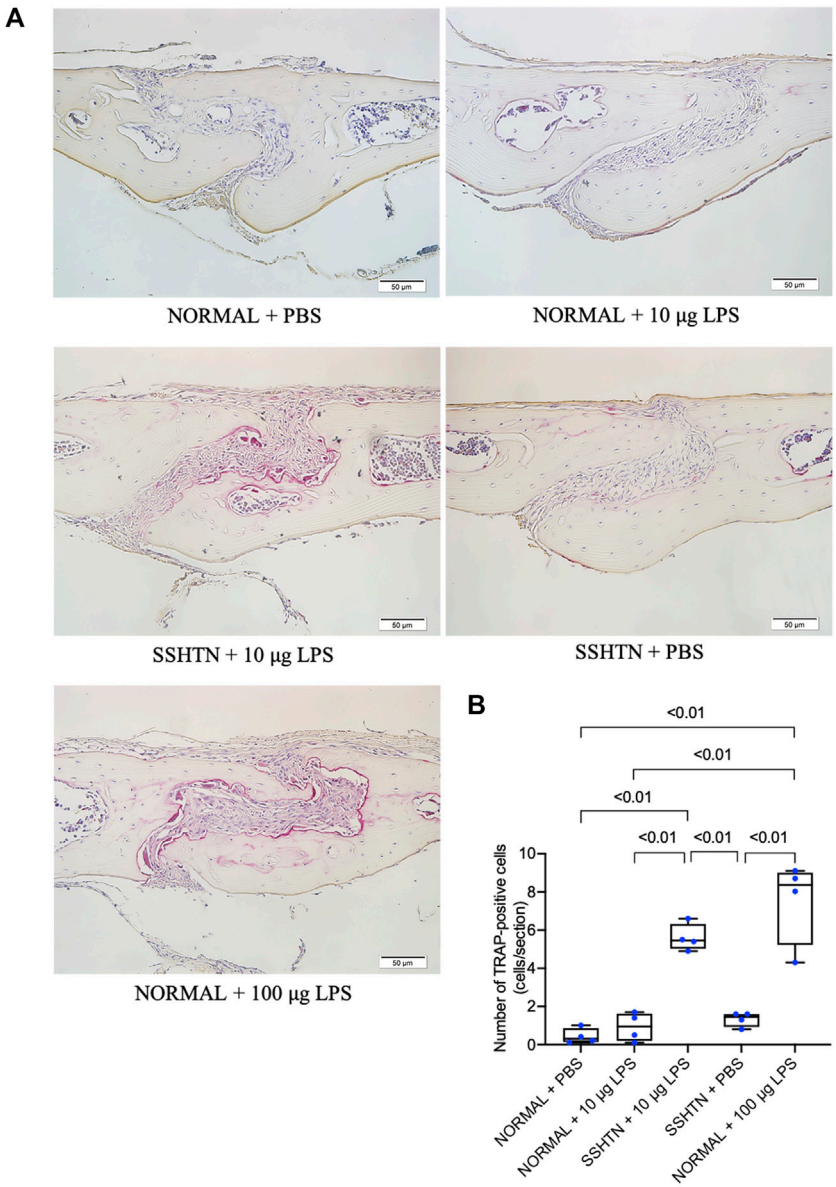

FIGURE 7 | SSHTN mice showed elevated osteoclastogenesis induced by LPS *in vivo*. **(A)** Histological sections of calvariae were obtained from normal control or SSHTN mice after 5 days of daily supracalvarial injection with PBS or LPS. TRAP staining was performed to identify osteoclasts. **(B)** Numbers of multinucleated TRAP-positive cells in the sagittal suture mesenchyme of calvariae were quantified. Scale bar = 50 μm (n = 4).

postmenopausal osteoporosis (Abuohashish et al., 2017b). In addition, the use of AGTR1 antagonists was shown to have therapeutic and protective effects on bone (Abuohashish et al., 2017c; Donmez et al., 2017; Birocale et al., 2019; Dionísio et al., 2020), and ACE inhibitors were shown to have beneficial effects on bone in both experimental and clinical studies (Abuohashish et al., 2017a; Rianon et al., 2017; Chen et al., 2018). Therefore, we also examined whether SSHTN promoted the activation of bone RAS. SSHTN mice showed elevated mRNA and protein expression of the bone RAS component, AGTR1. Indeed, increased AGTR1 mRNA and protein expression were detected in the joint tissues in a transgenic mouse model overexpressing human TNF-α (Akagi et al., 2020). These observations suggest that excessive TNF-α in SSHTN could promote local bone RAS activation, which may have important synergistic effects in SSHTN-induced bone loss.

To further elucidate whether upregulation of TNF-α mRNA expression in SSHTN activates local bone RAS activation resulting in bone loss, we examined the effect of TNF-α on AGTR1 mRNA expression in bone cells. Stimulation with TNF-α did not promote AGTR1 mRNA expression in murine

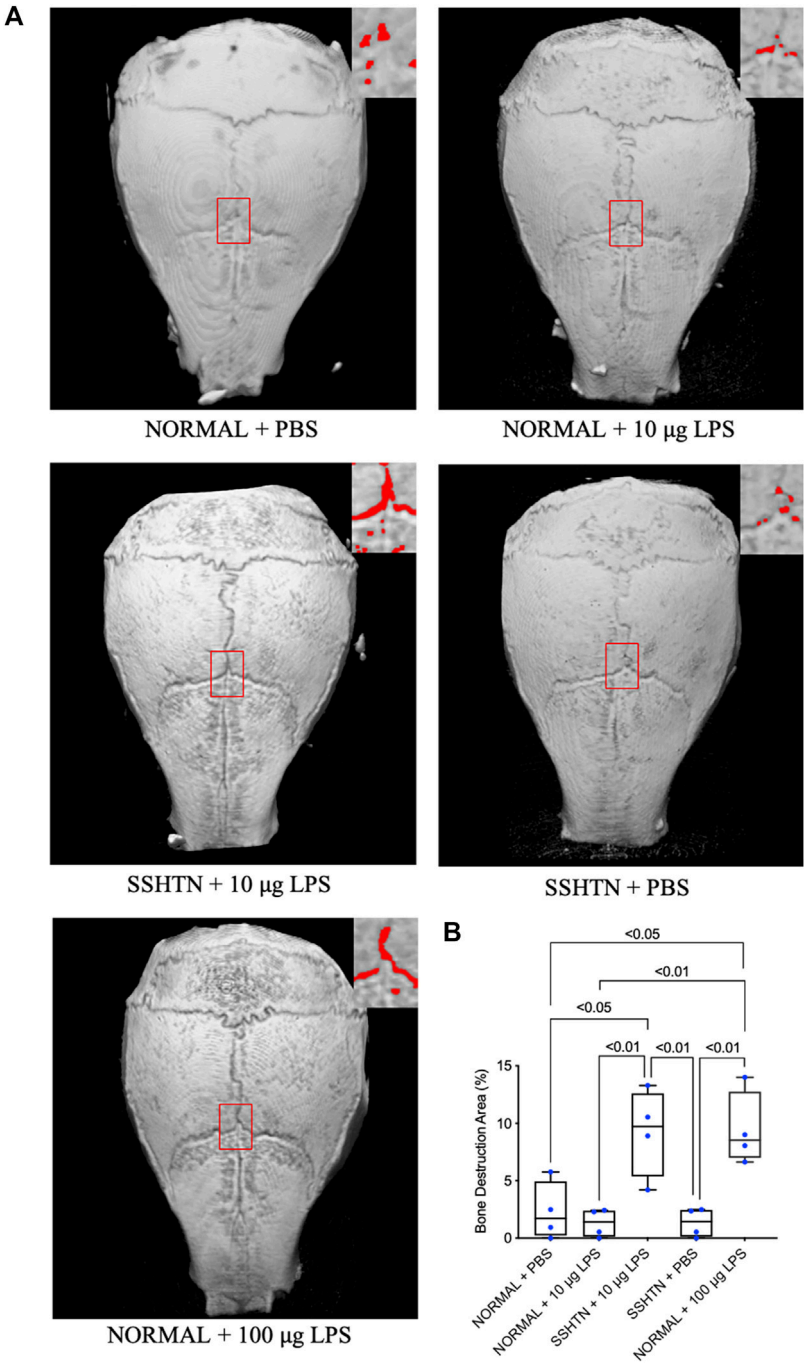

FIGURE 8 | SSHTN mice showed increased bone resorption area induced by LPS *in vivo*. **(A)** Micro-CT reconstructed images of calvariae from normal control or SSHTN mice after daily supracalvarial injection of PBS or LPS for 5 days. Bone resorption areas are shown in red. **(B)** The ratio of bone resorption area to total area was quantified (n = 4).

primary osteoclast precursors in culture, while TNF-α enhanced AGTR1 mRNA expression in murine primary osteoblast cultures. TNF-α has been reported to induce AGTR1 expression in cardiac fibroblasts (Peng et al., 2002; Gurantz et al., 2005) and chondrocytes (Tsukamoto et al., 2014). In addition, the transcription factor, NF-κB, and possibly p38 MAPK, were shown to be required for TNF-α-induced AGTR1 upregulation in cardiac fibroblasts (Cowling et al., 2002). Therefore, we also examined the downstream inhibitory effects of TNF-α on ERK1/2, p38, JNK MAPKs, and NF-κB activation using selective inhibitors (U0126, SB 203580, JNK inhibitor II, and BAY11-7082, respectively). However, only the p38 MAPK inhibitor, SB

203580, attenuated AGTR1 protein expression in TNF-α-treated osteoblasts. Angiotensin II has been reported to induce osteoclastogenesis indirectly *via* stromal cells by increasing RANKL expression via AGTR1 receptors (Shimizu et al., 2008). Therefore, we assumed that angiotensin II enhanced TNF-α-induced osteoblast AGTR1 expression and promoted osteoclastogenesis indirectly through TNF-α-mediated osteoblast osteoclastogenic capability. Therefore, we primed osteoblasts with TNF-α followed by treatment with angiotensin II. Stimulation of TNF-α-primed osteoblasts with angiotensin II led to an increase in RANKL/OPG ratio. Furthermore, we also evaluated the effects of TNF-α priming on osteoclastogenesis in osteoblast/osteoclast precursor co-culture and showed that TNF-α priming upregulated osteoclastogenesis compared to untreated controls. The increase in osteoclastogenesis in the TNF-α-primed group was likely due to the increased RANKL/OPG ratio, stimulation by angiotensin II in TNF-α priming osteoblast was shown to markedly increase the RANKL/OPG ratio. These results suggested that angiotensin II stimulation and increased expression of AGTR1 by TNF-α may induce RANKL expression, thus leading to osteoclastogenesis.

It has been reported that subcutaneous administration of LPS at a dose of 100 μg/day for 5 days can promote osteoclastogenesis and bone resorption in calvariae, while daily injection of LPS at 10 μg/day failed to increase osteoclast number and stimulate bone resorption *in vivo* (Ishida et al., 2015; Shima et al., 2018). Consistent with these findings, administration of LPS at a dose of 10 μg/day did not increase osteoclast number *in vivo*. However, SSHTN mice injected with LPS at a dose of 10 μg/day showed an increase in osteoclast number. These observations suggested that SSHTN exacerbates inflammation-induced osteoclastogenesis *in vivo*. In addition, we also examined whether SSHTN exacerbates LPS-induced bone resorption by micro-CT. Increased bone resorption area was only found in normal control mice injected with 100 μg/day LPS and SSHTN mice injected with 10 μg/day LPS, but not in SSHTN mice injected with PBS. These observations suggested that SSHTN exacerbates inflammation-induced osteoclastogenesis and bone resorption, and therefore SSHTN could be a risk factor for progressive bone resorption in inflammatory bone disease.

5 CONCLUSION

The results of the present study demonstrated the detrimental effects of SSHTN on bone health. These hypertensive mice showed deterioration of the bone microstructure, possibly due to increased expression of the proinflammatory cytokine, TNF-α, together with excessive bone RAS activation. Our results may facilitate the development of novel therapeutic strategies to protect bone health under conditions of long-term high-salt intake and hypertension.

DATA AVAILABILITY STATEMENT

The original contributions presented in the study are included in the article/supplementary material, further inquiries can be directed to the corresponding author.

ETHICS STATEMENT

The animal study was reviewed and approved by the Tohoku University of Science Animal Care and Use Committee.

AUTHOR CONTRIBUTIONS

AP and HK contributed to the conception and design of the study, data acquisition, data analysis, data interpretation, and drafting the manuscript. HK contributed to critical revision of the manuscript. AP, FO, TN, AM, YN, RJ, JM, KK, and YT collected the samples and performed data analysis. HK and IM supervised the project. All authors provided final approval and agree to be accountable for all aspects of the work.

FUNDING

This work was supported by the JSPS KAKENHI grants from the Japan Society for the Promotion of Science (No. 19K10397 to HK).

REFERENCES

Abu-Amer, Y., Ross, F. P., Edwards, J., and Teitelbaum, S. L. (1997). Lipopolysaccharide-stimulated Osteoclastogenesis Is Mediated by Tumor Necrosis Factor via its P55 Receptor. *J. Clin. Invest.* 100, 1557–1565. doi:10.1172/JCI119679

Abuohashish, H. M., Ahmed, M. M., Sabry, D., Khattab, M. M., and Al-Rejaie, S. S. (2017a). ACE-2/Ang1-7/Mas cascade Mediates ACE Inhibitor, Captopril, Protective Effects in Estrogen-Deficient Osteoporotic Rats. *Biomed. Pharmacother.* 92, 58–68. doi:10.1016/j.biopha.2017.05.062

Abuohashish, H. M., Ahmed, M. M., Sabry, D., Khattab, M. M., and Al-Rejaie, S. S. (2017b). Angiotensin (1-7) Ameliorates the Structural and Biochemical Alterations of Ovariectomy-Induced Osteoporosis in Rats via Activation of ACE-2/Mas Receptor axis. *Sci. Rep.* 7, 1–11. doi:10.1038/s41598-017-02570-x

Abuohashish, H. M., Ahmed, M. M., Sabry, D., Khattab, M. M., and Al-Rejaie, S. S. (2017c). The ACE-2/Ang1-7/Mas cascade Enhances Bone Structure and Metabolism Following Angiotensin-II Type 1 Receptor Blockade. *Eur. J. Pharmacol.* 807, 44–55. doi:10.1016/j.ejphar.2017.04.031

Ahn, Y. M., Choi, Y. H., Yoon, J. J., Lee, Y. J., Cho, K. W., Kang, D. G., et al. (2017). Oleanolic Acid Modulates the Renin-Angiotensin System and Cardiac Natriuretic Hormone Concomitantly with Volume and Pressure Balance in Rats. *Eur. J. Pharmacol.* 809, 231–241. doi:10.1016/j.ejphar.2017.05.030

Akagi, T., Mukai, T., Mito, T., Kawahara, K., Tsuji, S., Fujita, S., et al. (2020). Effect of Angiotensin II on Bone Erosion and Systemic Bone Loss in Mice with Tumor Necrosis Factor-Mediated Arthritis. *Int. J. Mol. Sci.* 21, 4145. doi:10.3390/ijms21114145

Amarasekara, D. S., Yu, J., and Rho, J. (2015). Bone Loss Triggered by the Cytokine Network in Inflammatory Autoimmune Diseases. *J. Immunol. Res.* 2015, 1–12. doi:10.1155/2015/832127

Arvanitakis, Z., Capuano, A. W., Lamar, M., Shah, R. C., Barnes, L. L., Bennett, D. A., et al. (2018). Late-life Blood Pressure Association with Cerebrovascular and Alzheimer Disease Pathology. *Neurology* 91, e517–e525. doi:10.1212/WNL.0000000000005951

Asaba, Y., Ito, M., Fumoto, T., Watanabe, K., Fukuhara, R., Takeshita, S., et al. (2009). Activation of Renin-Angiotensin System Induces Osteoporosis Independently of Hypertension. *J. Bone Mineral Res.* 24, 241–250. doi:10.1359/jbmr.081006

Asano, Y., Matsumoto, Y., La Rose, J., He, F., Katsuyama, T., Ziyi, W., et al. (2021). Endonuclease Increases Efficiency of Osteoblast Isolation from Murine Calvariae. *Sci. Rep.* 11, 8502. doi:10.1038/s41598-021-87716-8

Baum, R., and Gravallese, E. M. (2014). Impact of Inflammation on the Osteoblast in Rheumatic Diseases. *Curr. Osteoporos. Rep.* 12, 9–16. doi:10.1007/s11914-013-0183-y

Birocale, A. M., Ferreira de Melo, A., Peixoto, P., Costalonga Oliveira, P. W., Gonçalves Ruffoni, L. D., Takayama, L. M., et al. (2019). Telmisartan Use in Rats with Preexisting Osteoporotics Bone Disorders Increases Bone Microarchitecture Alterations via PPARγ. *Life Sci.* 237, 116890. doi:10.1016/j.lfs.2019.116890

Chen, X.-F., Li, X.-L., Liu, J.-X., Xu, J., Zhao, Y.-Y., Yang, M., et al. (2018). Inhibition on Angiotensin-Converting Enzyme Exerts Beneficial Effects on Trabecular Bone in Orchidectomized Mice. *Pharmacol. Rep.* 70, 705–711. doi:10.1016/j.pharep.2018.02.008

Chen, J., Bundy, J. D., Hamm, L. L., Hsu, C.-y., Lash, J., Miller, E. R., et al. (2019). Inflammation and Apparent Treatment-Resistant Hypertension in Patients with Chronic Kidney Disease. *Hypertension* 73, 785–793. doi:10.1161/HYPERTENSIONAHA.118.12358

Cowling, R. T., Gurantz, D., Peng, J., Dillmann, W. H., and Greenberg, B. H. (2002). Transcription Factor NF-κB Is Necessary for Up-Regulation of Type 1 Angiotensin II Receptor mRNA in Rat Cardiac Fibroblasts Treated with Tumor Necrosis Factor-α or Interleukin-1β. *J. Biol. Chem.* 277, 5719–5724. doi:10.1074/jbc.M107515200

Dai, B., Wang, Z.-Z., Zhang, H., Han, M.-X., Zhang, G.-X., and Chen, J.-W. (2020). Antihypertensive Properties of a Traditional Chinese Medicine GAO-ZI-YAO in Elderly Spontaneous Hypertensive Rats. *Biomed. Pharmacother.* 131, 110739. doi:10.1016/j.biopha.2020.110739

Dionísio, T. J., Souza, G. P., Colombini-Ishikiriama, B. L., Garbieri, T. F., Parisi, V. A., Oliveira, G. M., et al. (2020). AT1 Receptor Antagonism Promotes Bone Loss Attenuation in Experimental Periodontitis, Blocks Inflammatory Mediators, and Upregulates Antioxidant Enzymes and Bone Formation Markers. *J. Periodontol.* 91, 533–544. doi:10.1002/JPER.19-0064

Donmez, B. O., Unal, M., Ozdemir, S., Ozturk, N., Oguz, N., and Akkus, O. (2017). Effects of Losartan Treatment on the Physicochemical Properties of Diabetic Rat Bone. *J. Bone Miner. Metab.* 35, 161–170. doi:10.1007/s00774-016-0748-9

Ettehad, D., Emdin, C. A., Kiran, A., Anderson, S. G., Callender, T., Emberson, J., et al. (2016). Blood Pressure Lowering for Prevention of Cardiovascular Disease and Death: A Systematic Review and Meta-Analysis. *Lancet* 387, 957–967. doi:10.1016/S0140-6736(15)01225-8

Gurantz, D., Cowling, R. T., Varki, N., Frikovsky, E., Moore, C. D., and Greenberg, B. H. (2005). IL-1β and TNF-α Upregulate Angiotensin II Type 1 (AT1) Receptors on Cardiac Fibroblasts and Are Associated with Increased AT1 Density in the post-MI Heart. *J. Mol. Cell Cardiol.* 38, 505–515. doi:10.1016/j.yjmcc.2004.12.015

Han, W., Sun, N., Chen, L., Jiang, S., Chen, Y., Li, M., et al. (2017). Relationship of Renin-Angiotensin System Polymorphisms with Ambulatory and central Blood Pressure in Patients with Hypertension. *J. Clin. Hypertens.* 19, 1081–1087. doi:10.1111/jch.13061

Ishida, M., Kitaura, H., Kimura, K., Sugisawa, H., Aonuma, T., Takada, H., et al. (2015). Muramyl Dipeptide Enhances Lipopolysaccharide-Induced Osteoclast Formation and Bone Resorption through Increased RANKL Expression in Stromal Cells. *J. Immunol. Res.* 2015, 1–12. doi:10.1155/2015/132765

Ishida, M., Shen, W.-R., Kimura, K., Kishikawa, A., Shima, K., Ogawa, S., et al. (2019). DPP-4 Inhibitor Impedes Lipopolysaccharide-Induced Osteoclast Formation and Bone Resorption *In Vivo*. *Biomed. Pharmacother.* 109, 242–253. doi:10.1016/j.biopha.2018.10.052

Javed, F., Khan, S. A., Ayers, E. W., Aziz, E. F., Akram, M. S., Nadkarni, G. N., et al. (2012). Association of Hypertension and Bone mineral Density in an Elderly African American Female Population. *J. Natl. Med. Assoc.* 104, 172–178. doi:10.1016/S0027-9684(15)30140-1

Jayedi, A., Rahimi, K., Bautista, L. E., Nazarzadeh, M., Zargar, M. S., and Shab-Bidar, S. (2019). Inflammation Markers and Risk of Developing Hypertension: A Meta-Analysis of Cohort Studies. *Heart* 105, 686–692. doi:10.1136/heartjnl-2018-314216

Jiang, E., Chapp, A. D., Fan, Y., Larson, R. A., Hahka, T., Huber, M. J., et al. (2018). Expression of Proinflammatory Cytokines Is Upregulated in the Hypothalamic Paraventricular Nucleus of Dahl Salt-Sensitive Hypertensive Rats. *Front. Physiol.* 9, 104. doi:10.3389/fphys.2018.00104

Jiménez, M. C., Rexrode, K. M., Kotler, G., Everett, B. M., Glynn, R. J., Lee, I.-M., et al. (2016). Association between Markers of Inflammation and Total Stroke by Hypertensive Status Among Women. *Am. J. Hypertens.* 29, 1117–1124. doi:10.1093/ajh/hpw050

Kearney, P. M., Whelton, M., Reynolds, K., Muntner, P., Whelton, P. K., and He, J. (2005). Global burden of Hypertension: Analysis of Worldwide Data. *Lancet* 365, 217–223. doi:10.1016/S0140-6736(05)17741-1

Kishikawa, A., Kitaura, H., Kimura, K., Ogawa, S., Qi, J., Shen, W.-R., et al. (2019). Docosahexaenoic Acid Inhibits Inflammation-Induced Osteoclast Formation and Bone Resorption *In Vivo* through GPR120 by Inhibiting TNF-α Production in Macrophages and Directly Inhibiting Osteoclast Formation. *Front. Endocrinol.* 10, 1–13. doi:10.3389/fendo.2019.00157

Kitaura, H., Sands, M. S., Aya, K., Zhou, P., Hirayama, T., Uthgenannt, B., et al. (2004). Marrow Stromal Cells and Osteoclast Precursors Differentially Contribute to TNF-α-Induced Osteoclastogenesis *In Vivo*. *J. Immunol.* 173, 4838–4846. doi:10.4049/jimmunol.173.8.4838

Li, Y., Xia, P., Xu, L., Wang, Y., and Chen, L. (2016). A Meta-Analysis on Prehypertension and Chronic Kidney Disease. *PLoS One* 11, e0156575. doi:10.1371/journal.pone.0156575

Li, C., Zeng, Y., Tao, L., Liu, S., Ni, Z., Huang, Q., et al. (2017). Meta-analysis of Hypertension and Osteoporotic Fracture Risk in Women and Men. *Osteoporos. Int.* 28, 2309–2318. doi:10.1007/s00198-017-4050-z

Lian, X. L., Zhang, Y. P., Li, X., Jing, L. D., Cairang, Z. M., and Gou, J. Q. (2017). Exploration on the Relationship between the Elderly Osteoporosis and Cardiovascular Disease Risk Factors. *Eur. Rev. Med. Pharmacol. Sci.* 21, 4386–4390.

Liu, X., Chen, K., Zhuang, Y., Huang, Y., Sui, Y., Zhang, Y., et al. (2019). Paeoniflorin Improves Pressure Overload-Induced Cardiac Remodeling by Modulating the MAPK Signaling Pathway in Spontaneously Hypertensive Rats. *Biomed. Pharmacother.* 111, 695–704. doi:10.1016/j.biopha.2018.12.090

Lopez Gelston, C. A., Balasubbramanian, D., Abouelkheir, G. R., Lopez, A. H., Hudson, K. R., Johnson, E. R., et al. (2018). Enhancing Renal Lymphatic Expansion Prevents Hypertension in Mice. *Circ. Res.* 122, 1094–1101. doi:10.1161/CIRCRESAHA.118.312765

Lu, J., Liu, F., Chen, F., Jin, Y., Chen, H., Liu, D., et al. (2016). Amlodipine and Atorvastatin Improve Ventricular Hypertrophy and Diastolic Function via Inhibiting TNF-α, IL-1β and NF-κB Inflammatory Cytokine Networks in Elderly Spontaneously Hypertensive Rats. *Biomed. Pharmacother.* 83, 330–339. doi:10.1016/j.biopha.2016.06.034

Marahleh, A., Kitaura, H., Ishida, M., Shima, K., Kishikawa, A., Ogawa, S., et al. (2019). Effect of Anti-c-fms Antibody on Osteoclast Formation and Proliferation of Osteoclast Precursor *In Vitro*. *JoVE* 145, 1–6. doi:10.3791/59089

Mills, K. T., Bundy, J. D., Kelly, T. N., Reed, J. E., Kearney, P. M., Reynolds, K., et al. (2016). Global Disparities of Hypertension Prevalence and Control. *Circulation* 134, 441–450. doi:10.1161/CIRCULATIONAHA.115.018912

Nara, Y., Kitaura, H., Ogawa, S., Shen, W.-R., Qi, J., Ohori, F., et al. (2020). Anti-C-FMS Antibody Prevents Osteoclast Formation and Bone Resorption in Co-culture of Osteoblasts and Osteoclast Precursors *In Vitro* and in Ovariectomized Mice. *Int. J. Mol. Sci.* 21, 6120–6216. doi:10.3390/ijms21176120

Noguchi, T., Kitaura, H., Ogawa, S., Qi, J., Shen, W.-R., Marahleh, A., et al. (2020). TNF-α Stimulates the Expression of RANK during Orthodontic Tooth Movement. *Arch. Oral Biol.* 117, 104796. doi:10.1016/j.archoralbio.2020.104796

Ohori, F., Kitaura, H., Marahleh, A., Kishikawa, A., Ogawa, S., Qi, J., et al. (2019). Effect of TNF-α-Induced Sclerostin on Osteocytes during Orthodontic Tooth Movement. *J. Immunol. Res.* 2019, 1–10. doi:10.1155/2019/9716758

Ohori, F., Kitaura, H., Ogawa, S., Shen, W.-R., Qi, J., Noguchi, T., et al. (2020). IL-33 Inhibits TNF-α-Induced Osteoclastogenesis and Bone Resorption. *Int. J. Mol. Sci.* 21, 1130–1213. doi:10.3390/ijms21031130

Peng, J., Gurantz, D., Tran, V., Cowling, R. T., and Greenberg, B. H. (2002). Tumor Necrosis Factor-α-Induced at 1 Receptor Upregulation Enhances Angiotensin II-Mediated Cardiac Fibroblast Responses that Favor Fibrosis. *Circ. Res.* 91, 1119–1126. doi:10.1161/01.RES.0000047090.08299.D5

Pouvreau, C., Dayre, A., Butkowski, E., De Jong, B., and Jelinek, H. F. (2018). Inflammation and Oxidative Stress Markers in Diabetes and Hypertension. *J. Inflamm. Res.* 11, 61–68. doi:10.2147/JIR.S148911

Rianon, N., Ambrose, C. G., Pervin, H., Garcia, M., Mama, S. K., Schwartz, A. V., et al. (2017). Long-term Use of Angiotensin-Converting Enzyme Inhibitors Protects against Bone Loss in African-American Elderly Men. *Arch. Osteoporos.* 12, 1–8. doi:10.1007/s11657-017-0387-3

Sakuma, Y., Tanaka, K., Suda, M., Yasoda, A., Natsui, K., Tanaka, I., et al. (2000). Crucial Involvement of the EP4 Subtype of Prostaglandin E Receptor in Osteoclast Formation by Proinflammatory Cytokines and Lipopolysaccharide. *J. Bone Miner. Res.* 15, 218–227. doi:10.1359/jbmr.2000.15.2.218

Shen, W.-R., Kimura, K., Ishida, M., Sugisawa, H., Kishikawa, A., Shima, K., et al. (2018). The Glucagon-like Peptide-1 Receptor Agonist Exendin-4 Inhibits Lipopolysaccharide-Induced Osteoclast Formation and Bone Resorption via Inhibition of TNF-αExpression in Macrophages. *J. Immunol. Res.* 2018, 1–10. doi:10.1155/2018/5783639

Shima, K., Kimura, K., Ishida, M., Kishikawa, A., Ogawa, S., Qi, J., et al. (2018). C-X-C Motif Chemokine 12 Enhances Lipopolysaccharide-Induced Osteoclastogenesis and Bone Resorption *In Vivo*. *Calcif. Tissue Int.* 103, 431–442. doi:10.1007/s00223-018-0435-z

Shimizu, H., Nakagami, H., Osako, M. K., Hanayama, R., Kunugiza, Y., Kizawa, T., et al. (2008). Angiotensin II Accelerates Osteoporosis by Activating Osteoclasts. *FASEB J.* 22, 2465–2475. doi:10.1096/fj.07-098954

Titze, J., Rittweger, J., Dietsch, P., Krause, H., Schwind, K. H., Engelke, K., et al. (2004). Hypertension, Sodium Retention, Calcium Excretion and Osteopenia in Dahl Rats. *J. Hypertens.* 22, 803–810. doi:10.1097/00004872-200404000-00024

Tiyasatkulkovit, W., Promruk, W., Rojviriya, C., Pakawanit, P., Chaimongkolnukul, K., Kengkoom, K., et al. (2019). Impairment of Bone Microstructure and Upregulation of Osteoclastogenic Markers in Spontaneously Hypertensive Rats. *Sci. Rep.* 9, 1–12. doi:10.1038/s41598-019-48797-8

Tsuda, K., Nishio, I., and Masuyama, Y. (2001). Bone mineral Density in Women with Essential Hypertension. *Am. J. Hypertens.* 14, 704–707. doi:10.1016/S0895-7061(01)01303-6

Tsukamoto, I., Akagi, M., Inoue, S., Yamagishi, K., Mori, S., and Asada, S. (2014). Expressions of Local Renin-Angiotensin System Components in Chondrocytes. *Eur. J. Histochem.* 58, 132–138. doi:10.4081/ejh.2014.2387

Uchikawa, Y., Hosomichi, J., Suzuki, J.-i., Yamaguchi, H., Ishida, Y., Hatano, K., et al. (2019). Differential Growth of Craniofacial and Tibial Bones to Sympathetic Hyperactivity-Related Hypertension in Rats. *Arch. Oral Biol.* 99, 73–81. doi:10.1016/j.archoralbio.2019.01.001

Xie, X., Atkins, E., Lv, J., Bennett, A., Neal, B., Ninomiya, T., et al. (2016). Effects of Intensive Blood Pressure Lowering on Cardiovascular and Renal Outcomes: Updated Systematic Review and Meta-Analysis. *Lancet* 387, 435–443. doi:10.1016/S0140-6736(15)00805-3

Xiong, J., Piemontese, M., Thostenson, J. D., Weinstein, R. S., Manolagas, S. C., and O'Brien, C. A. (2014). Osteocyte-derived RANKL Is a Critical Mediator of the Increased Bone Resorption Caused by Dietary Calcium Deficiency. *Bone* 66, 146–154. doi:10.1016/j.bone.2014.06.006

Ye, Z., Lu, H., and Liu, P. (2017). Association between Essential Hypertension and Bone mineral Density: a Systematic Review and Meta-Analysis. *Oncotarget* 8, 68916–68927. doi:10.18632/oncotarget.20325

Yu, H., Shao, H., Yan, J., Tsoukias, N. M., and Zhou, M.-S. (2012). Bone Marrow Transplantation Improves Endothelial Function in Hypertensive Dahl Salt-Sensitive Rats. *J. Am. Soc. Hypertens.* 6, 331–337. doi:10.1016/j.jash.2012.08.003

Zhou, Y., Guan, X., Chen, X., Yu, M., Wang, C., Chen, X., et al. (2017). Angiotensin II/Angiotensin II Receptor Blockade Affects Osteoporosis via the AT1/AT2-Mediated cAMP-dependent PKA Pathway. *Cells Tissues Organs* 204, 25–37. doi:10.1159/000464461

Conflict of Interest: The authors declare that the research was conducted in the absence of any commercial or financial relationships that could be construed as a potential conflict of interest.

Publisher's Note: All claims expressed in this article are solely those of the authors and do not necessarily represent those of their affiliated organizations, or those of the publisher, the editors and the reviewers. Any product that may be evaluated in this article, or claim that may be made by its manufacturer, is not guaranteed or endorsed by the publisher.

frontiers | Frontiers in Cell and Developmental Biology

REVIEW
published: 11 April 2022
doi: 10.3389/fcell.2022.873226

Multinucleated Giant Cells: Current Insights in Phenotype, Biological Activities, and Mechanism of Formation

Kourosh Ahmadzadeh[1*†], *Margot Vanoppen*[1†], *Carlos D. Rose*[2], *Patrick Matthys*[1‡] *and Carine Helena Wouters*[1,3,4*‡]

[1]*Laboratory of Immunobiology, Department Microbiology and Immunology, Rega Institute, KU Leuven – University of Leuven, Leuven, Belgium,* [2]*Division of Pediatric Rheumatology Nemours Children's Hospital, Thomas Jefferson University, Philadelphia, PA, United States,* [3]*Division Pediatric Rheumatology, UZ Leuven, Leuven, Belgium,* [4]*European Reference Network for Rare Immunodeficiency, Autoinflammatory and Autoimmune Diseases (RITA) at University Hospital Leuven, Leuven, Belgium*

Monocytes and macrophages are innate immune cells with diverse functions ranging from phagocytosis of microorganisms to forming a bridge with the adaptive immune system. A lesser-known attribute of macrophages is their ability to fuse with each other to form multinucleated giant cells. Based on their morphology and functional characteristics, there are in general three types of multinucleated giant cells including osteoclasts, foreign body giant cells and Langhans giant cells. Osteoclasts are bone resorbing cells and under physiological conditions they participate in bone remodeling. However, under pathological conditions such as rheumatoid arthritis and osteoporosis, osteoclasts are responsible for bone destruction and bone loss. Foreign body giant cells and Langhans giant cells appear only under pathological conditions. While foreign body giant cells are found in immune reactions against foreign material, including implants, Langhans giant cells are associated with granulomas in infectious and non-infectious diseases. The functionality and fusion mechanism of osteoclasts are being elucidated, however, our knowledge on the functions of foreign body giant cells and Langhans giant cells is limited. In this review, we describe and compare the phenotypic aspects, biological and functional activities of the three types of multinucleated giant cells. Furthermore, we provide an overview of the multinucleation process and highlight key molecules in the different phases of macrophage fusion.

Keywords: multinucleated giant cell (MGC), osteoclast, foreign body giant cell (FBGC), Langhans giant cell (LGC), macrophage, cell fusion, migration, multinucleation

OPEN ACCESS

Edited by:
Yoshihiro Komatsu,
University of Texas Medical School at Houston, United States

Reviewed by:
Teun J. De Vries,
VU Amsterdam, Netherlands
Niroshani Soysa,
University of Peradeniya, Sri Lanka
'Vincent Everts,
VU Amsterdam, Netherlands

***Correspondence:**
Kourosh Ahmadzadeh
kourosh.ahmadzadeh@kuleuven.be
Carine Helena Wouters
carine.wouters@uzleuven.be

†These authors have contributed equally to this work and share first authorship

‡These authors have contributed equally to this work and share last authorship

Specialty section:
This article was submitted to Cell Growth and Division, a section of the journal Frontiers in Cell and Developmental Biology

Received: *10 February 2022*
Accepted: *17 March 2022*
Published: *11 April 2022*

Citation:
Ahmadzadeh K, Vanoppen M, Rose CD, Matthys P and Wouters CH (2022) Multinucleated Giant Cells: Current Insights in Phenotype, Biological Activities, and Mechanism of Formation. Front. Cell Dev. Biol. 10:873226. doi: 10.3389/fcell.2022.873226

INTRODUCTION

Cell-cell fusion is the process in which the outer plasma membranes of two cells merge together forming a new syncytial cell (Pereira et al., 2018). In mammalians, both homotypic and heterotypic cell-cell fusion are crucial to multiple physiological processes (Skokos et al., 2011). It is essential for reproduction through fusion of a sperm cell with an oocyte, resulting in a diploid zygote (Georgadaki et al., 2016), development of the embryo (fusion of cytotrophoblast cells into the syncytiotrophoblast, required for proper functioning of the placenta) (Ma et al., 2020), development of muscle fibers (fusion of myoblasts into myofibrils) (Deng et al., 2017), and tissue repair (e.g. neuronal cell-cell fusion during axonal regeneration) (Giordano-Santini et al., 2016). However, cell-cell fusion may

also contribute to pathological conditions including homotypic cancer cell fusion in which cancer cells fuse with each other or heterotypic cancer cell fusion where cancer cells fuse with other cell types like macrophages, endothelial cells or stem cells (Strick et al., 2007; Xue et al., 2015; Fernandes et al., 2019).

Among all immune cell types, macrophages possess great ability to undergo fusion with themselves and with other cell types (Pereira et al., 2018). Macrophages are innate immune cells that belong to the myeloid cell lineage (Gentek et al., 2014; Varol et al., 2015). For many years, it was thought that all macrophages originate from adult hematopoiesis in bone marrow, giving rise to mature monocytes that circulate in the bloodstream. During inflammation, monocytes extravasate the blood vessels and enter the affected tissue where they differentiate into macrophages (Varol et al., 2015; Wynn and Vannella, 2016). This theory was revised when recent findings showed that many tissue-resident macrophages have an embryonic origin (Epelman et al., 2014; Gentek et al., 2014), developed through embryonic hematopoiesis in the yolk sac (Epelman et al., 2014; Gentek et al., 2014; Wynn and Vannella, 2016). Due to their longevity and capacity for self-renewal, these macrophages can populate various tissues with minimal contribution of monocyte-derived macrophages (Gentek et al., 2014; Varol et al., 2015).

Macrophages are highly versatile and modulate the immunological response from initiation to termination of inflammation and subsequent tissue repair (Shapouri-Moghaddam et al., 2018). To this end, macrophages adapt to the micro-environment and acquire diverse phenotypes with modified functions. Two main subtypes of macrophages are distinguished: classically activated macrophages M1 and alternatively activated macrophages M2 (Martinez et al., 2008; Atri et al., 2018). During T helper type 1 (Th1) immune responses, macrophages polarize towards M1 macrophages, which are pro-inflammatory in nature, characterized by their release of pro-inflammatory mediators (Martinez et al., 2008; Timmermans et al., 2016; Atri et al., 2018; Le and Crouser, 2018; Yunna et al., 2020). Moreover, M1 macrophages are capable of antigen presentation and pathogen clearance (Shapouri-Moghaddam et al., 2018). During Th2 immune responses, macrophages shift towards the M2 phenotype, which are involved in termination of inflammation, tissue homeostasis, and repair (Martinez et al., 2008; Shapouri-Moghaddam et al., 2018; Yunna et al., 2020). The immunomodulatory capacities are accomplished through production of anti-inflammatory mediators and removal of inflammatory triggers, such as pathogens and apoptotic cells, by phagocytosis (Shapouri-Moghaddam et al., 2018; Yunna et al., 2020).

Under certain circumstances, macrophages can fuse resulting in formation of multinucleated giant cells (MGCs) (Pereira et al., 2018). In general, these polykaryons are subdivided into three main subtypes: osteoclasts, foreign body giant cells (FBGCs), and Langhans giant cells (LGCs) (Anderson, 2000). Osteoclasts are found under physiological conditions in bone, where they function as bone resorbing cells (Novack and Teitelbaum, 2008; Drissi and Sanjay, 2016). However, osteoclasts are also involved in the pathogenesis of rheumatoid arthritis (RA) and osteoporosis, indicating that proper osteoclast regulation is

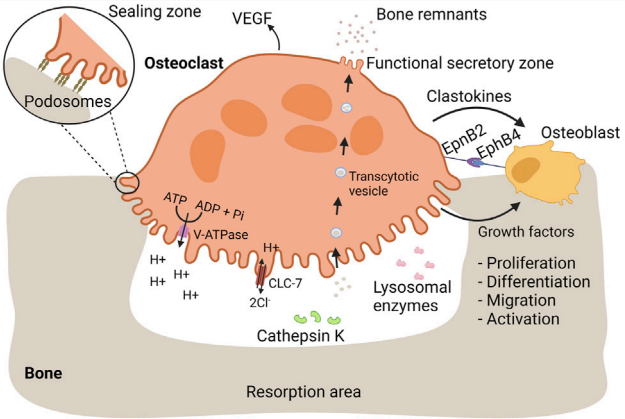

FIGURE 1 | Osteoclasts mediate bone resorption and proper bone replacement by osteoblasts. Bone is a dynamic tissue that is remodeled by interplay of bone-resorbing osteoclasts and bone-generating osteoblasts. During bone resorption, osteoclasts firmly adhere to bone mediated by podosomes. Each podosome is composed of a central core of a dense F-actin network and actin polymerization activators. The core is surrounded by a loose F-actin network interspersed with regulatory proteins and adaptor proteins linking the podosome structure with integrins, referred as the podosome cloud. Podosomes are organized in an extensive circular pattern, the sealing zone, isolating an extracellular compartment in which bone resorbing substances are released. Bone-resorbing osteoclasts are characterized by a ruffled border, essential for bone resorption. The ruffled border is enriched with V-ATPase proton pumps, pumping hydrogen protons into the resorption lacunae, required for dissolution of bone minerals. During proton secretion, electroneutrality is maintained by release of chloride ions through CLC-7. Lysosomal enzymes, including cathepsin K, are released at the ruffled border and mediate the degradation of bone proteins, such as collagen I. Bone remnants are taken up in transcytotic vesicles and transported across the osteoclast cytoplasm towards the functional secretory zone where they are released. In order to ensure proper bone replacement, osteoclasts stimulate bone formation by osteoblasts. During bone resorption, osteoblastic growth factors are released from the bone matrix. Additionally, osteoclasts secrete clastokines, soluble factors that support osteoblast proliferation, differentiation, migration, activity, and survival. EpnB2 is expressed on osteoclast and is a transmembrane protein that stimulates osteoblast differentiation through interaction with EphB4 on osteoblasts. Vasculogenesis is stimulated through the release of VEGF.

crucial to prevent pathological conditions (Drissi and Sanjay, 2016). By contrast to osteoclasts, FBGCs and LGCs are exclusively found under pathological conditions. FBGCs are formed during inflammatory reactions against foreign material, including implants and protheses (McNally and Anderson, 2002; Jay et al., 2007). LGCs are part of granulomas, which are focal clusters of immune cells (Zumla and James, 1996), in both infectious and non-infectious diseases (Wang et al., 2020).

Although MGCs have been described over 150 years ago (Mizuno et al., 2001; Pagán and Ramakrishnan, 2018), our understanding of these cells, except from osteoclasts, has not been further improved. Whereas osteoclasts are well-characterized, little knowledge is available on the phenotype and functionality of FBGCs and LGCs. In this respect, it is worth mentioning that in literature, FBGCs and LGCs are often seen or regarded as one cell type, making it difficult to obtain good understanding of their characteristics and biological

activities. Furthermore, the macrophage fusion process remains poorly understood, especially for LGCs. In the first part of this review, we focus on the phenotypic characteristics of distinct MGC subtypes and on the current knowledge of MGC function and biological activity. In the second part, we provide an overview of the mechanisms of MGC formation with a focus on the key players in the different fusion steps. Finally, a general conclusion is drawn and remaining questions are discussed.

OSTEOCLAST PHENOTYPE, FUNCTIONS, AND BIOLOGICAL ACTIVITIES

Osteoclasts are well-known as bone resorbing cells contributing to skeletal remodeling and homeostasis throughout life (Novack and Teitelbaum, 2008; Drissi and Sanjay, 2016). During active bone resorption, osteoclasts are characterized by a ruffled border facing the bone surface and the nuclei are located close to the apical membrane, opposite to the ruffled border (Novack and Teitelbaum, 2008; Brooks et al., 2019). Today, increasing evidence is found that osteoclasts act in multiple processes beyond bone resorption. In the next sections, we will focus on the contribution of osteoclasts in bone resorption, promotion of bone formation, vasculogenesis, and immune regulation.

Bone Resorption

Bone is a dynamic tissue consisting of an organic phase, which is predominantly type I collagen, and an inorganic phase, mainly composed of minerals in the form of hydroxyapatite (Buck and Dumanian, 2012). Throughout life, bone is remodeled by interplay of bone resorbing osteoclasts and osteoblasts generating new bone tissue (Chiu et al., 2012; Chen et al., 2018). Osteoclasts are equipped with a specialized bone-resorbing mechanism, resulting in external degradation of bone tissue and subsequent uptake of bone remnants for further processing (Mulari et al., 2003; Cappariello et al., 2014). An overview of the osteoclastic bone resorption process is depicted in **Figure 1**.

Extracellular Bone Degradation

During bone resorption, osteoclasts firmly adhere to bone tissue which is mediated by specialized actin-based membrane extensions, called podosomes (Touaitahuata et al., 2013). Each podosome is composed of a central core of a dense F-actin network and actin polymerization activators (Jurdic et al., 2006). The core is surrounded by a loose F-actin network interspersed with regulatory proteins and adaptor proteins linking the podosome structure with integrins, referred as the podosome cloud (Jurdic et al., 2006; Georgess et al., 2014). At the onset of bone resorption, podosomes are organized into an extensive circular pattern: the sealing zone (Georgess et al., 2014), which is of great importance and essential for bone resorption (Jurdic et al., 2006). It defines an isolated extracellular compartment, the resorption lacunae, where bone tissue is degraded (Helming and Gordon, 2009). Therefore, the resorption lacunae could be seen as an extracellular lysosome, able to destroy bone matrix (Vignery, 2005a; Helming and Gordon, 2009). Since bone is too large to internalize, the formation of this extracellular lysosome is a crucial step in bone resorption (Cappariello et al., 2014).

Active bone-resorbing osteoclasts are characterized by a ruffled border facing the bone surface (Novack and Teitelbaum, 2008; Brooks et al., 2019). By contrast, LGCs and FBGCs do not have a ruffled border and are not considered to resorb bone, illustrating the importance of the ruffled border in bone resorption. This border originates from fusion of lysosomes or storage of granule-like structures with the plasma membrane, enabling the insertion of lysosomal membrane proteins into the plasma membrane and the release of lysosomal enzymes into the resorption lacunae (Stenbeck, 2002; Na et al., 2020).

Resorption of the Inorganic Bone Fraction

Resorption of the mineral bone phase is mediated by vacuolar (V)-ATPase proton pump, a lysosomal protein inserted into the ruffled border during bone resorption (Stenbeck, 2002). V-ATPase mediates the release of hydrogen protons in the resorption lacunae, leading to the dissolution of bone minerals (Väänänen et al., 1990; Supanchart and Kornak, 2008). During proton secretion, electroneutrality is maintained by chloride channel 7 (ClC-7) as it allows the release of chloride ions into the extracellular environment (Sørensen et al., 2007). Pharmacological inhibition of V-ATPase diminishes the acidification of the resorption lacunae and bone resorption (Woo et al., 1996; Karsdal et al., 2005; Sørensen et al., 2007), illustrating the importance of V-ATPase in bone degradation. Additionally, patients with mutations in osteoclastic V-ATPase a3 subunit or in ClC-7, suffer from osteopetrosis, a condition characterized by increased bone density, due to impaired acidification and bone resorption (Karsdal et al., 2005, 2007).

Resorption of the Organic Bone Fraction

Once the mineral fraction is resolved, osteoclasts switch their degrading capacities towards the organic bone phase (Blair et al., 1986). In order to break down bone proteins, osteoclasts release several lysosomal enzymes, such as proteases, acid phosphatases and hydrolases (Na et al., 2020).

Cathepsin K. Cathepsin K is a cysteine protease able to cleave collagen type I, the most abundant protein in bone (Zaidi et al., 2001; Kiesel et al., 2009; Gradin et al., 2012; Drake et al., 2017). A major role for cathepsin K in breakdown of bone matrix proteins has been illustrated by multiple findings. In activated osteoclasts, cathepsin K is highly enriched at the ruffled border (Zaidi et al., 2001). In addition, absence of cathepsin K in humans leads to pycnodysostosis, a heritable disease characterized by osteopetrosis and a short stature (Gelb et al., 1996; Zaidi et al., 2001; Drake et al., 2017). Likewise, cathepsin K knock-out (KO) mice develop osteopetrosis (Saftig et al., 1998; Zaidi et al., 2001). Finally, pharmacological inhibition of cathepsin K reduces extensive bone resorption and can be used as a treatment of osteoporosis (Novinec and Lenarčič, 2013).

Matrix Metalloproteases. Matrix metalloproteases (MMPs) have been implicated in the resorption process as well (Stenbeck, 2002). This notion is supported by the localization of MMP1, MMP9 and MT1-MMP in the ruffled border. However, bone resorption by osteoclasts derived from MMP9 or MT1-MMP KO mice is not abrogated, suggesting that these MMPs are not crucial for osteoclast activity. It is worth noting that the involvement of MMPs in bone resorption depends on the anatomical location of osteoclasts (Everts et al., 1999, 2006). Everts et al. reported that MMP inhibitors affect bone-resorbing activity of cranial osteoclasts, whereas the bone-degrading capacities of long bone osteoclasts remain unaltered (Everts et al., 1999). By contrast, in conditions of suppressed cathepsin K expression, MMP inhibitors further deteriorate the bone resorption activity of long bone osteoclast, indicating that MMPs may partly compensate for cathepsin K deficiency (Everts et al., 2006).

Tartrate Resistant Acid Phosphatase. Tartrate Resistant Acid Phosphatase (TRAP) is a non-specific phosphatase (Fleckenstein and Drexler, 1997) that is extensively expressed in osteoclasts (Kirstein et al., 2006). TRAP secretion is positively correlated with bone resorption (Kirstein et al., 2006; Hayman, 2008) and serum level of TRAP is often used as a biomarker for bone resorption (Kirstein et al., 2006; Mira-Pascual et al., 2020). Mice lacking TRAP display mild osteopetrosis and *in vitro* bone resorption is impaired in osteoclasts derived from these mice (Hayman et al., 1996; Hayman, 2008). Additionally, transgenic mice overexpressing TRAP show mild osteoporosis, further pointing towards a role for TRAP in bone resorption (Angel et al., 2000). TRAP has been detected in transcytotic vesicles (Mira-Pascual et al., 2020), referring to vesicles that originate from endocytosis of bone degradation products by osteoclasts (Madel et al., 2019). Within these vesicles, TRAP contributes to the degradation bone remnants by catalyzing the production of reactive oxygen species (ROS) that in turn damages the internalized bone proteins (Halleen et al., 1999; Halleen et al., 2003).

Intracellular Degradation

As mentioned before, osteoclasts are able to internalize bone remnants for intracellular degradation (Stenbeck, 2002; Mulari et al., 2003; Madel et al., 2019). Lysosomal enzymes are secreted at the periphery of the ruffled border, whereas uptake of degradation products takes place at the center (Mulari et al., 2003). The internalization is coordinated by the regular clathrin-mediated endocytosis machinery (Mulari et al., 2003) and results in the formation of intracellular vesicles filled with bone remnants: transcytotic vesicles (Madel et al., 2019). By transcytotic trafficking, vesicles are transported to the functional secretory zone (i.e., the membrane in opposite of the ruffled border) where the content is released into the extracellular environment.

Promotion of Bone Formation

A tight regulation between osteoclast and osteoblast activity is crucial to maintain healthy bone tissue over time (Chen et al., 2018). Hyperactivation of osteoclasts leads to a condition characterized by low bone density and an increased risk of fractures, called osteoporosis (Armas and Recker, 2012), whereas osteoclast insufficiency may induce osteopetrosis (Stark and Savarirayan, 2009). In order to keep the right balance between bone resorption and formation, osteoclasts and osteoblasts mediate each other's activity (Chen et al., 2018). Whereas osteoblasts modulate osteoclast differentiation and function, several osteoclastic mechanisms regulate osteoblast differentiation (Matsuo and Irie, 2008; Teti, 2013; Chen et al., 2018).

The bone matrix forms a reservoir for several growth factors, including transforming growth factor (TGF)-β, insulin like growth factor (IGF)-I, and bone morphogenic proteins (BMPs) (Matsuo and Irie, 2008; Teti, 2013). During bone resorption, these factors are released from the bone matrix and become activated through the acidic pH and/or enzymatic cleavage within the resorption lacunae (Teti, 2013). The activated growth factors in turn enhance osteoblastic bone formation, guaranteeing proper replacement of old bone tissue (Matsuo and Irie, 2008).

Clastokines

Osteoclasts also stimulate bone formation directly through the release of various soluble osteogenic factors, called clastokines (Lotinun et al., 2013). Amongst others, sphingosine-1 phosphate (SP-1 P), BMP6, TRAP, platelet-derived growth factor (PDGF), and hepatocyte growth factor (HGF) are well-described clastokines (DiGiovanni et al., 2012; Teti, 2013; Cappariello et al., 2014). SP-1 P is a signaling sphingolipid that enhances bone regeneration through multiple mechanisms (Higashi et al., 2016; Meshcheryakova et al., 2017). SP-1 P recruits osteoblast precursors (Meshcheryakova et al., 2017), promotes osteoblast proliferation, differentiation, activity, and survival (Higashi et al., 2016; Meshcheryakova et al., 2017). BMP6 induces osteoblast differentiation (Demirtaş et al., 2016) and bone mineralization (Luo et al., 2011; Zhu et al., 2012). In addition to its role in bone resorption, TRAP acts as a clastokine by facilitating osteoblast proliferation and differentiation (Gradin et al., 2012). PDGF acts as a chemotactic and mitogenic factor for osteoblasts (DiGiovanni et al., 2012), whereas HGF facilitates osteoblast proliferation and differentiation (Hossain et al., 2005; Frisch et al., 2016). Together, these factors facilitate the migration of osteoblast precursors, osteoblast proliferation, differentiation, and/or activity (Gradin et al., 2012; Cappariello et al., 2014).

Osteoclasts also promote bone formation through direct cell contact with osteoblasts, mediated by members of the Eph receptor family and their ephrin ligands (Zhao et al., 2006; Edwards and Mundy, 2008; Matsuo and Otaki, 2012; Tamma and Zallone, 2012). Eph receptors are tyrosine kinase receptors that are involved in multiple biological processes, including neuronal development (Kania and Klein, 2016). Interaction between Eph receptors and ephrin ligands results into bi-directional signaling, meaning that signaling pathways are activated in both receptor-expressing and ligand-expressing cells (Edwards and Mundy, 2008; Kania and Klein, 2016). Signal transduction from ephrin ligands to Eph receptors is

referred as forward signaling, whereas reverse signaling points to signal transduction from Eph receptors to ephrin ligands (Kania and Klein, 2016). Several reports indicate that ephrinB2 ligand and EphB4 receptor are involved in osteoclast-osteoblast intercommunication (Zhao et al., 2006; Edwards and Mundy, 2008; Matsuo and Otaki, 2012; Tamma and Zallone, 2012). Differentiating and mature osteoclasts express ephrinB2, whereas osteoblasts express EphB4 (Zhao et al., 2006; Edwards and Mundy, 2008; Matsuo and Otaki, 2012). Forward signaling stimulates osteoblast differentiation (Zhao et al., 2006; Edwards and Mundy, 2008; Matsuo and Otaki, 2012), facilitating the formation of new bone tissue, whereas reverse signaling inhibits osteoclast maturation (Zhao et al., 2006). The combined action of both signaling cascades ensures efficient bone replacement by mediating simultaneously cessation of bone resorption and generation of new bone tissue (Edwards and Mundy, 2008).

Vasculogenesis

Mounting evidence is emerging that osteoclasts and their precursors stimulate angiogenesis (Kiesel et al., 2007; Drissi and Sanjay, 2016; Han et al., 2018). It has been observed that bone vascularization and ossification is disturbed in the absence of osteoclasts (Matsuo and Otaki, 2012). Vascularization is important during bone development for the migration of bone cells involved in degradation of cartilage and subsequent bone deposition (Tombran-Tink and Barnstable, 2004). Furthermore, bone remodeling and repair depend on well-developed vascular networks (Grosso et al., 2017) to provide bone tissue with oxygen and nutrients (Kiesel et al., 2007; Grosso et al., 2017), to remove bone remnants (e.g. calcium and phosphate ions) (Kiesel et al., 2007; Grosso et al., 2017), and to recruit hematopoietic stem cells, bone cells and immune cells (Grosso et al., 2017). Various pro-angiogenic factors such as endothelial growth factor and PDGF isoform BB are upregulated during osteoclastogenesis (Kiesel et al., 2007), with some remaining expressed in mature osteoclasts (Tombran-Tink and Barnstable, 2004). Vascular endothelial growth factor (VEGF) (Tombran-Tink and Barnstable, 2004; Kiesel et al., 2007; Grosso et al., 2017), a key regulator of angiogenesis (Grosso et al., 2017), induces migration, proliferation, and survival of endothelial cells (Grosso et al., 2017; Han et al., 2018), whereas PDGF isoform BB (PDGF-BB) (Xie et al., 2014; Gao et al., 2017) promotes the recruitment of endothelial progenitor cells (Xie et al., 2014; Gao et al., 2017; Han et al., 2018) and their differentiation into mature endothelial cells (Gao et al., 2017). The pro-angiogenic action of PDGF-BB probably involves the induction of VEGF in endothelial progenitor cells (Gao et al., 2017), which in turn stimulates vessel formation. Furthermore, ephrinB2 regulates VEGF-induced endothelial cell migration and angiogenesis (Sawamiphak et al., 2010; Wang et al., 2010). Since osteoclasts express ephrinB2, it is tempting to hypothesize that osteoclasts also mediate angiogenesis through ephrin2B (Matsuo and Otaki, 2012). Next to direct stimulation of vessel formation, osteoclasts establish the required space for blood vessels to grow (through bone-resorption) (Grüneboom et al., 2019). To provide bone marrow of sufficient oxygen, nutrients and to establish efficient emigration of newly generated blood cells from the bone marrow to the external circulation, a well-established vascular network is indispensable. Therefore, a multitude of trans-cortical vessels cross the bone shaft in order to connect the bone marrow with the external circulation. The transcortical vessels require small channels through or small channels in the bone tissue, which are maintained by osteoclasts.

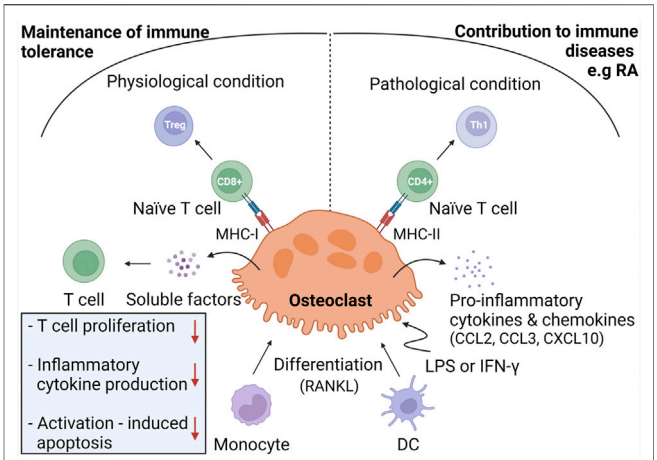

FIGURE 2 | Immunoregulation by osteoclasts. Under physiological conditions, osteoclasts are considered to be derived from monocyte progenitor cells and exhibit immunomodulatory activities in order to maintain immune tolerance to bone remnants. To do so, osteoclasts induce Treg cells through antigen presentation in MHC-I complexes towards $CD8^+$ T cells. Osteoclasts inhibit T cell proliferation, production of inflammatory cytokines, and activation-induced apoptosis through release of soluble mediators. Under inflammatory conditions, osteoclasts are hypothesized to derive from DC and to contribute to immune diseases, including RA. In response to LPS or IFN-γ, osteoclasts produce pro-inflammatory mediators and differentiate naïve T cells into Th1 cells through antigen presentation in MHC-II molecules.

Immunomodulation

It has been established that bone and the immune system are interconnected (Okamoto and Takayanagi, 2019). Hematopoietic stem cells and immune cell precursors originate from bone marrow (Okamoto and Takayanagi, 2019; Guder et al., 2020). Several signaling molecules, including cytokines, receptors, and transcription factors, are shared between the skeletal and immune system (Okamoto and Takayanagi, 2019). Also, many auto-immune and inflammatory disorders are characterized by bone destruction, including RA and Crohn's disease (Veauthier and Hornecker, 2018; Madel et al., 2019; Ashai and Harvey, 2020). At last, a spectrum of bone alterations has been described in several genetically defined autoimmune conditions, caused by mutations in innate immune components (Bader-Meunier et al., 2018).

It has been demonstrated that immune cells mediate osteoclast differentiation and activity. For example, T cells are able to promote osteoclastogenesis through the expression of RANKL (Kiesel et al., 2009; Grassi et al., 2011; Shashkova et al., 2016). Osteoclasts can be differentiated from monocytes, macrophages, or dendritic cells (DCs) (Speziani et al., 2007; Nishida et al., 2018;

Lou et al., 2019; Wu et al., 2019; Narisawa et al., 2021). Since these osteoclast precursors are well-known for their immunological activities, it would not be surprising that osteoclasts may participate in immunological processes as well. Recently, accumulating evidence has shown that osteoclasts indeed perform immunological tasks, including phagocytosis, antigen presentation, and T cell activation (Li et al., 2010; Meng et al., 2010). The role of osteoclasts within the immune system is depicted in **Figure 2**.

Phagocytosis

Phagocytosis is the internalization of particles larger than 0.5 μm (Hirayama et al., 2001) in size by plasma membrane-derived vesicles (Rosales and Uribe-Querol, 2017). Professional phagocytes, including macrophages and DCs, internalize foreign particles for degradation purposes or in advance of antigen preparation and presentation (Madel et al., 2019). Osteoclasts engulf bone remnants for the purpose of bone degradation through clathrin-mediated endocytosis (Mulari et al., 2003). Other than bone remnants, osteoclasts have been reported to internalize many other particles through phagocytosis, including latex, polymethylmethacrylate, and titanium (Wang et al., 1997; Meng et al., 2010; Madel et al., 2019). Whether phagocytosis of particles other than bone remnants influences bone resorption remains unclear as conflicting results have been reported (Wang et al., 1997; Meng et al., 2010). Wang et al. showed that osteoclasts still exert bone resorption after they have internalized latex or polymethylmethacrylate particles, whereas Meng et al. suggested that bone resorption decreases upon phagocytosis of titanium particles (Meng et al., 2010). Moreover, several reports indicate that osteoclasts are able to phagocytose apoptotic cells (Taniwaki and Katchburian, 1998; Bronckers et al., 2000; Boabaid et al., 2001; Cerri et al., 2003; Harre et al., 2012). Apoptosis is a sterile form of programmed cell death, such that it does not elicit an inflammatory response (Xu et al., 2019). During apoptosis, various molecules are exposed to the cell surface that label the cell as being apoptotic (Savill, 1997). These molecules are recognized by phagocytic receptors on phagocytes followed by the internalization of the apoptotic cell (Savill, 1997). Macrophages and DCs are well-equipped to clear apoptotic cells through phagocytosis (Harre et al., 2012). Moreover, Harre et al. reported that osteoclasts express multiple proteins that are involved in the engulfment of apoptotic cells, to a similar or even higher extend than macrophages and DCs (Harre et al., 2012). This is reflected by the high phagocytic capacity of osteoclasts for murine apoptotic thymocytes *in vitro*. In contrast to macrophages, osteoclasts internalized the cells independently from serum, indicating that they do not use opsonization or that they make the opsins themselves. *In vivo* evidence has also been provided that osteoclasts perform phagocytosis under physiological conditions (Taniwaki and Katchburian, 1998; Bronckers et al., 2000; Boabaid et al., 2001; Cerri et al., 2003). Osteoclasts are able to engulf apoptotic bone cells, including chondrocytes, osteocytes, and osteoblasts (Taniwaki and Katchburian, 1998; Bronckers et al., 2000; Boabaid et al., 2001; Cerri et al., 2003). Osteocytes and chondrocytes are tightly surrounded by bone and cartilage matrices respectively, making them difficult to reach by classical phagocytes, such as macrophages (Harre et al., 2012). Therefore, osteoclasts are crucial to remove dying bone cells to prevent chronic inflammation or autoimmunity. Not only the accessibility renders osteoclasts more suitable for clearance of dying bone cells, also the fact that they do not rely on serum-derived opsins is important since bone tissue is poorly vascularized.

Antigen Presentation and T Cell Activation

Growing evidence indicates that osteoclasts interact with T cells. In bone marrow, T cells are in close proximity to osteoclasts (Grassi et al., 2011), suggesting that osteoclasts attract T cells. This hypothesis is supported by the finding that osteoclasts secrete T cell-attracting chemokines, including CC chemokine ligand (CCL)2, CCL3, and CXCL10 (Kiesel et al., 2009; Grassi et al., 2011). Adhesion assays showed that osteoclasts are able to recruit and retain T cells (Grassi et al., 2011). Next to mediating chemotaxis, osteoclasts can also regulate T cell activity and differentiation. In order to become activated, naïve T cells need to be primed with antigens presented on the surface of antigen presenting cells (APCs) (Sprent, 2005). Several reports demonstrated that osteoclasts can act as APCs. Indeed, osteoclasts cross present exogenous antigens in MHC-I molecules to $CD8^+$ T cells (Buchwald et al., 2013; Le Goff et al., 2013). Characterization of these $CD8^+$ T cells revealed that osteoclasts induce a regulatory T cell (Treg) phenotype, thereby inducing an immune modulatory effect (Buchwald et al., 2013; Le Goff et al., 2013; Shashkova et al., 2016). In addition, osteoclasts have been reported to present antigens in MHC-II molecules to $CD4^+$ T cells, which in turn differentiate into Th1 cells (Le Goff et al., 2013; Ibáñez et al., 2016) (**Figure 2**).

It should be noted that not all studies that have examined the APC function of osteoclasts reached the same conclusion. Kiesel et al. reported that osteoclasts cannot present antigens to $CD4^+$ T cells since they do not express MHC-II molecules (Kiesel et al., 2009). By contrast, other reports demonstrated that osteoclasts do express MHC-II molecules (Li et al., 2010, 2014; Le Goff et al., 2013; Ibáñez et al., 2016) and that they are able to present antigens to $CD4^+$ T cells (Li et al., 2010, 2014; Le Goff et al., 2013). Furthermore, conflicting results about the expression of co-stimulatory molecules have been reported (Kiesel et al., 2009; Li et al., 2010, 2014; Ibáñez et al., 2016). Kiesel et al. reported that osteoclasts only express CD80 but not CD86 (Kiesel et al., 2009), whereas other groups found that osteoclasts express both molecules (Li et al., 2010, 2014; Ibáñez et al., 2016). These discrepancies could be explained by the immune environment in which osteoclast-T cell interactions take place (Le Goff et al., 2013; Ibáñez et al., 2016). Under physiological conditions, osteoclasts exhibit an immune-modulatory phenotype, characterized by the secretion of anti-inflammatory cytokines, such as IL-10 (Ibáñez et al., 2016). These osteoclasts induce Tregs by antigen cross presentation to $CD8^+$ T cells (Buchwald et al., 2013; Le Goff et al., 2013; Shashkova et al., 2016). Additionally, they secrete soluble factors that inhibit T cell proliferation, inflammatory cytokine production, and activation-induced

apoptosis of T cells (Grassi et al., 2011). It is assumed that these immunomodulatory functions of osteoclasts are crucial to maintain immune tolerance to bone remnants in order to prevent autoinflammation (Ibáñez et al., 2016). Conversely, under inflammatory conditions, osteoclasts may exacerbate the ongoing inflammation. Upon stimulation with LPS or IFN-γ, MHC-II expression is upregulated in osteoclasts (Grassi et al., 2011; Le Goff et al., 2013), which leads to increased Th1 cell induction. Furthermore, osteoclasts merely produce pro-inflammatory cytokines (TNF-α, IL-1β, IL-6 and IL-23) and chemokines (CCL2, CCL5 and CCL7) in an inflammatory environment (Ibáñez et al., 2016).

The differences in osteoclast activity might be also explained by the different origin of osteoclasts in various milieus (Ibáñez et al., 2016). Under physiological conditions, osteoclasts are considered to be derived from monocytes, whereas under inflammatory conditions they may originate from immature DCs. Therefore, the inflammatory osteoclast can be seen as an intermediate between the monocyte-derived osteoclast and the DC and probably plays a role in many immune diseases, including RA (Narisawa et al., 2021).

Osteoclasts may also indirectly regulate the activity of immune cells (van Niekerk et al., 2018). Bone tissue forms a reservoir for calcium, phosphate and magnesium ions, which are released during bone resorption. These ions are crucial for many immune related processes, such as immune cell proliferation, chemotaxis, and signaling.

Taken together, osteoclasts exert multiple functions within the human body of which bone resorption is the best recognized (Drissi and Sanjay, 2016). Throughout the last decades, increasing evidence was found that osteoclasts cannot longer be regarded as solely bone-resorbing cells and that they contribute to multiple processes, including osteoblast stimulation, vasculogenesis and immune regulation (Le Goff et al., 2013; Cappariello et al., 2014; Drissi and Sanjay, 2016). Compared to osteoclasts, the functionality of FBGCs and LGCs is less well established, and will be discussed in the next two sections.

FOREIGN BODY GIANT CELL PHENOTYPE, FUNCTIONS, AND BIOLOGICAL ACTIVITIES

Among all MGC subtypes, FBGCs are the largest reaching up to 1 mm in size (Wang et al., 2020). They have an irregular shape and contain hundreds of nuclei, scattered throughout the cytoplasm (Anderson, 2000; Quinn and Schepetkin, 2009; Lemaire et al., 2012; Sakai et al., 2012; Wang et al., 2020). FBGCs are formed in foreign body reactions (FBRs), which are chronic inflammatory reactions against non-infectious foreign body material, including implants, protheses, and medical devices (McNally and Anderson, 2002; Anderson et al., 2008). FBRs involve a series of events that eventually leads to the formation of FBGCs and fibrotic encapsulation of the foreign body (Anderson et al., 2008; Sheikh et al., 2015). Upon implantation of biomaterial, host tissue is injured resulting into blood-material interactions. These interactions involve the adsorption of host proteins onto the surface of the biomaterial and thrombus formation at the tissue-material interface (Anderson et al., 2008). The deposited cloth of proteins is referred as the provisional matrix, which plays an important role in shaping the subsequent immunological reactions (Sheikh et al., 2015). The provisional matrix forms a docking site for immune cells and contains several bioactive agents, such as mitogens, cytokines, and chemokines, supporting chemotaxis, proliferation, and activation of immune cells. Among the recruited cell types, macrophages are prominent in shaping the FBR through production of immunological mediators (Anderson et al., 2008) and through their fusogenic capacity to form FBGCs over time in the presence of a conditioned cytokine milieu (**Figure 3**).

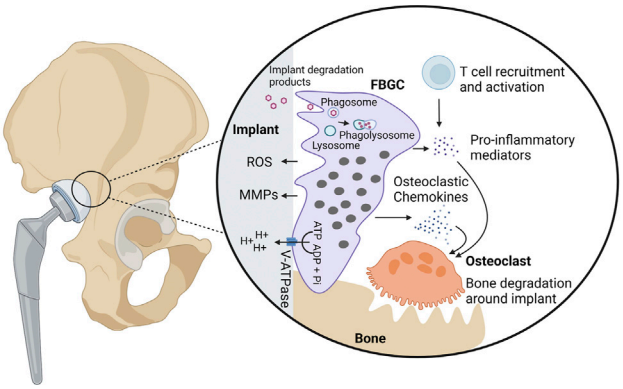

FIGURE 3 | Biological activities of foreign body giant cells. FBGCs are formed on the surface of foreign bodies, including implants and protheses, and are thought to contribute to the degradation of foreign particles through phagocytosis or secretion of ROS, MMPs, and hydrogen protons. In case of bone implants, FBGCs are hypothesized to contribute to aseptic loosening, bone destruction around the implant. Hydrogen protons released from FBGCs dissolve bone minerals in proximity to the implant. Additionally, FBGCs recruit and activate osteoclasts through secretion of chemokines and pro-inflammatory cytokines. Finally, FBGCs are thought to recruit and activate T cells, which in turn produce osteoclast-stimulating mediators.

Particle Degradation

It is assumed that FBGCs arise when individual macrophages are unable to remove foreign particles (Jay et al., 2010). In such conditions, macrophages fuse together in expectation that the bigger cell size and excess plasma membrane (Whitlock and Chernomordik, 2021) enable them to remove the threat (Han et al., 2000; Vignery, 2000; Milde et al., 2015).

Intracellular Degradation

One possible mechanism by which FBGCs may destroy their substrate is phagocytosis and intracellular degradation (Lee et al., 1981; Milde et al., 2015). Several researchers demonstrated that FBGCs are able to engulf particles that single macrophages cannot (Moreno et al., 2007; Milde et al., 2015). Milde et al. showed that FBGCs are more efficient in phagocytosing beads of 20 μm compared to macrophages and that beads of 45 μm are exclusively taken up by FBGCs (Milde et al., 2015). In addition,

Moreno et al. showed that fusion of macrophages into FBGCs is crucial to be able to phagocytose 25 μm beads while IL-4 stimulated macrophages failed to phagocytose these beads. (Moreno et al., 2007). Inhalation experiments in rats, hamsters and guinea pigs provided *in vivo* evidence that alveolar macrophages preferably internalize small dust fibers (i.e. particles smaller than 5 μm in size), whereas particles larger than 10 μm are phagocytosed by FBGCs (Lee et al., 1981).

Protein adsorption on biomaterial surfaces plays probably an important role in the phagocytic properties of FBGCs. Milde et al. found that FBGCs are highly phagocytic for complement-opsonized particles (Milde et al., 2015). Indeed, the excessive phagocytic capacity was diminished when medium was depleted of complement component 3 (C3) or when FBGCs did not express the complement receptor 3 subunit CD11b. Complement-mediated phagocytosis is very efficient in FBGCs since the complement receptor 3 (CR3) localizes into membrane rumples, which provide excess cellular membrane to engulf large particles. Complement opsonization may be of great importance in phagocytosis of foreign bodies, such as polymer or metal particles, that do not have any ligands for phagocytic receptors. Since the nature of the biomaterial highly influences protein adsorption (Anderson et al., 2008), it can be speculated that it also interferes with the phagocytic capacity of FBGCs. Further research is required to investigate whether other phagocytic receptors are involved in the internalization of foreign bodies and whether the contribution of the receptors is altered by the nature of the biomaterial.

Extracellular Degradation

Next to phagocytosis, FBGCs destroy foreign bodies through the secretion of ROS and matrix metalloproteases (MMPs) (Jones et al., 2007). Release of these deleterious substances was found to lead to the failure of medical implants (Anderson et al., 2008), stressing the need for the development of resistant biomaterials (Ebert et al., 2005). Microscopic analyses revealed that FBGCs firmly adhere to their substrate thereby creating an isolated extracellular environment between the FBGC plasma membrane and the particle surface, called the sealing zone (ten Harkel et al., 2015; ten Harkel et al., 2016). The sealing zone can be regarded as an extracellular lysosome in which harmful substances are released in order to degrade the biomaterial (Vignery, 2005a). Evidence has been provided that FBGCs degrade collagen, which is often used as biomaterial for medical devices (van Wachem et al., 1991; Ye et al., 2011; ten Harkel et al., 2016). At sites where FBGCs are in close proximity to collagen bundles, the collagen structure loosens and fibrils look thinner, pointing to extracellular degradation (ten Harkel et al., 2016). FBGCs are also able to break down gelatin (i.e. denatured collagen) (Ye et al., 2011). The degradation of collagen and gelatin both rely on MMP13, an active collagenase and gelatinase. Furthermore, collagen and gelatin can be phagocytosed, suggesting that they undergo additional intracellular degradation.

Whether FBGCs preferably degrade their substrate internally (i.e. through phagocytosis) or externally (i.e. through secretion of ROS and MMPs) depends on the size of the particle (Sheikh et al., 2015). Existing data suggest that FBGCs efficiently phagocytose particles up to 100 μm in diameter. Though the phagocytic efficiency decreases with increased particle size and if needed, FBGCs could switch to external degradation.

Aseptic Loosening

Peri-implant bone loss, referred as aseptic loosening, is often observed after implantation of biomaterials (Wang et al., 1997; Meng et al., 2010) and is considered as a main cause of implant failure (Wooley and Schwarz, 2004). After implantation, microparticles are often released from the bone implant and elicit a chronic inflammatory response (Gu et al., 2012; Goodman and Gallo, 2019). In case of a bone-anchored prothesis, the inflammatory reaction stimulates osteoclastogenesis and activity, thereby facilitating bone destruction around the implant (Wooley and Schwarz, 2004; Gu et al., 2012; Goodman and Gallo, 2019). In addition to osteoclasts, FBGCs are hypothesized to contribute to aseptic loosening by massive excess of hydrogen protons (ten Harkel et al., 2015). FBGCs, like osteoclasts, highly express the vacuolar V-ATPase proton pump which enables them to secrete massive amounts of hydrogen protons. Whether the release of protons by FBGCs contributes to bone destruction around implants *in vivo* needs to be elucidated. Apart from the possibility to dissolve bone minerals, FBGCs are suspected to promote aseptic loosening by stimulation of bone degradation by osteoclasts. FBGCs produce various osteoclastic chemokines, including CCL2, CCL3, and CCL9, which together promote osteoclast formation and survival (Khan et al., 2014).

Shaping of the Foreign Body Reaction

FBGCs may contribute to the establishment and maintenance of foreign body reactions through the production of many inflammatory mediators. It has been reported that FBGCs express CCL2, CCL3, and CCL5, which are very potent macrophage chemoattractants (Khan et al., 2014). Next to macrophage attraction, FBGCs regulate the FBR through interaction with T cells (Chang et al., 2009). During FBRs, newly recruited T cells attach to macrophages and FBGCs than to the surface of the foreign particle. After docking, the recruited T cells become activated which may be mediated by FBGCs as they express several cytokines and inflammatory surface molecules, including MHC molecules. Depending on the nature of the biomaterial, FBGCs express a different repertoire or concentrations of inflammatory factors (Jones et al., 2007). Therefore, the FBR slightly differs between distinct biomaterials. For example, cells present on hydrophobic biomaterial produce small amounts of IL-1β and IL-6, whereas the production of these cytokines is enhanced on hydrophilic surfaces. The secretion of cytokines and chemokines is also time-dependent since FBGCs undergo a phenotypic switch (Hernandez-Pando et al., 2000; Jones et al., 2007). Initially, FBGCs merely produce pro-inflammatory cytokines, thereby stimulating inflammation. Later on, pro-inflammatory mediators are downregulated and the expression of anti-inflammatory cytokines increases (Jones et al., 2007). These phenotypic changes have been described in mice that were subcutaneously injected with nitrocellulose particles (Hernandez-Pando et al., 2000). Within the first 4 weeks,

FBGCs produced high amounts of IL-1 and tumor necrosis factor (TNF)-α, two major cytokines involved in the recruitment and activation of immune cells. After 2 months, the inflammatory profile of FBGCs switched towards an anti-inflammatory phenotype, characterized by massive expression of TGF-β, a key factor in tissue repair and fibrosis (Hernandez-Pando et al., 2000; Pagán and Ramakrishnan, 2018; Weiskirchen et al., 2019). Apart from its capacity to promote fibroblast proliferation, TGF-β also stimulates fibroblasts, epithelial, and mesenchymal cells to produce extracellular matrix components, like collagen and fibronectin (Mornex et al., 1994; Wynn and Ramalingam, 2012; Pagán and Ramakrishnan, 2018; Weiskirchen et al., 2019). As aforementioned, FBGCs could be involved in the encapsulation of foreign bodies, which is characteristic for FBRs (Sheikh et al., 2015). However, Kyriakides et al. reported that the production of TGF-β is unaltered and that extensive fibrosis also takes place when FBGC formation is impaired, suggesting that other immune cells, such as macrophages, suffice to establish the fibrous capsule (Kyriakides et al., 2004).

LANGHANS GIANT CELLS PHENOTYPE, FUNCTIONS, AND BIOLOGICAL ACTIVITIES

LGCs are circular or ovoid shaped and contain generally less than 20 nuclei, arranged in a circular or horseshoe pattern along the cell border (Anderson, 2000; Quinn and Schepetkin, 2009; Sakai et al., 2012; Pagán and Ramakrishnan, 2018; Wang et al., 2020). They were first described in 1868 by Theodor Langhans in his studies of granulomas in tuberculosis (Mizuno et al., 2001; Helming et al., 2009; Pagán and Ramakrishnan, 2018). Subsequently, LGCs have been described in various infectious and non-infectious granulomatous conditions (Sakai et al., 2012; Wang et al., 2020).

Langhans Giant Cells in Infectious Diseases

In infectious diseases, LGCs are formed when individual macrophages fail to eradicate persistent pathogens (Pagán and Ramakrishnan, 2018). Because of their increased cell size compared to macrophages, it could be assumed that LGCs dispose better phagocytic properties (Rose et al., 2014). However, the phagocytic capacity of IL-15 induced LGCs for bacille Calmette-Guérin and *M. leprae* bacteria is similar to that of macrophages (Wang et al., 2020). Lay et al. even reported that human LGCs, derived from M. tuberculosis-induced granulomas, are unable to phagocytose beads coated with *M. tuberculosis* antigens (Lay et al., 2007). The impaired phagocytic capacity of LGCs was associated with downregulation of the mannose receptor and CD11b (a subunit of the C3 receptor), two phagocytic receptors. Taken together, these findings suggest that LGCs cannot to be considered as superior phagocytes.

The killing capacities of LGCs to pathogens remain a matter of debate as different research groups reported conflicting results. Yasui et al. demonstrated that LGCs produce decreased levels of superoxide anions, which may enable *M. tuberculosis* to survive within granulomas (Yasui et al., 2011). On the other hand, LGCs

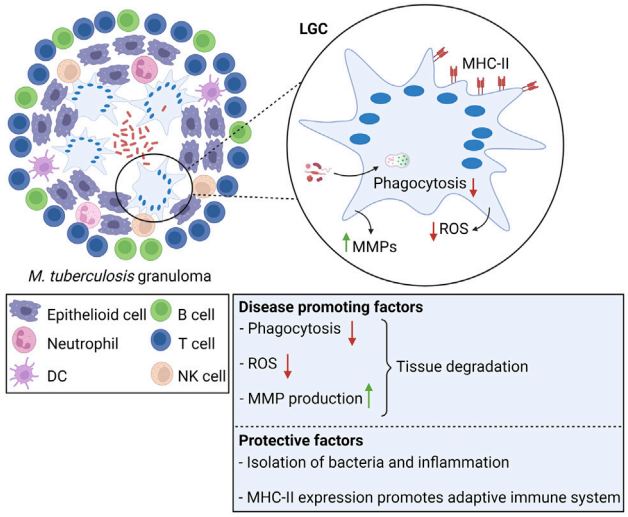

FIGURE 4 | Langhans giant cells in tuberculosis. LGCs are a hallmark of M. tuberculosis-induced granulomas. In tuberculosis, LGCs exhibit both protective and disease promoting factors. Clearance of *M. tuberculosis* is inefficient since LGCs cannot mediate bacterial uptake or sufficient ROS production for pathogen killing. Additionally, LGCs secrete MMPs leading to tissue destruction. On the other hand, LGCs are involved in isolation of bacteria and inflammation from the surrounding tissue. LGCs highly express MHC-II molecules, suggesting that they promote the adaptive immune response through antigen presentation.

may have better fungicidal capacities than macrophages (do Nascimento et al., 2011; Enelow et al., 1992). Enelow et al. demonstrated that LGCs stimulated with phorbol myristate acetate, display enhanced fungicidal capacities against *C. albicans* due to elevated oxidative activity (Enelow et al., 1992). It is worth noting that Enelow et al. differentiated human monocytes into LGCs by stimulation with IFN-γ and IL-3, but that Yasui et al. did not use IFN-γ or IL-3 for the production of LGCs (Enelow et al., 1992; Yasui et al., 2011). As IFN-γ and IL-3 are able to promote superoxide anion production by monocytes (Jendrossek et al., 1993), the different microbicidal activity of LGCs in both reports might be due to differences in the differentiation protocol.

Role of LGCs in *Mycobacterium tuberculosis* Infection

LGCs are most studied within the context of tuberculosis (**Figure 4**). Although LGCs are inefficient in destroying *M. tuberculosis*, either through phagocytosis or through production of microbicidal oxidants (Lay et al., 2007; Yasui et al., 2011), they still may exert protective functions. Within the granulomatous structure, LGCs form a barrier that shields *M. tuberculosis* from the rest of the body, and prevent cell-to-cell spread and growth of bacteria (Byrd, 1998; Brooks et al., 2019). Furthermore, LGCs express high amounts of MHC-II molecules, enabling them to function as antigen presenting cells, capable to prime the adaptive immune response (Lay et al., 2007). Conversely, tuberculosis-associated LGCs produce MMPs thereby inducing tissue destruction (Helming et al., 2009). LGCs may be involved in the inflammatory reaction of the

granuloma through the production of cytokines and chemokines. In a murine model for pulmonary tuberculosis, immunostaining for TNF-α and IL-1α, two cytokines that have been reported to be crucial for granuloma formation (Huaux et al., 2015; Pereira et al., 2018), was strongly positive in LGCs (Hernandez-Pando et al., 1997). In addition to initiation and maintenance of granulomas, LGCs may also be involved in resolution of inflammation and development of fibrosis. As for FBGCs, LGCs undergo a phenotypic switch with time, characterized by reduced expression of TNF-α and IL-1β, and simultaneous upregulation of TGF-β, a major regulator of tissue repair and fibrosis (Hernandez-Pando et al., 1997; Wynn and Ramalingam, 2012).

Although LGCs are a major morphological characteristic of infectious granulomas, their specific biological activity and function still needs further elucidation.

Langhans Giant Cells in Non-Infectious Diseases

The role of LGCs in non-infectious diseases is less understood. LGCs are a pathological hallmark in granulomatous inflammatory diseases, such as sarcoidosis and Blau syndrome (Okamoto et al., 2003; Janssen et al., 2012; Sakai et al., 2012; Wouters et al., 2014). Although these disorders have no infectious cause and are considered auto-inflammatory granulomatous conditions, DNA fragments of *Mycobacteria* are occasionally found within the granulomatous lesions through PCR-based detection methods (Dow and Ellingson, 2010; Lee et al., 2019; Poline et al., 2020). Whether the LGC-granulomas are formed in response to the bacteria or whether the lesions form the ideal environment for the pathogen to survive remains unclear.

In some cases, LGCs can be found in close proximity to cancer cells (Bigotti et al., 2002) and may be involved in the clearance of tumor cells. Wang et al. reported that LGCs are able to phagocytose malignant cells in esophageal cancer (Wang et al., 2021). The precise role of LGCs or granulomas within malignant diseases is not elucidated. In Hodgkin disease, the presence of granulomas is associated with more beneficial outcomes (Pagán and Ramakrishnan, 2018), whereas intravascular granulomas may worsen the clinical outcome in testicular seminomas (Downes et al., 2016).

FORMATION OF MULTINUCLEATED GIANT CELLS THROUGH MACROPHAGE FUSION

Throughout the decades, scientists have been searching for the mechanism of MGC formation and several hypotheses have been proposed, the most plausible being endoreplication, "frustrated" phagocytosis, and cell fusion (McNally et al., 1996; DeFife et al., 1997; McNally and Anderson, 2005; Herrtwich et al., 2016). Endoreplication refers to the failure of the actual cell division after the nucleus has been replicated (Herrtwich et al., 2016). "Frustrated" phagocytosis was suggested to be a mechanism of multinucleation after the observation that proteins involved in phagocytosis seemed to be important for MGC formation as well (McNally et al., 1996; DeFife et al., 1997; McNally and Anderson, 2005). In this model of macrophage fusion, MGCs originate from macrophages that phagocytose particles in close proximity to other macrophages (DeFife et al., 1999). When individual macrophages are unable to engulf a foreign particle, this may eventually lead to "frustrated" phagocytosis and internalization of surrounding macrophages (DeFife et al., 1999). Although it is difficult to exclude the above mechanisms, it is nowadays accepted that MGCs originate from fusion of cells of the monocyte-macrophage lineage.

Macrophage fusion is a complex, not well understood multistep process. Before the real fusion process can be initiated, macrophages have to undergo a series of events: acquirement of a fusion competent state, chemotaxis and adhesion, and finally fusion (Brooks et al., 2019; Faust et al., 2019). Although all derived from macrophage fusion, distinct MGC subtypes are induced by different stimuli (Anderson, 2000). Combined action of M-CSF and RANKL has been well established for fusion of macrophages into osteoclasts (Asagiri and Takayanagi, 2007). IL-4 and IL-13 are efficient inducers of FBGCs *in vitro* (Anderson, 2000; Yang et al., 2014), whereas biomaterial implantation leads to generation of FBGCs *in vivo* (Yang et al., 2014). Fusion of macrophages into LGCs is triggered by cytokines, such as combinations of IFN-γ plus IL-3 or GM-CSF (Anderson, 2000), pathogens and derivates, including *M. tuberculosis* and muramyl dipeptide (Mizuno et al., 2001), and concanavalin A (Sakai et al., 2012). Whereas the stimuli vary between the different MGC subtypes, it is supposed that the actual fusion process relies on a common fusion machinery (Pereira et al., 2018). It should be noted that our insights in macrophage fusion are incomplete and highly dependent on MGC subtype, stressing the need for additional and in-depth analysis of this phenomenon in all MGCs. Especially our knowledge on LGC formation remains unsatisfactory, reflected by sparse literature on this topic. In the next section, we provide an overview of the current knowledge on the molecular pathways and key molecules involved in macrophage fusion (**Figure 5**).

Fusion Competency by Upregulation of Fusogens

Initially, macrophages have to become fusion competent, through upregulation of essential fusogens (Pereira et al., 2018), which are proteins required for cell fusion (Brukman et al., 2019). Fusogens are induced by signaling through so-called prefusion mediators expressed on macrophages, including DNAX-activating protein of 12 kDa, triggering receptor expressed on myeloid cells 2 (TREM2), and P2X7 receptor (P2RX7) (Pereira et al., 2018).

DAP12 – TREM2 Interaction

DNAX-activating protein of 12 kDa (DAP12) is a transmembrane adaptor protein (Paloneva et al., 2003) predominantly expressed on NK cells (Takaki et al., 2006; Tessarz and Cerwenka, 2008) and on cells of the myeloid lineage (Takaki et al., 2006), including monocytes (Tessarz and Cerwenka, 2008), macrophages, neutrophils (Tessarz and

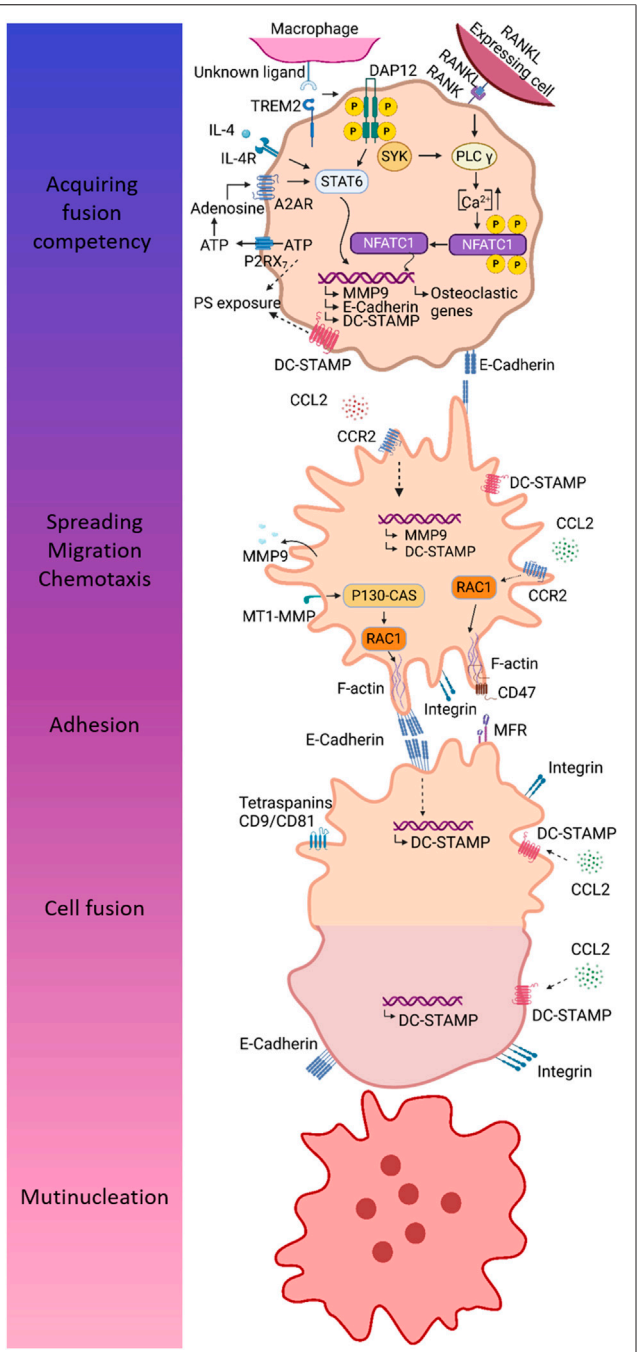

FIGURE 5 | Different steps in the multinucleation process mainly based on findings in osteoclasts. MGCs originate from macrophage fusion, a multi-step process comprising acquirement of fusion competency, chemotaxis and adhesion, and finally cell fusion resulting into multinucleation. Fusion competency is accomplished through upregulation of fusogens downstream of signaling through so-called prefusion mediators. DAP12 and its associated receptor TREM2 are well-established prefusion mediators. After binding of its unknown ligand, TREM2 associates with DAP12 leading to phosphorylation of DAP12 and downstream signaling via SYK. In IL-4 induced fusion, DAP12-mediated signaling results in activation of STAT6 and subsequent induction of several fusogens, including MMP9, E-cadherin, and DC-STAMP. During osteoclastogenesis, combined action of RANK- and DAP12-mediated signaling leads to Ca^{2+} signaling downstream of PLCγ, resulting in an increase

(*Continued*)

FIGURE 5 | of intracellular Ca^{2+} concentration enabling translocation of NFATc1 to the nucleus. Fusogens are induced by combined action of P2RX7 and A2A receptor. ATP release through P2RX7 provides extracellular ATP for biosynthesis of adenosine, which in turn induces fusion competency by binding to A2A receptor. Fusing macrophages are characterized by exposure of PS, a lipid that is normally localized in the inner membrane leaflet. The mechanism of PS externalization may involve P2RX7 and DC-STAMP. Macrophage chemotaxis is driven by CCL2 and is essential to bring the membranes of two individual cells in close proximity for fusion. Next to chemotaxis, CCL2 is hypothesized to mediate the induction of fusogens, including MMP9 and DC-STAMP. In order to allow cell migration and subsequent cell adhesion, macrophages undergo cytoskeletal arrangements, which are mediated by RAC1, a major regulator of the cytoskeleton. It has been established that MT-MMP1 activates RAC1. Furthermore, CCL2 signaling has also been associated with RAC1 activation. Homotypic cell-cell adhesion is mediated by integrins and E-cadherin. The latter might also be involved in induction of fusogens, such as DC-STAMP. Cell-cell attachment is dependent on interaction between CD47 and MFR. Once macrophages are firmly attached to each other, the real fusion process can proceed. DC-STAMP is considered a main fusion regulator; however, its ligand and mechanism of action remain to be defined. Several putative ligands for DC-STAMP has been proposed, including CCL2, MFR, and CD47.

Cerwenka, 2008), and DCs (Humphrey et al., 2004). DAP12 is expressed as a homodimer at the cell surface, where it associates with DAP12-associated receptors to exert its function (Humphrey et al., 2004). In DAP12-deficient mice, bone mass is increased (Humphrey et al., 2004), suggesting a role for DAP12 in osteoclast formation and/or function. Osteoclast fusion is inefficient in monocytes derived from patients with loss-of-function mutations in DAP12 (Paloneva et al., 2003) and in bone marrow macrophages derived from DAP12-deficient mice (Humphrey et al., 2004). By contrast, stimulation of DAP12 in RAW264.7 cells (a monocyte/macrophage cell line derived from mice) enhances fusion, resulting in more multinucleated osteoclasts with increased cell size and number of nuclei (Humphrey et al., 2004). A role for DAP12 in fusion is not exclusive to osteoclasts as Helming et al. demonstrated that IL-4 induced fusion is also impaired in human macrophages silenced for DAP12 (Helming et al., 2008). Triggering receptor expressed on myeloid cells 2 (TREM2) functions as a DAP12-associated receptor in osteoclasts (Takaki et al., 2006; Peng et al., 2010; Zou and Teitelbaum, 2015) and has also been reported to mediate osteoclast multinucleation (Paloneva et al., 2003). It is hypothesized that macrophages themselves express a TREM2 ligand and thus that TREM2/DAP12-mediated signaling relies on the interaction between macrophages (Peng et al., 2010). During osteoclastogenesis, TREM2 is upregulated and its expression positively correlates with the number of nuclei in mature osteoclasts (Humphrey et al., 2006). Stimulation of TREM2 enhances multinucleation (Humphrey et al., 2004), whereas silencing or blockade of TREM2 inhibits osteoclast multinucleation (Humphrey et al., 2006; Peng et al., 2010). Finally, human PBMCs derived from TREM2-deficient patients, show impaired fusion when differentiated into osteoclasts (Paloneva et al., 2003). Together, these results demonstrate that combined action of DAP12 and TREM2 is important to macrophage fusion. After recognition of its unknown ligand, TREM2 associates with DAP12 leading to

the phosphorylation of the immunoreceptor tyrosine-based activation motif (ITAM) in the cytoplasmic domain of DAP12 (Paloneva et al., 2003; Pereira et al., 2018). Once phosphorylated, DAP12 interacts with the cytoplasmic protein tyrosine kinases SYK and ZAP70, thereby triggering several downstream pathways (Paloneva et al., 2003). Although both FBGCs and osteoclasts rely on DAP12/TREM2-signaling, distinct downstream pathways are involved to acquire a fusion competent state (Pereira et al., 2018). In FBGC precursors, cooperation of IL-4 and ITAM signaling results in the activation of transcription factor STAT6 which in turn induces the expression of essential fusogens, including E-cadherin, DC-STAMP, and MMP9 (Moreno et al., 2007; Helming and Gordon, 2009; Van den Bossche et al., 2012; Pereira et al., 2018). In osteoclast precursors, recruitment of SYK to DAP12 leads to Ca^{2+} signaling downstream of PLCγ (Koga et al., 2004). Ca^{2+} signaling enhances the induction of nuclear factor of activated T cells c1 (NFATc1), the master transcription factor of osteoclastogenesis, through an autoamplification mechanism (Koga et al., 2004; Kameda et al., 2013).

It is worth mentioning that DAP12-depleted mice still form multinucleated osteoclasts *in vivo*, whereas multinucleation is severely inhibited *in vitro* (Humphrey et al., 2004). Therefore, other mechanisms compensate for fusion in case of DAP12 deficiency *in vivo*. Zou et al. demonstrated that FcRγ, another ITAM-containing signaling adaptor that activates SYK signaling, can rescue osteoclast multinucleation in absence of DAP12 (Zou and Teitelbaum, 2015).

P2X7 Receptor

P2RX7 is an ATP-gated ion channel that belongs to the family of P2X purinergic receptors (Di Virgilio et al., 1999; Gartland et al., 2003; Lemaire et al., 2006). Although P2RX7 functions as a cation-selective channel under transient stimulation with ATP, the receptor transforms into a nonselective pore for hydrophilic molecules of a molecular mass up to 900 Da upon repetitive ATP stimulation (Di Virgilio et al., 1999; Falzoni et al., 2000). During macrophage fusion, P2RX7 localizes at sites of cell-cell contact in podosomes (Falzoni et al., 2000; Lemaire et al., 2012), indicating that the receptor plays a role in macrophage fusion. The involvement of P2RX7 in fusion is further supported by the finding that mouse J774 macrophages expressing high levels of P2RX7 spontaneously form MGCs (Chiozzi et al., 1997; Di Virgilio et al., 1999; Falzoni et al., 2000). Previously, it was assumed that P2RX7 drives fusion through the formation of a "fusion pore", thereby connecting the cytoplasm of two neighboring cells (Falzoni et al., 2000; Lemaire et al., 2012). This hypothesis was supported by the finding that P2RX7 pore-forming activity is required for macrophage fusion (Lemaire et al., 2012). Blockade of the pore activity with P2RX7 neutralizing antibodies or with the receptor antagonist oxidized ATP, impairs fusion of human and murine macrophages (Chiozzi et al., 1997; Di Virgilio et al., 1999; Falzoni et al., 2000; Gartland et al., 2003; Steinberg and Hiken, 2007). Additionally, polymyxin B, a natural cationic peptide that potentiates pore activity in response to ATP, facilitates fusion of HEK293 cells transfected with P2RX7 (Lemaire et al., 2006). By contrast, HEK293 cells transfected with a truncated form of P2RX7 that lacks ATP-induced pore-forming activity, show impaired fusion even in presence of polymyxin B. Interestingly, hydrolyzation of extracellular ATP, by hexokinase or apyrase, accelerates MGC formation, which conflicts with the idea of ATP-induced pore formation during fusion (Di Virgilio et al., 1999; Pellegatti et al., 2011). These observations may be explained by receptor desensitization when stimulated with high ATP concentrations as degradation of ATP by hexokinase or apyrase might restore the responsiveness of P2RX7 (Falzoni et al., 2000). More recently, Pellegatti et al. proposed a new concept in which P2RX7 solely functions as a receptor for local ATP release to provide extracellular ATP for biosynthesis of adenosine, the actual fusogen (Pellegatti et al., 2011). Indeed, small amounts of extracellular ATP restore fusion in presence of anti-P2RX7 antibodies. Moreover, extracellular degradation of adenosine abolishes fusion, whereas addition of adenosine has the opposite effect. During macrophage fusion, adenosine likely acts at the adenosine receptor A2A as pharmacological inhibition of the A2A receptor reduces fusion, whereas A2A receptor agonists increase fusion. The finding that combined action of a P2RX7 inhibitor and A2A receptor agonists allows fusion, indicates that proper adenosine supply is required for MGC formation.

Chemotaxis

Chemotaxis and migration of macrophages towards each other is a crucial step before cell-cell fusion. CCL2 and its receptor CCR2 mediate chemotaxis of monocytes/macrophages (Li et al., 2007; Khan et al., 2016; Guicciardi et al., 2018) and their role in macrophage fusion has been established. CCL2 potentiates RANKL-induced osteoclast formation in human and mice (Kim et al., 2005; Li et al., 2007) and even induces the formation of osteoblast-like cells in absence of RANKL or when NFATc1 is inhibited (Kim et al., 2005). Osteoclast-like cells are multinucleated, but lack bone resorbing activity, suggesting that CCL2 stimulates the fusion process rather than osteoclast differentiation (Kim et al., 2005). Furthermore, CCL2 or CCR2-deficient mice display impaired osteoclast fusion *in vivo* and *in vitro* (Miyamoto et al., 2009; Khan et al., 2016) and exogenous CCL2 restores fusion in cultures derived from CCL2-deficient mice (Khan et al., 2016). Several findings illustrate the involvement of CCL2 and CCR2 in FBGC formation as well. Blocking of CCL2, either by an inhibitory peptide or neutralizing antibodies, diminishes IL-4 induced fusion of human monocytes (Kyriakides et al., 2004). In addition, bone marrow cultures derived from CCL2 or CCR2-deficient mice, display impaired FBGC multinucleation, whereas exogenous CCL2 rescues fusion in CCL2-deficient cultures (Khan et al., 2016). *In vivo* macrophage fusion on implanted biomaterials is also abrogated in CCL2-deficient mice (Kyriakides et al., 2004; Skokos et al., 2011), probably due to reduced macrophage accumulation and migration (Skokos et al., 2011). Next to chemotaxis, CCL2 is thought to contribute to the fusion competency through induction of essential fusogens, including DC-STAMP and MMP9 (Helming and Gordon, 2009; Miyamoto et al., 2009; Skokos et al., 2011), and through

activation of Rac1 (Skokos et al., 2011), a major cytoskeleton regulator (Touaitahuata et al., 2014).

Adhesion

After chemotaxis, macrophages attach to each other to bring their membranes in close proximity prior to cell fusion. The homotypic cell-cell contacts are partly mediated by E-cadherins and some studies elucidate that integrins might be involved as well (Helming and Gordon, 2009).

E-Cadherin

E-cadherin belongs to the family of the cadherins, which are transmembrane or membrane-associated glycoproteins that mediate calcium-dependent cell-cell adhesions (Mbalaviele et al., 1995; van Roy and Berx, 2008). During FBGC formation, E-cadherin is upregulated at the macrophage cell surface downstream of IL-4 or IL-13 signaling (Moreno et al., 2007; Van den Bossche et al., 2009, 2012; Wanat et al., 2014; Fiorino and Harrison, 2016), suggesting for a role in macrophage fusion. Moreover, E-cadherin neutralizing antibodies impair IL-4 induced macrophage fusion, especially in early stages of differentiation (Moreno et al., 2007), and fusion is diminished in macrophages derived from E-cadherin deficient mice (Van de Bossche et al., 2009; Van de Bossche et al., 2012). Fusion-efficient macrophages are characterized by membrane extension, called podosomes, which form zipper-like structures at cell fusion sites (Balabiyev et al., 2020). E-cadherin is probably implicated in the generation of these zipper-like structures as neutralizing antibodies disrupt formation of these structures and subsequent fusion (Balabiyev et al., 2020). E-cadherin is also upregulated during osteoclastogenesis, especially at early differentiation stages, suggesting that E-cadherin is involved in early osteoclastogenesis (Fiorino and Harrison, 2016). Blocking of E-cadherin, either by neutralizing antibodies (Mbalaviele et al., 1995; Fiorino and Harrison, 2016; Sun et al., 2020) or synthetic peptides containing the cell adhesion recognition sequence of cadherins (Mbalaviele et al., 1995), diminishes osteoclast fusion (Mbalaviele et al., 1995; Fiorino and Harrison, 2016), whereas E-cadherin overexpression transiently accelerates fusion (Fiorino and Harrison, 2016). Although E-cadherin is upregulated at membrane extensions and cell-cell contact sites, the protein is not detected at fusion sites, indicating that it does not make part of the fusion machinery (Fiorino and Harrison, 2016). Instead, E-cadherin neutralizing antibodies impact migration and expression of fusogens, including DC-STAMP, suggesting that cell-cell contact mediated through E-cadherin alters macrophage proliferation and induce the transition to cell migration and fusion.

Integrins

Integrins are a superfamily of heterodimeric transmembrane proteins comprised of α and β subunits, which mediate both cell-extracellular matrix and cell-cell adhesions (Campbell and Humphries, 2011; Aghbali et al., 2017). The integrin subunits β1, β2, and β5 have been reported to contribute to FBGC formation. Anti-β1 and anti-β2 antibodies impair the adhesion of human monocyte/macrophage to biomaterials, an essential prerequisite for FBGC formation (McNally and Anderson, 2002). Although blockage of β1 dramatically reduces the number of adherent monocyte/macrophages, some FBGCs are still formed, indicating that fusion competency is remained. By contrast, β2 neutralizing antibodies also abolishes fusion, suggesting that β2 mediates both intercellular and cell-biomaterial interactions during FBGC formation. αMβ2 is involved in IL-4 induced fusion of murine peritoneal macrophages both *in vivo* and *in vitro*. Indeed, blocking of αMβ2 results in less FBGCs formation and the remaining FBGCs are smaller in size and contain less nuclei (Podolnikova et al., 2016). αDβ2 might also contribute to IL-4 induced fusion of murine macrophages, however to a lower extend as αMβ2. Finally, IL-4 has been reported to increase the expression of β5 on human monocytes, suggesting a role for this integrin in FBGC fusion (Aghbali et al., 2017). Integrins are also involved in the formation of multinucleated osteoclasts (Rao et al., 2006). It has been found that α9β1 contributes to osteoclast multinucleation, reflected by reduced osteoclast formation in human bone marrow cultures treated with anti-α9 antibodies and smaller osteoclast size in α9-deficient mice.

Macrophage Fusion Receptor and CD47

Macrophage fusion receptor (MFR), also called signal regulatory protein α (SIRPα), and CD47 are transmembrane proteins that belong to the superfamily of immunoglobulins (Igs) (Han et al., 2000; Gautam and Acharya, 2014; Zhang et al., 2020). It was demonstrated that MFR and CD47 are induced at the onset of fusion both *in vivo* and *in vitro*, suggesting that these proteins contribute to macrophage fusion (Saginario et al., 1995; Saginario et al., 1998; Han et al., 2000; Podolnikova et al., 2019). Moreover, blocking of MFR or CD47, either by monoclonal antibodies or engineered proteins containing the extracellular domain of MFR or CD47, impairs fusion. Finally, IL-4 induced fusion is abrogated in RAW264.7 cells depleted for MRF by short hairpin (sh)RNA (Podolnikova et al., 2019). Han et al. proposed a model for MFR and CD47 mediated fusion. In order to guarantee cell-cell attachment, CD47 may initially interact with a "long" form of MFR on the neighboring macrophage, consisting of an extracellular immunoglobulin V domain and two adjacent immunoglobulin constant domains (Han et al., 2000; Vignery, 2005a). Afterwards, CD47 switches to a poorly expressed "short" form of MFR, only containing the immunoglobulin V domain. This homotypic interaction brings the plasma membranes of the two cells to a distance of 5–10 nm, allowing cell fusion (Han et al., 2000; Vignery, 2000, 2005a). MFR can also interact with the integrin CD11b contributing to fusion (Podolnikova et al., 2019). In macrophages, MFR and CD11b are detected at sites of cell-cell contact. Furthermore, IL-4 induced fusion has been observed in co-cultures of MFR and CD11b expressing HEK293 cells. Despite the findings favoring a role for MFR and CD47 in macrophage fusion, van Beek et al. reported that the number of nuclei remains unaltered in mice lacking the cytoplasmic signaling region of MFR, indicating that MFR or at least MFR signaling is dispensable for osteoclast fusion (van Beek et al., 2009). Additionally, osteoclasts derived from bone marrow cells of CD47 KO mice or differentiated in presence of MFR neutralizing antibodies do not differ in size or number of

nuclei (Lundberg et al., 2007). Together, these findings suggest that MFR and CD47 may be involved in macrophage fusion other that osteoclast formation.

Cytoskeletal Alterations

Cytoskeletal alterations are implicated in many aspects of macrophage fusion, including chemotaxis/migration, adhesion, the actual fusion process, and cellular reorganization (Wang et al., 2008, 2015; Pereira et al., 2018). Fusing macrophages are characterized by actin-based membrane protrusions and these structures have been shown to induce fusion (Wang et al., 2015; Faust et al., 2019). Indeed, almost all fusion events take place at membrane protrusions and impaired formation of these structures prevents macrophage fusion (Faust et al., 2019). The actin cytoskeleton is a dynamic structure that is constitutively remodeled by actin organizing proteins (Fritzsche et al., 2017). An important group of actin organizers are the Rho-related small GTPases with Rac1, Cdc42, and RhoA as the best characterized members to mediate macrophage fusion (Wang et al., 2008; Touaitahuata et al., 2014). Pharmacological inhibition or genetic depletion of Rac1 impairs the fusion of mouse macrophages into FBGCs and osteoclasts (Jay et al., 2007, 2010; Wang et al., 2008; Takito et al., 2015). Furthermore, release of Rac1 inhibitor from implanted biomaterials reduces FBGC formation *in vivo* (Jay et al., 2007). Next to Rac1, Cdc42 positively regulates fusion of mouse macrophages into FBGCs and osteoclasts (Leung et al., 2010; Faust et al., 2019; Park et al., 2019). The effect of RhoA on macrophage fusion is less straightforward. RhoA activation leads to more but smaller osteoclasts, whereas inhibition of its downstream effector Rho kinase elevates the formation of large osteoclasts (Takito et al., 2015). By contrast, inhibition of Rho kinase induces more but smaller FBGCs (Jay et al., 2007). Contradictory results have also been published on the involvement of actin in macrophage adhesion and migration prior to fusion. DeFife et al. reported that cytochalasin B and D, two substances that disrupt actin dynamics, prevent the formation of multinucleated FBGCs without affecting macrophage adhesion, spreading, and motility (DeFife et al., 1999). Inhibition of Rac1 reduces macrophage fusion on implanted biomaterials *in vivo* without affecting macrophage recruitment (Jay et al., 2007). The formation of FBGCs in response to implanted biomaterials is also affected in Cdc42-deficient mice, but depletion of Cdc42 has no effect on macrophage recruitment or adhesion (Faust et al., 2019). By contrast, osteoclast precursors from Rac1-depleted mice display, next to impaired fusion, reduced cell spreading and motility (Wang et al., 2008). Furthermore, cytochalasin D abolishes macrophage migration during osteoclastogenesis (Wang et al., 2015). Together, these illustrations suggest that macrophage adhesion, spreading and motility can be maintained during FBGC formation even though the actin network is dysregulated, whereas this is not the case during osteoclastogenesis.

Lipid Alterations

During macrophage fusion, the lipid composition of the cytoplasmic and extracellular plasma membrane leaflet is altered to allow fusion. Phosphatidylserine (PS) is normally located in the cytoplasmic membrane leaflet (Shin and Takatsu, 2020), but is externalized during fusion (Verma et al., 2018; Kang et al., 2020). The importance of PS exposure during osteoclast multinucleation is illustrated by PS neutralization at the cell surface, either by antibodies or PS-binding protein, leading to diminished fusion (Verma et al., 2018; Kang et al., 2020; Whitlock and Chernomordik, 2021). Moreover, silencing or pharmacological inhibition of lipid transporters involved in outer translocation of PS, prevents PS externalization and subsequent fusion of osteoclast precursors. DC-STAMP and P2RX7, two well-described fusion proteins, might be implicated in PS exposure during macrophage fusion as PS externalization is abrogated by anti-DC-STAMP antibodies and brief activation of P2RX7 channels causes reversible PS exposure on the cell surface (Helming and Gordon, 2009; Lemaire et al., 2012; Verma et al., 2018). During FBGC formation, fusion probably depends on recognition of PS by the lipid receptor CD36 (Helming et al., 2009). CD36 localizes at sites of cell contact and IL-4 induced fusion of macrophages derived from CD36-deficient mice is impaired. Although CD36 is required for FBGC formation, the receptor is dispensable for osteoclast fusion as anti-CD36 antibodies nor CD36 KO macrophages display reduced osteoclast multinucleation.

Next to PS, phosphatidylethanolamine (PE) is also involved in osteoclast formation (Irie et al., 2017; Whitlock and Chernomordik, 2021). Under normal conditions, PE is located in the inner plasma membrane leaflet (Shin and Takatsu, 2020), but clusters in the extracellular leaflet at fusion sites during osteoclastogenesis (Irie et al., 2017). Moreover, inhibition of PE synthesis or translocation to the outer plasma membrane impairs PE exposure and osteoclast fusion (Irie et al., 2017).

Fusion

After successful acquirement of fusion competency, chemotaxis and adhesion, and essential cytoskeletal and lipid alterations, the fusion process goes into its final execution. In this final stage, it is worth to mention a few key players, including dendritic cell-specific transmembrane protein (DC-STAMP), tetraspanins, and matrix metalloproteases (MMPs).

Dendritic Cell-Specific Transmembrane Protein

Dendritic cell-specific transmembrane protein (DC-STAMP) is a seven-transmembrane protein (Chiu et al., 2012) that is essential for macrophage fusion in human and mice (Yagi et al., 2005, 2006; Kim et al., 2008; Miyamoto, 2011; Zeng et al., 2013; Møller et al., 2020). The expression of DC-STAMP in human osteoclast precursors is positively correlated with the number of nuclei in mature osteoclasts (Møller et al., 2020). Moreover, suppression of DC-STAMP in human monocytes through lentivirus-mediated RNA interference impairs the formation of multinucleated osteoclasts (Zeng et al., 2013). Depletion of DC-STAMP in mice abrogates fusion of preosteoclasts into multinucleated osteoclasts both *in vivo* and *in vitro* (Yagi et al., 2005, 2006; Kim et al., 2008; Miyamoto, 2011) and reintroduction of DC-STAMP in osteoclast precursors derived from DC-STAMP-deficient mice rescues multinucleation (Yagi et al., 2005, 2006).

Although osteoclast precursors isolated from DC-STAMP-deficient mice are unable to fuse, the expression of osteoclast markers, including TRAP (Yagi et al., 2005, 2006) and NFATc1, is not impaired (Yagi et al., 2006). Furthermore, ruffled borders and actin rings, typical morphological features of osteoclasts, are observed and cells exhibit minor bone-resorbing capacities (Yagi et al., 2005, 2006). These findings suggest that DC-STAMP is required for macrophage fusion without mediating osteoclast differentiation. Next to osteoclast multinucleation, DC-STAMP is indispensable for the formation of multinucleated FBGCs and LGCs (Yagi et al., 2005, 2006; Kim et al., 2008; Miyamoto, 2011; Sakai et al., 2012). Generation of multinucleated FBGCs is abolished in mice deficient for DC-STAMP *in vivo* and *in vitro* (Yagi et al., 2005, 2006; Kim et al., 2008; Miyamoto, 2011). Additionally, DC-STAMP is upregulated during LGC formation and siRNA-mediated knock-down of DC-STAMP inhibits fusion of human monocytes into LGCs (Sakai et al., 2012). Taken together, DC-STAMP is considered a common fusion mediator, yet different signaling mechanisms are responsible for induction of DC-STAMP in osteoclasts, FBGCs, and LGCs. During osteoclastogenesis, DC-STAMP is induced downstream of c-FOS and NFATc1 signaling (Yagi et al., 2007; Kim et al., 2008; Miyamoto, 2011; Sakai et al., 2012; Zhang et al., 2014), whereas PU.1 and NF-κB mediate the expression of DC-STAMP during FBGC formation (Yagi et al., 2007; Sakai et al., 2012), and probably NF-κB and MAP kinases during LGC formation (Sakai et al., 2012). It is speculated that DC-STAMP promotes macrophage fusion in a receptor-ligand fashion (Yagi et al., 2005), but the ligand for DC-STAMP required for macrophage fusion remains currently unknown (Quinn and Schepetkin, 2009). Since DC-STAMP shows structural similarities with chemokine receptors, it is speculated that a certain chemokine, such as CCL2, serves as ligand for DC-STAMP (Yagi et al., 2007; Quinn and Schepetkin, 2009). Other possible candidates include MFR and CD47. The exact mechanism by which DC-STAMP mediates macrophage fusion remains speculative as well. It is hypothesized that DC-STAMP induces the expression of fusogens (Zhang et al.), including MFR, and therefore indirectly mediates macrophage fusion (Vignery, 2005b).

Tetraspanins

Tetraspanins are four-span transmembrane proteins (Sangsri et al., 2020) that bind to one another and to a variety of other transmembrane proteins (Parthasarathy et al., 2009). Because of their ability to interact with several molecules, tetraspanins act as membrane organizers, mediating the generation of functional protein clusters in tetraspanin-enriched microdomains (Parthasarathy et al., 2009) of which some may modulate macrophage fusion. CD9 and CD81 are the best studied tetraspanins in the context of macrophage fusion, but whether they regulate fusion in a positive or negative manner remains controversial. For example, CD81 neutralizing antibodies support fusion of mouse macrophages infected with *B. thailandensis*, whereas inhibition of CD81 diminishes fusion upon infection with *B. pseudomallei* (Elgawidi et al., 2020; Sangsri et al., 2020). Additionally, CD9 neutralizing antibodies promote the formation of multinucleated osteoclast from murine bone marrow cells (Takeda et al., 2003), whereas blocking of CD9, either by neutralizing antibodies or small interfering RNA (siRNA), impairs the formation of multinucleated osteoclasts in RAW264.7 cells (Ishii et al., 2006). Although the effect of CD9 and CD81 on macrophage fusion remains unclear, CD63 seems to be a positive regulator (Takeda et al., 2003; Parthasarathy et al., 2009). CD63 is upregulated in human monocytes stimulated with Concanavalin A, and monoclonal antibodies directed against CD63 abrogate MGC formation. Tspan-5 and NET-6 have also been suggested to influence macrophage fusion as Tspan-5 is upregulated during osteoclastogenesis and NET-6 is downregulated (Iwai et al., 2007). Furthermore, silencing of Tspan-5 impairs fusion of RAW264.7 into multinucleated osteoclasts, whereas the opposite is true for NET-6.

Matrix Metalloproteases

Matrix metalloproteases (MMPs) compromise a family of endopeptidases known to degrade various extracellular matrix components (EMCs) (Gonzalo et al., 2010; Kim and Lee, 2020). MMPs may modulate macrophage fusion by degrading EMCs and/or cell-surface bound molecules involved in cell fusion (Jones et al., 2008). *In vitro* and *in vivo* fusion of macrophages into osteoclasts and FBGCs is abolished in mice deficient for MT1-MMP, a membrane-anchored MMP (Gonzalo and Arroyo, 2010; Gonzalo et al., 2010). Depletion of MT1-MMP affects macrophage spreading, formation of lamellipodia, and Rac1 activity, indicating that impaired migration lies at the basis of reduced fusion events in these cells (Gonzalo and Arroyo, 2010). MT1-MMP probably promotes fusion through its interaction with adaptor protein p130Crk-associated substrate (CAS), which in turn triggers Rac1 activation (Gonzalo and Arroyo, 2010; Gonzalo et al., 2010). Although MT1-MPP positively regulates macrophage fusion (Gonzalo and Arroyo, 2010; Gonzalo et al., 2010), MMP8 and MMP13 have been described to negatively impact fusion (Kim and Lee, 2020). RANKL decreases the expression of MMP8 and MMP13 in murine bone marrow macrophages, indicating that their down-regulation is required for proper osteoclastogenesis. Targeting these MMPs, either through siRNA or pharmacological inhibition, facilitates osteoclast fusion without altering differentiation (Kim and Lee, 2020). These findings are in contrast to data from Fu et al. who demonstrated that MMP13 promotes osteoclast formation starting from mouse bone marrow macrophages and that fusion is abrogated in macrophages derived from MMP13-deficient mice (Fu et al., 2016). Several reports indicate that MMPs also regulate FBGC formation. Pharmacological inhibition experiments suggested that MMP1, -8, -13, and -18 act as positive regulators of IL-4 induced fusion in human monocytes, whereas MMP2, -3, -9, and -12 do not influence fusion (Jones et al., 2008). Notwithstanding the observation that MMP9 is not implicated in human macrophage fusion, MMP9 neutralizing antibodies reduce IL-4 induced fusion of mouse macrophages and MMP9-deficient mice display reduced FBGC formation after implantation of biomaterials (Maclauchlan et al., 2009). The impaired fusion observed in MMP9-deficient mouse macrophages may result from defective cytoskeletal dynamics

prior to cell fusion. The discrepancy on the effect of MMP-9 on macrophage fusion between human and mice may be explained by suboptimal specificity of pharmacological MMP inhibitors used in human experiments.

CONCLUSION AND REMAINING KEY QUESTIONS

MGCs are polykaryons that originate from fusion of cells of the monocyte-macrophage lineage and are subdivided into three main subtypes: osteoclasts, FBGCs, and LGCs (Anderson, 2000). Osteoclasts are well-known for their bone-resorbing capacities and increasing evidence is found that they contribute to multiple processes beyond bone resorption, including osteoblast stimulation, vasculogenesis and immune regulation (Novack and Teitelbaum, 2008; Le Goff et al., 2013; Cappariello et al., 2014; Drissi and Sanjay, 2016). FBGCs are formed during inflammatory reactions against foreign body material to remove particles that single macrophages cannot (Han et al., 2000; Vignery, 2000). Among all MGC subtypes, LGCs are the least characterized in terms of function and mechanism of formation. In infectious granulomatous diseases, LGCs are thought to be formed in response to a persistent pathogen as a final attempt to remove or isolate the irritant from the surrounding tissue (Byrd, 1998; Pagán and Ramakrishnan, 2018). In non-infectious granulomatous diseases, little is known about LGCs and multiple questions remain unresolved, like: What drives LGC formation and which mediators are essential to the fusion process? What are the mechanisms of macrophage fusion? Why do LGCs arise and what is their role in disease development and outcome? All MGCs have a common feature, namely a high number of nuclei. In osteoclasts, bone resorption is positively correlated with the number of nuclei, indicating that increased cell size empowers osteoclasts to degrade bone tissue (Yagi et al., 2006). In FBGCs, the acquisition of multiple nuclei may facilitate the engulfment of large particles (Milde et al., 2015). For LGCs, the functional consequences of multinucleation remain elusive. Furthermore, the nuclei of the three multinucleated subtypes are arranged in a unique fashion within the cytoplasm but to what extend the nuclear pattern influences the functionality of these cells has yet to be determined. Also, there is limited understanding of how these cells operate considering the many nuclei. In addition, it would be interesting to investigate whether MGCs are terminally differentiated or whether these cells still show plasticity. Implantation experiments in rats revealed that LGCs are the initial MGC subtype to be formed on the implanted particle, which over time fuse together to form FBGCs (van der Rhee et al., 1979; Smetana, 1987). It should be mentioned that these experiments date back from more than 30 years ago and that, to our knowledge, no recent reports about MGC plasticity have been published. In conclusion, despite being described over 150 years ago (Pagán and Ramakrishnan, 2018), multiple questions on MGCs remain unanswered, especially for LGCs. Since LGCs occur in a myriad of infectious and non-infectious diseases (Wang et al., 2020), in-depth analysis of the function, biological activity, and multinucleation of LGCs will provide us insights into the contribution of these cells to the pathogenesis of these diseases.

AUTHOR CONTRIBUTIONS

KA and MV wrote the first draft of the manuscript. KA designed figures with Biorender software (BioRender.com). CR, PM, and CW critically read and edited the manuscript. All authors contributed to the article and approved the submitted version.

FUNDING

This study received funding from the FWO-Flanders (G0C3420N). KA obtained a FWO PhD fellowship strategic basic research (1S75320N). Images were designed with BioRender.com This review was funded by Fond Wetenschappelijk Onderzoek Vlaanderen (Research Foundation Flanders, FWO-Vlaanderen).

REFERENCES

Aghbali, A., Rafieyan, S., Mohamed-Khosroshahi, L., Baradaran, B., Shanehbandi, D., and Kouhsoltani, M. (2016). IL-4 Induces the Formation of Multinucleated Giant Cells and Expression of β5 Integrin in central Giant Cell Lesion. *Med. Oral Patol Oral Cir Bucal.* 22 (1), e1–e6. doi:10.4317/medoral.20935

Anderson, J. M. (2000). Multinucleated Giant Cells. *Med. Oral* 7, 40–47. doi:10.1097/00062752-200001000-00008

Anderson, J. M., Rodriguez, A., and Chang, D. T. (2008). Foreign Body Reaction to Biomaterials. *Semin. Immunol.* 20, 86–100. doi:10.1016/j.smim.2007.11.004

Angel, N. Z., Walsh, N., Forwood, M. R., Ostrowski, M. C., Cassady, A. I., and Hume, D. A. (2000). Transgenic Mice Overexpressing Tartrate-Resistant Acid Phosphatase Exhibit an Increased Rate of Bone Turnover. *J. Bone Miner Res.* 15, 103–110. doi:10.1359/jbmr.2000.15.1.103

Armas, L. A. G., and Recker, R. R. (2012). Pathophysiology of Osteoporosis. *Endocrinol. Metab. Clin. North America* 41, 475–486. doi:10.1016/j.ecl.2012.04.006

Asagiri, M., and Takayanagi, H. (2007). The Molecular Understanding of Osteoclast Differentiation. *Bone* 40, 251–264. doi:10.1016/j.bone.2006.09.023

Ashai, S., and Harvey, N. C. (2020). Rheumatoid Arthritis and Bone Health. *Clin. Med.* 20, 565–567. doi:10.7861/clinmed.20.6.rabh

Atri, C., Guerfali, F., and Laouini, D. (2018). Role of Human Macrophage Polarization in Inflammation during Infectious Diseases. *Ijms* 19, 1801. doi:10.3390/ijms19061801

Bader-Meunier, B., Van Nieuwenhove, E., Breton, S., and Wouters, C. (2018). Bone Involvement in Monogenic Autoinflammatory Syndromes. *Rheumatology (Oxford)* 57, 606–618. doi:10.1093/rheumatology/kex306

Balabiyev, A., Podolnikova, N. P., Mursalimov, A., Lowry, D., Newbern, J. M., Roberson, R. W., et al. (2020). Transition of Podosomes into Zipper-like Structures in Macrophage-Derived Multinucleated Giant Cells. *MBoC* 31, 2002–2020. doi:10.1091/mbc.E19-12-0707

Bigotti, G., Coli, A., Magistrelli, P., De Ninno, M., Antonacci, V., Crucitti, A., et al. (2002). Gastric Adenocarcinoma Associated with Granulomatous Gastritis. Case Report and Review of the Literature. *Tumori* 88, 163–166. doi:10.1177/030089160208800216

Blair, H. C., Kahn, A. J., Crouch, E. C., Jeffrey, J. J., and Teitelbaum, S. L. (1986). Isolated Osteoclasts Resorb the Organic and Inorganic Components of Bone. *J. Cel Biol* 102, 1164–1172. doi:10.1083/jcb.102.4.1164

Boabaid, F., Cerri, P. S., and Katchburian, E. (2001). Apoptotic Bone Cells May Be Engulfed by Osteoclasts during Alveolar Bone Resorption in Young Rats. *Tissue and Cell* 33, 318–325. doi:10.1054/tice.2001.0179

Bronckers, A. L. J. J., Goei, W., van Heerde, W. L., Dumont, E. A. W. J., Reutelingsperger, C. P. M., and van den Eijnde, S. M. (2000). Phagocytosis of Dying Chondrocytes by Osteoclasts in the Mouse Growth Plate as Demonstrated by Annexin-V Labelling. *Cel Tissue Res.* 301, 267–272. doi:10.1007/s004410000238

Brooks, P. J., Glogauer, M., and Mcculloch, C. A. (2019). An Overview of the Derivation and Function of Multinucleated Giant Cells and Their Role in Pathologic Processes. *Am. J. Pathol.* 189, 1145–1158. doi:10.1016/j.ajpath.2019.02.006

Brukman, N. G., Uygur, B., Podbilewicz, B., and Chernomordik, L. V. (2019). How Cells Fuse. *J. Cel Biol.* 218, 1436–1451. doi:10.1083/jcb.201901017

Buchwald, Z. S., Kiesel, J. R., Yang, C., DiPaolo, R., Novack, D. V., and Aurora, R. (2013). Osteoclast-Induced FOXP3+ CD8 T-Cells Limit Bone Loss in Mice. *Bone* 56, 163–173. doi:10.1016/j.bone.2013.05.024

Buck, D. W., and Dumanian, G. A. (2012). Bone Biology and Physiology. *Plast. Reconstr. Surg.* 129, 1314–1320. doi:10.1097/PRS.0b013e31824eca94

Byrd, T. F. (1998). Multinucleated Giant Cell Formation Induced by IFN-γ/IL-3 Is Associated with Restriction of VirulentMycobacterium tuberculosisCell to Cell Invasion in Human Monocyte Monolayers. *Cell Immunol.* 188, 89–96. doi:10.1006/cimm.1998.1352

Campbell, I. D., and Humphries, M. J. (2011). Integrin Structure, Activation, and Interactions. *Cold Spring Harbor Perspect. Biol.* 3, a004994. doi:10.1101/cshperspect.a004994

Cappariello, A., Maurizi, A., Veeriah, V., and Teti, A. (2014). The Great Beauty of the Osteoclast. *Arch. Biochem. Biophys.* 558, 70–78. doi:10.1016/j.abb.2014.06.017

Cerri, P. S., Boabaid, F., and Katchburian, E. (2003). Combined TUNEL and TRAP Methods Suggest that Apoptotic Bone Cells Are inside Vacuoles of Alveolar Bone Osteoclasts in Young Rats. *J. Periodontal Res.* 38, 223–226. doi:10.1034/j.1600-0765.2003.02006.x

Chang, D. T., Colton, E., Matsuda, T., and Anderson, J. M. (2009). Lymphocyte Adhesion and Interactions with Biomaterial Adherent Macrophages and Foreign Body Giant Cells. *J. Biomed. Mater. Res.* 91A, 1210–1220. doi:10.1002/jbm.a.32218

Chen, X., Wang, Z., Duan, N., Zhu, G., Schwarz, E. M., and Xie, C. (2018). Osteoblast-Osteoclast Interactions. *Connect. Tissue Res.* 59, 99–107. doi:10.1080/03008207.2017.1290085

Chiozzi, P., Sanz, J. M., Ferrari, D., Falzoni, S., Aleotti, A., Buell, G. N., et al. (1997). Spontaneous Cell Fusion in Macrophage Cultures Expressing High Levels of the P2Z/P2X7 Receptor. *J. Cel Biol* 138, 697–706. doi:10.1083/jcb.138.3.697

Chiu, Y.-H., Mensah, K. A., Schwarz, E. M., Ju, Y., Takahata, M., Feng, C., et al. (2012). Regulation of Human Osteoclast Development by Dendritic Cell-specific Transmembrane Protein (DC-STAMP). *J. Bone Miner Res.* 27, 79–92. doi:10.1002/jbmr.531

DeFife, K. M., Jenney, C. R., McNally, A. K., Colton, E., and Anderson, J. M. (1997). Interleukin-13 Induces Human Monocyte/Macrophage Fusion and Macrophage Mannose Receptor Expression. *J. Immunol.* 158, 3385–3390.

DeFife, K. M., Jenney, C. R., Colton, E., and Anderson, J. M. (1999). Disruption of Filamentous Actin Inhibits Human Macrophage Fusion. *FASEB j.* 13, 823–832. doi:10.1096/fasebj.13.8.823

Demirtaş, T. T., Göz, E., Karakeçili, A., and Gümüşderelioğlu, M. (2016). Combined Delivery of PDGF-BB and BMP-6 for Enhanced Osteoblastic Differentiation. *J. Mater. Sci. Mater. Med.* 27, 12. doi:10.1007/s10856-015-5626-9

Deng, S., Azevedo, M., and Baylies, M. (2017). Acting on Identity: Myoblast Fusion and the Formation of the Syncytial Muscle Fiber. *Semin. Cel Developmental Biol.* 72, 45–55. doi:10.1016/j.semcdb.2017.10.033

Di Virgilio, F., Falzoni, S., Chiozzi, P., Sanz, J. M., Ferrari, D., and Buell, G. N. (1999). ATP Receptors and Giant Cell Formation. *J. Leukoc. Biol.* 66, 723–726. doi:10.1002/jlb.66.5.723

DiGiovanni, C. W., Lin, S., and Pinzur, M. (2012). Recombinant Human PDGF-BB in Foot and Ankle Fusion. *Expert Rev. Med. Devices* 9, 111–122. doi:10.1586/erd.11.76

Dow, C. T., and Ellingson, J. L. E. (2010). Detection ofMycobacterium Avium Ss. Paratuberculosisin Blau Syndrome Tissues. *Autoimmune Dis.* 2010, 1–5. doi:10.4061/2010/127692

Downes, M. R., Cheung, C. C., Pintilie, M., Chung, P., and van der Kwast, T. H. (2016). Assessment of Intravascular Granulomas in Testicular Seminomas and Their Association with Tumour Relapse and Dissemination. *J. Clin. Pathol.* 69, 47–52. doi:10.1136/jclinpath-2015-202997

Drake, M. T., Clarke, B. L., Oursler, M. J., and Khosla, S. (2017). Cathepsin K Inhibitors for Osteoporosis: Biology, Potential Clinical Utility, and Lessons Learned. *Endocr. Rev.* 38, 325–350. doi:10.1210/er.2015-1114

Drissi, H., and Sanjay, A. (2016). The Multifaceted Osteoclast; Far and beyond Bone Resorption. *J. Cel. Biochem.* 117, 1753–1756. doi:10.1002/jcb.25560

Ebert, M., Ward, B., Anderson, J., McVenes, R., and Stokes, K. (2005). *In Vivo* Biostability of Polyether Polyurethanes with Polyethylene Oxide Surface-Modifying End Groups; Resistance to Biologic Oxidation and Stress Cracking. *J. Biomed. Mater. Res.* 75A, 175–184. doi:10.1002/jbm.a.30396

Edwards, C. M., and Mundy, G. R. (2008). Eph Receptors and Ephrin Signaling Pathways: A Role in Bone Homeostasis. *Int. J. Med. Sci.* 5, 263–272. doi:10.7150/ijms.5.263

Elgawidi, A., Mohsin, M. I., Ali, F., Watts, A., Monk, P. N., Thomas, M. S., et al. (2020). A Role for Tetraspanin Proteins in Regulating Fusion Induced by Burkholderia Thailandensis. *Med. Microbiol. Immunol.* 209, 473–487. doi:10.1007/s00430-020-00670-6

Endow, R. I., Sullivan, G. W., Carper, H. T., and Mandell, G. L. (1992). Induction of Multinucleated Giant Cell Formation fromIn VitroCulture of Human Monocytes with Interleukin-3 and Interferon-γ: Comparison with Other Stimulating Factors. *Am. J. Respir. Cel Mol Biol* 6, 57–62. doi:10.1165/ajrcmb/6.1.57

Epelman, S., Lavine, K. J., and Randolph, G. J. (2014). Origin and Functions of Tissue Macrophages. *Immunity* 41, 21–35. doi:10.1016/j.immuni.2014.06.013

Everts, V., Korper, W., Hoeben, K. A., Jansen, I. D., Bromme, D., Cleutjens, K. B., et al. (2006). Osteoclastic Bone Degradation and the Role of Different Cysteine Proteinases and Matrix Metalloproteinases: Differences between Calvaria and Long Bone. *J. Bone Miner Res.* 21, 1399–1408. doi:10.1359/jbmr.060614

Everts, V., Korper, W., Jansen, D. C., Steinfort, J., Lammerse, I., Heera, S., et al. (1999). Functional Heterogeneity of Osteoclasts: Matrix Metalloproteinases Participate in Osteoclastic Resorption of Calvarial Bone but Not in Resorption of Long Bone. *FASEB j.* 13, 1219–1230. doi:10.1096/fasebj.13.10.1219

Falzoni, S., Chiozzi, P., Ferrari, D., Buell, G., and Di Virgilio, F. (2000). P2X7Receptor and Polykarion Formation. *MBoC* 11, 3169–3176. doi:10.1091/mbc.11.9.3169

Faust, J. J., Balabiyev, A., Heddleston, J. M., Podolnikova, N. P., Baluch, D. P., Chew, T.-L., et al. (2019). An Actin-Based Protrusion Originating from a Podosome-Enriched Region Initiates Macrophage Fusion. *MBoC* 30, 2254–2267. doi:10.1091/mbc.E19-01-0009

Fernandes, C., Prabhu, P., Juvale, K., Suares, D., and Yc, M. (2019). Cancer Cell Fusion: A Potential Target to Tackle Drug-Resistant and Metastatic Cancer Cells. *Drug Discov. Today* 24, 1836–1844. doi:10.1016/j.drudis.2019.05.024

Fiorino, C., and Harrison, R. E. (2016). E-cadherin Is Important for Cell Differentiation during Osteoclastogenesis. *Bone* 86, 106–118. doi:10.1016/j.bone.2016.03.004

Fleckenstein, E., and Drexler, H. (1997). Tartrate-Resistant Acid Phosphatase: Gene Structure and Function. *Leukemia* 11, 10–13. doi:10.1038/sj.leu.2400532

Frisch, R. N., Curtis, K. M., Aenlle, K. K., and Howard, G. A. (2016). Hepatocyte Growth Factor and Alternative Splice Variants - Expression, Regulation and Implications in Osteogenesis and Bone Health and Repair. *Expert Opin. Ther. Targets* 20, 1087–1098. doi:10.1517/14728222.2016.1162293

Fritzsche, M., Li, D., Colin-York, H., Chang, V. T., Moeendarbary, E., Felce, J. H., et al. (2017). Self-Organizing Actin Patterns Shape Membrane Architecture but Not Cell Mechanics. *Nat. Commun.* 8, 14347. doi:10.1038/ncomms14347

Fu, J., Li, S., Feng, R., Ma, H., Sabeh, F., Roodman, G. D., et al. (2016). Multiple Myeloma-Derived MMP-13 Mediates Osteoclast Fusogenesis and Osteolytic Disease. *J. Clin. Invest.* 126, 1759–1772. doi:10.1172/JCI80276

Gao, S.-Y., Zheng, G.-S., Wang, L., Liang, Y.-J., Zhang, S.-E., Lao, X.-M., et al. (2017). Zoledronate Suppressed Angiogenesis and Osteogenesis by Inhibiting Osteoclasts Formation and Secretion of PDGF-BB. *PLoS One* 12, e0179248. doi:10.1371/journal.pone.0179248

Gartland, A., Buckley, K. A., Bowler, W. B., and Gallagher, J. A. (2003). Blockade of the Pore-Forming P2X 7 Receptor Inhibits Formation of Multinucleated Human Osteoclasts *In Vitro*. *Calcified Tissue Int.* 73, 361–369. doi:10.1007/s00223-002-2098-y

Gautam, P. K., and Acharya, A. (2014). Suppressed Expression of Homotypic Multinucleation, Extracellular Domains of CD172α(SIRP-α) and CD47 (IAP) Receptors in TAMs UpRegulated by Hsp70-Peptide Complex in Dalton's Lymphoma. *Scand. J. Immunol.* 80, 22–35. doi:10.1111/sji.12180

Gelb, B. D., Shi, G.-P., Chapman, H. A., and Desnick, R. J. (1996). Pycnodysostosis, a Lysosomal Disease Caused by Cathepsin K Deficiency. *Science* 273, 1236–1238. doi:10.1126/science.273.5279.1236

Gentek, R., Molawi, K., and Sieweke, M. H. (2014). Tissue Macrophage Identity and Self-Renewal. *Immunol. Rev.* 262, 56–73. doi:10.1111/imr.12224

Georgadaki, K., Khoury, N., Spandidos, D. A., and Zoumpourlis, V. (2016). The Molecular Basis of Fertilization (Review). *Int. J. Mol. Med.* 38, 979–986. doi:10.3892/ijmm.2016.2723

Georgess, D., Machuca-Gayet, I., Blangy, A., and Jurdic, P. (2014). Podosome Organization Drives Osteoclast-Mediated Bone Resorption. *Cell Adhes. Migration* 8, 192–204. doi:10.4161/cam.27840

Giordano-Santini, R., Linton, C., and Hilliard, M. A. (2016). Cell-Cell Fusion in the Nervous System: Alternative Mechanisms of Development, Injury, and Repair. *Semin. Cel Developmental Biol.* 60, 146–154. doi:10.1016/j.semcdb.2016.06.019

Gonzalo, P., and Arroyo, A. G. (2010). Mt1-Mmp. *Communicative Integr. Biol.* 3, 256–259. doi:10.4161/cib.3.3.11456

Gonzalo, P., Guadamillas, M. C., Hernández-Riquer, M. V., Pollán, Á., Grande-García, A., Bartolomé, R. A., et al. (2010). MT1-MMP Is Required for Myeloid Cell Fusion via Regulation of Rac1 Signaling. *Developmental Cel* 18, 77–89. doi:10.1016/j.devcel.2009.11.012

Goodman, S. B., and Gallo, J. (2019). Periprosthetic Osteolysis: Mechanisms, Prevention and Treatment. *Jcm* 8, 2091. doi:10.3390/jcm8122091

Gradin, P., Hollberg, K., Cassady, A. I., Lång, P., and Andersson, G. (2012). Transgenic Overexpression of Tartrate-Resistant Acid Phosphatase Is Associated with Induction of Osteoblast Gene Expression and Increased Cortical Bone Mineral Content and Density. *Cells Tissues Organs* 196, 68–81. doi:10.1159/000330806

Grassi, F., Manferdini, C., Cattini, L., Piacentini, A., Gabusi, E., Facchini, A., et al. (2011). T Cell Suppression by Osteoclasts *In Vitro*. *J. Cel. Physiol.* 226, 982–990. doi:10.1002/jcp.22411

Grosso, A., Burger, M. G., Lunger, A., Schaefer, D. J., Banfi, A., and Di Maggio, N. (2017). It Takes Two to Tango: Coupling of Angiogenesis and Osteogenesis for Bone Regeneration. *Front. Bioeng. Biotechnol.* 5, 68. doi:10.3389/fbioe.2017.00068

Grüneboom, A., Hawwari, I., Weidner, D., Culemann, S., Müller, S., Henneberg, S., et al. (2019). A Network of Trans-cortical Capillaries as Mainstay for Blood Circulation in Long Bones. *Nat. Metab.* 1, 236–250. doi:10.1038/s42255-018-0016-5

Gu, Q., Shi, Q., and Yang, H. (2012). The Role of TLR and Chemokine in Wear Particle-Induced Aseptic Loosening. *J. Biomed. Biotechnol.* 2012, 1–9. doi:10.1155/2012/596870

Guder, C., Gravius, S., Burger, C., Wirtz, D. C., and Schildberg, F. A. (2020). Osteoimmunology: A Current Update of the Interplay between Bone and the Immune System. *Front. Immunol.* 11, 58. doi:10.3389/fimmu.2020.00058

Guicciardi, M. E., Trussoni, C. E., Krishnan, A., Bronk, S. F., Lorenzo Pisarello, M. J., O'Hara, S. P., et al. (2018). Macrophages Contribute to the Pathogenesis of Sclerosing Cholangitis in Mice. *J. Hepatol.* 69, 676–686. doi:10.1016/j.jhep.2018.05.018

Halleen, J. M., Räisänen, S. R., Alatalo, S. L., and Väänänen, H. K. (2003). Potential Function for the ROS-Generating Activity of TRACP. *J. Bone Miner Res.* 18, 1908–1911. doi:10.1359/jbmr.2003.18.10.1908

Halleen, J. M., Räisänen, S., Salo, J. J., Reddy, S. V., Roodman, G. D., Hentunen, T. A., et al. (1999). Intracellular Fragmentation of Bone Resorption Products by Reactive Oxygen Species Generated by Osteoclastic Tartrate-Resistant Acid Phosphatase. *J. Biol. Chem.* 274, 22907–22910. doi:10.1074/jbc.274.33.22907

Han, X., Sterling, H., Chen, Y., Saginario, C., Brown, E. J., Frazier, W. A., et al. (2000). CD47, a Ligand for the Macrophage Fusion Receptor, Participates in Macrophage Multinucleation. *J. Biol. Chem.* 275, 37984–37992. doi:10.1074/jbc.M002334200

Han, Y., You, X., Xing, W., Zhang, Z., and Zou, W. (2018). Paracrine and Endocrine Actions of Bone-The Functions of Secretory Proteins from Osteoblasts, Osteocytes, and Osteoclasts. *Bone Res.* 6, 16. doi:10.1038/s41413-018-0019-6

Harre, U., Keppeler, H., Ipseiz, N., Derer, A., Poller, K., Aigner, M., et al. (2012). Moonlighting Osteoclasts as Undertakers of Apoptotic Cells. *Autoimmunity* 45, 612–619. doi:10.3109/08916934.2012.719950

Hayman, A. R., Jones, S. J., Boyde, A., Foster, D., Colledge, W. H., Carlton, M. B., et al. (1996). Mice Lacking Tartrate-Resistant Acid Phosphatase (Acp 5) Have Disrupted Endochondral Ossification and Mild Osteopetrosis. *Development* 122, 3151–3162. doi:10.1242/dev.122.10.3151

Hayman, A. R. (2008). Tartrate-Resistant Acid Phosphatase (TRAP) and the Osteoclast/Immune Cell Dichotomy. *Autoimmunity* 41, 218–223. doi:10.1080/08916930701694667

Helming, L., and Gordon, S. (2009). Molecular Mediators of Macrophage Fusion. *Trends Cel Biol.* 19, 514–522. doi:10.1016/j.tcb.2009.07.005

Helming, L., Tomasello, E., Kyriakides, T. R., Martinez, F. O., Takai, T., Gordon, S., et al. (2008). Essential Role of DAP12 Signaling in Macrophage Programming into a Fusion-Competent State. *Sci. Signal.* 1, ra11. doi:10.1126/scisignal.1159665

Helming, L., Winter, J., and Gordon, S. (2009). The Scavenger Receptor CD36 Plays a Role in Cytokine-Induced Macrophage Fusion. *J. Cel Sci.* 122, 453–459. doi:10.1242/jcs.037200

Hernandez-pando, R., Orozco, H., Arriaga, E. K., Sampieri, A., Larriva-sahd, J., and Madrid-marina, V. (1997). Analysis of the Local Kinetics and Localization of Interleukin-1 α , Tumour Necrosis'qc Factor- α and Transforming Growth Factor- β , during the Course of Experimental Pulmonary Tuberculosis. *Immunology* 90, 607–617. doi:10.1046/j.1365-2567.1997.00193.x

Hernandez-Pando, R., Bornstein, Q. L., Aguilar Leon, D., Orozco, E. H., Madrigal, V. K., and Martinez Cordero, E. (2000). Inflammatory Cytokine Production by Immunological and Foreign Body Multinucleated Giant Cells. *Immunology* 100, 352–358. doi:10.1046/j.1365-2567.2000.00025.x

Herrtwich, L., Nanda, I., Evangelou, K., Nikolova, T., Horn, V., Sagar, D., et al. (2016). DNA Damage Signaling Instructs Polyploid Macrophage Fate in Granulomas. *Cell* 167, 1264–1280. e18. doi:10.1016/j.cell.2016.09.054

Higashi, K., Matsuzaki, E., Hashimoto, Y., Takahashi-Yanaga, F., Takano, A., Anan, H., et al. (2016). Sphingosine-1-Phosphate/S1PR2-Mediated Signaling Triggers Smad1/5/8 Phosphorylation and Thereby Induces Runx2 Expression in Osteoblasts. *Bone* 93, 1–11. doi:10.1016/j.bone.2016.09.003

Hirayama, T., Fujikawa, Y., Itonaga, I., and Torisu, T. (2001). Effect of Particle Size on Macrophage-Osteoclast Differentiation *In Vitro*. *J. Orthopaedic Sci.* 6, 53–58. doi:10.1007/s007760170025

Hossain, M., Irwin, R., Baumann, M. J., and McCabe, L. R. (2005). Hepatocyte Growth Factor (HGF) Adsorption Kinetics and Enhancement of Osteoblast Differentiation on Hydroxyapatite Surfaces. *Biomaterials* 26, 2595–2602. doi:10.1016/j.biomaterials.2004.07.051

Huaux, F., Lo ReGiordano, S. G., Giordano, G., Uwambayinema, F., Devosse, R., Yakoub, Y., et al. (2015). IL-1α Induces CD11blow Alveolar Macrophage Proliferation and Maturation during Granuloma Formation. *J. Pathol.* 235, 698–709. doi:10.1002/path.4487

Humphrey, M. B., Daws, M. R., Spusta, S. C., Niemi, E. C., Torchia, J. A., Lanier, L. L., et al. (2006). TREM2, a DAP12-Associated Receptor, Regulates Osteoclast Differentiation and Function. *J. Bone Miner. Res.* 21, 237–245. doi:10.1359/jbmr.051016

Humphrey, M. B., Ogasawara, K., Yao, W., Spusta, S. C., Daws, M. R., Lane, N. E., et al. (2004). The Signaling Adapter Protein DAP12 Regulates Multinucleation during Osteoclast Development. *J. Bone Miner. Res.* 19, 224–234. doi:10.1359/jbmr.0301234

Ibáñez, L., Abou-Ezzi, G., Ciucci, T., Amiot, V., Belaïd, N., Obino, D., et al. (2016). Inflammatory Osteoclasts Prime TNFα-Producing CD4+T Cells and Express CX3CR1. *J. Bone Miner. Res.* 31, 1899–1908. doi:10.1002/jbmr.2868

Irie, A., Yamamoto, K., Miki, Y., and Murakami, M. (2017). Phosphatidylethanolamine Dynamics Are Required for Osteoclast Fusion. *Sci. Rep.* 7, 46715. doi:10.1038/srep46715

Ishii, M., Iwai, K., Koike, M., Ohshima, S., Kudo-Tanaka, E., Ishii, T., et al. (2006). RANKL-induced Expression of Tetraspanin CD9 in Lipid Raft Membrane Microdomain Is Essential for Cell Fusion during Osteoclastogenesis. *J. Bone Miner. Res.* 21, 965–976. doi:10.1359/jbmr.060308

Iwai, K., Ishii, M., Ohshima, S., Miyatake, K., and Saeki, Y. (2007). Expression and Function of Transmembrane-4 Superfamily (Tetraspanin) Proteins in Osteoclasts: Reciprocal Roles of Tspan-5 and NET-6 during Osteoclastogenesis. *Allergol. Int.* 56, 457–463. doi:10.2332/allergolint.O-07-488

Janssen, C. E. I., Rose, C. D., De Hertogh, G., Martin, T. M., Bader Meunier, B., Cimaz, R., et al. (2012). Morphologic and Immunohistochemical Characterization of Granulomas in the Nucleotide Oligomerization Domain

2-Related Disorders Blau Syndrome and Crohn Disease. *J. Allergy Clin. Immunol.* 129, 1076–1084. doi:10.1016/j.jaci.2012.02.004

Jay, S. M., Skokos, E. A., Zeng, J., Knox, K., and Kyriakides, T. R. (2009). Macrophage Fusion Leading to Foreign Body Giant Cell Formation Persists under Phagocytic Stimulation by Microspheresin Vitroandin Vivoin Mouse Models. *J. Biomed. Mater. Res.* 93, 189–199. doi:10.1002/jbm.a.32513

Jay, S. M., Skokos, E., Laiwalla, F., Krady, M.-M., and Kyriakides, T. R. (2007). Foreign Body Giant Cell Formation Is Preceded by Lamellipodia Formation and Can Be Attenuated by Inhibition of Rac1 Activation. *Am. J. Pathol.* 171, 632–640. doi:10.2353/ajpath.2007.061213

Jendrossek, V., Peters, A., Buth, S., Liese, J., Wintergerst, U., Belohradsky, B., et al. (1993). Improvement of Superoxide Production in Monocytes from Patients with Chronic Granulomatous Disease by Recombinant Cytokines. *Blood* 81, 2131–2136. doi:10.1182/blood.v81.8.2131.bloodjournal8182131

Jones, J. A., Chang, D. T., Meyerson, H., Colton, E., Kwon, I. K., Matsuda, T., et al. (2007). Proteomic Analysis and Quantification of Cytokines and Chemokines from Biomaterial Surface-Adherent Macrophages and Foreign Body Giant Cells. *J. Biomed. Mater. Res.* 83A, 585–596. doi:10.1002/jbm.a.31221

Jones, J. A., Mcnally, A. K., Chang, D. T., Qin, L. A., Meyerson, H., Colton, E., et al. (2008). Matrix Metalloproteinases and Their Inhibitors in the Foreign Body Reaction on Biomaterials. *J. Biomed. Mater. Res.* 84A, 158–166. doi:10.1002/jbm.a.31220

Jurdic, P., Saltel, F., Chabadel, A., and Destaing, O. (2006). Podosome and Sealing Zone: Specificity of the Osteoclast Model. *Eur. J. Cel Biol.* 85, 195–202. doi:10.1016/j.ejcb.2005.09.008

Kameda, Y., Takahata, M., Komatsu, M., Mikuni, S., Hatakeyama, S., Shimizu, T., et al. (2013). Siglec-15 Regulates Osteoclast Differentiation by Modulating RANKL-Induced Phosphatidylinositol 3-Kinase/Akt and Erk Pathways in Association with Signaling Adaptor DAP12. *J. Bone Miner. Res.* 28, 2463–2475. doi:10.1002/jbmr.1989

Kang, J.-H., Ko, H.-M., Han, G.-D., Lee, S.-Y., Moon, J.-S., Kim, M.-S., et al. (2020). Dual Role of Phosphatidylserine and its Receptors in Osteoclastogenesis. *Cell Death Dis* 11, 497. doi:10.1038/s41419-020-2712-9

Kania, A., and Klein, R. (2016). Mechanisms of Ephrin-Eph Signalling in Development, Physiology and Disease. *Nat. Rev. Mol. Cel Biol.* 17, 240–256. doi:10.1038/nrm.2015.16

Karsdal, M. A., Henriksen, K., Sørensen, M. G., Gram, J., Schaller, S., Dziegiel, M. H., et al. (2005). Acidification of the Osteoclastic Resorption Compartment Provides Insight into the Coupling of Bone Formation to Bone Resorption. *Am. J. Pathol.* 166, 467–476. doi:10.1016/S0002-9440(10)62269-9

Karsdal, M. A., Martin, T. J., Bollerslev, J., Christiansen, C., and Henriksen, K. (2007). Are Nonresorbing Osteoclasts Sources of Bone Anabolic Activity? *J. Bone Miner. Res.* 22, 487–494. doi:10.1359/jbmr.070109

Khan, U. A., Hashimi, S. M., Bakr, M. M., Forwood, M. R., and Morrison, N. A. (2016). CCL2 and CCR2 Are Essential for the Formation of Osteoclasts and Foreign Body Giant Cells. *J. Cel. Biochem.* 117, 382–389. doi:10.1002/jcb.25282

Khan, U. A., Hashimi, S. M., Khan, S., Quan, J., Bakr, M. M., Forwood, M. R., et al. (2014). Differential Expression of Chemokines, Chemokine Receptors and Proteinases by Foreign Body Giant Cells (FBGCs) and Osteoclasts. *J. Cel. Biochem.* 115, 1290–1298. doi:10.1002/jcb.24781

Kiesel, J., Miller, C., Abu-Amer, Y., and Aurora, R. (2007). Systems Level Analysis of Osteoclastogenesis Reveals Intrinsic and Extrinsic Regulatory Interactions. *Dev. Dyn.* 236, 2181–2197. doi:10.1002/dvdy.21206

Kiesel, J. R., Buchwald, Z. S., and Aurora, R. (2009). Cross-Presentation by Osteoclasts Induces FoxP3 in CD8+T Cells. *J. Immunol.* 182, 5477–5487. doi:10.4049/jimmunol.0803897

Kim, H. J., and Lee, Y. (2020). Endogenous Collagenases Regulate Osteoclast Fusion. *Biomolecules* 10, 705. doi:10.3390/biom10050705

Kim, K., Lee, S.-H., Ha Kim, J., Choi, Y., and Kim, N. (2008). NFATc1 Induces Osteoclast Fusion via Up-Regulation of Atp6v0d2 and the Dendritic Cell-specific Transmembrane Protein (DC-STAMP). *Mol. Endocrinol.* 22, 176–185. doi:10.1210/me.2007-0237

Kim, M. S., Day, C. J., and Morrison, N. A. (2005). MCP-1 Is Induced by Receptor Activator of Nuclear Factor-Kb Ligand, Promotes Human Osteoclast Fusion, and Rescues Granulocyte Macrophage Colony-stimulating Factor Suppression of Osteoclast Formation. *J. Biol. Chem.* 280, 16163–16169. doi:10.1074/jbc.M412713200

Kirstein, B., Chambers, T. J., and Fuller, K. (2006). Secretion of Tartrate-Resistant Acid Phosphatase by Osteoclasts Correlates with Resorptive Behavior. *J. Cel. Biochem.* 98, 1085–1094. doi:10.1002/jcb.20835

Koga, T., Inui, M., Inoue, K., Kim, S., Suematsu, A., Kobayashi, E., et al. (2004). Costimulatory Signals Mediated by the ITAM Motif Cooperate with RANKL for Bone Homeostasis. *Nature* 428, 758–763. doi:10.1038/nature02444

Kyriakides, T. R., Foster, M. J., Keeney, G. E., Tsai, A., Giachelli, C. M., Clark-Lewis, I., et al. (2004). The CC Chemokine Ligand, CCL2/MCP1, Participates in Macrophage Fusion and Foreign Body Giant Cell Formation. *Am. J. Pathol.* 165, 2157–2166. doi:10.1016/S0002-9440(10)63265-8

Lay, G., Poquet, Y., Salek-Peyron, P., Puissegur, M.-P., Botanch, C., Bon, H., et al. (2007). Langhans Giant Cells fromM. Tuberculosis-Induced Human Granulomas Cannot Mediate Mycobacterial Uptake. *J. Pathol.* 211, 76–85. doi:10.1002/path.2092

Le Goff, B., Berthelot, J.-M., Maugars, Y., and Heymann, D. (2013). Osteoclasts in RA: Diverse Origins and Functions. *Jt. Bone Spine* 80, 586–591. doi:10.1016/j.jbspin.2013.04.002

Le, V., and Crouser, E. D. (2018). Potential Immunotherapies for Sarcoidosis. *Expert Opin. Biol. Ther.* 18, 399–407. doi:10.1080/14712598.2018.1427727

Lee, H., Eom, M., Kim, S. H., Wang, H. Y., Lee, H., and Choi, E. H. (2019). Identification of *Mycobacterium tuberculosis* and Non-tuberculous Mycobacteria from Cutaneous Sarcoidosis Lesions by Reverse Blot Hybridization Assay. *J. Dermatol.* 46, 917–921. doi:10.1111/1346-8138.15042

Lee, K. P., Barras, C. E., Griffith, F. D., and Waritz, R. S. (1981). Pulmonary Response and Transmigration of Inorganic Fibers by Inhalation Exposure. *Am. J. Pathol.* 102, 314–323.

Lemaire, I., Falzoni, S., and Adinolfi, E. (2012). Purinergic Signaling in Giant Cell Formation. *Front. Biosci.* E4, 41–55. doi:10.2741/e359

Lemaire, I., Falzoni, S., Leduc, N., Zhang, B., Pellegatti, P., Adinolfi, E., et al. (2006). Involvement of the Purinergic P2X7Receptor in the Formation of Multinucleated Giant Cells. *J. Immunol.* 177, 7257–7265. doi:10.4049/jimmunol.177.10.7257

Leung, R., Wang, Y., Cuddy, K., Sun, C., Magalhaes, J., Grynpas, M., et al. (2010). Filamin A Regulates Monocyte Migration through Rho Small GTPases during Osteoclastogenesis. *J. Bone Mineral Res.* 25, 091123192444063–36. doi:10.1359/jbmr.091114

Li, H., Hong, S., Qian, J., Zheng, Y., Yang, J., and Yi, Q. (2010). Cross Talk between the Bone and Immune Systems: Osteoclasts Function as Antigen-Presenting Cells and Activate CD4+ and CD8+ T Cells. *Blood* 116, 210–217. doi:10.1182/blood-2009-11-255026

Li, H., Lu, Y., Qian, J., Zheng, Y., Zhang, M., Bi, E., et al. (2014). Human Osteoclasts Are Inducible Immunosuppressive Cells in Response to T Cell-Derived IFN-γ and CD40 Ligand *In Vitro*. *J. Bone Miner. Res.* 29, 2666–2675. doi:10.1002/jbmr.2294

Li, X., Qin, L., Bergenstock, M., Bevelock, L. M., Novack, D. V., and Partridge, N. C. (2007). Parathyroid Hormone Stimulates Osteoblastic Expression of MCP-1 to Recruit and Increase the Fusion of Pre/Osteoclasts. *J. Biol. Chem.* 282, 33098–33106. doi:10.1074/jbc.M611781200

Lotinun, S., Kiviranta, R., Matsubara, T., Alzate, J. A., Neff, L., Lüth, A., et al. (2013). Osteoclast-specific Cathepsin K Deletion Stimulates S1P-dependent Bone Formation. *J. Clin. Invest.* 123, 666–681. doi:10.1172/JCI64840

Lou, Z., Peng, Z., Wang, B., Li, X., Li, X., and Zhang, X. (2019). miR-142-5p Promotes the Osteoclast Differentiation of Bone Marrow-Derived Macrophages via PTEN/PI3K/AKT/FoxO1 Pathway. *J. Bone Miner. Metab.* 37, 815–824. doi:10.1007/s00774-019-00997-y

Lundberg, P., Koskinen, C., Baldock, P. A., Löthgren, H., Stenberg, Å., Lerner, U. H., et al. (2007). Osteoclast Formation Is Strongly Reduced Both *In Vivo* and *In Vitro* in the Absence of CD47/SIRPα-Interaction. *Biochem. Biophysical Res. Commun.* 352, 444–448. doi:10.1016/j.bbrc.2006.11.057

Luo, W., Friedman, M. S., Hankenson, K. D., and Woolf, P. J. (2011). Time Series Gene Expression Profiling and Temporal Regulatory Pathway Analysis of BMP6 Induced Osteoblast Differentiation and Mineralization. *BMC Syst. Biol.* 5, 82. doi:10.1186/1752-0509-5-82

Ma, Z., Sagrillo-Fagundes, L., Mok, S., Vaillancourt, C., and Moraes, C. (2020). Mechanobiological Regulation of Placental Trophoblast Fusion and Function through Extracellular Matrix Rigidity. *Sci. Rep.* 10, 5837. doi:10.1038/s41598-020-62659-8

Maclauchlan, S., Skokos, E. A., Meznarich, N., Zhu, D. H., Raoof, S., Shipley, J. M., et al. (2009). Macrophage Fusion, Giant Cell Formation, and the Foreign Body Response Require Matrix Metalloproteinase 9. *J. Leukoc. Biol.* 85, 617–626. doi:10.1189/jlb.1008588

Madel, M.-B., Ibáñez, L., Wakkach, A., de Vries, T. J., Teti, A., Apparailly, F., et al. (2019). Immune Function and Diversity of Osteoclasts in Normal and Pathological Conditions. *Front. Immunol.* 10, 1408. doi:10.3389/fimmu.2019.01408

Martinez, F. O., Sica, A., Mantovani, A., and Locati, M. (2008). Macrophage Activation and Polarization. *Front. Biosci.* 13, 453–461. doi:10.2741/2692

Matsuo, K., and Irie, N. (2008). Osteoclast-Osteoblast Communication. *Arch. Biochem. Biophys.* 473, 201–209. doi:10.1016/j.abb.2008.03.027

Matsuo, K., and Otaki, N. (2012). Bone Cell Interactions through Eph/ephrin. *Cel Adhes. Migration* 6, 148–156. doi:10.4161/cam.20888

Mbalaviele, G., Chen, H., Boyce, B. F., Mundy, G. R., and Yoneda, T. (1995). The Role of Cadherin in the Generation of Multinucleated Osteoclasts from Mononuclear Precursors in Murine Marrow. *J. Clin. Invest.* 95, 2757–2765. doi:10.1172/JCI117979

McNally, A. K., DeFife, K. M., and Anderson, J. M. (1996). Interleukin-4-Induced Macrophage Fusion Is Prevented by Inhibitors of Mannose Receptor Activity. *Am. J. Pathol.* 149, 975–85.

McNally, A. K., and Anderson, J. M. (2002). β1 and β2 Integrins Mediate Adhesion during Macrophage Fusion and Multinucleated Foreign Body Giant Cell Formation. *Am. J. Pathol.* 160, 621–630. doi:10.1016/S0002-9440(10)64882-1

McNally, A. K., and Anderson, J. M. (2005). Multinucleated Giant Cell Formation Exhibits Features of Phagocytosis with Participation of the Endoplasmic Reticulum. *Exp. Mol. Pathol.* 79, 126–135. doi:10.1016/j.yexmp.2005.06.008

Meng, B., Liang, X., Yang, X., Chen, Y., Zhai, J., and Liang, X. (2010). Effect of Titanium Particles on Osteoclast Activity *In Vitro*. *Mol. Med. Rep.* 3, 1065–1069. doi:10.3892/mmr.2010.368

Meshcheryakova, A., Mechtcheriakova, D., and Pietschmann, P. (2017). Sphingosine 1-Phosphate Signaling in Bone Remodeling: Multifaceted Roles and Therapeutic Potential. *Expert Opin. Ther. Targets* 21, 725–737. doi:10.1080/14728222.2017.1332180

Milde, R., Ritter, J., Tennent, G. A., Loesch, A., Martinez, F. O., Gordon, S., et al. (2015). Multinucleated Giant Cells Are Specialized for Complement-Mediated Phagocytosis and Large Target Destruction. *Cel Rep.* 13, 1937–1948. doi:10.1016/j.celrep.2015.10.065

Mira-Pascual, L., Patlaka, C., Desai, S., Paulie, S., Näreoja, T., Lång, P., et al. (2020). A Novel Sandwich ELISA for Tartrate-Resistant Acid Phosphatase 5a and 5b Protein Reveals that Both Isoforms Are Secreted by Differentiating Osteoclasts and Correlate to the Type I Collagen Degradation Marker CTX-I *In Vivo* and *In Vitro*. *Calcif. Tissue Int.* 106, 194–207. doi:10.1007/s00223-019-00618-w

Miyamoto, K., Ninomiya, K., Sonoda, K.-H., Miyauchi, Y., Hoshi, H., Iwasaki, R., et al. (2009). MCP-1 Expressed by Osteoclasts Stimulates Osteoclastogenesis in an Autocrine/Paracrine Manner. *Biochem. Biophysical Res. Commun.* 383, 373–377. doi:10.1016/j.bbrc.2009.04.020

Miyamoto, T. (2011). Regulators of Osteoclast Differentiation and Cell-Cell Fusion. *Keio J. Med.* 60, 101–105. doi:10.2302/kjm.60.101

Mizuno, K., Okamoto, H., and Horio, T. (2001). Muramyl Dipeptide and Mononuclear Cell Supernatant Induce Langhans-type Cells from Human Monocytes. *J. Leukoc. Biol.* 70, 386–94. doi:10.1189/jlb.70.3.386

Møller, A. M. J., Delaissé, J.-M., Olesen, J. B., Canto, L. M., Rogatto, S. R., Madsen, J. S., et al. (2020). Fusion Potential of Human Osteoclasts *In Vitro* Reflects Age, Menopause, and *In Vivo* Bone Resorption Levels of Their Donors-A Possible Involvement of DC-STAMP. *Ijms* 21, 6368. doi:10.3390/ijms21176368

Moreno, J. L., Mikhailenko, I., Tondravi, M. M., and Keegan, A. D. (2007). IL-4 Promotes the Formation of Multinucleated Giant Cells from Macrophage Precursors by a STAT6-dependent, Homotypic Mechanism: Contribution of E-Cadherin. *J. Leukoc. Biol.* 82, 1542–1553. doi:10.1189/jlb.0107058

Mornex, J. F., Leroux, C., Greenland, T., and Ecochard, D. (1994). From Granuloma to Fibrosis in Interstitial Lung Diseases: Molecular and Cellular Interactions. *Eur. Respir. J.* 7, 779–785. doi:10.1183/09031936.94.07040779

Mulari, M. T. K., Zhao, H., Lakkakorpi, P. T., and Väänänen, H. K. (2003). Osteoclast Ruffled Border Has Distinct Subdomains for Secretion and Degraded Matrix Uptake. *Traffic* 4, 113–125. doi:10.1034/j.1600-0854.2003.40206.x

Na, W., Lee, E.-J., Kang, M.-K., Kim, Y.-H., Kim, D. Y., Oh, H., et al. (2020). Aesculetin Inhibits Osteoclastic Bone Resorption through Blocking Ruffled Border Formation and Lysosomal Trafficking. *Ijms* 21, 8581. doi:10.3390/ijms21228581

Narisawa, M., Kubo, S., Okada, Y., Yamagata, K., Nakayamada, S., Sakata, K., et al. (2021). Human Dendritic Cell-Derived Osteoclasts with High Bone Resorption Capacity and T Cell Stimulation Ability. *Bone* 142, 115616. doi:10.1016/j.bone.2020.115616

Nascimento, M. P. P. D., Bannwart, C. F., Nakaira-Takahagi, E., and Peraçoli, M. T. S. (2011). Granulocyte Macrophage Colony-Stimulating Factor Enhances the Modulatory Effect of Cytokines on Monocyte-Derived Multinucleated Giant Cell Formation and Fungicidal Activity against Paracoccidioides Brasiliensis. *Mem. Inst. Oswaldo Cruz* 106, 735–741. doi:10.1590/s0074-02762011000600014

Nishida, M., Saegusa, J., Tanaka, S., and Morinobu, A. (2018). S100A12 Facilitates Osteoclast Differentiation from Human Monocytes. *PLoS One* 13, e0204140. doi:10.1371/journal.pone.0204140

Novack, D. V., and Teitelbaum, S. L. (2008). The Osteoclast: Friend or Foe? *Annu. Rev. Pathol. Mech. Dis.* 3, 457–484. doi:10.1146/annurev.pathmechdis.3.121806.151431

Novinec, M., and Lenarčič, B. (2013). Cathepsin K: A Unique Collagenolytic Cysteine Peptidase. *Biol. Chem.* 394, 1163–1179. doi:10.1515/hsz-2013-0134

Okamoto, H., Mizuno, K., and Horio, T. (2003). Monocyte-Derived Multinucleated Giant Cells and Sarcoidosis. *J. Dermatol. Sci.* 31, 119–128. doi:10.1016/s0923-1811(02)00148-2

Okamoto, K., and Takayanagi, H. (2019). Osteoimmunology. *Cold Spring Harb Perspect. Med.* 9, a031245. doi:10.1101/cshperspect.a031245

Pagán, A. J., and Ramakrishnan, L. (2018). The Formation and Function of Granulomas. *Annu. Rev. Immunol.* 36, 639–665. doi:10.1146/annurev-immunol-032712-100022

Paloneva, J., Mandelin, J., Kiialainen, A., Böhling, T., Prudlo, J., Hakola, P., et al. (2003). DAP12/TREM2 Deficiency Results in Impaired Osteoclast Differentiation and Osteoporotic Features. *J. Exp. Med.* 198, 669–675. doi:10.1084/jem.20030027

Park, S. J., Lee, J. Y., Lee, S. H., Koh, J.-M., and Kim, B.-J. (2019). SLIT2 Inhibits Osteoclastogenesis and Bone Resorption by Suppression of Cdc42 Activity. *Biochem. Biophysical Res. Commun.* 514, 868–874. doi:10.1016/j.bbrc.2019.05.046

Parthasarathy, V., Martin, F., Higginbottom, A., Murray, H., Moseley, G. W., Read, R. C., et al. (2009). Distinct Roles for Tetraspanins CD9, CD63 and CD81 in the Formation of Multinucleated Giant Cells. *Immunology* 127, 237–248. doi:10.1111/j.1365-2567.2008.02945.x

Pellegatti, P., Falzoni, S., Donvito, G., Lemaire, I., and Di Virgilio, F. (2011). P2X7 Receptor Drives Osteoclast Fusion by Increasing the Extracellular Adenosine Concentration. *FASEB j.* 25, 1264–1274. doi:10.1096/fj.10-169854

Peng, Q., Malhotra, S., Torchia, J. A., Kerr, W. G., Coggeshall, K. M., and Humphrey, M. B. (2010). TREM2- and DAP12-dependent Activation of PI3K Requires DAP10 and Is Inhibited by SHIP1. *Sci. Signal.* 3, ra38. doi:10.1126/scisignal.2000500

Pereira, M., Petretto, E., Gordon, S., Bassett, J. H. D., Williams, G. R., and Behmoaras, J. (2018). Common Signalling Pathways in Macrophage and Osteoclast Multinucleation. *J. Cel Sci.* 131, jcs216267. doi:10.1242/jcs.216267

Podolnikova, N. P., Hlavackova, M., Wu, Y., Yakubenko, V. P., Faust, J., Balabiyev, A., et al. (2019). Interaction between the Integrin Mac-1 and Signal Regulatory Protein α (SIRPα) Mediates Fusion in Heterologous Cells. *J. Biol. Chem.* 294, 7833–7849. doi:10.1074/jbc.RA118.006314

Podolnikova, N. P., Kushchayeva, Y. S., Wu, Y., Faust, J., and Ugarova, T. P. (2016). The Role of Integrins αMβ2 (Mac-1, CD11b/CD18) and αDβ2 (CD11d/CD18) in Macrophage Fusion. *Am. J. Pathol.* 186, 2105–2116. doi:10.1016/j.ajpath.2016.04.001

Poline, J., Fogel, O., Pajot, C., Miceli-Richard, C., Rybojad, M., Galeotti, C., et al. (2020). Early-onset Granulomatous Arthritis, Uveitis and Skin Rash: Characterization of Skin Involvement in Blau Syndrome. *J. Eur. Acad. Dermatol. Venereol.* 34, 340–348. doi:10.1111/jdv.15963

Quinn, M. T., and Schepetkin, I. A. (2009). Role of NADPH Oxidase in Formation and Function of Multinucleated Giant Cells. *J. Innate Immun.* 1, 509–526. doi:10.1159/000228158

Rao, H., Lu, G., Kajiya, H., Garcia-Palacios, V., Kurihara, N., Anderson, J., et al. (2006). α9β1: A Novel Osteoclast Integrin that Regulates Osteoclast Formation and Function. *J. Bone Miner Res.* 21, 1657–1665. doi:10.1359/jbmr.060718

Rosales, C., and Uribe-Querol, E. (2017). Phagocytosis: A Fundamental Process in Immunity. *Biomed. Res. Int.* 2017, 1–18. doi:10.1155/2017/9042851

Rose, C. D., Neven, B., and Wouters, C. (2014). Granulomatous Inflammation: The Overlap of Immune Deficiency and Inflammation. *Best Pract. Res. Clin. Rheumatol.* 28, 191–212. doi:10.1016/j.berh.2014.03.006

Saftig, P., Hunziker, E., Wehmeyer, O., Jones, S., Boyde, A., Rommerskirch, W., et al. (1998). Impaired Osteoclastic Bone Resorption Leads to Osteopetrosis in Cathepsin-K-Deficient Mice. *Proc. Natl. Acad. Sci. U.S.A.* 95, 13453–13458. doi:10.1073/pnas.95.23.13453

Saginario, C., Qian, H. Y., and Vignery, A. (1995). Identification of an Inducible Surface Molecule Specific to Fusing Macrophages. *Proc. Natl. Acad. Sci. U.S.A.* 92, 12210–12214. doi:10.1073/pnas.92.26.12210

Saginario, C., Sterling, H., Beckers, C., Kobayashi, R., Solimena, M., Ullu, E., et al. (1998). MFR, a Putative Receptor Mediating the Fusion of Macrophages. *Mol. Cel Biol* 18, 6213–6223. doi:10.1128/MCB.18.11.6213

Sakai, H., Okafuji, I., Nishikomori, R., Abe, J., Izawa, K., Kambe, N., et al. (2012). The CD40-Cd40l axis and IFN- Play Critical Roles in Langhans Giant Cell Formation. *Int. Immunol.* 24, 5–15. doi:10.1093/intimm/dxr088

Sangsri, T., Saiprom, N., Tubsuwan, A., Monk, P., Partridge, L. J., and Chantratita, N. (2020). Tetraspanins Are Involved in Burkholderia Pseudomallei-Induced Cell-To-Cell Fusion of Phagocytic and Non-phagocytic Cells. *Sci. Rep.* 10, 17972. doi:10.1038/s41598-020-74737-y

Savill, J. (1997). Recognition and Phagocytosis of Cells Undergoing Apoptosis. *Br. Med. Bull.* 53, 491–508. doi:10.1093/oxfordjournals.bmb.a011626

Sawamiphak, S., Seidel, S., Essmann, C. L., Wilkinson, G. A., Pitulescu, M. E., Acker, T., et al. (2010). Ephrin-B2 Regulates VEGFR2 Function in Developmental and Tumour Angiogenesis. *Nature* 465, 487–491. doi:10.1038/nature08995

Shapouri-Moghaddam, A., Mohammadian, S., Vazini, H., Taghadosi, M., Esmaeili, S. A., Mardani, F., et al. (2018). Macrophage Plasticity, Polarization, and Function in Health and Disease. *J. Cel. Physiol.* 233, 6425–6440. doi:10.1002/jcp.26429

Shashkova, E. V., Trivedi, J., Cline-Smith, A. B., Ferris, C., Buchwald, Z. S., Gibbs, J., et al. (2016). Osteoclast-Primed Foxp3+ CD8 T Cells Induce T-Bet, Eomesodermin, and IFN-γ to Regulate Bone Resorption. *J.I.* 197, 726–735. doi:10.4049/jimmunol.1600253

Sheikh, Z., Brooks, P., Barzilay, O., Fine, N., and Glogauer, M. (2015). Macrophages, Foreign Body Giant Cells and Their Response to Implantable Biomaterials. *Materials* 8, 5671–5701. doi:10.3390/ma8095269

Shin, H.-W., and Takatsu, H. (2020). Phosphatidylserine Exposure in Living Cells. *Crit. Rev. Biochem. Mol. Biol.* 55, 166–178. doi:10.1080/10409238.2020.1758624

Skokos, E. A., Charokopos, A., Khan, K., Wanjala, J., and Kyriakides, T. R. (2011). Lack of TNF-α-Induced MMP-9 Production and Abnormal E-Cadherin Redistribution Associated with Compromised Fusion in MCP-1-Null Macrophages. *Am. J. Pathol.* 178, 2311–2321. doi:10.1016/j.ajpath.2011.01.045

Smetana, K. (1987). Multinucleate Foreign-Body Giant Cell Formation. *Exp. Mol. Pathol.* 46, 258–265. doi:10.1016/0014-4800(87)90048-7

Sørensen, M. G., Henriksen, K., Neutzsky-Wulff, A. V., Dziegiel, M. H., and Karsdal, M. A. (2007). Diphyllin, a Novel and Naturally Potent V-ATPase Inhibitor, Abrogates Acidification of the Osteoclastic Resorption Lacunae and Bone Resorption. *J. Bone Miner. Res.* 22, 1640–1648. doi:10.1359/JBMR.070613

Speziani, C., Rivollier, A., Gallois, A., Coury, F., Mazzorana, M., Azocar, O., et al. (2007). Murine Dendritic Cell Transdifferentiation into Osteoclasts Is Differentially Regulated by Innate and Adaptive Cytokines. *Eur. J. Immunol.* 37, 747–757. doi:10.1002/eji.200636534

Sprent, J. (2005). Direct Stimulation of Naïve T Cells by Antigen-Presenting Cell Vesicles. *Blood Cell Mol. Dis.* 35, 17–20. doi:10.1016/j.bcmd.2005.04.004

Stark, Z., and Savarirayan, R. (2009). Osteopetrosis. *Orphanet J. Rare Dis.* 4, 5. doi:10.1186/1750-1172-4-5

Steinberg, T. H., and Hiken, J. F. (2007). P2 Receptors in Macrophage Fusion and Osteoclast Formation. *Purinergic Signal.* 3, 53–57. doi:10.1007/s11302-006-9036-9

Stenbeck, G. (2002). Formation and Function of the Ruffled Border in Osteoclasts. *Semin. Cel Developmental Biol.* 13, 285–292. doi:10.1016/s1084952102000587

Strick, R., Ackermann, S., Langbein, M., Swiatek, J., Schubert, S. W., Hashemolhosseini, S., et al. (2006). Proliferation and Cell-Cell Fusion of Endometrial Carcinoma Are Induced by the Human Endogenous Retroviral Syncytin-1 and Regulated by TGF-β. *J. Mol. Med.* 85, 23–38. doi:10.1007/s00109-006-0104-y

Sun, Q., Liu, C., Bai, X., and Huo, B. (2020). Cell-substrate Traction Force Regulates the Fusion of Osteoclast Precursors through Cell-Cell Interaction. *Biomech. Model. Mechanobiol.* 19, 481–492. doi:10.1007/s10237-019-01223-4

Supanchart, C., and Kornak, U. (2008). Ion Channels and Transporters in Osteoclasts. *Arch. Biochem. Biophys.* 473, 161–165. doi:10.1016/j.abb.2008.03.029

Takaki, R., Watson, S. R., and Lanier, L. L. (2006). DAP12: An Adapter Protein with Dual Functionality. *Immunol. Rev.* 214, 118–129. doi:10.1111/j.1600-065X.2006.00466.x

Takeda, Y., Tachibana, I., Miyado, K., Kobayashi, M., Miyazaki, T., Funakoshi, T., et al. (2003). Tetraspanins CD9 and CD81 Function to Prevent the Fusion of Mononuclear Phagocytes. *J. Cel Biol.* 161, 945–956. doi:10.1083/jcb.200212031

Takito, J., Otsuka, H., Yanagisawa, N., Arai, H., Shiga, M., Inoue, M., et al. (2015). Regulation of Osteoclast Multinucleation by the Actin Cytoskeleton Signaling Network. *J. Cel. Physiol.* 230, 395–405. doi:10.1002/jcp.24723

Tamma, R., and Zallone, A. (2012). Osteoblast and Osteoclast Crosstalks: From OAF to Ephrin. *Iadt* 11, 196–200. doi:10.2174/187152812800392670

Taniwaki, N. N., and Katchburian, E. (1998). Ultrastructural and Lanthanum Tracer Examination of Rapidly Resorbing Rat Alveolar Bone Suggests that Osteoclasts Internalize Dying Bone Cells. *Cel Tissue Res.* 293, 173–176. doi:10.1007/s004410051109

ten Harkel, B., Koopsen, J., van Putten, S. M., van Veen, H., Picavet, D. I., de Vries, T. J., et al. (2016). Ultrastructural Aspects of Foreign Body Giant Cells Generated on Different Substrates. *J. Struct. Biol.* 195, 31–40. doi:10.1016/j.jsb.2016.04.016

ten Harkel, B., Schoenmaker, T., Picavet, D. I., Davison, N. L., de Vries, T. J., and Everts, V. (2015). The Foreign Body Giant Cell Cannot Resorb Bone, but Dissolves Hydroxyapatite like Osteoclasts. *PLoS One* 10, e0139564. doi:10.1371/journal.pone.0139564

Tessarz, A. S., and Cerwenka, A. (2008). The TREM-1/DAP12 Pathway. *Immunol. Lett.* 116, 111–116. doi:10.1016/j.imlet.2007.11.021

Teti, A. (2013). Mechanisms of Osteoclast-dependent Bone Formation. *Bonekey Rep.* 2, 449. doi:10.1038/bonekey.2013.183

Timmermans, W. M. C., van Laar, J. A. M., van Hagen, P. M., and van Zelm, M. C. (2016). Immunopathogenesis of Granulomas in Chronic Autoinflammatory Diseases. *Clin. Trans. Immunol.* 5, e118. doi:10.1038/cti.2016.75

Tombran-Tink, J., and Barnstable, C. J. (2004). Osteoblasts and Osteoclasts Express PEDF, VEGF-A Isoforms, and VEGF Receptors: Possible Mediators of Angiogenesis and Matrix Remodeling in the Bone. *Biochem. Biophysical Res. Commun.* 316, 573–579. doi:10.1016/j.bbrc.2004.02.076

Touaitahuata, H., Blangy, A., and Vives, V. (2014). Modulation of Osteoclast Differentiation and Bone Resorption by Rho GTPases. *Small GTPases* 5, e28119. doi:10.4161/sgtp.28119

Touaitahuata, H., Planus, E., Albiges-Rizo, C., Blangy, A., and Pawlak, G. (2013). Podosomes Are Dispensable for Osteoclast Differentiation and Migration. *Eur. J. Cel Biol.* 92, 139–149. doi:10.1016/j.ejcb.2013.03.001

Väänänen, H. K., Karhukorpi, E. K., Sundquist, K., Wallmark, B., Roininen, I., Hentunen, T., et al. (1990). Evidence for the Presence of a Proton Pump of the Vacuolar H(+)-ATPase Type in the Ruffled Borders of Osteoclasts. *J. Cel Biol.* 111, 1305–1311. doi:10.1083/jcb.111.3.1305

van Beek, E. M., Vries, T. J., Mulder, L., Schoenmaker, T., Hoeben, K. A., Matozaki, T., et al. (2009). Inhibitory Regulation of Osteoclast Bone Resorption by Signal Regulatory Protein α. *FASEB J.* 23, 4081–4090. doi:10.1096/fj.09-131557

Van den Bossche, J., Bogaert, P., van Hengel, J., Guérin, C. J., Berx, G., Movahedi, K., et al. (2009). Alternatively Activated Macrophages Engage in Homotypic and Heterotypic Interactions through IL-4 and Polyamine-Induced E-Cadherin/Catenin Complexes. *Blood* 114, 4664–4674. doi:10.1182/blood-2009-05-221598

Van den Bossche, J., Malissen, B., Mantovani, A., De Baetselier, P., and Van Ginderachter, J. A. (2012). Regulation and Function of the E-Cadherin/Catenin Complex in Cells of the Monocyte-Macrophage Lineage and DCs. *Blood* 119, 1623–1633. doi:10.1182/blood-2011-10-384289

van der Rhee, H. J., van der Burgh-de Winter, C. P. M., and Daems, W. T. (1979). The Transformation of Langhans Giant Cells into Foreign Body Giant Cells. *Ultramicroscopy* 4, 147. doi:10.1016/0304-3991(79)90092-5

van Niekerk, G., Mitchell, M., and Engelbrecht, A.-M. (2018). Bone Resorption: Supporting Immunometabolism. *Biol. Lett.* 14, 20170783. doi:10.1098/rsbl.2017.0783

van Roy, F., and Berx, G. (2008). The Cell-Cell Adhesion Molecule E-Cadherin. *Cell. Mol. Life Sci.* 65, 3756–3788. doi:10.1007/s00018-008-8281-1

van Wachem, P. B., van Luyn, M. J. A., Nieuwenhuis, P., Koerten, H. K., Damink, L. O., Hoopen, H. T., et al. (1991). *In Vivo* Degradation of Processed Dermal Sheep Collagen Evaluated with Transmission Electron Microscopy. *Biomaterials* 12, 215–223. doi:10.1016/0142-9612(91)90203-m

Varol, C., Mildner, A., and Jung, S. (2015). Macrophages: Development and Tissue Specialization. *Annu. Rev. Immunol.* 33, 643–675. doi:10.1146/annurev-immunol-032414-112220

Veauthier, B., and Hornecker, J. R. (2018). Crohn's Disease: Diagnosis and Management. *Am. Fam. Physician* 98, 661–669. doi:10.1016/j.imlet.2007.11.021

Verma, S. K., Leikina, E., Melikov, K., Gebert, C., Kram, V., Young, M. F., et al. (2018). Cell-Surface Phosphatidylserine Regulates Osteoclast Precursor Fusion. *J. Biol. Chem.* 293, 254–270. doi:10.1074/jbc.M117.809681

Vignery, A. (2005b). Macrophage Fusion. *J. Exp. Med.* 202, 337–340. doi:10.1084/jem.20051123

Vignery, A. (2005a). Macrophage Fusion: Are Somatic and Cancer Cells Possible Partners? *Trends Cel Biol.* 15, 188–193. doi:10.1016/j.tcb.2005.02.008

Vignery, A. (2000). Osteoclasts and Giant Cells: Macrophage-Macrophage Fusion Mechanism Current Status Review: Granulatomous Disease. *Int. J. Exp. Pathol.* 81, 291–304. doi:10.1046/j.1365-2613.2000.00164.x

Wanat, K. A., Rosenbach, M., Zoiber, A. F., Zhang, P. J., and Schaffer, A. (2014). E-cadherin Is Expressed by Mono- and Multinucleated Histiocytes in Cutaneous Sarcoidal and Foreign Body Granulomas. *Am. J. Dermatopathol* 36, 651–654. doi:10.1097/DAD.0b013e31828de7e0

Wang, H., Jiang, H., Teles, R. M. B., Chen, Y., Wu, A., Lu, J., et al. (2020). Cellular, Molecular, and Immunological Characteristics of Langhans Multinucleated Giant Cells Programmed by IL-15. *J. Invest. Dermatol.* 140, 1824–1836. e7. doi:10.1016/j.jid.2020.01.026

Wang, H., Zhou, J., Li, J., Geng, Y., Meng, P., Ma, C., et al. (2021). A Study of Multinucleated Giant Cells in Esophageal Cancer. *Clin. Immunol.* 222, 108600. doi:10.1016/j.clim.2020.108600

Wang, W., Ferguson, D. J. P., Quinn, J. M. W., Simpson, A. H. R. W., and Athanasou, N. A. (1997). Osteoclasts Are Capable of Particle Phagocytosis and Bone Resorption. *J. Pathol.* 182, 92–98. doi:10.1002/(sici)1096-9896(199705)182:1<92::aid-path813>3.0.co;2-e

Wang, Y., Brooks, P. J., Jang, J. J., Silver, A. S., Arora, P. D., Mcculloch, C. A., et al. (2015). Role of Actin Filaments in Fusopod Formation and Osteoclastogenesis. *Biochim. Biophys. Acta (Bba) - Mol. Cel Res.* 1853, 1715–1724. doi:10.1016/j.bbamcr.2015.04.001

Wang, Y., Lebowitz, D., Sun, C., Thang, H., Grynpas, M. D., and Glogauer, M. (2008). Identifying the Relative Contributions of Rac1 and Rac2 to Osteoclastogenesis. *J. Bone Miner Res.* 23, 260–270. doi:10.1359/JBMR.071013

Wang, Y., Nakayama, M., Pitulescu, M. E., Schmidt, T. S., Bochenek, M. L., Sakakibara, A., et al. (2010). Ephrin-B2 Controls VEGF-Induced Angiogenesis and Lymphangiogenesis. *Nature* 465, 483–486. doi:10.1038/nature09002

Weiskirchen, R., Weiskirchen, S., and Tacke, F. (2019). Organ and Tissue Fibrosis: Molecular Signals, Cellular Mechanisms and Translational Implications. *Mol. Aspects Med.* 65, 2–15. doi:10.1016/j.mam.2018.06.003

Whitlock, J. M., and Chernomordik, L. V. (2021). Flagging Fusion: Phosphatidylserine Signaling in Cell-Cell Fusion. *J. Biol. Chem.* 296, 100411. doi:10.1016/j.jbc.2021.100411

Woo, J., Ohba, Y., Tagami, K., Sumitani, K., Yamaguchi, K., and Tsuji, T. (1996). Concanamycin B, a Vacuolar H+-ATPase Specific Inhibitor Suppresses Bone Resorption *In Vitro*. *Biol. Pharm. Bull.* 19, 297–299. doi:10.1248/bpb.19.297

Wooley, P., and Schwarz, E. (2004). Aseptic Loosening. *Gene Ther.* 11, 402–407. doi:10.1038/sj.gt.3302202

Wouters, C. H., Maes, A., Foley, K. P., Bertin, J., and Rose, C. D. (2014). Blau Syndrome, the Prototypic Auto-Inflammatory Granulomatous Disease. *Pediatr. Rheumatol.* 12, 33. doi:10.1186/1546-0096-12-33

Wu, L., Luo, Z., Liu, Y., Jia, L., Jiang, Y., Du, J., et al. (2019). Aspirin Inhibits RANKL-Induced Osteoclast Differentiation in Dendritic Cells by Suppressing NF-Kb and NFATc1 Activation. *Stem Cel Res. Ther.* 10, 375. doi:10.1186/s13287-019-1500-x

Wynn, T. A., and Ramalingam, T. R. (2012). Mechanisms of Fibrosis: Therapeutic Translation for Fibrotic Disease. *Nat. Med.* 18, 1028–1040. doi:10.1038/nm.2807

Wynn, T. A., and Vannella, K. M. (2016). Macrophages in Tissue Repair, Regeneration, and Fibrosis. *Immunity* 44, 450–462. doi:10.1016/j.immuni.2016.02.015

Xie, H., Cui, Z., Wang, L., Xia, Z., Hu, Y., Xian, L., et al. (2014). PDGF-BB Secreted by Preosteoclasts Induces Angiogenesis during Coupling with Osteogenesis. *Nat. Med.* 20, 1270–1278. doi:10.1038/nm.3668

Xu, X., Lai, Y., and Hua, Z.-C. (2019). Apoptosis and Apoptotic Body: Disease Message and Therapeutic Target Potentials. *Biosci. Rep.* 39, BSR20180992. doi:10.1042/BSR20180992

Xue, J., Zhu, Y., Sun, Z., Ji, R., Zhang, X., Xu, W., et al. (2015). Tumorigenic Hybrids between Mesenchymal Stem Cells and Gastric Cancer Cells Enhanced Cancer Proliferation, Migration and Stemness. *BMC Cancer* 15, 793. doi:10.1186/s12885-015-1780-1

Yagi, M., Miyamoto, T., Sawatani, Y., Iwamoto, K., Hosogane, N., Fujita, N., et al. (2005). DC-STAMP Is Essential for Cell-Cell Fusion in Osteoclasts and Foreign Body Giant Cells. *J. Exp. Med.* 202, 345–351. doi:10.1084/jem.20050645

Yagi, M., Miyamoto, T., Toyama, Y., and Suda, T. (2006). Role of DC-STAMP in Cellular Fusion of Osteoclasts and Macrophage Giant Cells. *J. Bone Miner Metab.* 24, 355–358. doi:10.1007/s00774-006-0697-9

Yagi, M., Ninomiya, K., Fujita, N., Suzuki, T., Iwasaki, R., Morita, K., et al. (2007). Induction of DC-STAMP by Alternative Activation and Downstream Signaling Mechanisms. *J. Bone Miner Res.* 22, 992–1001. doi:10.1359/JBMR.070401

Yang, J., Jao, B., Mcnally, A. K., and Anderson, J. M. (2014). In Vivoquantitative and Qualitative Assessment of Foreign Body Giant Cell Formation on Biomaterials in Mice Deficient in Natural Killer Lymphocyte Subsets, Mast Cells, or the Interleukin-4 Receptorα and in Severe Combined Immunodeficient Mice. *J. Biomed. Mater. Res.* 102, 2017–2023. doi:10.1002/jbm.a.35152

Yasui, K., Yashiro, M., Tsuge, M., Kondo, Y., Saito, Y., Nagaoka, Y., et al. (2011). Tumor Necrosis Factor-α Can Induce Langhans-type Multinucleated Giant Cell Formation Derived from Myeloid Dendritic Cells. *Microbiol. Immunol.* 55, 809–816. doi:10.1111/j.1348-0421.2011.00380.x

Ye, Q., Harmsen, M. C., Ren, Y., and Bank, R. A. (2011). The Role of Collagen Receptors Endo180 and DDR-2 in the Foreign Body Reaction against Non-crosslinked Collagen and Gelatin. *Biomaterials* 32, 1339–1350. doi:10.1016/j.biomaterials.2010.09.076

Yunna, C., Mengru, H., Lei, W., and Weidong, C. (2020). Macrophage M1/M2 Polarization. *Eur. J. Pharmacol.* 877, 173090. doi:10.1016/j.ejphar.2020.173090

Zaidi, M., Troen, B., Moonga, B. S., and Abe, E. (2001). Cathepsin K, Osteoclastic Resorption, and Osteoporosis Therapy. *J. Bone Miner Res.* 16, 1747–1749. doi:10.1359/jbmr.2001.16.10.1747

Zeng, Z., Zhang, C., and Chen, J. (2013). Lentivirus-Mediated RNA Interference of DC-STAMP Expression Inhibits the Fusion and Resorptive Activity of Human Osteoclasts. *J. Bone Miner Metab.* 31, 409–416. doi:10.1007/s00774-013-0434-0

Zhang, C., Dou, C., Xu, J., and Dong, S. (2014). DC-STAMP, the Key Fusion-Mediating Molecule in Osteoclastogenesis. *J. Cel. Physiol* 229, 1330–1335. doi:10.1002/jcp.24553

Zhang, W., Huang, Q., Xiao, W., Zhao, Y., Pi, J., Xu, H., et al. (2020). Advances in Anti-tumor Treatments Targeting the CD47/SIRPα Axis. *Front. Immunol.* 11, 18. doi:10.3389/fimmu.2020.00018

Zhao, C., Irie, N., Takada, Y., Shimoda, K., Miyamoto, T., Nishiwaki, T., et al. (2006). Bidirectional EphrinB2-EphB4 Signaling Controls Bone Homeostasis. *Cel Metab.* 4, 111–121. doi:10.1016/j.cmet.2006.05.012

Zhu, F., Friedman, M. S., Luo, W., Woolf, P., and Hankenson, K. D. (2012). The Transcription Factor Osterix (SP7) Regulates BMP6-Induced Human Osteoblast Differentiation. *J. Cel. Physiol.* 227, 2677–2685. doi:10.1002/jcp.23010

Zou, W., and Teitelbaum, S. L. (2015). Absence of Dap12 and the αvβ3 Integrin Causes Severe Osteopetrosis. *J. Cel Biol.* 208, 125–136. doi:10.1083/jcb.201410123

Zumla, A., and James, D. G. (1996). Granulomatous Infections: Etiology and Classification. *Clin. Infect. Dis.* 23, 146–158. doi:10.1093/clinids/23.1.146

Conflict of Interest: CW obtained unrestricted grants to KU Leuven from Novartis, Roche, GSK immuno-inflammation and Pfizer.

The remaining authors declare that the research was conducted in the absence of any commercial or financial relationships that could be construed as a potential conflict of interest.

Publisher's Note: All claims expressed in this article are solely those of the authors and do not necessarily represent those of their affiliated organizations, or those of the publisher, the editors and the reviewers. Any product that may be evaluated in this article, or claim that may be made by its manufacturer, is not guaranteed or endorsed by the publisher.

frontiers | Frontiers in Cell and Developmental Biology

ORIGINAL RESEARCH
published: 19 April 2022
doi: 10.3389/fcell.2022.796227

Acacetin Prevents Bone Loss by Disrupting Osteoclast Formation and Promoting Type H Vessel Formation in Ovariectomy-Induced Osteoporosis

Xiao Lin[1], Fang Xu[1], Ke-Wen Zhang[1], Wu-Xia Qiu[1], Hui Zhang[1], Qiang Hao[2], Meng Li[2], Xiao-Ni Deng[1], Ye Tian[1], Zhi-Hao Chen[1]* and Ai-Rong Qian[1]**

[1]Lab for Bone Metabolism, Xi'an Key Laboratory of Special Medicine and Health Engineering, Key Lab for Space Biosciences and Biotechnology, Research Center for Special Medicine and Health Systems Engineering, NPU-UAB Joint Laboratory for Bone Metabolism, School of Life Sciences, Northwestern Polytechnical University, Xi'an, China, [2]State Key Laboratory of Cancer Biology, Biotechnology Center, School of Pharmacy, Fourth Military Medical University, Xi'an, China

OPEN ACCESS

Edited by:
Stefania Mariggiò, National Research Council (CNR), Italy

Reviewed by:
Julia Charles, Brigham and Women's Hospital and Harvard Medical School, United States
Raj Gopalakrishnan, University of Minnesota Twin Cities, United States

***Correspondence:**
Ye Tian
tianye@nwpu.edu.cn
Zhi-Hao Chen
chenzhihao@nwpu.edu.cn
Ai-Rong Qian
qianair@nwpu.edu.cn

Specialty section:
This article was submitted to Cellular Biochemistry, a section of the journal Frontiers in Cell and Developmental Biology

Received: *16 October 2021*
Accepted: *01 April 2022*
Published: *19 April 2022*

Citation:
Lin X, Xu F, Zhang K-W, Qiu W-X, Zhang H, Hao Q, Li M, Deng X-N, Tian Y, Chen Z-H and Qian A-R (2022) Acacetin Prevents Bone Loss by Disrupting Osteoclast Formation and Promoting Type H Vessel Formation in Ovariectomy-Induced Osteoporosis. Front. Cell Dev. Biol. 10:796227. doi: 10.3389/fcell.2022.796227

Osteoporosis, characterized by the destruction of bone resorption and bone formation, is a serious disease that endangers human health. Osteoporosis prevention and treatment has become one of the important research contents in the field of medicine. Acacetin, a natural flavonoid compound, could promote osteoblast differentiation, and inhibit osteoclast formation *in vitro*. However, the mechanisms of acacetin on osteoclast differentiation and type H vessel formation, as well as the effect of preventing bone loss, remain unclear. Here, we firstly used primary bone marrow derived macrophages (BMMs), endothelial progenitor cells (EPCs), and ovariectomized (OVX) mice to explore the function of acacetin on bone remodeling and H type vessel formation. In this study, we found that acacetin inhibits osteoclast formation and bone resorption of BMMs induced by the macrophage colony stimulating factor (M-CSF) and receptor activator of nuclear factor-κB ligand (RANKL) in a concentration of 20 μM without exerting cytotoxic effects. It was accompanied by downregulation of osteoclast differentiation marker genes (*Ctsk*, *Acp5*, and *Mmp9*) and cell fusion genes (*CD9*, *CD47*, *Atp6v0d2*, *Dc-stamp*, and *Oc-stamp*). Moreover, acacetin disrupted actin ring formation and extracellular acidification in osteoclasts. Mechanistic analysis revealed that acacetin not only inhibits the expression of the major transcription factor NFATc1 and NF-κB during RANKL-induced osteoclast formation, but also suppresses RANKL-induced the phosphorylation of Akt, GSK3β, IκBα, and p65. Additionally, acacetin enhanced the ability of M-CSF and RANKL-stimulated BMMs to promote angiogenesis and migration of EPCs. We further established that, *in vivo*, acacetin increased trabecular bone mass, decreased the number of osteoclasts, and showed more type H vessels in OVX mice. These data demonstrate that acacetin prevents OVX-induced bone loss in mice through inhibition of osteoclast function and promotion of type H vessel formation *via* Akt/GSK3β and NF-κB signalling pathway, suggesting that acacetin may be a novel therapeutic agent for the treatment of osteoporosis.

Keywords: acacetin, osteoporosis, osteoclasts, type H vessel, Akt/GSK3β, NF-κB

1 INTRODUCTION

Osteoporosis is a chronic bone disease characterized by destruction of bone microstructure and low bone mass, leading to increased bone fragility and thus increased fracture susceptibility (Chujiao Lin et al., 2019). Bone resorption mediated by osteoclasts exceeds bone formation mediated by osteoblasts, which is one of the potential mechanisms of osteoporosis (Qiang Xu et al., 2021). Studies have shown that 50% of women will suffer fractures due to osteoporosis in their lifetimes (Beekman et al., 2019). Therefore, the prevention and treatment of osteoporosis has become a focus of medical and health research. In the treatment of osteoporosis, antiresorptive drugs, including bisphosphonates (alendronate, zoledronate, etc.) and denosumab, increase bone mineral density and reduce the risk of fracture by inhibiting osteoclast-mediated resorption (Leder et al., 2020). However, the cost of Western medicine therapy is high, and the clinical side effects are uncertain, such as fever, joint myalgia, hypocalcaemia, and other potential adverse events (Meng et al., 2020). Therefore, the use of traditional Chinese medicine, which has the concomitant function of both medicine and foodstuff in the treatment of osteoporosis, has the advantages of low cost and fewer side effects (Shi et al., 2020).

Osteoclasts are multinucleated cells, that differentiate from monocytes/macrophages in the presence of M-CSF and RANKL (Xiao Lin et al., 2019). When RANKL activates the receptor activator of nuclear factor-κB (RANK), the inner membrane portion of RANK reacts with tumour necrosis factor receptor-associated factor 6 (TRAF6) and activates a series of downstream signalling pathways, including AKT, nuclear factor-κB (NF-κB), mitogen-activated protein kinase (MAPK), and calcium signalling pathways (Delong Chen et al., 2020). Furthermore, the differentiation, survival, multinucleation, and activation of osteoclasts are regulated by these pathways (Dai et al., 2017). In recent years, type H vessels, a special subtype of vessel with strong expression of CD31 and EMCN in endothelial cells, have been identified to couple the balance of bone absorption and formation (Xie et al., 2014). Mononuclear preosteoclasts can promote the growth of type H vessels by releasing platelet-derived growth factor-BB (PDGF-BB) prior to multinucleated osteoclast formation (Xiaoqun Li et al., 2020). Moreover, the number of type H vessels decreases with age to a degree consistent with the severity of bone loss (Song et al., 2020). Therefore, by simultaneously interrupting the maturation and activation of osteoclasts, inhibiting bone resorption and promoting the formation of type H blood vessels, osteoporosis can be effectively prevented.

Flavonoids are abundant in many common vegetables, fruits, grains, and herbs. They have potential therapeutic properties due to their antioxidant, anti-inflammatory, differentiation, and apoptotic properties (Bellavia et al., 2021). The intake of flavonoids increases bone mineral density (BMD), reduces bone resorption in perimenopausal women, and maintains bone health (Hardcastle et al., 2011; Zhang et al., 2014). Many flavonoid compounds have been evaluated as potential alternative therapeutic candidates against bone resorptive diseases, such as cladrin, icariin, petunidin, and epiafzelechin (Bellavia et al., 2021; Yingxing Xu et al., 2021). Acacetin (5,7-dihydroxy-4-methoxyflavone) is a flavonoid compound that can be isolated from Damiana, Saussurea involucrata plant, and black locust plants (Ren et al., 2020). It exerts pronounced anti-inflammatory, anti-peroxidative, and anti-cancer activities (Wang et al., 2020). Interestingly, acacetin has been reported to promote osteoblastic differentiation and mineralization (Li et al., 2016) and inhibit osteoclastic differentiation *in vitro* (Kim et al., 2020). However, the effect of acacetin on the formation of osteoclasts and type H vessels, and its protective function in boss loss *in vivo* are still unclear.

In this study, we investigated the effects and mechanism of acacetin on RANKL-mediated osteoclastogenesis and elucidated whether this compound could attenuate osteoclast formation and promote type H vessel formation in OVX mice. Our results demonstrated that acacetin inhibits osteoclastogenesis and bone resorption through suppression of the Akt/GSK3β and NF-κB signalling pathways, as well as stimulation of type H vessels cocultured with osteoclasts, thereby preventing the OVX-induced bone loss *in vivo*.

2 MATERIALS AND METHODS

2.1 Reagents and Antibodies

Acacetin (PubChem CID: 5280442) (purity >98%, HPLC) was purchased from Herbest Bio-Tech Co., Ltd. (Baoji, China). Alpha-minimal essential medium (α-MEM) was obtained from Gibco (Rockville, MD, United States). Foetal bovine serum (FBS) was obtained from HyClone (MA, United States). M-CSF and RANKL were provided by R&D (R&D Systems, MN, United States). Sodium carboxymethyl cellulose (CMC-Na), peroxidase conjugate-wheat germ agglutinin (WGA) (L3892), FITC-WGA (L4895), acid phosphatase, leukocyte (TRAP) kit, rhodamine-conjugated phalloidin, acridine orange, and dimethylsulfoxide (DMSO) were obtained from Sigma-Aldrich (St Louis, MO, United States). Antibodies against CTSK (sc-48353), ACP5 (sc-376875), MMP9 (sc-13520), NFATc1 (sc-7294), PI3K (sc-376112), p-Akt (sc-293125), Akt (sc-81434), p-GSK3β (sc-373800), GSK3β (sc-53931), p-IκBα (sc-8404), IκBα (sc-1643), p-NF-κB p65 (sc-136548), NF-κB p65 (sc-8008), p-ERK (sc-81492), ERK (sc-514302), p-JNK (sc-6254), JNK (sc-7345), p-p38 (sc-7973), p38 (sc-7972), CD31 (365804), EMCN (sc-65495), PDGF-BB (sc-365805), TRAP (sc-376875), and GAPDH (sc-166574) were obtained from Santa Cruz Biotechnology (CA, United States). ECL chemiluminescence reagents were obtained from Pierce Biotechnology (Rockford, IL, United States). The DAB Horseradish Peroxidase Colour Development Kit, One Step TUNEL Apoptosis Assay Kit, Calcein AM, 4′,6-diamidino-2-phenylindole (DAPI), paraformaldehyde (PFA), ethylenediaminetetraacetic acid (EDTA), Haematoxylin and Eosin (H&E) Staining Kit, horseradish peroxidase (HRP)-conjugated IgG, RIPA Lysis Buffer, Calcein AM, and Triton X-100 were obtained from Beyotime Biotechnology (Jiangsu, China). Matrigel was obtained from BD (Franklin Lakes, NJ, United States). TRIzol reagent and methyl thiazolyl tetrazolium (MTT) were obtained

from Invitrogen (Rockville, MD, United States). A one-step PrimeScript RT reagent kit and SYBR Premix Ex TaqIIkit were provided by TaKaRa (Dalian, China). A mouse PDGF-BB ELISA kit was obtained from Jingmei Biotechnology (Jiangsu, China). A glutamic-oxalacetic transaminase (GOT/AST) activity assay kit, glutamic-pyruvic transaminase (GPT/ALT) activity assay kit, urea nitrogen assay kit, and creatinine (CREA) assay kit were obtained from Sangon Biotech (Shanghai, China).

2.2 Cell Culture

Primary bone marrow derived macrophages (BMMs) were isolated from the femur and tibia of six-week-old C57BL/6J mice by flushing the marrow with a syringe and then cultured in α-MEM supplemented with 10% FBS, 100 U/mL penicillin and 100 μg/ml streptomycin in the presence of 5 ng/mL M-CSF for 24 h. Then, cells in the supernatant were collected as primary BMMs and seeded for osteoclastogenic differentiation induction. Osteoclastogenesis of BMMs was induced by conditioned medium in α-MEM supplemented with 10% FBS, 100 μg/ml streptomycin and 100 U/mL penicillin in the presence of 10 ng/mL M-CSF and 10 ng/ml RANKL. The cells were seeded into 24-well plates at a density of 2×10^5/well and induced with conditioned medium for 4 days in a 5% CO_2 incubator at 37°C.

Endothelial progenitor cells (EPCs) (Newgainbio, China) were culture in endothelial growth medium-2 (EGM-2) (Lonza). Endothelial basal medium-2 (EBM-2; Lonza) was used for experiments that do not require growth factors. The cells were incubated at 37°C in a 5% CO_2 incubator.

The MC3T3-E1 osteoblastic cell line were cultured in α-MEM supplemented with 10% FBS, 100 U/mL penicillin and 100 μg/ml streptomycin and incubated at 37°C in a 5% CO_2 incubator.

2.3 Cytotoxicity Assay

BMMs were seeded into 96-well plates at a density of 4×10^4/well, and cultured with α-MEM supplied with 5 ng/mL M-CSF and treated with various concentrations of acacetin (0, 1, 5, 10, 20, 50, and 100 μM). After 24 and 48 h of incubation, 0.5 mg/ml MTT was added to each well and incubated for 3 h at 37°C. Then, DMSO was used to dissolve the formazan crystals, and the optical density was measured at a wavelength of 490 nm using a microplate analyser (BioTek, United States).

2.4 TUNEL Staining

BMMs were seeded into 24-well plates at a density of 2×10^5/well, cultured with α-MEM supplied with 5 ng/mL M-CSF and treated with various concentrations of acacetin (0, 5, 10, 20, 50, and 100 μM). After 24 and 48 h of incubation, the TUNEL staining assay was performed using a One Step TUNEL Apoptosis Assay Kit. In brief, BMMs were washed once with precooled PBS for 3–5 min. Then, the cells were fixed in 4% PFA for 30 min and washed again with precooled PBS. The cells were permeabilized with 0.3% Triton X-100 for 5 min and washed with PBS twice. After adding 50 μL TUNEL solution/well, the samples were developed in the dark for 1 h at 37°C, washed 3 times with precooled PBS and observed using an inverted fluorescence microscope (Leica, Wetzlar, Germany). The apoptosis rate of in randomly chosen areas was quantified using ImageJ software.

TABLE 1 | Primer sequences used in real-time PCR.

Gene	Primer sequences
Acp5	Forward: 5′-TCCGTGCTCGGCGATGGACCAGA-3′
	Reverse: 5′-CTGGAGTGCACGATGCCAGCGACA-3′
CtsK	Forward: 5′-AGGCATTGACTCTGAAGATGCT-3′
	Reverse: 5′-TCCCCACAGGAATCTCTCTG-3′
Mmp9	Forward: 5′-GCGGCCCTCAAAGATGAACGG-3′
	Reverse: 5′-GCTGACTACGATAAGGACGGCA-3′
CD9	Forward: 5′-CGGTCAAAGGAGGTAG-3′
	Reverse: 5′-GGAGCCATAGTCCAATA-3′
CD47	Forward: 5′-TGGTGGGAAACTACACTTGCGA-3′
	Reverse: 5′-AGGCTGATCCTTGGTCAGTGTTG-3′
Atp6v0d2	Forward: 5′-TCAGATCTCTTCAAGGCTGTGCTG-3′
	Reverse: 5′-GTGCCAAATGAGTTCAGAGTGATG-3′
Dc-stamp	Forward: 5′-GGGCACCAGTATTTTCCTGA-3′
	Reverse: 5′-CAGAACGGCCAGAAGAATGA-3′
Oc-stamp	Forward: 5′-GGGCTACTGGCATTGCTCTTAGT-3′
	Reverse: 5′-CCAGAACCTTATATGAGGCGTCA-3′
Atp6i	Forward: 5′-CACAGGGTCTGCTTACAACTG-3′
	Reverse: 5′-CGTCTACCACGAAGCGTCTC-3′
c-Fos	Forward: 5′ACTTCTTGTTTCCGGC-3′
	Reverse: 5′-AGCTTCAGGGTAGGTG-3′
Pu.1	Forward: 5′-ACTCCTTCGTGGGCAGCGATGGAG-3′
	Reverse: 5′-GGGAAGCACATCCGGGGCATGTAG-3′
Nfatc1	Forward: 5′-GAGAATCGAGATCACCTCCTAC-3′
	Reverse: 5′-TTGCAGCTAGGAAGTACGTCTT-3′
Nf-κb p65	Forward: 5′-CAAAGACAAAGAGGAAGTGCAA-3′
	Reverse: 5′-GATGGAATGTAATCCCACCGTA-3′
Rankl	Forward: 5′-GGAAGCGTACCTACAGACTATC-3′
	Reverse: 5′-AAAGTGGAATTCAGAATTGCCC-3′
Opg	Forward: 5′-ACCAGTGATGAGTGTGTGTATT-3′
	Reverse: 5′-AGAATTCGATCTCCAGGTAACG-3′
Runx2	Forward: 5′-CGCCCCTCCCTGAACTCT-3′
	Reverse: 5′-TGCCTGCCTGGGATCTGTA-3′
Alp	Forward: 5′-GTTGCCAAGCTGGGAAGAACAC-3′
	Reverse: 5′-CCCACCCCGCTATTCCAAAC-3′
Ocn	Forward: 5′-GAACAGACTCCGGCGCTA-3′
	Reverse: 5′-AGGGAGGATCAAGTCCCG-3′
Gapdh	Forward: 5′-TGCACCACCAACTGCTTAG-3′
	Reverse: 5′-GGATGCAGGGATGATGTTC-3′

2.5 TRAP Staining

BMMs (2×10^5 cells/well) were seeded into 24-well plates, incubated with 10 ng/ml RANKL and 10 ng/mL M-CSF and treated with various concentrations of acacetin (0, 5, 10, and 20 μM) for 4 days. After fixation in 4% PFA for 20 min, the cells were subjected to TRAP staining using the acid phosphatase, leukocyte (TRAP) kit according to the manufacturer's instructions. The number of $TRAP^+$ osteoclasts containing more than 3 nuclei was counted using an optical microscope (Leica, Wetzlar, Germany).

Femurs of sham, OVX and OVX + Acacetin mice were sectioned in 4-μm-thick tissue sections for TRAP staining using the same kit. The stained sections were scanned using an Aperio AT2 Digital Whole Slide Scanner (Leica, Wetzlar, Germany). The osteoclast number/endocortical surface (N.Oc/BS, 1/mm) was measured using ImageJ.

2.6 RNA Extraction and Real-Time PCR Analysis

BMMs were induced with conditioned medium and treated with acacetin (0, 5, 10, 20 μM) for 4 days. Total RNA was isolated from cells and tibiae using TRIzol reagent according to the manufacturer's instructions. Reverse transcription was performed using the one-step PrimeScript RT reagent kit for mRNA analysis. Real-time PCR assays for mRNA analysis were performed using a SYBR Premix Ex TaqII kit with a Thermal Cycler C-1000 Touch System (Bio-Rad, Hercules, CA). The primers used for real-time PCR are listed in **Table 1**. *Gapdh* was used as an internal control for mRNA detection. All primers were purchased from Sangon Biotech (Shanghai, China).

2.7 Western Blotting

Whole-cell lysates for western blotting were prepared by extracting proteins from the cells using RIPA lysis buffer, and then blotting them on a polyvinylidene fluoride membrane. The membranes were incubated with antibodies against CTSK (1:1,000), ACP5 (1:1,000), MMP9 (1:1,000), NFATc1 (1:1,000), PI3K (1:1,000), p-Akt (1:1,000), Akt (1:1,000), p-GSK3β (1:1,000), GSK3β (1:1,000), p-IκBα (1:1,000), IκBα (1:1,000), p-NF-κB p65 (1:1,000), NF-κB p65 (1:1,000), p-ERK (1:1,000), ERK (1:1,000), p-JNK (1:1,000), JNK (1:1,000), p-p38 (1:1,000), p38 (1:1,000), and GAPDH (1:5,000). Secondary antibodies conjugated with HRP (1:10,000) were used for signal detection. The blots were visualized using ECL chemiluminescence reagents.

2.8 Bone Resorption Assay

Bone resorption assays were performed using Osteo Assay surface (Corning, NY, United States). BMMs were seeded onto osteo surface and induced with 10 ng/mL M-CSF and 10 ng/ml RANKL for 5 days. Bone resorption pits were sonicated in PBS to remove adherent cells. The bone resorption pits on the osteo surface were visualized using optical microscope (Leica, Wetzlar, Germany).

2.9 Actin Staining

Primary BMMs on bone slices or glass chamber slides were induced with 10 ng/mL M-CSF and 10 ng/ml RANKL and treated with various concentrations of acacetin for 4 days. The cells were washed 2–3 times with PBS, and fixed in 4% PFA for 15 min and washed again with precooled PBS 2–3 times. Then, the cells were permeabilized with 0.5% Triton X-100 for 10 min and washed 2–3 times with precooled PBS for 3–5 min each. The cells were stained with 0.5 μg/ml rhodamine-conjugated phalloidin in the dark for 40 min. After incubation, the cells were washed twice with precooled PBS for 3–5 min each. Finally, the nuclei were counterstained with 1 μg/ml DAPI in the dark for 3 min, washed twice with precooled PBS for 3–5 min and observed under fluorescence microscopy (Nikon 80i, Japan).

2.10 Acridine Orange Staining

Primary BMMs on glass chamber slides were induced with 10 ng/mL M-CSF and 10 ng/ml RANKL for 4 days and then treated with acacetin (0 and 20 μM) for another 24 h. The cells were washed 2–3 times with PBS and incubated with 5 μg/ml acridine orange for 15 min at 37°C. Then, the cells were washed with PBS and chased with fresh medium for 10 min, and stained cells were observed under fluorescence microscopy (Nikon 80i, Japan).

2.11 Preparation of Conditioned Media From Osteoclasts

Conditioned media from osteoclasts treated with acacetin (0, 5, 10, 20 μM) was prepared. BMMs (2×10^5 cells/well) were seeded into 24-well plates, incubated with 10 ng/mL M-CSF and 10 ng/ml RANKL, and treated with various concentrations of acacetin (0, 5, 10, and 20 μM) for 4 days. At the end of induction, serum-containing conditioned medium from the mature osteoclasts was collected. Serum-free conditioned medium containing the same concentrations of M-CSF, RANKL, and acacetin was harvested after another day of culture. All the aliquoted conditioned media were centrifuged at 2,500 rpm for 10 min and stored at −80°C.

2.12 Tube Formation Assay

EPCs were seeded onto Matrigel-coated 24-well plates and incubated with acacetin or serum-containing conditioned medium from osteoclasts cultured with acacetin (0, 5, 10, and 20 μM). After 6 h, the cells were stained with calcein AM, and network formation was imaged using an inverted fluorescence microscope (Leica, Wetzlar, Germany). The total tube lengths and numbers of intersections in randomly chosen areas were quantified using ImageJ software.

2.13 Wound Healing Assay

EPCs were seeded into 6-well plates and grown to 90% confluence. An injury was created in the cell monolayer using a sterile 200 ml pipette, and unattached cells were removed by washing twice with PBS. Then, the cells were allowed to migrate into the empty space for 18 h in acacetin or serum-free conditioned medium from osteoclasts cultured with acacetin (0, 5, 10, and 20 μM). The cells were imaged during migration using an inverted optical microscope (Leica, Wetzlar, Germany). The width of the injury was measured using ImageJ software.

2.14 ELISA

BMMs (2×10^5 cells/well) were seeded into 24-well plates, incubated with 10 ng/mL M-CSF and 10 ng/ml RANKL, and treated with various concentrations of acacetin (0, 5, 10, and 20 μM) for 4 days. The conditioned medium was subjected to PDGF-BB ELISA analysis using a mouse PDGF-BB ELISA kit according to the manufacturers' instructions.

2.15 Animals

Eight-week-old C57BL/6 female mice were purchased from Beijing Vital River Laboratory (Beijing, China). Mice were randomly divided into three groups ($n = 6$ in each group), including the sham-operated (sham) group, the OVX group, and the OVX with acacetin (OVX +

Acacetin) group. The sham group was treated with 0.5% CMC-Na with a sham operation, while both the OVX and OVX + Acacetin groups were ovariectomized, and orally administered 0.5% CMC-Na or 20 mg/kg/d acacetin for 8 weeks, respectively. The choice of dosage was based on previous studies (Ren et al., 2020; Wei et al., 2020). All animal experiments were performed in accordance with the Guiding Principles for the Care and Use of Laboratory Animals, and all experimental procedures were approved by the Institutional Experimental Animal Committee of Northwestern Polytechnical University (Xi'an, China).

2.16 Tissue Collection and Sample Preparation

Blood was collected from the hearts of mice before euthanasia after a 4-h fast. The collected blood was centrifuged at 1,500 g for 15 min, and the supernatant was collected and stored in a refrigerator at −80°C for later use. The femurs, tibiae and vertebrae were collected, and the attached muscles were removed. The left femurs were fixed in 4% PFA for 2 days and then embedded in paraffin after 4 weeks of decalcification with 10% EDTA. They were prepared for subsequent H&E staining, TRAP staining, immunohistochemical staining, and immunofluorescent staining. The right femurs and vertebrae were fixed in 4% PFA for micro-CT analysis. The left and right tibiae were collected and placed in a freezer at −80°C for real-time PCR analysis of acid phosphatase 5 (Acp5) and Rankl/osteoprotegerin (Opg) mRNA expression.

2.17 Serum Analysis

Serum was evaluated for AST, ALT, BUN, and CREA content using assay kits according to the manufacturer's guidelines for each.

2.18 Micro-CT Analysis

The distal metaphysis of the femur and 5th lumbar vertebrae were fixed in 4% PFA and scanned using a Bruker SkyScan 1,276 Micro-CT device (Allentown, PA, United States). In brief, the scanning parameters were set as following, energy: 70 kV, 114 μA; angle of increment: 0.2°, exposure time: 810 ms/frame, scanning time: 14 min, and the scanning resolution were set as 10 μm. For femur, a region of interest (ROI) that start from the growth plate to 1.5 mm below the growth plate was selected for analysis (threshold = 117.4 mg HA/ccm) using CTvox software (Blue Scientific, Cambridge, United Kingdom), and three-dimensional (3D) reconstruct by NRecon Reconstruction software (Micro Photonics, Allentown, PA, United States). For vertebrae, the ROI of trabecular bone of 5th vertebral body was selected for analysis (threshold = 282.15 mg HA/ccm) and 3D reconstruction. The following parameters of trabecular bone and vertebrae were calculated using the direct three-dimensional measurement method: bone mineral density (BMD; g/cm^3), bone surface area/bone volume (BS/BV; 1/mm), bone surface to tissue volume (BS/TV; 1/mm), bone volume to tissue volume (BV/TV; %), trabecular number (Tb.N; 1/mm), trabecular spacing (Tb.Sp; mm), and trabecular thickness (Tb.Th; mm).

2.19 Immunofluorescence, Immunohistochemistry, and Histomorphometry

Femurs of sham, OVX and OVX + Acacetin mice were embedded in paraffin and sectioned into 4-μm-thick tissue sections. For immunofluorescence analyses, sections were treated with 3% H_2O_2 for 25 min and then blocked with 3% BSA for 30 min. Then bone sections were incubated with individual primary antibodies against mouse CD31 (1:100), EMCN (1:100), PDGF-BB (1:100), and TRAP (1:100) overnight at 4°C. Then, the sections were washed and incubated with secondary antibodies conjugated with fluorescence in the dark for 1 h. Finally, the nuclei were counterstained with 1 μg/ml DAPI in the dark for 3 min and washed twice with precooled PBS for 3–5 min. CD31^{hi}EMCN^{hi} vessels were quantitatively analysed as previously described (Xie et al., 2014). The number of positively stained cells in the field of distal femoral metaphysis was calculated and normalized to the number per square millimetre (N·mm^{-2}) of bone marrow area in the trabecular bone. For immunohistochemistry analyses (Zhihao Chen et al., 2020), sections were processed for antigen retrieval for 15 min and blocked in 3% BSA for 30 min. The sections were then incubated overnight with primary antibody against CTSK (1:100) at 4°C, and incubated with HRP-conjugated IgG (1:400) for 50 min after three washes with PBS. A DAB Horseradish Peroxidase Colour Development Kit was used to detect immunoactivity, followed by counterstaining with haematoxylin. Sections were examined under a fluorescence microscope (Nikon, Japan). For bone histomorphometry, sections were stained with H&E. All sections were scanned using an Aperio AT2 Digital Whole Slide Scanner (Leica, Wetzlar, Germany).

2.20 Osteoblast Osteoclast Co-Culture

A transwell assay with polycarbonate membranes (0.4 μm pore size) (Corning Costar, MA, United States) was used for osteoblast-osteoclast co-culture. MC3T3-E1 cells (5×10^4) were added to the upper compartment of the transwell system in α-MEM complete medium, and BMMs were added into lower chamber in α-MEM complete medium without RANKL or M-CSF. After 5 days co-culture, the cells in both upper and lower chamber were selected for further study.

2.21 Statistical analysis

The data are presented as the mean ± s.d. Analyses were performed using GraphPad Prism software. A Student's *t*-test or ANOVA was performed to assess statistical significance of differences. Values were considered statistically significant at $^*p < 0.05$ or $^{**}p < 0.01$.

3 RESULTS

3.1 The Cytotoxic Effect of Acacetin on BMMs

To evaluate the concentration range in which acacetin is not toxic to BMMs, BMMs were treated with different concentrations of acacetin (**Figure 1A**), and cell viability was evaluated by the MTT assay. The

results showed that acacetin did not exert a cytotoxic effect on BMMs at concentrations ranging from 0–20 μM after cultured for 24 h (**Figure 1B**) and 48 h (**Figure 1C**). Moreover, the TUNEL staining assay showed that acacetin at concentrations of 50 and 100 μM significantly increased the proportion of apoptotic cells, while 0–20 μM acacetin had no effect on cell apoptosis at either 24 h or 48 h (**Figures 1D–G**), consistent with the MTT results. Therefore, acacetin was used in the concentration range of 0–20 μM in subsequent study.

3.2 Acacetin Attenuates RANKL-Induced Osteoclastogenesis and NFATc1 and NF-κB Expression

To investigate the potential role of acacetin in RANKL-induced osteoclast differentiation, freshly harvested BMMs were cultured with 10 ng/mL M-CSF and 10 ng/ml RANKL with or without different concentrations of acacetin. After 4 days of induction, TRAP staining revealed that acacetin inhibited the size and number of osteoclasts, and the formation of multinucleated osteoclasts (≥3 nuclei), and the effect was most obvious at 20 μM (**Figures 2A–C**). Interestingly, real-time PCR results showed that the osteoclastic marker genes *Acp5*, *CtsK*, and *Mmp9* were significantly downregulated in the 10 and 20 μM acacetin-treated groups (**Figures 2D–F**). Additionally, western blotting analysis indicated that 20 μM acacetin had the most obvious inhibitory effect on the protein expression of CTSK, ACP5, and MMP9 (**Figure 2G**). Taken together, these results demonstrate that 20 μM acacetin inhibits RANKL-induced osteoclast differentiation.

To investigate the signalling pathways by which acacetin inhibits osteoclast formation, M-CSF- and RANKL- induced osteoclasts were examined for expression of osteoclast-related transcription factors in response to different concentrations of

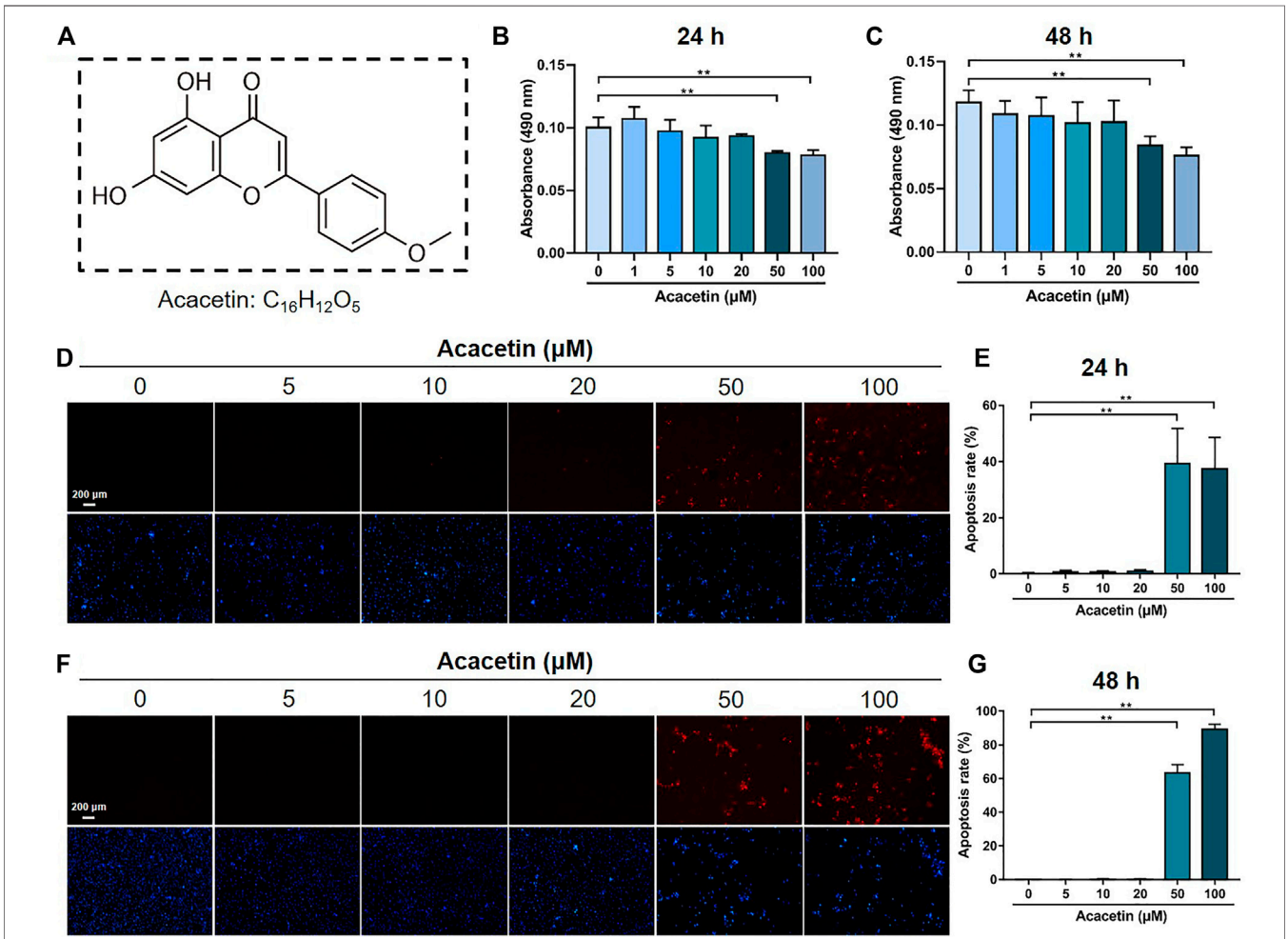

FIGURE 1 | The cytotoxic effect of acacetin on BMMs. **(A)** Chemical structure of acacetin. **(B,C)** BMMs were treated with M-CSF and different concentrations of acacetin (0, 1, 5, 10, 20, 50, and 100 μM) for 24 h **(B)** and 48 h (C), and cell viability was measured by MTT assay ($n = 6$). **(D,F)** TUNEL staining of BMMs treated with M-CSF and different concentrations of acacetin (0, 5, 10, 20, 50, and 100 μM) for 24 h **(D)** and 48 h **(F)**. **(E,G)** Quantification of apoptotic cells in **(D)** and **(F)** ($n = 4$). The data are presented as the mean ± s.d.; A Student's *t*-test or ANOVA was performed to assess statistical significance of differences; $^{*}p < 0.05$ and $^{**}p < 0.01$ versus control group.

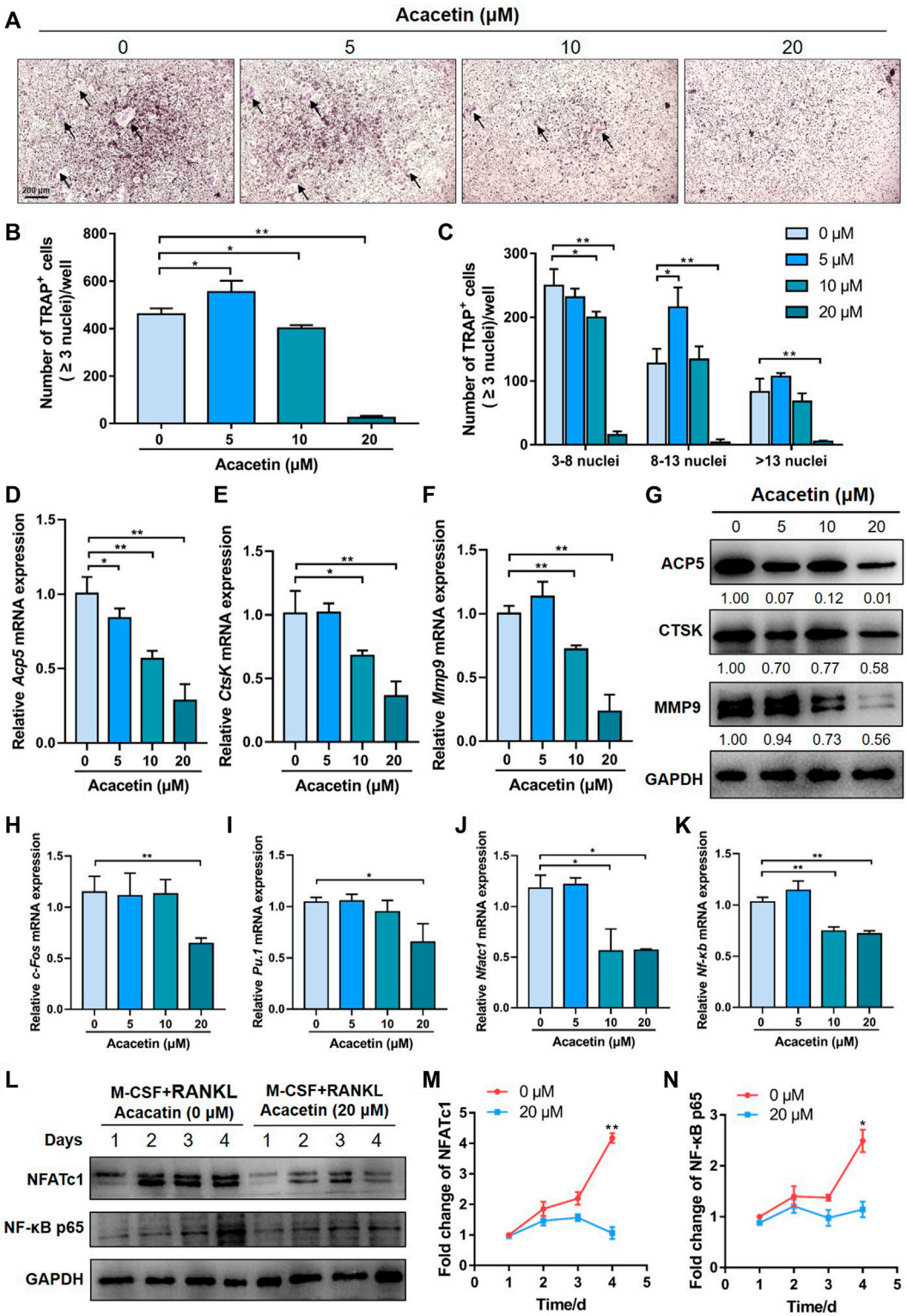

FIGURE 2 | Acacetin attenuates RANKL-induced osteoclastogenesis. **(A)** Representative images of TRAP staining with the indicated concentrations of acacetin (0, 5, 10, and 20 μM) for 4 days. (Scale bar = 200 μm). **(B,C)** Quantification of multinucleated cells (≥3 nuclei) is shown in **(A)** ($n = 3$). **(D–F)** Real-time PCR analysis of *Acp5*, *Ctsk*, and *Mmp9* expression in osteoclasts treated with different concentrations of acacetin (0, 5, 10, and 20 μM) (n = 4) (G) Western blotting analysis of Acp5, Ctsk, and Mmp9 expression in osteoclasts treated with acacetin (0, 5, 10, and 20 μM). **(H–K)** Real-time PCR analysis of *c-fos*, *Pu.1*, *Nfatc1*, and *Nf-κb* expression in osteoclasts treated with 20 μM acacetin ($n = 3$). **(L)** Western blotting analysis of NFATc1 and NF-κB expression during osteoclastogenesis treated with 20 μM acacetin. **(M,N)** Quantification of NFATc1 and NF-κB levels versus GAPDH levels ($n = 3$). The data are presented as the mean ± s.d.; A Student's *t*-test or ANOVA was performed to assess statistical significance of differences; $^{*}p < 0.05$ and $^{**}p < 0.01$ versus control group.

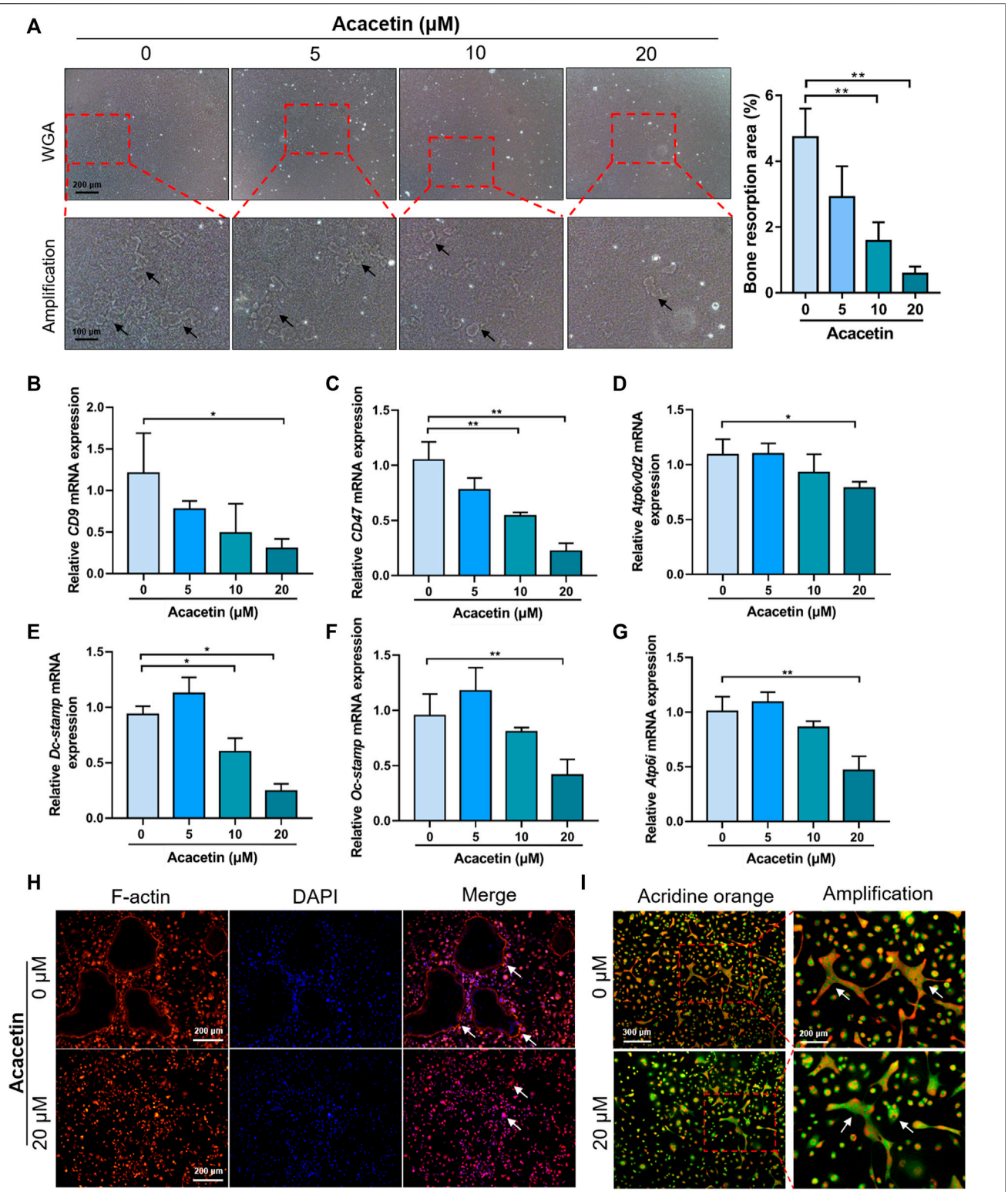

FIGURE 3 | Acacetin attenuates bone resorption and acidification of osteoclasts**. (A)** Representative images and quantitative analyses of bone resorption area of osteoclasts on osteo assay surface treated with acacetin (0, 5, 10, and 20 μM). (Upper: scale bar = 200 μm, lower: scale bar = 100 μm). **(B–G)** Real-time PCR analysis of *CD9*, *CD47*, *Atp6v0d2*, *Dc-stamp*, *Oc-stamp*, and *Atp6i* expression in osteoclasts treated with different concentrations of acacetin (0, 5, 10, and 20 μM) (n = 3). **(H)** Representative images of actin ring staining of osteoclasts treated with 20 μM acacetin. (Scale bar = 200 μm). **(I)** Representative images of acridine orange staining of osteoclasts treated with 20 μM acacetin. (Upper: scale bar = 300 μm, lower: scale bar = 200 μm). The data are presented as the mean ± s.d.; A Student's t-test or ANOVA was performed to assess statistical significance of differences; A Student's t-test or ANOVA was performed to assess statistical significance of differences; $^{*}p < 0.05$ and $^{**}p < 0.01$ versus control group.

acacetin (0, 5, 10, and 20 μM). Real-time PCR results showed that expression of *c-Fos* and *Pu.1* were reduced by 20 μM acacetin after 4 days of induction (**Figures 2H, I**), while the expression of *Nfatc1* and *Nf-κb* was significantly reduced by acacetin at both 10 and 20 μM (**Figures 2J, K**). Furthermore, the western blotting results was consistent, and the protein expression of NFATc1 and NF-κB p65 was significantly reduced by 20 μM acacetin during the osteoclastogenesis process (**Figures 2L–N**). These data indicate that acacetin abrogates RANKL-induced NFATc1 and NF-κB expression.

3.3 Acacetin Attenuates Bone Resorption and Acidification of Osteoclasts

To further study the role of acacetin in osteoclast function, we performed a bone resorption assay. Equal numbers of BMMs were cultured on the osteo assay surface and treated with 10 ng/mL M-CSF, 10 ng/ml RANKL for 5 days, and treated with acacetin at concentrations of 0, 5, 10, and 20 μM for another 2 days. Bone resorption assays indicate that the total resorption area was significantly reduced in the acacetin treatment groups (10 and 20 μM) (**Figure 3A**).

The fusion of pre-osteoclast is the key step of osteoclast function. To determine the effect of acacetin on osteoclast fusion, osteoclast fusion genes were further examined by real-time PCR. The results showed that expression of *CD9*, *CD47*, *Atp6v0d2*, *Dc-stamp*, and *Oc-stamp* was reduced in response to 20 μM acacetin treatment after 4 days of induction (**Figures 3B–F**). Moreover, small F-actin belts and few nuclei were observed in osteoclasts after 20 μM acacetin treatment (**Figure 3H**). Additionally, the expression of *Atp6i*, which determines extracellular acidification, was downregulated in acacetin-treated osteoclasts (**Figure 3G**). These results are consistent with those of acridine orange staining, that is, the level of extracellular acidification was lower after 20 μM acacetin treatment (**Figure 3I**). Taken together, these data indicate that 20 μM acacetin inhibits osteoclast acidification and bone resorption.

3.4 Acacetin Attenuates RANKL-Induced Osteoclastogenesis Through Akt/GSK3β and NF-κB Signalling

To further explore the molecular mechanism by which acacetin inhibits RANKL-induced osteoclast formation, BMMs were induced with 10 ng/mL M-CSF and 10 ng/ml RANKL for 3 days. Then, the cells were starved for 5 h and stimulated with 50 ng/ml RANKL or RANKL + acacetin for 5–60 min. Western blotting results demonstrated that phosphorylation of Akt, GSK3β, IκBα, and p65, which was increased by RANKL, was markedly attenuated by acacetin treatment (**Figures 4A, C–G**). However, RANKL-induced early signalling pathways, such as activation of ERK, JNK, and p38, were not altered by acacetin treatment (**Figures 4B, H–J**). These data suggest that acacetin attenuates RANKL-induced osteoclastogenesis by inhibiting the Akt/GSK3β and NF-κB signalling pathways.

3.5 Acacetin Promotes Preosteoclast-Induced Angiogenesis

To validate the effects of acacetin on preosteoclast-induced angiogenesis, the concentration of PDGF-BB in serum-containing conditioned medium from acacetin (0, 5, 10, and 20 μM) treated osteoclasts was measured. As evidenced by ELISA, the production of PDGF-BB in conditioned medium was increased by acacetin treatment at a concentration of 20 μM (**Figure 5A**). Furthermore, EPCs were cultured on Matrigel, incubated with serum-containing conditioned medium, and allowed to form capillary-like tubes. The results showed that acacetin promoted the angiogenesis process of EPCs with enhanced tube length and a higher number of intersections (**Figures 5B, C**). Additionally, wound healing assays revealed that serum-containing conditioned medium from acacetin treated osteoclasts promotes the migration of EPCs in a concentration-dependent manner (**Figures 5D, E**). To exclude the direct effect of acacetin on EPCs, the acacetin (0, 5, 10, and 20 μM) treated EPCs was measured. It was showed that acacetin inhibited both the angiogenesis and migration of EPCs (**Supplementary Figure S1**). Taken together, these findings indicate that acacetin promotes preosteoclast-induced angiogenesis.

3.6 Intragastric Administration of Acacetin Prevents Bone Loss Induced by OVX

To evaluate the effects of acacetin on osteolytic disease, OVX mice were generated and intragastrically administered acacetin (20 mg/kg/d) or vehicle (CMC-Na) for 2 months. Serum analysis revealed that acacetin did not exert liver or kidney toxicity in mice because there was no significant change in AST, ALT, BUN, or CREA content (**Supplementary Figures S2A–D**). Micro-CT analysis revealed that the trabecular bone mass of OVX mice was markedly lower in the distal metaphysis of the femur than in the sham group, but the acacetin alleviated bone loss in OVX mice (**Figure 6A**). Quantitative analyses of BMD, BS/BV, BS/TV, BV/TV, Tb.N, Tb.Sp, and Tb.Th confirmed the preventive effect of acacetin on OVX-induced bone loss (**Figures 6B–H**). Moreover, micro-CT and quantitative analyses of vertebrae also demonstrated that acacetin inhibited bone loss in OVX mice (**Supplementary Figures S2E–L**). H&E staining showed that acacetin induced bone area and prevented fat cell accumulation in the bone marrow of OVX mice (**Figures 6I, J**). Additionally, immunofluorescence staining of osteocalcin (OCN) showed an increased number of osteoblasts on the surface of trabecular bone in acacetin-treated mice (**Figures 6K, L**). To determine whether acacetin treatment regulates osteoclasts through osteoblasts, BMMs were co-cultured with osteoblasts treated with acacetin (0, 5, 10, and 20 μM) without RANKL or M-CSF. The osteoblast differentiation marker genes including *Runx2*, *Alp* and *Ocn* were upregulated by acacetin, while the expression of *Rankl*/*Opg* was not changed (**Supplementary Figure S3A**). Furthermore, the osteoclastic marker genes *Acp5*, *CtsK*, and *Mmp9* were not changed in osteoclast co-cultured with osteoblasts treated with acacetin (**Supplementary Figure S3**).

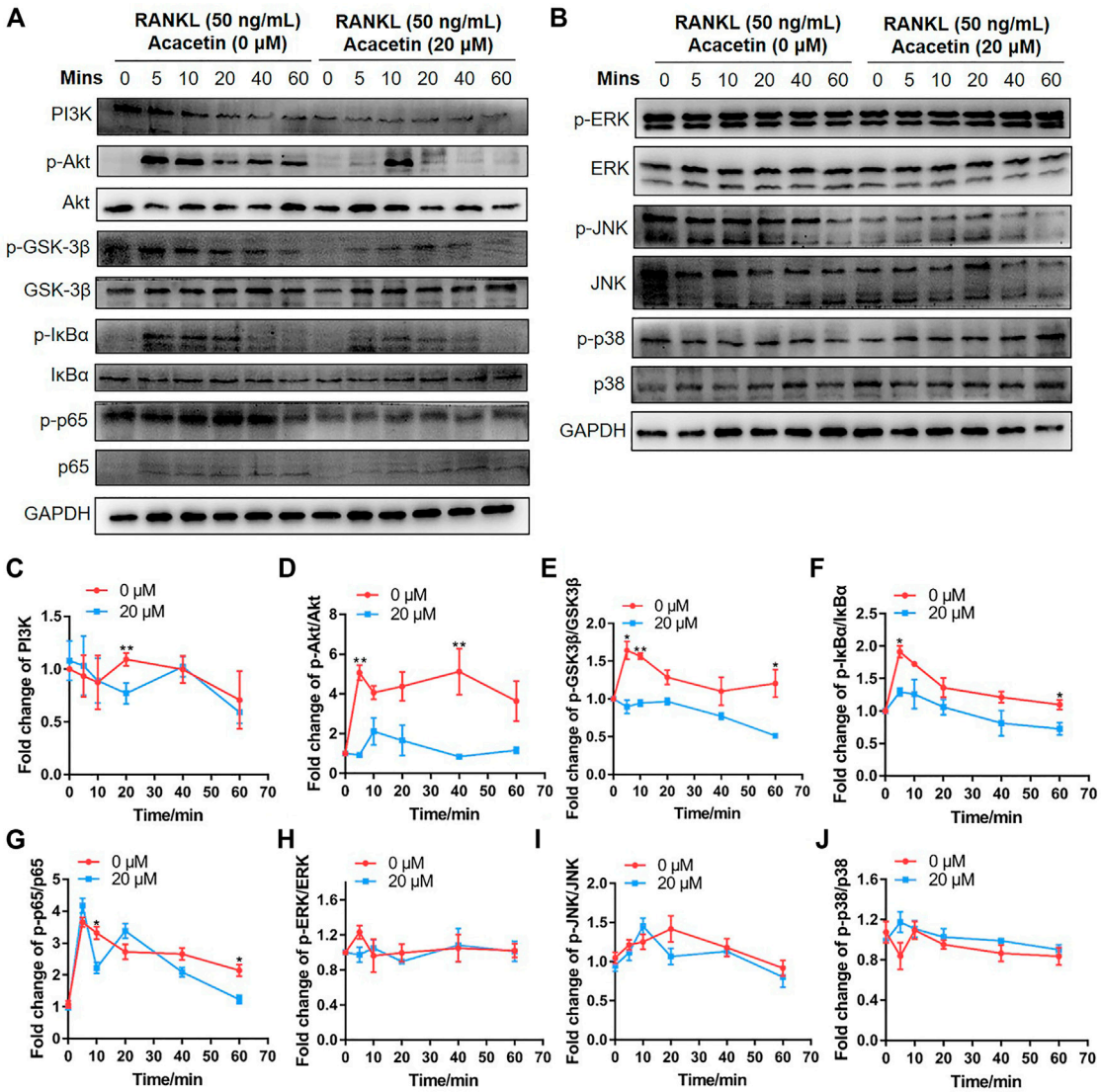

FIGURE 4 | Acacetin attenuates RANKL-induced osteoclastogenesis through Akt/GSK3β and NF-κB signalling. **(A,B)** BMMs were induced with M-CSF and RANKL for 3 days, and starved for 5 h and stimulated with 50 ng/ml RANKL for the indicated times. Western blotting analysis with specific antibodies was performed as indicated. **(C–J)** Quantification of PI3K level versus GAPDH level, phospho-Akt level versus total Akt level, phospho-GSK3β level versus total GSK3β level, phospho-IκBα level versus total IκBα level, phospho-p65 level versus total p65 level, phospho-ERK level versus total ERK level, phospho-JNK level versus total JNK level, and phospho-p38 level versus total p38 level (n = 3). The data are presented as the mean ± s.d.; A Student's t-test was performed to assess statistical significance of differences; $^{*}p < 0.05$ and $^{**}p < 0.01$ versus control group.

These results indicate that the inhibition of osteoclast differentiation by acacetin is direct. Altogether, these results indicate that acacetin effectively protects against OVX-induced osteoporosis *in vivo*.

3.7 Acacetin Represses Osteoclasts and Stimulates Type H Vessel Formation in OVX Mice

To investigate osteoclast development *in vivo*, we analysed sections of the femora by TRAP staining. The results showed that $TRAP^{+}$ osteoclasts on the trabecular bone of distal femurs and cortical bone were increased, while acacetin reduced the number of osteoclasts in OVX mice (**Figures 7A–C**). Immunohistochemical staining for CTSK revealed that osteoclastogenic activity was promoted in OVX mice but significantly inhibited when OVX mice were treated with acacetin (**Figure 7D**). Moreover, the expression of *Acp5* and *Rankl*/*Opg* in the femurs of OVX mice was upregulated in response to acacetin treatment (**Figure 7E**).

An increase in the number of preosteoclasts induces the formation of $CD31^{hi}Emcn^{hi}$ vessels (Xie et al., 2014). Immunofluorescence staining showed that acacetin promoted the formation of $CD31^{hi}EMCN^{hi}$ vessels adjacent to the

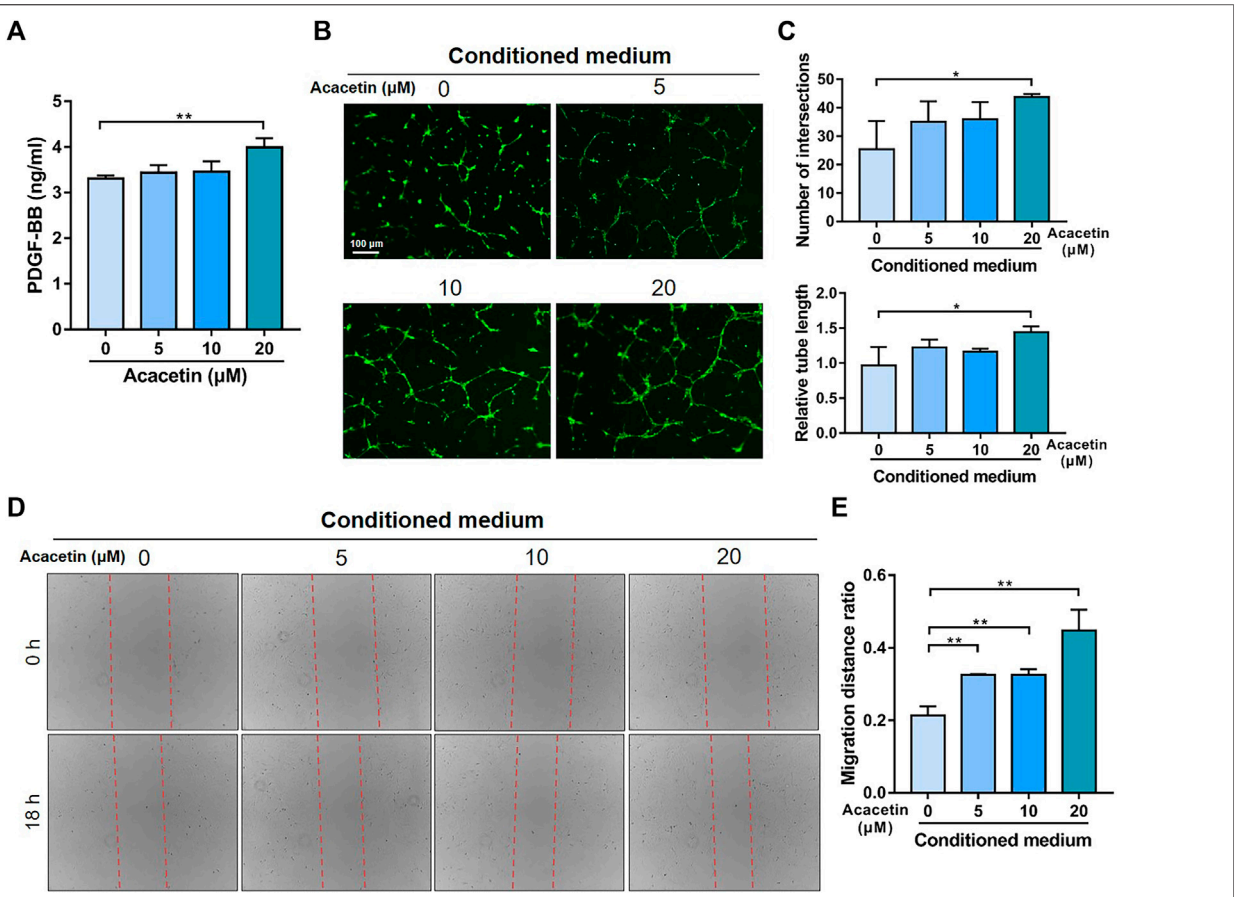

FIGURE 5 | Acacetin promotes preosteoclast induced angiogenesis. **(A)** ELISA analysis of PDGF-BB levels in serum-containing conditioned medium from osteoclasts treated with acacetin (0, 5, 10, and 20 μM) ($n = 3$). **(B)** Representative Matrigel tube formation assay images with cultures of EPCs using conditioned medium from acacetin-treated osteoclast as indicated. (Scale bar = 100 μm). **(C)** Quantification of tube length and number of intersections in **(B)** using ImageJ ($n = 3$). **(D)** The mobility of EPCs in conditioned medium from acacetin-treated osteoclast as indicated was assessed by wound healing assays. **(E)** Quantification of migration distance in **(D)** using ImageJ ($n = 3$). The data are presented as the mean ± s.d.; A Student's *t*-test or ANOVA was performed to assess statistical significance of differences; $^{*}p < 0.05$ and $^{**}p < 0.01$ versus control group.

growth plate (GP) of OVX mice, which was similar to the sham-operated mice (**Figures 7F, G**). Preosteoclasts couple angiogenesis and bone formation by secreting PDGF-BB (Xie et al., 2014). Therefore, PDGF-BB and TRAP immunofluorescence double staining was performed to further evaluate the distribution of preosteoclasts expressing PDGF-BB in the femur. The results revealed that OVX mice had a significantly lower proportion of $TRAP^+$ cells that were positive for PDGF-BB than sham-operated mice, while acacetin rescued the proportion of $PDGF\text{-}BB^+/TRAP^+$ cells in OVX mice (**Figures 7H, I**). Collectively, these results suggest that acacetin reduces the number of multinuclear osteoclasts and increases the number of $PDGF\text{-}BB^+/TRAP^+$ preosteoclasts that stimulate angiogenesis and bone formation in OVX mice.

4 DISCUSSION

Osteoporosis is a common bone disease characterized by excessive bone resorption mediated by osteoclasts and resulting in bone loss (Qiang Xu et al., 2021). It is estimated that more than 200 million people currently suffer from osteoporosis (Tatangelo et al., 2019). As the population continues to age and live longer, the number of people affected will increase significantly. Therefore, osteoporosis is considered a serious public health problem worldwide (Akbar et al., 2017).

To prevent the development of osteoporosis, a great deal of work has been done to identify effective treatments. Overactivation of osteoclasts plays a major role in bone destruction, therefore, osteoclast differentiation is considered as a major therapeutic target for developing new drugs (Ono and Nakashima, 2018). Clinically, antiresorptive agents, such as alendronate, zoledronate, and denosumab, are widely used for the treatment of osteoporosis (Leder et al., 2020). Unfortunately, these drugs can cause a number of side effects, including stroke, gastrointestinal discomfort, hypokalaemia, and osteonecrosis of the jaw (Chen et al., 2019; Delong Chen et al., 2020). Considering these shortcomings, it is imperative to find effective drugs to treat unbalanced bone remodelling caused by excessive osteoclast activity (Huang et al., 2015; Wantao Li et al., 2020).

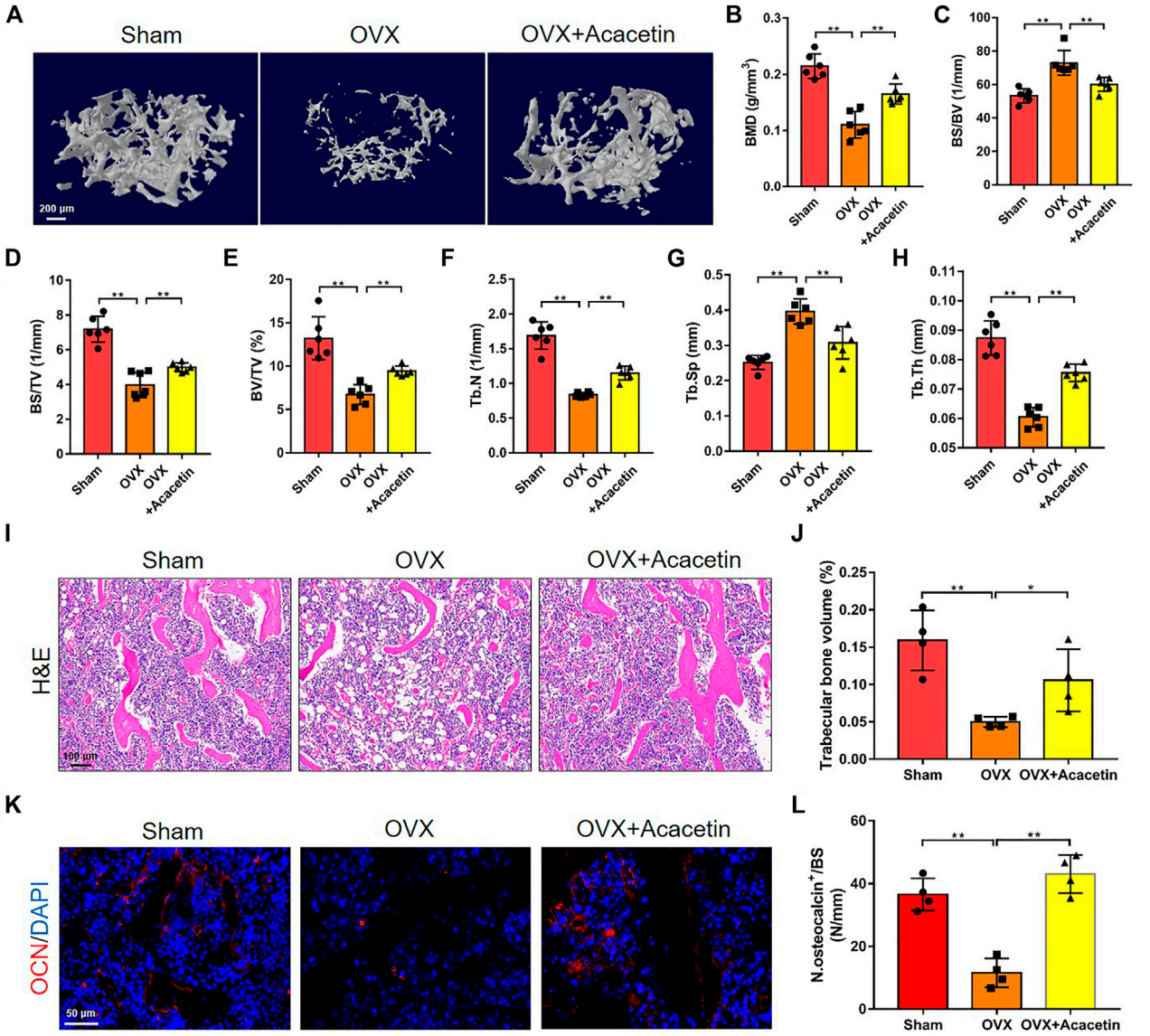

FIGURE 6 | Intragastric administration of acacetin prevents bone loss induced by OVX. **(A)** Representative 3D reconstruction micro-CT images of femur trabecular bone in the different groups. (Scale bar = 200 μm). **(B–H)** Quantitative analyses of femur trabecular bone-related parameters, including BMD, BS/BV, BS/TV, BV/TV, Tb.N, Tb.Sp, and Tb.Th (n = 6). **(I)** Representative H&E staining images of distal femurs in sham group, OVX group, and OVX group treated with 20 mg/kg acacetin. (Scale bar = 100 μm). **(J)** Quantitative analyses of trabecular bone volume in **(I)** (n = 4). **(K)** Representative immunostaining of OCN on the trabecular bone surface. (Scale bar = 50 μm). **(L)** Quantitative analyses of OCN^+ cell numbers on the trabeculae in **(K)** (n = 4). The ROI of microCT, H&E, and OCN is in the region that start from the growth plate to 1.5 mm below the growth plate. The data are presented as the mean ± s.d.; A Student's t-test or ANOVA was performed to assess statistical significance of differences; $^*p < 0.05$ and $^{**}p < 0.01$ versus control group.

Flavonoids have antioxidant, anti-inflammatory, differentiation, and apoptotic properties (Bellavia et al., 2021), which make them important in maintaining bone health (Hardcastle et al., 2011; Zhang et al., 2014). Recently, studies have shown that a large number of compounds, such as cladrin, icariin, and petunidin have inhibitory effects on osteoclast function and represent potential therapies for bone resorption diseases (Bellavia et al., 2021). Acacetin has been reported to promote osteoblastic differentiation and mineralization (Li et al., 2016) and inhibit osteoclastic differentiation through regulating CD44 and integrins *in vitro* (Kim et al., 2020). However, the effect and mechanism of acacetin on the formation of osteoclasts and type H vessels in OVX-induced bone loss have not yet been elucidated. In this study, we found that acacetin inhibits macrophages from differentiating into multinucleated osteoclasts. Relative expression of osteoclast marker genes, including *Acp5*, *Ctsk*, and *Mmp9*, also demonstrated the inhibitory effects of acacetin on osteoclastogenesis. Next, we tested the role of acacetin in osteoclast function. The bone resorption assay, actin-ring staining, and acridine orange staining confirmed

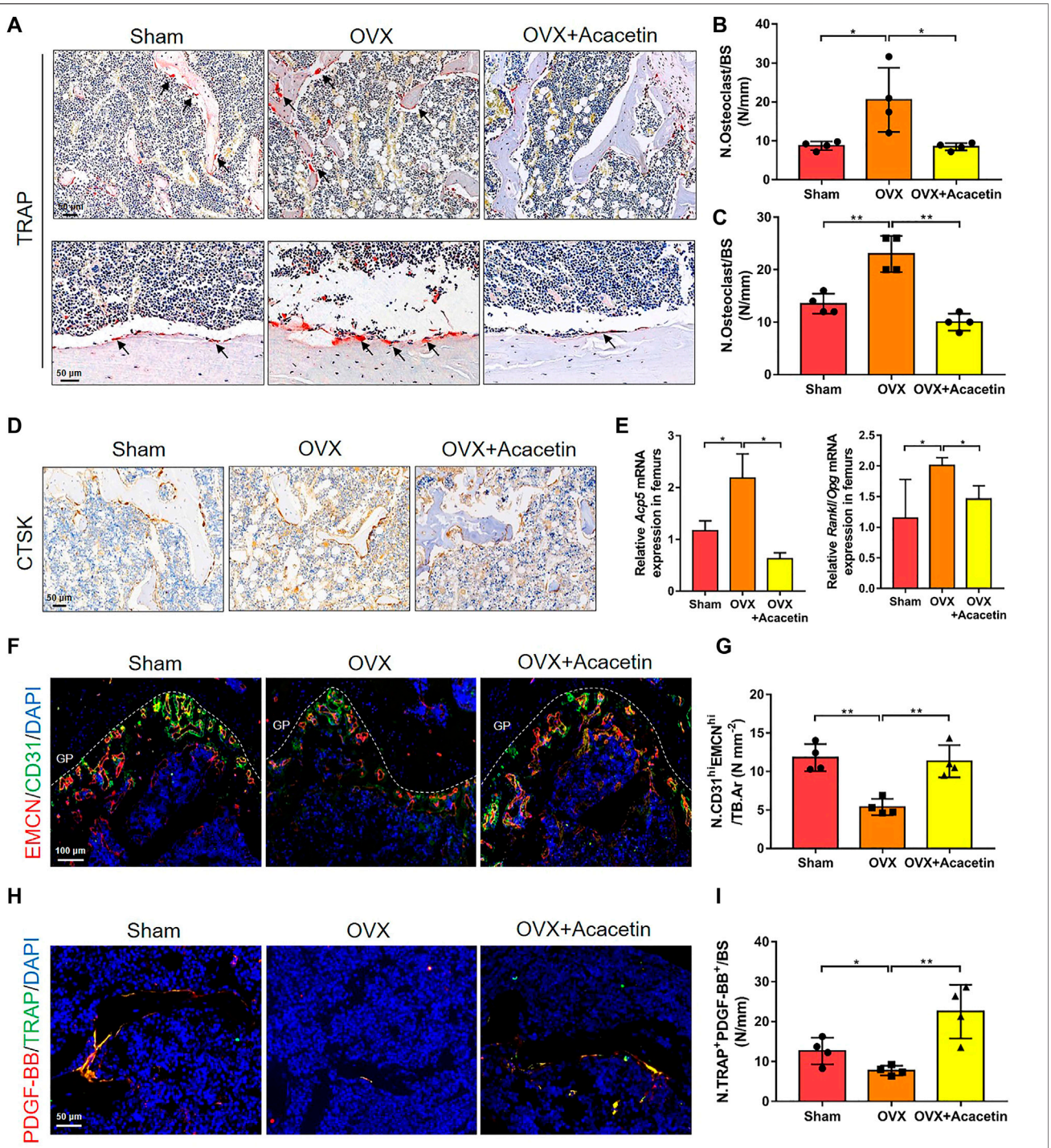

FIGURE 7 | Acacetin represses osteoclasts and stimulates type H vessel formation in OVX mice. **(A)** Representative TRAP$^+$ cells on the trabecular bones of distal femurs (upper) and cortical bone of diaphyseal femurs (below). (Scale bar = 50 μm). **(B,C)** Quantification of TRAP staining in trabecular bones of distal femurs **(B)** and cortical bone of diaphyseal femurs **(C)** (n = 4). **(D)** Representative immunohistochemistry of CTSK$^+$ cells on the trabecular bone surface. (Scale bar = 100 μm). **(E)** Real-time PCR analysis of *Acp5* and *Rankl/Opg* expression in bone tissues (n = 3). **(F)** Representative images of immunostaining of endomucin (EMCN) (red) and CD31 (green) on trabecular bone (Scale bar = 100 μm). **(G)** Quantification of CD31^{hi}EMCN^{hi} (yellow) cells in bone marrow in **(F)** (n = 4). **(H)** Representative images of immunostaining of PDGF-BB (red) and TRAP (green) on the trabecular bone (Scale bar = 50 μm). **(I)** Quantification of PDGF-BB$^+$ TRAP$^+$ (yellow) cells in bone marrow in **(H)** (n = 4). The ROI of TRAP, Ctsk, and PDGF-BB/TRAP staining was in the region that start from the growth plate to 1.5 mm below the growth plate. The ROI of EMCN/CD31 staining is in the region of growth plate. The data are presented as the mean ± s.d.; A Student's t-test or ANOVA was performed to assess statistical significance of differences; $^*p < 0.05$ and $^{**}p < 0.01$ versus control group.

that acacetin inhibited the bone resorption and extracellular acidification of osteoclasts. These results indicate that acacetin suppresses RANKL-induced osteoclast formation and function *in vitro*.

The binding of RANKL to RANK during osteoclast differentiation activates key downstream signalling pathways, such as Akt and NF-κB (Moon et al., 2012; Chen et al., 2018; Ilchovska and Barrow, 2021). Previous studies have shown that Akt induces osteoclast differentiation by inhibiting the GSK3β signalling cascade (Wu et al., 2017). Acacetin has been reported to bind with the p110α subunit of PI3K (Jung et al., 2014). Here, we found that acacetin limits the phosphorylation of Akt and GSK3β, which are downstreams of PI3K, in response to RANKL stimulation and that acacetin regulates expression of the transcription factor NFATc1 expression during the late stage of osteoclast differentiation. Moreover, acacetin inhibited NF-κB signalling in inflammation-associated tumorigenesis and osteoarthritis (Pan et al., 2006; Jian Chen et al., 2020). In our study, acacetin inhibited p65 and IκBα phosphorylation at 10 and 60 min of RANKL stimulation, suggesting that acacetin responds to RANKL signaling during the early and late stages of osteoclast formation. c-Fos and pu.1 can be activated by RANKL and induce gene expression with NFATc1 during osteoclast formation (Takayanagi et al., 2002). c-Fos deficient mice exhibit reduced NFATc1 expression and an osteoporotic phenotype (Grigoriadis et al., 1994). Furthermore, the development of osteoclasts and macrophages is inhibited in the pu.1-deficient mice, inducing an osteosclerosis phenotype (Tondravi et al., 1997). Here, we found that the mRNA expression of c-Fos and pu.1 was significantly reduced in RANKL-stimulated BMMs in response to acacetin treatment. This expression trend was consistent with the marker genes for osteoclast differentiation.

Type H vessels play an important role in maintaining normal bone structure (Kusumbe et al., 2014; Ramasamy et al., 2016). Previous studies have shown that preosteoclasts significantly affect bone formation, and the destruction of type H blood vessels is one of the primary causes of reduced bone formation (Xie et al., 2014; Yang et al., 2018; Gao et al., 2019). The number of type H endothelial cells and bone progenitor cells was significantly reduced in the bone of osteoporosis (Wang et al., 2017; Zhu et al., 2019). Therefore, type H vessels play an important role in bone formation and osteoporosis. It has been reported that acacetin could inhibit angiogenesis *in vitro* and *in vivo* (Bhat et al., 2013). However, the influence of acacetin on the formation of type H vessels through osteoclasts is unclear. In this study, we found that conditioned medium from osteoclasts incubated with RANKL and acacetin enhanced the migratory ability and tube structure formation of EPCs. These results are consistent with previous reports that reduced multinucleated osteoclasts and enhanced preosteoclasts contributed to type H vessel formation.

Finally, a preclinical study using an OVX mouse model of osteoporosis confirmed the role of acacetin in reducing bone loss. The micro-CT results showed that treatment with acacetin restored OVX-induced damage to the trabecular bone architecture of the femur and vertebrae via increases in BMD, BS/TV, BV/TV, Tb.N, and Tb.Th, and a decrease in the BS/BV and Tb. Sp parameters. Moreover, acacetin increased the number of osteoprogenitor cells in the femurs. Our results demonstrated that OVX-induced increases in the number of osteoclasts and enhanced expression of *Acp5* and *Rankl*/*Opg* in bone were significantly reduced by acacetin treatment. Type H vessels play an important role in maintaining normal bone structure (Kusumbe et al., 2014; Ramasamy et al., 2016). Previous studies have shown that preosteoclasts significantly affect bone formation through PDGF-BB, and the destruction of type H blood vessels is one of the primary causes of reduced bone formation (Xie et al., 2014; Yang et al., 2018; Gao et al., 2019). The number of type H endothelial cells and bone progenitor cells was significantly reduced in the bone of osteoporosis (Wang et al., 2017; Zhu et al., 2019). Therefore, type H vessels play an important role in bone formation and osteoporosis. However, the influence of acacetin on the formation of type H vessels is unclear. In this study, we found that type H vessels and $TRAP^{+}PDGF\text{-}BB^{+}$ cells were induced by acacetin in OVX mice. Taken together, these observations demonstrated that acacetin exerts a protective effect on bone loss *in vivo*.

5 CONCLUSION

In summary, we demonstrated that acacetin prevents OVX-induced bone loss by regulating bone resorption and type H vessel formation. Notably, our results reveal that acacetin treatment inhibits osteoclastogenesis and bone resorption through suppression of the Akt/GSK3β and NF-κB signalling pathways. Therefore, this study provides potential application prospects for the pharmacological countermeasures of acacetin in osteoporosis treatment.

DATA AVAILABILITY STATEMENT

The original contributions presented in the study are included in the article/**Supplementary Material**, further inquiries can be directed to the corresponding authors.

ETHICS STATEMENT

The animal study was reviewed and approved by the Institutional Experimental Animal Committee of Northwestern Polytechnical University.

AUTHOR CONTRIBUTIONS

Study conception and design: XL, Z-HC, and A-RQ. Acquisition, analysis, and interpretation of data: XL, FX, K-WZ, W-XQ, and

HZ. Drafting the manuscript: XL, Z-HC, and A-RQ. Revision of the work: XL, QH, ML, and YT. Final approval and overall responsibility for the published work: Z-HC and A-RQ. All authors read and approved the final manuscript.

FUNDING

This work was supported by the National Natural Science Foundation of China (Grant number 81700784), the Key R&D Projects in Shaanxi Province (Grant number 2021SF-242), the China Postdoctoral Science Foundation (Grant numbers 2017M613196, 2020M683573), the Natural Science Basic Research Plan of Shaanxi Province of China (Grant number 2021JQ-128), and the key grant BKJ17J004.

SUPPLEMENTARY MATERIAL

The Supplementary Material for this article can be found online at: https://www.frontiersin.org/articles/10.3389/fcell.2022.796227/full#supplementary-material

REFERENCES

Akbar, M. A., Nardo, D., Chen, M.-J., Elshikha, A. S., Ahamed, R., Elsayed, E. M., et al. (2017). α-1 Antitrypsin Inhibits RANKL-Induced Osteoclast Formation and Functions. *Mol. Med.* 23, 57–69. doi:10.2119/molmed.2016.00170

Beekman, K. M., Veldhuis-Vlug, A. G., den Heijer, M., Maas, M., Oleksik, A. M., Tanck, M. W., et al. (2019). The Effect of Raloxifene on Bone Marrow Adipose Tissue and Bone Turnover in Postmenopausal Women with Osteoporosis. *Bone* 118, 62–68. doi:10.1016/j.bone.2017.10.011

Bellavia, D., Dimarco, E., Costa, V., Carina, V., De Luca, A., Raimondi, L., et al. (2021). Flavonoids in Bone Erosive Diseases: Perspectives in Osteoporosis Treatment. *Trends Endocrinol. Metab.* 32 (2), 76–94. doi:10.1016/j.tem.2020.11.007

Bhat, T. A., Nambiar, D., Tailor, D., Pal, A., Agarwal, R., and Singh, R. P. (2013). Acacetin Inhibits *In Vitro* and *In Vivo* Angiogenesis and Downregulates Stat Signaling and VEGF Expression. *Cancer Prev. Res.* 6 (10), 1128–1139. doi:10.1158/1940-6207.CAPR-13-0209

Chen, D., Ye, Z., Wang, C., Wang, Q., Wang, H., Kuek, V., et al. (2020). Arctiin Abrogates Osteoclastogenesis and Bone Resorption via Suppressing RANKL-Induced ROS and NFATc1 Activation. *Pharmacol. Res.* 159, 104944. doi:10.1016/j.phrs.2020.104944

Chen, J., Wang, C., Huang, K., Chen, S., and Ma, Y. (2020). Acacetin Suppresses IL-1β-Induced Expression of Matrix Metalloproteinases in Chondrocytes and Protects against Osteoarthritis in a Mouse Model by Inhibiting NF-κB Signaling Pathways. *Biomed. Res. Int.* 2020, 1–12. doi:10.1155/2020/2328401

Chen, X., Zhi, X., Yin, Z., Li, X., Qin, L., Qiu, Z., et al. (2018). 18β-Glycyrrhetinic Acid Inhibits Osteoclastogenesis *In Vivo* and *In Vitro* by Blocking RANKL-Mediated RANK-TRAF6 Interactions and NF-κB and MAPK Signaling Pathways. *Front. Pharmacol.* 9, 647. doi:10.3389/fphar.2018.00647

Chen, L.-R., Ko, N.-Y., and Chen, K.-H. (2019). Medical Treatment for Osteoporosis: From Molecular to Clinical Opinions. *Ijms* 20 (9), 2213. doi:10.3390/ijms20092213

Chen, Z., Zhao, F., Liang, C., Hu, L., Li, D., Zhang, Y., et al. (2020). Silencing of miR-138-5p Sensitizes Bone Anabolic Action to Mechanical Stimuli. *Theranostics* 10 (26), 12263–12278. doi:10.7150/thno.53009

Dai, Q., Xie, F., Han, Y., Ma, X., Zhou, S., Jiang, L., et al. (2017). Inactivation of Regulatory-Associated Protein of mTOR (Raptor)/Mammalian Target of Rapamycin Complex 1 (mTORC1) Signaling in Osteoclasts Increases Bone Mass by Inhibiting Osteoclast Differentiation in Mice. *J. Biol. Chem.* 292 (1), 196–204. doi:10.1074/jbc.M116.764761

Gao, B., Deng, R., Chai, Y., Chen, H., Hu, B., Wang, X., et al. (2019). Macrophage-lineage TRAP+ Cells Recruit Periosteum-Derived Cells for Periosteal Osteogenesis and Regeneration. *J. Clin. Invest.* 129 (6), 2578–2594. doi:10.1172/JCI98857

Grigoriadis, A. E., Wang, Z.-Q., Cecchini, M. G., Hofstetter, W., Felix, R., Fleisch, H. A., et al. (1994). c-Fos: a Key Regulator of Osteoclast-Macrophage Lineage Determination and Bone Remodeling. *Science* 266 (5184), 443–448. doi:10.1126/science.7939685

Hardcastle, A. C., Aucott, L., Reid, D. M., and Macdonald, H. M. (2011). Associations between Dietary Flavonoid Intakes and Bone Health in a Scottish Population. *J. Bone Miner Res.* 26 (5), 941–947. doi:10.1002/jbmr.285

Huang, Q., Shi, J., Gao, B., Zhang, H.-Y., Fan, J., Li, X.-J., et al. (2015). Gastrodin: an Ancient Chinese Herbal Medicine as a Source for Anti-osteoporosis Agents via Reducing Reactive Oxygen Species. *Bone* 73, 132–144. doi:10.1016/j.bone.2014.12.059

Ilchovska, D., and Barrow, D. M. (2021). An Overview of the NF-kB Mechanism of Pathophysiology in Rheumatoid Arthritis, Investigation of the NF-kB Ligand RANKL and Related Nutritional Interventions. *Autoimmun. Rev.* 20 (2), 102741. doi:10.1016/j.autrev.2020.102741

Jung, S. K., Kim, J. E., Lee, S.-Y., Lee, M. H., Byun, S., Kim, Y. A., et al. (2014). The P110 Subunit of PI3-K Is a Therapeutic Target of Acacetin in Skin Cancer. *Carcin* 35 (1), 123–130. doi:10.1093/carcin/bgt266

Kim, S.-I., Kim, Y.-H., Kang, B. G., Kang, M.-K., Lee, E.-J., Kim, D. Y., et al. (2020). Linarin and its Aglycone Acacetin Abrogate Actin Ring Formation and Focal Contact to Bone Matrix of Bone-Resorbing Osteoclasts through Inhibition of αvβ3 Integrin and Core-Linked CD44. *Phytomedicine* 79, 153351. doi:10.1016/j.phymed.2020.153351

Kusumbe, A. P., Ramasamy, S. K., and Adams, R. H. (2014). Coupling of Angiogenesis and Osteogenesis by a Specific Vessel Subtype in Bone. *Nature* 507 (7492), 323–328. doi:10.1038/nature13145

Leder, B. Z., Mitlak, B., Hu, M.-y., Hattersley, G., and Bockman, R. S. (2020). Effect of Abaloparatide vs Alendronate on Fracture Risk Reduction in Postmenopausal Women with Osteoporosis. *J. Clin. Endocrinol. Metab.* 105 (3), 938–943. doi:10.1210/clinem/dgz162

Lin, C., Yu, S., Jin, R., Xiao, Y., Pan, M., Pei, F., et al. (2019). Circulating miR-338 Cluster Activities on Osteoblast Differentiation: Potential Diagnostic and Therapeutic Targets for Postmenopausal Osteoporosis. *Theranostics* 9 (13), 3780–3797. doi:10.7150/thno.34493

Li, J., Lin, X., Zhang, Y., Liu, W., Mi, X., Zhang, J., et al. (2016). Preparative Purification of Bioactive Compounds fromFlos Chrysanthemi Indiciand Evaluation of its Antiosteoporosis Effect. *Evid.-Based Complement. Altern. Med.* 2016, 1–12. doi:10.1155/2016/2587201

Li, W., Zhou, X., Jiang, T., He, H., and Wen, T. (2020). Positive Effect of Gushukang on Type-H Vessel and Bone Formation. *Front. Cel Dev. Biol.* 8, 265. doi:10.3389/fcell.2020.00265

Lin, X., Xiao, Y., Chen, Z., Ma, J., Qiu, W., Zhang, K., et al. (2019). Microtubule Actin Crosslinking Factor 1 (MACF1) Knockdown Inhibits RANKL-Induced Osteoclastogenesis via Akt/GSK3β/NFATc1 Signalling Pathway. *Mol. Cell Endocrinol.* 494, 110494. doi:10.1016/j.mce.2019.110494

Meng, J., Zhang, W., Wang, C., Zhang, W., Zhou, C., Jiang, G., et al. (2020). Catalpol Suppresses Osteoclastogenesis and Attenuates Osteoclast-Derived Bone Resorption by Modulating PTEN Activity. *Biochem. Pharmacol.* 171, 113715. doi:10.1016/j.bcp.2019.113715

Moon, J. B., Kim, J. H., Kim, K., Youn, B. U., Ko, A., Lee, S. Y., et al. (2012). Akt Induces Osteoclast Differentiation through Regulating the GSK3β/NFATc1 Signaling Cascade. *J.I.* 188 (1), 163–169. doi:10.4049/jimmunol.1101254

Ono, T., and Nakashima, T. (2018). Recent Advances in Osteoclast Biology. *Histochem. Cel. Biol.* 149 (4), 325–341. doi:10.1007/s00418-018-1636-2

Pan, M.-H., Lai, C.-S., Wang, Y.-J., and Ho, C.-T. (2006). Acacetin Suppressed LPS-Induced Up-Expression of iNOS and COX-2 in Murine Macrophages and TPA-Induced Tumor Promotion in Mice. *Biochem. Pharmacol.* 72 (10), 1293–1303. doi:10.1016/j.bcp.2006.07.039

Ramasamy, S. K., Kusumbe, A. P., Schiller, M., Zeuschner, D., Bixel, M. G., Milia, C., et al. (2016). Blood Flow Controls Bone Vascular Function and Osteogenesis. *Nat. Commun.* 7, 13601. doi:10.1038/ncomms13601

Ren, J., Yue, B., Wang, H., Zhang, B., Luo, X., Yu, Z., et al. (2020). Acacetin Ameliorates Experimental Colitis in Mice via Inhibiting Macrophage Inflammatory Response and Regulating the Composition of Gut Microbiota. *Front. Physiol.* 11, 577237. doi:10.3389/fphys.2020.577237

Shi, Y., Shu, H., Wang, X., Zhao, H., Lu, C., Lu, A., et al. (2020). Potential Advantages of Bioactive Compounds Extracted from Traditional Chinese Medicine to Inhibit Bone Destructions in Rheumatoid Arthritis. *Front. Pharmacol.* 11, 561962. doi:10.3389/fphar.2020.561962

Song, C., Cao, J., Lei, Y., Chi, H., Kong, P., Chen, G., et al. (2020). Nuciferine Prevents Bone Loss by Disrupting Multinucleated Osteoclast Formation and Promoting Type H Vessel Formation. *FASEB j.* 34 (3), 4798–4811. doi:10.1096/fj.201902551R

Takayanagi, H., Kim, S., Koga, T., Nishina, H., Isshiki, M., Yoshida, H., et al. (2002). Induction and Activation of the Transcription Factor NFATc1 (NFAT2) Integrate RANKL Signaling in Terminal Differentiation of Osteoclasts. *Dev. Cel.* 3 (6), 889–901. doi:10.1016/s1534-5807(02)00369-6

Tatangelo, G., Watts, J., Lim, K., Connaughton, C., Abimanyi-Ochom, J., Borgström, F., et al. (2019). The Cost of Osteoporosis, Osteopenia, and Associated Fractures in Australia in 2017. *J. Bone Miner Res.* 34 (4), 616–625. doi:10.1002/jbmr.3640

Tondravi, M. M., McKercher, S. R., Anderson, K., Erdmann, J. M., Quiroz, M., Maki, R., et al. (1997). Osteopetrosis in Mice Lacking Haematopoietic Transcription Factor PU.1. *Nature* 386 (6620), 81–84. doi:10.1038/386081a0

Wang, L., Zhou, F., Zhang, P., Wang, H., Qu, Z., Jia, P., et al. (2017). Human Type H Vessels Are a Sensitive Biomarker of Bone Mass. *Cell Death Dis.* 8 (5), e2760. doi:10.1038/cddis.2017.36

Wang, S., Lin, B., Liu, W., Wei, G., Li, Z., Yu, N., et al. (2020). Acacetin Induces Apoptosis in Human Osteosarcoma Cells by Modulation of ROS/JNK Activation. *Dddt* 14, 5077–5085. doi:10.2147/DDDT.S275148

Wei, Y., Yuan, P., Zhang, Q., Fu, Y., Hou, Y., Gao, L., et al. (2020). Acacetin Improves Endothelial Dysfunction and Aortic Fibrosis in Insulin-Resistant SHR Rats by Estrogen Receptors. *Mol. Biol. Rep.* 47 (9), 6899–6918. doi:10.1007/s11033-020-05746-3

Wu, M., Chen, W., Lu, Y., Zhu, G., Hao, L., and Li, Y.-P. (2017). Gα13 Negatively Controls Osteoclastogenesis through Inhibition of the Akt-GSK3β-NFATc1 Signalling Pathway. *Nat. Commun.* 8, 13700. doi:10.1038/ncomms13700

Xiaoqun Li, X., Wang, L., Huang, B., Gu, Y., Luo, Y., Zhi, X., et al. (2020). Targeting Actin-Bundling Protein L-Plastin as an Anabolic Therapy for Bone Loss. *Sci. Adv.* 6 (47), eabb7135. doi:10.1126/sciadv.abb7135

Xie, H., Cui, Z., Wang, L., Xia, Z., Hu, Y., Xian, L., et al. (2014). PDGF-BB Secreted by Preosteoclasts Induces Angiogenesis during Coupling with Osteogenesis. *Nat. Med.* 20 (11), 1270–1278. doi:10.1038/nm.3668

Xu, Q., Chen, G., Xu, H., Xia, G., Zhu, M., Zhan, H., et al. (2021). Celastrol Attenuates RANKL-Induced Osteoclastogenesis *In Vitro* and Reduces Titanium Particle-Induced Osteolysis and Ovariectomy-Induced Bone Loss *In Vivo*. *Front. Pharmacol.* 12, 682541. doi:10.3389/fphar.2021.682541

Yang, P., Lv, S., Wang, Y., Peng, Y., Ye, Z., Xia, Z., et al. (2018). Preservation of Type H Vessels and Osteoblasts by Enhanced Preosteoclast Platelet-Derived Growth Factor Type BB Attenuates Glucocorticoid-Induced Osteoporosis in Growing Mice. *Bone* 114, 1–13. doi:10.1016/j.bone.2018.05.025

Yingxing Xu, Y., Jiang, Y., Jia, B., Wang, Y., and Li, T. (2021). Icariin Stimulates Osteogenesis and Suppresses Adipogenesis of Human Bone Mesenchymal Stem Cells via miR-23a-Mediated Activation of the Wnt/β-Catenin Signaling Pathway. *Phytomedicine* 85, 153485. doi:10.1016/j.phymed.2021.153485

Zhang, Z.-q., He, L.-p., Liu, Y.-h., Liu, J., Su, Y.-x., and Chen, Y.-m. (2014). Association between Dietary Intake of Flavonoid and Bone mineral Density in Middle Aged and Elderly Chinese Women and Men. *Osteoporos. Int.* 25 (10), 2417–2425. doi:10.1007/s00198-014-2763-9

Zhu, Y., Ruan, Z., Lin, Z., Long, H., Zhao, R., Sun, B., et al. (2019). The Association between CD31(hi)Emcn(hi) Endothelial Cells and Bone mineral Density in Chinese Women. *J. Bone Miner Metab.* 37 (6), 987–995. doi:10.1007/s00774-019-01000-4

Conflict of Interest: The authors declare that the research was conducted in the absence of any commercial or financial relationships that could be construed as a potential conflict of interest.

Publisher's Note: All claims expressed in this article are solely those of the authors and do not necessarily represent those of their affiliated organizations, or those of the publisher, the editors and the reviewers. Any product that may be evaluated in this article, or claim that may be made by its manufacturer, is not guaranteed or endorsed by the publisher.

frontiers | Frontiers in Cell and Developmental Biology

REVIEW
published: 13 May 2022
doi: 10.3389/fcell.2022.886305

The Osteoclast Traces the Route to Bone Tumors and Metastases

Sharon Russo†, *Federica Scotto di Carlo*† *and Fernando Gianfrancesco* *

Institute of Genetics and Biophysics "Adriano Buzzati-Traverso", National Research Council of Italy, Naples, Italy

Osteoclasts are highly specialized cells of the bone, with a unique apparatus responsible for resorption in the process of bone remodeling. They are derived from differentiation and fusion of hematopoietic precursors, committed to form mature osteoclasts in response to finely regulated stimuli produced by bone marrow–derived cells belonging to the stromal lineage. Despite a highly specific function confined to bone degradation, emerging evidence supports their relevant implication in bone tumors and metastases. In this review, we summarize the physiological role of osteoclasts and then focus our attention on their involvement in skeletal tumors, both primary and metastatic. We highlight how osteoclast-mediated bone erosion confers increased aggressiveness to primary tumors, even those with benign features. We also outline how breast and pancreas cancer cells promote osteoclastogenesis to fuel their metastatic process to the bone. Furthermore, we emphasize the role of osteoclasts in reactivating dormant cancer cells within the bone marrow niches for manifestation of overt metastases, even decades after homing of latent disseminated cells. Finally, we point out the importance of counteracting tumor progression and dissemination through pharmacological treatments based on a better understanding of molecular mechanisms underlying osteoclast lytic activity and their recruitment from cancer cells.

Keywords: osteoclast bone resorption, skeletal tumors, bone metastases, vicious cycle, tumor dormancy

OPEN ACCESS

Edited by:
Stefania Mariggiò,
Institute of Biochemistry and Cell Biology (CNR), Italy

Reviewed by:
Wei Zou,
Washington University in St. Louis, United States
Helen Knowles,
University of Oxford, United Kingdom
Miranda Clements,
National Institutes of Health (NIH), United States

***Correspondence:**
Fernando Gianfrancesco
fernando.gianfrancesco@igb.cnr.it

†*These authors have contributed equally to this work and share first authorship*

Specialty section:
This article was submitted to Cellular Biochemistry, a section of the journal Frontiers in Cell and Developmental Biology

Received: *28 February 2022*
Accepted: *24 March 2022*
Published: *13 May 2022*

Citation:
Russo S, Scotto di Carlo F and Gianfrancesco F (2022) The Osteoclast Traces the Route to Bone Tumors and Metastases. Front. Cell Dev. Biol. 10:886305. doi: 10.3389/fcell.2022.886305

INTRODUCTION

Bone is a dynamic tissue that constantly requires removal of old and damaged bone and generation of newly synthesized bone to restore structural integrity. For this purpose, two main cell types have evolved: osteoclasts and osteoblasts. The former are polykaryon of hematopoietic origin, which form as a result of the fusion of mononuclear precursors driven by the production of two pivotal cytokines derived from the marrow microenvironment: the macrophage colony-stimulating factor (M-CSF) and the receptor activator of nuclear factor kappa B ligand (RANKL) (Suda et al., 1992; Teitelbaum, 2000). Osteoclasts possess an efficient machinery responsible for mineral dissolution and degradation of large quantity of organic bone matrix and mineralized cartilage (Boyle et al., 2003). Multiple pathologies are associated with osteoclast dysfunction, including Paget's disease of bone, where genetic determinants lead to higher sensitivity of osteoclast precursors to pro-differentiation cytokines, formation of giant and hyper-nucleated osteoclasts, and increased ability to resorb bone matrix (Divisato et al., 2016; Scotto di Carlo et al., 2020a). Given the variety of cells present within bone marrow, it is not surprising that the bone is also the site of several tumors and metastases (Coleman et al., 2020). Although it is widely accepted that osteoclasts do not undergo neoplastic transformation, increasing evidence has demonstrated their indirect involvement in the process of tumorigenesis and their support to cancer cells. In this review, starting from the

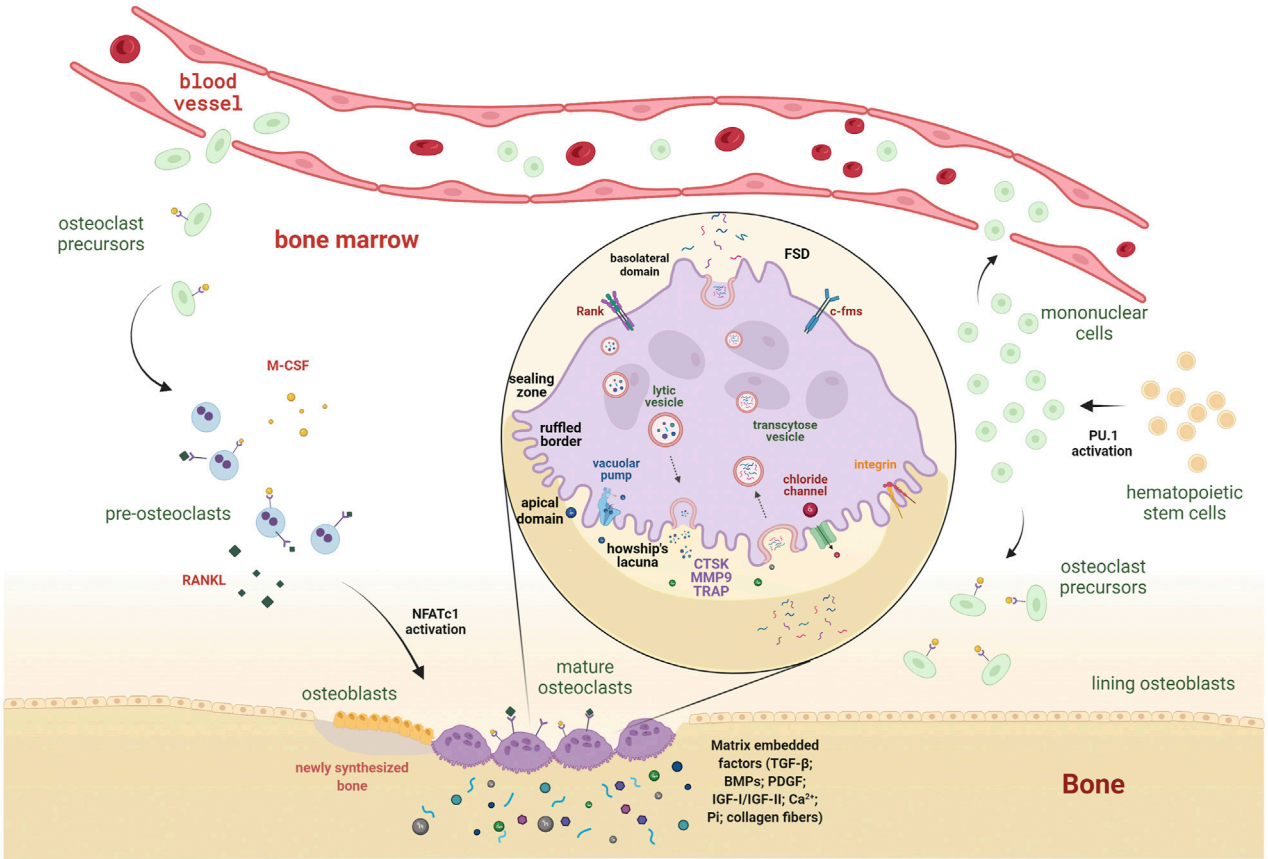

FIGURE 1 | From hematopoietic stem cells to mature osteoclasts: behind the scene of osteoclastogenesis. Following the expression of *PU.1*, hematopoietic stem cells differentiate in mononuclear cells. The latter become osteoclast precursors upon the M-CSF stimulus. They reach the bone site to be resorbed either by recruitment from the surrounding bone marrow or the bloodstream and become mature osteoclasts through stimulation of M-CSF and RANKL, released by the stromal/osteoblastic compartment. The binding of these cytokines to their receptors, c-Fms and RANK, triggers the downstream activation of osteoclastogenic transcriptional factors (e.g., NFATc1), inducing the expression of genes involved in osteoclast-mediated bone erosion. Magnification of mature osteoclast shows functional membrane domains defining an apicobasal polarity. Osteoclasts closely adhere to the bone through the F-actin reach sealing zone, surrounded by integrins ($\alpha_v\beta_3$), which delineates the ruffled border. The resorption area under the ruffled border, the Howship's lacunae, is an acidic compartment due to release of H^+ and Cl^- ions. The acidic environment degrades inorganic structures, while organic components require extracellular release of lysosomal enzymes, such as CTSK, MMP9, and TRAP, for their degradation. Osteoclasts release growth and osteotropic factors (i.e., TGF-β, BMPs, PDGF, IGF-I, and IGF-II) trapped within the matrix. Inorganic products (i.e., Ca^{2+} and Pi) and organic molecules (e.g., collagen fibers) are packaged into transcytoses vesicles, which are transported to the functional secretory domain (FSD) at the basolateral domain of osteoclasts and secreted *via* exocytosis. M-CSF, macrophage colony-stimulating factor; RANKL, receptor activator of nuclear factor kappa B ligand; c-Fms, colony-stimulating factor 1 receptor; RANK, receptor activator of nuclear factor kappa B; NFATc1, nuclear factor of activated T cells 1; H^+, proton; Cl^-, chloride ion; CTSK, cathepsin K; MMP9, matrix metallopeptidase 9; TRAP, tartrate-resistant acid phosphatase; TGF-β, transforming growth factor-β; BMPs, bone morphogenetic proteins; PDGF, platelet-derived growth factor; IGF-I and IGF-II, insulin-like growth factor I and II; Ca^{2+}, calcium ion; Pi, inorganic phosphate.

description of physiological role of osteoclasts, we will deepen their involvement in bone tumors and metastases. In particular, we will focus on the effects of these cells on the creation and maintenance of cancer microenvironment and their cooperation with tumor cells.

BIOLOGY OF OSTEOCLASTS

Osteoclast formation. Osteoclastogenesis begins with the stimulation of bone marrow–derived hematopoietic stem cells to turn into mononuclear cells (Tondravi et al., 1997). This phase requires activation of the PU.1 transcription factor, belonging to the Ets family. In fact, mice harboring the *PU.1* gene disruption manifest complete absence of osteoclasts, resulting in osteopetrotic features (Tondravi et al., 1997). Mononuclear cells are either present in the bone marrow and stimulated to become osteoclast precursors or introduced in the bloodstream to circulate until they return to the bone to be resorbed and there differentiate into mature osteoclasts (Muto et al., 2011; Warde, 2011) (**Figure 1**). The survival, proliferation, and differentiation of osteoclasts and their precursors are provided by M-CSF signaling, which results in the activation of ERK and PI3K/Akt pathways (Nakamura et al., 2001; Glantschnig et al., 2003). Indispensable for osteoclast maturation and their complete activation is RANKL, a type II transmembrane protein

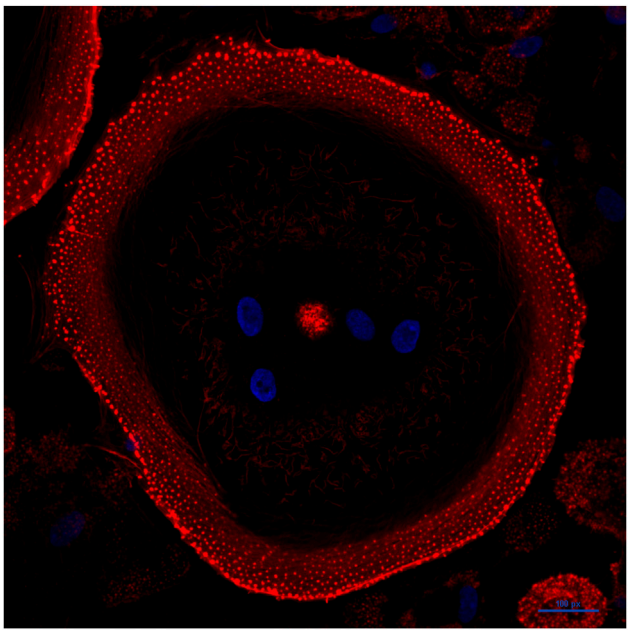

FIGURE 2 | Mature osteoclasts assemble an F-actin ring. Confocal image of a human osteoclast derived from stimulation of peripheral blood mononuclear cells of a healthy donor with M-CSF and RANKL. Nuclei are shown in blue (stained with Hoechst 33342); F-actin is shown in red (stained with phalloidin). The cell is grown on glass and displays a mature actin ring that surrounds the ruffled border and has evolved into a large peripheral podosome belt.

produced by osteoblasts as a proteolytically released soluble molecule (Boyle et al., 2003). In response to binding to its receptor RANK, a cascade signaling pathway is triggered, which determines the recruitment of TRAF6 to the intracellular domain of RANK and culminates in the downstream activation of osteoclastogenic transcription factors, such as NF-κB, activator protein 1 (AP-1), cyclic adenosine monophosphate response element–binding protein (CREB), and nuclear factor of activated T cells 1 (NFATc1) (Kobayashi et al., 2001; Gohda et al., 2005) (**Figure 1**). The process of fusion is essential for the formation of large and multinucleated osteoclasts (Teitelbaum, 2000). Several factors regulate osteoclast fusion, which can be divided into molecules regulated by RANKL (CD9, ATP6V0d2, and DC-STAMP) and those that are not dependent on RANKL stimulation (CD44, CD47, and TREM2) (Xing et al., 2012). Among them, DC-STAMP is the master fusion factor, and its abrogation results in mononuclear TRAP-positive cells, indicating that cell fusion is hampered (Yagi et al., 2005). Mature osteoclasts reach a huge diameter (20–100 μm), essential for the attachment to the site of bone resorption and matrix degradation, drilling a pit into the bone tissue (Tiedemann et al., 2017).

Osteoclast structure. Active bone-resorbing osteoclasts show a peculiar cellular polarization, with the apical membrane facing the bone surface—consisting of the *sealing zone* and the *ruffled border*—and the basolateral plasma membrane (**Figure 1**). The sealing zone is the result of cytoskeleton reorganization aimed at forming an F actin–rich ring to mediate the tight attachment of the osteoclast to the extracellular matrix (Teitelbaum, 2000) (**Figure 2**). As osteoclast prepares itself to resorb the bone, it forms a ruffled border, a resorbing organelle consisting of intracellular acidified fused vesicles, which represents the site where bone resorption takes place (Blair et al., 1989; Huizing et al., 2008) (**Figure 1**). Unlike other lytic cells (e.g., macrophages), osteoclasts arrange an extracellular lysosomal acidified compartment, generally called Howship's lacuna, in which lytic enzymes, such as cathepsin K (CTSK), matrix metalloproteinase-9 (MMP9), and tartrate-resistant acid phosphatase (TRAP), are secreted through protease-bearing vesicles (Abu-Amer et al., 1999; Teitelbaum, 2000; Luzio et al., 2014). Thus, osteoclasts have evolved to utilize lysosomes to carry out one of the most difficult jobs in our body, namely, to excavate the mineralized bone.

Osteoclast function. The dissolution of minerals initiates with the secretion of chloride ions (Cl^-) and the activation of H^+- and ATP-consuming vacuolar pumps through the ruffled border into the lacuna (Blair et al., 1989) (**Figure 1**). The chloride ions passively follow protons (H^+) through the chloride channel present on the ruffled border, and the combined exit of H^+ and Cl^- acidifies the resorption compartment, reaching a low pH environment (~4) (Blair and Schlesinger, 1990) (**Figure 1**). The creation of an acidic compartment not only fosters the beginning of matrix dissolution and activation of lytic enzymes (e.g., CTSK) but also directly stimulates osteoclasts, inducing a significant increase in intracellular Ca^{2+} concentration, which acts through calmodulin to stimulate calcineurin activity. Calcineurin, in fact, moves the autoinhibitory domain away from its catalytic site for the dephosphorylation of NFATc1 nuclear localization signal (Park et al., 1995; Wesselborg et al., 1996). As a consequence, the translocation of NFATc1 to the nucleus further stimulates resorption, allowing the expression of osteoclastogenic markers, such as *DC-STAMP, TRAP, CTSK*, and several integrins, which determine full osteoclast maturation (Kobayashi et al., 2001; Mizukami et al., 2002; Komarova et al., 2005). The main enzyme involved in matrix digestion is CTSK, with the participation of other proteolytic enzymes belonging to big families of cysteine proteinases and matrix metalloproteinases (MMPs) (Bossard et al., 1996; Everts et al., 2006). The depletion or inhibition of CTSK results in an overall reduction in bone resorption efficiency interrupting intracellular vesicular trafficking while maintaining all the other osteoclast functions, such as, cell formation, activation, and secretory process (Leung et al., 2011). Of interest, bone site-specific osteoclasts exist, which use a different enzyme repertoire during the bone resorption function (Everts et al., 2009). For example, osteoclasts residing in calvaria or scapular bone, despite expressing cathepsins, preferentially use MMPs for degradation (Shorey et al., 2004; Everts et al., 2006). Another remarkable difference between osteoclast groups that populate different bone sites is the amount of TRAP enzyme released at bone remodeling sites (Everts et al., 2009). Calvarial osteoclasts show increased levels of TRAP activity—up to 25-fold higher—compared to the levels detected at long bone sites, likely to compensate for the

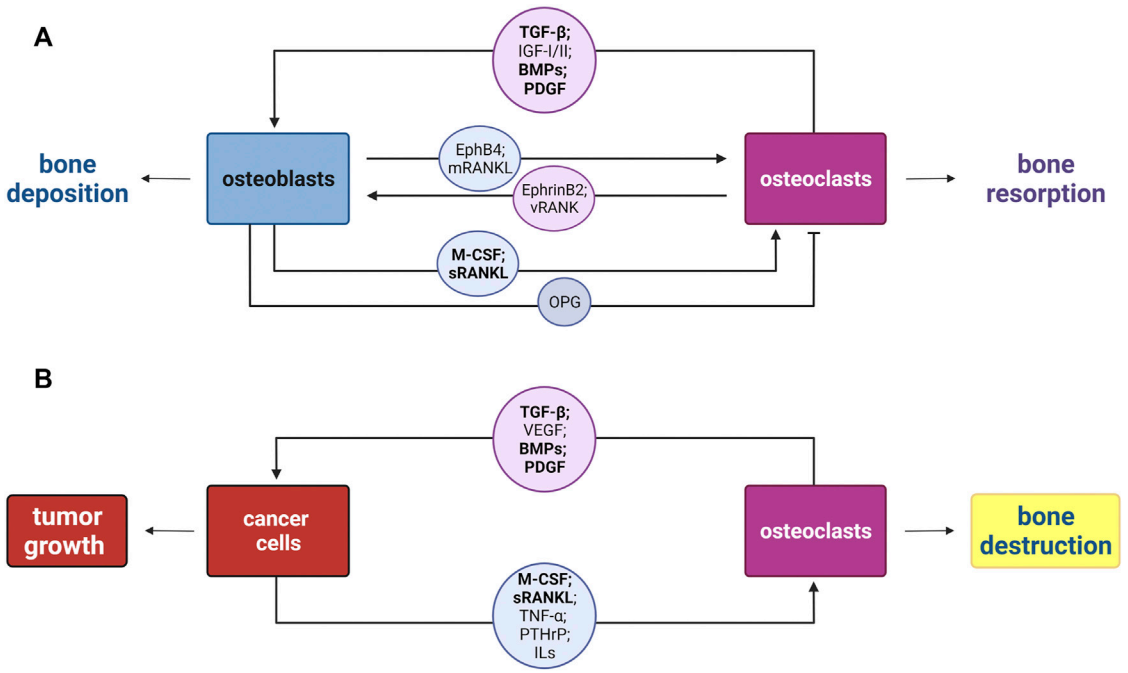

FIGURE 3 | Schematic representation of the osteoclast–osteoblast coupling in bone remodeling *versus* the vicious cycle in bone tumors. **(A)** New bone deposition occurs at bone resorption sites in each cycle of bone remodeling by the osteoblast–osteoclast coupling. Osteoblasts mediate both osteoclasts activation and inhibition, *via* secretion of M-CSF, soluble RANKL (sRANKL), and OPG. Instead, osteoclasts are able to mediate bone deposition by the release of matrix-embedded factors upon bone erosion (TGF-β, IGF-I/II, BMPs, and PDGF), through the secretion of extracellular vesicles carrying the receptor RANK (vRANK), and direct interaction through the membrane protein ephrinB2 with the osteblastic EphB4. **(B)** Disruption of the osteoblast–osteoclast coupling by the vicious cycle of bone. Tumor cells secrete soluble factors including M-CSF, sRANKL, TNF-α, PTHrP, and several interleukins (ILs), which act on osteoclast to enhance their bone destruction activity. Consequently, osteoclasts contribute to tumor growth and progression releasing TGF-β, pro-angiogenic factor VEGF, different BMPs, and PDGF. In bold are highlighted the molecules shared by the two cycles. M-CSF, macrophage colony-stimulating factor; RANKL, receptor activator of nuclear factor kappa B ligand; OPG, osteoprotegerin; TGF-β, transforming growth factor-β; IGF-I and IGF-II, insulin-like growth factor I and II; BMPs, bone morphogenetic proteins; PDGF, platelet-derived growth factor; RANK, receptor activator of nuclear factor kappa B; EphB4 and Eph receptor B4; TNF-α, tumor necrosis factor-α; PTHrP, parathyroid hormone-related protein; VEGF, vascular endothelial growth factor.

aforementioned lower cysteine proteinase activity and also to degrade non-collagenous proteins of this type of bone (Perez-Amodio et al., 2006).

Osteoclast–osteoblast coupling activities. The osteoclast resorbing activity needs to be neutralized to avoid excessive bone erosion. To this end, osteoblasts—in addition to the aforementioned RANKL—produce Osteoprotegerin (OPG), the soluble decoy receptor for RANKL that selectively inhibits RANK and RANKL binding, due to the homology to the members of the TNF receptor family, thereby blocking osteoclastogenesis (Simonet et al., 1997; Lacey et al., 1998; Robling et al., 2006) (**Figure 3A**). Thus, osteoblasts can be thought of as regulators of both osteoclast activation and inhibition.

Osteoclasts act upon osteoblast lineage cells producing multiple proteins, either associated with exosomes (e.g., RANK), released from the resorbed bone, or secreted, and they also directly interact with osteoblasts through membrane-bound proteins (Sims and Martin, 2020) (**Figure 3A**). The ability of osteoclasts to regulate osteoblasts, even independent of their resorption activity, was observed with the formation of mineralized nodules in osteoblast cultures in the presence of conditioned medium derived from osteoclasts grown on plastic, and hence not releasing products from degradation (Karsdal et al., 2008). Nevertheless, the byproducts of bone degradation certainly impact osteoblast differentiation. Indeed, released transforming growth factor-β (TGF-β) is able to promote the recruitment of BMSCs at the remodeled site, by activating mammalian target of rapamycin (mTOR) (Tang et al., 2009). Also, the release of insulin-like growth factors, that is, IGF-I and IGF-II, together with BMPs and the homodimeric platelet-derived growth factor (PDGF) additionally support BMSCs recruitment and stimulate osteoblast progenitor expansion, migration, and differentiation, thus enhancing bone formation (Mitlak et al., 1996; Xian et al., 2012; Xie et al., 2014). Furthermore, a recent seminal work highlighted that the RANK and RANKL axis works as *reverse signaling* to allow osteoclasts to communicate with osteoblasts, utilizing the same molecules, which they are target thereof (Ikebuchi et al., 2018). Osteoclasts release small extracellular vesicles that carry the receptor RANK (vesicular RANK), which binds RANKL molecules present on pre-osteoblast and early osteoblast membranes (membranous RANKL) (Ikebuchi et al., 2018). This binding triggers intracellular signaling, culminating in the expression of the master regulator of osteoblastogenesis, *RUNX2*

(Ikebuchi et al., 2018; Zaidi and Cardozo, 2018). Of note, the proline-rich motif in the RANKL cytoplasmic tail is fundamental for the reverse signaling to occur. In fact, mice harboring a point mutation in this domain showed reduced activation of osteoblasts stimulated by RANK-exposed microvesicles released by osteoclasts (Ikebuchi et al., 2018). Despite the ability to regulate osteoblasts at a distance, osteoclasts also developed mechanisms to directly interact with osteoblast precursors. An example of this class of direct cell–cell communication is EphrinB2–EphB4, where osteoclast-derived ephrinB2 contact with osteoblastic EphB4 enhances osteoblast differentiation, by lowering RhoA activity (Zhao et al., 2006).

Once completed bone deposition, osteoblasts remain trapped within the matrix and become osteocytes, showing extensive dendritic processes through which they communicate with other bone cells. Indeed, osteocytes are the main cells able to sense mechanical and hormonal stimuli, to which they respond by regulating osteoblast and osteoclast activity (Bellido, 2014). In this regard, osteocytes express the RANKL cytokine to support osteoclastogenesis, even in a higher amount than bone marrow stromal cells (Nakashima et al., 2011). Accordingly, mice lacking RANKL specifically in osteocytes manifest a dramatic osteopetrotic phenotype (Nakashima et al., 2011).

Therefore, osteoclast and osteoblast formation and activity are strictly regulated to ensure a physiological bone remodeling and the maintenance of the quality and quantity of bone through the entire life-course, where osteoclastic bone erosion is generally always followed by osteoblastic bone deposition (Martin, 2014).

ROLE OF OSTEOCLASTS IN TUMOR BIOLOGY

Primary Bone Tumors

Although most bone cancers have a mesenchymal origin, osteoclasts frequently contribute to increase their aggressiveness, conferring lytic features to tumors (Valastyan and Weinberg, 2011). The pivotal role of osteoclasts in the creation and maintenance of a favorable tumor microenvironment stems from initial studies in animal models supporting this evidence. Mice harboring a deletion in the integrin β3—an essential protein for osteoclast activity—manifest resistance to bone tumor growth and osteolytic metastasis upon intra-tibial injection of cancer cell lines, which conversely promptly caused tumor-associated bone loss and tumor metastasis in the control group (Bakewell et al., 2003).

Among the bone tumors with a remarkable osteoclast activity, giant cell tumors (GCT), osteosarcomas (OS), and chondrosarcomas (CS) are the most common. These tumors have different origin and behavior, yet they share a low-to-high composition of osteoclasts that mediate the tumor-associated bone destruction.

Giant cell tumor. Giant cell tumor is a common benign tumor, mainly affecting the epiphysis of long bones in young adults (Goldenberg et al., 1970). Although the neoplastic cell has been undoubtedly identified as the stromal cell carrying mutations in *H3F3A*, osteoclast-like giant cells strongly influences the aggressiveness of the tumor, to the extent that these cells name the tumor (Behjati et al., 2013). These giant osteoclastic cells could comprise more than 50% of the total cell content of the tumor (Atkins et al., 2000; Morgan et al., 2005). Giant cells, albeit non-tumoral elements, are responsible for destructive osteolysis seen in GCT, even involving the bone cortex and resulting in pathological fractures in ~30% of patients (Campanacci et al., 1987). The lytic properties of osteoclast-like giant cells also allow the tumor to extend into soft tissues (Mavrogenis et al., 2017; Palmerini et al., 2019). Similar to osteoclasts, giant cells also express the RANK receptor on their surface, suggesting their formation as a result of fusion of monocytic precursors recruited by the stromal cells through the expression of RANKL, exactly as is the case for osteoclasts (Morgan et al., 2005). The high expression of RANKL within the tumor paved the way for the use of denosumab, a fully human monoclonal antibody to RANKL, as efficient treatment for GCT, reducing its lytic activity (Chawla et al., 2019; Alothman et al., 2020). Therefore, targeting giant cells is a more effective approach than targeting neoplastic stromal cells. GCT can also arise as severe degeneration of Paget's disease of bone (PDB), a bone remodeling disorder (GCT/PDB). GCT/PDB generally involves the axial skeleton and is caused by germline mutations in *ZNF687*, thus affecting both the stromal and osteoclastic compartments (Divisato et al., 2016; Divisato et al., 2018). *ZNF687* encodes a transcription factor with a key role in promoting osteoclast differentiation (Divisato et al., 2018). Consequently, giant cells found in GCT/PDB biopsies are even bigger than conventional GCT, and the tumor usually shows a worse prognosis (Divisato et al., 2017; Scotto di Carlo et al., 2020b). PDB patients harboring *ZNF687* mutations display a lower likelihood of developing the tumor when treated with bisphosphonates, strong inhibitors of osteoclast activity used to suppress the elevated bone resorption in PDB (Rendina et al., 2015; Divisato et al., 2018; Ralston, 2020). It seems that by controlling the progression of PDB, the neoplastic transformation is prevented (Scotto di Carlo et al., 2020b). This observation confirms that tumor development and aggressiveness might be reduced by decreasing osteoclast resorption.

Osteosarcoma. Osteosarcoma (OS) is the most common and aggressive bone tumor, primarily arising in long bones of children and adolescents (Mirabello et al., 2009). The great genetic heterogeneity that characterizes OS results in multiple histological appearances of the tumor (Kansara et al., 2014; Rickel et al., 2017). Common histological variants of OS include osteoblastic, chondroblastic, and fibroblastic types, depending on the main cellular atypia and the type of the extracellular matrix produced by neoplastic cells (Kansara et al., 2014). Giant cell OS is a rare histological variant (comprising less than 3% of all OS), characterized by numerous osteoclast-like giant cells in addition to osteoid matrix. In addition to making differential diagnosis difficult due to similarity with other giant cell rich lesions (e.g., GCT and aneurysmal bone cyst), the presence of osteoclasts within OS is a key driver of cancer-associated bone degradation (Domansk and Walther, 2017). However, bone

degradation is part of the pathological process for all OS subtypes, and a certain number of osteoclasts are consistently present in OS, both at the periphery of the tumor and within the tumor tissue (Avnet et al., 2008). High levels of PTHrP, IL-6, and RANKL have been detected in both OS samples and cell lines, suggesting local production of cytokines and growth factors as a mechanism for tumor cells to enhance osteoclastogenesis (Avnet et al., 2008). In support of this, OS-derived exosomes promote osteoclast differentiation and bone resorption activity (Raimondi et al., 2020). Under this respect, PTHrP seems to be of particular importance: through its secretion, the tumor cells can simultaneously stimulate the expression of RANKL and reduce the expression of OPG by osteoblast cells, overstimulating osteoclast differentiation (Guise et al., 2002). Consequently, it appears evident that targeting RANKL is one of the most suitable approaches in personalized medicine in order to contrast OS aggressiveness (Trinidad and Gonzalez-Suarez, 2016). Mice with osteolytic OS treated with OPG or RANK-Fc, a therapeutic antagonist for RANKL, showed decreased osteoclast number, although the therapy had no effect on cancer cells. However, OS-bearing mice displayed reduced tumor growth, increased survival, and significant reduction in tumor metastasis degeneration. In addition, preventive treatment with RANK-Fc completely inhibited OS development (Lamoureux et al., 2007; Lamoureux et al., 2008; Chen et al., 2015). To further underscore the importance of RANKL signaling in OS, crossing *Rankl*$^{-/-}$ mice with a mouse model with inactive p53 and Rb1, which spontaneously develops aggressive and metastatic OS, resulted in a marked suppression of OS development and reduced number of metastatic lesions (Chen et al., 2015). This emphasizes the role of bone-resorbing osteoclasts in the progression of OS.

In the elderly, OS typically associates with PDB (OS/PDB) and shows a 5-year survival rate almost nil (Deyrup et al., 2007). OS/PDB usually shows enrichment in osteoclasts within the tumor sites, perhaps as a result of recruitment of pre-existing hyperactive osteoclasts in the PDB sites (Hansen et al., 2006). Although genetically complex, the loss of the *PFN1* has been found as a recurrent theme in OS/PDB samples (Scotto di Carlo et al., 2020a; Scotto di Carlo et al., 2022). *PFN1* encodes Profilin 1, an essential actin-binding protein with a key role in cytoskeleton remodeling and intracellular trafficking (Pimm et al., 2020; Murk et al., 2021). Profilin 1 depletion in the RAW264.7 monocytic cell line resulted in higher sensitivity to RANKL and consequent formation of large and hyper-nucleated osteoclasts (Scotto di Carlo et al., 2020a). Accordingly, a mouse model carrying a loss-of-function mutation in *Pfn1* exhibits active bone resorption and bone loss (Wei et al., 2021). This underscores the effect of Profilin 1 downregulation in osteoclast formation in OS.

Chondrosarcoma and chondroblastoma. Chondrosarcomas are the second most common malignant bone sarcomas and constitute a heterogenous group of neoplasms where tumor cells produce cartilage matrix (Gelderblom et al., 2008; Valery et al., 2015). The main localization areas of chondrosarcomas are pelvic bone, scapula, and long bones (Brown et al., 2018). The bone microenvironment plays a pivotal role in chondrosarcoma development, as supported by histological examination of conventional chondrosarcoma revealing the presence of numerous bone cells (i.e., osteoclasts and osteoblasts) in close contact to the cartilaginous tumor cells (Grimaud et al., 2002). The infiltration of chondrosarcoma tumor cells into the bone tissue is associated with bone resorption through the stimulation of osteoclast formation (David et al., 2011). Accordingly, the presence of osteoclasts has been observed in the microenvironment of chondrosarcoma, responsible for the bone destruction behavior (David et al., 2011; Otero et al., 2014). Inherent in this observation, chondrosarcoma possesses an aggressive lytic activity, characterized by osteopenia, cortical erosion, and pathologic fractures, as detected by radiographic imaging (Ollivier et al., 2003; Littrell et al., 2004; Gelderblom et al., 2008). Because tumor cells lack the ability to resorb the bone, they take advantage of osteoclast activation in the tumor microenvironment for their propagation. Indeed, culture media conditioned by chondrosarcoma cell lines was able to trigger the formation of mature osteoclasts in the RAW264.7 monocytic cell line. Also, chondrosarcoma tumors formed by the injection of chondrosarcoma cells in nude mice contained a remarkable number of TRAP-positive osteoclasts (Clark et al., 2010). Furthermore, unlike subcutaneously formed chondrosarcomas, the intra-tibial tumors displayed increased tumor infiltration and bone destruction (Hamm et al., 2010). Interestingly, in these tumors high expression of osteoclast-related enzymes was detected, for example, cathepsins and metalloproteineases, presumably promoting tumor invasion (Hamm et al., 2010). In line with an osteoclast-promoting capacity of chondrosarcoma tumor cells, therapies aimed at targeting RANKL proved to be beneficial in chondrosarcoma treatment. Indeed, chondrosarcoma is highly resistant to current chemotherapy and radiation regimens, and surgical treatment leads to severe disability (Moussavi-Harami et al., 2006; Polychronidou et al., 2017). Therefore, the use of bisphosphonates as adjuvant therapy may have clinical utility in chondrosarcoma patients. In particular, two different studies demonstrated that treatment of chondrosarcoma-bearing rats with zoledronic acid—a potent bisphosphonate—prevented cortical destruction, inhibited trabecular resorption, and resulted in decreased tumor volume in the bone (Gouin et al., 2006; Otero et al., 2014). Thus, suppression of osteoclasts seems to be a key approach to inhibit local cancer growth.

Another bone tumor–producing chondroid matrix is chondroblastoma. However, chondroblastoma is a benign tumor, even though it is locally aggressive and affects younger patients (Kaim et al., 2002; McCarthy and Frassica, 2014). It characteristically occurs in the epiphyses of long bones, particularly the femur and tibia (McCarthy and Frassica, 2014). Histologically, chondroblastomas exhibit multinucleated osteoclast-like giant cells (Lucas, 1996). For this reason, it resembles giant cell tumor; in fact, in 1931, it was defined as "chondromatous giant cell tumor" (De Mattos et al., 2013). However, immunohistochemical positivity to protein S-100, marker of chondrocytes and cartilaginous differentiation, exclusively in chondroblastoma tumor cells, helps the differential diagnosis between the two tumors (Monda and

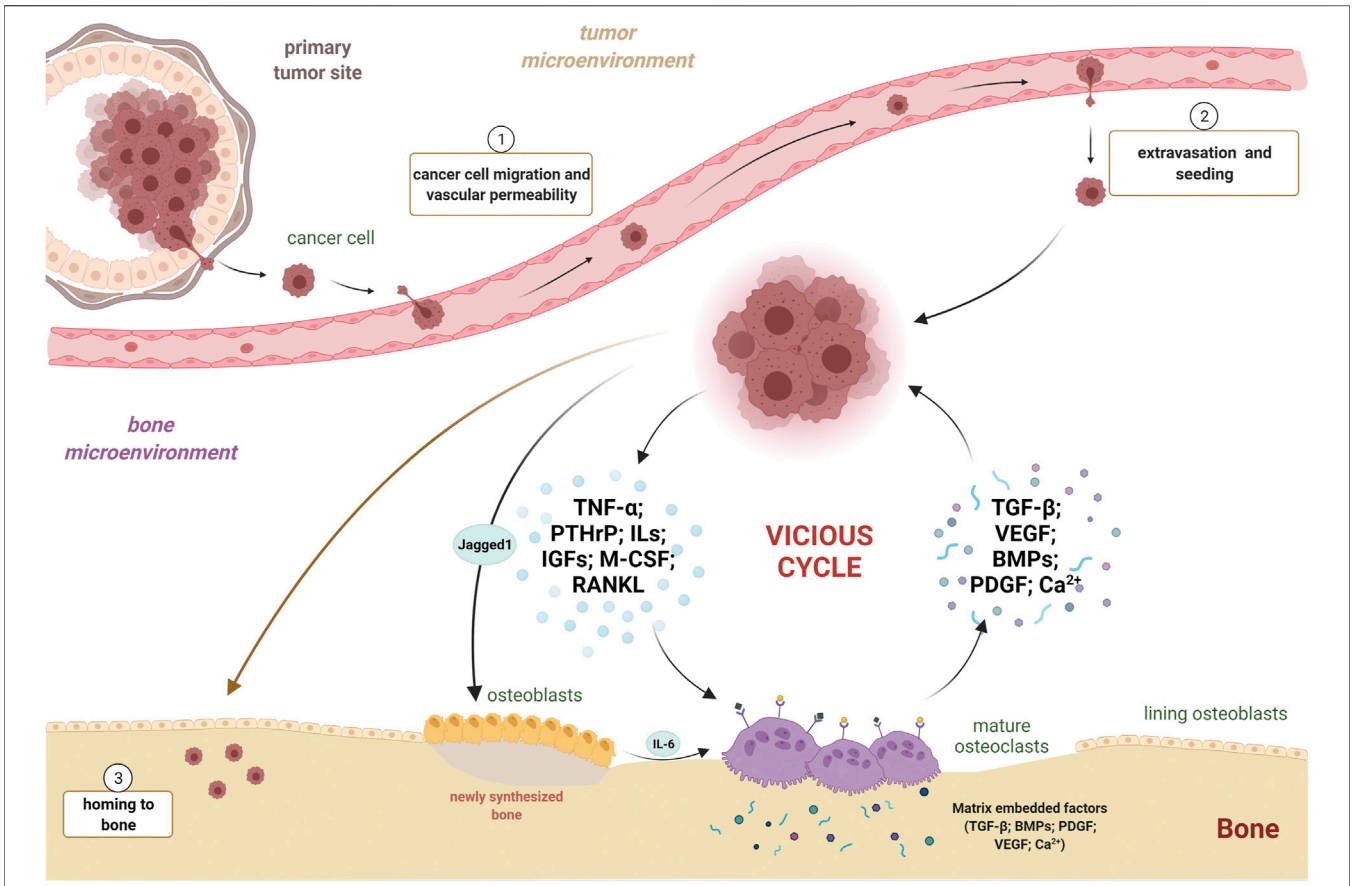

FIGURE 4 | Osteoclasts and cancer cells: partners in crime in the vicious cycle. Three principal steps are necessary for a bone metastasis to occur: 1) escape of the cancer cell from primary tumor site, migration, and vascular permeabilization; 2) extravasation from blood stream and bone marrow seeding; and 3) colonization and homing to bone. Once engrafted in the bone, neoplastic cells secrete pro-osteoclastogenic factors, such as TNF-α, PTHrP, ILs, IGFs, M-CSF, and RANKL, promoting osteoclast differentiation and activity. Jagged1 expression by neoplastic cells fuels IL-6 secretion by osteoblasts, exacerbating osteoclastogenesis and tumor growth. Mature osteoclasts, in turn, free several pro-tumorigenic factors, such as TGF-β, VEGF, BMPs, PDGF, and Ca^{2+} ions, all capable of stimulating tumor growth. This leads to the instauration and fueling of the vicious cycle between cancer cells and active osteoclasts. TNF-α, tumor necrosis factor-α; PTHrP, parathyroid hormone-related protein; ILs, interleukins; IGFs, insulin-like growth factors; M-CSF, macrophage colony-stimulating factor; RANKL, receptor activator of nuclear factor kappa B ligand; TGF-β, transforming growth factor-β; VEGF, vascular endothelial growth factor; BMPs, bone morphogenetic proteins; PDGF, platelet-derived growth factor; Ca^{2+}, calcium ion.

Wick, 1985; Nielsen et al., 2017). As expected, the presence of osteoclastic giant cells is responsible for the aggressive osteolytic characteristic of this tumor. In agreement with an osteoclast recruitment and consequent osteolytic bone destruction, RANKL, but not OPG, expression is found at high levels in chondroblastoma specimens, and denosumab has been used neoadjuvantly for the treatment of chondroblastomas with success (Huang et al., 2003; Visgauss et al., 2021).

Multiple myeloma. Multiple myeloma is a hematologic malignancy characterized by the accumulation of malignant plasma cells in the bone marrow due to a tropism for the bone medullary compartment, leading to impaired hematopoiesis (Terpos et al., 2018). Osteolytic bone disease is the hallmark of multiple myeloma that severely undermines the life quality of patients (Edwards et al., 2008). Similar to the process described for other tumor types, a vicious cycle exists when myeloma cells home to the marrow and release cytokines and factors that induce osteoclast activity and bone destruction, including TNF-α, IL-1, IL-3, and IL-6 (**Figures 3B**, **4**) (Edwards et al., 2008; Kawano et al., 1988; Lee et al., 2004). Osteoclasts contribute to multiple myeloma through different mechanisms. In addition to promoting bone destruction and, consequently, tumor growth, osteoclast activity promotes angiogenesis, required for cell survival and proliferation. Indeed, osteoclastic bone resorption releases the vascular endothelial growth factor (VEGF) from the bone matrix through the production of MMP9 (**Figure 4**) (Raje et al., 2019; Roodman, 2009; Mansour et al., 2017). Accordingly, zoledronate treatment to mice developing multiple myeloma after the intravenous injection of myeloma cells resulted in decreased osteolysis, tumor burden, and angiogenesis (Croucher et al., 2003). Furthermore, osteoclasts are able to remodel the endosteal niche within the bone marrow, thus activating dormant myeloma cells (Lawson et al., 2015). Last, osteoclasts are capable of inducing T cell apoptosis or suppression, maintaining an immune suppressive environment in multiple myeloma, *via* direct inhibition of proliferating $CD4^+$

and $CD8^+$ T cells. In addition, during osteoclastogenesis several molecules are upregulated, including Galectin-9, which specifically induces apoptosis of T cells while sparing monocytes and myeloma cells (An et al., 2016). Therefore, in multiple myeloma, osteoclasts participate in the regulation of angiogenesis, remodeling of marrow niches, and control of immune response; this creates a vicious cycle in which the bone resorptive process increases tumor burden, perpetuating the cycle (**Figure 4**). As one would expect, multiple myeloma samples and cell lines express high levels of RANKL, and mouse models of multiple myeloma exhibit deregulated RANKL/OPG balance (Pearse et al., 2001; Roux et al., 2002; Raje et al., 2019). Therefore, therapeutic options for multiple myeloma patients target bone remodeling. In addition to bisphosphonates and denosumab, hitherto described for other osteoclast-rich bone lesions, proteasome inhibitors have also been used in the clinical regimens for multiple myeloma (Morgan et al., 2013; Raje et al., 2016; Gandolfi et al., 2017; Raje et al., 2019). By preventing the degradation of IκBα, they decrease NF-κB expression and inhibit osteoclast differentiation and function (Kupperman et al., 2010). Indeed, the treatment with proteasome inhibitors in multiple myeloma patients decreased serum levels of both RANKL and bone resorption markers (Terpos et al., 2006).

Skeletal Metastases

Bone marrow is a frequent site of metastasis for a number of cancers—including breast, prostate, and lung cancer—and bone metastases are generally associated with increased morbidity and mortality (Harding et al., 2018; Weilbaecher et al., 2011). In order to metastasize, tumor cells must penetrate the blood or lymphatic circulatory system, where they exhibit a non-proliferative quiescent state and are arrested in G0-G1 (Fares et al., 2020). When tumor cells home to bone marrow, they encounter a unique microenvironment that contains a variety of cell types and growth factors that support their colonization (Wang et al., 2015; Yu-Lee et al., 2018) (**Figure 4**). Upon dissemination into the bone marrow, tumor cells may either grow as overt metastasis or enter a dormant state. The majority of dormant tumor cells enter a quiescent, non-proliferative state by exhibiting mitotic arrest through reversible G0-G1 arrest. Therefore, they remain viable but do not proliferate (Park and Nam, 2020). However, another way to reach dormancy is through a constant balance between proliferation and apoptosis, where tumor cells divide but do not increase in number. This occurs mainly when a dormant tumor cell grows into a micrometastasis and requires new vasculature: if angiogenesis is suppressed, poor vascularization leads to cell death ("angiogenic dormancy") (Sosa et al., 2014). Moreover, in the so-called "immune-mediated dormancy," the immune system keeps the number of proliferative tumor cells unchanged mostly via cytotoxic activity of $CD8^+$ cells (Romero et al., 2014).

Role of osteoclasts in bone metastases. The bone does not receive invading cancer cells passively. In fact, primary tumor cells selectively and actively prime the host microenvironment to promote the formation of a pre-metastatic niche. Disseminating cancer cells release factors and extracellular vesicles that induce vascular leakage, extracellular matrix remodeling, and immunosuppression (Peinado et al., 2017). For example, tumor cells secrete the parathyroid hormone-related peptide (PTHrP) to promote osteoclast differentiation and activity, by altering osteoblast production of RANKL and its antagonist OPG (Guise et al., 1996). The resultant bone degradation releases a number of growth factors embedded in the bone matrix, such as TGF-β, which further stimulates the malignancy of tumor cells (Buijs et al., 2012). Thus, tumor metastasis to bone is a complex process involving reciprocal interplay between cancer cells and host stroma (**Figure 4**). Another essential microenvironmental factor is represented by hypoxia, which activates signaling through hypoxia-inducible factor 1 (HIF-1) in response to low oxygen levels. Widely accepted, hypoxia strongly stimulates osteoclasts differentiation and activity *via* the regulation of RANKL/OPG ratio (Bozec et al., 2008). Previous studies have proven that activation of HIF-1 signaling in breast cancer cells fosters bone colonization and osteolysis following intracardiac and orthotopic injections of these cells (Hiraga et al., 2007; Lu et al., 2010). For example, mice injected with human breast cancer cells constitutively expressing active HIF-1 exhibited a more aggressive tumor growth and a greater osteolysis in long bones (Hiraga et al., 2007). It has been demonstrated that hypoxia is specifically related to bone metastasis in patients with estrogen-receptor negative breast cancer, where the analysis of breast cancer cell secretome identified lysil oxidase significantly associated with bone tropism and relapse (Cox et al., 2015). Interestingly, lysil oxidase was shown to promote NFATc1-dependent osteoclastogenesis, independent of RANK ligand, to favor bone resorption and provide disseminating cancer cells with a platform to colonize and form metastases (Cox et al., 2015). The evidence that bone-degrading osteoclasts aid the expansion of breast cancer metastatic lesions also came by the observation that circulating tumor cells express high levels of the Notch ligand, Jagged1 (Reedijk et al., 2005). Remarkably, Jagged1 promotes tumor growth by stimulating IL-6 release from osteoblasts, directly activating osteoclast differentiation and activity (**Figure 4**) (Sethi et al., 2011). Therefore, bone resorption appears to mediate proliferation of metastatic tumor cells within bone marrow. In fact, OPG treatment in mice decreased bone resorption and, importantly, significantly reduced tumor area and overall cancer-associated sclerotic bone lesion area after intra-tibial implantation of human breast cancer cells (Zheng et al., 2008). Intriguingly, a calcium deficient diet increased the levels of bone resorption and, in parallel, the size of tumors and osteosclerotic areas, confirming the effect of bone resorption in mediated tumor growth (Zheng et al., 2008). Breast cancer is not the only malignant tumor showing a substantial tropism for bone in metastatic process. Nearly 80% of patients with advanced-stage prostate cancer develop skeletal metastases, and this feature is associated with poor prognosis, with less than 50% of patients surviving 1 year after diagnosis of bone metastasis (Halabi et al., 2016; Macedo et al., 2017). Although bone metastases in prostate cancer patients are primarily sclerotic, and therefore characterized by deposition of new bone by osteoblasts, a critical role for osteoclasts has been described in the process of tumor growth (Macedo et al., 2017).

Indeed, osteoclast precursors isolated from the bone marrow of C57BL6 mice were able to fully differentiate into mature osteoclasts in the presence of conditioned medium of prostate cancer cell lines, suggesting that tumor cells secrete factors needed to promote osteoclastogenesis (Polavaram et al., 2021). In support of this observation, castration-induced bone loss in nude mice triggered growth of tumor cells within the skeleton after intracardiac injection of prostate cancer cells, even in 12-week-old animals where the low rate of bone turnover generally leads to only a moderate skeletal tumor growth (Ottewell et al., 2014). Similarly, ovariectomy of C57BL6 mice performed 1 week before the inoculation of the multiple myeloma cells in the tail vein simultaneously increased bone remodeling and accelerated the severity of the tumor, with an earlier development of osteolytic lesions in tibiae and femurs (Libouban et al., 2003). Further confirming an active role for osteoclasts in skeletal metastases, mice administered granulocyte colony-stimulating factor (G-CSF) demonstrated increased markers of osteoclast activity, decreased bone mineral density, and also significantly increased tumor growth in the marrow cavity after intra-tibial injection of melanoma cells (Hirbe et al., 2007). Therefore, osteoclasts are predominant actors in bone metastasis formation, mediating bone degradation and promoting skeletal tumor growth.

Role of osteoclasts in reactivation from tumor dormancy. Dormant cells exhibit prolonged survival in cell cycle arrest (for up to several decades) and have the potential ability to exit this state and start proliferating again, eventually leading to overt metastatic disease. Until that moment, they are clinically undetectable (Park and Nam, 2020). Furthermore, the lack of proliferation provides dormant cells with an inherent resistance to cytotoxic treatments, for example, chemotherapies and radiation, which generally target dividing cells (Santos-de-Frutos and Djouder, 2021). The notion that the bone might provide dormancy-inducing factors stems from the evidence that in prostate cancer patients, bone metastasis can occur years or decades after prostatectomy, suggesting that disseminated tumor cells had been dormant at the metastatic site in bone (Ahove et al., 2010; Yu-Lee et al., 2018; Yu-Lee et al., 2019). Central to the mechanisms of cellular dormancy and reactivation is the crosstalk between cancer cells and their microenvironment (Fares et al., 2020).

A key dormancy-promoting role is thought to be played by osteoblasts, which support cancer cell dormancy secreting the same signals used to regulate quiescence of hematopoietic stem cells (HSCs) (Taichman et al., 2013; Yu-Lee et al., 2018; Ren et al., 2019; Yu-Lee et al., 2019). Indeed, Shiozawa *et al.* demonstrated in a mouse model of metastasis that human prostate cancer cells colonize the marrow osteoblastic niche by directly competing with HSCs (Shiozawa et al., 2011). Among many other molecules, osteoblasts produce the growth arrest specific 6 (GAS6) protein, which binds to the tyrosine kinase receptor Axl (Taichman et al., 2013). Interestingly, disseminated tumor cells frequently show high expression of the Axl receptor and become growth arrested in response to GAS6 (Taichman et al., 2013; Yumoto et al., 2016).

Just like in bone remodeling, osteoblasts and osteoclasts have opposite role also in tumor dormancy. While osteoblasts are primarily associated with dormancy induction and maintenance, osteoclasts have been reported in reactivation of dormant cells and generation of osteolytic metastases. Thus, tumor dormancy is a reversible state controlled by the extrinsic bone microenvironment. In this regard, the process of osteoclastic bone resorption leads to changes in the cellular composition and signaling within the bone marrow, which can cause the exit of cancer cells from a dormant state. Indeed, treatment of multiple myeloma-bearing mice with soluble RANKL to stimulate osteoclast formation and resorption resulted in a significant decrease in the number of dormant tumor cells in the bone marrow. The observation that myeloma cells in the spleen were not affected by the RANKL treatment confirmed that the effect on dormant cells was a non-cell-autonomous effect mediated by osteoclasts in the bone (Lawson et al., 2015). Accordingly, patients with recurrent myeloma show increased serum levels of C-terminal telopeptide (CTX), a biochemical marker of bone resorption (Lawson et al., 2015). Mechanistically, osteoclast-mediated bone resorption releases several growth factors, including TGF-β and periostin, which are tumor-promoting factors (Buijs et al., 2012). Therefore, osteoclasts are crucial to reactivation of tumor cells from dormancy in the process of bone metastasis.

TARGETING OSTEOCLASTS TO LIMIT TUMOR PROGRESSION

The evidence that osteoclasts are key players in the formation of skeletal tumors provides the rationale for using antiresorptive drugs in the treatment of bone tumors and metastases. Hence, therapies commonly used to treat patients with bone remodeling disorders, for example, Paget's disease of bone, have been translated in the clinical practice of bone cancers to mitigate the vicious cycle (Mackiewicz-Wysocka et al., 2012; Satcher and Zhang, 2021). As described before, one of the most utilized molecules belongs to the class of bisphosphonates, which target the bone matrix by binding to hydroxyapatite crystals (Zhang et al., 2007; Russell et al., 2008; Zielinska et al., 2021). Once this drug has been internalized by bone-resorbing osteoclasts, bisphosphonate inhibits their polarization and cytoskeleton rearrangement, thus compromising bone erosion and inducing their apoptosis (Wang L. et al., 2020). Currently, a frequently administrated bisphosphonate drug is zoledronic acid (ZA), which interferes with the mevalonic pathway, involved in the synthesis of steroids, such as cholesterol (Thurnher et al., 2012; Gobel et al., 2016). By inhibiting the farnesyl pyrophosphate synthase enzyme, ZA triggers the stop of posttranslational modifications of proteins and small GTPases, such as Rho, Ras, and Rac, thus inducing osteoclast apoptosis *via* destruction of the actin cytoskeleton structure (Gobel et al., 2016). In addition to jeopardizing osteoclast activity, ZA also directly interferes with the life span of cancer cells within the bone. Indeed, ZA activates the caspase-dependent apoptosis pathway to kill cancer cells, blocking Ras-dependent Erk 1/2 and Akt pathways, and then reduces the phosphorylation of Bcl-2 and Bad proteins to increase the apoptotic function (Tassone et al., 2003; Wang L. et al., 2020). To overcome the adverse effects of prolonged and massive use of bisphosphonates, lower concentrations of the drug are used in combination with adjuvants. For example, the simultaneous administration of ZA and the adjuvant anticancer drug ifosfamide—used for the

treatment of human OS—showed decreased cancer-induced osteolytic lesions as well as efficient tumor growth arrest in a rat-transplantable model of osteosarcoma (Heymann et al., 2005).

In addition to bisphosphonates, other drugs are widely used to treat cancer-related osteoclastogenesis and to counteract metastasis formation. Denosumab is a fully human monoclonal antibody (IgG2) highly specific for RANKL and able to prevent its interaction with the receptor RANK, thereby blocking the osteoclastogenic process (Baron et al., 2011). Unlike other molecules interfering with RANK and RANKL binding (e.g., OPG-Fc), denosumab shows higher specificity to the substrate, a longer half-life, and no neutralizing antibodies have been identified (Baron et al., 2011). Interestingly, denosumab demonstrated superiority over ZA in preventing bone lesions in both breast and prostate cancers that metastasized to bone, by mimicking OPG action and minimizing pre-osteoclast and osteoclast survival and activity (Stopeck et al., 2010; Fizazi et al., 2011; Lipton and Goessl, 2011).

Additional molecules have been described as effective in limiting bone metastases by targeting osteoclast activity rather than osteoclasts themselves. Given the aforementioned role of TGF-β as a released factor promoting cancer proliferation, it is not surprising that TGF-β inhibitors represent another class of novel molecules utilized to prevent bone metastases, blocking the vicious cycle between cancer cells and the bone (Buijs et al., 2012; Hu et al., 2012; Wan et al., 2012). Neutralizing TGF-β antibodies have been developed to target individual ligands and all three TGF-β isomers (Baselga et al., 2008; Biswas et al., 2011). Athymic mice inoculated with MCF-7 breast cancer cells and then treated with neutralizing anti-TGF-β antibodies displayed total abrogation of cancer growth and metastasis (Arteaga et al., 1993). Notably, the use of these inhibitors does not affect the osteoblastic compartment, therefore preserving bone volume and architecture (Biswas et al., 2011). Likewise, inhibitors targeting integrin β3 have been developed for the treatment of breast cancer metastases to bone because of high expression of this molecule by breast cancer cells and its association with promoting skeletal tumor metastasis (Desgrosellier and Cheresh, 2010; Kovacheva et al., 2021). Of interest, by exploiting the specific overexpression of integrin β3 in the metastatic site, these molecules might be delivered in conjugation with nanoparticles that selectively target cancer cells (Ross et al., 2017). Recently, an emerging immunotherapy based on the use of nivolumab, an anti-PD-1 monoclonal antibody, has evidenced positive effect on tumor suppression and tumor-induced osteolysis (Wang K. et al., 2020). In fact, neoplastic cells produce high levels of PD-1 ligand, and monocytes/macrophages and pre-osteoclast present within bone tumor microenvironment express high levels of the PD-1 receptor. The binding of PD-1 ligand to its receptor leads to JNK activation and chemokine C-C motif ligand 2 (CCL2) secretion, thus promoting osteoclastogenesis. Strikingly, tumor-bearing mice treated with nivolumab showed total abolishment of bone osteolytic lesions, even though the tumor growth and progression were not totally neutralized (Wang K. et al., 2020). Patients with advanced-stage cancer experience intense pain owing to bone fractures or lesions as a consequence of bone metastases and accelerated osteolysis. To counteract these detrimental conditions, the use of STING (stimulator of interferon genes) agonists reduces bone cancer–induced pain and, equally important, through the induction of the STING/IFN-1 signaling, allows protection against bone destruction and tumor growth (Wang et al., 2021).

A common challenge for all the aforementioned therapies is to face potential toxicity caused by the pleiotropic roles of the targeted pathways. A new therapeutic approach could benefit from the positively charged bone matrix of the acidic environment. For example, conjugation of antibodies or inhibitors with bisphosphonates, which are negatively charged, can significantly enrich these molecules in the bone microenvironment, thereby reducing side effects on other organs (Cole et al., 2016; Farrell et al., 2018; Tian et al., 2021).

CONCLUSION

A widely accepted view in biology implies osteoclasts as highly specialized cells quite exclusively implicated in bone resorption during the remodeling. However, although never described as the neoplastic cell, several studies agree that the osteoclast influences the development, progression, and aggressiveness of bone tumors, both primary and metastatic. Therefore, better understanding of the molecular mechanisms governing the osteoclast function may result in the development of novel diagnostic and therapeutic approaches. Here, we underline that the skeleton should not be overlooked in patients with primary tumors in other sites (e.g., breast and pancreas), even when the mass has been completely eradicated through pharmacological or surgical approaches. Indeed, the osteoclast-mediated bone resorption activity might promote either the growth of metastatic cells within the marrow or the reactivation from tumor dormancy. Serum markers of bone resorption should be routinely tested in periodic follow-ups for the assessment of osteoclast activity in patients with bone tumors or metastases. In conclusion, we highlight that the osteoclast could be considered as a pro-cancer cell due to its ability to degrade bone matrix and release tumorigenic factors, thus creating a pro-tumoral microenvironment.

AUTHOR CONTRIBUTIONS

All authors listed have made a substantial, direct, and intellectual contribution to the work and approved it for publication.

FUNDING

This work in the Gianfrancesco lab was supported by grants from the Italian Association for Cancer Research to FG (IG 2020; project ID. 25110) and the Italian Society for Osteoporosis, Mineral Metabolism and Bone Diseases (SIOMMMS), to FSdC. FSdC was supported by Fondazione Umberto Veronesi.

REFERENCES

Abu-Amer, Y., Teitelbaum, S. L., Chappel, J. C., Schlesinger, P., and Ross, F. P. (1999). Expression and Regulation of RAB3 Proteins in Osteoclasts and Their Precursors. *J. Bone Miner Res.* 14, 1855–1860. doi:10.1359/jbmr.1999.14.11.1855

Ahove, D. A., Hoffman, K. E., Hu, J. C., Choueiri, T. K., D'Amico, A. V., and Nguyen, P. L. (2010). Which Patients with Undetectable PSA Levels 5 Years after Radical Prostatectomy Are Still at Risk of Recurrence?-Implications for a Risk-Adapted Follow-Up Strategy. *Urology* 76, 1201–1205. doi:10.1016/j.urology.2010.03.092

Alothman, M., Althobaity, W., Asiri, Y., Alreshoodi, S., Alismail, K., and Alshaalan, M. (2020). Giant Cell Tumor of Bone Following Denosumab Treatment: Assessment of Tumor Response Using Various Imaging Modalities. *Insights Imaging* 11, 41. doi:10.1186/s13244-020-00845-y

An, G., Acharya, C., Feng, X., Wen, K., Zhong, M., Zhang, L., et al. (2016). Osteoclasts Promote Immune Suppressive Microenvironment in Multiple Myeloma: Therapeutic Implication. *Blood* 128, 1590–1603. doi:10.1182/blood-2016-03-707547

Arteaga, C. L., Hurd, S. D., Winnier, A. R., Johnson, M. D., Fendly, B. M., and Forbes, J. T. (1993). Anti-transforming Growth Factor (TGF)-beta Antibodies Inhibit Breast Cancer Cell Tumorigenicity and Increase Mouse Spleen Natural Killer Cell Activity. Implications for a Possible Role of Tumor Cell/host TGF-Beta Interactions in Human Breast Cancer Progression. *J. Clin. Invest.* 92, 2569–2576. doi:10.1172/jci116871

Atkins, G. J., Haynes, D. R., Graves, S. E., Evdokiou, A., Hay, S., Bouralexis, S., et al. (2000). Expression of Osteoclast Differentiation Signals by Stromal Elements of Giant Cell Tumors. *J. Bone Miner Res.* 15, 640–649. doi:10.1359/jbmr.2000.15.4.640

Avnet, S., Longhi, A., Salerno, M., Halleen, J. M., Perut, F., Granchi, D., et al. (2008). Increased Osteoclast Activity Is Associated with Aggressiveness of Osteosarcoma. *Int. J. Oncol.* 33, 1231–1238.

Bakewell, S. J., Nestor, P., Prasad, S., Tomasson, M. H., Dowland, N., Mehrotra, M., et al. (2003). Platelet and Osteoclast β 3 Integrins Are Critical for Bone Metastasis. *Proc. Natl. Acad. Sci. U.S.A.* 100, 14205–14210. doi:10.1073/pnas.2234372100

Baron, R., Ferrari, S., and Russell, R. G. G. (2011). Denosumab and Bisphosphonates: Different Mechanisms of Action and Effects. *Bone* 48, 677–692. doi:10.1016/j.bone.2010.11.020

Baselga, J., Rothenberg, M. L., Tabernero, J., Seoane, J., Daly, T., Cleverly, A., et al. (2008). TGF-β Signalling-Related Markers in Cancer Patients with Bone Metastasis. *Biomarkers* 13, 217–236. doi:10.1080/13547500701676019

Behjati, S., Tarpey, P. S., Presneau, N., Scheipl, S., Pillay, N., Van Loo, P., et al. (2013). Distinct H3F3A and H3F3B Driver Mutations Define Chondroblastoma and Giant Cell Tumor of Bone. *Nat. Genet.* 45, 1479–1482. doi:10.1038/ng.2814

Bellido, T. (2014). Osteocyte-driven Bone Remodeling. *Calcif Tissue Int.* 94, 25–34. doi:10.1007/s00223-013-9774-y

Biswas, S., Nyman, J. S., Alvarez, J., Chakrabarti, A., Ayres, A., Sterling, J., et al. (2011). Anti-transforming Growth Factor Ss Antibody Treatment Rescues Bone Loss and Prevents Breast Cancer Metastasis to Bone. *PLoS One* 6, e27090. doi:10.1371/journal.pone.0027090

Blair, H. C., and Schlesinger, P. H. (1990). Purification of a Stilbene Sensitive Chloride Channel and Reconstitution of Chloride Conductivity into Phospholipid Vesicles. *Biochem. Biophysical Res. Commun.* 171, 920–925. doi:10.1016/0006-291x(90)90771-e

Blair, H. C., Teitelbaum, S. L., Ghiselli, R., and Gluck, S. (1989). Osteoclastic Bone Resorption by a Polarized Vacuolar Proton Pump. *Science* 245, 855–857. doi:10.1126/science.2528207

Bossard, M. J., Tomaszek, T. A., Thompson, S. K., Amegadzie, B. Y., Hanning, C. R., Jones, C., et al. (1996). Proteolytic Activity of Human Osteoclast Cathepsin K. *J. Biol. Chem.* 271, 12517–12524. doi:10.1074/jbc.271.21.12517

Boyle, W. J., Simonet, W. S., and Lacey, D. L. (2003). Osteoclast Differentiation and Activation. *Nature* 423, 337–342. doi:10.1038/nature01658

Bozec, A., Bakiri, L., Hoebertz, A., Eferl, R., Schilling, A. F., Komnenovic, V., et al. (2008). Osteoclast Size Is Controlled by Fra-2 through LIF/LIF-receptor Signalling and Hypoxia. *Nature* 454, 221–225. doi:10.1038/nature07019

Brown, H. K., Schiavone, K., Gouin, F., Heymann, M.-F., and Heymann, D. (2018). Biology of Bone Sarcomas and New Therapeutic Developments. *Calcif Tissue Int.* 102, 174–195. doi:10.1007/s00223-017-0372-2

Buijs, J. T., Stayrook, K. R., and Guise, T. A. (2012). The Role of TGF-β in Bone Metastasis: Novel Therapeutic Perspectives. *Bonekey Rep.* 1, 96. doi:10.1038/bonekey.2012.96

Campanacci, M., Baldini, N., Boriani, S., and Sudanese, A. (1987). Giant-cell Tumor of Bone. *J. Bone Jt. Surg.* 69, 106–114. doi:10.2106/00004623-198769010-00018

Chawla, S., Blay, J.-Y., Rutkowski, P., Le Cesne, A., Reichardt, P., Gelderblom, H., et al. (2019). Denosumab in Patients with Giant-Cell Tumour of Bone: a Multicentre, Open-Label, Phase 2 Study. *Lancet Oncol.* 20, 1719–1729. doi:10.1016/s1470-2045(19)30663-1

Chen, Y., Di Grappa, M. A., Molyneux, S. D., Mckee, T. D., Waterhouse, P., Penninger, J. M., et al. (2015). RANKL Blockade Prevents and Treats Aggressive Osteosarcomas. *Sci. Transl Med.* 7, 317ra197. doi:10.1126/scitranslmed.aad0295

Clark, J. C., Akiyama, T., Dass, C. R., and Choong, P. F. (2010). New Clinically Relevant, Orthotopic Mouse Models of Human Chondrosarcoma with Spontaneous Metastasis. *Cancer Cel Int* 10, 20. doi:10.1186/1475-2867-10-20

Cole, L. E., Vargo-Gogola, T., and Roeder, R. K. (2016). Targeted Delivery to Bone and mineral Deposits Using Bisphosphonate Ligands. *Adv. Drug Deliv. Rev.* 99, 12–27. doi:10.1016/j.addr.2015.10.005

Coleman, R. E., Croucher, P. I., Padhani, A. R., Clézardin, P., Chow, E., Fallon, M., et al. (2020). Bone Metastases. *Nat. Rev. Dis. Primers* 6, 83. doi:10.1038/s41572-020-00216-3

Cox, T. R., Rumney, R. M. H., Schoof, E. M., Perryman, L., Høye, A. M., Agrawal, A., et al. (2015). The Hypoxic Cancer Secretome Induces Pre-metastatic Bone Lesions through Lysyl Oxidase. *Nature* 522, 106–110. doi:10.1038/nature14492

Croucher, P. I., De Raeve, H., Perry, M. J., Hijzen, A., Shipman, C. M., Lippitt, J., et al. (2003). Zoledronic Acid Treatment of 5T2MM-Bearing Mice Inhibits the Development of Myeloma Bone Disease: Evidence for Decreased Osteolysis, Tumor burden and Angiogenesis, and Increased Survival. *J. Bone Miner Res.* 18, 482–492. doi:10.1359/jbmr.2003.18.3.482

David, E., Blanchard, F., Heymann, M. F., De Pinieux, G., Gouin, F., Rédini, F., et al. (2011). The Bone Niche of Chondrosarcoma: A Sanctuary for Drug Resistance, Tumour Growth and Also a Source of New Therapeutic Targets. *Sarcoma* 2011, 932451. doi:10.1155/2011/932451

De Mattos, C. B. R., Angsanuntsukh, C., Arkader, A., and Dormans, J. P. (2013). Chondroblastoma and Chondromyxoid Fibroma. *J. Am. Acad. Orthopaedic Surgeons* 21, 225–233. doi:10.5435/jaaos-21-04-225

Desgrosellier, J. S., and Cheresh, D. A. (2010). Integrins in Cancer: Biological Implications and Therapeutic Opportunities. *Nat. Rev. Cancer* 10, 9–22. doi:10.1038/nrc2748

Deyrup, A. T., Montag, A. G., Inwards, C. Y., Xu, Z., Swee, R. G., and Krishnan Unni, K. (2007). Sarcomas Arising in Paget Disease of Bone: a Clinicopathologic Analysis of 70 Cases. *Arch. Pathol. Lab. Med.* 131, 942–946. doi:10.5858/2007-131-942-saipdo

Divisato, G., di Carlo, F. S., Pazzaglia, L., Rizzo, R., Coviello, D. A., Benassi, M. S., et al. (2017). The Distinct Clinical Features of Giant Cell Tumor of Bone in Pagetic and Non-pagetic Patients Are Associated with Genetic, Biochemical and Histological Differences. *Oncotarget* 8, 63121–63131. doi:10.18632/oncotarget.18670

Divisato, G., Formicola, D., Esposito, T., Merlotti, D., Pazzaglia, L., Del Fattore, A., et al. (2016). ZNF687 Mutations in Severe Paget Disease of Bone Associated with Giant Cell Tumor. *Am. J. Hum. Genet.* 98, 275–286. doi:10.1016/j.ajhg.2015.12.016

Divisato, G., Scotto di Carlo, F., Petrillo, N., Esposito, T., and Gianfrancesco, F. (2018). ZNF687 Mutations Are Frequently Found in Pagetic Patients from South Italy: Implication in the Pathogenesis of Paget's Disease of Bone. *Clin. Genet.* 93, 1240–1244. doi:10.1111/cge.13247

Domansk, H. A., and Walther, C. S. (2017). Giant Cell Tumor of Bone and Other Giant Cell-Rich Lesions. *Monogr. Clin. Cytol.* 22, 165–170. doi:10.1159/000475109

Edwards, C. M., Zhuang, J., and Mundy, G. R. (2008). The Pathogenesis of the Bone Disease of Multiple Myeloma. *Bone* 42, 1007–1013. doi:10.1016/j.bone.2008.01.027

Everts, V., De Vries, T. J., and Helfrich, M. H. (20091792). Osteoclast Heterogeneity:. *Biochim. Biophys. Acta (Bba) - Mol. Basis Dis.* 1792, 757–765. doi:10.1016/j.bbadis.2009.05.004

Everts, V., Korper, W., Hoeben, K. A., Jansen, I. D., Bromme, D., Cleutjens, K. B., et al. (2006). Osteoclastic Bone Degradation and the Role of Different Cysteine Proteinases and Matrix Metalloproteinases: Differences between Calvaria and Long Bone. *J. Bone Miner Res.* 21, 1399–1408. doi:10.1359/jbmr.060614

Fares, J., Fares, M. Y., Khachfe, H. H., Salhab, H. A., and Fares, Y. (2020). Molecular Principles of Metastasis: a Hallmark of Cancer Revisited. *Sig Transduct Target. Ther.* 5, 28. doi:10.1038/s41392-020-0134-x

Farrell, K. B., Karpeisky, A., Thamm, D. H., and Zinnen, S. (2018). Bisphosphonate Conjugation for Bone Specific Drug Targeting. *Bone Rep.* 9, 47–60. doi:10.1016/j.bonr.2018.06.007

Fizazi, K., Carducci, M., Smith, M., Damião, R., Brown, J., Karsh, L., et al. (2011). Denosumab versus Zoledronic Acid for Treatment of Bone Metastases in Men with Castration-Resistant Prostate Cancer: a Randomised, Double-Blind Study. *The Lancet* 377, 813–822. doi:10.1016/s0140-6736(10)62344-6

Gandolfi, S., Laubach, J. P., Hideshima, T., Chauhan, D., Anderson, K. C., and Richardson, P. G. (2017). The Proteasome and Proteasome Inhibitors in Multiple Myeloma. *Cancer Metastasis Rev.* 36, 561–584. doi:10.1007/s10555-017-9707-8

Gelderblom, H., Hogendoorn, P. C. W., Dijkstra, S. D., Van Rijswijk, C. S., Krol, A. D., Taminiau, A. H. M., et al. (2008). The Clinical Approach towards Chondrosarcoma. *Oncologist* 13, 320–329. doi:10.1634/theoncologist.2007-0237

Glantschnig, H., Fisher, J. E., Wesolowski, G., Rodan, G. A., and Reszka, A. A. (2003). M-CSF, TNFα and RANK Ligand Promote Osteoclast Survival by Signaling through mTOR/S6 Kinase. *Cell Death Differ* 10, 1165–1177. doi:10.1038/sj.cdd.4401285

Göbel, A., Thiele, S., Browne, A. J., Rauner, M., Zinna, V. M., Hofbauer, L. C., et al. (2016). Combined Inhibition of the Mevalonate Pathway with Statins and Zoledronic Acid Potentiates Their Anti-tumor Effects in Human Breast Cancer Cells. *Cancer Lett.* 375, 162–171. doi:10.1016/j.canlet.2016.03.004

Gohda, J., Akiyama, T., Koga, T., Takayanagi, H., Tanaka, S., and Inoue, J.-i. (2005). RANK-mediated Amplification of TRAF6 Signaling Leads to NFATc1 Induction during Osteoclastogenesis. *EMBO J.* 24, 790–799. doi:10.1038/sj.emboj.7600564

Goldenberg, R. R., Campbell, C. J., and Bonfiglio, M. (1970). Giant-Cell Tumor of Bone. *J. Bone Jt. Surg.* 52, 619–664. doi:10.2106/00004623-197052040-00001

Gouin, F., Ory, B., Rédini, F., and Heymann, D. (2006). Zoledronic Acid Slows Down Rat Primary Chondrosarcoma Development, Recurrent Tumor Progression after Intralesional Curretage and Increases Overall Survival. *Int. J. Cancer* 119, 980–984. doi:10.1002/ijc.21951

Grimaud, E., Damiens, C., Rousselle, A. V., Passuti, N., Heymann, D., and Gouin, F. (2002). Bone Remodelling and Tumour Grade Modifications Induced by Interactions between Bone and Swarm Rat Chondrosarcoma. *Histol. Histopathol* 17, 1103–1111. doi:10.14670/HH-17.1103

Guise, T. A., Yin, J. J., Taylor, S. D., Kumagai, Y., Dallas, M., Boyce, B. F., et al. (1996). Evidence for a Causal Role of Parathyroid Hormone-Related Protein in the Pathogenesis of Human Breast Cancer-Mediated Osteolysis. *J. Clin. Invest.* 98, 1544–1549. doi:10.1172/jci118947

Guise, T. A., Yin, J. J., Thomas, R. J., Dallas, M., Cui, Y., and Gillespie, M. T. (2002). Parathyroid Hormone-Related Protein (PTHrP)-(1-139) Isoform Is Efficiently Secreted *In Vitro* and Enhances Breast Cancer Metastasis to Bone *In Vivo*. *Bone* 30, 670–676. doi:10.1016/s8756-3282(02)00685-3

Halabi, S., Kelly, W. K., Ma, H., Zhou, H., Solomon, N. C., Fizazi, K., et al. (2016). Meta-Analysis Evaluating the Impact of Site of Metastasis on Overall Survival in Men with Castration-Resistant Prostate Cancer. *Jco* 34, 1652–1659. doi:10.1200/jco.2015.65.7270

Hamm, C. A., Stevens, J. W., Xie, H., Vanin, E. F., Morcuende, J. A., Abdulkawy, H., et al. (2010). Microenvironment Alters Epigenetic and Gene Expression Profiles in Swarm Rat Chondrosarcoma Tumors. *BMC Cancer* 10, 471. doi:10.1186/1471-2407-10-471

Hansen, M. F., Seton, M., and Merchant, A. (2006). Osteosarcoma in Paget's Disease of Bone. *J. Bone Miner Res.* 21 Suppl 2 (Suppl. 2), P58–P63. doi:10.1359/jbmr.06s211

Harding, J. J., Abu-Zeinah, G., Chou, J. F., Owen, D. H., Ly, M., Lowery, M. A., et al. (2018). Frequency, Morbidity, and Mortality of Bone Metastases in Advanced Hepatocellular Carcinoma. *J. Natl. Compr. Canc Netw.* 16, 50–58. doi:10.6004/jnccn.2017.7024

Heymann, D., Ory, B., Blanchard, F., Heymann, M.-F., Coipeau, P., Charrier, C., et al. (2005). Enhanced Tumor Regression and Tissue Repair when Zoledronic Acid Is Combined with Ifosfamide in Rat Osteosarcoma. *Bone* 37, 74–86. doi:10.1016/j.bone.2005.02.020

Hiraga, T., Kizaka-Kondoh, S., Hirota, K., Hiraoka, M., and Yoneda, T. (2007). Hypoxia and Hypoxia-Inducible Factor-1 Expression Enhance Osteolytic Bone Metastases of Breast Cancer. *Cancer Res.* 67, 4157–4163. doi:10.1158/0008-5472.can-06-2355

Hirbe, A. C., Uluçkan, O., Morgan, E. A., Eagleton, M. C., Prior, J. L., Piwnica-Worms, D., et al. (2007). Granulocyte colony-stimulating Factor Enhances Bone Tumor Growth in Mice in an Osteoclast-dependent Manner. *Blood* 109, 3424–3431. doi:10.1182/blood-2006-09-048686

Hu, Z., Gupta, J., Zhang, Z., Gerseny, H., Berg, A., Chen, Y. J., et al. (2012). Systemic Delivery of Oncolytic Adenoviruses Targeting Transforming Growth Factor-β Inhibits Established Bone Metastasis in a Prostate Cancer Mouse Model. *Hum. Gene Ther.* 23, 871–882. doi:10.1089/hum.2012.040

Huang, L., Cheng, Y. Y., Chow, L. T., Zheng, M. H., and Kumta, S. M. (2003). Receptor Activator of NF-kappaB Ligand (RANKL) Is Expressed in Chondroblastoma: Possible Involvement in Osteoclastic Giant Cell Recruitment. *Mol. Pathol.* 56, 116–120. doi:10.1136/mp.56.2.116

Huizing, M., Helip-Wooley, A., Westbroek, W., Gunay-Aygun, M., and Gahl, W. A. (2008). Disorders of Lysosome-Related Organelle Biogenesis: Clinical and Molecular Genetics. *Annu. Rev. Genom. Hum. Genet.* 9, 359–386. doi:10.1146/annurev.genom.9.081307.164303

Ikebuchi, Y., Aoki, S., Honma, M., Hayashi, M., Sugamori, Y., Khan, M., et al. (2018). Coupling of Bone Resorption and Formation by RANKL Reverse Signalling. *Nature* 561, 195–200. doi:10.1038/s41586-018-0482-7

Kaim, A. H., Hügli, R., Bonél, H. M., and Jundt, G. (2002). Chondroblastoma and clear Cell Chondrosarcoma: Radiological and MRI Characteristics with Histopathological Correlation. *Skeletal Radiol.* 31, 88–95. doi:10.1007/s00256-001-0450-3

Kansara, M., Teng, M. W., Smyth, M. J., and Thomas, D. M. (2014). Translational Biology of Osteosarcoma. *Nat. Rev. Cancer* 14, 722–735. doi:10.1038/nrc3838

Karsdal, M. A., Neutzsky-Wulff, A. V., Dziegiel, M. H., Christiansen, C., and Henriksen, K. (2008). Osteoclasts Secrete Non-bone Derived Signals that Induce Bone Formation. *Biochem. Biophysical Res. Commun.* 366, 483–488. doi:10.1016/j.bbrc.2007.11.168

Kawano, M., Hirano, T., Matsuda, T., Taga, T., Horii, Y., Iwato, K., et al. (1988). Autocrine Generation and Requirement of BSF-2/IL-6 for Human Multiple Myelomas. *Nature* 332, 83–85. doi:10.1038/332083a0

Kobayashi, N., Kadono, Y., Naito, A., Matsumoto, K., Yamamoto, T., Tanaka, S., et al. (2001). Segregation of TRAF6-Mediated Signaling Pathways Clarifies its Role in Osteoclastogenesis. *EMBO J.* 20, 1271–1280. doi:10.1093/emboj/20.6.1271

Komarova, S. V., Pereverzev, A., Shum, J. W., Sims, S. M., and Dixon, S. J. (2005). Convergent Signaling by Acidosis and Receptor Activator of NF-Kb Ligand (RANKL) on the Calcium/calcineurin/NFAT Pathway in Osteoclasts. *Proc. Natl. Acad. Sci. U.S.A.* 102, 2643–2648. doi:10.1073/pnas.0406874102

Kovacheva, M., Zepp, M., Berger, S., and Berger, M. R. (2021). Conditional Knockdown of Integrin Beta-3 Reveals its Involvement in Osteolytic and Soft Tissue Lesions of Breast Cancer Skeletal Metastasis. *J. Cancer Res. Clin. Oncol.* 147, 361–371. doi:10.1007/s00432-020-03428-y

Kupperman, E., Lee, E. C., Cao, Y., Bannerman, B., Fitzgerald, M., Berger, A., et al. (2010). Evaluation of the Proteasome Inhibitor MLN9708 in Preclinical Models of Human Cancer. *Cancer Res.* 70, 1970–1980. doi:10.1158/0008-5472.can-09-2766

Lacey, D. L., Timms, E., Tan, H.-L., Kelley, M. J., Dunstan, C. R., Burgess, T., et al. (1998). Osteoprotegerin Ligand Is a Cytokine that Regulates Osteoclast Differentiation and Activation. *Cell* 93, 165–176. doi:10.1016/s0092-8674(00)81569-x

Lamoureux, F., Ory, B., Battaglia, S., Pilet, P., Heymann, M.-F., Gouin, F., et al. (2008). Relevance of a New Rat Model of Osteoblastic Metastases from Prostate Carcinoma for Preclinical Studies Using Zoledronic Acid. *Int. J. Cancer* 122, 751–760. doi:10.1002/ijc.23187

Lamoureux, F., Richard, P., Wittrant, Y., Battaglia, S., Pilet, P., Trichet, V., et al. (2007). Therapeutic Relevance of Osteoprotegerin Gene Therapy in

Osteosarcoma: Blockade of the Vicious Cycle between Tumor Cell Proliferation and Bone Resorption. *Cancer Res.* 67, 7308–7318. doi:10.1158/0008-5472.can-06-4130

Lawson, M. A., Mcdonald, M. M., Kovacic, N., Hua Khoo, W., Terry, R. L., Down, J., et al. (2015). Osteoclasts Control Reactivation of Dormant Myeloma Cells by Remodelling the Endosteal Niche. *Nat. Commun.* 6, 8983. doi:10.1038/ncomms9983

Lee, J. W., Chung, H. Y., Ehrlich, L. A., Jelinek, D. F., Callander, N. S., Roodman, G. D., et al. (2004). IL-3 Expression by Myeloma Cells Increases Both Osteoclast Formation and Growth of Myeloma Cells. *Blood* 103, 2308–2315. doi:10.1182/blood-2003-06-1992

Leung, P., Pickarski, M., Zhuo, Y., Masarachia, P. J., and Duong, L. T. (2011). The Effects of the Cathepsin K Inhibitor Odanacatib on Osteoclastic Bone Resorption and Vesicular Trafficking. *Bone* 49, 623–635. doi:10.1016/j.bone.2011.06.014

Libouban, H., Moreau, M.-F., Baslé, M. F., Bataille, R., and Chappard, D. (2003). Increased Bone Remodeling Due to Ovariectomy Dramatically Increases Tumoral Growth in the 5T2 Multiple Myeloma Mouse Model. *Bone* 33, 283–292. doi:10.1016/s8756-3282(03)00196-0

Lipton, A., and Goessl, C. (2011). Clinical Development of Anti-RANKL Therapies for Treatment and Prevention of Bone Metastasis. *Bone* 48, 96–99. doi:10.1016/j.bone.2010.10.161

Littrell, L. A., Wenger, D. E., Wold, L. E., Bertoni, F., Unni, K. K., White, L. M., et al. (2004). Radiographic, CT, and MR Imaging Features of Dedifferentiated Chondrosarcomas: a Retrospective Review of 174 De Novo Cases. *Radiographics* 24, 1397–1409. doi:10.1148/rg.245045009

Lu, X., Yan, C. H., Yuan, M., Wei, Y., Hu, G., and Kang, Y. (2010). *In Vivo* dynamics and Distinct Functions of Hypoxia in Primary Tumor Growth and Organotropic Metastasis of Breast Cancer. *Cancer Res.* 70, 3905–3914. doi:10.1158/0008-5472.can-09-3739

Lucas, D. R. (1996). Dahlin's Bone Tumors: General Aspects and Data on 11,087 Cases. *Am. J. Clin. Pathol.* 106, 693. doi:10.1093/ajcp/106.5.693

Luzio, J. P., Hackmann, Y., Dieckmann, N. M. G., and Griffiths, G. M. (2014). The Biogenesis of Lysosomes and Lysosome-Related Organelles. *Cold Spring Harbor Perspect. Biol.* 6, a016840. doi:10.1101/cshperspect.a016840

Macedo, F., Ladeira, K., Pinho, F., Saraiva, N., Bonito, N., Pinto, L., et al. (2017). Bone Metastases: An Overview. *Oncol. Rev.* 11, 321. doi:10.4081/oncol.2017.321

Mackiewicz-Wysocka, M., Pankowska, M., and Wysocki, P. J. (2012). Progress in the Treatment of Bone Metastases in Cancer Patients. *Expert Opin. Investig. Drugs* 21, 785–795. doi:10.1517/13543784.2012.679928

Mansour, A., Wakkach, A., and Blin-Wakkach, C. (2017). Emerging Roles of Osteoclasts in the Modulation of Bone Microenvironment and Immune Suppression in Multiple Myeloma. *Front. Immunol.* 8, 954. doi:10.3389/fimmu.2017.00954

Martin, T. J. (2014). Coupling Factors: How many Candidates Can There Be? *J. Bone Miner Res.* 29, 1519–1521. doi:10.1002/jbmr.2276

Mavrogenis, A. F., Igoumenou, V. G., Megaloikonomos, P. D., Panagopoulos, G. N., Papagelopoulos, P. J., and Soucacos, P. N. (2017). Giant Cell Tumor of Bone Revisited. *SICOT-J* 3, 54. doi:10.1051/sicotj/2017041

McCarthy, E. F., and Frassica, F. J. (2014). *Pathology of Bone and Joint Disorders: With Clinical and Radiographic Correlation*. 2 ed. Cambridge: Cambridge University Press.

Mirabello, L., Troisi, R. J., and Savage, S. A. (2009). Osteosarcoma Incidence and Survival Rates from 1973 to 2004. *Cancer* 115, 1531–1543. doi:10.1002/cncr.24121

Mitlak, B. H., Finkelman, R. D., Hill, E. L., Li, J., Martin, B., Smith, T., et al. (1996). The Effect of Systemically Administered PDGF-BB on the Rodent Skeleton. *J. Bone Miner Res.* 11, 238–247. doi:10.1002/jbmr.5650110213

Mizukami, J., Takaesu, G., Akatsuka, H., Sakurai, H., Ninomiya-Tsuji, J., Matsumoto, K., et al. (2002). Receptor Activator of NF-Kb Ligand (RANKL) Activates TAK1 Mitogen-Activated Protein Kinase Kinase Kinase through a Signaling Complex Containing RANK, TAB2, and TRAF6. *Mol. Cel Biol* 22, 992–1000. doi:10.1128/mcb.22.4.992-1000.2002

Monda, L., and Wick, M. R. (1985). S-100 Protein Immunostaining in the Differential Diagnosis of Chondroblastoma. *Hum. Pathol.* 16, 287–292. doi:10.1016/s0046-8177(85)80016-2

Morgan, G. J., Davies, F. E., Gregory, W. M., Bell, S. E., Szubert, A. J., Cook, G., et al. (2013). Long-term Follow-Up of MRC Myeloma IX Trial: Survival Outcomes with Bisphosphonate and Thalidomide Treatment. *Clin. Cancer Res.* 19, 6030–6038. doi:10.1158/1078-0432.ccr-12-3211

Morgan, T., Atkins, G. J., Trivett, M. K., Johnson, S. A., Kansara, M., Schlicht, S. L., et al. (2005). Molecular Profiling of Giant Cell Tumor of Bone and the Osteoclastic Localization of Ligand for Receptor Activator of Nuclear Factor κB. *Am. J. Pathol.* 167, 117–128. doi:10.1016/s0002-9440(10)62959-8

Moussavi-Harami, F., Mollano, A., Martin, J. A., Ayoob, A., Domann, F. E., Gitelis, S., et al. (2006). Intrinsic Radiation Resistance in Human Chondrosarcoma Cells. *Biochem. Biophysical Res. Commun.* 346, 379–385. doi:10.1016/j.bbrc.2006.05.158

Murk, K., Ornaghi, M., and Schiweck, J. (2021). Profilin Isoforms in Health and Disease - All the Same but Different. *Front. Cel Dev. Biol.* 9, 681122. doi:10.3389/fcell.2021.681122

Muto, A., Mizoguchi, T., Udagawa, N., Ito, S., Kawahara, I., Abiko, Y., et al. (2011). Lineage-committed Osteoclast Precursors Circulate in Blood and Settle Down into Bone. *J. Bone Miner Res.* 26, 2978–2990. doi:10.1002/jbmr.490

Nakamura, I., Lipfert, L., Rodan, G. A., and Duong, L. T. (2001). Convergence of αvβ3Integrin-And Macrophage Colony Stimulating Factor-Mediated Signals on Phospholipase Cγ in Prefusion Osteoclasts. *J. Cel Biol* 152, 361–374. doi:10.1083/jcb.152.2.361

Nakashima, T., Hayashi, M., Fukunaga, T., Kurata, K., Oh-Hora, M., Feng, J. Q., et al. (2011). Evidence for Osteocyte Regulation of Bone Homeostasis through RANKL Expression. *Nat. Med.* 17, 1231–1234. doi:10.1038/nm.2452

Nielsen, G. P., Rosenberg, A. E., Deshpande, V., Hornicek, F. J., Kattapuram, S. V., and Rosenthal, D. I. (2017). "Chondroblastoma," in *Diagnostic Pathology: Bone*. Editors G. P. Nielsen, A. E. ROSENBERG, V. DESHPANDE, F. J. HORNICEK, S. V. KATTAPURAM, and D. I. ROSENTHAL. Second Edition (Amsterdam, Netherlands: Elsevier). doi:10.1016/b978-0-323-47777-2.50023-9

Ollivier, L., Vanel, D., and Leclere, J. (2003). Imaging of Chondrosarcomas. *Cancer Imaging* 4, 36–38. doi:10.1102/1470-7330.2003.0022

Otero, J. E., Stevens, J. W., Malandra, A. E., Fredericks, D. C., Odgren, P. R., Buckwalter, J. A., et al. (2014). Osteoclast Inhibition Impairs Chondrosarcoma Growth and Bone Destruction. *J. Orthop. Res.* 32, 1562–1571. doi:10.1002/jor.22714

Ottewell, P. D., Wang, N., Meek, J., Fowles, C. A., Croucher, P. I., Eaton, C. L., et al. (2014). Castration-induced Bone Loss Triggers Growth of Disseminated Prostate Cancer Cells in Bone. *Endocr. Relat. Cancer* 21, 769–781. doi:10.1530/erc-14-0199

Palmerini, E., Picci, P., Reichardt, P., and Downey, G. (2019). Malignancy in Giant Cell Tumor of Bone: A Review of the Literature. *Technol. Cancer Res. Treat.* 18, 1533033819840000. doi:10.1177/1533033819840000

Park, J., Yaseen, N. R., Hogan, P. G., Rao, A., and Sharma, S. (1995). Phosphorylation of the Transcription Factor NFATp Inhibits its DNA Binding Activity in Cyclosporin A-Treated Human B and T Cells. *J. Biol. Chem.* 270, 20653–20659. doi:10.1074/jbc.270.35.20653

Park, S.-Y., and Nam, J.-S. (2020). The Force Awakens: Metastatic Dormant Cancer Cells. *Exp. Mol. Med.* 52, 569–581. doi:10.1038/s12276-020-0423-z

Pearse, R. N., Sordillo, E. M., Yaccoby, S., Wong, B. R., Liau, D. F., Colman, N., et al. (2001). Multiple Myeloma Disrupts the TRANCE/Osteoprotegerin Cytokine axis to Trigger Bone Destruction and Promote Tumor Progression. *Proc. Natl. Acad. Sci. U.S.A.* 98, 11581–11586. doi:10.1073/pnas.201394498

Peinado, H., Zhang, H., Matei, I. R., Costa-Silva, B., Hoshino, A., Rodrigues, G., et al. (2017). Pre-metastatic Niches: Organ-specific Homes for Metastases. *Nat. Rev. Cancer* 17, 302–317. doi:10.1038/nrc.2017.6

Perez-Amodio, S., Jansen, D. C., Schoenmaker, T., Vogels, I. M. C., Reinheckel, T., Hayman, A. R., et al. (2006). Calvarial Osteoclasts Express a Higher Level of Tartrate-Resistant Acid Phosphatase Than Long Bone Osteoclasts and Activation Does Not Depend on Cathepsin K or L Activity. *Calcif Tissue Int.* 79, 245–254. doi:10.1007/s00223-005-0289-z

Pimm, M. L., Hotaling, J., and Henty-Ridilla, J. L. (2020). Profilin Choreographs Actin and Microtubules in Cells and Cancer. *Int. Rev. Cel Mol Biol* 355, 155–204. doi:10.1016/bs.ircmb.2020.05.005

Polavaram, N. S., Dutta, S., Islam, R., Bag, A. K., Roy, S., Poitz, D., et al. (2021). Tumor- and Osteoclast-Derived NRP2 in Prostate Cancer Bone Metastases. *Bone Res.* 9, 24. doi:10.1038/s41413-021-00136-2

Polychronidou, G., Karavasilis, V., Pollack, S. M., Huang, P. H., Lee, A., and Jones, R. L. (2017). Novel Therapeutic Approaches in Chondrosarcoma. *Future Oncol.* 13, 637–648. doi:10.2217/fon-2016-0226

Raimondi, L., De Luca, A., Gallo, A., Costa, V., Russelli, G., Cuscino, N., et al. (2020). Osteosarcoma Cell-Derived Exosomes Affect Tumor Microenvironment by Specific Packaging of microRNAs. *Carcinogenesis* 41, 666–677. doi:10.1093/carcin/bgz130

Raje, N. S., Bhatta, S., and Terpos, E. (2019). Role of the RANK/RANKL Pathway in Multiple Myeloma. *Clin. Cancer Res.* 25, 12–20. doi:10.1158/1078-0432.ccr-18-1537

Raje, N., Vadhan-Raj, S., Willenbacher, W., Terpos, E., Hungria, V., Spencer, A., et al. (2016). Evaluating Results from the Multiple Myeloma Patient Subset Treated with Denosumab or Zoledronic Acid in a Randomized Phase 3 Trial. *Blood Cancer J.* 6, e378. doi:10.1038/bcj.2015.96

Ralston, S. H. (2020). Bisphosphonates in the Management of Paget's Disease. *Bone* 138, 115465. doi:10.1016/j.bone.2020.115465

Reedijk, M., Odorcic, S., Chang, L., Zhang, H., Miller, N., Mccready, D. R., et al. (2005). High-level Coexpression of JAG1 and NOTCH1 Is Observed in Human Breast Cancer and Is Associated with Poor Overall Survival. *Cancer Res.* 65, 8530–8537. doi:10.1158/0008-5472.can-05-1069

Ren, D., Dai, Y., Yang, Q., Zhang, X., Guo, W., Ye, L., et al. (2019). Wnt5a Induces and Maintains Prostate Cancer Cells Dormancy in Bone. *J. Exp. Med.* 216, 428–449. doi:10.1084/jem.20180661

Rendina, D., De Filippo, G., Ralston, S. H., Merlotti, D., Gianfrancesco, F., Esposito, T., et al. (2015). Clinical Characteristics and Evolution of Giant Cell Tumor Occurring in Paget's Disease of Bone. *J. Bone Miner Res.* 30, 257–263. doi:10.1002/jbmr.2349

Rickel, K., Fang, F., and Tao, J. (2017). Molecular Genetics of Osteosarcoma. *Bone* 102, 69–79. doi:10.1016/j.bone.2016.10.017

Robling, A. G., Castillo, A. B., and Turner, C. H. (2006). Biomechanical and Molecular Regulation of Bone Remodeling. *Annu. Rev. Biomed. Eng.* 8, 455–498. doi:10.1146/annurev.bioeng.8.061505.095721

Romero, I., Garrido, F., and Garcia-Lora, A. M. (2014). Metastases in Immune-Mediated Dormancy: a New Opportunity for Targeting Cancer. *Cancer Res.* 74, 6750–6757. doi:10.1158/0008-5472.can-14-2406

Roodman, G. D. (2009). Pathogenesis of Myeloma Bone Disease. *Leukemia* 23, 435–441. doi:10.1038/leu.2008.336

Ross, M. H., Esser, A. K., Fox, G. C., Schmieder, A. H., Yang, X., Hu, G., et al. (2017). Bone-Induced Expression of Integrin β3 Enables Targeted Nanotherapy of Breast Cancer Metastases. *Cancer Res.* 77, 6299–6312. doi:10.1158/0008-5472.can-17-1225

Roux, S., Meignin, V., Quillard, J., Meduri, G., Guiochon-Mantel, A., Fermand, J.-P., et al. (2002). RANK (Receptor Activator of Nuclear Factor-Kb) and RANKL Expression in Multiple Myeloma. *Br. J. Haematol.* 117, 86–92. doi:10.1046/j.1365-2141.2002.03417.x

Russell, R. G. G., Watts, N. B., Ebetino, F. H., and Rogers, M. J. (2008). Mechanisms of Action of Bisphosphonates: Similarities and Differences and Their Potential Influence on Clinical Efficacy. *Osteoporos. Int.* 19, 733–759. doi:10.1007/s00198-007-0540-8

Santos-de-Frutos, K., and Djouder, N. (2021). When Dormancy Fuels Tumour Relapse. *Commun. Biol.* 4, 747. doi:10.1038/s42003-021-02257-0

Satcher, R. L., and Zhang, X. H. (2021). Evolving Cancer-Niche Interactions and Therapeutic Targets during Bone Metastasis. *Nat. Rev. Cancer* 22, 85. doi:10.1038/s41568-021-00406-5

Scotto di Carlo, F., Pazzaglia, L., Esposito, T., and Gianfrancesco, F. (2020a). The Loss of Profilin 1 Causes Early Onset Paget's Disease of Bone. *J. Bone Miner Res.* 35, 1387–1398. doi:10.1002/jbmr.3964

Scotto di Carlo, F., Russo, S., Muyas, F., Mangini, M., Pazzaglia, L., Biamonte, F., et al. (2022). Profilin 1 Deficiency Drives Mitotic Defects and Impairs Genome Stability. *bioRxiv, 2022.02.01.478160*.

Scotto di Carlo, F., Whyte, M. P., and Gianfrancesco, F. (2020b). The Two Faces of Giant Cell Tumor of Bone. *Cancer Lett.* 489, 1–8. doi:10.1016/j.canlet.2020.05.031

Sethi, N., Dai, X., Winter, C. G., and Kang, Y. (2011). Tumor-derived JAGGED1 Promotes Osteolytic Bone Metastasis of Breast Cancer by Engaging Notch Signaling in Bone Cells. *Cancer Cell* 19, 192–205. doi:10.1016/j.ccr.2010.12.022

Shiozawa, Y., Pedersen, E. A., Havens, A. M., Jung, Y., Mishra, A., Joseph, J., et al. (2011). Human Prostate Cancer Metastases Target the Hematopoietic Stem Cell Niche to Establish Footholds in Mouse Bone Marrow. *J. Clin. Invest.* 121, 1298–1312. doi:10.1172/jci43414

Shorey, S., Heersche, J. N. M., and Manolson, M. F. (2004). The Relative Contribution of Cysteine Proteinases and Matrix Metalloproteinases to the Resorption Process in Osteoclasts Derived from Long Bone and Scapula. *Bone* 35, 909–917. doi:10.1016/j.bone.2004.06.002

Simonet, W. S., Lacey, D. L., Dunstan, C. R., Kelley, M., Chang, M.-S., Lüthy, R., et al. (1997). Osteoprotegerin: a Novel Secreted Protein Involved in the Regulation of Bone Density. *Cell* 89, 309–319. doi:10.1016/s0092-8674(00)80209-3

Sims, N. A., and Martin, T. J. (2020). Osteoclasts Provide Coupling Signals to Osteoblast Lineage Cells through Multiple Mechanisms. *Annu. Rev. Physiol.* 82, 507–529. doi:10.1146/annurev-physiol-021119-034425

Sosa, M. S., Bragado, P., and Aguirre-Ghiso, J. A. (2014). Mechanisms of Disseminated Cancer Cell Dormancy: an Awakening Field. *Nat. Rev. Cancer* 14, 611–622. doi:10.1038/nrc3793

Stopeck, A. T., Lipton, A., Body, J.-J., Steger, G. G., Tonkin, K., De Boer, R. H., et al. (2010). Denosumab Compared with Zoledronic Acid for the Treatment of Bone Metastases in Patients with Advanced Breast Cancer: a Randomized, Double-Blind Study. *Jco* 28, 5132–5139. doi:10.1200/jco.2010.29.7101

Suda, T., Takahashi, N., and Martin, T. J. (1992). Modulation of Osteoclast Differentiation [published Erratum Appears in Endocr Rev 1992 May;13(2):191]. *Endocr. Rev.* 13, 66–80. doi:10.1210/er.13.1.66

Taichman, R. S., Patel, L. R., Bedenis, R., Wang, J., Weidner, S., Schumann, T., et al. (2013). GAS6 Receptor Status Is Associated with Dormancy and Bone Metastatic Tumor Formation. *PLoS One* 8, e61873. doi:10.1371/journal.pone.0061873

Tang, Y., Wu, X., Lei, W., Pang, L., Wan, C., Shi, Z., et al. (2009). TGF-β1-induced Migration of Bone Mesenchymal Stem Cells Couples Bone Resorption with Formation. *Nat. Med.* 15, 757–765. doi:10.1038/nm.1979

Tassone, P., Tagliaferri, P., Viscomi, C., Palmieri, C., Caraglia, M., D'Alessandro, A., et al. (2003). Zoledronic Acid Induces Antiproliferative and Apoptotic Effects in Human Pancreatic Cancer Cells *In Vitro*. *Br. J. Cancer* 88, 1971–1978. doi:10.1038/sj.bjc.6600986

Teitelbaum, S. L. (2000). Bone Resorption by Osteoclasts. *Science* 289, 1504–1508. doi:10.1126/science.289.5484.1504

Terpos, E., Heath, D. J., Rahemtulla, A., Zervas, K., Chantry, A., Anagnostopoulos, A., et al. (2006). Bortezomib Reduces Serum Dickkopf-1 and Receptor Activator of Nuclear Factor-?B Ligand Concentrations and Normalises Indices of Bone Remodelling in Patients with Relapsed Multiple Myeloma. *Br. J. Haematol.* 135, 688–692. doi:10.1111/j.1365-2141.2006.06356.x

Terpos, E., Ntanasis-Stathopoulos, I., Gavriatopoulou, M., and Dimopoulos, M. A. (2018). Pathogenesis of Bone Disease in Multiple Myeloma: from Bench to Bedside. *Blood Cancer J.* 8, 7. doi:10.1038/s41408-017-0037-4

Thurnher, M., Nussbaumer, O., and Gruenbacher, G. (2012). Novel Aspects of Mevalonate Pathway Inhibitors as Antitumor Agents. *Clin. Cancer Res.* 18, 3524–3531. doi:10.1158/1078-0432.ccr-12-0489

Tian, Z., Wu, L., Yu, C., Chen, Y., Xu, Z., Bado, I., et al. (2021). Harnessing the Power of Antibodies to Fight Bone Metastasis. *Sci. Adv.* 7. doi:10.1126/sciadv.abf2051

Tiedemann, K., Le Nihouannen, D., Fong, J. E., Hussein, O., Barralet, J. E., and Komarova, S. V. (2017). Regulation of Osteoclast Growth and Fusion by mTOR/raptor and mTOR/rictor/Akt. *Front. Cel Dev. Biol.* 5, 54. doi:10.3389/fcell.2017.00054

Tondravi, M. M., Mckercher, S. R., Anderson, K., Erdmann, J. M., Quiroz, M., Maki, R., et al. (1997). Osteopetrosis in Mice Lacking Haematopoietic Transcription Factor PU.1. *Nature* 386, 81–84. doi:10.1038/386081a0

Trinidad, E. M., and González-Suárez, E. (2016). RANKL Inhibitors for Osteosarcoma Treatment: hope and Caution. *Ann. Transl. Med.* 4, 534. doi:10.21037/atm.2016.12.10

Valastyan, S., and Weinberg, R. A. (2011). Tumor Metastasis: Molecular Insights and Evolving Paradigms. *Cell* 147, 275–292. doi:10.1016/j.cell.2011.09.024

Valery, P. C., Laversanne, M., and Bray, F. (2015). Bone Cancer Incidence by Morphological Subtype: a Global Assessment. *Cancer Causes Control* 26, 1127–1139. doi:10.1007/s10552-015-0607-3

Visgauss, J. D., Lazarides, A., Dickson, B., Cardona, D., Sheth, M., Dewitt, S. B., et al. (2021). Treatment of Chondroblastoma with Denosumab: A Case Report with a Correlative Analysis of Effect on the RANK Signaling Pathway. *JBJS Case Connect.* 11. doi:10.2106/JBJS.CC.20.00178

Wan, X., Li, Z.-G., Yingling, J. M., Yang, J., Starbuck, M. W., Ravoori, M. K., et al. (2012). Effect of Transforming Growth Factor Beta (TGF-β) Receptor I Kinase Inhibitor on Prostate Cancer Bone Growth. *Bone* 50, 695–703. doi:10.1016/j.bone.2011.11.022

Wang, H., Yu, C., Gao, X., Welte, T., Muscarella, A. M., Tian, L., et al. (2015). The Osteogenic Niche Promotes Early-Stage Bone Colonization of Disseminated Breast Cancer Cells. *Cancer Cell* 27, 193–210. doi:10.1016/j.ccell.2014.11.017

Wang, K., Donnelly, C. R., Jiang, C., Liao, Y., Luo, X., Tao, X., et al. (2021). STING Suppresses Bone Cancer Pain via Immune and Neuronal Modulation. *Nat. Commun.* 12, 4558. doi:10.1038/s41467-021-24867-2

Wang, K., Gu, Y., Liao, Y., Bang, S., Donnelly, C. R., Chen, O., et al. (2020a). PD-1 Blockade Inhibits Osteoclast Formation and Murine Bone Cancer Pain. *J. Clin. Invest.* 130, 3603–3620. doi:10.1172/jci133334

Wang, L., Fang, D., Xu, J., and Luo, R. (2020b). Various Pathways of Zoledronic Acid against Osteoclasts and Bone Cancer Metastasis: a Brief Review. *BMC Cancer* 20, 1059. doi:10.1186/s12885-020-07568-9

Warde, N. (2011). The Odyssey of Osteoclast Precursors. *Nat. Rev. Rheumatol.* 7, 557. doi:10.1038/nrrheum.2011.140

Wei, Z., Li, S., Tao, X., Zhu, G., Sun, Z., Wei, Z., et al. (2021). Mutations in Profilin 1 Cause Early-Onset Paget's Disease of Bone with Giant Cell Tumors. *J. Bone Mineral. Res.* 36, 1088–1103. doi:10.1002/jbmr.4275

Weilbaecher, K. N., Guise, T. A., and Mccauley, L. K. (2011). Cancer to Bone: a Fatal Attraction. *Nat. Rev. Cancer* 11, 411–425. doi:10.1038/nrc3055

Wesselborg, S., Fruman, D. A., Sagoo, J. K., Bierer, B. E., and Burakoff, S. J. (1996). Identification of a Physical Interaction between Calcineurin and Nuclear Factor of Activated T Cells (NFATp). *J. Biol. Chem.* 271, 1274–1277. doi:10.1074/jbc.271.3.1274

Xian, L., Wu, X., Pang, L., Lou, M., Rosen, C. J., Qiu, T., et al. (2012). Matrix IGF-1 Maintains Bone Mass by Activation of mTOR in Mesenchymal Stem Cells. *Nat. Med.* 18, 1095–1101. doi:10.1038/nm.2793

Xie, H., Cui, Z., Wang, L., Xia, Z., Hu, Y., Xian, L., et al. (2014). PDGF-BB Secreted by Preosteoclasts Induces Angiogenesis during Coupling with Osteogenesis. *Nat. Med.* 20, 1270–1278. doi:10.1038/nm.3668

Xing, L., Xiu, Y., and Boyce, B. F. (2012). Osteoclast Fusion and Regulation by RANKL-dependent and Independent Factors. *Wjo* 3, 212–222. doi:10.5312/wjo.v3.i12.212

Yagi, M., Miyamoto, T., Sawatani, Y., Iwamoto, K., Hosogane, N., Fujita, N., et al. (2005). DC-STAMP Is Essential for Cell-Cell Fusion in Osteoclasts and Foreign Body Giant Cells. *J. Exp. Med.* 202, 345–351. doi:10.1084/jem.20050645

Yu-Lee, L.-Y., Lee, Y.-C., Pan, J., Lin, S.-C., Pan, T., Yu, G., et al. (2019). Bone Secreted Factors Induce Cellular Quiescence in Prostate Cancer Cells. *Sci. Rep.* 9, 18635. doi:10.1038/s41598-019-54566-4

Yu-Lee, L.-Y., Yu, G., Lee, Y.-C., Lin, S.-C., Pan, J., Pan, T., et al. (2018). Osteoblast-Secreted Factors Mediate Dormancy of Metastatic Prostate Cancer in the Bone via Activation of the TGFβRIII-p38MAPK-pS249/T252RB Pathway. *Cancer Res.* 78, 2911–2924. doi:10.1158/0008-5472.can-17-1051

Yumoto, K., Eber, M. R., Wang, J., Cackowski, F. C., Decker, A. M., Lee, E., et al. (2016). Axl Is Required for TGF-B2-Induced Dormancy of Prostate Cancer Cells in the Bone Marrow. *Sci. Rep.* 6, 36520. doi:10.1038/srep36520

Zaidi, M., and Cardozo, C. P. (2018). Receptor Becomes a Ligand to Control Bone Remodelling. *Nature* 561, 180–181. doi:10.1038/d41586-018-05960-x

Zhang, S., Wright, J. E. I., Özber, N., and Uludağ, H. (2007). The Interaction of Cationic Polymers and Their Bisphosphonate Derivatives with Hydroxyapatite. *Macromol. Biosci.* 7, 656–670. doi:10.1002/mabi.200600286

Zhao, C., Irie, N., Takada, Y., Shimoda, K., Miyamoto, T., Nishiwaki, T., et al. (2006). Bidirectional ephrinB2-EphB4 Signaling Controls Bone Homeostasis. *Cel Metab.* 4, 111–121. doi:10.1016/j.cmet.2006.05.012

Zheng, Y., Zhou, H., Fong-Yee, C., Modzelewski, J. R. K., Seibel, M. J., and Dunstan, C. R. (2008). Bone Resorption Increases Tumour Growth in a Mouse Model of Osteosclerotic Breast Cancer Metastasis. *Clin. Exp. Metastasis* 25, 559–567. doi:10.1007/s10585-008-9172-4

Zielińska, M., Chmielewska, E., Buchwald, T., Voelkel, A., and Kafarski, P. (2021). Determination of Bisphosphonates Anti-resorptive Properties Based on Three Forms of Ceramic Materials: Sorption and Release Process Evaluation. *J. Pharm. Anal.* 11, 364–373. doi:10.1016/j.jpha.2020.07.011

Conflict of Interest: The authors declare that the research was conducted in the absence of any commercial or financial relationships that could be construed as a potential conflict of interest.

The handling editor SM declared a past collaboration with the authors FG and FSdC.

Publisher's Note: All claims expressed in this article are solely those of the authors and do not necessarily represent those of their affiliated organizations, or those of the publisher, the editors, and the reviewers. Any product that may be evaluated in this article, or claim that may be made by its manufacturer, is not guaranteed or endorsed by the publisher.

frontiers | Frontiers in Molecular Biosciences

ORIGINAL RESEARCH
published: 14 June 2022
doi: 10.3389/fmolb.2022.896841

Spatial Organization of Osteoclastic Coupling Factors and Their Receptors at Human Bone Remodeling Sites

Xenia G. Borggaard[1,2]*, *Malene H. Nielsen*[1,2], *Jean-Marie Delaisse*[1,2], *Christina M. Andreasen*[1,2] *and Thomas L. Andersen*[1,2,3]*

[1]Research Unit of Pathology, Department of Clinical Research and Department of Molecular Medicine, Molecular Bone Histology Team, Clinical Cell Biology, University of Southern Denmark, Odense, Denmark, [2]Department of Pathology, Odense University Hospital, Odense, Denmark, [3]Department of Forensic Medicine, Aarhus University, Aarhus, Denmark

The strictly regulated bone remodeling process ensures that osteoblastic bone formation is coupled to osteoclastic bone resorption. This coupling is regulated by a panel of coupling factors, including clastokines promoting the recruitment, expansion, and differentiation of osteoprogenitor cells within the eroded cavity. The osteoprogenitor cells on eroded surfaces are called reversal cells. They are intermixed with osteoclasts and become bone-forming osteoblast when reaching a critical density and maturity. Several coupling factors have been proposed in the literature, but their effects and expression pattern vary between studies depending on species and experimental setup. In this study, we investigated the mRNA levels of proposed secreted and membrane-bound coupling factors and their receptors in cortical bone remodeling events within the femur of healthy adolescent human controls using high-sensitivity RNA *in situ* hybridization. Of the proposed coupling factors, human osteoclasts showed mRNA-presence of *LIF*, *PDGFB*, *SEMA4D*, but no presence of *EFNB2*, and *OSM*. On the other hand, the osteoblastic reversal cells proximate to osteoclasts presented with *LIFR*, *PDGFRA* and *PLXNB1*, but not *PDGFRB*, which are all known receptors of the proposed coupling factors. Although *EFNB2* was not present in mature osteoclasts, the mRNA of the ligand-receptor pair *EFNB2:EPHB4* were abundant near the central blood vessels within intracortical pores with active remodeling. *EPHB4* and *SEMA4D* were also abundant in mature bone-forming osteoblasts. This study highlights that especially *LIF:LIFR*, *PDGFB:PDGFRA*, *SEMA4D:PLXNB1* may play a critical role in the osteoclast-osteoblast coupling in human remodeling events, as they are expressed within the critical cells.

Keywords: bone remodeling, osteoclast (OC), coupling, osteoblast (OB), bone cells interaction

OPEN ACCESS

Edited by:
Maria-Bernadette Madel, Baylor College of Medicine, United States

Reviewed by:
Natalie A. Sims, University of Melbourne, Australia
Rupesh K. Srivastava, All India Institute of Medical Sciences, India
'Vincent Everts, VU Amsterdam, Netherlands

***Correspondence:**
Xenia G. Borggaard
xborggaard@health.sdu.dk
orcid.org/0000-0002-4922-2478
Thomas L. Andersen
Thomas.levin.andersen@rsyd.dk
orcid.org/0000-0002-6981-7276

Specialty section:
This article was submitted to Cellular Biochemistry, a section of the journal Frontiers in Molecular Biosciences

Received: *15 March 2022*
Accepted: *11 May 2022*
Published: *14 June 2022*

Citation:
Borggaard XG, Nielsen MH, Delaisse J-M, Andreasen CM and Andersen TL (2022) Spatial Organization of Osteoclastic Coupling Factors and Their Receptors at Human Bone Remodeling Sites. Front. Mol. Biosci. 9:896841. doi: 10.3389/fmolb.2022.896841

INTRODUCTION

Bone remodeling is responsible for maintenance of the adult human skeleton. Imbalances in bone resorption and formation during the bone remodeling process causes either a gain or loss of bone (Delaisse et al., 2020). Such imbalance may be due to uncoupled resorption and formation, as characteristic of ageing, osteoporosis and multiple myeloma (Andersen et al., 2010, 2013; Jensen et al., 2014; Andreasen et al., 2020). The bone remodeling process includes three different phases: First, the resorptive phase where osteoclasts start resorption of old bone. Second, the reversal-resorption phase, where osteoclasts expand the resorbed area. In the reversal-resorption phase,

osteoclasts are intermixed with osteoprogenitors recruited to the eroded bone surface. These osteoprogenitors, known as reversal cells, prepare the bone surface for bone formation, while gradually undergoing differentiation into mature bone forming osteoblasts. Third, the bone formation phase (Andersen et al., 2013; Lassen et al., 2017; Delaisse et al., 2020; Sims and Martin, 2020).

The proximity between osteoclasts and osteoblastic reversal cells during the reversal-resorption phase allows active interaction and signaling between these cell types. Furthermore, reversal cells comprise a possible target cell available for osteoclastic coupling factors. Osteoclastic coupling factors include: 1) matrix-derived factors released during resorption, 2) factors secreted by osteoclasts, 3) membrane-bound factors on osteoclasts, and 4) factors packed in exosomes released by osteoclasts (Charles and Aliprantis, 2014; Sims and Martin, 2020).

The discovery of reversal cells vacating eroded bone surfaces near osteoclasts have provided a potential bridge in the communication between osteoclasts and osteoblastic cells during bone remodeling, as bone-resorbing osteoclasts are rarely observed near bone-forming osteoblasts (Eriksen, Melsen and Mosekilde, 1984; Andersen et al., 2009; Lassen et al., 2017). Initially, reversal cells were described as mononucleated cells, covering approximately 80% of eroded surfaces in trabecular bone and proposed to be pre-osteoclasts due to the presence of TRAcP (Baron et al., 1983; Eriksen et al., 1984; Eriksen et al., 1984; Bianco et al., 1988; Mocetti et al., 2000). We now know that they are osteoblast-lineage cells, expressing markers specific for early osteogenic commitment (Andersen et al., 2009; Abdelgawad et al., 2016; Abdallah et al., 2017; Jafari et al., 2017; Lassen et al., 2017; Chen et al., 2019). Furthermore, we have shown that early reversal cells have direct cell-cell interactions with osteoclasts, they take up Tartrate-resistant acid phosphatase (TRAcP) released by osteoclasts, and they decompose resorption debris left by the osteoclast (Everts et al., 2002; Abdelgawad et al., 2016). Collectively, this supports the concept that osteoblastic reversal cells are a key recipient of osteoclastic coupling factors (Charles and Aliprantis, 2014; Delaisse et al., 2020).

The proposed osteoclastic coupling factors include secreted and membrane-bound coupling factors. Potential secreted coupling factors (clastokines) includes Leukemia Inhibitory Factor (LIF), Cardiotrophin-1 (CTF1) and Oncostatin M (OSM) from the IL-6 family of cytokines. These cytokines have been suggested to play a role in bone metabolism (Sims, 2009, 2021). An interesting feature of these cytokines is their dependency of the glycoprotein 130 subunit during signaling, and their ability to react with other receptors within this group of cytokines (Kishimoto et al., 1995). LIF has been associated with metabolic and immunological processes and especially with growth and bone metabolism (Ware et al., 1995; Jones and Jenkins, 2018). The receptor of LIF (LIFR) is expressed by murine osteoblastic cells *in vitro* (Allan et al., 1990; Reid et al., 1990; Bellido et al., 1997; Walker et al., 2010). The amino acid sequence of CTF1 is similar to LIF and able to bind and activate LIFR(Pennica et al., 1995). In primary murine osteoblastic cells, *Ctf1* expression increases with differentiation (Liu, Aubin and Malaval, 2002) whereas CTF1 protein has been reported in mature murine osteoclasts (Walker et al., 2008). OSM also has the ability to bind and activate LIFR (Rose and Bruce, 1991; Liu et al., 1992) besides the specific OSM receptor (OSMR) (Thoma et al., 1994). Murine osteoblastic cells express both *Lifr* and *Osmr*, but their expression levels differ throughout differentiation (Bellido et al., 1996). However, knowledge on how *LIF*, *CTF1*, *OSM*, *OSMR* and *LIFR* are expressed in human bone is scarce.

Platelet-Derived Growth Factor (PDGF) has also attracted attention as a possible secreted coupling factor regulating bone formation (Horner et al., 1996). PDGFs are dimeric proteins of two polypeptide chains, forming either homodimers (AA, BB) or heterodimers (AB). Likewise, PDGF receptors are dimeric and either homodimers or heterodimers (PDGFRA, PDGFRB or PDGFRAB). PDGF-BB is considered the universal PDGF with binding affinity for all PDGF receptors (Horner et al., 1996; Alvarez, Kantarjian and Cortes, 2006). In human trabecular bone, *PDGFB* expression was recently observed in osteoclasts, while its receptors *PDGFRA* and *PDGFRB* were expressed in proximate reversal cells and osteoblastic canopy cells, separating bone surface cells from the marrow cavity (Brun et al., 2020).

Proposed membrane-bound coupling factors include semaphorin 4D (SEMA4D), a transmembrane glycoprotein with high affinity to PlexinB1 (PLXNB1) (Kang and Kumanogoh, 2013). SEMA4D is believed to be a repressor of bone formation, as knockdown in mice leads to a high bone-mass phenotype with no effect on bone resorption (Negishi-Koga et al., 2011). In humans, high serum levels of SEMA4D has been associated with low BMD and decreased markers of bone formation (Zhang et al., 2015). However, not much is known about the spatial expression of *SEMA4D* and *PLXNB1* within the bone environment. EphrinB2 (EFNB2) is yet another proposed membrane-bound coupling factor. EFNB2 is a transmembrane ligand of the receptor tyrosine kinase EPHB4. Activation of receptor tyrosine kinases initiates bidirectional signaling, forward through the receptor and reverse through the ligand (Pasquale, 2010; Taylor, Campbell and Nobes, 2017). Expression of *Efnb2* has been shown in osteoclasts, osteoblasts and osteocytes of mice, whereas *Ephb4* expression has only been shown in osteoblasts (Arthur et al., 2011, 2018; Wang et al., 2014).

In this study we investigated spatial mRNA localization of several suggested coupling factors, secreted or membrane-bound in osteoclasts, and their receptors in osteoblastic reversal cells and osteoblasts within human intracortical bone remodeling events.

MATERIALS AND METHODS

Human bone specimens were collected from the proximal femur of nine adolescent patients aged 6–15 years undergoing corrective surgery for Coxa Valga. Collected specimens were fixated in 4% paraformaldehyde for 2 days and subsequently decalcified for 30 days in 0.5 M EDTA containing 0.4% paraformaldehyde. Decalcified specimens were dehydrated, paraffin-embedded and cut in series of 3.5-µm-thick adjacent sections. Every fifth section was Masson Trichrome stained to select samples with

active bone remodeling (identified as erosion or formation in cortical pores). Selected sections were stained with *in situ* hybridization combined with TRAcP. Spatial localization of each mRNA was validated in at least three different individuals. The study was approved by the Danish National Committee on Biomedical Research Ethics (Project-ID: S-2012-0193).

In situ Hybridization Combined With Immunostaining

Sections adjacent to Masson Trichrome stained sections were *in situ* hybridized for the mRNA abundance of proposed coupling factors *LIF*, *CTF1*, *OSM*, *SEMA4D*, *EPHB4* and *PDGFA*, as well as their receptors *LIFR*, *OSMR*, *PLXNB1*, *EFNB2*, *PDGFRA* and *PDGFRB*. *In situ* hybridization was performed using a modified RNAscope 2.5 high-definition procedure (R2283, Sigma-Aldrich). After deparaffinization and rehydration, sections were treated with 1.5% hydrogen peroxidase for 30 min at room temperature to inactivate endogenous peroxidases. Subsequently, sections were pretreated with RNAscope Target Retrieval for 15 min at 90°C and pepsin (322300, ACD Bioscience) for 20 min at 40°C. After pretreatment, sections were hybridized in a HybEZ™ hybridization oven at 40°C overnight with 20- probe-pairs for human *LIF* (cat. No: 445721, binding nt 839-1780 of NM_002309.4), *CTF1* (Cat. No. 895601, binding nt 40-1222 of NM_001330.5), *OSM* (Cat. No. 456381, binding nt 32-1175 of NM_020530.4), *SEMA4D* (Cat. No, 430711, binding nt 611-1623 of NM_006378.3), EPH receptor panel with high affinity for *EPHB4* and affinity for *EPHB1/EPHB2/EPHB3* (Cat. No. 516401, binding nt 2019-2577 of NM_004444.4), *PDGFB* (Cat. No. 406701, binding nt 665-2037 of NM_033016.2), *LIFR* (Cat. No. 441021, binding nt 2411-3421 of NM_001127671.1), *OSMR* (Cat. No. 537121, binding nt 307-1357 of NM_001323505.1), *PLXNB1* (Cat. No. 430681, binding nt 1208-2101 of NM_002673.5), *EFNB2* (Cat. No. 430651, binding nt 2-919 of NM_004093.3), *PDGFRA* (Cat. No. 604481, binding nt 844-1774 of NM_006206.4) and *PDGFRB* (Cat. No. 548991, binding 523-2984 of NM_002609.3) from ACD Bioscience. The probes were diluted 1:1 in probe diluent (449819, ACD Bioscience) and negative controls were with only probe diluent. Each probe was validated on a tissue array with 36 different anonymized tissue-samples. Hybridized probes were branch amplified through six steps in the HybEZ™ hybridization oven according to manufactures instructions, and further enhanced with digoxigenin-conjugated tyramide (NEL748001KT, PerkinElmer) detected with alkaline-phosphatase conjugated sheep anti-digoxigenin Fab fragments (11093274910, Roche) and visualized using Liquid Permanent Red (Agiliant). After the *in situ* procedure, osteoclasts were immunostained with mouse-anti-TRAcP IgG2B antibody (clone 9C5, MABF96, Merck Millipore) detected with horseradish peroxidase-conjugated anti-mouse IgG polymers (BrightVision, Immunologic, Duiven, Holland) and visualized using Deep Space Black (Biocare Medical Concord, CA, United States). Finally, sections were counterstained with Mayer's hematoxylin.

Microscopy

The stained sections were imaged on a VS200 slide scanner (Olympus) using Z-stack condensed into a single plane with optimal focus, which were investigated using the Olivia software (Olympus).

RESULTS

In this observational study, we examined the presence of mRNA encoding secreted and membrane-bound coupling factors proposed in the literature and their receptors in human cortical bone remodeling events. Here, we focused particularly on reversal cells situated adjacent to mature bone resorbing osteoclasts. We examined femur cortical bone specimens from nine adolescents and each mRNA was evaluated in at least three different individuals.

IL-6 Family Cytokines and Their Receptors are Present in Human Bone Remodeling Events

Analysis of the spatial mRNA localization of *LIF* and *LIFR* revealed a high abundance of *LIF* in mature bone-resorbing osteoclasts and a lower presence in osteocytes (**Figure 1A**). On the other hand, the *LIFR* mRNA was not detected in mature bone-resorbing osteoclasts (**Figure 1B**). Instead, *LIFR* was highly abundant in reversal cells near osteoclasts on the eroded surfaces, and in mononucleated cells within the pore lumen, which to a great extend reflect osteoprogenitors being recruited to the eroded surfaces as reversal cells (Lassen et al., 2017) (**Figure 1B**). *LIFR* was also abundant in mature bone-forming osteoblasts on osteoid surfaces and only weakly present in some osteocytes (**Figures 1D,F**). *LIF* was only weakly present in mature bone-forming osteoblasts (**Figure 1E**).

Bone-resorbing osteoclasts showed no presence of *CTF1* (**Figure 2B**) despite presence of *LIFR* in proximate reversal cells and mononucleated cells within the lumen (potential osteoprogenitors) (**Figure 2C**). *OSMR* was abundant in reversal cells and proximate mononucleated cells within the lumen (potential osteoprogenitors), as well as to some extend in osteocytes. In contrast to *LIFR*, *OSMR* was not notably present in bone-forming osteoblasts (**Figure 2D**). Surprisingly, bone-resorbing osteoclasts showed no evidence of *OSM* mRNA (**Figure 2E**), as the case for *CTF1*. Levels of *OSM* and *CFT1* was generally low and restricted to a few mononucleated cells within the intracortical pores. Both *OSM* and *CTF1* were detected in different tissues in the control tissue array (Suppl. 1).

PDGF and its Receptors are Present in Human Bone Remodeling Events

PDGFB was detected in osteoclasts and in cells near the vascular structures, not in reversal cells (**Figures 3A,E**). The two receptors were present at different levels in the tissue.

PDGFRA and *PDGFRB* were present in reversal cells on eroded surfaces (**Figures 3B, C**). Furthermore, *PDGFRA* was

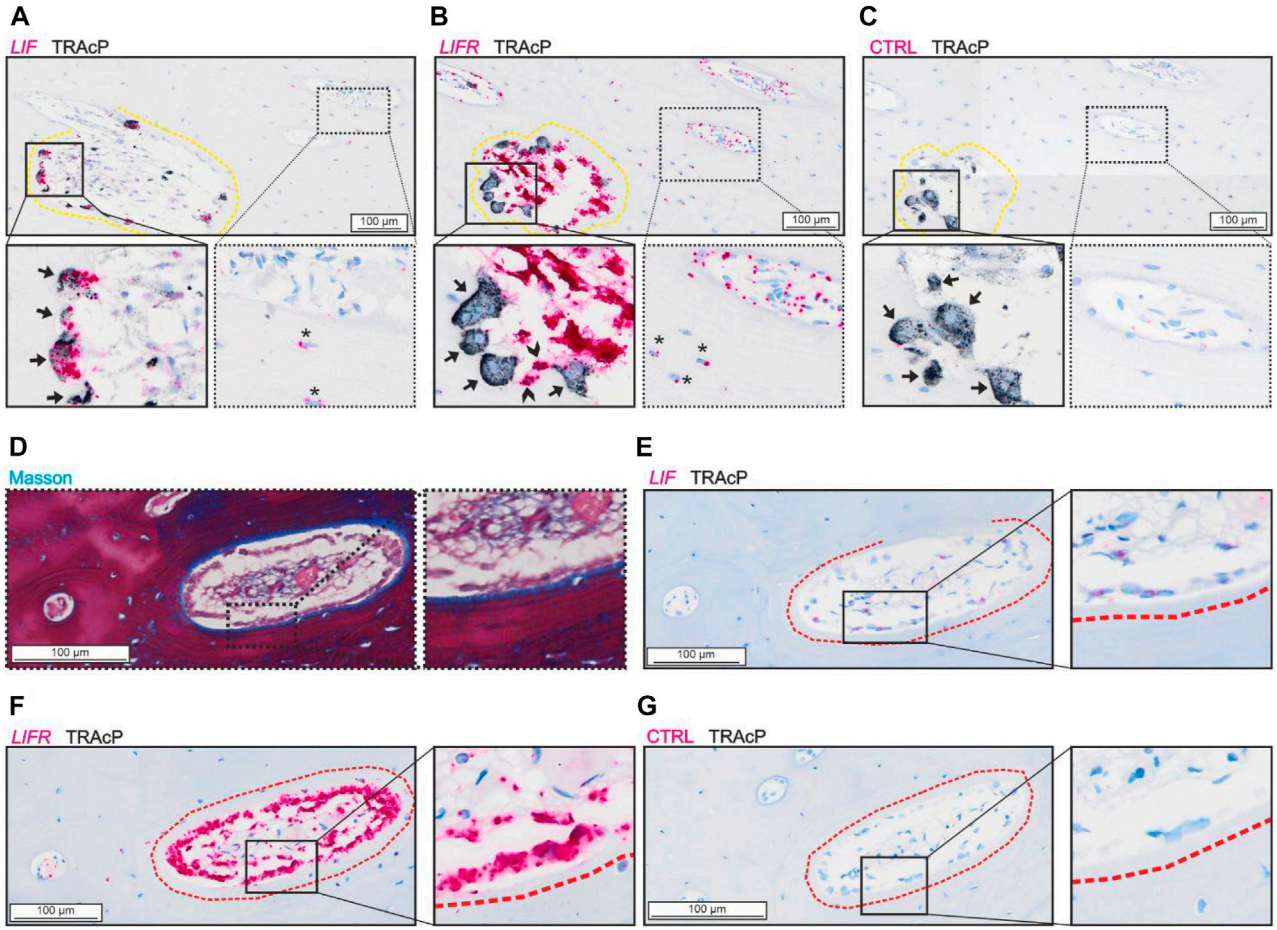

FIGURE 1 | LIF is present in osteoclasts and LIFR in osteoblasts and mononucleated cells in the lumen of adjacent sections of intracortical canals. **(A–C)** Adjacent sections of eroded pore with *in situ* hybridization (red) of LIF **(A)**, LIFR **(B)** and negative control **(C)** combined with immunostaining of TRAcP (black). **(D–G)** Adjacent sections of formative pore with masson **(D)** and *in situ* hybridization of LIF **(E)**, LIFR **(F)** or negative control **(G)** combined with immunostaining of TRAcP (black). Eroded surfaces are marked by a yellow dashed line, formative bone surfaces are marked by a red dashed line. Osteoclasts are indicated by black arrows in the zooms, Reversal cells are indicated by arrowheads and osteocytes with signal from *in situ* hybridization are shown with*.

present in osteocytes and osteoblasts (**Figures 3B,F**), whereas *PDGFRB* was primarily located near vascular structures within the lumen of intracortical pores and not in bone forming osteoblasts or osteocytes (**Figures 3C,G**).

SEMA4D and PLXNB1 are Present in Human Bone Remodeling Events

SEMA4D was present in mature bone-resorbing osteoclasts (**Figure 4A**) and in bone-forming osteoblasts on osteoid surfaces and in some osteocytes (**Figures 4D,E**). The few mononucleated cells within the lumen showing low levels of *SEMA4D*, appeared morphologically like endothelial cells instead of potential osteoprogenitors. Discrete levels of *PLXNB1* (receptor of SEMA4D) were observed in reversal cells next to *SEMA4D*-positive osteoclasts (**Figure 4B**), and in bone-forming osteoblasts on osteoid surfaces and in some osteocytes (**Figures 4E,F**). No *PLXNB1* was observed in mature bone-resorbing osteoclasts (**Figure 4B**).

Vascular Structures Express EFNB2 and EPHB4 in *Human Bone Remodeling Events*

We observed no presence of either *EPHB4* or *EFNB2* in osteoclasts, reversal cells or osteocytes (**Figure 5**), but some mature bone-forming osteoblasts contained *EPHB4* mRNA (**Figure 5A**). In contrast, both EPHB4 and EFNB2 were highly present in vascular structures within the intracortical pores (**Figure 5**).

DISCUSSION

The elusive coupling of bone formation to osteoclastic bone resorption is a critical step in the bone remodeling process, which we are only starting to understand (Delaisse et al., 2020). Osteoclastic coupling factors play a central role in the osteoclast-osteoblast coupling, ensuring the initiation of bone formation within the vacated resorption cavities (Sims and Martin, 2020). The present study examines *in situ* mRNA

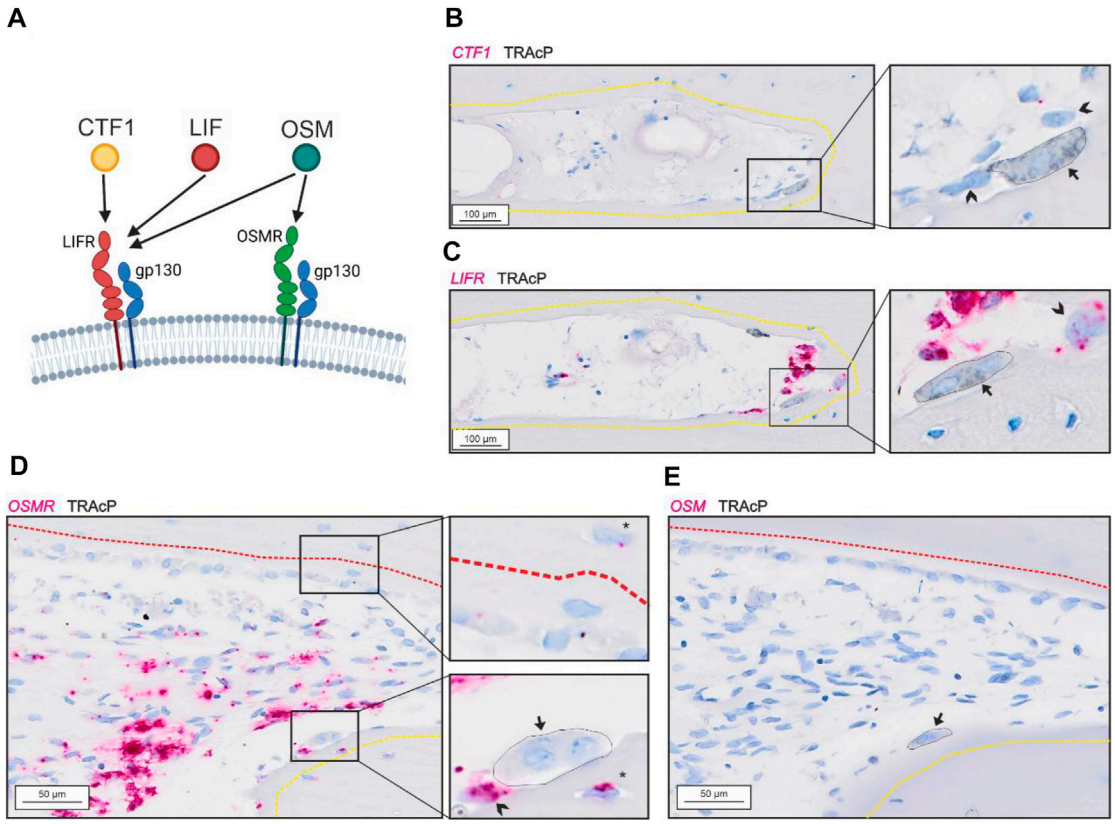

FIGURE 2 | Gp130-associating receptors are present within intracortical pores with active bone remodeling. **(A)** schematic illustration of the two gp130-associating receptors (LIFR and OSMR) and their affinity for CTF-1, LIF and OSM. **(A–B)** Adjacent sections of eroded pore with *in situ* hybridization (red) of *CTF1* **(A)** and *LIFR* **(B)** combined with immunostaining of TRAcP (black). **(D–E)** Adjacent sections of pore with resorption and formation with *in situ* hybridization (red) of *OSMR* **(D)** and *OSM* **(E)** combined with immunostaining of TRAcP (black). Eroded surfaces are marked by a yellow dashed line and formative surfaces are marked by a red dashed line. Osteoclasts are marked by a black arrow and outlined in the zooms, reversal cells are marked by arrowheads.

localization of potential membrane-bound and secreted osteoclastic coupling factors and their respective receptors in human cortical remodeling events. The study demonstrates that mRNA of several coupling factors are present in osteoclasts, while their receptors were present in neighboring osteoblastic reversal cells (e.g., osteoprogenitors) during the reversal-resorption phase. This supports the notion that interactions between osteoclasts and osteoprogenitors within the reversal-resorption phase play a key role in the coupling mechanism, potentially involving a dedicated panel of secreted and membrane-bound coupling factors.

Secreted Osteoclastic Coupling Factors and Their Receptors in Human Bone Remodeling

In human cortical remodeling events, the osteoclastic levels of *LIF* and high levels of *LIFR* in neighboring reversal cells and potential osteoprogenitors within the lumen, support that LIF:LIFR signaling may likely have a functional role in the coupling during human bone remodeling. This supports previous studies in genetic mice models, suggesting a pro-osteogenic effect of LIF:LIFR signaling during bone remodeling. These mice studies showed an increased bone volume when *Lif* was overexpressed (Metcalf and Gearing, 1989), and decreased bone volume and increased number of osteoclasts in *Lif* knockout mice (Bozec et al., 2008) and *Lifr* knockout mice (Ware et al., 1995). This skeletal effect is partly transferable to humans, where mutations in the *LIFR* gene cause Stüve-Wiedemann syndrome (OMIM #610559), characterized by bowing and thickening in the lower limbs and abnormal trabecular bone structure (Cormier-Daire et al., 1998; Dagoneau et al., 2004). Stüve-Wiedemann syndrome is often fatal and associated with early lethality, as also observed in *Lif* and *Lifr* knockout mice (Cormier-Daire et al., 1998; Sims, 2009). The early lethality makes the effects of LIF:LIFR signaling on remodeling versus modeling and growth hard to interpret, and differing roles of LIF signaling in bone development and remodeling has been reported (Poulton et al., 2012). Our findings of *LIF* and *LIFR* in interacting osteoclasts and osteoprogenitors, support that LIF:LIFR signaling plays a role in the osteoclast-osteoblast coupling within the reversal-resorption phase.

Importantly, LIFR signaling can also be activated by several other ligands of the IL-6 family cytokines (Kishimoto et al., 1995).

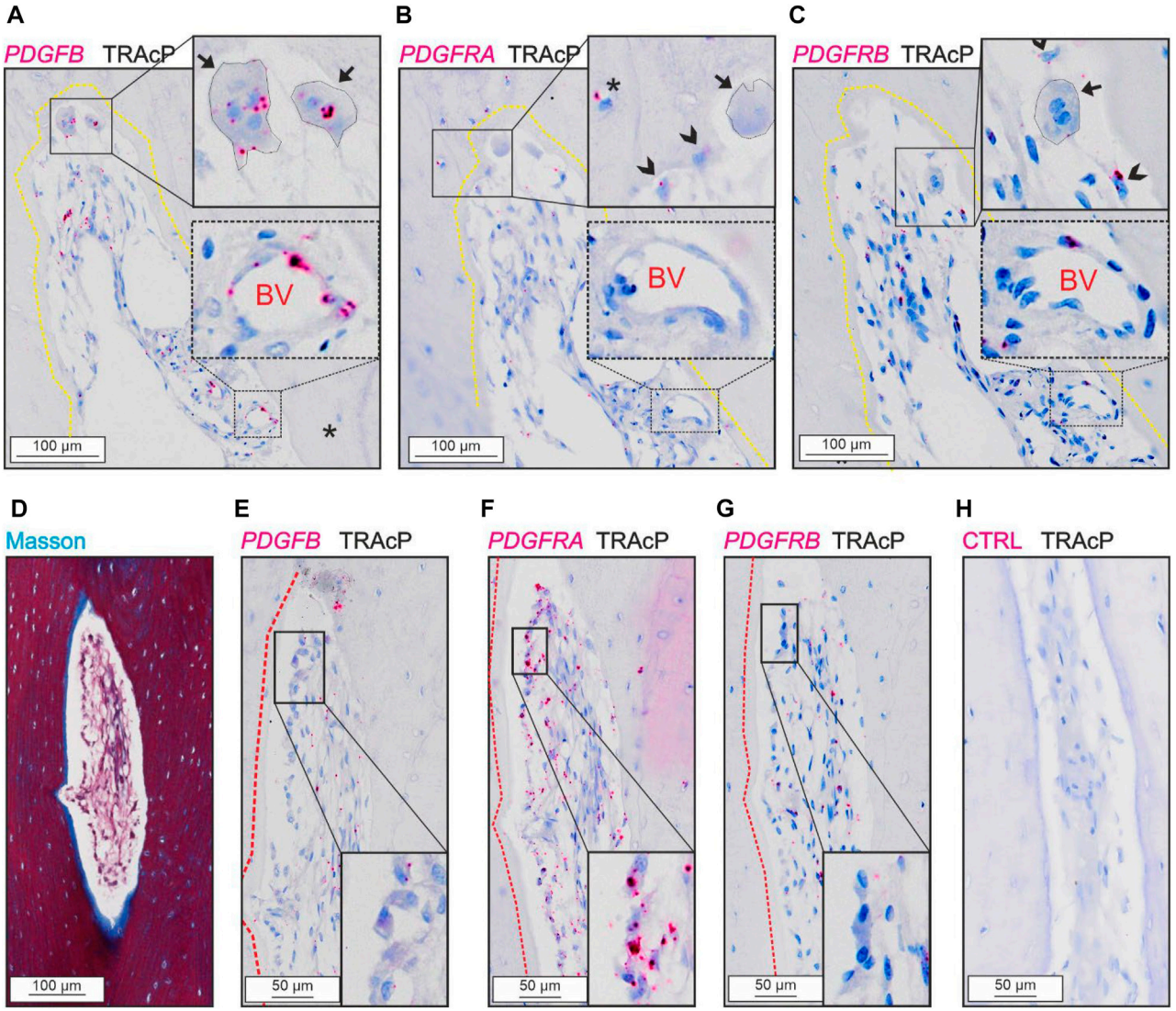

FIGURE 3 | Levels of *PDGFRA* and *PDGFRB* differ in cortical bone. **(A–C)** Adjacent sections of eroded pore with immunostaining of TRAcP (black) and *in situ* hybridization (red) of *PDGFB* **(A)**, *PDGFRA* **(B)** and *PDGFRB* **(C)**. **(D–H)** Adjacent sections of pore with bone formation with Masson Trichrome **(D)** or *in situ* hybridization of *PDGFB* **(E)**, *PDGFRA* **(F)**, *PDGFRB* **(G)** or negative control **(H)** combined with immunostaining of TRAcP (black). Eroded surfaces are marked by a yellow dotted line, formative surfaces are marked by a red dotted line. Osteoclasts are outlined and marked with black arrows, reversal cells with arrowheads and osteocytes with *in situ* signal are marked with (*), blood vessels are indicated with "BV".

CTF1 and OSM are two alternative ligands of LIFR, which have been suggested to play a regulatory role in bone remodeling. Like LIF, CTF1 might possess different roles in modeling versus remodeling events. Studies on *Ctf1* knockout mice have shown that they are osteopenic at birth but had a high bone mass phenotype at 10- and 26-weeks of age (Walker et al., 2008; Poulton et al., 2012). In the same study, CTF1 protein was observed in murine osteoclasts. We did not observe any notable levels of *CTF1* mRNA in osteoclasts, reversal cells or osteoblasts in human cortical bone remodeling events, questioning its importance in human bone remodeling. OSM is an alternative ligand of LIFR, which has been extensively studied. Studies treating mice with OSM has indicated both pro-osteogenic effects (Jay et al., 1996; Bellido et al., 1997; Walker et al., 2010), as well as an increased osteoclast formation and activity (Tamura et al., 1993; Palmqvist et al., 2002). Recently, it was suggested that OSM signaling through LIFR stimulates bone formation (Walker et al., 2010), consistent with a high bone mass phenotype observed in mice overexpressing bovine *Osm* (Malik et al., 1995). Conversely, OSM signaling through OSMR is suggested to induce osteoclastogenesis indirectly by upregulating RANKL expression (Walker et al., 2010). However, we did not observe any notable presence in osteoclasts, reversal cells or osteoblasts in human cortical bone remodeling events, questioning its importance in human bone remodeling. On the other hand,

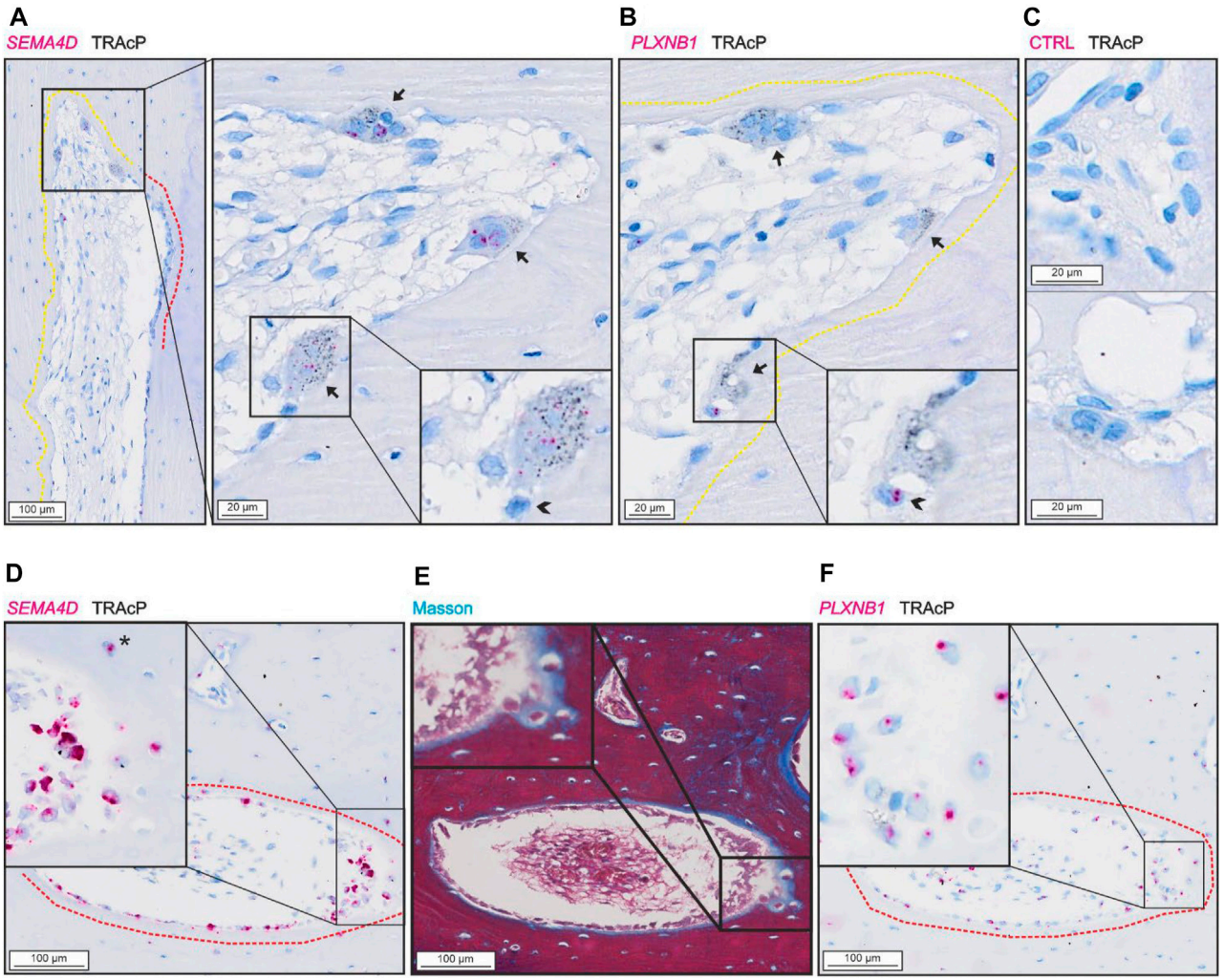

FIGURE 4 | *SEMA4D* is present in osteoclasts and mature osteoblasts and *PLXNB1* is present in osteoblasts. **(A–C)** Adjacent sections of pore with resorption with *in situ* hybridization (red) of *SEMA4D* **(A)**, *PLXNB1* **(B)** or negative control **(C)** combined with immunostaining of TRAcP (black). **(D–F)** Adjacent sections of pore with bone formation with masson trichrome staining **(E)** or *in situ* hybridization (red) of *SEMA4D* **(D)** or *PLXNB1* **(F)** combined with immunostaining of TRAcP (black). Eroded surfaces are marked by a yellow dotted line, formative surfaces are marked by a red dotted line. Osteoclasts are outlined and marked with black arrows, reversal cells with arrowheads (*).

we did observe *OSMR* mRNA in reversal cells and potential osteoprogenitors within the lumen of intracortical pores, which may respond to an alternative unknown ligand.

Another potential secreted osteoclastic coupling factor is PDGF homodimers or heterodimers, which have attracted attention as regulators of bone remodeling. This attention originates from clinical studies with the tyrosine kinase inhibitors Imatinib and Nilutinib observed to increase serum markers of bone formation, but not resorption (Grey et al., 2006). Subsequently, *in vitro* studies ascribed this effect of Imatinib and Nilutinib treatment to PDGFR-β signaling causing increased *Opg* expression (O'Sullivan et al., 2007, 2011, 2016). Treatment with PDGF-BB has also been shown to increase mesenchymal cell proliferation and osteoblast differentiation *in vitro*, but also the expression of pro-resorptive factors, such as *Csf1* and *Rankl* (Chen et al., 2015). In human trabecular bone, *PDGFB* was expressed by osteoclasts whereas both PDGF receptors (*PDGFRA* and *PDGFRB*) were expressed by osteoblastic canopy cells and reversal cells (Brun et al., 2020). In the present study, we observed expression of both receptors in reversal cells but differing expression pattern in other cells. Besides in reversal cells, *PDGFRA* was expressed by osteocytes and osteoblasts, whereas *PDGFRB* was expressed near vascular structures within intracortical pores.

Membrane-Bound Osteoclastic Coupling Factor and Their Receptors in Human Bone Remodeling

In human cortical bone remodeling events, *SEMA4D* was present in osteoclasts and *PLXNB1* was observed in reversal cells, supporting that SEMA4D:PLXNB1 binding may play a role in

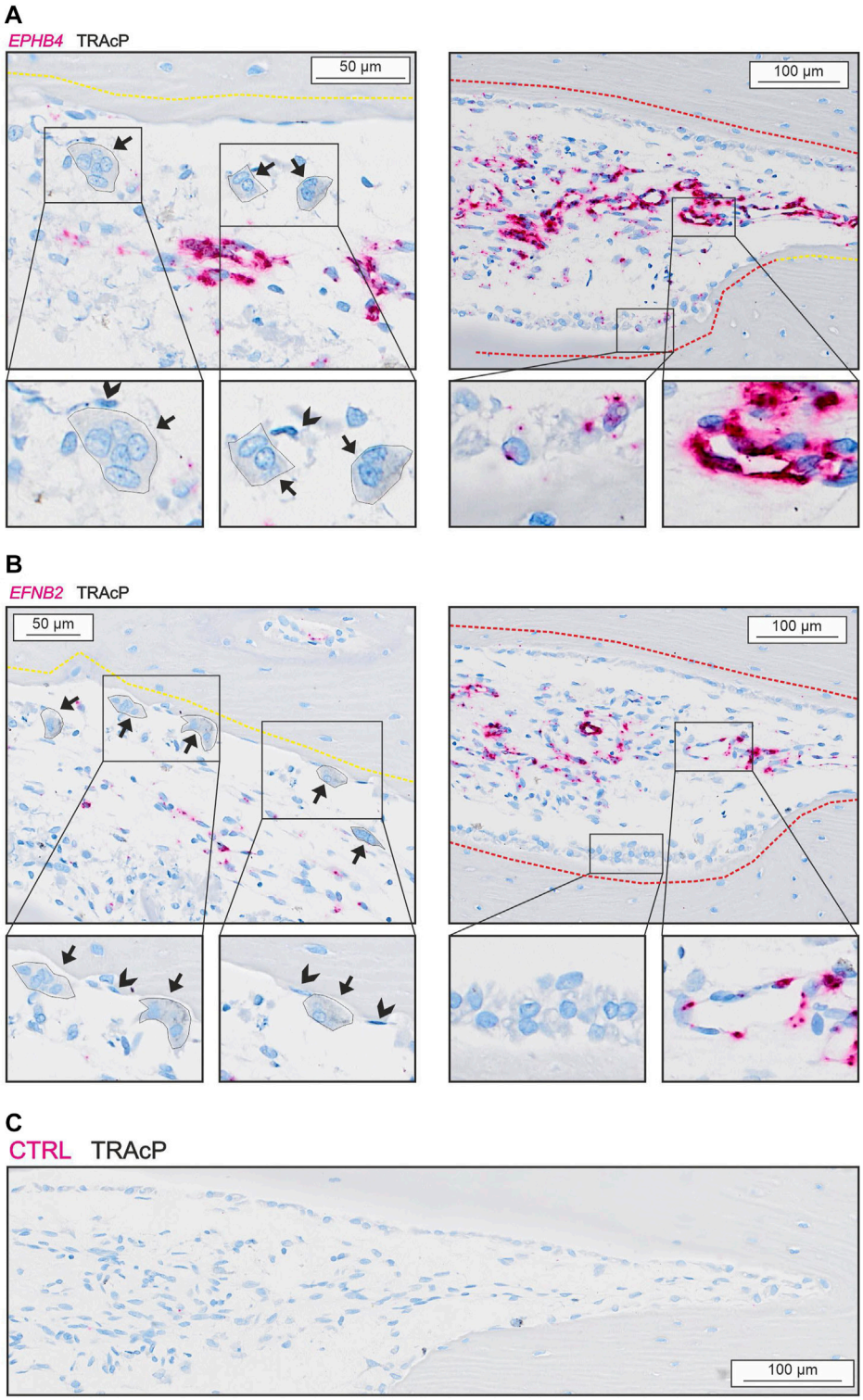

FIGURE 5 | *EFNB2* and *EPHB4* are mainly present near vascular structures. **(A)** *In situ* hybridization of *EPHB4* (red) and immunohistochemical staining of TRAcP (black). **(B)** *In situ* hybridization of *EFNB2* (red) and immunohistochemical staining of TRAcP (black). Eroded surfaces are marked by a yellow dotted line, formative surfaces are marked by a red dotted line. Osteoclasts are outlined and marked with black arrows, reversal cells with arrowheads.

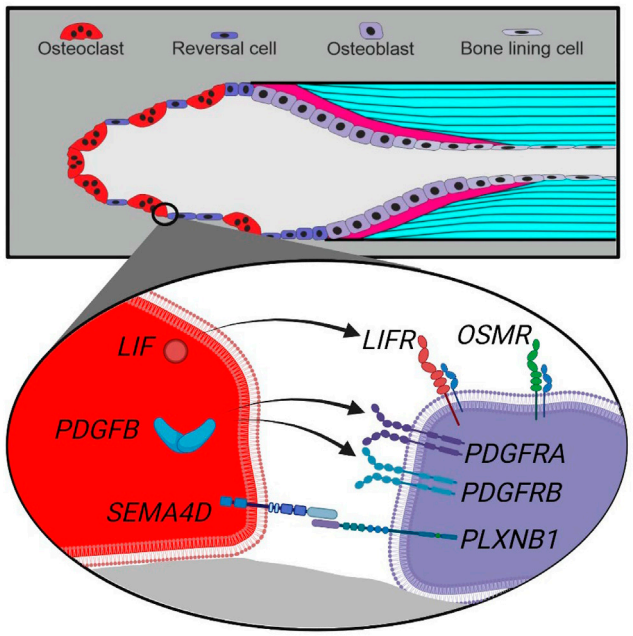

FIGURE 6 | Schematic presentation of a cutting cone with observed coupling factors and receptors in osteoclasts and reversal cells in human bone remodeling. Top, a cutting cone with initial resorption (left), reversal-resorption phase with osteoclasts intermixed with reversal cells (middle) followed by bone forming osteoblasts laying down osteoid (right). Bottom, zoom on the cell-cell interface between osteoclasts (red) and reversal cells (purple) with observed expression of coupling factors and receptors.

their communication. This is in line with murine studies, showing *Sema4d* expression in osteoclasts and osteoclast progenitors, and increased *Plxnb1* expression during osteoblast differentiation (Negishi-Koga et al., 2011). Functional studies in mice, suggest that Sema4D is a suppressor of bone formation with knockdown leading to a higher bone mass. However, the cause of high bone mass in knockout mice does not concur between studies. Negishi-Koga and colleagues reported increased bone formation without osteoclastic effect (Negishi-Koga et al., 2011) whereas Dacquin and colleagues observed reduced resorptive activity (Dacquin et al., 2011). In a clinical study, serum levels of SEMA4D positively correlated with serum markers of resorption in patients with multiple myeloma (Zhang et al., 2015; Terpos et al., 2018). Later, SEMA4D secreted from a human lung cancer cell line were shown to inhibit osteoblast differentiation *in vitro* (Chen et al., 2019). In contrast to this study, treatment of osteoporotic postmenopausal women with the antiresorptive Denosumab have been shown to increase serum levels of SEMA4D compared to controls (Anastasilakis et al., 2015), suggesting that SEMA4D is produced by other sources than osteoclasts. This study suggests that SEM4D originate from mature bone-forming osteoblasts, showing presence of *SEMA4D* mRNA at human bone remodeling sites.

EFNB2:EPHB4 signaling has also been proposed as a coupling pathway requiring cell-cell contact. *Efnb2* and *Ephb4* have been reported in several bone cells (Arthur et al., 2011, 2018; Wang et al., 2014) and EFNB2:EPHB4 signaling within the osteoblast lineage is believed to promote osteoblast differentiation (Takyar et al., 2013; Tonna et al., 2014). Nevertheless, we were unable to observe any notable presence of *EFNB2* and *EPHB4* in human osteoclasts and reversal cells questioning its direct importance in the osteoclast-osteoblasts coupling mechanism of human bone remodeling. On the other hand, *EFNB2* and *EPHB4* are highly expressed in the vascular structures within the lumen of intracortical pores, consistent with a role in the local vascularization and angiogenesis as shown in other studies (Wang et al., 2010). Vascularization is essential for osteoprogenitor recruitment and thereby indirectly the activation of bone formation on eroded bone surfaces vacated by the osteoclasts.

In this study, we qualitatively investigated the spatial *in situ* mRNA localization of proposed coupling factors and their receptors using bone specimens from adolescents undergoing corrective surgery for Coxa Valga. Therefore, we consider the analyzed cortical bone as healthy. By investigating intracortical pores, we ensure that well-defined remodeling processes were examined, despite the young age of patients. Our investigations are limited to the *in situ* cellular mRNA-levels, which are affected by expression and stability of each individual mRNA. Despite the use of a tissue array to validate probes, stability and retention time within bone may vary from other tissues. The study does not investigate the distribution of proteins or functional analyses of included coupling factors. In the applied mRNA detection-procedure we used probe pairs designed by ACD Bioscience. Each set of probe pairs included 20 different probe pairs targeting a specific region within the gene of interest. Levels of mRNA detected were described af high/low when compared to other probes or differing levels between cell types.

Further investigation of the mRNA and protein abundance, as well as functional significance of these coupling factors are needed in human bone remodeling.

CONCLUSION

Our mRNA analysis of human cortical bone remodeling events revealed presence of proposed coupling factors *LIF*, *SEMA4D* and *PDGFB* mRNA in mature bone-resorbing osteoclasts and presence of their respective receptors *LIFR*, *PLXNB1*, *PDGFRA* and *PDGFRB* mRNA in neighboring reversal cells. These results are complementary to previous functional studies, supporting a functional role in the coupling mechanism of human bone remodeling. Conversely, we did not observe presence of *CTF1* or *OSM* mRNA in mature osteoclasts, despite the presence of *OSMR* mRNA in neighboring reversal cells (**Figure 6**). Finally, presence of *EFNB2* and *EPHB4* mRNA was restricted to vascular structures within intracortical pores, with no indications of presence within osteoclasts nor reversal cells.

DATA AVAILABILITY STATEMENT

The original contributions presented in the study are included in the article/Supplementary Material, further inquiries can be directed to the corresponding author.

ETHICS STATEMENT

The studies involving human participants were reviewed and approved by the Danish National Committee on Biomedical Research Ethics. Written informed consent to participate in this study was provided by the participants' legal guardian/ next of kin. (Project-ID: S-2012-0193).

AUTHOR CONTRIBUTIONS

Authorship contribution statement: Conceptualization and design; TA, J-MD, and CA Acquisition of data: XB and MN Investigation and methodology: XB, MN, TA, and CA Analysis and interpretation of data: all authors Funding acquisition, project administration and supervision: TA, J-MD, CA, and XB Drafting: XB and TA Final approval: all authors.

FUNDING

Salary for PhD student Xenia Borggaard was covered by The Velux Foundation (Grant no. 25723) and Department of Clinical Research, University of Southern Denmark. Laboratory costs were covered by The Velux Foundation (Grant no. 25723), Aase og Ejnar Danielsens fond (Grant no. 18-10-0473) and The Danish National Association for Osteoporosis (Osteoporoseforeningen). Schematic figures in this publication were created with www.biorender.com.

ACKNOWLEDGMENTS

We acknowledge Dr Søren Harving, Aalborg University Hospital for collection of specimens.

REFERENCES

Abdallah, B. M., Figeac, F., Larsen, K. H., Ditzel, N., Keshari, P., Isa, A., et al. (2017). CRMP4 Inhibits Bone Formation by Negatively Regulating BMP and RhoA Signaling. *J. Bone Min. Res.* 32 (5), 913–926. doi:10.1002/jbmr.3069

Abdelgawad, M. E., Delaisse, J.-M., Hinge, M., Jensen, P. R., Alnaimi, R. W., Rolighed, L., et al. (2016). Early Reversal Cells in Adult Human Bone Remodeling: Osteoblastic Nature, Catabolic Functions and Interactions with Osteoclasts. *Histochem Cell Biol.* 145 (6), 603–615. doi:10.1007/s00418-016-1414-y

Allan, E. H., Hilton, D. J., Brown, M. A., Evely, R. S., Yumita, S., Metcalf, D., et al. (1990). Osteoblasts Display Receptors for and Responses to Leukemia-Inhibitory Factor. *J. Cell. Physiol.* 145 (1), 110–119. doi:10.1002/jcp.1041450116

Alvarez, R. H., Kantarjian, H. M., and Cortes, J. E. (2006). Biology of Platelet-Derived Growth Factor and its Involvement in Disease. *Mayo Clin. Proc.* 81 (9), 1241–1257. doi:10.4065/81.9.1241

Anastasilakis, A. D., Polyzos, S. A., Makras, P., Gkiomisi, A., Sakellariou, G., Savvidis, M., et al. (2015). Circulating semaphorin-4D and Plexin-B1 Levels in Postmenopausal Women with Low Bone Mass: The 3-month Effect of Zoledronic Acid, Denosumab or Teriparatide Treatment. *Expert Opin. Ther. Targets* 19 (3), 299–306. doi:10.1517/14728222.2014.983078

Andersen, T. L., Sondergaard, T. E., Skorzynska, K. E., Dagnaes-Hansen, F., Plesner, T. L., Hauge, E. M., et al. (2009). A Physical Mechanism for Coupling Bone Resorption and Formation in Adult Human Bone. *Am. J. Pathology* 174 (1), 239–247. doi:10.2353/ajpath.2009.080627

Andersen, T. L., Søe, K., Sondergaard, T. E., Plesner, T., and Delaisse, J.-M. (2010). Myeloma Cell-Induced Disruption of Bone Remodelling Compartments Leads to Osteolytic Lesions and Generation of Osteoclast-Myeloma Hybrid Cells. *Br. J. Haematol.* 148 (4), 551–561. doi:10.1111/j.1365-2141.2009.07980.x

Andersen, T. L., Abdelgawad, M. E., Kristensen, H. B., Hauge, E. M., Rolighed, L., Bollerslev, J., et al. (2013). Understanding Coupling between Bone Resorption and Formation: Are Reversal Cells the Missing Link?. *Am. J. Pathology* 183 (1), 235–246. doi:10.1016/j.ajpath.2013.03.006

Andreasen, C. M., Bakalova, L. P., Brüel, A., Hauge, E. M., Kiil, B. J., Delaisse, J.-M., et al. (2020). The Generation of Enlarged Eroded Pores upon Existing Intracortical Canals Is a Major Contributor to Endocortical Trabecularization. *Bone* 130, 115127. doi:10.1016/j.bone.2019.115127

Arthur, A., Zannettino, A., Panagopoulos, R., Koblar, S. A., Sims, N. A., Stylianou, C., et al. (2011). EphB/ephrin-B Interactions Mediate Human MSC Attachment, Migration and Osteochondral Differentiation. *Bone* 48 (3), 533–542. doi:10.1016/j.bone.2010.10.180

Arthur, A., Nguyen, T. M., Paton, S., Klisuric, A., Zannettino, A. C. W., and Gronthos, S. (2018). The Osteoprogenitor-specific Loss of ephrinB1 Results in an Osteoporotic Phenotype Affecting the Balance between Bone Formation and Resorption. *Sci. Rep.* 8 (1), 1–12. doi:10.1038/s41598-018-31190-2

Baron, R., Silverglate, A., Broadus, A., and Lang, R. (1983). Estimation of Trabecular Bone Resorption by Histomorphometry: Evidence for a Prolonged Reversal Phase with Normal Resorption in Post-menopausal Osteoporosis and Coupled Increased Resorption in Primary Hyperparathyroidism. *Clin. Disord. Bone Min. Metab.* 1 191–195.

Bellido, T., Stahl, N., Farruggella, T. J., Borba, V., Yancopoulos, G. D., and Manolagas, S. C. (1996). Detection of Receptors for Interleukin-6, Interleukin-11, Leukemia Inhibitory Factor, Oncostatin M, and Ciliary Neurotrophic Factor in Bone Marrow Stromal/osteoblastic Cells. *J. Clin. Invest.* 97 (2), 431–437. doi:10.1172/JCI118432

Bellido, T., Borba, V. Z. C., Roberson, P., and Manolagas, S. C. (1997). Activation of the Janus Kinase/STAT (Signal Transducer and Activator of Transcription) Signal Transduction Pathway by Interleukin-6-type Cytokines Promotes Osteoblast Differentiation*. *Endocrinology* 138 (9), 3666–3676. doi:10.1210/endo.138.9.5364

Bianco, P., Ballanti, P., and Bonucci, E. (1988). Tartrate-resistant Acid Phosphatase Activity in Rat Osteoblasts and Osteocytes. *Calcif. Tissue Int.* 43 (3), 167–171. doi:10.1007/BF02571315

Bozec, A., Bakiri, L., Hoebertz, A., Eferl, R., Schilling, A. F., Komnenovic, V., et al. (2008). Osteoclast Size Is Controlled by Fra-2 through LIF/LIF-receptor Signalling and Hypoxia. *Nature* 454 (7201), 221–225. doi:10.1038/nature07019

Brun, J., Andreasen, C. M., Ejersted, C., Andersen, T. L., Caverzasio, J., and Thouverey, C. (2020). PDGF Receptor Signaling in Osteoblast Lineage Cells Controls Bone Resorption through Upregulation of Csf1 Expression. *J. Bone Min. Res.* 35 (12), 2458–2469. doi:10.1002/jbmr.4150

Charles, J. F., and Aliprantis, A. O. (2014). Osteoclasts: More Than 'bone Eaters'. *Trends Mol. Med.* 20 (8), 449–459. doi:10.1002/nme.211010.1016/j.molmed.2014.06.001

Chen, W., Baylink, D. J., Brier-Jones, J., Neises, A., Kiroyan, J. B., Rundle, C. H., et al. (2015). PDGFB-based Stem Cell Gene Therapy Increases Bone Strength in the Mouse. *Proc. Natl. Acad. Sci. U.S.A.* 112 (29), E3893–E3900. doi:10.1073/pnas.1501759112

Chen, L., Shi, K., Andersen, T. L., Qiu, W., and Kassem, M. (2019). KIAA1199 is a Secreted Molecule that Enhances Osteoblastic Stem Cell Migration and Recruitment. *Cell Death Dis.* 10 (2). 126. doi:10.1038/s41419-018-1202-9

Chen, W.-g., Sun, J., Shen, W.-w., Yang, S.-z., Zhang, Y., Hu, X., et al. (2019). Sema4D Expression and Secretion Are Increased by HIF-1α and Inhibit Osteogenesis in Bone Metastases of Lung Cancer. *Clin. Exp. Metastasis* 36 (1), 39–56. doi:10.1007/s10585-018-9951-5

Cormier-Daire, V., Munnich, A., Lyonnet, S., Rustin, P., Delezoide, A.-L., Maroteaux, P., et al. (1998). Presentation of Six Cases of Stüve-Wiedemann Syndrome. *Pediatr. Radiol.* 28 (10), 776–780. doi:10.1007/s002470050464

Dacquin, R., Domenget, C., Kumanogoh, A., Kikutani, H., Jurdic, P., and Machuca-Gayet, I. (2011). Control of Bone Resorption by Semaphorin 4D Is Dependent on Ovarian Function. *PLoS ONE* 6 (10), e26627. doi:10.1371/journal.pone.0026627

Dagoneau, N., Scheffer, D., Huber, C., Al-Gazali, L. I., Di Rocco, M., Godard, A., et al. (2004). Null Leukemia Inhibitory Factor Receptor (LIFR) Mutations in Stüve-Wiedemann/Schwartz-Jampel Type 2 Syndrome. *Am. J. Hum. Genet.* 74 (2), 298–305. doi:10.1086/381715

Delaisse, J.-M., Andersen, T. L., Kristensen, H. B., Jensen, P. R., Andreasen, C. M., et al. (2020). Re-thinking the Bone Remodeling Cycle Mechanism and the Origin of Bone Loss. *Bone* 723 138028. doi:10.1016/j.scitotenv.2020.138028

Eriksen, E. F., Gundersen, H. J. G., Melsen, F., and Mosekilde, L. (1984). Reconstruction of the Formative Site in Iliac Trabecular Bone in 20 Normal Individuals Employing a Kinetic Model for Matrix and Mineral Apposition. *Metabolic Bone Dis. Relat. Res.* 5 (5), 243–252. doi:10.1016/0221-8747(84)90066-3

Eriksen, E. F., Melsen, F., and Mosekilde, L. (1984). Reconstruction of the Resorptive Site in Iliac Trabecular Bone: A Kinetic Model for Bone Resorption in 20 Normal Individuals. *Metabolic Bone Dis. Relat. Res.* 5 (5), 235–242. doi:10.1016/0221-8747(84)90065-1

Everts, V., Delaissé, J. M., Korper, W., Jansen, D. C., Tigchelaar-Gutter, W., Saftig, P., et al. (2002). The Bone Lining Cell: Its Role in Cleaning Howship's Lacunae and Initiating Bone Formation. *J. Bone Min. Res.* 17 (1), 77–90. doi:10.1359/jbmr.2002.17.1.77

Grey, A., O'Sullivan, S., Reid, I. R., and Browett, P. (2006). Imatinib Mesylate, Increased Bone Formation, and Secondary Hyperparathyroidism. *N. Engl. J. Med.* 355 (23), 2494–2495. doi:10.1056/nejmc062388

Horner, A., Bord, S., Kemp, P., Grainger, D., and Compston, J. E. (1996). Distribution of Platelet-Derived Growth Factor (PDGF) a Chain mRNA, Protein, and PDGF-α Receptor in Rapidly Forming Human Bone. *Bone* 19 (4), 353–362. doi:10.1016/S8756-3282(96)00217-7

Jafari, A., Qanie, D., Andersen, T. L., Zhang, Y., Chen, L., Postert, B., et al. (2017). Legumain Regulates Differentiation Fate of Human Bone Marrow Stromal Cells and Is Altered in Postmenopausal Osteoporosis. *Stem Cell Rep.* 8 (2), 373–386. doi:10.1016/j.stemcr.2017.01.003

Jay, P. R., Centrella, M., Lorenzo, J., Bruce, A. G., and Horowitz, M. C. (1996). Oncostatin-M: a New Bone Active Cytokine that Activates Osteoblasts and Inhibits Bone Resorption. *Endocrinology* 137 (4), 1151–1158. doi:10.1210/endo.137.4.8625883

Jensen, P. R., Andersen, T. L., Hauge, E.-M., Bollerslev, J., and Delaissé, J.-M. (2014). A Joined Role of Canopy and Reversal Cells in Bone Remodeling - Lessons from Glucocorticoid-Induced Osteoporosis. *Bone* 73, 16–23. doi:10.1016/j.bone.2014.12.004

Jones, S. A., and Jenkins, B. J. (2018). Recent Insights into Targeting the IL-6 Cytokine Family in Inflammatory Diseases and Cancer. *Nat. Rev. Immunol.* 18 (12), 773–789. doi:10.1038/s41577-018-0066-7

Kang, S., and Kumanogoh, A. (2013). Semaphorins in Bone Development, Homeostasis, and Disease. *Seminars Cell & Dev. Biol.* 24 (3), 163–171. doi:10.1016/j.semcdb.2012.09.008

Kishimoto, T., Akira, S., Narazaki, M., and Taga, T. (1995). Interleukin-6 Family of Cytokines and Gp130. *Blood* 86 (4), 1243–1254. doi:10.1182/blood.v86.4.1243.bloodjournal8641243

Lassen, N. E., Andersen, T. L., Pløen, G. G., Søe, K., Hauge, E. M., Harving, S., et al. (2017). Coupling of Bone Resorption and Formation in Real Time: New Knowledge Gained from Human Haversian BMUs. *J. Bone Min. Res.* 32 (7), 1395–1405. doi:10.1002/jbmr.316910.1002/jbmr.3091

Liu, J., Modrell, B., Aruffo, A., Marken, J. S., Taga, T., Yasukawa, K., et al. (1992). Interleukin-6 Signal Transducer Gp130 Mediates Oncostatin M Signaling. *J. Biol. Chem.* 267 (24), 16763–16766. doi:10.1016/s0021-9258(18)41845-5

Liu, F., Aubin, J. E., and Malaval, L. (2002). Expression of Leukemia Inhibitory Factor (LIF)/interleukin-6 Family Cytokines and Receptors during *In Vitro* Osteogenesis: Differential Regulation by Dexamethasone and LIF. *Bone* 31 (1), 212–219. doi:10.1016/S8756-3282(02)00806-2

Malik, N., Haugen, H. S., Modrell, B., Shoyab, M., and Clegg, C. H. (1995). Developmental Abnormalities in Mice Transgenic for Bovine Oncostatin M. *Mol. Cell Biol.* 15 (5), 2349–2358. doi:10.1128/mcb.15.5.2349

Metcalf, D., and Gearing, D. P. (1989). Fatal Syndrome in Mice Engrafted with Cells Producing High Levels of the Leukemia Inhibitory Factor. *Proc. Natl. Acad. Sci. U.S.A.* 86 (15), 5948–5952. doi:10.1073/pnas.86.15.5948

Mocetti, P., Ballanti, P., Zalzal, S., Silvestrini, G., Bonucci, E., and Nanci, A. (2000). A Histomorphometric, Structural, and Immunocytochemical Study of the Effects of Diet-Induced Hypocalcemia on Bone in Growing Rats. *J. Histochem Cytochem.* 48 (8), 1059–1077. doi:10.1177/002215540004800804

Negishi-Koga, T., Shinohara, M., Komatsu, N., Bito, H., Kodama, T., Friedel, R. H., et al. (2011). Suppression of Bone Formation by Osteoclastic Expression of Semaphorin 4D. *Nat. Med.* 17 (11), 1473–1480. doi:10.1038/nm.2489

O'Sullivan, S., Naot, D., Callon, K., Porteous, F., Horne, A., Wattie, D., et al. (2007). Imatinib Promotes Osteoblast Differentiation by Inhibiting PDGFR Signaling and Inhibits Osteoclastogenesis by Both Direct and Stromal Cell-dependent Mechanisms. *J. Bone Min. Res.* 22 (11), 1679–1689. doi:10.1359/jbmr.070719

O'Sullivan, S., Lin, J.-M., Watson, M., Callon, K., Tong, P. C., Naot, D., et al. (2011). The Skeletal Effects of the Tyrosine Kinase Inhibitor Nilotinib. *Bone* 49 (2), 281–289. doi:10.1016/j.bone.2011.04.014

O'Sullivan, S., Tay, M. L., Lin, J.-M., Bava, U., Callon, K., Cornish, J., et al. (2016). Tyrosine Kinase Inhibitors Regulate OPG through Inhibition of PDGFRβ. *PLoS ONE* 11 (10), e0164727–13. doi:10.1371/journal.pone.0164727

Palmqvist, P., Persson, E., Conaway, H. H., and Lerner, U. H. (2002). IL-6, Leukemia Inhibitory Factor, and Oncostatin M Stimulate Bone Resorption and Regulate the Expression of Receptor Activator of NF-Kb Ligand, Osteoprotegerin, and Receptor Activator of NF-Kb in Mouse Calvariae. *J. Immunol.* 169 (6), 3353–3362. doi:10.4049/jimmunol.169.6.3353

Pasquale, E. B. (2010). Eph Receptors and Ephrins in Cancer: Bidirectional Signalling and beyond. *Nat. Rev. Cancer* 10 (3), 165–180. doi:10.1038/nrc2806

Pennica, D., King, K. L., Shaw, K. J., Luis, E., Rullamas, J., Luoh, S. M., et al. (1995). Expression Cloning of Cardiotrophin 1, a Cytokine that Induces Cardiac Myocyte Hypertrophy. *Proc. Natl. Acad. Sci. U.S.A.* 92 (4), 1142–1146. doi:10.1073/pnas.92.4.1142

Poulton, I. J., McGregor, N. E., Pompolo, S., Walker, E. C., and Sims, N. A. (2012). Contrasting Roles of Leukemia Inhibitory Factor in Murine Bone Development and Remodeling Involve Region-specific Changes in Vascularization. *J. Bone Min. Res.* 27 (3), 586–595. doi:10.1002/jbmr.1485

Reid, I. R., Lowe, C., Cornish, J., Skinner, S. J. M., Hilton, D. J., Willson, T. A., et al. (1990). Leukemia Inhibitory Factor: A Novel Bone-Active Cytokine*. *Endocrinology* 126 (3), 1416–1420. doi:10.1210/endo-126-3-1416

Rose, T. M., and Bruce, A. G. (1991). Oncostatin M Is a Member of a Cytokine Family that Includes Leukemia-Inhibitory Factor, Granulocyte Colony-Stimulating Factor, and Interleukin 6. *Proc. Natl. Acad. Sci. U.S.A.* 88 (19), 8641–8645. doi:10.1073/pnas.88.19.8641

Sims, N. A., and Martin, T. J. (2020). Osteoclasts Provide Coupling Signals to Osteoblast Lineage Cells through Multiple Mechanisms. *Annu. Rev. Physiol.* 82 (1), 507–529. doi:10.1146/annurev-physiol-021119-034425

Sims, N. A. (2009). gp130 Signaling in Bone Cell Biology: Multiple Roles Revealed by Analysis of Genetically Altered Mice. *Mol. Cell. Endocrinol.* 310 (1–2), 30–39. doi:10.1016/j.mce.2008.08.025

Sims, N. A. (2021). Influences of the IL-6 Cytokine Family on Bone Structure and Function. *Cytokine* 146, 155655. doi:10.1016/j.cyto.2021.155655

Takyar, F. M., Tonna, S., Ho, P. W., Crimeen-Irwin, B., Baker, E. K., Martin, T. J., et al. (2013). EphrinB2/EphB4 Inhibition in the Osteoblast Lineage Modifies the Anabolic Response to Parathyroid Hormone. *J. Bone Min. Res.* 28 (4), 912–925. doi:10.1002/jbmr.1820

Tamura, T., Udagawa, N., Takahashi, N., Miyaura, C., Tanaka, S., Yamada, Y., et al. (1993). Soluble Interleukin-6 Receptor Triggers Osteoclast Formation by Interleukin 6. *Proc. Natl. Acad. Sci. U.S.A.* 90 (24), 11924–11928. doi:10.1073/pnas.90.24.11924

Taylor, H., Campbell, J., and Nobes, C. D. (2017). Ephs and Ephrins. *Curr. Biol.* 27 (3), R90–R95. doi:10.1016/j.cub.2017.01.003

Terpos, E., Ntanasis-Stathopoulos, I., Christoulas, D., Bagratuni, T., Bakogeorgos, M., Gavriatopoulou, M., et al. (2018). Semaphorin 4D Correlates with Increased Bone Resorption, Hypercalcemia, and Disease Stage in Newly Diagnosed Patients with Multiple Myeloma. *Blood Cancer J.* 8 (5). 42. doi:10.1038/s41408-018-0075-6

Thoma, B., Bird, T. A., Friend, D. J., Gearing, D. P., and Dower, S. K. (1994). Oncostatin M and Leukemia Inhibitory Factor Trigger Overlapping and Different Signals through Partially Shared Receptor Complexes. *J. Biol. Chem.* 269 (8), 6215–6222. doi:10.1016/s0021-9258(17)37590-7

Tonna, S., Takyar, F. M., Vrahnas, C., Crimeen-Irwin, B., Ho, P. W. M., Poulton, I. J., et al. (2014). EphrinB2 Signaling in Osteoblasts Promotes Bone Mineralization by Preventing Apoptosis. *FASEB J.* 28 (10), 4482–4496. doi:10.1096/fj.14-254300

Walker, E. C., McGregor, N. E., Poulton, I. J., Pompolo, S., Allan, E. H., Quinn, J. M., et al. (2008). Cardiotrophin-1 Is an Osteoclast-Derived Stimulus of Bone Formation Required for Normal Bone Remodeling. *J. Bone Mineral Res.* 23 (12), 2025–2032. doi:10.1359/jbmr.080706

Walker, E. C., McGregor, N. E., Poulton, I. J., Solano, M., Pompolo, S., Fernandes, T. J., et al. (2010). Oncostatin M Promotes Bone Formation Independently of Resorption when Signaling through Leukemia Inhibitory Factor Receptor in Mice. *J. Clin. Invest.* 120 (2), 582–592. doi:10.1172/JCI40568

Wang, Y., Nakayama, M., Pitulescu, M. E., Schmidt, T. S., Bochenek, M. L., Sakakibara, A., et al. (2010). Ephrin-B2 Controls VEGF-Induced Angiogenesis and Lymphangiogenesis. *Nature* 465 (7297), 483–486. doi:10.1038/nature09002

Wang, Y., Menendez, A., Fong, C., ElAlieh, H. Z., Chang, W., and Bikle, D. D. (2014). Ephrin B2/EphB4 Mediates the Actions of IGF-I Signaling in Regulating Endochondral Bone Formation. *J. Bone Min. Res.* 29 (8), 1900–1913. doi:10.1002/jbmr.2196

Ware, C. B., Horowitz, M. C., Renshaw, B. R., Hunt, J. S., Liggitt, D., Koblar, S. A., et al. (1995). Targeted Disruption of the Low-Affinity Leukemia Inhibitory Factor Receptor Gene Causes Placental, Skeletal, Neural and Metabolic Defects and Results in Perinatal Death. *Development* 121 (5), 1283–1299. doi:10.1242/dev.121.5.1283

Zhang, Y., Feng, E., Xu, Y., Wang, W., Zhang, T., Xiao, L., et al. (2015). Serum Sema4D Levels Are Associated with Lumbar Spine Bone Mineral Density and Bone Turnover Markers in Patients with Postmenopausal Osteoporosis. *Int. J. Clin. Exp. Med.* 8 (9), 16352–16357.

Conflict of Interest: The authors declare that the research was conducted in the absence of any commercial or financial relationships that could be construed as a potential conflict of interest.

Publisher's Note: All claims expressed in this article are solely those of the authors and do not necessarily represent those of their affiliated organizations, or those of the publisher, the editors and the reviewers. Any product that may be evaluated in this article, or claim that may be made by its manufacturer, is not guaranteed or endorsed by the publisher.

frontiers | Frontiers in Cell and Developmental Biology

METHODS
published: 05 July 2022
doi: 10.3389/fcell.2022.941542

Automated Quantification of Human Osteoclasts Using Object Detection

Sampsa Kohtala[1], Tonje Marie Vikene Nedal[2], Carlo Kriesi[1,3], Siv Helen Moen[2], Qianli Ma[2], Kristin Sirnes Ødegaard[4], Therese Standal[2,5] and Martin Steinert[1]*

[1]TrollLABS, Department of Mechanical and Industrial Engineering, Faculty of Engineering, Norwegian University of Science and Technology (NTNU), Trondheim, Norway, [2]Centre of Molecular Inflammation Research, Department of Clinical and Molecular Medicine, Faculty of Medicine and Health Sciences, Norwegian University of Science and Technology (NTNU), Trondheim, Norway, [3]Vitroscope AS, Trondheim, Norway, [4]Department of Mechanical and Industrial Engineering, Faculty of Engineering, Norwegian University of Science and Technology (NTNU), Trondheim, Norway, [5]Department of Hematology, St. Olavs University Hospital, Trondheim, Norway

A balanced skeletal remodeling process is paramount to staying healthy. The remodeling process can be studied by analyzing osteoclasts differentiated *in vitro* from mononuclear cells isolated from peripheral blood or from buffy coats. Osteoclasts are highly specialized, multinucleated cells that break down bone tissue. Identifying and correctly quantifying osteoclasts in culture are usually done by trained personnel using light microscopy, which is time-consuming and susceptible to operator biases. Using machine learning with 307 different well images from seven human PBMC donors containing a total of 94,974 marked osteoclasts, we present an efficient and reliable method to quantify human osteoclasts from microscopic images. An open-source, deep learning-based object detection framework called Darknet (YOLOv4) was used to train and test several models to analyze the applicability and generalizability of the proposed method. The trained model achieved a mean average precision of 85.26% with a correlation coefficient of 0.99 with human annotators on an independent test set and counted on average 2.1% more osteoclasts per culture than the humans. Additionally, the trained models agreed more than two independent human annotators, supporting a more reliable and less biased approach to quantifying osteoclasts while saving time and resources. We invite interested researchers to test their datasets on our models to further strengthen and validate the results.

Keywords: osteoclasts, object detection, machine learning, artificial intelligence, automatic image analysis

OPEN ACCESS

Edited by:
Venkaiah Betapudi, United States Department of Health and Human Services, United States

Reviewed by:
Helen Knowles, University of Oxford, United Kingdom
Domitilla Mandatori, University of Studies G.d'Annunzio Chieti and Pescara, Italy

****Correspondence:***
Sampsa Kohtala
sampsa.kohtala@ntnu.no

Specialty section:
This article was submitted to Cellular Biochemistry, a section of the journal Frontiers in Cell and Developmental Biology

Received: *11 May 2022*
Accepted: *15 June 2022*
Published: *05 July 2022*

Citation:
Kohtala S, Nedal TMV, Kriesi C, Moen SH, Ma Q, Ødegaard KS, Standal T and Steinert M (2022) Automated Quantification of Human Osteoclasts Using Object Detection. Front. Cell Dev. Biol. 10:941542. doi: 10.3389/fcell.2022.941542

1 INTRODUCTION

In order to be healthy, the skeleton is constantly undergoing a balanced remodeling process where bone is removed by osteoclasts (OCs) before osteoblasts are recruited to build new bone (Charles and Aliprantis, 2014; Marino et al., 2014). Overactivation of osteoclasts may lead to unbalanced bone remodeling and excessive loss of bone. This is seen in diseases such as rheumatoid arthritis, multiple myeloma and cancers metastasizing to bone (Yahara et al., 2022).

Osteoclasts are highly specialized, multinucleated cells originating from cells of the monocyte-macrophage lineage. Two key cytokines, macrophage colony-stimulating factor (M-CSF) and receptor activator of NFkB ligand (RANKL), are essential for osteoclast formation. M-CSF is important for survival and proliferation of osteoclast precursors and leads to the expression of RANK

(Marino et al., 2014). Signaling through RANK by RANKL is required for fusion of the osteoclast precursors and differentiation into mature osteoclasts (Marino et al., 2014; Pereira et al., 2018).

Human osteoclasts can be differentiated *in vitro* from mononuclear cells isolated from peripheral blood or from buffy coat (Marino et al., 2014). Typically, monocytes are isolated from peripheral blood mononuclear cells (PBMCs) by adhesion to plastic or by anti-CD14 coated beads. The cells are subsequently cultured in the presence of M-CSF and RANKL for about 14–16 days until multinucleated cells appear (Sørensen et al., 2007; Marino et al., 2014). Osteoclasts are defined as cells containing three or more nuclei and are tartrate-resistant acid phosphatase (TRAP) positive (Marino et al., 2014). TRAP is an acid phosphatase secreted by osteoclasts during bone resorption (Hayman, 2008). As the name indicates, TRAP is resistant to tartrate inhibition, which makes it distinguishable from other acid phosphatases, a property exploited during TRAP-staining (Burstone, 1959; Filgueira, 2004; Hayman, 2008). TRAP-staining is one of the most common methods to characterize osteoclasts *in vitro* cell cultures (Filgueira, 2004; Hayman, 2008; Marino et al., 2014).

While the definition of osteoclasts may be straightforward, identifying and correctly quantifying the number of osteoclasts in culture is a challenge. The number and size of osteoclasts are usually evaluated under a light microscope, which requires trained personnel. It is time-consuming and subjective. To avoid operator bias, each sample must be counted blind by at least two individuals. Osteoclast number and size may also be evaluated after imaging of the cultures. The nuclei in each cell can be difficult to see using the traditional TRAP-staining protocol, but this challenge can be overcome by adding nuclear stains such as Hoechst 33,342. Using combined fluorescence and transmitted light imaging systems, digital brightfield images and fluorescence images can be merged. Still, counting osteoclasts based on such images is difficult and the same challenges with time consumption and operator bias exist. Thus, there is a great need for a more unbiased, efficient, and reliable method to quantify osteoclasts in culture.

A few previous studies have attempted to quantify OCs from microscopic images of animal cells automatically. Cohen-Karlik et al. (2021) used machine learning (ML) to train an object detection model for measuring the number and area of OCs in cell cultures of mice. Their approach achieved a high correlation with trained human annotators for detecting subclasses of OCs with different numbers of nuclei. However, they do not mention the model performance (accuracy, precision, etc.). The "OC_Finder" system by Wang et al. (2021) also detects osteoclasts from mice. It uses an automated cell segmentation approach before applying deep learning to classify the cells as OCs or non-OCs. Their system achieved 98.1% accuracy and correlated well with a human examiner. Emmanuel et al. (2021) used an artificial intelligence-assisted method through proprietary software to identify and count OC from Wistar rats, with no significant difference in accuracy compared to manual methods while saving time. To our knowledge, OCs from humans have not been analyzed using ML. Our images also contain more variation than the other methods' datasets. Therefore, we have developed a method to quantify human osteoclast from a variety of experiments using ML-based object detection.

Object detection combines computer vision and ML techniques to locate and classify objects in images. Using samples of images with labeled objects, we can train an object detection model to detect the objects in new images automatically. The model consists of several parts, where a convolutional neural network (backbone) can learn and extract features from images, which is connected to a predictor (head) for estimating object location (bounding box) and class probabilities. We use an open-source object detection (deep learning) framework called Darknet (Alexey et al., 2021). Darknet has achieved state-of-the-art results with its recent YOLOv4 model (Bochkovskiy et al., 2020) and is known for its training and prediction speed on a single graphics processing unit (GPU). Darknet and versions of the YOLO models have been used in multiple fields, including medicine and diagnosis (Elgendi et al., 2020; Yao et al., 2022), agriculture (Zheng et al., 2021), construction and industry (Nath and Behzadan, 2020; Kohtala and Steinert, 2021), and autonomous vehicles (Cai et al., 2021) to name a few.

We trained, validated, and tested multiple object detection models using osteoclasts generated from seven human PBMC donors, resulting in 307 different wells. Each well was marked using Fiji (Schindelin et al., 2012), with 94,974 OCs in total, and automatically converted to training and test datasets. The models are thoroughly evaluated using various training scenarios to analyze their performance compared to human annotators and to discuss their potential for replacing the labor-intensive process of manually counting OCs.

2 METHODS

2.1 *In Vitro* Methods

2.1.1 Differentiation of Osteoclasts From $CD14^+$ Cells—Dataset I

Human buffy coats were provided by the Blood bank at St. Olavs Hospital (REK #2009/2245). PBMCs were isolated using a Lymphoprep density gradient (Alere), and $CD14^+$ cells were isolated from these using CD14 microbeads (#130-050-201, Miltenyi Biotech). 13,000 $CD14^+$ cells per well were seeded out in transparent plastic 96-well plates (#3599, Corning). The cells were cultured in α-minimum essential medium without phenol red (αMEM, #41061-029, Gibco) with 10% heat-inactivated pooled human serum supplemented with M-CSF (30 ng/ml, R&D Systems), RANKL (10 ng/ml, R&D Systems) and transforming growth factor-β (TGF β, 1 ng/ml, R&D Systems). The number of days used to differentiate the cells varied from donor to donor. Pre-osteoclasts were observed after 5–9 days. At this point, the cells were stimulated with various stimulants as part of an experiment. Mature osteoclasts were observed after about 12–16 days and the cells were TRAP stained. Six PBMC donors were used for dataset I, one per experiment presented in **Figure 1**.

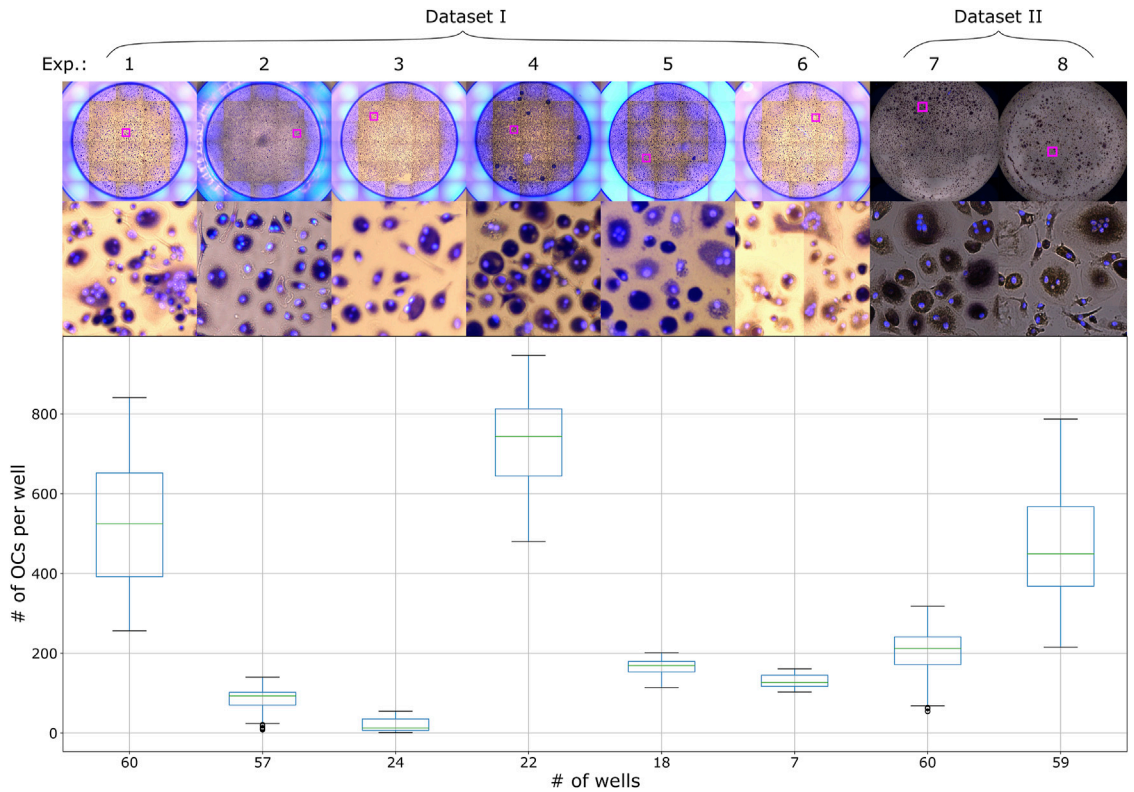

FIGURE 1 | Distribution of the number of OCs per well with an example well image from each experiment in Dataset I and II.

2.1.2 Differentiation of Osteoclasts From Macrophages—Dataset II

PBMCs were isolated as described above. The $CD16^+$ patrolling monocytes (pMos) and $CD16^-CD14^+$ inflammatory monocytes (iMos) were isolated from one PBMC donor using $CD16^+$ monocytes isolation kit (#130-091-765, Miltenyi Biotec) and CD14 microbeads in sequence. The purified cells were seeded out at 30,000 cells per well in black 96-well plates with glass bottom (#P96-1.5H-N, Cellvis). The cells were cultured in α-MEM medium with 10% heat-inactivated pooled human serum and M-CSF (10 ng/ml) for 7 days to form macrophages. At this point, the cells were stimulated with various stimulants as part of an experiment. Media was also changed to pre-osteoclastogenic differentiation medium containing M-CSF (30 ng/ml), RANKL (10 ng/ml) and TGF-β (1 ng/ml) before seven additional days of culture. The media supplements were then adjusted to M-CSF (10 ng/ml) and RANKL (50 ng/ml) and cells cultured three more days before TRAP staining. One PBMC donor was used for dataset II, the same donor for both experiments 7 and 8 presented in **Figure 1**. Experiment 7 represents pMos differentiated osteoclasts and experiment 8 represents iMos differentiated osteoclasts.

2.1.3 Differentiation of Osteoclasts From Human Osteoclast Precursor Cells—Retraining Dataset

Human osteoclast precursor cells (#2T-110, Lonza) were plated at 10,000 cells per well in a transparent plastic 96-well plate and cultured according to the manufacturer's instructions in OCP medium (#PT-8021, Lonza) in the presence of M-CSF (33 ng/ml) and RANKL (66 ng/ml). The cells were stimulated with various stimulants as part of an experiment during culture. When mature osteoclasts were present, the cells were TRAP stained. Two wells from this experiment were used for a small retraining of the model, described in **Section 3.4**.

2.1.4 Staining

Mature osteoclasts were stained for TRAP using the Acid Phosphatase, Leukocyte (TRAP) Kit (#387A, Sigma-Aldrich) following the manufacturer's instructions, with the following exceptions: osteoclasts were fixed with 4% paraformaldehyde (#43368, Alfa Aesar) in phosphate-buffered saline (PBS) for 15 min and appropriate TRAP staining was observed after incubation for up to 1.5 h. Cells were then washed twice with deionized H_2O, before nuclei were stained with Hoechst 33,342 (#H3570, Life Technologies) 1:5,000 in PBS. Cells were kept in this solution during imaging.

2.1.5 Imaging

Images were acquired with an EVOS FL Auto 2 Microscope (Invitrogen by Thermo Fisher Scientific) using a ×10 objective. TRAP staining was imaged using transmission microscopy, capturing a brightfield image of the well with a color camera. The EVOS light cube tagBFP was used for fluorescent detection of Hoechst. The microscope captured several smaller images of different regions of the well, which could later be arranged

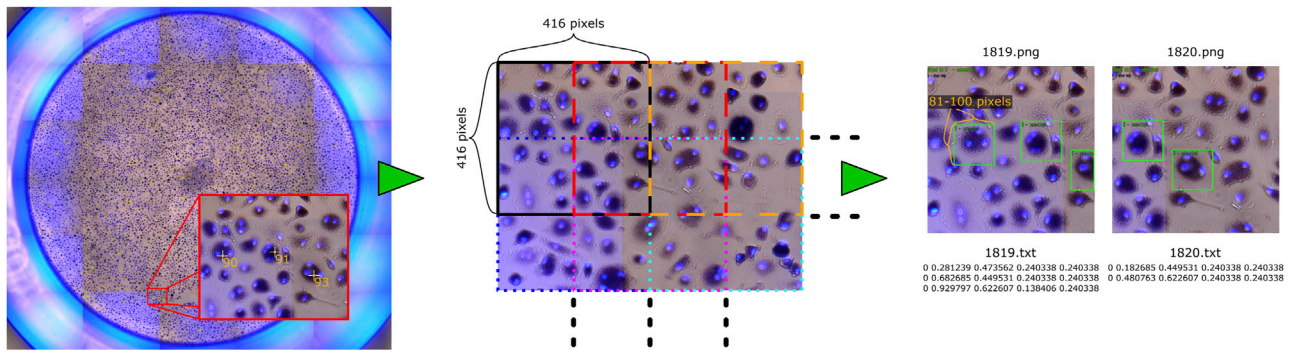

FIGURE 2 | Sample image with processing steps, where each well image is split into overlapping segments that are saved as separate images, with each mark converted to a bounding box stored in a text file.

next to each other resulting in one larger image of the whole well, this process is called tiling. For dataset I and the Retraining dataset, tiling of the images was done in the EVOS software (Invitrogen EVOS FL Auto 2 Imaging System), creating two images per well, one TRAP image and one Hoechst image. For dataset II, tiling of the already merged images was done using a custom script in Fiji. TRAP and Hoechst images were merged using either the EVOS software or Fiji for all datasets, generating one image of the whole well. The edges of the wells were not imaged completely in dataset II, which resulted in these images being smaller than the images from dataset I. All images were saved as TIF files. The datasets I and II contain a total of 307 well images from eight different experiments, with their OC distribution and sample images shown in **Figure 1**. The Retraining dataset contain two wells from one experiment.

2.1.6 Manual Osteoclast Counting

The merged images from EVOS were used for the human counting. Prior to counting, the images from an experiment were given random names using a Fiji script to make the counting unbiased. Fiji was used to count the osteoclasts by manually marking each osteoclast using the multi-point tool. When clicking on osteoclasts in an image, the multi-point tool leaves a mark and keeps track of the number of total markings in the image. When all wells of an experiment had been counted, the images could be decoded, revealing the results of the experiment.

2.2 Datasets and Training Procedures

2.2.1 Data Preparation

The two datasets (I and II) were initially intended for different research topics and purposes. This provided us the opportunity to test our approach on various OCs in a large number of images, and thus improve and thoroughly evaluate the algorithm. The well images were marked prior to this study, and their placements relative to the OCs are therefore not optimized for training an object detection model. We have not edited the marks due to the large number of samples (94,974 marked OCs) and the time required to correct each label manually. Therefore, several scripts were made to automatically create and prepare the data before training a model for detecting OCs. Each image of a well was processed, as illustrated in **Figure 2**.

First, a Fiji script converted the TIF images into PNG and exported every marked OC's pixel coordinate to a CSV file. The PNG format removed the metadata (markings) and reduced file size for further processing. Because the object detection framework can only process small images, each image of a well was further split into segments of 416 × 416 pixels with 50% overlap, resulting in 2,200 segments for each image (10,248 × 9,122 pixels) in dataset I and 1,520 segments for each image (8,320 × 7,760 pixels) in dataset II. An overlap of 50% was used to ensure that each cell could be viewed entirely at least once while increasing the number and variation of training data. Object detection also requires a bounding box that covers the region of interest for detection. Based on observations, most cells would fit inside a box that is approximately 0.9756% of the width of the whole well image, which we used to automatically create bounding boxes covering roughly 100 pixels in height and width for dataset I and 81 pixels for dataset II. The bounding box coordinates around each marked OC were then saved to a text file corresponding to each image segment, described by its center, width, and height relative to the segment. Bounding boxes extending the perimeter of an image segment were reduced to fit within the segment. The two additional wells in the Retraining dataset with large variation in cell sizes were manually labeled with bounding boxes using LabelImg (Tzutalin, 2022) to ensure that each OC was covered entirely.

2.2.2 Training Procedure

Transfer learning was used by training the OC detection models using an existing weights file for the convolutional layers [yolov4. conv.137 from Alexey et al. (2021)], which is pre-trained on the MS COCO (common objects in context) dataset (Lin et al., 2014). The pre-trained weights have learned to recognize many useful features from images to increase the training speed for detecting new objects. Training and prediction were performed locally on a laptop with an Intel i9-8950HK 2.9 GHz CPU connected to an external NVIDIA GeForce RTX 2080 Ti GPU.

TABLE 1 | Number of samples used for each model.

Models	Train		Validation		Test		Sum	
	Wells	Segments	Wells	Segments	Wells	Segments	Wells	Segments
M1	183	354,320	64	124,480	60	115,680	307	594,480
M2_exp1, 2, 4	16	35,200	2	4,400	2	4,400	80	162,400
M2_exp8	16	24,320	2	3,040	2	3,040		
M3_P1, M3_P2	4	8,800	2	4,400	2	4,400	8	17,600

We applied the same configuration file provided for the YOLOv4 model, with batch size 64, input width and height set to 416 pixels, and a learning rate of 0.001 for the first 80% training iterations, which is reduced by a factor of 10 for each remaining 10% of training iterations. Darknet also provides methods for using data augmentation during training, which will randomly alter the input images to increase the variability of the data and improve generalization. For data augmentation, we used random hue, saturation, exposure, cropping, aspect ratio, and mosaic data augmentation (randomly mixing four training images).

2.2.3 Training Scenarios

Four separate training scenarios were analyzed. In the first scenario, a single model (M1) was trained and optimized for the entire dataset, where the well images from each experiment (see **Figure 1**) were split into a training (~60%), validation (~20%), and test (~20%) set, with the total number of samples in the final datasets shown in **Table 1**. We trained the model for 11,073 iterations, i.e., two epochs when using a batch size of 64, and evaluated the validation set every 500 iterations for selecting the best model after training is complete. Finally, using the test set with M1, we can assess how closely the trained model can match the annotators (ground truth) for OC detection and counting. The 60/20/20 data split is the most common approach used to train (fit the model), validate (tune and select the best model), and test (unbiased measure of performance) ML models, and represents how the method would usually be applied in practice. Thus, our goal is to evaluate the applicability of using an open-source object detection framework to detect human OCs from microscopic images. By comparing the validation and test accuracies, we can also assess the model's degree of bias (underfitting) and variance (overfitting).

In many cases of ML, the available data does not represent the variation found in the wild (unseen samples), and it is uncertain how the chosen method generalizes to this new, unforeseen variation. However, with a large dataset from different experiments, it is possible to simulate this scenario by only training and validating the model on a subset of the available data and then testing it against "unseen" subsets. Thus, to assess the ability of our approach to generalize across different experiments (different donors and image appearance), we randomly picked 20 well images from experiments 1, 2, 4, and 8 for the second training scenario. A model was then trained (16 wells) and validated (2 wells) for each experiment (denoted by M2_exp1, M2_exp2, M2_exp4, and M2_exp8) and then tested against each other's remaining two test wells. Each model was trained for 2500 iterations, i.e., 6.5 epochs for M2_exp8 and 4.5 epochs for the other models. This training scenario was performed to test how a model trained on only one experiment generalizes to other 'unseen' experiments or if the models tend to overfit if not introduced to more variation.

In the third scenario, we analyzed eight wells from experiment 4 that were marked independently by two annotators (P1 and P2). Two models were trained for each annotated dataset, where models M3_P1 and M3_P2 are trained on P1 and P2's labels, respectively. We used 4-fold cross-validation (CV), using four training wells and two validation and test wells, to analyze each well without being part of the training and thus reduce bias. The models were trained for 3,000 iterations for each CV step (roughly 20 epochs). We can then directly compare both human-human and model-human agreements to assess if the proposed object detection method for automatic OC counting can replace humans and further evaluate the proposed method's applicability and generalizability.

A fourth scenario was included to test if model M1 can be retrained to work on different-sized cells with larger variation. We labeled two wells from the Retraining dataset with large and small OCs containing at least three and up to more than 20 nuclei. The labels (bounding boxes used as ground truth) had to be made manually using a labeling tool since the auto-generated labels used for training the other models would not fit these cells. The cells ranged from 40 to 1,600 pixels in width and height, with an average of 260 pixels. The image segments were increased to 650 pixels in width and height to ensure that at least 95% of the labeled cells would fit inside. One of the wells was used to retrain and validate the model, while the other well was used to test the accuracy.

2.3 Evaluation

Since the human-labeled marks from Fiji were not perfectly centered on the cells, and the bounding boxes were given a fixed size around the marks, we used a relatively low Intersection over Union (IoU) threshold of 0.1 for considering a detection a true positive. The mean average precision (mAP) is then calculated through Darknet, which employs the average precision (AP) calculation procedure provided by the PASCAL VOC2010 challenge (Everingham et al., 2015). Here, AP is the area under the monotonically decreasing precision-recall curve ranked by detection confidence. Subsequent detections of the same ground truth label are counted as false positives in the calculation. The mAP is the mean of the APs for all classes, and since we only consider one class, AP is equal to mAP. The mAP with an IoU threshold of 0.1 is referred to as mAP@0.1, which we calculate for the validation set during training to select the best

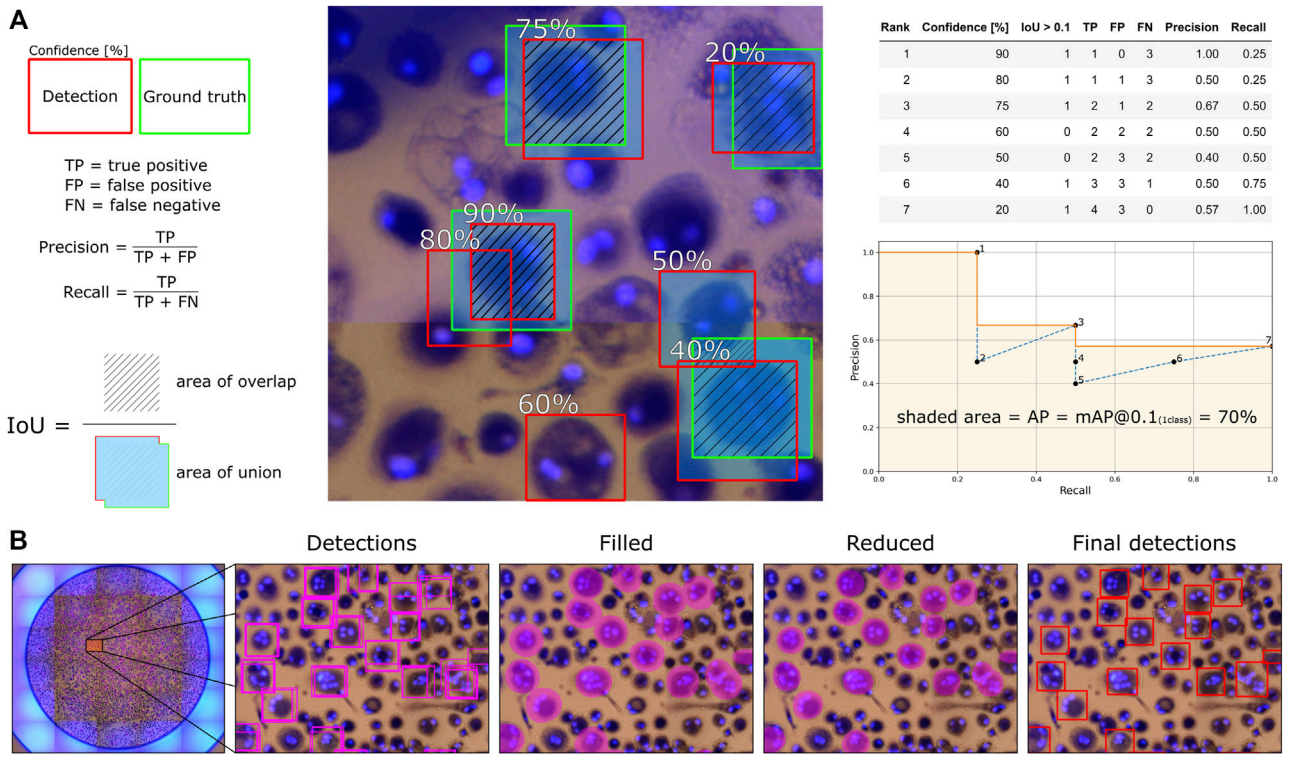

FIGURE 3 | An illustrative example for how **(A)** average precision (mAP@0.1) is calculated and how **(B)** the total number of detected OCs are counted and segmented for each well with overlapping image segments.

model and then for the test set to report model performance. We also report mAP@0.5 results since an IoU threshold of 0.5 is commonly used for object detection models. An illustrative example of how mAP@0.1 is calculated for one sample image is shown in **Figure 3A**, where the same approach is used when multiple images are analyzed.

With the mAP metric considering every detection confidence and representing how accurately the trained model can locate, classify, and recall the marked OCs, we need to find a detection threshold for detecting OCs in new images. Therefore, we also calculate precision and recall values for the validation set to find the detection threshold that achieves the highest F1-score (harmonic mean of the precision and recall). We can then use this threshold value to detect and count the total number of OCs for each well in the test set by evaluating all corresponding image segments. Since the training images (segments) are overlapping, we compare the detection accuracy with and without overlapping segments to determine which approach is better suited. The number of segments in **Table 1** is thus reduced by 75% in the case of only using non-overlapping segments. We created a simple algorithm using OpenCV (Bradski, 2000) to prevent multiple detections of the same OC when using overlapping segments. The algorithm first fills an ellipse-shaped region within the detected bounding boxes reduced by 20% in height and width to differentiate compact OCs with overlapping detections. The connected ellipses are then fused to reduce multiple detections of the same OC to one, finally creating bounding boxes around the merged ellipse shapes. The procedure is illustrated in **Figure 3B**.

After analyzing each whole well, we can compare the total number of OCs detected by the model and annotators and measure their agreement by calculating the root-mean-squared error (RMSE). *Python* (version 3.7.9) with the Scipy library (version 1.7.1) was used for calculating Pearson correlation coefficients between the models and annotators and perform normality tests.

3 RESULTS

3.1 Scenario 1: Model Performance Using the Entire Datasets

The first model (M1) was trained for approximately 2 days and 14 h, including validation-set evaluations every 500 iterations taking roughly 2 h each time. Although the total training duration can be substantially reduced by excluding the validation set, selecting the best model based on training loss may cause overfitting. Since the validation set is not used to fit the model, it will reduce bias and better indicate model performance and generalization. **Figure 4** shows the training loss and validation accuracy for the entire training duration. The best models were selected based on the highest validation accuracies and then evaluated on the test set, with results presented in **Table 2**. The mAP values were acquired on

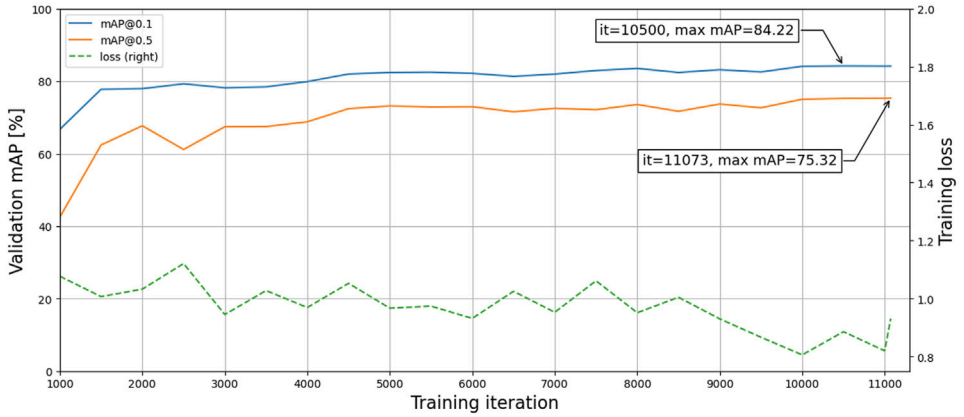

FIGURE 4 | Training loss and validation accuracies during training.

TABLE 2 | Validation and test results for the best models.

IoU threshold	Validation					Test			
	mAP [%]	P	R	F1	DT	mAP [%]	P	R	F1
0.1	84.22	0.79	0.81	0.80	0.25	85.26	0.80	0.82	0.81
0.5	75.32	0.75	0.75	0.75	0.26	75.92	0.76	0.74	0.75

P, precision; R, recall; F1, F1 score; DT, detection threshold.

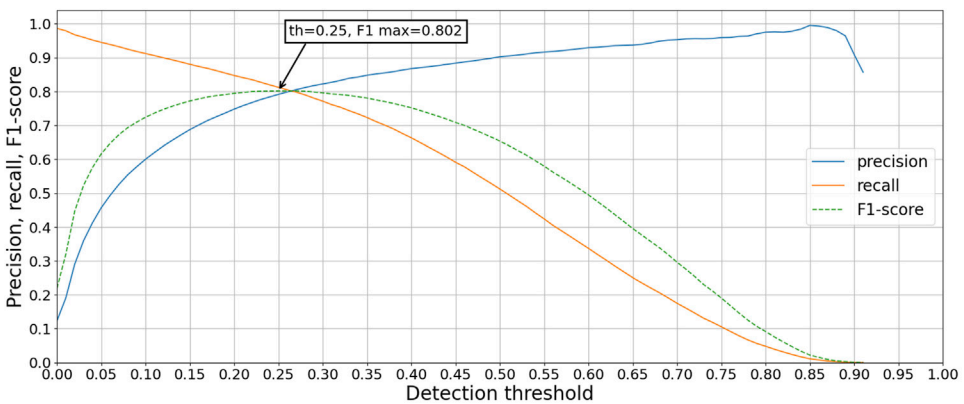

FIGURE 5 | Precision, recall, and F1-score for the validation set using the model that achieved the highest mAP@0.1 score.

overlapping and non-overlapping validation and test images, with a mean absolute difference of only 0.2% between the approaches. Thus, the effect of the segmentation method does not significantly affect the mAP values. Furthermore, the similar and high validation and test accuracies indicate that the trained model has both low variance and bias, respectively, thus having generalized properly. The mAP@0.5 values are consistently lower than the mAP@0.1 values, which is expected due to the stricter evaluation criteria.

The precision, recall, and F1 scores were calculated for every detection threshold incremented by 0.05, with the results shown in **Figure 5** for the validation set using the best model (highest mAP@0.1 score). The highest F1 score was achieved with a detection threshold of 0.25.

Using the best model based on mAP@0.1 and a detection threshold of 0.25, the number of OCs was detected and counted for each validation well. The process shown in **Figure 3B**, applied to overlapping segments, resulted in a combined RMSE of 51.87 while detecting directly on non-overlapping segments resulted in a combined RMSE of 32.37. Therefore, the approach of using overlapping segments for detection was disregarded, as it deviates more from the

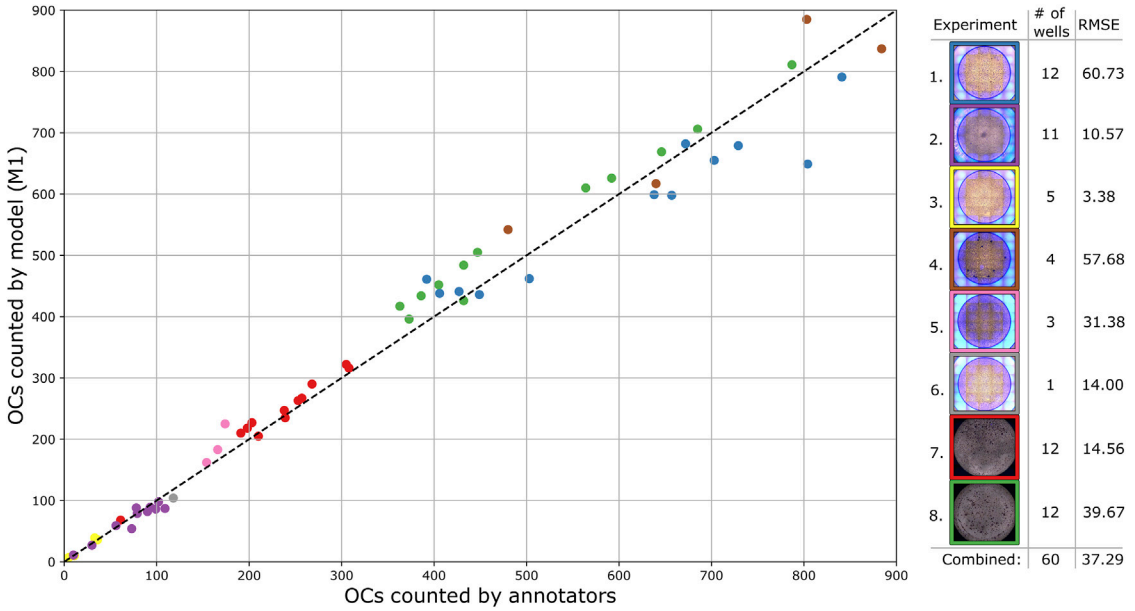

FIGURE 6 | Comparison of the total number of detected OCs by the trained model and annotators for each test well, with each experiment separated by color. The dashed diagonal line represents the line of perfect agreement.

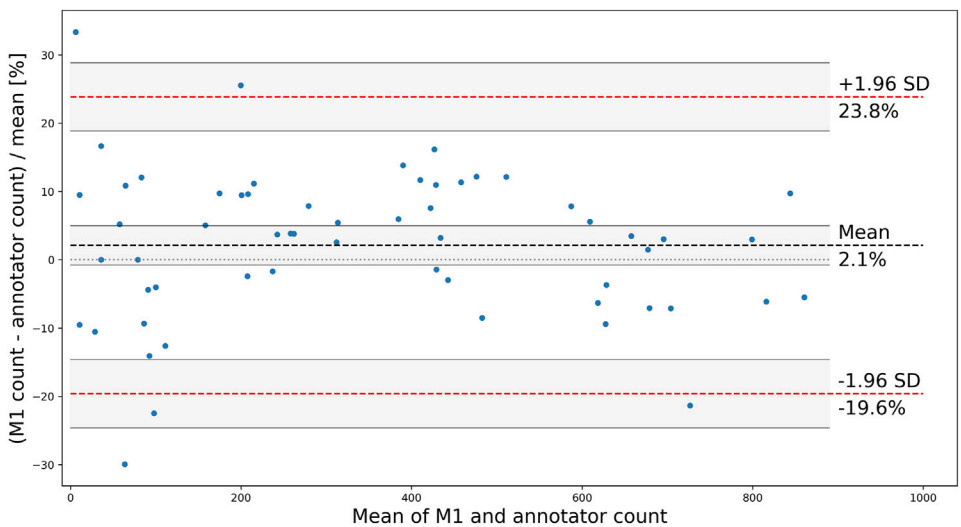

FIGURE 7 | Bland and Altman plot showing the difference between M1 and annotators for each counted test well, with the limits of agreement shown as red, dashed lines, mean (bias) shown as a black dashed line, and CIs shaded in grey.

annotators than using non-overlapping segments without the extra step of combining detections. **Figure 6** shows the number of OCs counted by the model compared to the annotators for each test well, with RMSE calculated for every experiment. The combined RMSE of all test wells is 37.29, with a Pearson correlation coefficient of 0.99 ($p < 0.001$, from scipy. stats.pearsonr) between M1 and annotators. These results support the applicability of using object detection to match human-level accuracy for counting OCs.

Although the correlation between the trained model and human annotators is high and positive, it does not necessarily imply a good agreement on the total number of counted OCs. To further analyze the applicability of the proposed method, a Bland and Altman plot is shown in **Figure 7** with confidence interval (CI) calculations based on Giavarina (2015). The plot shows the difference (in the percentage of the mean) between measurements for the test wells, for which the residuals are normally distributed ($p > 0.18$, from scipy. stats.normaltest). The limits of agreement

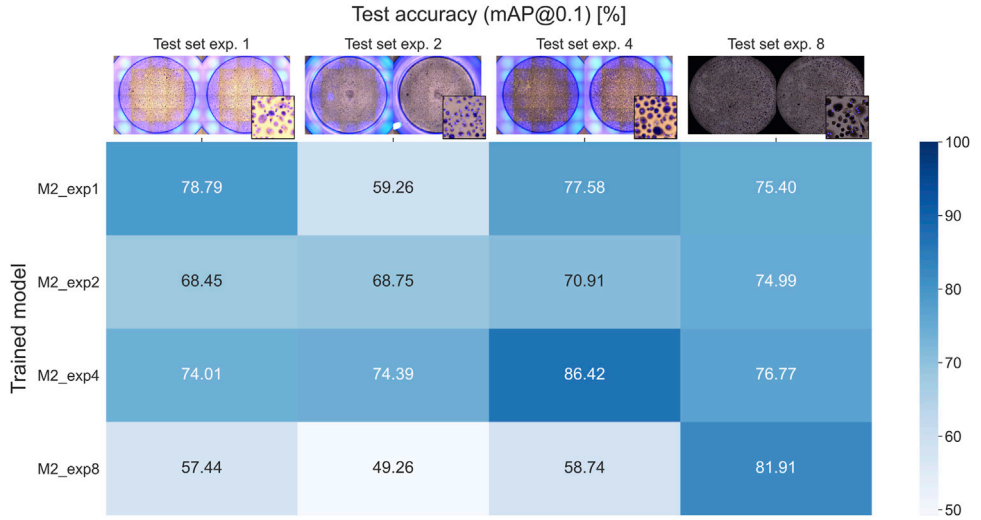

FIGURE 8 | Test accuracies for models trained and validated on one experiment each.

(mean difference ±1.96 SD) are 23.8% and −19.6%, which contain 95% of the differences. The bias of 2.1% is not significant since the line of equality (representing perfect agreement) is within its CI, indicating that the model consistently counts the number of OCs close to the human annotators without a systematic difference. However, the agreement interval is relatively wide, with the most considerable deviations found for the wells containing the fewest OCs. One outlier having a mean of three (one annotated and five detected OCs) and a difference of 133.3% was removed from the analysis.

3.2 Scenario 2: Generalization Across Experiments

Four models were trained, each using 16 samples from only one experiment (1, 2, 4, and 8 in **Figure 1**), and then evaluated against test wells from each experiment. The resulting mAP@0.1 values are shown in **Figure 8**. It is expected that a model trained, validated, and tested on the same experiment will achieve higher test accuracy compared to the other experiments since the training and test data are more related. However, this is not the case for model M2_exp2, which scored higher on experiments 4 and 8.

Additionally, each model achieves high accuracies on the test wells from experiment 8. In contrast, the model trained with images from experiment 8 has the lowest accuracies when tested on the other experiments. The dark appearance of the images in experiment 8 reduced the effectiveness of data augmentation (random hue, saturation, and exposure) when training M2_exp8, resulting in the model not being able to generalize properly. At the same time, the other experiments are not affected on the same level and were, therefore, able to generalize sufficiently to detect OCs from experiment 8 with reasonable accuracy. These results show that the method can produce models able to detect OCs from different experiments that were not part of the training and validation, thus showing generalizable tendencies of the trained models.

3.3 Scenario 3: Cross-Validation With Two Human Annotators

Two models were trained with a 4-fold CV using eight wells from experiment 4, marked independently by two annotators. The trained models, M3_P1 and M3_P2, had an average test accuracy (mAP@0.1) of 85.5 and 77.78%, respectively. The total numbers of OCs counted by the annotators and models are shown in **Figure 9**, with RMSE and correlation coefficients between each OC counter shown in **Table 3**. As seen in **Table 3**, the models agree more with the person marking the dataset, and the models agree more than the two annotators.

3.4 Scenario 4: Retraining and Detection of Varying OC Sizes

Model M1 applied directly to the two wells of the Retraining dataset with large variation in osteoclast size resulted in 66.27% mAP@0.1, an F1-score of 0.66, and counted 16% fewer OCs than the annotator. M1 was then retrained using one of the wells for 50 min, where the highest validation accuracy (88.77%) was found at the 25 min mark. This resulted in a new test accuracy of 91.71% mAP@0.1, an F1-score of 0.85, and counted 11% more OCs than the annotator. These promising results support the applicability of the proposed method for detecting OCs with various shapes and sizes. A few sample detections from the test well are shown in **Figure 10**, with OCs ranging from 626 pixels to 64 pixels in width.

4 DISCUSSION

4.1 Automatic OC Counting Accuracy

Our approach can automatically detect and count human OCs from microscopic images with good accuracy. The Pearson correlation coefficient of 0.99 indicates that the trained model

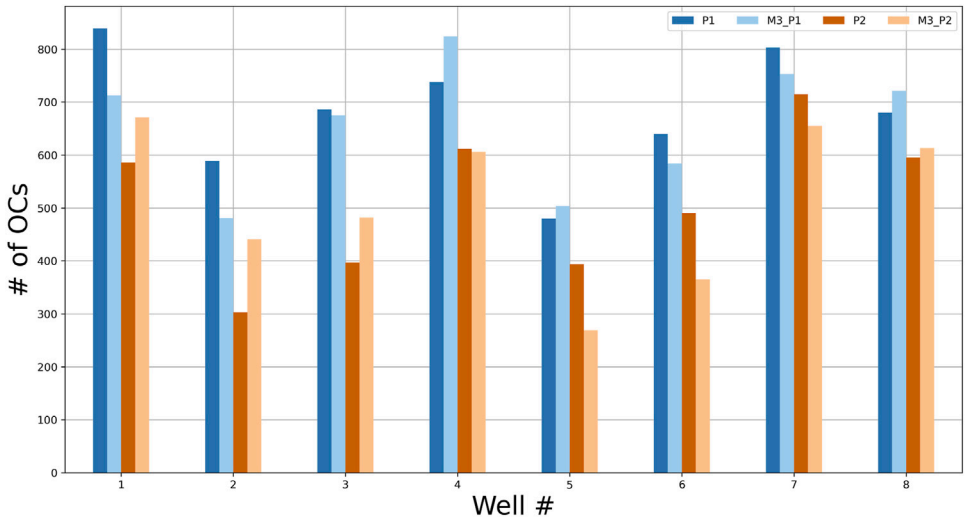

FIGURE 9 | The number of OCs counted by two annotators (P1 and P2) and the two models M3_P1 and M3_P2 for each test well from experiment 4.

TABLE 3 | Agreement between each OC counter, ranked by lowest RMSE.

	RMSE	Mean difference ±SD	Pearson correlation coefficient
P1 vs. M3_P1	73.27	25.00 ± 73.63	0.81
P2 vs. M3_P2	92.67	−1.25 ± 99.06	0.76
P2 vs. M3_P1	161.36	−145.38 ± 74.86	0.84
M3_P1 vs. M3_P2	163.01	144.13 ± 81.43	0.83
P1 vs. M3_P2	178.78	169.13 ± 61.97	0.92
P1 vs. P2	190.42	170.38 ± 90.90	0.76

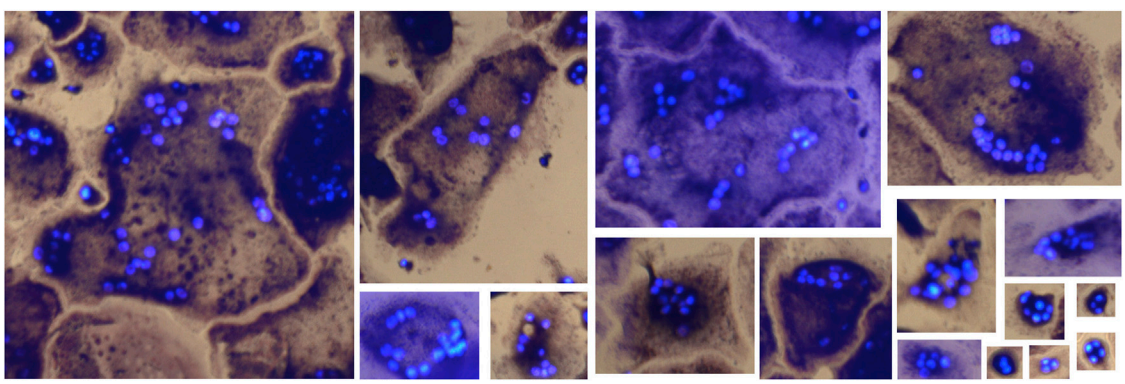

FIGURE 10 | OCs of various sizes detected (true positives) by the retrained model.

can reliably count the number of OCs compared to human annotators, which is essential when comparing the amount of OCs between experiments. Furthermore, the trained model can locate and classify OCs in various images with a mAP@0.1 accuracy of 85.26% and count the number of OCs with a bias of only 2.1%. However, the limits of agreement found in **Figure 7** ranges from −19.6 to 23.8%, and their acceptability must be based on the study being conducted. These results are auspicious when considering the suboptimal labels used for training, suggesting that the model can be improved further by optimizing the labels. The model can also be retrained to account for various cell sizes, as shown in scenario four. However, due to the few samples used, more manually labeled data is needed to further improve detection of various OC sizes.

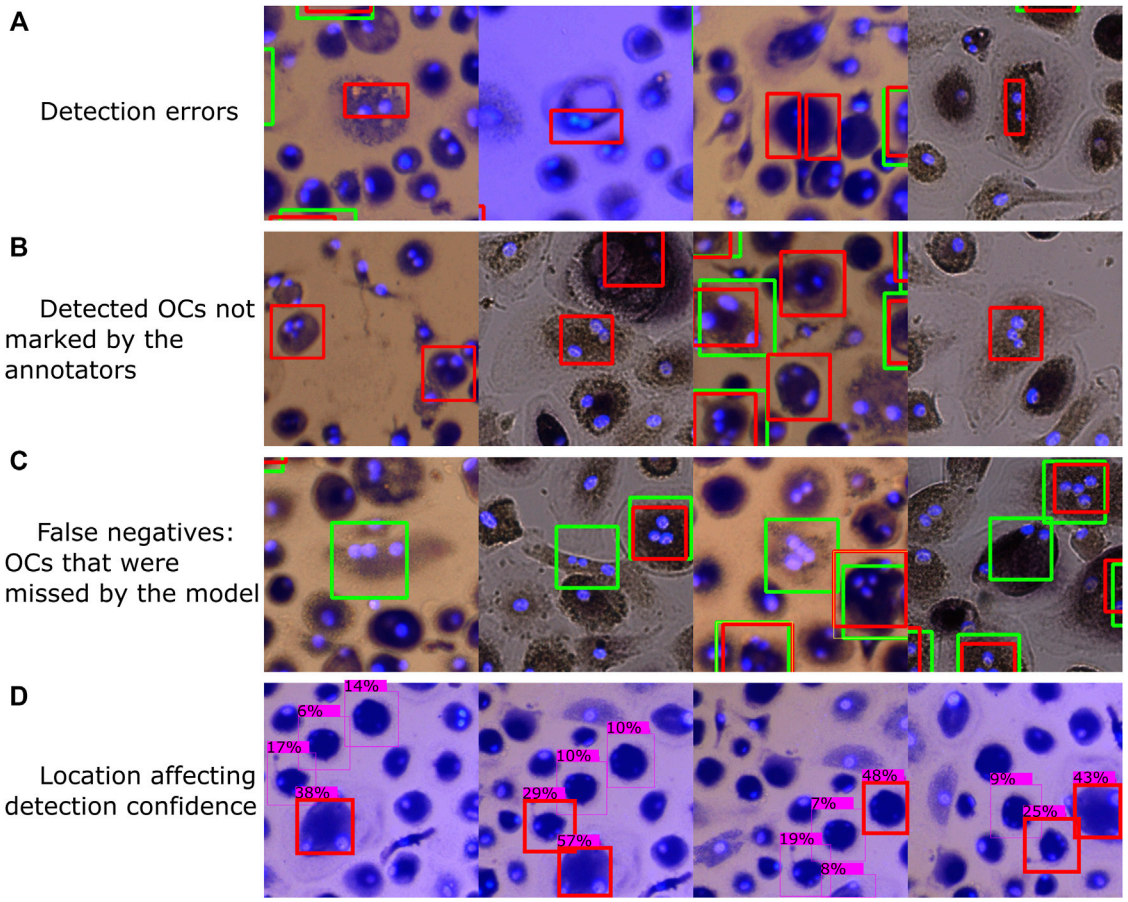

FIGURE 11 | Typical errors, including **(A)** classifying parts of a cell as an OC, **(B)** OCs regarded as false positives during evaluation due to the annotators missing some OCs during manual counting, **(C)** OCs differing in shape and appearance from most OCs in our dataset that were found by the annotators but not by the model, and **(D)** cell location affecting detection confidence. Red bounding boxes represent detections made by model M1, with green representing the annotated labels (ground truth).

One well image (550 segments without overlap) takes about 49 s to analyze, including 28s for splitting the image and saving each segment to a folder and 21s to perform detection (~26 frames per second) and count the total number of OCs. Manual counting takes 15–40 min depending on the number of cells, whereas our approach takes around 6 min on the CPU. Even without GPU acceleration, our approach can save a lot of time and manual labor, especially when analyzing multiple wells.

By training several models using only one experiment each, we showed in scenario two that the method will still produce models able to detect OCs on different experiments and images with reasonable accuracy. Therefore, we expect that the model (M1) trained on all our experiments will work well on completely new experiments that may look slightly different. It is, however, essential to validate the model and tune the detection threshold on new images before relying on the reported accuracy. We also found that the darker images produced the least accurate models due to the reduced effect of data augmentation, which should be considered when capturing new data and training new models for cell analysis.

A trained model will naturally agree more with the person annotating the dataset, as seen in **Figure 9** and **Table 3**. However, the trained models agreed more than the two annotators, indicating that the models have consistency at least as good as the human annotators and were able to learn the essential features for detecting OCs without overfitting on erroneous or missing labels. This further supports the use of trained object detection models to replace the manual process without losing accuracy.

4.2 Limitations and Typical Errors

A few samples of typical errors are shown in **Figure 11**. Since the object detection models can only process small images, thus having to divide each well image into smaller segments, some of the training images will contain incomplete OCs that remain marked. The model has thus learned to recognize such incomplete OCs, resulting in detection errors, as shown in **Figure 11A**. A segmentation algorithm that considers the labeled OCs so that none of the segments contain incomplete OCs could be developed, which would remove such erroneous samples from the training data.

Figures 11B,C shows some false positives and false negatives with respect to the human-marked OCs. After going through some of the automatically analyzed wells, we found several false positive detections by the trained model that should be considered true positives, resulting from the annotators not detecting each OC during manual counting. Although this is not a limitation of the trained model, it shows that human error can affect the evaluation of the model. To further improve the detection accuracy, a manual evaluation of the model's and human's detections can be performed to correct erroneous and missing labels in the training data and then retrain the model. Many false negatives, i.e., human-labeled OCs that the model did not detect, had different shapes and appearances than most of the OCs in our dataset. In addition, a few faulty labels were caused by accidental clicks using the Fiji marking tool.

A small translation was applied to the first three image segments shown in **Figure 11D**, with the fourth segment being rotated, which resulted in different detection confidences for the same cells. Since a detection threshold is required to filter out erroneous detections and improve accuracy, the well images' segmentation approach can affect the results. For example, the method of detecting OCs using overlapping image segments, as shown in **Figure 2** and **Figure 3B**, resulted in more detections (a significant, 12.5% bias) compared to using non-overlapping segments (2.1% bias). Therefore, it is important to validate the model and segmentation approach to tune the detection threshold.

It is required that the cells are approximately the same size relative to the image segments when using our trained model. Darknet models can be trained with image sizes between 320 and 608 pixels in width and height, where we used 416 pixels. Using images with different sizes is also possible, as demonstrated in scenario four, which will be resized accordingly when processed through Darknet. Therefore, the image segmentation strategy must be adjusted based on cell size and the size of the whole well image. If detection of larger cells or the number of nuclei per cell is required, our model can be retrained with new labeled data to increase accuracy. The approach can also be used on completely different cell types by training new models and can be used in real-time systems with a prediction time of roughly 26 images per second, depending on hardware.

5 CONCLUSION

An approach for automatically detecting and counting osteoclasts in microscopic images has been developed and evaluated. Several object detection (deep learning) models were trained, validated, and tested using 307 different wells from seven human PBMC donors, containing a total of 94,974 marked OCs. The first model was optimized for the OC counting task by utilizing a train, validation, and test split on all the available data, resulting in a test accuracy of 85.26% mAP@0.1. The model counted on average 2.1% more OCs per well than the human annotators, with limits of agreement between 23.8% and -19.6%, an RMSE of 37.29, and a correlation coefficient of 0.99. The approach can generalize across different experiments with effective data augmentation, supporting the potential adaptation of the model in different studies. Furthermore, two independent annotators agreed less than the trained models on the same dataset. A substantial amount of labor and time can thus be saved by automatically detecting OCs with (at least) human-level accuracy and reliability while reducing operator bias. Additionally, the trained model can be continuously improved by introducing new data from different experiments.

DATA AVAILABILITY STATEMENT

The raw data supporting the conclusions of this article will be made available by the authors, without undue reservation.

AUTHOR CONTRIBUTIONS

SK trained models, analyzed data, and wrote the paper. TN provided experimental data, evaluated results, and wrote the paper. SM and QM provided experimental data. CK, KØ, TS, and MS contributed to conception and design of the study. All authors contributed to manuscript revision, read, and approved the submitted version.

FUNDING

The project was supported by funding from the Research Council of Norway (#274991) and the Regional Health Authorities in Central Norway (Samarbeidsorganet #90485500). Imaging using EVOS FL Auto 2 Microscope was performed at the Cellular and Molecular Imaging Core Facility (CMIC), Norwegian University of Science and Technology (NTNU). CMIC is funded by the Faculty of Medicine at NTNU and Central Norway Regional Health Authority.

REFERENCES

Alexey, J. R., Sinigardi, S., Hager, T., JaledMCMaaz, M., Zhang, V., et al. (2021). "AlexeyAB/darknet: YOLOv4," in *Zenodo*. doi:10.5281/ZENODO.3693998

Bochkovskiy, A., Wang, C.-Y., and Liao, H.-Y. M. (2020). YOLOv4: Optimal Speed and Accuracy of Object Detection. 10934. arXiv:2004.10934 [cs, eess]. Available at: http://arxiv.org/abs/2004 (Accessed June 10, 2021).

Bradski, G. (2000). The openCV Library. *Dr. Dobb's J. Softw. Tools Prof. Program* 25, 120–123.

Burstone, M. S. (1959). HISTOCHEMICAL DEMONSTRATION OF ACID PHOSPHATASE ACTIVITY IN OSTEOCLASTS. *J. Histochem Cytochem.* 7, 39–41. doi:10.1177/7.1.39

Cai, Y., Luan, T., Gao, H., Wang, H., Chen, L., Li, Y., et al. (2021). YOLOv4-5D: An Effective and Efficient Object Detector for Autonomous Driving. *IEEE Trans. Instrum. Meas.* 70, 1–13. doi:10.1109/TIM.2021.3065438

Charles, J. F., and Aliprantis, A. O. (2014). Osteoclasts: More Than 'bone Eaters'. *Trends Mol. Med.* 20, 449–459. doi:10.1016/j.molmed.2014.06.001

Cohen-Karlik, E., Awida, Z., Bergman, A., Eshed, S., Nestor, O., Kadashev, M., et al. (2021). Quantification of Osteoclasts in Culture, Powered by Machine Learning. *Front. Cell Dev. Biol.* 9, 674710. doi:10.3389/fcell.2021.674710

Elgendi, M., Nasir, M. U., Tang, Q., Fletcher, R. R., Howard, N., Menon, C., et al. (2020). The Performance of Deep Neural Networks in Differentiating Chest X-Rays of COVID-19 Patients from Other Bacterial and Viral Pneumonias. *Front. Med.* 7, 550. doi:10.3389/fmed.2020.00550

Emmanuel, T., Brüel, A., Thomsen, J. S., Steiniche, T., and Brent, M. B. (2021). Artificial Intelligence-Assisted Identification and Quantification of Osteoclasts. *MethodsX* 8, 101272. doi:10.1016/j.mex.2021.101272

Everingham, M., Eslami, S. M. A., Van Gool, L., Williams, C. K. I., Winn, J., and Zisserman, A. (2011). The Pascal Visual Object Classes Challenge: A Retrospective. *Int. J. Comput. Vis.* 111, 98–136. doi:10.1007/s11263-014-0733-5

Filgueira, L. (2004). Fluorescence-based Staining for Tartrate-Resistant Acidic Phosphatase (TRAP) in Osteoclasts Combined with Other Fluorescent Dyes and Protocols. *J. Histochem Cytochem.* 52, 411–414. doi:10.1177/002215540405200312

Giavarina, D. (2015). Understanding Bland Altman Analysis. *Biochem. Med.* 25, 141–151. doi:10.11613/BM.2015.015

Hayman, A. R. (2008). Tartrate-resistant Acid Phosphatase (TRAP) and the Osteoclast/immune Cell Dichotomy. *Autoimmunity* 41, 218–223. doi:10.1080/08916930701694667

Kohtala, S., and Steinert, M. (2021). Leveraging Synthetic Data from CAD Models for Training Object Detection Models - a VR Industry Application Case. *Procedia CIRP* 100, 714–719. doi:10.1016/j.procir.2021.05.092

Lin, T.-Y., Maire, M., Belongie, S., Hays, J., Perona, P., Ramanan, D., et al. (2014). Microsoft COCO: Common Objects in Context, in *Computer Vision – ECCV 2014*, Lecture Notes in Computer Science, Editors D. Fleet, T. Pajdla, B. Schiele, and T. Tuytelaars (Cham: Springer International Publishing), 740–755. doi:10.1007/978-3-319-10602-1_48

Marino, S., Logan, J. G., Mellis, D., and Capulli, M. (2014). Generation and Culture of Osteoclasts. *Bonekey Rep.* 3, 570. doi:10.1038/bonekey.2014.65

Nath, N. D., and Behzadan, A. H. (2020). Deep Convolutional Networks for Construction Object Detection Under Different Visual Conditions. *Front. Built Environ.* 6, 97. doi:10.3389/fbuil.2020.00097

Pereira, M., Petretto, E., Gordon, S., Bassett, J. H. D., Williams, G. R., and Behmoaras, J. (2018). Common Signalling Pathways in Macrophage and Osteoclast Multinucleation. *J. Cell Sci.* 131, jcs216267. doi:10.1242/jcs.216267

Schindelin, J., Arganda-Carreras, I., Frise, E., Kaynig, V., Longair, M., Pietzsch, T., et al. (2012). Fiji: an Open-Source Platform for Biological-Image Analysis. *Nat. Methods* 9, 676–682. doi:10.1038/nmeth.2019

Sørensen, M. G., Henriksen, K., Schaller, S., Henriksen, D. B., Nielsen, F. C., Dziegiel, M. H., et al. (2007). Characterization of Osteoclasts Derived from CD14+ Monocytes Isolated from Peripheral Blood. *J. Bone Min. Metab.* 25, 36–45. doi:10.1007/s00774-006-0725-9

Tzutalin (2022). LabelImg. Available at: https://github.com/tzutalin/labelImg (Accessed June 10, 2022).

Wang, X., Kittaka, M., He, Y., Zhang, Y., Ueki, Y., and Kihara, D. (2021). OC_Finder: A Deep Learning-Based Software for Osteoclast Segmentation, Counting, and Classification. *biorxiv* 1025, 465786. doi:10.1101/2021.10.25.465786

Yahara, Y., Nguyen, T., Ishikawa, K., Kamei, K., and Alman, B. A. (2022). The Origins and Roles of Osteoclasts in Bone Development, Homeostasis and Repair. *Development* 149, dev199908. doi:10.1242/dev.199908

Yao, Z., Jin, T., Mao, B., Lu, B., Zhang, Y., Li, S., et al. (2022). Construction and Multicenter Diagnostic Verification of Intelligent Recognition System for Endoscopic Images from Early Gastric Cancer Based on YOLO-V3 Algorithm. *Front. Oncol.* 12, 815951. doi:10.3389/fonc.2022.815951

Zheng, Z., Xiong, J., Lin, H., Han, Y., Sun, B., Xie, Z., et al. (2021). A Method of Green Citrus Detection in Natural Environments Using a Deep Convolutional Neural Network. *Front. Plant Sci.* 12, 705737. doi:10.3389/fpls.2021.705737

Conflict of Interest: The authors declare that the research was conducted in the absence of any commercial or financial relationships that could be construed as a potential conflict of interest.

frontiers | Frontiers in Cell and Developmental Biology

TYPE Mini Review
PUBLISHED 08 August 2022
DOI 10.3389/fcell.2022.957800

OPEN ACCESS

EDITED BY
Claudine Blin-Wakkach,
UMR7370 Laboratoire de Physio Médecine Moléculaire (LP2M), France

REVIEWED BY
Axel Vater,
Aptarion Biotech AG, Germany

*CORRESPONDENCE
Pier Giorgio Amendola,
piergiorgio.amendola@dompe.com

†These authors have contributed equally to this work and share first authorship

SPECIALTY SECTION
This article was submitted to Cellular Biochemistry, a section of the journal Frontiers in Cell and Developmental Biology

RECEIVED 31 May 2022
ACCEPTED 11 July 2022
PUBLISHED 08 August 2022

CITATION
Ruocco A, Sirico A, Novelli R, Iannelli S, Van Breda SV, Kyburz D, Hasler P, Aramini A and Amendola PG (2022), The role of C5a-C5aR1 axis in bone pathophysiology: A mini-review. *Front. Cell Dev. Biol.* 10:957800. doi: 10.3389/fcell.2022.957800

The role of C5a-C5aR1 axis in bone pathophysiology: A mini-review

Anna Ruocco[1†], Anna Sirico[1†], Rubina Novelli[2], Silvia Iannelli[1], Shane Vontelin Van Breda[3], Diego Kyburz[3], Paul Hasler[4], Andrea Aramini[5] and Pier Giorgio Amendola[1*]

[1]R&D, Dompé Farmaceutici SpA, Naples, Italy, [2]R&D, Dompé Farmaceutici SpA, Milan, Italy, [3]Departement Biomedizin, University of Basel, Basel, Switzerland, [4]Division of Rheumatology, Kantonsspital Aarau AG, Aarau, Switzerland, [5]R&D, Dompé Farmaceutici SpA, L'Aquila, Italy

Bone remodeling is a physiological, dynamic process that mainly depends on the functions of 2 cell types: osteoblasts and osteoclasts. Emerging evidence suggests that complement system is crucially involved in the regulation of functions of these cells, especially during inflammatory states. In this context, complement component 5a (C5a), a powerful pro-inflammatory anaphylatoxin that binds the receptor C5aR1, is known to regulate osteoclast formation and osteoblast inflammatory responses, and has thus been proposed as potential therapeutic target for the treatment of inflammatory bone diseases. In this review, we will analyze the role of C5a-C5aR1 axis in bone physiology and pathophysiology, describing its involvement in the pathogenesis of some of the most frequent inflammatory bone diseases such as rheumatoid arthritis, and also in osteoporosis and bone cancer and metastasis. Moreover, we will examine C5aR1-based pharmacological approaches that are available and have been tested so far for the treatment of these conditions. Given the growing interest of the scientific community on osteoimmunology, and the scarcity of data regarding the role of C5a-C5aR1 axis in bone pathophysiology, we will highlight the importance of this axis in mediating the interactions between skeletal and immune systems and its potential use as a therapeutic target.

KEYWORDS

C5a, C5aR1, bone, rheumatoid arthritis, osteoclasts, osteoblasts

Introduction

Complement component 5a (C5a) is one of the most potent inflammatory proteins of the complement system. It results from the cleavage of the precursor protein C5 by the enzyme C5 convertases and binds to C5a receptor 1 (C5aR1 or CD88) (Ehrnthaller et al., 2011) and C5aR2 (C5a receptor-like two or C5L2), which are expressed on the surface of immune cells and, also, ubiquitously on other cell types (Monk et al., 2007). As complement component 3a (C3a), C5a is an anaphylatoxin, whose activation leads to clearance of foreign cells, vasodilation, chemotaxis of inflammatory cells, cytokine and

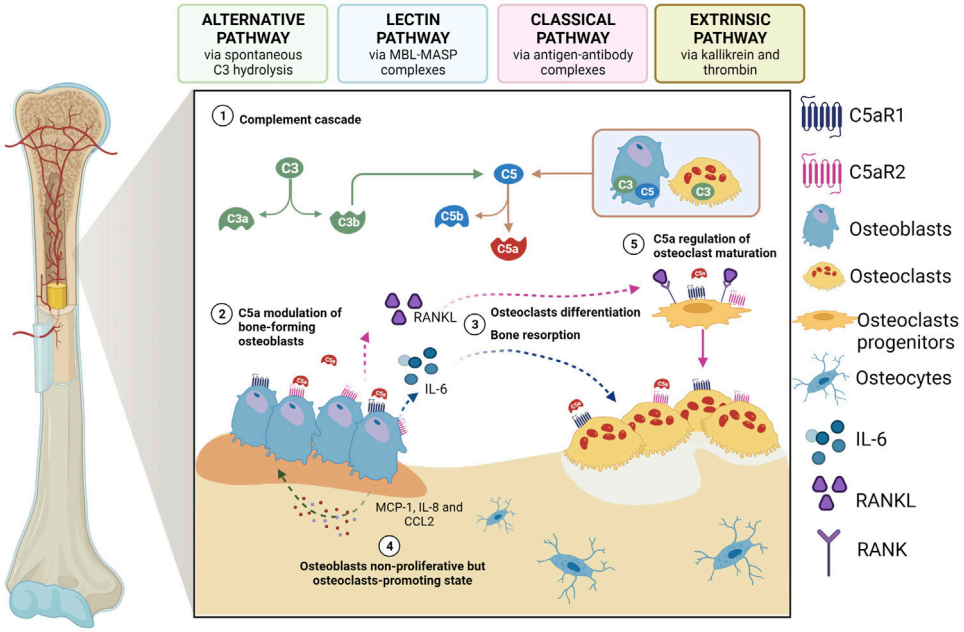

FIGURE 1
The role of C5a as a modulator of osteoblast-osteoclast interplay. 1) Activated complement system leads to the generation of C5a which can bind to C5aR1/2 on osteoblasts; 2) once activated by C5a, osteblasts start to release IL-6 and RANKL, thus inducing 3) osteoclastogenesis and bone resorption as well as differentiation of osteoclast progenitors; 4) activated osteoblasts can also secrete other chemokines and cytokines, such as MCP-1, CCL2 and IL-8, which in turn act on osteoblasts inducing a non-proliferative osteoclast-promoting state; 5) C5a also regulates the first phase of osteoclastogenesis maturation. Created with BioRender.com.

chemokine release, oxidative burst of immune cells (Guo and Ward, 2005) and induction and amplification of inflammatory reactions (Ricklin et al., 2010).

Besides its crucial role in the immune system-mediated protection from internal and external threats, C5a and its widely expressed receptors are also emerging as important players in different pathophysiological processes (Zheng et al., 2019; Carvelli et al., 2020; Giorgio et al., 2021; Wu et al., 2022). In addition to its activation in response to pathogens in fact, C5a formation can be also triggered by complement-independent enzymes, such as thrombin, neutrophil elastase and a macrophage serine protease, which have C5 convertase (C5a-generating) activity (Huber-Lang et al., 2015) and can thus activate C5a in tissues in response to several stimuli. Among the processes and tissues that are targets of C5a functions, growing evidence has shown that C5a-C5aR axis has an impact on the skeletal system, where it regulates bone metabolism and turnover both under physiological and pathophysiological conditions (Modinger et al., 2018).

In this mini-review, we will discuss the role of the C5a-C5aR1 axis in bone physiology and pathology, focusing on its involvement in the pathogenesis of inflammatory disorders of the skeletal system, as in particular rheumatoid arthritis, and also osteoporosis and cancer metastasis to the bones.

The role of C5a in bone physiology

Bone is an extremely dynamic tissue that undergoes continuous remodeling during the lifetime, and this process is carried out by three types of cells (Ponzetti and Rucci, 2019): osteoclasts, which are bone-resorbing cells deriving from stem cells of the macrophage-hematopoietic lineage; osteoblasts, that are bone-forming cells (Matsuoka et al., 2014); and osteocytes, which are former osteoblasts buried in the bone mineral matrix (Metzger and Narayanan, 2019).

In physiological conditions, studies have been indicating a direct involvement of complement system in bone development and homeostasis. In support of this, osteoblasts express both C3 and C5, while osteoclasts express only C3, but both cells are able to cleave C5 (and not C3) and generate C5a. Moreover, the receptors C3aR, C5aR1 and C5aR2 are expressed on both cell types (Ignatius et al., 2011a) (Figure 1). Multiple complement components, including C3 and C5, were described to have a characteristic expression pattern in distinct zones of the epiphyseal growth plate, suggesting a role for complement during bone development (Andrades et al., 1996). The specific expression of C5 in the hypertrophic zone of the growth plate together with the evidence that C5-deficient mice have thicker epiphyseal growth plates, potentially due to delayed endochondral ossification, suggest in fact that C5 requirement

is important during bone formation and longitudinal bone growth (Ehrnthaller et al., 2013). Finally, C3a, C3aR, and C5aR have shown to be crucial for the regulation of calcified cartilage matrix degradation mediated by osteoclasts, the formation — but not the resorption activity — of which is significantly enhanced in the presence of C3a and C5a (Ignatius et al., 2011a; Kovtun et al., 2017).

Although no observations on bone malformations in development or bone density have been published in humans carrying C5 deficiency, and this is most probably due to the rarity of such condition and its lethality (i.e., Leiner`s disease, which is particularly fatal if not corrected at infancy) (Guenther, 1983), the relevance of the C5a-C5aR axis in bone formation and regulation of its structure has been confirmed in preclinical studies. Twelve-week-old C5aR1-knockout (ko) and C5aR2-ko mice showed in fact a higher bone-mass phenotype compared to wild-type controls, and this effect was more pronounced in C5aR1-ko mice, where it was associated with decreased osteoclasts in trabecular bone (Kovtun et al., 2017). Moreover, pharmacological inhibition of C5a pathway during embryo-foetal development using avacopan, a small molecule C5aR antagonist (Harigai and Takada, 2022), induced an increased incidence of skeletal variations in hamsters, further confirming the role of the complement during bone development (European Medicines Agency, 2022).

In the adult skeleton, osteoclasts and osteoblasts, and their respective mesenchymal and haematopoietic precursors, closely interact and communicate in a fine-tuned balance that is a prerequisite for bone homeostasis. The C5a-C5aR1 axis plays a role in this context, as it can regulate the expression of different mediators that are involved in this process (Modinger et al., 2018). C5a can, for example, modulate the release of interleukin (IL)-6 from osteoblasts (Pobanz et al., 2000), thus inducing osteoclastogenesis and bone resorption (Ishimi et al., 1990), and this can happen *via* the induction of the expression of receptor activator of nuclear factor kappa-B (RANK) ligand (RANKL) in osteoblasts (Ishimi et al., 1990) or without its induction (Figure 1). Secreted by osteoblasts, RANKL stimulates osteoclastogenic differentiation by binding to its receptor RANK on the membrane of osteoclast-committed monocytes (Lacey et al., 1998), while other chemokines (e.g., monocyte chemoattractant protein-1 (MCP-1; CCL2) and cytokines, including IL-8 (CXCL8), act on osteoblasts inducing a non-proliferative but osteoclast-promoting state (Pathak et al., 2015) (Figure 1). Indeed, *in vitro* IL-8 stimulation has been shown to enhance IL-6 gene expression and protein production by human osteoblasts obtained from bone biopsies, indicating that IL-8-stimulated osteoblasts can produce factors that are essential for osteoclast formation (Pathak et al., 2015). Notably, the role of C5aR in regulating the first phases of osteoclast maturation has also been recently demonstrated in RAW264.7 cells (D'Angelo et al., 2020), which are murine monocytes/macrophages that upon treatment with RANKL can form multinucleated and functionally active osteoclast-like cells. Indeed, in these cells, both C5aR downregulation and antagonism—by C5aR antagonist PMX-53 and two newly synthesized allosteric C5aR antagonists, DF2593A and DF3016A—inhibited osteoclast maturation, as demonstrated by the reduced RANKL-triggered transcription of the most important osteoclast differentiation markers, such as NFATc1, MMP-9, cathepsin-K, and TRAP. Interestingly, it was observed that, as osteoclast differentiation progressed, C5aR mRNA expression decreased, with a consequent less impact of C5aR on the regulation of later events of osteoclast fusion (D'Angelo et al., 2020).

C5a can also induce the production of macrophage-colony stimulating factor (M-CSF) and plays a chemotactic role, together with the anaphylatoxin C3a, for immune cells, human mesenchymal stem cells (MSCs) (Schraufstatter et al., 2009; Moll et al., 2011), osteoclast and osteoblast precursors, and, at an even higher rate, for mature osteoblasts (Ignatius et al., 2011b).

Thus, complement proteins, and especially C5a-C5aR1 axis, are directly and indirectly involved in the physiology of the bone tissue during development and homeostasis (Pobanz et al., 2000; Ignatius et al., 2011a), as well as in its pathology, especially when a pro-inflammatory status develops in the bone environment (DiScipio et al., 2013). Indeed, the state of complement activation has been found to play a role in the development and progression of several bone-related inflammatory disorders, and in particular rheumatoid arthritis (RA), which is an excellent model of osteoimmunology because of the extensive involvement of the immune system in its pathogenesis, and also osteoporosis and cancer bone metastasis.

C5a in Rheumatoid Arthritis

Rheumatoid Arthritis (RA) is a systemic autoimmune disease that affects 0.24% of the general population worldwide, according to the Global Burden of Disease 2017 study (Disease, 2018; Safiri et al., 2019), with a higher prevalence in females than males. The risk to develop RA is age-dependent, with an incidence peak between 65 and 80 years of age and a lifetime risk of 1.7% in men compared to 3.6% in women (Crowson et al., 2011; Eriksson et al., 2013; World Health Organization, 2018). RA main clinical manifestations include pain and swelling of hands, wrists, and foot and knee (polyarthritis) joints. Some patients may also develop manifestations in other organs, even with no articular involvement, such as interstitial lung disease (ILD), pericarditis, pleural effusion, or bronchiectasis (Littlejohn and Monrad, 2018; Conforti et al., 2021). Treatment of RA is aimed at reducing joint inflammation and pain, preventing joint destruction and maximizing joint function: first-line RA treatments are nonsteroidal anti-inflammatory drugs (NSAIDs) (Bullock et al., 2018), and corticosteroids are also used, but for a short

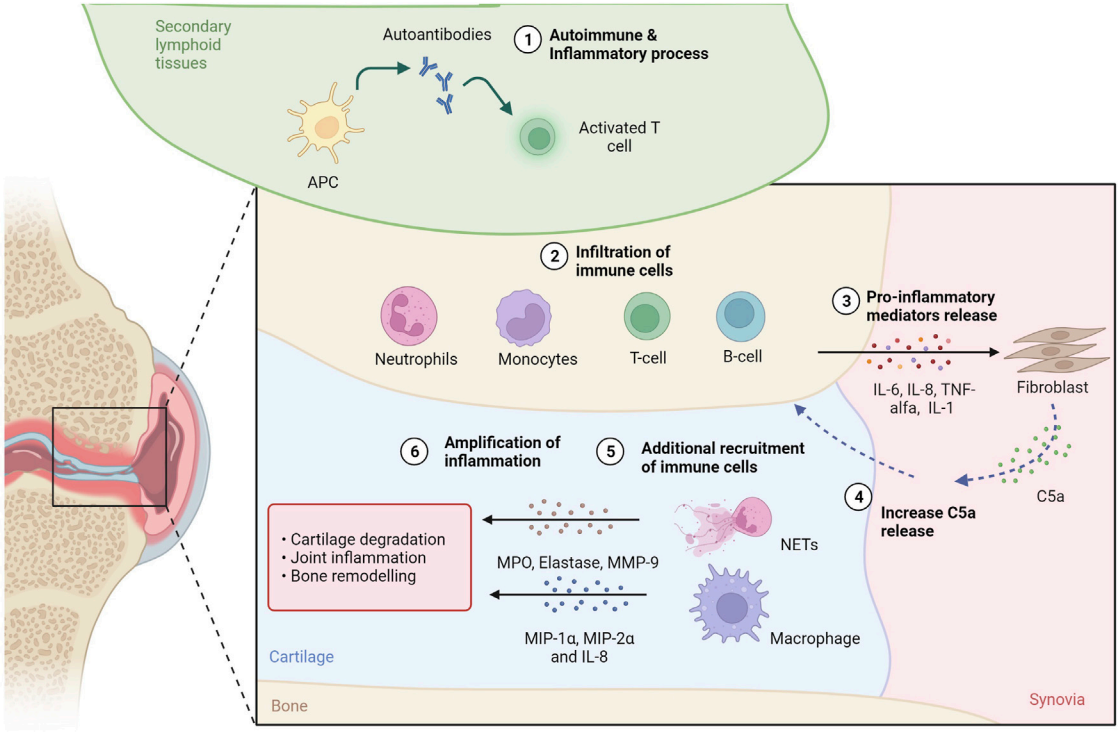

FIGURE 2
C5a in rheumatoid arthritis. In secondary tissues of RA patients, production of autoantibodies 1) activates inflammation and attracts immune cells 2), such as T and B lymphocytes, neutrophils and monocytes, to the inflammation site. The release of proinflammatory molecules 3) drives the proliferation of synovial tissue fibroblasts, which can contribute to the increase of C5a levels in the synovial fluid (SF) 4). C5a contributes to additional immune cell recruitment 5) and activation: neutrofils can undergo NETosis releasing proteaseses (i.e., MPO, elastase, MMP-9), while macrophages can release inflammatory proteins (i.e., MIP-1α, MIP-2α and IL-8). The release of proteases and proinflammatory proteins supports cartilage degradation, joint inflammation and bone remodeling, amplyfing the inflammatory state 6). Created with BioRender.com.

period of time and at low doses due to their greater side effects (Lim and Bolster, 2019). In addition, there are the disease-modifying antirheumatic drugs (DMARDs) that can be synthetic (small chemical molecules given orally) or biologic (proteins administered parenterally).

The etiology of RA remains unknown; however, it is generally accepted that it results from the combined effects of patients' genotype and environment (Klareskog et al., 2006). In RA patients, the persistent articular inflammation is driven by the proliferation of synovial tissue fibroblasts and by the infiltration of immune cells, such as T and B lymphocytes, neutrophils and monocytes, and induces the formation of the pannus, an abnormal synovial tissue, which invades and destroys local articular structures. The infiltrating cells of the pannus express pro-inflammatory cytokines, chemokines (as IL-6, IL-8, TNF-alfa and IL-1) and matrix metalloproteinases, such as MMP-2 and MMP-9, that contribute to a progressive distruction of both cartilage and bone (McInnes et al., 2016; Zhang, 2021).

Synovitis, swelling and joint damage are caused by a complex autoimmune and inflammatory process mediated by both the innate and adaptive immune systems (Gibofsky, 2014). Inflammatory cell recruitment into the synovial fluid and tissue occurs as a result of the organized action of chemoattractants (e.g., RANTES) and macrophage inflammatory proteins (i.e., MIP-1α, MIP-2α and IL-8) produced by activated macrophages, synovial fibroblasts, and other cells in the inflamed joint. The increase in inflammatory cells is also due to the chemotactic action of complement activation products, such as C5a, the level of which is increased in synovial fluid (SF) compared to plasma concentration (Moxley and Ruddy, 1985; Jose et al., 1990; Boackle, 2003) (Figure 2).

C5a is a potent neutrophil chemoattractant and priming agent that induces oxidative bursts and release of effector molecules from neutrophils and of cytokines from monocytes and macrophages (Hogasen et al., 1995). In RA, neutrophils and macrophages are the cells that primarily express C5aR (Hornum et al., 2017), also described as a key initiator of neutrophil adhesion (Miyabe et al., 2017). Interestingly, when neutrophils *in vitro* were exposed to GM-CSF and C5a, which are both abundant factors in RA, neutrophil extracellular traps (NETs) formation has been observed. NETs are networks of modified

histones (citH3), DNA fiber and antimicrobial proteins (MPO, elastase, others) released by neutrophils to entrap and facilitate the killing of pathogens in a process named NETosis (Disease, 2018). In RA pathogenesis, the role of NETosis has been investigated (Crowson et al., 2011; Eriksson et al., 2013), demonstrating that when NETosis occurs, citrullinated proteins are released and, when recognized by anti-citrullinated protein antibodies (ACPAs), initiate and propagate the aberrant immune responses and inflammation that is characteristic of RA (World Health Organization, 2018; Safiri et al., 2019). NETs have also been shown to provide a scaffold for the alternative complement pathway, leading to C5a generation. In addition, properdin, which is an essential positive regulator of the complement pathway that allows for the formation of the C3 convertase C3bBb of the alternative pathway and thus the formation of C5a, has also been observed to be present on NETs (Wang et al., 2015).

C5a/C5aR1 axis acts also on the luminal endothelium surface of the joint vasculature, where immune complexes that deposit in the joint can trigger C5a generation. Interestingly, the inhibition of NETosis by DNase one abrogated C5a production, ultimately reducing endothelial cell damage *in vitro* (Schreiber et al., 2017). C5a then binds to heparan sulfate proteoglycan (HSPG) on synovial endothelium, leading to the arrest of neutrophils *via* ß$_2$ integrin activation. This signalling causes the release of leukotriene B$_4$ (LTB$_4$), initiating autocrine/paracrine actions *via* the BLT1 receptor and allowing neutrophils to move from the blood vessel lumen into the interstitium. Neutrophils in the joint space can then propagate their survival *via* CXCL2-CXCR2 signaling (Sadik et al., 2018).

Thus, not only is C5a responsible for NET formation, but it can also be important for diapedisis into the joint, where the NETs can further damage cartilage and bone. Apart from causing damage in RA joints, NETs can further provide a scaffold for the alternative pathway, increasing formation of C5a and acting as an amplification loop for C5a production, recruitment of neutrophils into the joint, NET production, and cartilage and bone damage (Figure 2). Targeting C5a or the C5aR might thus be a viable solution for modulating NET formation in RA, thus preventing the destruction of cartilage (Carmona-Rivera et al., 2020) and bone (O'Neil et al., 2020) and reducing endothelial cell damage (Schreiber et al., 2017). In agreement, both genetic ablation or pharmacological inhibition of the C5a-C5aR axis improved arthritis or prevented the disease in animal studies (Wang et al., 1995; Goodfellow et al., 2000; Ames et al., 2001; Grant et al., 2002; Ji et al., 2002; Woodruff et al., 2002; Katschke et al., 2007; Banda et al., 2012). This strategy could be effective as it can target also the pro-osteoclastogenic effect of C5a that in the inflammed bone, as happens in RA and bone healing, enhances the inflammatory response of osteoblasts and increases osteoclast formation (Hornum et al., 2017; Modinger et al., 2018).

Other diseases

C5a/C5aR1 axis in osteoporosis-related bone fracture

Osteoporosis is a bone disease characterized by a decrease of bone mineral density and bone mass (Nikolaou et al., 2009). The etiologic determinants of osteoporosis include endocrine and metabolic conditions and mechanical factors, including sex, body size, race, family history, changes of hormones (postmenopausal hormonal condition, pregnancy), diet (insufficient vitamin D and calcium intake), lifestyle and long term use of certain medications (Yun and Lee, 2004). Specific pathologies, such as gastrointestinal diseases, RA, certain types of cancer, HIV/AIDS and anorexia nervosa, have also been considered as triggers of osteoporosis (Ginaldi et al., 2005). In osteoporosis patients, risk of bone fractures is raised and frequently associated with healing complications, prolonged hospitalization, and increased morbidity and mortality (Nikolaou et al., 2009; von Rüden and Augat, 2016; Giannoudis et al., 2007).

Emerging clinical and molecular data, along with a growing understanding of bone remodeling processes, have suggested that inflammation is crucially involved in bone turnover (Lorenzo, 2000) and healing, and thus in the onset of osteoporosis and recovery after fractures in these patients (Kiecolt-Glaser et al., 2003). Following an isolated fracture, the complement system critically modulates bone regeneration and healing (Huber-Lang et al., 2015), particularly through the C5a/C5aR1 axis (Bergdolt et al., 2017). C5a in fact is a strong activator of mast cells and triggers the rapid release of pre-formed granular factors (Moon et al., 2014; Erdei et al., 2004; el-Lati et al., 1994) that mediate osteoclastogenic effects (Kroner et al., 2017). C5aRs, on the other hand, are strongly expressed in the fracture callus, not only by immune cells, but also by bone cells and chondroblasts (Huber-Lang et al., 2015), and the relative spatial expression and functionality of the two C5a receptors on bone and immune cells during the healing period crucially influences post-fracture outcome (Ehrnthaller et al., 2013).

Genetically modified animal models have allowed to investigate and demonstrate the crucial role of the C5a/C5aR axis in fracture healing (Ehrnthaller et al., 2013). C5-deficient mice for example displayed a reduced volume and mechanical properties in fracture calluses, indicating impaired healing (Ehrnthaller et al., 2013). In addition, C5aR1 knockout mice showed a decrease of early inflammation in the fracture callus but also a disturbed final healing outcome in late healing stages, including the cartilage-to-bone transition (Kovtun et al., 2017). Interestingly, similarly disturbed fracture healing was also observed in C5aR2-ko mice subjected to a femur fracture (Kovtun et al., 2017). On the other hand, osteoblast-specific C5aR1-overexpression disturbed fracture healing in mice subjected to a femur fracture, with or without the induction of an additional systemic inflammation by thoracic trauma,

diminishing mechanical properties of the healed femur, reducing bone content of the fracture callus, and increasing impairment following severe trauma compared to wild-type littermates (Bergdolt et al., 2017). These data strongly suggest that the C5a/C5aR axis directly affect osteoblasts activity on bone healing and regeneration, exerting a fine and tight regulation of fracture healing during the entire process (Bergdolt et al., 2017).

C5a, bone cancer and neutrophil extracellular traps

Bone tumors represent a real challenge in oncology (Ferguson and Turner, 2018). They can grow as primary cancers or as consequence of metastatic colonization (Ferguson and Turner, 2018). Primary bone cancers are rare, accounting for about 0.2% of all malignancies worldwide, while secondary bone tumors represent one of the most common type of metastasis following advanced stages of lungs, liver, breast and prostate cancers (Coleman, 2001; Pullan and Budh, 2021). There are two main types of bone metastasis: the osteolytic lesions that are caused by the cancer cell-induced activation of osteoclastogenesis, which results in the complete destruction of bone and its substitution with cancer cells (Guise et al., 2006); and the osteosclerotic lesions, which are instead caused by aberrant osteoblast activation that produces low quality extra bone tissues (Ibrahim et al., 2010). Notably, the latter are also characterized by an increased osteoclast activity and bone resorption, which is needed to create the space for cancer cells to growth (Maurizi and Rucci, 2018).

C5a plays a crucial role in regulating tumor growth, metastasis, and drug resistance (Ajona et al., 2019). Expression of C5aR1 on cancer cells enhances their motility, invasiveness and epithelial to mesenchymal transition (Nitta et al., 2013; Maeda et al., 2015; Hu et al., 2016). In non-small-cell lung cancer (NSCLC) for example, higher C5aR1 levels in the primary tumor predict bone metastasis and result in decreased overall survival and relapse free survival (Ajona et al., 2018a). Accordingly, activation of the C5a/C5aR1 axis induced a pro-metastatic phenotype in lung cancer cells in culture, while favoring bone colonization *via* regulation of CXCL16 release, which in turns promotes a proosteoclastogenic environment in bone metastasis (Ajona et al., 2018a). In addition to cancer cells, osteoblasts also highly express C5aR1 (Bergdolt et al., 2017) further promoting a pro-metastatic environment. In response to C5a in fact, C5aR1 interacts with TLR2 in osteoblasts, promoting the upregulation of CXCL10 (Kwak et al., 2008; Mödinger et al., 2018), a chemokine that is critical for bone cancer cells recruitment, to support osteoclast differentiation and to promote the formation of osteolytic bone metastases (Lee et al., 2012).

Beside the direct actions on the bone, C5a/C5aR axis also exerts indirect pro-metastatic effects by inducing C5a-dependent recruitment of PMN-MDSCs (Corrales et al., 2012) that has been observed to facilitate metastasis. PMN-MDSCs can in fact suppress effector $CD8^+$ and $CD4^+$ T-cells responses in the lungs and livers of mice with breast malignancy (Vadrevu, 2014) and undergo NETosis. C5a enhances PMN-MDSC migration and invasion and, together with the costimulatory factor nuclear protein high mobility group box 1 (HMGB1) produced by cancer cells, induces the formation of NETs that in turn promote cancer cell dissemination and lung metastasis (Ortiz-Espinosa et al., 2022). Since NETs levels were shown to be elevated in multiple advanced cancer patients (Tohme et al., 2016; Rayes et al., 2019), further studies should be pursued to understand more in depth the contribution of C5a/C5aR1 axis and NETosis specifically during skeletal colonization.

C5a/C5aR targeting pharmacological approaches

Activation of the complement system is a major pathogenic event that drives various inflammatory responses in numerous diseases. For this reason, a large number of anti-complement drugs are in development, providing tools for blocking specific complement activation pathways, or isolated complement fragments, such as C5a (Floege and Feehally, 2013; Thurman and Le Quintrec, 2016; Thurman and Yapa, 2019).

Among the drugs targeting the C5a/C5aR1/C5aR2 axis that have reached the clinical phases of development for the treatment of various immunological disorders, some are still under evaluation in clinical trials (e.g., Zimura, Nomacopan, Tesidolumab and MOR-210), while some of them have been discontinued (e.g., PMX-53, MEDI-7814, Olendalizumab and others). Approved for clinical use is avacopan, a selective C5a receptor inhibitor, that has been tested for the treatment of ANCA-associated vasculitis with positive results (Jayne et al., 2017). Another available approach to block C5a biological activity is eculizumab, a monoclonal antibody targeting C5 that thus prevents the generation of both C5a and the terminal complement complex (Volokhina et al., 2015). Notably, a trial with eculizumab has been conducted in RA patients (Sadik et al., 2018), and the results from phase II suggested that inhibiting C5 might be a promising approach for the treatment of this disease. These data are in contrast with those of another study reporting that C5aR blockade by PMX-53 in RA patients failed to reduce effectively synovial inflammation (Vergunst et al., 2007), implying that further investigations are necessary to fully explore the role of C5a-C5aR inhibition in human RA.

Preclinical data have also shown that antagonizing C5aR1 after bone fracture in rats by a single application of PMX-53 immediately reversed the negative effect of the trauma-induced systemic inflammation on fracture healing outcome. However, when inhibiting C5aR1 in the early

inflammatory phase in a model of uneventful fracture healing with no additional traumatic injury, bone regeneration was unaffected (Takayanagi, 2012). Due to the paucity of data and in light of the fact that PMX-53 has being discontinued, further pre-clinical and clinical studies with novel drugs targeting C5a/C5aR axis for the treatment of fracture healing would be very useful.

Given the involvement of C5a/C5aR1 axis in the development of bone metastasis, studies have also aimed at finding the effect of C5aR1 inactivation in this context. In a syngeneic model of breast cancer for example, C5aR knockout mice or pharmacologic inhibition of C5aR1 reduced lung and liver metastatic burden, while CD8 T cells and inhibiting regulatory T cells were increased. In contrast, there was no significant effect on the growth of primary breast tumors (Ajona et al., 2018a). Moreover, both genetic ablation and pharmacological inhibition of C5a decreased bone metastasis in an *in vivo* mouse cancer model (Ajona et al., 2018b). Interestingly, incubation with DF3016A, a C5aR inhibitor, has been shown to diminish osteoclast-resorbing activity *in vitro* (D'Angelo et al., 2020). Thus, it has been suggested that DF3016A may be used as a potential double-edged blade treatment to fight bone metastases from several tumors, as it can both decrease the osteoclast activity required for the formation of the bone metastatic niche and act at the level of tumor cells by reducing their homing to bone (D'Angelo et al., 2020). Finally, blocking C5aR signaling promotes the anti-tumor efficacy of PD-1/PD-L1 blockade, while the combined immunotherapy based on C5a and PD-1 blockade has shown synergistic effects on both lung cancer growth and metastatic progression (Ajona et al., 2017).

Notably, from the available clinical data, chronic therapies with antagonists of the C5a/C5aR1/C5aR2 axis did not show consistent evident adverse effects on bone density and bone formation when administered in adult patients (Eschbach, 2000; Takata et al., 2004; ClinicalTrials.gov, 2021), thus suggesting that the use of C5 antagonists — even chronically — for related pathologies during post-natal/adult life can be relatively safe from the bone/skeletal point of view.

Conclusion

Growing evidence has demonstrated the role that C5a-C5aR1 axis plays in mediating the interactions between skeletal and immune systems, both in physiological conditions and in the pathogenesis of several bone inflammatory disorders. Thus, the combined used of standard therapies and of inhibitors of C5a-C5aR1 axis might be a successful strategy for the treatment of bone pathologies in which inflammation and complement system are known to be crucially involved, as rheumatoid arthritis in particular, for which also clinical trials have been conducted using C5aR1 inhibitors, but also for osteopenia and osteoporosis, fracture healing and metastatic bone disease. First preclinical and clinical data indicate that this approach has promises for all these conditions. Taking advantage of the numerous C5aR1 inhibitory compounds that are already available — and even approved for the clinical application — further studies are urgently needed to deeply investigate the effects of such approaches in the treatment of bone inflammatory conditions.

Author contributions

AR, AS, and SI performed data collection (literature reviewing) and prepared the original draft of the manuscript. RN revised and wrote the final version of the manuscript. SB, DK, PH, and AA revised and edited the manuscript for critically important intellectual content. PA conceptualized the study and reviewed and edited the manuscript.

Conflict of interest

AR, AS, RN, SI, AA, and PA are employees of Dompé Farmaceutici SpA.

The remaining authors declare that the research was conducted in the absence of any commercial or financial relationships that could be construed as a potential conflict of interest.

Publisher's note

References

Ajona, D., Ortiz-Espinosa, S., Moreno, H., Lozano, T., Pajares, M. J., Agorreta, J., et al. (2017). A combined PD-1/C5a blockade synergistically protects against lung cancer growth and metastasis. *Cancer Discov.* 7 (7), 694–703. doi:10.1158/2159-8290.CD-16-1184

Ajona, D., Ortiz-Espinosa, S., and Pio, R. (2019). Complement anaphylatoxins C3a and C5a: Emerging roles in cancer progression and treatment. *Semin. Cell Dev. Biol.* 85, 153–163. doi:10.1016/j.semcdb.2017.11.023

Ajona, D., Zandueta, C., Corrales, L., Moreno, H., Pajares, M. J., Ortiz-Espinosa, S., et al. (2018). Blockade of the complement C5a/C5aR1 axis impairs lung cancer bone metastasis by CXCL16-mediated effects. *Am. J. Respir. Crit. Care Med.* 197 (9), 1164–1176. doi:10.1164/rccm.201703-0660OC

Ajona, D., Zandueta, C., Corrales, L., Moreno, H., Pajares, M. J., Ortiz-Espinosa, S., et al. (2018). Blockade of the complement C5a/C5aR1 Axis impairs lung cancer

bone metastasis by CXCL16-mediated effects. *Am. J. Respir. Crit. Care Med.* 197 (9), 1164–1176. doi:10.1164/rccm.201703-0660OC

Ames, R. S., Lee, D., Foley, J. J., Jurewicz, A. J., Tornetta, M. A., Bautsch, W., et al. (2001). Identification of a selective nonpeptide antagonist of the anaphylatoxin C3a receptor that demonstrates antiinflammatory activity in animal models. *J. Immunol.* 166 (10), 6341–6348. doi:10.4049/jimmunol.166.10.6341

Andrades, J. A., Nimni, M. E., Becerra, J., Eisenstein, R., Davis, M., Sorgente, N., et al. (1996). Complement proteins are present in developing endochondral bone and may mediate cartilage cell death and vascularization. *Exp. Cell Res.* 227 (2), 208–213. doi:10.1006/excr.1996.0269

Banda, N. K., Hyatt, S., Antonioli, A. H., White, J. T., Glogowska, M., Takahashi, K., et al. (2012). Role of C3a receptors, C5a receptors, and complement protein C6 deficiency in collagen antibody-induced arthritis in mice. *J. Immunol.* 188 (3), 1469–1478. doi:10.4049/jimmunol.1102310

Bergdolt, S., Kovtun, A., Hagele, Y., Liedert, A., Schinke, T., Amling, M., et al. (2017). Osteoblast-specific overexpression of complement receptor C5aR1 impairs fracture healing. *PLoS One* 12 (6), e0179512. doi:10.1371/journal.pone.0179512

Boackle, S. A. (2003). Complement and autoimmunity. *Biomed. Pharmacother.* 57 (7), 269–273. doi:10.1016/s0753-3322(03)00084-2

Bullock, J., Rizvi, S. A. A., Saleh, A. M., Ahmed, S. S., Do, D. P., Ansari, R. A., et al. (2018). Rheumatoid arthritis: A brief overview of the treatment. *Med. Princ. Pract.* 27 (6), 501–507. doi:10.1159/000493390

Carmona-Rivera, C., Carlucci, P. M., Goel, R. R., James, E., Brooks, S. R., Rims, C., et al. (2020). Neutrophil extracellular traps mediate articular cartilage damage and enhance cartilage component immunogenicity in rheumatoid arthritis. *JCI Insight* 5 (13), 139388. doi:10.1172/jci.insight.139388

Carvelli, J., Demaria, O., Vely, F., Batista, L., Chouaki Benmansour, N., Fares, J., et al. (2020). Association of COVID-19 inflammation with activation of the C5a-C5aR1 axis. *Nature* 588 (7836), 146–150. doi:10.1038/s41586-020-2600-6

ClinicalTrials.gov (2021). *Identifier NCT03301467, controlled trial evaluating avacopan in C3 glomerulopathy (ACCOLADE).* Bethesda (MD): National Library of Medicine US. Available at: https://clinicaltrials.gov/ct2/show/NCT03301467.

Coleman, R. E. (2001). Metastatic bone disease: Clinical features, pathophysiology and treatment strategies. *Cancer Treat. Rev.* 27 (3), 165–176. doi:10.1053/ctrv.2000.0210

Conforti, A., Di Cola, I., Pavlych, V., Ruscitti, P., Berardicurti, O., Ursini, F., et al. (2021). Beyond the joints, the extra-articular manifestations in rheumatoid arthritis. *Autoimmun. Rev.* 20 (2), 102735. doi:10.1016/j.autrev.2020.102735

Corrales, L., Ajona, D., Rafail, S., Lasarte, J. J., Riezu-Boj, J. I., Lambris, J. D., et al. (2012). Anaphylatoxin C5a creates a favorable microenvironment for lung cancer progression. *J. Immunol.* 189 (9), 4674–4683. doi:10.4049/jimmunol.1201654

Crowson, C. S., Matteson, E. L., Myasoedova, E., Michet, C. J., Ernste, F. C., Warrington, K. J., et al. (2011). The lifetime risk of adult-onset rheumatoid arthritis and other inflammatory autoimmune rheumatic diseases. *Arthritis Rheum.* 63 (3), 633–639. doi:10.1002/art.30155

D'Angelo, R., Mangini, M., Fonderico, J., Fulle, S., Mayo, E., Aramini, A., et al. (2020). Inhibition of osteoclast activity by complement regulation with DF3016A, a novel small-molecular-weight C5aR inhibitor. *Biomed. Pharmacother.* 123, 109764. doi:10.1016/j.biopha.2019.109764

DiScipio, R., Khaldoyanidi, S., Moya-Castro, R., and Schraufstatter, I. (2013). Complement C3a signaling mediates production of angiogenic factors in mesenchymal stem cells. *J. Biomed. Sci. Eng.* 6, 1–13. doi:10.4236/jbise.2013.68a1001

Disease, G. B. D. (2018). Injury I, prevalence C. Global, regional, and national incidence, prevalence, and years lived with disability for 354 diseases and injuries for 195 countries and territories, 1990-2017: A systematic analysis for the global burden of disease study 2017. *Lancet* 392 (10159), 1789–1858. doi:10.1016/S0140-6736(18)32279-7

Ehrnthaller, C., Huber-Lang, M., Nilsson, P., Bindl, R., Redeker, S., Recknagel, S., et al. (2013). Complement C3 and C5 deficiency affects fracture healing. *PloS one* 8 (11), e81341. doi:10.1371/journal.pone.0081341

Ehrnthaller, C., Ignatius, A., Gebhard, F., and Huber-Lang, M. (2011). New insights of an old defense system: Structure, function, and clinical relevance of the complement system. *Mol. Med.* 17 (3-4), 317–329. doi:10.2119/molmed.2010.00149

el-Lati, S. G., Dahinden, C. A., and Church, M. K. (1994). Complement peptides C3a- and C5a-induced mediator release from dissociated human skin mast cells. *J. Invest. Dermatol.* 102 (5), 803–806. doi:10.1111/1523-1747.ep12378589

Erdei, A., Andrásfalvy, M., Péterfy, H., Tóth, G., and Pecht, I. (2004). Regulation of mast cell activation by complement-derived peptides. *Immunol. Lett.* 92 (1), 39–42. doi:10.1016/j.imlet.2003.11.019

Eriksson, J. K., Neovius, M., Ernestam, S., Lindblad, S., Simard, J. F., Askling, J., et al. (2013). Incidence of rheumatoid arthritis in Sweden: A nationwide population-based assessment of incidence, its determinants, and treatment penetration. *Arthritis Care Res.* 65 (6), 870–878. doi:10.1002/acr.21900

Eschbach, J. W. (2000). Current concepts of anemia management in chronic renal failure: Impact of NKF-doqi. *Semin. Nephrol.* 20 (4), 320–329.

European Medicines Agency (2022). EMEA/H/C/005523 Summary of product characteristics. Available at: https://www.ema.europa.eu/en/documents/product-information/tavneos-epar-product-information_en.pdf.

Ferguson, J. L., and Turner, S. P. (2018). Bone cancer: Diagnosis and treatment principles. *Am. Fam. Physician* 98 (4), 205–213.

Floege, J., and Feehally, J. (2013). Treatment of IgA nephropathy and henoch–schönlein nephritis. *Nat. Rev. Nephrol.* 9 (6), 320–327. doi:10.1038/nrneph.2013.59

Giannoudis, P., Tzioupis, C., Almalki, T., and Buckley, R. (2007). Fracture healing in osteoporotic fractures: Is it really different? A basic science perspective. *Injury* 38 (1), S90–S99. doi:10.1016/j.injury.2007.02.014

Gibofsky, A. (2014). Epidemiology, pathophysiology, and diagnosis of rheumatoid arthritis: A synopsis. *Am. J. Manag. Care* 20 (7), S128–S135.

Ginaldi, L., Di Benedetto, M. C., and De Martinis, M. (2005). Osteoporosis, inflammation and ageing. *Immun. Ageing* 2, 14. doi:10.1186/1742-4933-2-14

Giorgio, C., Zippoli, M., Cocchiaro, P., Castelli, V., Varrassi, G., Aramini, A., et al. (2021). Emerging role of C5 complement pathway in peripheral neuropathies: Current treatments and future perspectives. *Biomedicines* 9 (4), 399. doi:10.3390/biomedicines9040399

Goodfellow, R. M., Williams, A., Levin, J., Williams, B. D., and Morgan, B. (2000). Soluble complement receptor one (sCR1) inhibits the development and progression of rat collagen-induced arthritis. *Clin. Exp. Immunol.* 119 (1), 210–216. doi:10.1046/j.1365-2249.2000.01129.x

Grant, E. P., Picarella, D., Burwell, T., Delaney, T., Croci, A., Avitahl, N., et al. (2002). Essential role for the C5a receptor in regulating the effector phase of synovial infiltration and joint destruction in experimental arthritis. *J. Exp. Med.* 196 (11), 1461–1471. doi:10.1084/jem.20020205

Guenther, L. C. (1983). Inherited disorders of complement. *J. Am. Acad. Dermatol.* 9 (6), 815–839. doi:10.1016/s0190-9622(83)70195-7

Guise, T. A., Mohammad, K. S., Clines, G., Stebbins, E. G., Wong, D. H., Higgins, L. S., et al. (2006). Basic mechanisms responsible for osteolytic and osteoblastic bone metastases. *Clin. Cancer Res.* 12 (20), 6213s–6s. doi:10.1158/1078-0432.CCR-06-1007

Guo, R. F., and Ward, P. A. (2005). Role of C5a in inflammatory responses. *Annu. Rev. Immunol.* 23, 821–852. doi:10.1146/annurev.immunol.23.021704.115835

Harigai, M., and Takada, H. (2022). Avacopan, a selective C5a receptor antagonist, for anti-neutrophil cytoplasmic antibody-associated vasculitis. *Mod. Rheumatol.* 32 (3), 475–483. doi:10.1093/mr/roab104

Hogasen, K., Mollnes, T. E., Harboe, M., Gotze, O., Hammer, H. B., Oppermann, M., et al. (1995). Terminal complement pathway activation and low lysis inhibitors in rheumatoid arthritis synovial fluid. *J. Rheumatol.* 22 (1), 24–28.

Hornum, L., Hansen, A. J., Tornehave, D., Fjording, M. S., Colmenero, P., Watjen, I. F., et al. (2017). C5a and C5aR are elevated in joints of rheumatoid and psoriatic arthritis patients, and C5aR blockade attenuates leukocyte migration to synovial fluid. *PLoS One* 12 (12), e0189017. doi:10.1371/journal.pone.0189017

Hu, W-H., Hu, Z., Shen, X., Dong, L-Y., Zhou, W-Z., Yu, X-X., et al. (2016). C5a receptor enhances hepatocellular carcinoma cell invasiveness via activating ERK1/2-mediated epithelial–mesenchymal transition. *Exp. Mol. Pathol.* 100 (1), 101–108. doi:10.1016/j.yexmp.2015.10.001

Huber-Lang, M., Ignatius, A., and Brenner, R. E. *Role of complement on broken surfaces after Trauma2015.* Cham: Springer International Publishing.

Ibrahim, T., Flamini, E., Mercatali, L., Sacanna, E., Serra, P., Amadori, D., et al. (2010). Pathogenesis of osteoblastic bone metastases from prostate cancer. *Cancer* 116 (6), 1406–1418. doi:10.1002/cncr.24896

Ignatius, A., Ehrnthaller, C., Brenner, R. E., Kreja, L., Schoengraf, P., Lisson, P., et al. (2011). The anaphylatoxin receptor C5aR is present during fracture healing in rats and mediates osteoblast migration *in vitro*. *J. Trauma* 71 (4), 952–960. doi:10.1097/TA.0b013e3181f8aa2d

Ignatius, A., Schoengraf, P., Kreja, L., Liedert, A., Recknagel, S., Kandert, S., et al. (2011). Complement C3a and C5a modulate osteoclast formation and inflammatory response of osteoblasts in synergism with IL-1β. *J. Cell. Biochem.* 112 (9), 2594–2605. doi:10.1002/jcb.23186

Ishimi, Y., Miyaura, C., Jin, C. H., Akatsu, T., Abe, E., Nakamura, Y., et al. (1990). IL-6 is produced by osteoblasts and induces bone resorption. *J. Immunol.* 145 (10), 3297–3303.

Jayne, D. R. W., Bruchfeld, A. N., Harper, L., Schaier, M., Venning, M. C., Hamilton, P., et al. (2017). Randomized trial of C5a receptor inhibitor avacopan in ANCA-associated vasculitis. *J. Am. Soc. Nephrol.* 28 (9), 2756–2767. doi:10.1681/ASN.2016111179

Ji, H., Ohmura, K., Mahmood, U., Lee, D. M., Hofhuis, F. M., Boackle, S. A., et al. (2002). Arthritis critically dependent on innate immune system players. *Immunity* 16 (2), 157–168. doi:10.1016/s1074-7613(02)00275-3

Jose, P., Moss, I., Maini, R., and Williams, T. (1990). Measurement of the chemotactic complement fragment C5a in rheumatoid synovial fluids by radioimmunoassay: Role of C5a in the acute inflammatory phase. *Ann. Rheum. Dis.* 49 (10), 747–752. doi:10.1136/ard.49.10.747

Katschke, K. J., Jr, Helmy, K. Y., Steffek, M., Xi, H., Yin, J., Lee, W. P., et al. (2007). A novel inhibitor of the alternative pathway of complement reverses inflammation and bone destruction in experimental arthritis. *J. Exp. Med.* 204 (6), 1319–1325. doi:10.1084/jem.20070432

Kiecolt-Glaser, J. K., Preacher, K. J., MacCallum, R. C., Atkinson, C., Malarkey, W. B., Glaser, R., et al. (2003). Chronic stress and age-related increases in the proinflammatory cytokine IL-6. *Proc. Natl. Acad. Sci. U. S. A.* 100 (15), 9090–9095. doi:10.1073/pnas.1531903100

Klareskog, L., Padyukov, L., Ronnelid, J., and Alfredsson, L. (2006). Genes, environment and immunity in the development of rheumatoid arthritis. *Curr. Opin. Immunol.* 18 (6), 650–655. doi:10.1016/j.coi.2006.06.004

Kovtun, A., Bergdolt, S., Hägele, Y., Matthes, R., Lambris, J. D., Huber-Lang, M., et al. (2017). Complement receptors C5aR1 and C5aR2 act differentially during the early immune response after bone fracture but are similarly involved in bone repair. *Sci. Rep.* 7 (1), 14061. doi:10.1038/s41598-017-14444-3

Kroner, J., Kovtun, A., Kemmler, J., Messmann, J. J., Strauss, G., Seitz, S., et al. (2017). Mast cells are critical regulators of bone fracture–induced inflammation and osteoclast formation and activity. *J. Bone Min. Res.* 32 (12), 2431–2444. doi:10.1002/jbmr.3234

Kwak, H. B., Ha, H., Kim, H. N., Lee, J. H., Kim, H. S., Lee, S., et al. (2008). Reciprocal cross-talk between RANKL and interferon-γ–inducible protein 10 is responsible for bone-erosive experimental arthritis. *Arthritis Rheum.* 58 (5), 1332–1342. doi:10.1002/art.23372

Lacey, D. L., Timms, E., Tan, H. L., Kelley, M. J., Dunstan, C. R., Burgess, T., et al. (1998). Osteoprotegerin ligand is a cytokine that regulates osteoclast differentiation and activation. *Cell* 93 (2), 165–176. doi:10.1016/s0092-8674(00)81569-x

Lee, J-H., Kim, H-N., Kim, K-O., Jin, W. J., Lee, S., Kim, H-H., et al. (2012). CXCL10 promotes osteolytic bone metastasis by enhancing cancer outgrowth and osteoclastogenesis. *Cancer Res.* 72 (13), 3175–3186. doi:10.1158/0008-5472.CAN-12-0481

Lim, S. Y., and Bolster, M. B. (2019). *Corticosteroids. Neurorheumatology*. New York: Springer, 261–267.

Littlejohn, E. A., and Monrad, S. U. (2018). Early diagnosis and treatment of rheumatoid arthritis. *Prim. Care* 45 (2), 237–255. doi:10.1016/j.pop.2018.02.010

Lorenzo, J. (2000). Interactions between immune and bone cells: New insights with many remaining questions. *J. Clin. Invest.* 106 (6), 749–752. doi:10.1172/JCI11089

Maeda, Y., Kawano, Y., Wada, Y., Yatsuda, J., Motoshima, T., Murakami, Y., et al. (2015). C5aR is frequently expressed in metastatic renal cell carcinoma and plays a crucial role in cell invasion via the ERK and PI3 kinase pathways. *Oncol. Rep.* 33 (4), 1844–1850. doi:10.3892/or.2015.3800

Matsuoka, K., Park, K. A., Ito, M., Ikeda, K., and Takeshita, S. (2014). Osteoclast-derived complement component 3a stimulates osteoblast differentiation. *J. Bone Min. Res.* 29 (7), 1522–1530. doi:10.1002/jbmr.2187

Maurizi, A., and Rucci, N. (2018). The osteoclast in bone metastasis: Player and target. *Cancers* 10 (7), 218. doi:10.3390/cancers10070218

McInnes, I. B., Buckley, C. D., and Isaacs, J. D. (2016). Cytokines in rheumatoid arthritis - shaping the immunological landscape. *Nat. Rev. Rheumatol.* 12 (1), 63–68. doi:10.1038/nrrheum.2015.171

Metzger, C. E., and Narayanan, S. A. (2019). The role of osteocytes in inflammatory bone loss. *Front. Endocrinol.* 10, 285. doi:10.3389/fendo.2019.00285

Miyabe, Y., Miyabe, C., Murooka, T. T., Kim, E. Y., Newton, G. A., Kim, N. D., et al. (2017). Complement C5a receptor is the key initiator of neutrophil adhesion igniting immune complex–induced arthritis. *Sci. Immunol.* 2 (7), eaaj2195. doi:10.1126/sciimmunol.aaj2195

Modinger, Y., Loffler, B., Huber-Lang, M., and Ignatius, A. (2018). Complement involvement in bone homeostasis and bone disorders. *Semin. Immunol.* 37, 53–65. doi:10.1016/j.smim.2018.01.001

Mödinger, Y., Rapp, A., Pazmandi, J., Vikman, A., Holzmann, K., Haffner-Luntzer, M., et al. (2018). C5aR1 interacts with TLR 2 in osteoblasts and stimulates the osteoclast-inducing chemokine CXCL 10. *J. Cell. Mol. Med.* 22 (12), 6002–6014. doi:10.1111/jcmm.13873

Moll, G., Jitschin, R., Von Bahr, L., Rasmusson-Duprez, I., Sundberg, B., Lönnies, L., et al. (2011). Mesenchymal stromal cells engage complement and complement receptor bearing innate effector cells to modulate immune responses. *PloS one* 6 (7), e21703. doi:10.1371/journal.pone.0021703

Monk, P. N., Scola, A. M., Madala, P., and Fairlie, D. P. (2007). Function, structure and therapeutic potential of complement C5a receptors. *Br. J. Pharmacol.* 152 (4), 429–448. doi:10.1038/sj.bjp.0707332

Moon, T. C., Befus, A. D., and Kulka, M. (2014). Mast cell mediators: Their differential release and the secretory pathways involved. *Front. Immunol.* 5, 569. doi:10.3389/fimmu.2014.00569

Moxley, G., and Ruddy, S. (1985). Elevated C3 anaphylatoxin levels in synovial fluids from patients with rheumatoid arthritis. *Arthritis Rheum.* 28 (10), 1089–1095. doi:10.1002/art.1780281003

Nikolaou, V. S., Efstathopoulos, N., Kontakis, G., Kanakaris, N. K., and Giannoudis, P. V. (2009). The influence of osteoporosis in femoral fracture healing time. *Injury* 40 (6), 663–668. doi:10.1016/j.injury.2008.10.035

Nitta, H., Wada, Y., Kawano, Y., Murakami, Y., Irie, A., Taniguchi, K., et al. (2013). Enhancement of human cancer cell motility and invasiveness by anaphylatoxin C5a via aberrantly expressed C5a receptor (CD88). *Clin. Cancer Res.* 19 (8), 2004–2013. doi:10.1158/1078-0432.CCR-12-1204

O'Neil, L. J., Barrera-Vargas, A., Sandoval-Heglund, D., Merayo-Chalico, J., Aguirre-Aguilar, E., Aponte, A. M., et al. (2020). Neutrophil-mediated carbamylation promotes articular damage in rheumatoid arthritis. *Sci. Adv.* 6 (44), eabd2688. doi:10.1126/sciadv.abd2688

Ortiz-Espinosa, S., Morales, X., Senent, Y., Alignani, D., Tavira, B., Macaya, I., et al. (2022). Complement C5a induces the formation of neutrophil extracellular traps by myeloid-derived suppressor cells to promote metastasis. *Cancer Lett.* 529, 70–84. doi:10.1016/j.canlet.2021.12.027

Pathak, J. L., Bakker, A. D., Verschueren, P., Lems, W. F., Luyten, F. P., Klein-Nulend, J., et al. (2015). CXCL8 and CCL20 enhance osteoclastogenesis via modulation of cytokine production by human primary osteoblasts. *PLOS ONE* 10 (6), e0131041. doi:10.1371/journal.pone.0131041

Pobanz, J. M., Reinhardt, R. A., Koka, S., and Sanderson, S. D. (2000). C5a modulation of interleukin-1 beta-induced interleukin-6 production by human osteoblast-like cells. *J. Periodontal Res.* 35 (3), 137–145. doi:10.1034/j.1600-0765.2000.035003137.x

Ponzetti, M., and Rucci, N. (2019). Updates on osteoimmunology: What's new on the cross-talk between bone and immune system. *Front. Endocrinol.* 10, 236. doi:10.3389/fendo.2019.00236

Pullan, J. E., and Budh, D. P. (2021). *Primary bone cancer. StatPearls*. statpearls: StatPearls Publishing.

Rayes, R. F., Mouhanna, J. G., Nicolau, I., Bourdeau, F., Giannias, B., Rousseau, S., et al. (2019). Primary tumors induce neutrophil extracellular traps with targetable metastasis-promoting effects. *JCI insight* 4 (16), 128008. doi:10.1172/jci.insight.128008

Ricklin, D., Hajishengallis, G., Yang, K., and Lambris, J. D. (2010). Complement: A key system for immune surveillance and homeostasis. *Nat. Immunol.* 11 (9), 785–797. doi:10.1038/ni.1923

Sadik, C. D., Miyabe, Y., Sezin, T., and Luster, A. D. (2018). The critical role of C5a as an initiator of neutrophil-mediated autoimmune inflammation of the joint and skin. *Semin. Immunol.* 37, 21–29. doi:10.1016/j.smim.2018.03.002

Safiri, S., Kolahi, A. A., Hoy, D., Smith, E., Bettampadi, D., Mansournia, M. A., et al. (2019). Global, regional and national burden of rheumatoid arthritis 1990-2017: A systematic analysis of the global burden of disease study 2017. *Ann. Rheum. Dis.* 78 (11), 1463–1471. doi:10.1136/annrheumdis-2019-215920

Schraufstatter, I. U., DiScipio, R. G., Zhao, M., and Khaldoyanidi, S. K. (2009). C3a and C5a are chemotactic factors for human mesenchymal stem cells, which cause prolonged ERK1/2 phosphorylation. *J. Immunol.* 182 (6), 3827–3836. doi:10.4049/jimmunol.0803055

Schreiber, A., Rousselle, A., Becker, J. U., von Massenhausen, A., Linkermann, A., Kettritz, R., et al. (2017). Necroptosis controls NET generation and mediates complement activation, endothelial damage, and autoimmune vasculitis. *Proc. Natl. Acad. Sci. U. S. A.* 114 (45), E9618-E9625. doi:10.1073/pnas.1708247114

Takata, H., Tomiyama, H., Fujiwara, M., Kobayashi, N., and Takiguchi, M. (2004). Cutting edge: Expression of chemokine receptor CXCR1 on human effector CD8+ T cells. *J. Immunol.* 173 (4), 2231–2235. doi:10.4049/jimmunol.173.4.2231

Takayanagi, H. (2012). New developments in osteoimmunology. *Nat. Rev. Rheumatol.* 8 (11), 684–689. doi:10.1038/nrrheum.2012.167

Thurman, J. M., and Le Quintrec, M. (2016). Targeting the complement cascade: Novel treatments coming down the pike. *Kidney Int.* 90 (4), 746–752. doi:10.1016/j.kint.2016.04.018

Thurman, J. M., and Yapa, R. (2019). Complement therapeutics in autoimmune disease. *Front. Immunol.* 10, 672. doi:10.3389/fimmu.2019.00672

Tohme, S., Yazdani, H. O., Al-Khafaji, A. B., Chidi, A. P., Loughran, P., Mowen, K., et al. (2016). Neutrophil extracellular traps promote the development and progression of liver metastases after surgical stress. *Cancer Res.* 76 (6), 1367–1380. doi:10.1158/0008-5472.CAN-15-1591

Vadrevu, C. (2014). C5a receptor facilitates cancer metastasis by altering T-cell responses in the metastatic niche. *Cancer Res.* 74, 3454. doi:10.1158/0008-5472.CAN-14-0157

Vergunst, C., Gerlag, D., Dinant, H., Schulz, L., Vinkenoog, M., Smeets, T., et al. (2007). Blocking the receptor for C5a in patients with rheumatoid arthritis does not reduce synovial inflammation. *Rheumatology* 46 (12), 1773–1778. doi:10.1093/rheumatology/kem222

Volokhina, E. B., Bergseth, G., van de Kar, N. C., van den Heuvel, L. P., and Mollnes, T. E. (2015). Eculizumab treatment efficiently prevents C5 cleavage without C5a generation *in vivo*. *Blood* 126 (2), 278–279. doi:10.1182/blood-2015-03-637645

von Rüden, C., and Augat, P. (2016). Failure of fracture fixation in osteoporotic bone. *Injury* 47, S3-S10. doi:10.1016/S0020-1383(16)47002-6

Wang, H., Wang, C., Zhao, M. H., and Chen, M. (2015). Neutrophil extracellular traps can activate alternative complement pathways. *Clin. Exp. Immunol.* 181 (3), 518–527. doi:10.1111/cei.12654

Wang, Y., Rollins, S. A., Madri, J. A., and Matis, L. A. (1995). Anti-C5 monoclonal antibody therapy prevents collagen-induced arthritis and ameliorates established disease. *Proc. Natl. Acad. Sci. U. S. A.* 92 (19), 8955–8959. doi:10.1073/pnas.92.19.8955

Woodruff, T. M., Strachan, A. J., Dryburgh, N., Shiels, I. A., Reid, R. C., Fairlie, D. P., et al. (2002). Antiarthritic activity of an orally active C5a receptor antagonist against antigen-induced monarticular arthritis in the rat. *Arthritis Rheum.* 46 (9), 2476–2485. doi:10.1002/art.10449

World Health Organization (2018). *Global health estimates 2016: Disease burden by cause, age, sex, by country and by region, 2000–2016*. Geneva: World Health Organization.

Wu, K. Y., Cao, B., Wang, C. X., Yang, X. L., Zhao, S. J., Diao, T. Y., et al. (2022). The C5a/C5aR1 Axis contributes to the pathogenesis of acute cystitis through enhancement of adhesion and colonization of uropathogenic *E. coli*. *Front. Cell. Infect. Microbiol.* 12, 824505. doi:10.3389/fcimb.2022.824505

Yun, A. J., and Lee, P. Y. (2004). Maldaptation of the link between inflammation and bone turnover may be a key determinant of osteoporosis. *Med. Hypotheses* 63 (3), 532–537. doi:10.1016/S0306-9877(03)00326-8

Zhang, C. (2021). Flare-up of cytokines in rheumatoid arthritis and their role in triggering depression: Shared common function and their possible applications in treatment (Review). *Biomed. Rep.* 14 (1), 16. doi:10.3892/br.2020.1392

Zheng, Q. Y., Liang, S. J., Xu, F., Li, G. Q., Luo, N., Wu, S., et al. (2019). C5a/C5aR1 pathway is critical for the pathogenesis of psoriasis. *Front. Immunol.* 10, 1866. doi:10.3389/fimmu.2019.01866

frontiers | Frontiers in Cell and Developmental Biology

TYPE Review
PUBLISHED 12 August 2022
DOI 10.3389/fcell.2022.932065

OPEN ACCESS

EDITED BY
Maria-Bernadette Madel,
Baylor College of Medicine,
United States

REVIEWED BY
Tim Cundy,
The University of Auckland,
New Zealand
Omar Albagha,
Hamad Bin Khalifa University, Qatar
Ian R. Reid,
The University of Auckland,
New Zealand

*CORRESPONDENCE
Luigi Gennari,
luigi.gennari@unisi.it
Alberto Falchetti,
alberto.falchetti@auxologico.it

SPECIALTY SECTION
This article was submitted to Cellular Biochemistry,
a section of the journal
Frontiers in Cell and Developmental Biology

RECEIVED 29 April 2022
ACCEPTED 25 July 2022
PUBLISHED 12 August 2022

CITATION
Gennari L, Rendina D, Merlotti D, Cavati G, Mingiano C, Cosso R, Materozzi M, Pirrotta F, Abate V, Calabrese M and Falchetti A (2022), Update on the pathogenesis and genetics of Paget's disease of bone. *Front. Cell Dev. Biol.* 10:932065. doi: 10.3389/fcell.2022.932065

Update on the pathogenesis and genetics of Paget's disease of bone

Luigi Gennari[1]*, Domenico Rendina[2], Daniela Merlotti[3], Guido Cavati[1], Christian Mingiano[1], Roberta Cosso[4], Maria Materozzi[1,5], Filippo Pirrotta[1], Veronica Abate[2], Marco Calabrese[1] and Alberto Falchetti[6]*

[1]Department of Medicine Surgery and Neurosciences, University of Siena Italy, Siena, Italy, [2]Department of Clinical Medicine and Surgery, Federico II University, Naples, Italy, [3]Department of Medical Sciences, Azienda Ospedaliera Universitaria Senese, Siena, Italy, [4]Unit of Rehabilitation Medicine, San Giuseppe Hospital, Istituto Auxologico Italiano, Piancavallo, Italy, [5]Age Related Diseases Unit, Division of Genetics and Cell Biology, San Raffaele Scientific Institute, Milano, Italy, [6]Experimental Research Laboratory on Bone Metabolism, Istituto di Ricovero e Cura a Carattere Scientifico (IRCCS), Istituto Auxologico Italiano, Milano, Italy

Studies over the past two decades have led to major advances in the pathogenesis of Paget's disease of bone (PDB) and particularly on the role of genetic factors. Germline mutations of different genes have been identified, as a possible cause of this disorder, and most of the underlying pathways are implicated in the regulation of osteoclast differentiation and function, whereas other are involved in cell autophagy mechanisms. In particular, about 30 different germline mutations of the *Sequestosome 1* gene (*SQSTM1*) have been described in a significant proportion of familial and sporadic PDB cases. The majority of *SQSTM1* mutations affect the ubiquitin-binding domain of the protein and are associated to a more severe clinical expression of the disease. Also, germline mutations in the *ZNF687* and *PFN1* genes have been associated to severe, early onset, polyostotic PDB with increased susceptibly to neoplastic degeneration, particularly giant cell tumor. Mutations in the *VCP* (Valosin Containing Protein) gene cause the autosomal dominant syndrome "Inclusion Body Myopathy, PDB, Fronto-temporal Dementia," characterized by pagetic manifestations, associated with myopathy, amyotrophic lateral sclerosis and fronto-temporal dementia. Moreover, germline mutations in the *TNFRSF11A* gene, which encodes for RANK, were associated with rare syndromes showing some histopathological, radiological, and clinical overlap with PDB and in two cases of early onset PDB-like disease. Likewise, genome wide association studies performed in unrelated PDB cases identified other potential predisposition genes and/or susceptibility loci. Thus, it is likely that polygenic factors are involved in the PDB pathogenesis in many individuals and that modifying genes may contribute in refining the clinical phenotype. Moreover, the contribution of somatic mutations of *SQSTM1* gene and/or epigenetic mechanisms in the pathogenesis of skeletal pagetic abnormalities and eventually neoplastic degeneration, cannot be excluded. Indeed, clinical and experimental observations indicate that genetic susceptibility might not be a sufficient condition for the clinical development of PDB without the

concomitant intervention of viral infection, in primis paramixoviruses, and/or other environmental factors (e.g., pesticides, heavy metals or tobacco exposure), at least in a subset of cases. This review summarizes the most important advances that have been made in the field of cellular and molecular biology PDB over the past decades.

KEYWORDS

Paget's disease of bone, osteoclast (OCs), genetics, viral inclusion, environmental factors

1 Introduction

Paget's disease of bone (PDB) is a chronic focal disorder of bone remodeling, affecting one (monostotic form) or more bones (polyostotic form) which are typically enlarged and deformed. The affected skeletal sites are generally asymmetric and most frequently include the pelvis, spine, skull, femur and tibia (one or more of these skeletal sites are affected in up to 90% of cases) (Gennari et al., 2019). The disease was first described in England, in 1877, by Sir James Paget who defined it with the name of "osteitis deformans" (Paget, 1877). However, this morbid picture is certainly older, so much that the first pagetic femur dates back to about three thousand years ago (Ortner and Putschar, 1981). Indeed, albeit with limits, lesions somewhat suggestive of the disease have even been supposed in vertebral bodies of dinosaurs from the late Palaeozoic to the mid Mesozoic eras (Witzmann et al., 2011; Haridy et al., 2019).

The prevalence of PDB is difficult to quantify due to the fact that it is often asymptomatic, especially in the first years after onset. It is very rare in people under the age of 30 years and it is generally diagnosed after the age of 50. On the basis of initial autopsy findings reported in the 1930s, prevalence rates around 2%–4% have been estimated for subjects over the age of 50, and the probability of its occurrence increased with age reaching 10% or above in very elderly subjects (Cooper et al., 2006; Gennari et al., 2018). No more up-to-date data is available from autopsy studies. Moreover PDB appears to be prevalent in males (male to female ratio variable between 1.5 and 2) and was more frequently described in European Countries, with a particularly higher prevalence in UK (reaching 4%–6%), or in North America (up to 3% in subjects of European origin), Australia and New Zealand, where it mainly affects the descendants of the colonizers (Cooper et al., 2006; Gennari et al., 2018). Conversely it was more rarely described in Africa, Asia and the Scandinavian countries. However, information about PDB prevalence in non-Caucasian populations is very limited, and patient series of Asian and Indian ancestry have very recently been described (Asirvatham et al., 2020; Wang et al., 2020). There are also restricted geographic areas with a particularly high PDB prevalence such as the Lancashire region in England, the "La Cabrera" district in Spain and some districts of the Campania region in Italy, where an increased disease severity was also reported (Barker et al., 1980; Lopez-Abente et al., 2003; Gennari et al., 2006; Rendina et al., 2006). Most epidemiological studies have documented a gradual decrease in the prevalence and incidence of PDB over the years, which is associated with a parallel decline in mortality and clinical severity (Cundy et al., 1997; Cooper et al., 1999; Cook et al., 2021). More recent estimates in subjects aged 45 years and over suggested a PDB prevalence below 1%, including the high prevalence areas of United Kingdom (Abdulla et al., 2018; Mazières et al., 2018). In a last report from UK primary care records, the overall standardized incidence of clinically diagnosed PDB decreased from 0.75/10,000 person-years in 1999 to 0.20/10,000 person-years in 2015 (Cook et al., 2021).

The peculiar feature of PDB is represented by an exaggerated increase in bone resorption followed by a phase of increased formation; it is believed that this is due to a defect in the osteoclasts which are increased in number, size and quantity of nuclei per cell (Reddy et al., 1999; Roodman and Windle, 2005). Pagetic bone is the site of intense metabolic activity and is richly vascularized; however, despite the increase in size the pagetic tissue still has poor biomechanical efficiency due to its structural disorganization. These features can result in various clinical consequences, such as a tendency to compress the nerve structures within the affected bones, the presence of bone deformities, a greater risk of fracture, and a frequent association with forms of osteoarthritis secondary to skeletal deformity and abnormal joint load (Gennari et al., 2019). In some cases (less than 1%) neoplastic degeneration of pagetic tissue in osteosarcomas, fibrosarcomas, chondrosarcomas, or giant cell tumor (GCT) is also described (Hansen et al., 2006; Rendina et al., 2015).

The cause of PDB remains in part unknown. Two main hypotheses have been originally proposed, the genetic one and the one linked to the presence of environmental triggers (Roodman and Windle, 2005; Ralston et al., 2008; Gennari et al., 2019). Over the past two decades, important advances have been made in the field of cellular and molecular biology of PDB, and some genetic mutations have been identified as a possible cause of the disorder in up to 20%–30% of cases (Gennari et al., 2019; Makaram and Ralston, 2021). However, at least in a subset of cases, genetic susceptibility might not be a sufficient condition for the clinical development of PDB without

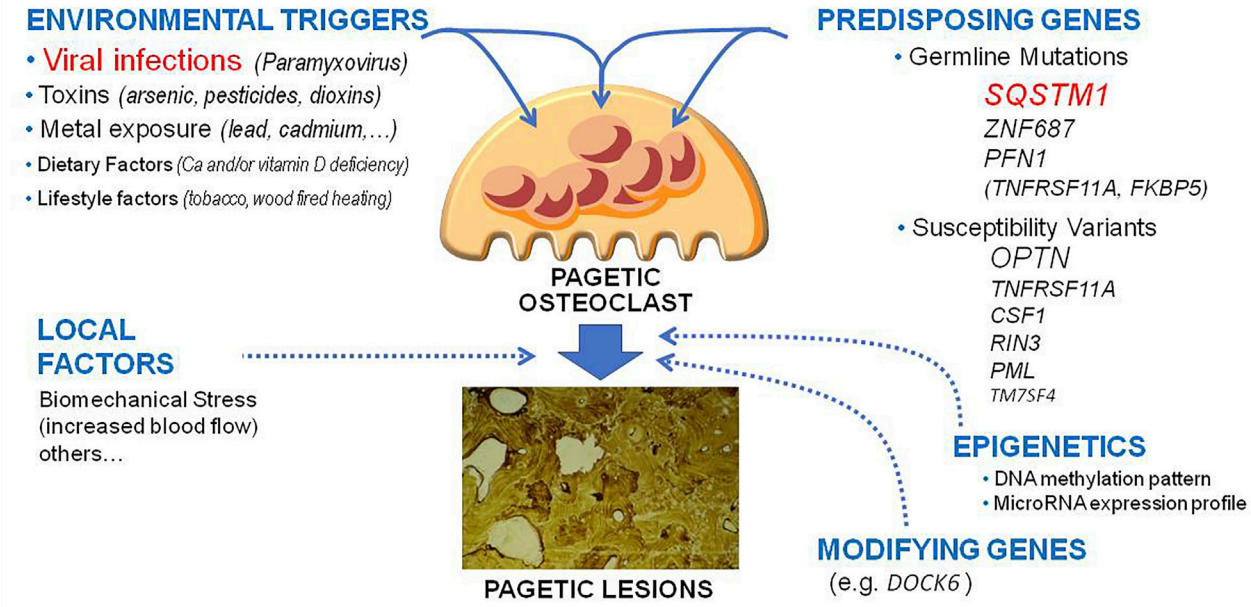

FIGURE 1
Updated pathogenetic model of Paget's disease of bone. The figure underlines the different genetic, environmental lifestyle and epigenetic factors and their potential reciprocal interactions in the pathogenesis of pagetic lesions.

the concomitant intervention of other factors, such as those related to a viral infection (Figure 1).

2 Genetics of Paget's disease of bone

The presence of a familial predisposition in PDB has been known for many years. Numerous epidemiological studies have in fact indicated a familial clustering in 15%–30% of patients, suggesting the possible role of genetic factors (Montagu, 1949; Siris et al., 1991), even though lower estimates have been also reported in some other studies (Eekhoff et al., 2004). Indeed, it is likely that the percentage of familial cases is underestimated, since the disease generally arises after 40 years of age and can remain asymptomatic for a long time. In this regard, an in-depth study in which detailed clinical research was carried out in first degree relatives of patients with the disease would have shown familial clustering in up to 40% of cases (Morales-Piga et al., 1995). It has also been estimated that the risk of PDB in first degree relatives of subjects suffering from the disease is about 7–10 times higher than in subjects without a family history (Siris et al., 1991), regardless of whether germline mutations of genes currently known related to PDB have been identified in affected subjects. The mode of inheritance appears to be autosomal dominant, although the existence of families with few affected members suggests incomplete penetrance and variable expression of the responsible gene or genes. A number of rare genetic disorders sharing some histopathological, radiological, and clinical overlap with PDB and even a similar genetic background have been also described (Ralston and Taylor, 2019). In the past two decades germline mutations in more than one gene and a number of predisposing common variants (i.e., polymorphisms) have been identified as the likely pathogenetic cause of PDB in a relevant number of patients (Table 1). Most of them affect the nuclear factor kappa-light-chain-enhancer of activated B cells (NFκB) signalling pathway and are implicated in the regulation of osteoclast differentiation and function, albeit at least three mutated genes are also involved in cell autophagy. Among the many functions attributed to NFκB, the one inherent osteoclastic pathophysiology is its modulating role in the differentiation of preosteoclasts into mature osteoclasts and their functional activation (Boyce et al., 2015).

2.1 Genetic mutations associated with Paget's disease of bone

2.1.1 Sequestosome 1 gene

Mutations affecting the sequestosome 1 gene (*SQSTM1*, within the PDB3 locus on chromosome 5q35 emerged from initial linkage analysis studies) currently represent the major

TABLE 1 Germline Mutations associated with PDB and/or PDB related disorders and their functions.

Gene	Encoded product	Bone related functions	PDB and PDB-related disease
SQSTM1	P62/sequestosome1	regulation of autophagy and NFκB signaling	Familial PDB
TNFRSF11A	RANK	master regulator of osteoclast formation and survival	Early onset PDB (rarely)
VCP	Valosin containing protein	role in protein degradation and autophagy, intracellular membrane fusion, DNA repair and replication; regulation of the cell cycle; activation of the NF-kB pathway	Inclusion Body Myopathy, PDB, FTD" (IBMPFD, now renamed MSP1)
ZNF687	Zink Finger Protein 687	unknown (part of the transcriptional regulator complex Z3)	Severe, early onset, PDB with higher risk of neoplastic degeneration in GCT
FKBP5	FK506-binding protein 51 (FKBP51)	regulator of NF-κB activation and Akt phosphorylation; scaffolding protein and autophagy inducer; regulation of microtubule dynamics	Polyostotic PDB (described in 2 Chinese Han families)
PFN1	Profilin 1	negative regulator of the NF-kB signaling; also involved in the turnover and restructuring of the actin cytoskeleton	Severe, early onset, PDB with higher risk of neoplastic degeneration

genetic cause of adult PDB and have been described in approximately 25%–40% of familial cases and in up to 10%–15% sporadic cases (i.e., those patients without documented familial clustering) in various patient series (Hocking et al., 2002; Laurin et al., 2002; Johnson-Pais et al., 2003a; Eekhoff et al., 2004; Good et al., 2004; Hocking et al., 2004; Falchetti et al., 2009; Rea et al., 2009; Gennari et al., 2010). The most common of these mutations is represented by the proline-leucine amino acid substitution in codon 392 (P392L) at the level of exon 8 (Gennari et al., 2010). These *SQSTM1* mutations are generally heterozygous mutations, but rare cases of homozygosity have been described, with both alleles of the *SQSTM1* gene mutated (Rea et al., 2009). Following the two positional cloning studies in 2002 (Hocking et al., 2002; Laurin et al., 2002), at least 30 different mutations is *SQSTM1* have been associated with PDB. The majority of these mutations affect the terminal portion of the gene and in particular the ubiquitin-binding domain (UBA domain) of the protein. In most of the series analyzed to date, it has been shown that patients with the *SQSTM1* mutation generally have a more severe form of the disease than patients without the mutation, with an earlier onset and a greater number of bones involved (Falchetti et al., 2009; Rea et al., 2009; Gennari et al., 2010; Visconti et al., 2010; Chung et al., 2011). Furthermore, genotype-phenotype correlation have suggested that patients with mutations that cause a stop codon and therefore the lack of synthesis or the synthesis of a truncated form of the protein (missing most of the UBA domain), tend to have a more severe and extensive disease compared to patients with "missense" mutations causing the change in one or more amino acids (Gennari et al., 2010; Visconti et al., 2010). However, there is considerable heterogeneity in the clinical manifestations of the disease even in patients with the same mutation, and even within the same family (Laurin et al., 2002; Gennari et al., 2010). Moreover, in keeping with the secular trends, the clinical expressiveness seems to have decreased over time in *SQSTM1* mutation carriers, so that the phenotype of PDB is attenuated and less extensive in the more recent generations, and it is delayed by at least 10 years (Bolland et al., 2007; Cundy et al., 2015; Dessay et al., 2020). The reasons for the delayed penetrance of PDB in these offspring remain unknown, but could be likely justified by a reduction in exposure to the putative environmental trigger(s).

The *SQSTM1* gene encodes a protein called p62, which is ubiquitously expressed and contains many structural domains, including the SH2-binding domain (Src homology 2), the atypical-PKC-interacting domain (AID), a ZZ domain, the TRAF6 ligand (TNFR-associated factor 6) two PEST motifs and the UBA domain (Joung et al., 1996). These domains exert several functions in different signaling and ubiquitin binding pathways that are relevant for cell autophagy, survival, or response to inflammatory and oxidative stress but also regulate the transcriptional activation and protein recruitment to endosomes (Joung et al., 1996; Duran et al., 2004). It is also known that p62 acts as an adaptor protein in the NFκB signaling pathway, downstream of the receptor activator of NFκB (RANK, a signaling receptor that plays a relevant role in osteoclast differentiation and function), where it binds molecules such as RIP (receptor interacting with proteins) and TRAF6 to the aPKC or other factors such as CYLD (a deubiquinating factor exerting an inhibitory effect on RANKL signaling) (Layfield et al., 2006; Jin et al., 2008; Sundaram et al., 2011). Most of the know *SQSTM1* mutations associated with PDB have deleterious effects on ubiquitin binding by p62 *in vitro* (causing either reduced UBA domain stability or affecting the ubiquitin binding interface) and there is evidence of an inverse relationship between ubiquitin binding function or the ability of different mutations to activate NFκB signaling *in vitro* and disease severity (Layfield et al., 2006; Goode et al., 2014). Thus, it has been speculated that the loss of ubiquitin binding by the mutated p62 protein might affect its interaction with ubiquitylated osteoclast proteins, leading to overstimulation of NFκB pathway and enhanced osteoclast formation and activity (Duran et al., 2004; Rea et al., 2013). Consistent with this hypothesis, osteoclasts derived from peripheral blood monocytes of *SQSTM1* mutation carriers showed increased

sensitivity to RANKL and high bone resorption capacity *in vitro* when compared with those derived from control monocytes (Chamoux et al., 2009; Rea et al., 2013). However, PDB-causing *SQSTM1* mutations located outside the UBA domain with little or no effects on ubiquitin binding have been described, and other domains of the p62 protein, such as AID, ZZ and the one binding TRAF6, also exert a relevant effect on osteoclasts (Goode and Layfield, 2010; Rea et al., 2013), suggesting more complex pathogenetic mechanisms in the presence of *SQSTM1* mutation. This might also explain the conflicting results emerged to date from studies in *SQSTM1* knockout (KO) mice or animal models with the p62 P394L mutation, corresponding to the P392L mutation observed in human (Duran et al., 2004; Hiruma et al., 2008; Daroszewska et al., 2011; Kurihara et al., 2011; Zach et al., 2018). In fact, while a first study in *SQSTM1* KO mice showed defective osteoclastogenesis due to impaired activation of Nfatc1 and NFκB, without a clear skeletal phenotype (Duran et al., 2004), a more recent and detailed analysis of an independently generated *SQSTM1* KO model reported enhanced activation of osteoclastogenesis and osteoclast activity (with a robust activation of Nfatc1 and NFκB), together with the development of PDB-like osteolytic lesions (Zach et al., 2018). Likewise, albeit there is general consensus about an increased sensitivity to RANKL in osteoclasts derived from the *SQSTM1* P394L mice model, there are still contrasting data about the development of PDB-like lesion in these mice (Hiruma et al., 2008; Daroszewska et al., 2011; Kurihara et al., 2011). A potential explanation for the divergent results might be related to the age differences between the studies and the different skeletal sites tested for the presence of pagetic lesions (vertebral vs. lower extremity bone). Very recently, a new interactor protein of p62, Ajuba, has been identified as an additional component of the SQSTM1/p62 protein complexes involved in NFκB signaling (Sultana et al., 2021). *In vitro*, Ajuba was shown to activate NFκB activity, while co-expression with SQSTM1/p62 inhibited this activation in an UBA domain dependent manner. Thus, either the lack of *SQSTM1* expression or the presence of p62 forms with inactive UBA domain (as occurs with typical, PDB-related *SQSTM1* mutations) might lead to increased or prolonged Ajuba-induced NFκB signaling and enhanced osteoclastogenesis.

While heritable mutations occurring in the germ cells (so called germline mutations) involve all nucleated cells deriving from them, somatic mutations may occur at any cell division from the first cleavage of the zygote to the lifelong cell divisions in an individual, and consequently affect all somatic cells descended from the original mutated cell. Interestingly, evidence of somatic *SQSTM1* mutations in sporadic PDB and pagetic osteosarcoma suggested a role for *SQSTM1* in both sporadic and inherited PDB (Merchant et al., 2009) and might in part explain the focal nature of the disorder. In particular, the *SQSTM1* (C1215T) mutation was reported at somatic level in samples from sporadic pagetic osteosarcoma patients, with the normal adjacent tissue from these tumors lacking this mutation, as expected for somatic mutational events. Equally interesting is the fact that *SQSTM1* mutations were not found in primary adolescent, non pagetic, osteosarcomas (Merchant et al., 2009). Conversely, a similar analysis in osteoblast and bone marrow cells cultures from 28 PDB patients did not identify somatic mutations (Matthews et al., 2009). About 6 years after these preliminary reports, another study identified SQSTM1/P392L mutation at post-zygotic level, restricted to the monocytic lineage, in about 5% of analyzed PDB patients and 1.5% of controls. Interestingly, PDB patients carrying such a mutation exhibited a bone phenotype milder than PDB patients with the same mutation but at germline level (Guay-Bélanger et al., 2015).

2.1.2 TNFRSF11A gene

Mutations in the *TNFRSF11A* gene, which encodes for RANK, were the first to be associated with isolated PDB cases and other, so called, PDB-like disorders, such as familial expansile osteolysis (FEO) and expansile skeletal hyperphosphatasia (ESH) (Hughes et al., 2000). This gene is located within the chromosomal region 18q21.1-22, containing the PDB2 locus. The RANK protein is a member of the TNFR (tumor necrosis factor receptor) superfamily, strongly expressed on osteoclasts and their precursors and essential for osteoclastic differentiation and activity (Hofbauer and Heufelder, 2000). Mutational screening of the *TNFRSF11A* gene revealed different insertions at the level of exon 1, mutations that result in the duplication of amino acid sequences in the RANK signal peptide (Hughes et al., 2000). To date, different heterozygous in-frame tandem duplications of variable length, elongating the signal peptide of RANK, have been described, most of them associated with rare PDB-like disorders (Ralston and Taylor, 2019). The 84dup18 (duplication of 18 base pairs in position 84) and the closely related one, 83dup18, have been found in most of the cases of FEO described so far (Hughes et al., 2000; Palenzuela et al., 2002; Johnson-Pais et al., 2003b); the 84dup15 mutation was found families with ESH (Whyte and Hughes, 2002); the 90dup12 was associated with panostotic expansile bone disease (Schafer et al., 2014); while the 75dup27 mutation was described in a Japanese family with an early and severe form of PDB, associated with unexplained tooth loss and bony enlargement of the small joints of the hands (Nakatsuka et al., 2003; Merchant et al., 2009). Of interest, in these disorders, the severity of the associated skeletal disease appears inversely related to the duplication's length. Moreover, a different duplication, 87dup15, has been more recently described in a 13-year-old Bolivian girl affected with the so called "Juvenile PDB" (also named familial idiopathic hyperphosphatasia) (Whyte et al., 2014), an autosomal recessive disorder manifesting extremely fast skeletal remodeling, which is usually caused by loss-of-function mutations within *TNFRSF11B* gene, encoding

osteoprotegerin (OPG), the decoy receptor of RANK-ligand (Whyte et al., 2002). Consequently, the hypothesis that FEO, ESH, and the few cases of early-onset PDB associated with *TNFRSF11A* mutation might represent slightly different manifestations of a common condition (that is different from classical PDB) cannot be excluded.

Initial functional studies suggested that both 84dup18 and 75dup27 mutations cause a defective cleavage of the RANK signal peptide resulting in the activation of the NFκB signal cascade, although the exact mechanism of these processes was unclear (Merchant et al., 2009). More recently a mouse model carrying the 75dup27 mutation was generated, which prospects a different pathogenetic mechanism (Alonso et al., 2021). Consistent with the clinical reports, mice heterozygous for the mutation developed a PDB-like disease with focal osteolytic lesions in the hind limbs with increasing age. However, functional *in vitro* studies showed that RANK ligand-induced osteoclast formation and signaling was impaired, while osteoclast survival was increased independent of RANKL stimulation. Surprisingly, 75dup27 homozygous mice showed osteopetrosis at birth, with complete absence of osteoclasts and an impaired osteoclastogenesis in response to RANKL and macrophage colony-stimulating factor (M-CSF) stimulation.

To date, apart from two additional forms of early onset PDB and different 27bp duplications (78dup27 and 77dup27) described, respectively, in single kindreds of Chinese and Mexican descent (Ke et al., 2009; Iwamoto et al., 2020), no other cases of mutations of the *TNFRSF11A* gene have been described in both familial and sporadic cases of PDB, although some polymorphisms of this gene might be associated with the risk of developing the classic form of the disorder (see Section 2.2, below) (Chung et al., 2010).

2.1.3 Valosin containing protein gene and other multisystem proteinopathy genes

Mutations in the VCP gene (encoding valosin containing protein), at the 9p21 locus, were identified as the cause of the autosomal dominant syndrome "Inclusion Body Myopathy, Paget's disease of bone, Fronto-temporal Dementia" (IBMPFD), characterized by skeletal manifestations similar to classical PDB, associated with myopathy, amyotrophic lateral sclerosis (ALS) and fronto-temporal dementia (Kovach et al., 2001; Watts et al., 2004). Myopathy is the most frequent feature in IBMPFD families, occurring in up to 90% of individuals, while PDB and dementia have been described in 43% and 37% of cases, respectively (Ralston and Taylor, 2019). Albeit the clinical and radiologic features are similar to classical PDB (including the presence of asymptomatic cases), the skeletal manifestation often occur at an earlier age (around 40–45 years). Moreover, increased mortality has been reported in IBMPFD patients due to respiratory insufficiency and/or cardiac failure, with a life expectancy around 58 years (Ralston and Taylor, 2019).

Since its original description, IBMPFD has been reclassified and included among the group of "Multisystem Proteinopathies" (MSP), disorders with a broader phenotypic spectrum in which different neuromuscular disfunctions (also including parkinsonism and motor neuron disease) may be accompanied by pagetic lesions (Taylor, 2015). The *VCP* gene encodes for an enzymatic protein involved in cell division, fusion of membranes within cells, reassembling cell structures after cell division, prevention of cells apoptosis, and repair of the damaged DNA. In particular, this protein is also linked to the ubiquitin-proteasome system, and therefore, most likely, contributes to the regulation of a correct autophagy process. To date, more than 45 different pathogenic *VCP* mutations have now been identified in patients with IBMPFD (now classified as MSP1) (Ralston and Taylor, 2019). Most of them affect exons 3–5, encoding the N-terminal domain of the protein, which is responsible for binding to ubiquitin-complexed proteins, which will be degraded by the proteasome (Ralston and Taylor, 2019). Thus, likewise *SQSTM1* mutations, disease-causing mutations in *VCP* may impair the scaffold function required to transport proteins to the proteasome for degradation, causing them to accumulate in the cytoplasm as inclusion bodies which are typically observed in myocites and neurons. In osteoclasts this also determines a reduced degradation of proteins involved in the NFκB signaling pathway, with prolonged activation of this pathway and consequent cell hyperactivity and bone resorption (Ralston and Taylor, 2019). An increased avidity of VCP mutant proteins for the NFκB inhibitor IkB has been also described as an additional mechanism of increased NFκB activity. In order to better understand the pathogenesis of MSP disorders, transgenic mice models overexpressing known VCP mutations have been generated. Together with muscle weakness and behavioural abnormalities these mice showed an osteopenic phenotype and developed focal osteosclerotic lesions within the internal cavity of long bones (Custer et al., 2010).

Overall, VCP mutations are estimated to account for about 50% of cases of MSP (the so called MSP1 form) and other mutations have been described involving hnRNPA2B1, hnRNPA1, and MATR3 genes (Taylor, 2015; Ralston and Taylor, 2019). The mechanisms by which these mutations cause the pagetic degenerations observed in some affected members remain to be established. Of interest, mutations in *SQSTM1* were also rarely described in patients with neuromuscular degeneration and other typical clinical features of MSP, either in the presence or absence of PDB (Teyssou et al., 2013; Bucelli et al., 2015). Likewise, *SQSTM1* mutations have been also detected in a limited number of patients with only frontotemporal dementia or ALS (Fecto and Siddique, 2012; Le Ber et al., 2013). The reason for such a different clinical presentation, even in the presence of a same *SQSTM1* mutation, remains unknown but it is likely that other genetic mutations or susceptibility alleles might predispose *SQSTM1*-mutated patients to one ore more clinical manifestations

described in MSP, including PDB. In keeping with this hypothesis a N357S genetic variant of *TIA1* gene (encoding for a key component of cytosolic stress granules) has been shown to interact with *SQSTM1* mutations to cause distal myopathy, whereas both *SQSTM1* mutation and the N357S genetic variant alone do not cause myopathy (Lee et al., 2018). Somatic mutations of the *VCP* gene have not been identified neither in pagetic tissue nor in bone tumors, although some human cancers exhibited them (Tate et al., 2019).

2.1.4 ZNF687 gene

In 2016, a whole-exome sequencing analysis of a large Italian PDB-pedigree with 14 affected members (four of whom developed GCTs at multiple pagetic skeletal sites) identified a missense P937R mutation in a new gene, *ZNF687* (Divisato et al., 2016). The mutation co-segregated with the clinical phenotype in all affected family members of the pedigree and was also identified in 2 out of 615 Italian PDB patients, in 2 out of 339 PDB cases from a multiethnic North-American cohort, and in seven unrelated cases with giant cell tumor degeneration at pagetic bones (Divisato et al., 2016). Moreover, a different mutation of *ZNF687* (S242I) was also described in another PDB family (Divisato et al., 2016). In a subsequent analysis, the P937 mutation was also found in a 45-year-old black American woman with polyostotic PDB and in tumor tissue derived from 1 undifferentiated pagetic sarcoma, while a new *ZNF687* mutation (R331W) was identified in 1 of 28 pagetic osteosarcomas (Scotto di Carlo et al., 2020a). From the clinical point of view, PDB cases harboring *ZNF687* mutations generally have a severe form of PDB, with an earlier onset and greater number of affected skeletal sites than other PDB cases, including patients with *SQSTM1* mutation (Divisato et al., 2016). Of interest, remarkable clinical and molecular differences have been reported between pagetic and non pagetic GCTs (Rendina et al., 2015). In fact, GCT generally complicates a longstanding, active, and polyostotic PDB, involving only skeletal sites affected by the disease or, rarely, extra-skeletal tissues adjacent to them. In contrast with the prevalent involvement of axial the skeleton in adults with PDB, GCT unrelated to PDB preferentially occurs in Asian females aged below 40 years and mostly involves the epi-metaphysis of long bones, in particular femurs and tibiae (Werner, 2006). In addition, pagetic GCT is frequently multifocal (in up to 25% of cases) and is associated with severe disease and reduced life expectancy, with a 5-years survival rate below 50% as compared to 96%–100% described in non-pagetic GCT (Rendina et al., 2015). These clinical differences might also be related to a different genetic background, since more than 90% of non pagetic GCT are associated with recurrent somatic mutations of the *H3F3A* gene, encoding the histone variant H3.3, that have rarely described in pagetic GCTs (Scotto di Carlo et al., 2020b). The increased prevalence of PDB-GCT cases in families from Southern Italy (up to 50% of pagetic GCT cases described so far) also suggests a strong genetic basis with a founder effect.

The *ZNF687* gene encodes for a zinc finger protein that is part of the transcriptional regulator complex Z3 (Malovannaya et al., 2011), is highly expressed during osteoclastogenesis and is upregulated in pagetic GCTs (Divisato et al., 2016). The exact function of this gene in bone metabolism and the pathogenetic mechanism leading to the development of PDB in *ZNF687* mutation carriers and/or to neoplastic degeneration of pagetic tissue remain unknown.

2.1.5 FKBP5 gene

In 2017 a missense mutation in *FKBP5* gene (V55L) was related to PDB in a single Chinese pedigree with four affected polyostotic cases (Lu et al., 2017). The gene encodes for FK506-binding protein 51 (FKBP51), a known regulator of NFκB activation and Akt phosphorylation (Bouwmeester et al., 2004; Lu et al., 2017). A *FKBP51*^{V55L} knock-in transgenic mice model was also generated to better characterize the skeletal implications of the mutation. Of interest, osteoclast precursors derived from the transgenic mice showed enhanced Akt phosphorylation and RANKL sensitivity, while mature osteoclasts exhibited a more intensive bone resorbing capacity than osteoclasts derived from the control mice (Lu et al., 2017). In keeping with the *in vitro* data, osteolytic lesions resembling the initial phase of PDB were also evidenced by micro-CT in three-dimensional reconstruction of distal femurs of *FKBP51*^{V55L} mice. However, at least in 10-months old animals, the focal increase in bone resorption was not followed by aberrant osteoblastic activity, osteosclerosis and increase in bone size, as typically observed in human PDB. To date the pathogenetic mechanism of *FKBP5* mutations in PDB is unknown and this finding remains restricted to a single PDB pedigree of Asian descent. Intriguingly, FKBP51 also acts as a scaffolding protein organizing protein complexes and functions as an autophagy inducer (Gassen et al., 2015; Fries et al., 2017), albeit no aberrant autophagy was described in the A *FKBP51*^{V55L} mice during osteoclast differentiation *in vitro* (Lu et al., 2017). In addition, *FKBP51* is also involved in the regulation of the cytoskeleton, more specifically microtubule dynamics (Fries et al., 2017).

2.1.6 PFN1 gene

Very recently, mutations in the *PFN1* gene were separately described in two Italian pedigrees affected with an early onset form of PDB (Scotto di Carlo et al., 2020c; Merlotti et al., 2020) and in two Chinese Han PDB families complicated by GCT (Wei et al., 2021). The same 4-nucleotide deletion giving rise to a frameshift mutation (D107Rfs*3) was found in the Italian families and in one out two Chinese families, as well as in a sporadic Italian PDB case without know family history for the disease. Novel *PFN1* mutations were described in the second

Chinese family (L112P) and in a sporadic early-onset PDB patient of Asian ancestry (heterozygous 1-bp deletion c.324_324delG) with GCT. Remarkably, all patients had early onset, polyostotic PDB with skull involvement, which appears a typical characteristic of the disease caused by *PFN1* mutation, since hyperostosis and osteolytic lesions of the skull were also found in a 17 years old, asymptomatic, unaffected carrier of the D107Rfs*3 mutation (Merlotti et al., 2020). Other peculiar phenotype characteristics included a rather symmetrical and extensive skeletal involvement, the presence of severe, early onset, osteoarthritis at the spine and major joints (occurring between 25 and 50 years) and an increased prevalence of fractures or neoplastic degeneration in either osteosarcoma (described in 21% of Italian patients) or GCT (described in 31% of Chinese cases). Moreover, reduced response to aminobisphosphonates, including zoledronic acid, requiring multiple infusions to control bone pain and achieve biochemical remission over a long term was described in most of these cases (Merlotti et al., 2020; Wei et al., 2021). Osteoclasts derived from peripheral blood mononuclear cells of *PFN1* mutation carriers showed PDB-like features such as a larger size and a higher number of nuclei (Scotto di Carlo et al., 2020c; Merlotti et al., 2020; Wei et al., 2021).

The *PFN1* gene encodes for profilin 1, a highly conserved and ubiquitously expressed protein among vertebrates, and member of the profilin family of small actin-binding proteins involved in the turnover and restructuring of the actin cytoskeleton (Carlsson et al., 1977; Alkam et al., 2017), that might be relevant for osteoblast biology (Luxenburg et al., 2007; Han et al., 2019). In addition, profilin 1 was shown to suppress NFκB activity in the regulation of osteoclast differentiation and to prevent the degradation of the phosphatase PTEN, a known negative modulator of osteoclast differentiation (Zaidi and Manna, 2016). Of interest, previous experimental evidences already underlined the relevance of profilin 1 for bone biology, since osteoclast specific deletion of *PFN1* increased cell motility, podosome formation, size, and bone resorptive activity of osteoclasts *in vitro* and caused several bone abnormalities *in vivo*, including dwarfism, reduced trabecular bone mass and osteolytic lesions (Shirakawa et al., 2019). Moreover, as for other PDB genes (e.g., *SQSTM1* or *VCP*), *PFN1* mutations were previously described in patients with familial ALS (Wu et al., 2012).

After the discovery of *PFN1* mutations in PDB, a transgenic mice model with the truncating D107Rfs*3 mutation of *PFN1* gene was recently established (Wei et al., 2021). While the homozygous mutation was embrionically lethal (likewise in the *PFN1* KO mice), heterozygous transgenic mice were smaller in size, and showed accelerated osteoclast differentiation, with deformed craniofacial bones and the presence of focal PDB-like lesions (Wei et al., 2021). Reduced profilin 1 expression was also demonstrated in femur sections from transgenic mice using immunohistochemistry staining (Wei et al., 2021). Taken all together these experimental observations suggest that the *PFN1* mutations associated with PDB might confer a loss of function in profilin 1 activity and cause PDB-like features in the osteoclasts, likely due to enhanced cell motility, increased Nf-kB activity, and actin ring formation.

2.2 Other genetic pathways associated with Paget's disease of bone: Genome wide association studies, single nucleotide polymorphisms association analysis, and modifying genes

Despite *SQSTM1* and other rarer mutations have been found in a relevant number of familial PDB-cases from different Countries, their prevalence remains very low in patients with sporadic disease, and at up to 40%–50% of familial cases do not yet have a recognized mutation. This suggests the presence of additional predisposition genes. Over the past years, molecular genetic studies in animal models of PDB, in cellular models of "pagetic" osteoclasts, and Genome Wide Association Studies (GWAS) in unrelated PDB individuals have contributed to identify other several potential genes and loci enabling the predisposition to develop PDB (Table 2).

Thus, in 2010 and 2011 a GWAS approach was applied to large and multiethnic populations of PDB in order to identify novel genetic variants predisposing to the disease (Albagha et al., 2010; Albagha et al., 2011). Overall, the following candidate regions were identified, accounting for about 13% of the familial risk of PDB in *SQSTM1* negative patients: 1) 10p13 (rs1561570, within *OPTN* gene); 2) 1p13 (rs484959, near the *CSF1* gene); 3) 18q21 (rs3018362, near *TNFRSF11A* gene); 4) 15q24 (rs5742915, within *PML* gene); 5) 14q32 (rs10498635 within *RIN3* gene); 6) 7q33 (rs4294134, within*NUP205* gene); and 7) 8q22 (rs2458413, within *TM7SF4* gene). Remarkably, some of these regions such as *TNFRSF11A* (encoding for RANK, as described in Section 2.1.2), *CSF1* (encoding for macrophage colony-stimulating factor, MCSF), and *TM7SF4* (encoding for the dendritic cell-specific transmembrane protein, DC-STAMP) have a well-recognized role in regulating osteoclast formation and activity, making their pathogenic effect on PDB biologically plausible. In fact, while MCSF and RANKL are the key regulators of osteoclast formation and activity (Boyce et al., 2015), DC-STAMP is necessary for the fusion of osteoclast precursors into multinucleated, mature osteoclasts (Kukita et al., 2004; Yagi et al., 2005). The implication of other genes such as *OPTN*, *RIN3*, and *PML*, in bone physiology has been more recently suggested.

The *OPTN* gene encodes for optineurin, a protein that, likewise p62/SQSTM1, is involved in the regulation of autophagy and NFκB signaling (Zhu et al., 2007). A first

TABLE 2 PDB-predisposing genetic variants (with chromosome location), reference SNP identification, encoded proteins, bone related functions and associated diseases different than PDB and/or PDB-related diseases.

Gene/ chromosome region	References SNP (rs)	Encoded product	Methodological approach	Bone related functions	Diseases associated other than PDB or PDB-related diseases
OPTN gene/10p13	rs1561570	Optineurin	GWAS	regulation of autophagy and NFκB signaling	Glaucoma, Primary Open Angle and Amyotrophic Lateral Sclerosis 12 With or Without Frontotemporal Dementia (https://www.genecards.org/cgi-bin/carddisp.pl?gene=OPTN)
CSF1/1p13	rs484959	MCSF	GWAS	master regulator of osteoclast formation and survival	Pigmented Villonodular Synovitis and Tenosynovial Giant Cell Tumor (https://www.genecards.org/cgi-bin/carddisp.pl?gene=CSF1)
TNFRSF11A/18q21	rs3018362	RANK	GWAS	master regulator of osteoclast formation and survival	Osteopetrosis, Autosomal Recessive 7 (https://www.genecards.org/cgi-bin/carddisp.pl?gene=TNFRSF11A)
TNFRSF11A/18q21	rs1805034 (*V192A*)	RANK	Whole exome scanning	greater activation of NFκB signaling *in vitro* and with increased disease severity *in vivo*	Osteopetrosis, Autosomal Recessive 7 (https://www.genecards.org/cgi-bin/carddisp.pl?gene=TNFRSF11A)
PML/15q24	rs5742915	Phosphoprotein member of TRIM	GWAS	differentiation, survival and resorptive activity of osteoclasts (mice)	Acute Promyelocytic Leukemia and Rabies (https://www.genecards.org/cgi-bin/carddisp.pl?gene=PML)
RIN3/14q32	rs10498635 rs117068593	Ras and Rab 3 interactor protein	GWAS/fine mapping analysis	vesicular trafficking, expressed particularly in osteoclasts	Ciliary Dyskinesia, Primary, 6 (https://www.genecards.org/cgi-bin/carddisp.pl?gene=RIN3)
NUP205/7q33	rs4294134	Nucleoporin 205	GWAS	unknown	Nephrotic Syndrome, Type 13 and Genetic Steroid-Resistant Nephrotic Syndrome (https://www.genecards.org/cgi-bin/carddisp.pl?gene=NUP205)
TM7SF4/8q22	rs2458413	DC-STAMP	GWAS	fusion of osteoclast precursors to form multinucleated mature osteoclasts	Osteopetrosis, Autosomal Recessive 8 (https://www.genecards.org/cgi-bin/carddisp.pl?gene=DCSTAMP)
DOCK6/19p13.2 (p.Val45Ile)	—	Dedicator Of CytoKinesis (DOCK) family of atypical guanine nucleotide exchange factors	Whole exome scanning	role in actin cytoskeletal reorganization by activating the Rho GTPases Cdc42 and Rac1 p.Val45Ile variant may decrease SRF-TF-like activity	Adams-Oliver Syndrome 2 and Adams-Oliver Syndrome (https://www.genecards.org/cgi-bin/carddisp.pl?gene=DOCK6)
VCP/9p13.3	rs565070	Valosin Containing Protein	SNPs association study	role in protein degradation, intracellular membrane fusion, DNA repair and replication, regulation of the cell cycle, and activation of the NF-kappa B pathway	Frontotemporal Dementia and/o (https://www.genecards.org/cgi-bin/carddisp.pl?gene=VCP r Amyotrophic Lateral Sclerosis 6)

study indicated that mice harboring a loss of function mutation in the ubiquitin-binding domain of *Optn* (*OptnD477N/D477N*) have enhanced bone turnover and that in osteoclast precursors optineurin acts as a negative regulator of RANK-induced NFκB activation (Obaid et al., 2015). Thus, since the risk rs1561570 allelic variant of *OPTN* was associated with reduced optineurin expression (Obaid et al., 2015), a plausible pathogenetic mechanism could be represented by an increase in NFκB activity and osteoclast formation and activity. However, only a limited number of these mice (10%) developed PDB like lesions (Obaid et al., 2015), making difficult the understanding of mechanistic process underlying the OPTN-PDB axis. Then, other animal studies using *Optn* KO model evidenced a recapitulation of the key clinical features observed in PDB patients, such as polyostotic osteolytic lesions, mixed-phase lesions, and increased bone turnover, and affecting all the

studied animals between 16 and 22 months of age (Wong et al., 2020). Interestingly, when the authors investigated the *ex vivo* differentiation of primary osteoclasts noted that the absence of *Optn* caused an increased osteoclastogenesis. Moreover, *Optn*-deficient osteoclasts displayed a significantly decreased type I interferon (IFN) signature, due to both defective production of IFNβ and impaired signaling via the IFNα/βR, acting as a negative feedback loop for osteoclastogenesis and survival. Such data lead to the hypothesis that optineurin may have dual roles in the type-I IFN response to restrain osteoclast activation and bone resorption, thus representing a potential novel therapeutic target for PDB. Very recently, it has been also suggested that OPTN interacts with nuclear factor erythroid-derived factor 2-related factor 2 (NRF2), acting as a master regulator of the antioxidant response, hypothesizing a pathway through which RANKL-induced reactive oxygen species (ROS) might be relevant for osteoclastogenesis. A study on monocytes from mice knock out for *Optn* (*Optn*−/−) compared with the wild-type (*Optn*+/+) counterpart revealed that *OPTN* deficiency decreased the basal expression of NRF2, inhibited the expression of NRF2-responsive antioxidants, and increased basal and RANKL-induced intracellular ROS levels, thus leading to enhanced osteoclastogenesis. Such findings contribute to sustain a novel OPTN-mediated molecular mechanism to regulate the NRF2-mediated antioxidant response in osteoclasts, thus extending the therapeutic potential of optineurin in the aging process resulting from ROS-triggered oxidative stress, known to be also associated with PDB (Xue et al., 2021). While germline *OPTN* mutations were previously described in patients with primary open-angle glaucoma and ALS (Toth and Atkin, 2018), they have never been detected in PDB patients.

The *PML* gene encodes for a phosphoprotein member of the tripartite motif (TRIM) family. Such a protein localizes to nuclear bodies where it acts both as a transcription factor and tumor suppressor. It exhibits a cell-cycle related expression, and it enables the regulation of p53 response to oncogenic signals. *PML* is often involved in the translocation with the retinoic acid receptor alpha gene associated with acute promyelocytic leukemia (Bernardi and Pandolfi, 2007). Recently, it has been reported that the PDB-risk allele of rs5742915, located within the *PML* gene by the GWAS, associates with a lower PML expression and that PML expression in blood cells from PDB patients is lower than in non pagetic controls (Wani et al., 2022). In a mice model of *Pml* KO, the differentiation, survival and resorptive activity of osteoclasts was increased compared to wild type animals. Moreover, in KO animals, the inhibitory effect of IFN-γ on osteoclast formation resulted to be significantly blunted when compared to wild type mice, while the bone nodule formation was increased. Bone histomorphometry analysis revealed that *Pml* KO mice had also a high bone turnover with a parallel increase in bone resorption and mineral apposition rate indices, whereas micro-CT analysis of trabecular bone showed no differences with respect to the wild type animals. Thus, such findings strongly suggest that reduced expression of *PML* may predispose to PDB, identifying this protein as a novel regulator of bone metabolism (Wani et al., 2022).

Although, the exact function of *RIN3* in bone metabolism and the pathogenesis of PDB remains unknown, this gene encodes for the Ras and Rab three interactor protein which is involved in vesicular trafficking and is expressed in bone, particularly in osteoclasts (Vallet et al., 2015; Shen et al., 2022). Albeit *RIN3* mutations have not been detected so far in PDB patients, a fine mapping analysis within the *RIN3* locus on chromosome 14q32 identified some rare missense variants predicted to be highly pathogenic and resulting remarkably more prevalent in PDB cases than in controls (Vallet et al., 2015). Particularly, the rs10498635C allele on chromosome 14q32.12 was significantly associated with PDB in several European populations. Eighteen PDB-associated variants in *RIN3* locus, including 16 missense variants were studied by targeted sequencing of the 60 kb region in the *RIN3* gene in 741 PDB patients and 2,699 healthy controls. Three missense variants, the rs117068593T allele, the rs117068593C allele and the rs10498635C allele, were found to be most common in PDB than controls (Vallet et al., 2015). However, this study identified other several rare variants being more common in PDB cases than healthy controls, and although individually they did not reach statistically significant results, their combination did. Lately, 22 distinct variants were identified in a Belgian population of unrelated pagetic and healthy subjects. Eight of these variants were newly recognized missense variants, and 2 were in the 5' untranslated region (De Ridder et al., 2019). Even though their results substantially confirmed the findings of the British cohort, the Belgian study strongly suggested a potentially modifying effect of the rs117068593, p. R279C variant on the age of onset of the disease, confirming *RIN3* as a potential gene modifier of the age of onset of the PDB. Moreover, albeit some of the variants described above affect the functional domains of the RIN3 protein, most of the variants associated with PDB are located in the noncoding regions of the RIN3 gene, likely altering its expression (Shen et al., 2022). While the mechanism by which these variants interact in the pathogenesis of PDB remains unknown, it has been shown that the targeted inactivation of the mouse *Rin3* gene leads to a reduction in osteoclast number and interferes with osteoclast activity, thus reducing bone resorption and leading to increased bone mass (Vallet et al., 2021). Thus, it is likely that PDB-predisposing variants of RIN3 in humans probably acts through a gain of function mechanism.

Despite the well recognized role of DC-STAMP in osteoclast biology, there is still limited and contrasting information about

the mechanism through which the rs2458413 variant of its encoding gene (*TM7SF4*) identified in GWAS or other rare variants affect osteoclast phenotype and cause PDB (Laurier et al., 2017; Mullin et al., 2019; Sultana et al., 2019).

Importantly, an interaction between the novel variants identified by the GWAS or other polymorphic variants in the same candidate regions and *SQSTM1* mutations on the pagetic phenotype was described in different reports. In a first study assessing the effects of a *T575C* polymorphic variant of *TNFRSF11A* (rs1805034, which results in a *V192A* substitution in the RANK protein), the presence of the *C* allele (*A192*) was shown to synergistically interact with *SQSTM1* mutations on the PDB phenotype, leading to greater activation of NFκB signaling *in vitro* and with increased disease severity in PDB patients (Gianfrancesco et al., 2012). A subsequent, more detailed study investigated the clinical effects of all the seven allelic variants identified by the GWAS in a large multiethnic sample of 1940 PDB patients (Albagha et al., 2013). A cumulative risk allele score was specifically constructed by adding the GWAS variants together and relating this to disease severity, alone or in combination with *SQSTM1* mutations. In *SQSTM1*-negative patients, risk allele scores in the highest tertiles (thus bearing most of the GWAS variants related to PDB) were associated with enhanced disease severity compared with the lowest tertile, either in terms of number of affected sites or in disease severity score. Importantly, the risk allele score remained a significant predictor of disease severity when *SQSTM1*-positive individuals were considered. Likewise, in 2011, a study on 196 Belgian cases with sporadic PDB searched for possible correlation between single nucleotide polymorphisms (SNPs) of candidate genes, *TNFSF11A*, *VCP*, and *IL-6*, and disease development susceptibility (Chung et al., 2011). The latter gene was selected since IL-6 is known to be a stimulator of osteoclast formation, possibly acting as an autocrine/paracrine factor to enhance osteoclastogenesis in PDB patients (Kurihara et al., 1990; de la Mata et al., 1995). A total of 20 SNPs were used, nine for *TNFSF11A*, three for *VCP*, and eight for *IL-6*, respectively. Authors concluded that SNPs in *TNFSF11A* or *IL-6* were very unlikely to play a role in the of sporadic PDB in their study population. Interestingly, one SNP of *VCP* gene, referred to as rs565070, showed association with PDB, even if, as suggested by Authors themselves, replication of this finding in other populations is needed before it can be included in the list of PDB-associated genes (Chung et al., 2011).

Always remaining in the context of modifying genes, very recently Dessay et al. (2022) elegantly identified, by whole exome sequencing in two large unrelated French Canadian PDB families with germline P392L *SQSTM1* mutation, a clinically attenuating effect on PDB severity exerted by a V45I rare variant in the *DOCK6* gene. Remarkably, albeit both variants were separately found in PDB patients and gave rise to a pagetic phenotype of osteoclasts *in vitro* versus healthy controls, the *DOCK6* variant was found to delay the onset of PDB and attenuate the severity of osteoclast phenotype of PDB caused by the P392L mutation of *SQSTM1*, when both variants were present. DOCK6 protein belongs to the dedicator of cytokinesis (DOCK) family of atypical guanine nucleotide exchange factors, components of intracellular signaling networks and by interacting with small GTPases they probably play a role in actin cytoskeletal reorganization by activating the Rho GTPases Cdc42 and Rac1 (Miyamoto et al., 2007). The same Authors performed a structural bioinformatics analyses showing that the *SQSTM1* P392L mutation may decrease its possible intramolecular interaction with the serum response factor–transcription factor (SRF-TF)-like domain, while at the same time the V45I variant of *DOCK6* gene may decrease SRF-TF-like activity (Dessay et al., 2022). Indeed, homozygous or dominant negative heterozygous mutations of DOCK6 gene account for the Adams-Oliver syndrome-2, an autosomal recessive multiple congenital anomaly syndrome featured by aplasia cutis congenita and terminal transverse limb defects, in association with variable involvement of the brain, eyes, and cardiovascular system (Shaheen et al., 2011).

3 Environmental factors

Clinical and experimental evidences support the hypotheses that one or more environmental factors are necessary for the complete clinical expression of PDB. Indeed, the incomplete penetrance of disease in families with a documented genetic predisposition, the clinical observation that PDB does not affect the entire skeleton but involves only one or more skeletal sites, as well as the declining trends in the PDB incidence and severity observed over the years, strongly support the hypothesis that non-genetic factors are involved in the disease etiopathogenesis (Cooper et al., 2006; Singer, 2015; Gennari et al., 2019). Even though this assumption is generally accepted, the exact nature of these factors and whether or how they might interact with the genetic factors in the pathogenesis of PDB is poorly understood.

3.1 Viral factors

The possible involvement of viral factors in the pathogenesis of PDB has been reported since the early 1970s (Mills and Singer, 1976; Rebel et al., 1981), when virus-like inclusions were demonstrated first in the nucleus and then in the cytoplasm of pagetic osteoclasts using electron microscopy. These inclusions consist of groups of microtubules, which are present either in a compact paracrystalline array or are scattered in a more random fashion (Singer, 2015). The pagetic microtubules are similar to the nucleocapsids of two paramyxoviruses, measles virus (MV) and respiratory syncytial virus (RSV), showed identical dimension, and have been found in

several studies in the past years (Mills et al., 1984; Basle et al., 1985; Basle et al., 1986; Mills et al., 1994; Reddy et al., 1995). More recently, Friedrichs et al. (2002) also identified the full-length sequence for the MV nucleocapsid gene in bone marrow obtained from a skeletal site showing the PDB pathognomonic changes from a PDB patient and more than 700 base pairs (bps) of MV sequence in three other PDB patients. These sequences were undetectable in four normal marrow samples studied simultaneously. Similar inclusions have been described in osteoclasts from patients with pycnodysostosis, osteopetrosis, and in foreign body giant cells of cases with primary oxalosis (Mills et al., 1988; Bianco et al., 1992). Other research groups have hypothesized an association between another paramyxovirus, the canine distemper virus (CDV), and PDB. The CDV is generally transmitted from infected dogs to humans through a bite or scratch and, indeed, several reports indicated that dog ownership was significantly more common in the PDB patients than in the control subjects (Anderson and O'Driscoll, 1986; O'Driscoll et al., 1990; Khan et al., 1996). Thus, Gordon et al. (1991) first demonstrated the presence of CDV mRNA in 11 of 25 bone biopsies from PDB patients using *in situ* hybridization analysis. These results were subsequently confirmed by Mee et al. (1998) that found the presence of CDV in all the tested samples from 15 PDB patients, using the *in situ* reverse transcriptase-polymerase chain reaction (IS-RT-PCR). Furthermore, *in vitro* reports suggested that CDV may induce osteoclastogenesis in human osteoclast precursors by activation of nuclear NFκB and SQSTM1/p62 (Selby et al., 2006), and more recently fusion and hemagglutinin proteins of CDV were shown to promote osteoclast formation through NFκB dependent and independent mechanisms (Wang et al., 2019). Altogether these results suggest that paramyxoviruses could induce in osteoclasts morphological changes resembling those described in PDB patients. However, many other attempts were made to replicate these findings in bone and blood samples from PDB patients, with negative results (Ralston et al., 1991; Birch et al., 1994; Helfrich et al., 2000; Ooi et al., 2000; Ralston et al., 2007; Matthews et al., 2008). While a different ability to detect the viral inclusions according to the technique used (from immunohistochemistry to *in situ* hybridization or RT-PCR) might in part explain such discordant findings (Hoyland et al., 2003), it has been also speculated that these inclusions might indeed originate from cell aggregates of undegraded proteins resulting from the dysregulation of cell autophagy consequent to an abnormal p62/SQSTM1 function (Vallet and Ralston, 2016a). However, the MV may persist for long time in cell types different form osteoclasts and osteoclast precursors and promote the disease in patients at a later time point. In this regard, Reddy et al. (1996) demonstrated that, in PDB patients, the MV nucleocapsid transcript expression is not restricted only to the osteoclast lineage but that also immature multipotent hematopoietic cells leading to granulocyte, erythrocyte, macrophage, and platelet expressed these transcripts. These results suggest that the pluripotent hematopoietic stem cells could be the initial target for MV infection in PDB patients.

In the last 20 years, animal models have been used to evaluate whether MV infection can induce the development of pagetic-like osteoclast and bone lesions. The MV genome consists of six genes encoding for the nucleocapsid, the matrix, the fusion, and hemagglutinin proteins, as well as the proteins L and P which both constitute the viral polymerase. Kurihara et al. (2000) first demonstrated that the transfection of normal human osteoclast precursors with the MV nucleocapsid protein (MVNP) caused the development of osteoclasts showing several functional and morphological characteristics of PDB osteoclasts. These characteristics include the increased cells size, the increased number of nuclei per cell, the increased capacity of bone resorption, the hypersensitivity to 1,25-$(OH)_2D_3$, and the increased TAF II-17 expression (Table 3). All these features were also described in osteoclasts developed *in vitro* from marrow samples of pagetic patients and were not observed when normal human osteoclast precursors were transfected with the MV matrix and fusion genes (Kurihara et al., 2000). Additional studies were performed using transgenic mice in which the human MV receptor, CD46, has been transfected in preosteoclastic cells. In effect, normal mice do not express the CD46 and are therefore resistant to MV infection. In CD46 transgenic mice the MV infection caused the development of osteoclasts showing functional and morphological properties similar both to those expressed by PDB osteoclasts and to those observed in normal human osteoclast' precursors transfected *in vitro* (Reddy et al., 2001). Then, similar evidences were provided by the development of a transgenic mice model expressing the MVNP in the osteoclast lineage (TRAP-MVNP-mice). These mice not only had osteoclasts sharing all the phenotype characteristics of pagetic osteoclasts, but up to 30%–40% of them developed localized bone lesions in the L1-L4 vertebrae resembling those seen in patients with PDB (Kurihara et al., 2006; Miyagawa et al., 2020). Remarkably, later experiments in the same mice model demonstrated that, likewise observed in osteoclast from PDB patients (Roodman et al., 1992), MVNP expression induces the production of high levels of IL-6 from the osteoclast, which in turn increases expression of osteoclast IGF-1 in an autocrine manner (Teramachi et al., 2016). This increase in IGF-1 then upregulate the expression of coupling factors such as ephrinB2 in osteoclasts and EphB4 in osteoblasts (Teramachi et al., 2016; Miyagawa et al., 2020), leading to a parallel increase in bone formation that is a hallmark of PDB. Not only conditional deletion of IGF-1 in osteoclast of TRAP-MVNP-mice (MVNP/Igf1-cKO) totally blocked the increase in bone formation and the development of pagetic lesions, but, of interest mice harboring the knockin P394L mutation of *SQSTM1*, only exhibited increased bone resorption, but not formation (Teramachi et al., 2016; Miyagawa et al., 2020). In a different set of studies, the same Authors bred the TRAP-

TABLE 3 Major *in vitro* characteristics of pagetic osteoclasts from PDB patients, *SQSTM1* P394L mice or transgenic MVNP mice models.

Phenotype characteristic	Human pagetic osteoclasts	SQSTM1 P394L osteoclasts	Transgenic MVNP osteoclasts
Increased size	+	+	+
Increased number of nuclei	+	+	+
Increased sensitivity to RANKL	+	+	+
Increased sensitivity to 1,25(OH)2 vitamin D	+	−	+
Increased IL-6 production	+/−[a]	−	+

[a]Described by some but not all studies.

MVNP-mice to the knockin P394L mice to generate a p62KI/MVNP mice model, in order to assess the potential interaction between genetic and viral factors (Kurihara et al., 2011). While osteoclast precursors from p62KI/MVNP and TRAP-MVNP mice models showed all the typical features of pagetic osteoclast precursors, an incomplete phenotype was observed in osteoclasts from the knockin P394L animals (mainly characterized by the increased RANKL sensitivity of osteoclast precursors). Moreover, p62KI/MVNP mice generated the highest number of hyper-multinucleated PDB-like osteoclasts and up to 40% of them, between 18 and 26 months of age, developed focal bone lesions within vertebral bone, that completely replicated those seen in human PDB, with the presence of thickened trabeculae, woven bone and extensive marrow fibrosis (Kurihara et al., 2011). It was concluded that, at least in mice, *SQSTM1* mutation was mainly able to increase RANKL sensitivity of osteoclast precursors, whereas MVNP was responsible for most of the PDB-like features (Kurihara et al., 2011), including the increased IL-6 production that is necessary for the coupling of osteoclast and osteoblast activity, leading the parallel increase in bone formation.

Other viruses, such as the swine influenza virus and the pig vesicular disease virus might also be implicated in the pathogenesis of PDB. These viruses are very difficult to identify and can persist in the asymptomatic phase for a long time in infected carriers (Marschall et al., 1996; Lin et al., 1998). In this regard, other epidemiological studies carried out in Italy and Spain have shown a higher prevalence of the disease in rural areas, especially in subjects in close contact with dogs and other animal species such as cattle and pigs (Lopez-Abente et al., 1997; Merlotti et al., 2005). It is therefore plausible that different viral infections, carried by different animal species, may be involved as possible triggers in the etiopathogenesis of PDB.

3.2 Other environmental risk factors

Environmental toxins such as arsenic or lead have been suggested as possible etiological agents of PDB. In 1974, a survey performed in the United Kingdom identified a cluster of six Lancashire towns where the average age-standardized prevalence of PDB was 6.3% compared with 4.3% in the remaining 25 and pointed out a possible link with the cotton industry (Barker et al., 1980). Considering that the two towns of the six with highest PDB prevalence are situated on estuaries whereas the two towns of the six with lowest PDB prevalence are above sea level, Barker and colleagues suggested a waterborne agent, the calcium arsenate [$Ca_3(AsO_4)_2$], as the possible causative PDB agent. Indeed, $Ca_3(AsO_4)_2$ was a pesticide largely used to protect the cotton crops against the boll weevils (*Anthonomus grandis*) until 1945, when it was progressively replaced by the less toxic Dichlorodiphenyltrichloroethane (DDT). Since the use of $Ca_3(AsO_4)_2$ as pesticide and the PDB incidence in Lancashire significantly both diminished in parallel in the last decades of 20th century, it has been hypothesized a pathogenic link between $Ca_3(AsO_4)_2$ use as pesticide and PDB (Lever, 2002). However, no direct evidence supports this hypothesis (Singer, 2015). On the other hand, Spencer et al. (1992) demonstrated a considerable occupational and environmental exposure to lead in 54 PDB patients. The lead amount was then determined in the bone specimen from PDB patients in two studies. In the first study, Barker et al. (1982) measured the lead levels in autopsy bone specimens form subject affected or unaffected by PDB and found that lead levels were lower in bone macroscopically affected by PDB compared to either normal bone from control individuals or bone from pagetic patients macroscopically unaffected by the disease. In the second study, Adachi et al. (1998), using bone biopsy samples, demonstrated that lead content in cortical bone was higher in PDB patients compared to patients with osteoporosis or with renal osteodystrophy. More recently, significant lower levels of some heavy metals, including arsenic and lead, were detected in urinary samples from PDB patients compared to healthy controls. Also, urinary cesium levels were lower in PDB compared to controls (Numan et al., 2019). However, in cellular models, an inhibitory effect of arsenic, lead, and cesium on osteoclast formation, on mean number of nuclei per cell, and on bone resorption were observed (Numan et al., 2019). An interaction with *SQSTM1* mutation was also described. In fact, in presence of cadmium, *SQSTM1* gene expression was upregulated in osteoclasts from patients with PDB versus healthy controls, particularly in

osteoclasts from carriers of the *SQSTM1* mutation (Numan et al., 2019). Taken together, all the above results do not allow to reach a definitive conclusion about the possible involvement of heavy metals in the PDB pathogenesis.

Environmental factors other than metals have been also proposed as potential PDB triggers. Analysing self-reported medical questionnaires compiled by 864 pagetic patients and 500 healthy controls, all enrolled between spouses and friends of PDB patients, Siris observed that dietary calcium intake during childhood and adolescence (estimated by number of milk glasses consumed each day) was significantly lower in PDB patients compared to controls, suggesting a potential link between the low milk and calcium intake in childhood and adolescence and the susceptibility to PDB (Siris, 1994). Analysing the hospital discharges collected in England, Wales, and Scotland from 1966 to 1972, Barker and Gardner (1974) proposed a significant association between the occurrence of vitamin D deficiency related rickets in childhood and the development of PDB in elderly age. Despite this hypothesis is very intriguing considering the pleiotropic biological activities of vitamin D, evidences for an association between PDB and vitamin D deprivation in childhood are inconclusive at the present time. Likewise, excessive biomechanical loading has been proposed as potential trigger for PDB development (Solomon, 1979). This should also explain the focal nature of the disease. More recently, Michou et al. (2012), analysing all members of 18 French-Canadian pagetic families, established a significant association between current or past tobacco exposure and PDB occurrence. In fact, 43% of PDB patients were current or past smokers versus 18% of relatives unaffected by PDB. The same study group demonstrated that, in *in vitro* models, likewise observed for cadmium, *SQSTM1* expression was upregulated by tobacco smoke condensates, particularly in the presence of *SQSTM1* mutation (Numan et al., 2019). Using data from a French-Canadian cohort, Audet et al. (2017) demonstrated a significant association between wood fired heating in childhood and/or adolescence and both familial and no-familial form of PDB. In addition, familial form of PDB was significantly associated with residency near a mine and hunting. However, despite all these environmental factors have been associated to an increased risk of PBD in some patient cohorts, no conclusive evidence can be drawn.

4 MicroRNAs and epigenetics

As emerged above about the genetics of PDB, an incomplete penetrance of PDB has been reported in familial PDB, thus limiting the role of *SQSTM1* mutational analysis to the clinical practice (Falchetti et al., 2010). Moreover, the genetic heterogeneity of PDB and/or the presence of still unknown modifier genes or triggers able to control its clinical expression in subjects with germline mutations (e.g., in *SQSTM1* gene, as also in other of the above-mentioned genes) complicate our understanding of the genetic mechanisms of the disorder. Indeed, as previously described, exposure to several environmental triggers has been postulated, which could act as disease modifying agents affecting the susceptibility to develop PDB, especially in subjects who may be in some way genetically predisposed. In this respect, a potential unifying mechanism linking genetic and environmental factor in the pathogenesis of PDB, yet to be demonstrated as such, could be represented by epigenetics. Specifically, epigenetics deals with changes in gene expression not resulting directly from mutations of genomic DNA but possibly leading to inherited traits both at intra-generational and inter-generational level. In example, it was shown that DNA methylation can modulate the expression of *POMC* gene, encoding for the pro-opiomelanocortin molecule, thus representing a biological link between early childhood exposures and subsequent obese phenotype development (Candler et al., 2019).

Among the more investigated epigenetic mechanisms are DNA methylation, and histone modifications, both mechanisms capable of influencing the ability of one or more genes to be transcribed adequately or completely. Even bone tissue and bone cells may undergo these problems deriving from exposure to food and environmental factors (especially when prolonged over time) capable of negatively modulating the correct expression of relevant genes, for example, in the regulation of osteoclast differentiation, maturation and metabolic activation. Regarding PDB, a combined genomic analysis and machine learning approach identified several chemical signatures, which appeared remarkably different in the DNA of PDB patients (Diboun et al., 2021). In this study, a complex and technologically refined genome-wide profiling of DNA methylation at CpG islands was performed in a cohort of 253 PDB patients also including subject carriers of germline *SQSTM1* mutation, and 280 controls, in order to detect a predictive role of epigenetic markers to differentiate pagetic patients from non-pagetic controls. Combining genomic analysis and machine learning revealed 14 genome-wide significant differentially methylated sites between PDB patients and controls. Interestingly, most of these CpGs resides within/near genes with known to be functionally relevant in the pathogenesis of PDB, including osteoclast differentiation, or related to environmental triggers associated with PDB such as viral infection and mechanical loading. This further suggested the hypothesis that PDB pathogenesis could partly depend by environmental factors.

Likewise, microRNAs are small, non-coding, single-stranded RNAs that post-transcriptionally regulate gene expression, with an essential role in vertebrate development and different biological processes. Of interest a rising number of experimental reports suggested that miRNAs are involved in every step of osteogenesis and bone metabolism, by regulating

the growth, differentiation, and activity of different cell systems inside and outside the skeleton, including osteoclast formation and activity (Gennari et al., 2017). Very recently, two small preliminary studies compared the miRNA expression profile of human osteoclasts derived form peripheral blood mononuclear cells of PDB patients and controls (Stephens et al., 2020; Nguyen et al., 2021). Some miRNAs appeared differently expressed between patients and controls. Target genes and enriched pathway analysis identified possible interactions between these miRNAs and apoptotic pathways or osteoclast signaling pathways such as PI3K/Akt, IFNγ, TGFβ, and c-Fos (Nguyen et al., 2021).

5 Conclusion

PDB has long been considered the second most common disorder of bone metabolism after osteoporosis. However, a dramatic and progressive decline in its prevalence and severity has been observed in many countries, which have made PDB a less frequently diagnosed disease (Michou and Orcel, 2019). The reason for this phenomenon remains unknown, although the rapidity of change observed in geographical areas at elevated PDB prevalence, such as UK, points to an alteration in one or more environmental determinants (Cooper et al., 1999). Moreover, PDB is also considered a model of high turnover bone disease, mainly related to an increase in size and number of acting resorbing osteoclasts at the affected skeletal sites.

Since it first description 1876 either genetic or environmental factors have been implicated in the pathogenesis of this disorder. In the past two decades, thanks to the development in technology, relevant advances have been made in the pathogenesis of PDB, leading to the identification of genetic mutations or variants predisposing to the disease and allowing a better characterization of the role of environmental triggers, such as MV infection, through the development of specifically designed mice models. An update on the pathogenetic mechanisms of PDB and their potential interactions is given on Figure 1. However, despite this remarkable progresses, the molecular and cellular mechanisms leading to the development of this disorder remain in large part unknown. Hopefully, further developments in technology and more detailed studies in animal models and large cohorts of patients will cast additional light into disease mechanism over the next years. There are however important clinical implications relating to the experimental investigations carried out to date. In fact, it has been shown that patients who possess *SQSTM1* gene mutations or other mutations (e.g., *ZNF687* or *PFN1*) have a more severe form of the disease and might thus require more aggressive and continuous treatment. Moreover, the extension of genetic analysis to the relatives of these patients could also allow the identification of new cases of recent onset (even before deformities and other complications have developed) or even allow preventive treatment before the onset of pagetic lesions. Such hypothesis will be verified in the next few years by an international clinical trial in asymptomatic *SQSTM1* mutation carriers (Cronin et al., 2019; Porteous et al., 2020).

Intriguingly, a significant number of genes involved in the pathogenesis of PDB (namely *SQSTM1*, *VCP*, *PFN1*, and *OPTN*) have been also associated with neurodegenerative disorders (e.g., ALS or frontotemporal dementia) suggesting shared pathophysiological mechanisms. Indeed, the *OPTN* gene has been reported to originate from gene duplication of the NFκB regulator named NFκB essential modulator (NEMO), containing also two ubiquitin-binding motifs, all features shared with *SQSTM1* gene. (Tumbarello et al., 2015). Thus, *OPTN* mutations may contribute to both abnormal autophagy and vesicles trafficking, as reported in the ALS-related forms (Ryan and Tumbarello, 2018), and abnormal NFκB activation, as a possible cause of uncontrolled maturation and activation of pagetic osteoclasts. Similarly to *OPTN* and *SQSTM1*, also *VCP* and *PFN1* share common roles in autophagic degradation raising the hypothesis of a common pathogenic mechanism affecting the formation and clearance of misfolded proteins in PDB, ALS and, more generally, in lysosomal storage diseases (Hocking et al., 2012; Lieberman et al., 2012; Vallet and Ralston, 2016b). Indeed, all these genes predispose to a group of neurological conditions included among the MPS category, characterized by accumulation of abnormal protein aggregates within cells, either because the disease-causing mutations result in defects of protein degradation through the proteasome or because they act directly to increase the propensity of the mutated protein to form aggregates (Taylor, 2015). It remains unclear why some patients with these mutations develop PDB while others develop neurological or muscle disorders, but it is likely that the co-inheritance of other variants might affect the clinical phenotype (Ralston, 2020).

Enduring and intriguing mysteries of PDB are also represented by the asymmetric appearance of bone lesions, which are randomly distributed in the body, as well as the non-appearance of new bone lesions during the clinical course of the disease. In this respect, the findings from Diboun et al. (2021), demonstrating significant differentially DNA methylated sites within or near genes regulating osteoclast differentiation, or the response to viral infection and to mechanical loading, might in part explain the clinically anarchic phenotype of PDB.

Author contributions

Conceptualization, LG, DR, DM, and AF; methodology, LG, MM, and RC; data curation, DM, MM, LG, DR, and AF; literature search and writing of sub-sections and tables GC, CM, MM, FP, VA, and MC; original draft preparation, DM, AF, DR, and LG; review and editing, LG and AF; supervision,

DM, DR, MM, AF, and LG. All authors have read and agreed to the published version of the manuscript.

Conflict of interest

The authors declare that the research was conducted in the absence of any commercial or financial relationships that could be construed as a potential conflict of interest.

Publisher's note

References

Abdulla, O., Naqvi, M. J., Shamshuddin, S., Bukhari, M., and Proctor, R. (2018). Prevalence of Paget's disease of bone in lancaster: Time for an update. *Rheumatol. Oxf.* 57, 931–932. doi:10.1093/rheumatology/kex505

Adachi, J. D., Arlen, D., Webber, C. E., Chettle, D. R., Beaumont, L. F., and Gordon, C. L. (1998). Is there any association between the presence of bone disease and cumulative exposure to lead? *Calcif. Tissue Int.* 63, 429–432. doi:10.1007/s002239900552

Albagha, O. M., Visconti, M. R., Alonso, N., Langston, A. L., Cundy, T., Dargie, R., et al. (2010). Genome-wide association study identifies variants at CSF1, OPTN and TNFRSF11A as genetic risk factors for Paget's disease of bone. *Nat. Genet.* 42, 520–524. doi:10.1038/ng.562

Albagha, O. M., Visconti, M. R., Alonso, N., Wani, S., Goodman, K., Fraser, W. D., et al. (2013). Common susceptibility alleles and SQSTM1 mutations predict disease extent and severity in a multinational study of patients with Paget's disease. *J. Bone Min. Res.* 28, 2338–2346. doi:10.1002/jbmr.1975

Albagha, O. M., Wani, S. E., Visconti, M. R., Alonso, N., Goodman, K., Brandi, M. L., et al. (2011). Genome-wide association identifies three new susceptibility loci for Paget's disease of bone.Genetic Determinants of Paget's Disease(GDPD) Consortium. Genome-wide association identifies three new susceptibility loci for Paget's disease of bone. *Nat. Genet.* 43, 685–689. doi:10.1038/ng.845

Alkam, D., Feldman, E. Z., Singh, A., and Kiaei, M. (2017). Profilin 1 biology and its mutation, actin(g) in disease. *Cell. Mol. Life Sci.* 74, 967–981. doi:10.1007/s00018-016-2372-1

Alonso, N., Wani, S., Rose, L., Van't Hof, R. J., Ralston, S. H., and Albagha, O. M. E. (2021). Insertion mutation in Tnfrsf11a causes a Paget's disease-like phenotype in heterozygous mice and osteopetrosis in homozygous mice. *J. Bone Min. Res.* 36, 1376–1386. doi:10.1002/jbmr.4288

Anderson, D. C., and O'Driscoll, J. B. (1986). Dogs and Paget's disease. *Lancet* 1, 41. doi:10.1016/s0140-6736(86)91920-3

Asirvatham, A. R., Kannan, S., Mahadevan, S., Balachandran, K., Sampathkumar, G., Sadacharan, D., et al. (2020). Is Paget disease of bone a predominant disease of south India? Clinical characteristics, therapeutic outcome and follow up of 66 patients from Tamil nadu and brief review of epidemiology. *Indian J. Endocrinol. Metab.* 24, 554–555. doi:10.4103/ijem.IJEM_713_20

Audet, M. C., Jean, S., Beaudoin, C., Guay-Bélanger, S., Dumont, J., Brown, J. P., et al. (2017). Environmental factors associated with familial or non-familial forms of Paget's disease of bone. *Jt. Bone Spine* 84, 719–723. doi:10.1016/j.jbspin.2016.11.010

Barker, D. J., Chamberlain, A. T., Detheridge, F. M., Gardner, M. J., and Guyer, P. B. (1982). Low lead levels in pagetoid bone. *Metab. Bone Dis. Relat. Res.* 4, 243–247. doi:10.1016/0221-8747(82)90034-0

Barker, D. J., Chamberlain, A. T., Guyer, P. B., and Gardner, M. J. (1980). Paget's disease of bone: The Lancashire focus. *Br. Med. J.* 280, 1105–1107. doi:10.1136/bmj.280.6222.1105

Barker, D. J., and Gardner, M. J. (1974). Distribution of Paget's disease in England, Wales and Scotland and a possible relationship with vitamin D deficiency in childhood. *Br. J. Prev. Soc. Med.* 28, 226–232. doi:10.1136/jech.28.4.226

Basle, M. F., Fournier, J. G., Rozenblatt, S., Rebel, A., and Bouteille, M. (1986). Measles virus RNA detected in Paget's disease bone tissue by *in situ* hybridization. *J. Gen. Virol.* 67, 907–913. doi:10.1099/0022-1317-67-5-907

Basle, M. F., Russell, W. C., Goswami, K. K., Rebel, A., Giraudon, P., Wild, F., et al. (1985). Paramyxovirus antigens in osteoclasts from Paget's bone tissue detected by monoclonal antibodies. *J. Gen. Virol.* 66, 2103–2110. doi:10.1099/0022-1317-66-10-2103

Bernardi, R., and Pandolfi, P. P. (2007). Structure, dynamics and functions of promyelocytic leukaemia nuclear bodies. *Nat. Rev. Mol. Cell Biol.* 8, 1006–1016. doi:10.1038/nrm2277

Bianco, P., Silvestrini, G., Ballanti, P., and Bonucci, E. (1992). Paramyxovirus-like nuclear inclusions identical to those of Paget's disease of bone detected in giant cells of primary oxalosis. *Virchows Arch. A Pathol. Anat. Histopathol.* 421, 427–433. doi:10.1007/BF01606916

Birch, M. A., Taylor, W., Fraser, W. D., Ralston, S. H., Hart, C. A., and Gallagher, J. A. (1994). Absence of paramyxovirus RNA in cultures of pagetic bone cells and in pagetic bone. *J. Bone Min. Res.* 9, 11–16. doi:10.1002/jbmr.5650090103

Bolland, M. J., Tong, P. C., Naot, D., Callon, K. E., Wattie, D. J., Gamble, G. D., et al. (2007). Delayed development of Paget's disease in offspring inheriting *SQSTM1* mutations. *J. Bone Min. Res.* 22, 411–415. doi:10.1359/jbmr.061204–

Bouwmeester, T., Bauch, A., Ruffner, H., Angrand, P. O., Bergamini, G., Croughton, K., et al. (2004). A physical and functional map of the human TNF-alpha/NF-kappa B signal transduction pathway. *Nat. Cell Biol.* 6, 97–105. doi:10.1038/ncb1086

Boyce, B. F., Xiu, Y., Li, J., Xing, L., and Yao, Z. (2015). NF-κB-Mediated regulation of osteoclastogenesis. *Endocrinol. Metab. Seoul.* 30, 35–44. doi:10.3803/EnM.2015.30.1.35

Bucelli, R. C., Arhzaouy, K., Pestronk, A., Pittman, S. K., Rojas, L., Sue, C. M., et al. (2015). *SQSTM1* splice site mutation in distal myopathy with rimmed vacuoles. *Neurology* 85, 665–674. doi:10.1212/WNL.0000000000001864

Candler, T., Kühnen, P., Prentice, A. M., and Silver, M. (2019). Epigenetic regulation of POMC; implications for nutritional programming, obesity and metabolic disease. *Front. Neuroendocrinol.* 54, 100773. doi:10.1016/j.yfrne.2019.100773

Carlsson, L., Nyström, L. E., Sundkvist, I., Markey, F., and Lindberg, U. (1977). Actin polymerizability is influenced by profilin, a low molecular weight protein in non-muscle cells. *J. Mol. Biol.* 115, 465–483. doi:10.1016/0022-2836(77)90166-8

Chamoux, E., Couture, J., Bisson, M., Morissette, J., Brown, J. P., and Roux, S. (2009). The p62 P392L mutation linked to Paget's disease induces activation of human osteoclasts. *Mol. Endocrinol.* 23, 1668–1680. doi:10.1210/me.2009-0066

Chung, P. Y., Beyens, G., de Freitas, F., Boonen, S., Geusens, P., Vanhoenacker, F., et al. (2011). Indications for a genetic association of a VCP polymorphism with the pathogenesis of sporadic Paget's disease of bone, but not for TNFSF11 (RANKL) and IL-6 polymorphisms. *Mol. Genet. Metab.* 103, 287–292. doi:10.1016/j.ymgme.2011.03.021

Chung, P. Y., Beyens, G., Riches, P. L., Van Wesenbeeck, L., de Freitas, F., Jennes, K., et al. (2010). Genetic variation in the TNFRSF11A gene encoding RANK is associated with susceptibility to Paget's disease of bone. *J. Bone Min. Res.* 25, 2592–2605. doi:10.1002/jbmr.162

Cook, M. J., Pye, S. R., Lunt, M., Dixon, W. G., Ashcroft, D. M., and O'Neill, T. W. (2021). Incidence of Paget's disease of bone in the UK: Evidence of a continuing decline. *Rheumatol. Oxf.* 60, 5668–5676. doi:10.1093/rheumatology/keab232

Cooper, C., Harvey, N. C., Dennison, E. M., and van Staa, T. P. (2006). Update on the epidemiology of Paget's disease of bone. *J. Bone Min. Res.* 21, P3–P8. doi:10.1359/jbmr.06s201

Cooper, C., Schafheutle, K., Dennison, E., Kellingray, S., Guyer, P., and Barker, D. (1999). The epidemiology of Paget's disease in Britain: Is the prevalence decreasing? *J. Bone Min. Res.* 14, 192–197. doi:10.1359/jbmr.1999.14.2.192

Cronin, O., Forsyth, L., Goodman, K., Lewis, S. C., Keerie, C., Walker, A., et al. (2019). Zoledronate in the prevention of Paget's (ZiPP): Protocol for a randomised trial of genetic testing and targeted zoledronic acid therapy to prevent *SQSTM1*

mediated Paget's disease of bone. *BMJ Open* 9, e030689. doi:10.1136/bmjopen-2019-030689

Cundy, T., McAnulty, K., Wattie, D., Gamble, G., Rutland, M., and Ibbertson, H. K. (1997). Evidence for secular change in Paget's disease. *Bone* 20, 69–71. doi:10.1016/s8756-3282(96)00310-9

Cundy, T., Rutland, M. D., Naot, D., and Bolland, M. (2015). Evolution of Paget's disease of bone in adults inheriting *SQSTM1* mutations. *Clin. Endocrinol.* 83, 315–319. doi:10.1111/cen.12741

Custer, S. K., Neumann, M., Lu, H., Wright, A. C., and Taylor, J. P. (2010). Transgenic mice expressing mutant forms VCP/p97 recapitulate the full spectrum of IBMPFD including degeneration in muscle, brain and bone. *Hum. Mol. Genet.* 19, 1741–1755. doi:10.1093/hmg/ddq050

Daroszewska, A., van 't Hof, R. J., Rojas, J. A., Layfield, R., Landao-Basonga, E., Rose, L., et al. (2011). A point mutation in the ubiquitin-associated domain of SQSMT1 is sufficient to cause a Paget's disease-like disorder in mice. *Hum. Mol. Genet.* 20, 2734–2744. doi:10.1093/hmg/ddr172

de la Mata, J., Uy, H. L., Guise, T. A., Story, B., Boyce, B. F., Mundy, G. R., et al. (1995). Interleukin-6 enhances hypercalcemia and bone resorption mediated by parathyroid hormone-related protein *in vivo*. *J. Clin. Invest.* 95, 2846–2852. doi:10.1172/JCI117990

De Ridder, R., Boudin, E., Vandeweyer, G., Devogelaer, J. P., Fransen, E., Mortier, G., et al. (2019). Genetic variation in RIN3 in the Belgian population supports its involvement in the pathogenesis of Paget's disease of bone and modifies the age of onset. *Calcif. Tissue Int.* 104, 613–621. doi:10.1007/s00223-019-00530-3

Dessay, M., Couture, E., Maaroufi, H., Fournier, F., Gagnon, E., Droit, A., et al. (2022). Attenuated clinical and osteoclastic phenotypes of Paget's disease of bone linked to the p.Pro392Leu/SQSTM1 mutation by a rare variant in the DOCK6 gene. *BMC Med. Genomics* 15, 41. doi:10.1186/s12920-022-01198-9

Dessay, M., Jobin Gervais, F., Simonyan, D., Samson, A., Gleeton, G., Gagnon, E., et al. (2020). Clinical phenotype of adult offspring carriers of the p.Pro392Leu mutation within the *SQSTM1* gene in Paget's disease of bone. *Bone Rep.* 13, 100717. doi:10.1016/j.bonr.2020.100717

Diboun, I., Wani, S., Ralston, S. H., and Albagha, O. M. (2021). Epigenetic analysis of Paget's disease of bone identifies differentially methylated loci that predict disease status. *Elife* 10, e65715. doi:10.7554/eLife.65715

Divisato, G., Formicola, D., Esposito, T., Merlotti, D., Pazzaglia, L., Del Fattore, A., et al. (2016). *ZNF687* mutations in severe Paget disease of bone associated with giant cell tumor. *Am. J. Hum. Genet.* 98, 275–286. doi:10.1016/j.ajhg.2015.12.016

Duran, A., Serrano, M., Leitges, M., Flores, J. M., Picard, S., Brown, J. P., et al. (2004). The atypical PKC-interacting protein p62 is an important mediator of RANK-activated osteoclastogenesis. *Dev. Cell* 6, 303–309. doi:10.1016/s1534-5807(03)00403-9

Eekhoff, E. W., Karperien, M., Houtsma, D., Zwinderman, A. H., Dragoiescu, C., Kneppers, A. L., et al. (2004). Familial Paget's disease in The Netherlands: Occurrence, identification of new mutations in the sequestosome 1 gene, and their clinical associations. *Arthritis Rheum.* 50, 1650–1654. doi:10.1002/art.20224

Falchetti, A., Di Stefano, M., Marini, F., Ortolani, S., Ulivieri, M. F., Bergui, S., et al. (2009). Genetic epidemiology of Paget's disease of bone in Italy: sequestosome1/p62 gene mutational test and haplotype analysis at 5q35 in a large representative series of sporadic and familial Italian cases of Paget's disease of bone. *Calcif. Tissue Int.* 84, 20–37. doi:10.1007/s00223-008-9192-8

Falchetti, A., Marini, F., Masi, L., Amedei, A., Brandi, M. L., Laura, M., et al. (2010). Genetic aspects of the Paget's disease of bone: Concerns on the introduction of DNA-based tests in the clinical practice. Advantages and disadvantages of its application. *Eur. J. Clin. Invest.* 40, 655–667. doi:10.1111/j.1365-2362.2010.02312.x

Fecto, F., and Siddique, T. (2012). UBQLN2/P62 cellular recycling pathways in amyotrophic lateral sclerosis and frontotemporal dementia. *Muscle Nerve* 45, 157–162. doi:10.1002/mus.23278

Friedrichs, W., Reddy, S. V., Bruder, J. M., Cundy, T., Cornish, J., Singer, F. R., et al. (2002). Sequence analysis of measles virus nucleocapsid transcripts in patients with Paget's disease. *J. Bone Min. Res.* 17, 145–151. doi:10.1359/jbmr.2002.17.1.145

Fries, G. R., Gassen, N. C., and Rein, T. (2017). The FKBP51 glucocorticoid receptor Co-chaperone: Regulation, function, and implications in Health and disease. *Int. J. Mol. Sci.* 18, 2614. doi:10.3390/ijms18122614

Gassen, N. C., Hartmann, J., Schmidt, M. V., and Rein, T. (2015). FKBP5/FKBP51 enhances autophagy to synergize with antidepressant action. *Autophagy* 11, 578–580. doi:10.1080/15548627.2015.1017224

Gennari, L., Bianciardi, S., and Merlotti, D. (2017). MicroRNAs in bone diseases. *Osteoporos. Int.* 28, 1191–1213. doi:10.1007/s00198-016-3847-5

Gennari, L., Gianfrancesco, F., Di Stefano, M., Rendina, D., Merlotti, D., Esposito, T., et al. (2010). *SQSTM1* gene analysis and gene-environment interaction in Paget's disease of bone. *J. Bone Min. Res.* 25, 1375–1384. doi:10.1002/jbmr.31

Gennari, L., Merlotti, D., Martini, G., and Nuti, R. (2006). Paget's disease of bone in Italy. *J. Bone Min. Res.* 21, P14–P21. doi:10.1359/jbmr.06s203

Gennari, L., Rendina, D., Falchetti, A., and Merlotti, D. (2019). Paget's disease of bone. *Paget's Dis. Bone. Calcif. Tissue Int.* 104, 483–500. doi:10.1007/s00223-019-00522-3

Gennari, L., Rendina, D., Picchioni, T., Bianciardi, S., Materozzi, M., Nuti, R., et al. (2018). Paget's disease of bone: An update on epidemiology, pathogenesis and pharmacotherapy. *Expert Opin. Orphan Drugs* 8, 485–496. doi:10.1080/21678707.2018.1500691

Gianfrancesco, F., Rendina, D., Di Stefano, M., Mingione, A., Esposito, T., Merlotti, D., et al. (2012). A nonsynonymous TNFRSF11A variation increases NFκB activity and the severity of Paget's disease. *J. Bone Min. Res.* 27, 443–452. doi:10.1002/jbmr.542

Good, D. A., Busfield, F., Fletcher, B. H., Lovelock, P. K., Duffy, D. L., Kesting, J. B., et al. (2004). Identification of *SQSTM1* mutations in familial Paget's disease in Australian pedigrees. *Bone* 35, 277–282. doi:10.1016/j.bone.2004.01.010

Goode, A., and Layfield, R. (2010). Recent advances in understanding the molecular basis of Paget disease of bone. *J. Clin. Pathol.* 63, 199–203. doi:10.1136/jcp.2009.064428

Goode, A., Long, J. E., Shaw, B., Ralston, S. H., Visconti, M. R., Gianfrancesco, F., et al. (2014). Paget disease of bone-associated UBA domain mutations of SQSTM1 exert distinct effects on protein structure and function. *Biochim. Biophys. Acta* 1842, 992–1000. doi:10.1016/j.bbadis.2014.03.006

Gordon, M. T., Anderson, D. C., and Sharpe, P. T. (1991). Canine distemper virus localised in bone cells of patients with Paget's disease. *Bone* 12, 195–201. doi:10.1016/8756-3282(91)90042-h

Guay-Bélanger, S., Picard, S., Gagnon, E., Morissette, J., Siris, E. S., Orcel, P., et al. (2015). Detection of SQSTM1/P392L post-zygotic mutations in Paget's disease of bone. *Hum. Genet.* 134, 53–65. doi:10.1007/s00439-014-1488-3

Han, G., Zuo, J., and Holliday, L. S. (2019). Specialized roles for actin in osteoclasts: Unanswered questions and therapeutic opportunities. *Biomolecules* 9, E17. pii. doi:10.3390/biom9010017

Hansen, M. F., Seton, M., and Merchant, A. (2006). Osteosarcoma in Paget's disease of bone. *J. Bone Min. Res.* 21, P58–P63. doi:10.1359/jbmr.06s211

Haridy, Y., Witzmann, F., Asbach, P., and Reisz, R. R. (2019). Permian metabolic bone disease revealed by microCT: Paget's disease-like pathology in vertebrae of an early amniote. *PLoS One* 7 (14), e0219662. doi:10.1371/journal.pone.0219662

Helfrich, M. H., Hobson, R. P., Grabowski, P. S., Zurbriggen, A., Cosby, S. L., Dickson, G. R., et al. (2000). A negative search for a paramyxoviral etiology of Paget's disease of bone: Molecular, immunological, and ultrastructural studies in UK patients. *J. Bone Min. Res.* 15, 2315–2329. doi:10.1359/jbmr.2000.15.12.2315

Hiruma, Y., Kurihara, N., Subler, M. A., Zhou, H., Boykin, C. S., Zhang, H., et al. (2008). A SQSTM1/p62 mutation linked to Paget's disease increases the osteoclastogenic potential of the bone microenvironment. *Hum. Mol. Genet.* 17, 3708–3719. doi:10.1093/hmg/ddn266

Hocking, L. J., Lucas, G. J., Daroszewska, A., Cundy, T., Nicholson, G. C., Donath, J., et al. (2004). Novel UBA domain mutations of *SQSTM1* in Paget's disease of bone: Genotype phenotype correlation, functional analysis, and structural consequences. *J. Bone Min. Res.* 19, 1122–1127. doi:10.1359/JBMR.0403015

Hocking, L. J., Lucas, G. J., Daroszewska, A., Mangion, J., Olavesen, M., Cundy, T., et al. (2002). Domain-specific mutations in sequestosome 1 (SQSTM1) cause familial and sporadic Paget's disease. *Hum. Mol. Genet.* 11, 2735–2739. doi:10.1093/hmg/11.22.2735

Hocking, L. J., Whitehouse, C., and Helfrich, M. H. (2012). Autophagy: A new player in skeletal maintenance? *J. Bone Min. Res.* 27, 1439–1447. doi:10.1002/jbmr.1668

Hofbauer, L. C., and Heufelder, A. E. (2000). The role of receptor activator of nuclear factor-κB ligand and osteoprotegerin in the pathogenesis and treatment of metabolic bone diseases. *J. Clin. Endocrinol. Metab.* 85, 2355–2363. doi:10.1210/jcem.85.7.6702

Hoyland, J. A., Dixon, J. A., Berry, J. L., Davies, M., Selby, P. L., and Mee, A. P. (2003). A comparison of *in situ* hybridisation, reverse transcriptase-polymerase chain reaction (RT-PCR) and *in situ*-RT-PCR for the detection of canine distemper virus RNA in Paget's disease. *J. Virol. Methods* 109, 253–259. doi:10.1016/s0166-0934(03)00079-x

Hughes, A. E., Ralston, S. H., Marken, J., Bell, C., MacPherson, H., Wallace, R. G., et al. (2000). Mutations in *TNFRSF11A*, affecting the signal peptide of RANK, cause familial expansile osteolysis. *Nat. Genet.* 24, 45–48. doi:10.1038/71667

Iwamoto, S. J., Rothman, M. S., Duan, S., Baker, J. C., Mumm, S., and Whyte, M. P. (2020). Early-onset Paget's disease of bone in a Mexican family caused by a novel

tandem duplication (77dup27) in TNFRSF11A that encodes RANK. *Bone* 133, 115224. doi:10.1016/j.bone.2020.115224

Jin, W., Chang, M., Paul, E. M., Babu, G., Lee, A. J., Reiley, W., et al. (2008). Deubiquitinating enzyme CYLD negatively regulates RANK signaling and osteoclastogenesis in mice. *J. Clin. Invest.* 118, 1858–1866. doi:10.1172/JCI34257

Johnson-Pais, T. L., Singer, F. R., Bone, H. G., McMurray, C. T., Hansen, M. F., and Leach, R. J. (2003). Identification of a novel tandem duplication in exon 1 of the TNFRSF11A gene in two unrelated patients with familial expansile osteolysis. *J. Bone Min. Res.* 18, 376–380. doi:10.1359/jbmr.2003.18.2.376

Johnson-Pais, T. L., Wisdom, J. H., Weldon, K. S., Cody, J. D., Hansen, M. F., Singer, F. R., et al. (2003). Three novel mutations in SQSTM1 identified in familial Paget's disease of bone. *J. Bone Min. Res.* 18, 1748–1753. doi:10.1359/jbmr.2003.18.10.1748

Joung, I., Strominger, J. L., and Shin, J. (1996). Molecular cloning of a phosphotyrosine-independent ligand of the p56lck SH2 domain. *Proc. Natl. Acad. Sci. U. S. A.* 93, 5991–5995. doi:10.1073/pnas.93.12.5991

Ke, Y. H., Yue, H., He, J. W., Liu, Y. J., and Zhang, Z. L. (2009). Early onset Paget's disease of bone caused by a novel mutation (78dup27) of the TNFRSF11A gene in a Chinese family. *Acta Pharmacol. Sin.* 30, 1204–1210. doi:10.1038/aps.2009.90

Khan, S. A., Brennan, P., Newman, J., Gray, R. E., McCloskey, E. V., and Kanis, J. A. (1996). Paget's disease of bone and unvaccinated dogs. *Bone* 19, 47–50. doi:10.1016/8756-3282(96)00117-2

Kovach, M. J., Waggoner, B., Leal, S. M., Gelber, D., Khardori, R., Levenstien, M. A., et al. (2001). Clinical delineation and localization to chromosome 9p13.3-p12 of a unique dominant disorder in four families: Hereditary inclusion body myopathy, Paget disease of bone, and frontotemporal dementia. *Mol. Genet. Metab.* 74, 458–475. doi:10.1006/mgme.2001.3256

Kukita, T., Wada, N., Kukita, A., Kakimoto, T., Sandra, F., Toh, K., et al. (2004). RANKL-induced DC-STAMP is essential for osteoclastogenesis. *J. Exp. Med.* 200, 941–946. doi:10.1084/jem.20040518

Kurihara, N., Bertolini, D., Suda, T., Akiyama, Y., and Roodman, G. D. (1990). IL-6 stimulates osteoclast-like multinucleated cell formation in long term human marrow cultures by inducing IL-1 release. *J. Immunol.* 144, 4226–4230.

Kurihara, N., Hiruma, Y., Yamana, K., Michou, L., Rousseau, C., Morissette, J., et al. (2011). Contributions of the measles virus nucleocapsid gene and the SQSTM1/p62(P392L) mutation to Paget's disease. *Cell Metab.* 13, 23–34. doi:10.1016/j.cmet.2010.12.002

Kurihara, N., Reddy, S. V., Menaa, C., Anderson, D., and Roodman, G. D. (2000). Osteoclasts expressing the measles virus nucleocapsid gene display a pagetic phenotype. *J. Clin. Invest.* 105, 607–614. doi:10.1172/JCI8489

Kurihara, N., Zhou, H., Reddy, S. V., Garcia Palacios, V., Subler, M. A., Dempster, D. W., et al. (2006). Expression of measles virus nucleocapsid protein in osteoclasts induces Paget's disease-like bone lesions in mice. *J. Bone Min. Res.* 21, 446–455. doi:10.1359/JBMR.051108

Laurier, E., Amiable, N., Gagnon, E., Brown, J. P., and Michou, L. (2017). Effect of a rare genetic variant of TM7SF4 gene on osteoclasts of patients with Paget's disease of bone. *BMC Med. Genet.* 18, 133. doi:10.1186/s12881-017-0495-3

Laurin, N., Brown, J. P., Morissette, J., and Raymond, V. (2002). Recurrent mutation of the gene encoding sequestosome 1 (*SQSTM1/p62*) in Paget disease of bone. *Am. J. Hum. Genet.* 70, 1582–1588. doi:10.1086/340731

Layfield, R., Cavey, J. R., Najat, D., Long, J., Sheppard, P. W., Ralston, S. H., et al. (2006). p62 mutations, ubiquitin recognition and Paget's disease of bone. *Biochem. Soc. Trans.* 34, 735–737. doi:10.1042/BST0340735

Le Ber, I., Camuzat, A., Guerreiro, R., Bouya-Ahmed, K., Bras, J., Nicolas, G., et al. (2013). Genetic Research Network on FF-A*SQSTM1* mutations in French patients with frontotemporal dementia or frontotemporal dementia with amyotrophic lateral sclerosis. *JAMA Neurol.* 70, 1403–1410. doi:10.1001/jamaneurol.2013.3849

Lee, Y., Jonson, P. H., Sarparanta, J., Palmio, J., Sarkar, M., Vihola, A., et al. (2018). TIA1 variant drives myodegeneration in multisystem proteinopathy with SQSTM1 mutations. *J. Clin. Invest.* 128, 1164–1177. doi:10.1172/JCI97103

Lever, J. H. (2002). Paget's disease of bone in Lancashire and arsenic pesticide in cotton mill wastewater: A speculative hypothesis. *Bone* 31, 434–436. doi:10.1016/s8756-3282(02)00833-5

Lieberman, A. P., Puertollano, R., Raben, N., Slaugenhaupt, S., Walkley, S. U., and Ballabio, A. (2012). Autophagy in lysosomal storage disorders. *Autophagy* 8, 719–730. doi:10.4161/auto.19469

Lin, F., Mackay, D. K., and Knowles, N. J. (1998). The persistence of swine vesicular disease virus infection in pigs. *Epidemiol. Infect.* 121, 459–472. doi:10.1017/s0950268898001332

Lopez-Abente, G., Morales-Piga, A., Bachiller-Corral, F. J., Illera-Martín, O., Martín-Domenech, R., and Abraira, V. (2003). Identification of possible areas of high prevalence of Paget's disease of bone in Spain. *Clin. Exp. Rheumatol.* 21, 635–638.

Lopez-Abente, G., Morales-Piga, A., Helena-Ibanez, A., Rey-Rey, J. S., and Corres-Gonzalez, J. (1997). Cattle, pets and Paget's disease of bone. *Epidemiology* 8, 247–251. doi:10.1097/00001648-199705000-00004

Lu, B., Jiao, Y., Wang, Y., Dong, J., Wei, M., Cui, B., et al. (2017). A FKBP5 mutation is associated with Paget's disease of bone and enhances osteoclastogenesis. *Exp. Mol. Med.* 49, e336. doi:10.1038/emm.2017.64

Luxenburg, C., Geblinger, D., Klein, E., Anderson, K., Hanein, D., Geiger, B., et al. (2007). The architecture of the adhesive apparatus of cultured osteoclasts: From podosome formation to sealing zone assembly. *PLoS One* 2, e179. doi:10.1371/journal.pone.0000179

Makaram, N. S., and Ralston, S. H. (2021). Genetic determinants of Paget's disease of bone. *Curr. Osteoporos. Rep.* 19, 327–337. doi:10.1007/s11914-021-00676-w

Malovannaya, A., Lanz, R. B., Jung, S. Y., Bulynko, Y., Le, N. T., Chan, D. W., et al. (2011). Analysis of the human endogenous coregulator complexome. *Cell* 145, 787–799. doi:10.1016/j.cell.2011.05.006

Marschall, M., Schuler, A., and Meier-Ewert, H. (1996). Influenza C virus RNA is uniquely stabilized in a steady state during primary and secondary persistent infections. *J. Gen. Virol.* 77, 681–686. doi:10.1099/0022-1317-77-4-681

Matthews, B. G., Afzal, M. A., Minor, P. D., Bava, U., Callon, K. E., Pitto, R. P., et al. (2008). Failure to detect measles virus ribonucleic acid in bone cells from patients with Paget's disease. *J. Clin. Endocrinol. Metab.* 93, 1398–1401. doi:10.1210/jc.2007-1978

Matthews, B. G., Naot, D., Bava, U., Callon, K. E., Pitto, R. P., McCowan, S. A., et al. (2009). Absence of somatic SQSTM1 mutations in Paget's disease of bone. *J. Clin. Endocrinol. Metab.* 94, 691–694. doi:10.1210/jc.2008-1140

Mazières, B., Coste, J., Euller-Ziegler, L., Fardellone, P., Fautrel, B., Pouchot, J., et al. (2018). Prevalence of pelvic Paget's disease of bone in France. *Bone* 107, 143–144. doi:10.1016/j.bone.2017.11.017

Mee, A. P., Dixon, J. A., Hoyland, J. A., Davies, M., Selby, P. L., and Mawer, E. B. (1998). Detection of canine distemper virus in 100% of Paget's disease samples by *in situ*-reverse transcriptase-polymerase chain reaction. *Bone* 23, 171–175. doi:10.1016/s8756-3282(98)00079-9

Merchant, A., Smielewska, M., Patel, N., Akunowicz, J. D., Saria, E. A., Delaney, J. D., et al. (2009). Somatic mutations in SQSTM1 detected in affected tissues from patients with sporadic Paget's disease of bone. *J. Bone Min. Res.* 24, 484–494. doi:10.1359/jbmr.081105

Merlotti, D., Gennari, L., Galli, B., Martini, G., Calabro, A., De Paola, V., et al. (2005). Characteristics and familial aggregation of Paget's disease of bone in Italy. *J. Bone Min. Res.* 20, 1356–1364. doi:10.1359/JBMR.050322

Merlotti, D., Materozzi, M., Bianciardi, S., Guarnieri, V., Rendina, D., Volterrani, L., et al. (2020). Mutation of *PFN1* gene in an early onset, polyostotic paget-like disease. *J. Clin. Endocrinol. Metab.* 105, dgaa252. doi:10.1210/clinem/dgaa252

Michou, L., Collet, C., Morissette, J., Audran, M., Thomas, T., Gagnon, E., et al. (2012). Epidemiogenetic study of French families with Paget's disease of bone. *Jt. Bone Spine* 79, 393–398. doi:10.1016/j.jbspin.2011.07.005

Michou, L., and Orcel, P. (2019). Has Paget's bone disease become rare? *Jt. Bone Spine* 86, 538–541. doi:10.1016/j.jbspin.2019.01.015

Mills, B. G., Frausto, A., Singer, F. R., Ohsaki, Y., Demulder, A., and Roodman, G. D. (1994). Multinucleated cells formed *in vitro* from Paget's bone marrow express viral antigens. *Bone* 15, 443–448. doi:10.1016/8756-3282(94)90823-0

Mills, B. G., and Singer, F. R. (1976). Nuclear inclusions in Paget's disease of bone. *Science* 194, 201–202. doi:10.1126/science.959849

Mills, B. G., Singer, F. R., Weiner, L. P., Suffin, S. C., Stabile, E., and Holst, P. (1984). Evidence for both respiratory syncytial virus and measles virus antigens in the osteoclasts of patients with Paget's disease of bone. *Clin. Orthop. Relat. Res.* 183, 303–311. doi:10.1097/00003086-198403000-00044

Mills, B. G., Yabe, H., and Singer, F. R. (1988). Osteoclasts in human osteopetrosis contain viralnucleocapsid- like nuclear inclusions. *J. Bone Min. Res.* 3, 101–106. doi:10.1002/jbmr.5650030115

Miyagawa, K., Ohata, Y., Delgado-Calle, J., Teramachi, J., Zhou, H., Dempster, D. D., et al. (2020). Osteoclast-derived IGF1 is required for pagetic lesion formation *in vivo*. *JCI Insight* 5, e133113. doi:10.1172/jci.insight.133113

Miyamoto, Y., Yamauchi, J., Sanbe, A., and Tanoue, A. (2007). Dock6, a Dock-C subfamily guanine nucleotide exchanger, has the dual specificity for Rac1 and Cdc42 and regulates neurite outgrowth. *Exp. Cell Res.* 313, 791–804. doi:10.1016/j.yexcr.2006.11.017

Montagu, M. F. A. (1949). Paget's disease (osteitis deformans) and hereditary. *Am. J. Hum. Genet.* 1, 94–95.

Morales-Piga, A. A., Rey-Rey, J. S., Corres-Gonzalez, J., Garcia-Sagredo, J. M., and Lopez-Abente, G. (1995). Frequency and characteristics of familial aggregation of

Paget's disease of bone. *J. Bone Min. Res.* 10, 663–670. doi:10.1002/jbmr.5650100421

Mullin, B. H., Zhu, K., Brown, S. J., Mullin, S., Tickner, J., Pavlos, N. J., et al. (2019). Genetic regulatory mechanisms in human osteoclasts suggest a role for the STMP1 and DCSTAMP genes in Paget's disease of bone. *Sci. Rep.* 9, 1052. doi:10.1038/s41598-018-37609-0

Nakatsuka, K., Nishizawa, Y., and Ralston, S. H. (2003). Phenotypic characterization of early onset Paget's disease of bone caused by a 27-bp duplication in the *TNFRSF11A* gene. *J. Bone Min. Res.* 18, 1381–1385. doi:10.1359/jbmr.2003.18.8.1381

Nguyen, H. D., Bisson, M., Scott, M., Boire, G., Bouchard, L., and Roux, S. (2021). miR profile in pagetic osteoclasts: from large-scale sequencing to gene expression study. *J. Mol. Med.* 99, 1771–1781. doi:10.1007/s00109-021-02128-5

Numan, M. S., Jean, S., Dessay, M., Gagnon, E., Amiable, N., Brown, J. P., et al. (2019). Gene-environment interactions in Paget's disease of bone. *Jt. Bone Spine* 86, 373–380. doi:10.1016/j.jbspin.2018.12.007

O'Driscoll, J. B., Buckler, H. M., Jeacock, J., and Anderson, D. C. (1990). Dogs, distemper and osteitis deformans: A further epidemiological study. *Bone Min.* 11, 209–216. doi:10.1016/0169-6009(90)90060-s

Obaid, R., Wani, S., Azfer, A., Hurd, T., Jones, R., Cohen, P., et al. (2015). Optineurin negatively regulates osteoclast differentiation by modulating NF-κB and interferon signaling: Implications for Paget's disease. *Cell Rep.* 13, 1096–1102. doi:10.1016/j.celrep.2015.09.071

Ooi, C. G., Walsh, C. A., Gallagher, J. A., and Fraser, W. D. (2000). Absence of measles virus and canine distemper virus transcripts in long-term bone marrow cultures from patients with Paget's disease of bone. *Bone* 27, 417–421. doi:10.1016/s8756-3282(00)00343-4

Ortner, D. J., and Putschar, W. (1981). *Pathological conditions in human skeletal remains*, 28. City of Washington: Smithsonian Contributions to Anthropology SMITHSONIAN INSTITUTION PRESS, 315.

Paget, J. (1877). On a form of chronic inflammation of bones (osteitis deformans). *Med. Chir. Trans.* 60, 37–649. doi:10.1177/095952877706000105

Palenzuela, L., Vives-Bauza, C., Fernandez-Cadenas, I., Meseguer, A., Font, N., Sarret, E., et al. (2002). Familial expansile osteolysis in a large Spanish kindred resulting from an insertion mutation in the TNFRSF11A gene. *J. Med. Genet.* 39, E67. doi:10.1136/jmg.39.10.e67

Porteous, M., Cetnarskyj, R., Ranganath, L. R., Selby, P. L., Hampson, G., Chandra, R., et al. (2020). Characteristics of early Paget's disease in *SQSTM1* mutation carriers: Baseline analysis of the ZiPP study cohort. *J. Bone Min. Res.* 35, 1246–1252. doi:10.1002/jbmr.4007

Ralston, S. H. (2020). A new gene for susceptibility to Paget's disease of bone and for multisystem proteinopathy. *J. Bone Min. Res.* 35, 1385–1386. doi:10.1002/jbmr.4090

Ralston, S. H., Afzal, M. A., Helfrich, M. H., Fraser, W. D., Gallagher, J. A., Mee, A., et al. (2007). Multicenter blinded analysis of RT-PCR detection methods for paramyxoviruses in relation to Paget's disease of bone. *J. Bone Min. Res.* 22, 569–577. doi:10.1359/jbmr.070103

Ralston, S. H., Digiovine, F. S., Gallacher, S. J., Boyle, I. T., and Duff, G. W. (1991). Failure to detect paramyxovirus sequences in Paget's disease of bone using the polymerase chain reaction. *J. Bone Min. Res.* 6, 1243–1248. doi:10.1002/jbmr.5650061115

Ralston, S. H., Langston, A. L., and Reid, I. R. (2008). Pathogenesis and management of Paget's disease of bone. *Lancet* 372, 155–163. doi:10.1016/S0140-6736(08)61035-1

Ralston, S. H., and Taylor, J. P. (2019). Rare inherited forms of Paget's disease and related syndromes. *Calcif. Tissue Int.* 104, 501–516. doi:10.1007/s00223-019-00520-5

Rea, S. L., Walsh, J. P., Layfield, R., Ratajczak, T., and Xu, J. (2013). New insights into the role of sequestosome 1/p62 mutant proteins in the pathogenesis of Paget's disease of bone. *Endocr. Rev.* 34, 501–524. doi:10.1210/er.2012-1034

Rea, S. L., Walsh, J. P., Ward, L., Magno, A. L., Ward, B. K., Shaw, B., et al. (2009). Sequestosome 1 mutations in Paget's disease of bone in Australia: Prevalence, genotype/phenotype correlation, and a novel non-UBA domain mutation (P364S) associated with increased NF-kappaB signaling without loss of ubiquitin binding. *J. Bone Min. Res.* 24, 1216–1223. doi:10.1359/jbmr.090214

Rebel, A., Basle, M., Pouplard, A., Malkani, K., Filmon, R., and Lepatezour, A. (1981). Towards a viral etiology for Paget's disease of bone. *Metab. Bone Dis. Relat. Res.* 3, 235–238. doi:10.1016/0221-8747(81)90038-2

Reddy, S. V., Kurihara, N., Menaa, C., Landucci, G., Forthal, D., Koop, B. A., et al. (2001). Osteoclasts formed by measles virus-infected osteoclast precursors from hCD46 transgenic mice express characteristics of pagetic osteoclasts. *Endocrinology* 142, 2898–2905. doi:10.1210/endo.142.7.8255

Reddy, S. V., Menaa, C., Singer, F. R., Demulder, A., and Roodman, G. D. (1999). Cell biology of Paget's disease. *J. Bone Min. Res.* 14, 3–8. doi:10.1002/jbmr.5650140203

Reddy, S. V., Singer, F. R., Mallette, L., and Roodman, G. D. (1996). Detection of measles virus nucleocapsid transcripts in circulating blood cells from patients with Paget disease. *J. Bone Min. Res.* 11, 1602–1607. doi:10.1002/jbmr.5650111103

Reddy, S. V., Singer, F. R., and Roodman, G. D. (1995). Bone marrow mononuclear cells from patients with Paget's disease contain measles virus nucleocapsid messenger ribonucleic acid that has mutations in a specific region of the sequence. *J. Clin. Endocrinol. Metab.* 80, 2108–2111. doi:10.1210/jcem.80.7.7608263

Rendina, D., De Filippo, G., Ralston, S. H., Merlotti, D., Gianfrancesco, F., Esposito, T., et al. (2015). Clinical characteristics and evolution of giant cell tumor occurring in Paget's disease of bone. *J. Bone Min. Res.* 30, 257–263. doi:10.1002/jbmr.2349

Rendina, D., Gennari, L., De Filippo, G., Merlotti, D., de Campora, E., Fazioli, F., et al. (2006). Evidence for increased clinical severity of familial and sporadic Paget's disease of bone in Campania, southern Italy. *J. Bone Min. Res.* 21, 1828–1835. doi:10.1359/jbmr.060822

Roodman, G. D., Kurihara, N., Ohsaki, Y., Kukita, A., Hosking, D., Demulder, A., et al. (1992). Interleukin 6. A potential autocrine/paracrine factor in Paget's disease of bone. *J. Clin. Invest.* 89, 46–52. doi:10.1172/JCI115584

Roodman, G. D., and Windle, J. J. (2005). Paget disease of bone. *J. Clin. Invest.* 115, 200–208. doi:10.1172/JCI24281

Ryan, T. A., and Tumbarello, D. A. (2018). Optineurin: A coordinator of membrane-associated cargo trafficking and autophagy. *Front. Immunol.* 9, 1024. doi:10.3389/fimmu.2018.01024

Schafer, A. L., Mumm, S., El-Sayed, I., McAlister, W. H., Horvai, A. E., Tom, A. M., et al. (2014). Panostotic expansile bone disease with massive jaw tumor formation and a novel mutation in the signal peptide of RANK. *J. Bone Min. Res.* 29, 911–921. doi:10.1002/jbmr.2094

Scotto di Carlo, F., Whyte, M. P., and Gianfrancesco, F. (2020). The two faces of giant cell tumor of bone. *Cancer Lett.* 489, 1–8. doi:10.1016/j.canlet.2020.05.031

Scotto di Carlo, F., Pazzaglia, L., Esposito, T., and Gianfrancesco, F. (2020). The loss of profilin 1 causes early onset Paget's disease of bone. *J. Bone Min. Res.* 35, 1387–1398. doi:10.1002/jbmr.3964

Scotto di Carlo, F., Pazzaglia, L., Mumm, S., Benassi, M. S., De Chiara, A., Franchi, A., et al. (2020). *ZNF687* mutations in an extended cohort of neoplastic transformations in Paget's disease of bone: Implications for clinical pathology. *J. Bone Min. Res.* 35, 1974–1980. doi:10.1002/jbmr.3993

Selby, P. L., Davies, M., and Mee, A. P. (2006). Canine distemper virus induces human osteoclastogenesis through NF-kappaB and sequestosome 1/P62 activation. *J. Bone Min. Res.* 21, 1750–1756. doi:10.1359/jbmr.060805

Shaheen, R., Faqeih, E., Sunker, A., Morsy, H., Al-Sheddi, T., Shamseldin, H. E., et al. (2011). Recessive mutations in DOCK6, encoding the guanidine nucleotide exchange factor DOCK6, lead to abnormal actin cytoskeleton organization and Adams-Oliver syndrome. *Am. J. Hum. Genet.* 89, 328–333. doi:10.1016/j.ajhg.2011.07.009

Shen, R., Murphy, C. J., Xu, X., Hu, M., Ding, J., and Wu, C. (2022). Ras and Rab interactor 3: From cellular mechanisms to human diseases. *Front. Cell Dev. Biol.* 10, 824961. doi:10.3389/fcell.2022.824961

Shirakawa, J., Kajikawa, S., Böttcher, R. T., Costell, M., Izu, Y., Hayata, T., et al. (2019). Profilin 1 negatively regulates osteoclast migration in postnatal skeletal growth, remodeling, and homeostasis in mice. *JBMR Plus* 3, e10130. doi:10.1002/jbm4.10130

Singer, F. R. (2015). Paget's disease of bone-genetic and environmental factors. *Nat. Rev. Endocrinol.* 11, 662–671. doi:10.1038/nrendo.2015.138

Siris, E. S. (1994). Epidemiological aspects of Paget's disease: Family history and relationship to other medical conditions. *Semin. Arthritis Rheum.* 23, 222–225. doi:10.1016/0049-0172(94)90037-x

Siris, E. S., Ottman, R., Flaster, E., and Kelsey, J. L. (1991). Familial aggregation of Paget's disease of bone. *J. Bone Min. Res.* 6, 495–500. doi:10.1002/jbmr.5650060511

Solomon, L. R. (1979). Billiard-player's fingers: An unusual case of Paget's disease of bone. *Br. Med. J.* 1, 931. doi:10.1136/bmj.1.6168.931

Spencer, H., O'Sullivan, V., and Sontag, S. J. (1992). Does lead play a role in Paget's disease of bone? A hypothesis. *J. Lab. Clin. Med.* 120, 798–800.

Stephens, E., Roy, M., Bisson, M., Nguyen, H. D., Scott, M. S., Boire, G., et al. (2020). Osteoclast signaling-targeting miR-146a-3p and miR-155-5p are downregulated in Paget's disease of bone. *Biochim. Biophys. Acta. Mol. Basis Dis.* 1866, 165852. doi:10.1016/j.bbadis.2020.165852

Sultana, M. A., Cluning, C., Kwong, W. S., Polain, N., Pavlos, N. J., Ratajczak, T., et al. (2021). The SQSTM1/p62 UBA domain regulates Ajuba localisation,

degradation and NF-κB signalling function. *PLoS ONE* 16, e0259556. doi:10.1371/journal.pone.0259556

Sultana, M. A., Pavlos, N. J., Ward, L., Walsh, J. P., and Rea, S. L. (2019). Targeted sequencing of DCSTAMP in familial Paget's disease of bone. *Bone Rep.* 10, 100198. doi:10.1016/j.bonr.2019.100198

Sundaram, K., Shanmugarajan, S., Rao, D. S., and Reddy, S. V. (2011). Mutant p62P392L stimulation of osteoclast differentiation in Paget's disease of bone. *Endocrinology* 152, 4180–4189. doi:10.1210/en.2011-1225

Tate, J. G., Bamford, S., Jubb, H. C., Sondka, Z., Beare, D. M., Bindal, N., et al. (2019). Cosmic: The catalogue of somatic mutations in cancer. *Nucleic Acids Res.* 47, D941–D947. doi:10.1093/nar/gky1015

Taylor, J. P. (2015). Multisystem proteinopathy: Intersecting genetics in muscle, bone, and brain degeneration. *Neurology* 85, 658–660. doi:10.1212/WNL.0000000000001862

Teramachi, J., Nagata, Y., Mohammad, K., Inagaki, Y., Ohata, Y., Guise, T., et al. (2016). Measles virus nucleocapsid protein increases osteoblast differentiation in Paget's disease. *J. Clin. Invest.* 126, 1012–1022. doi:10.1172/JCI82012

Teyssou, E., Takeda, T., Lebon, V., Boillee, S., Doukoure, B., Bataillon, G., et al. (2013). Mutations in *SQSTM1* encoding p62 in amyotrophic lateral sclerosis: Genetics and neuropathology. *Acta Neuropathol.* 125, 511–522. doi:10.1007/s00401-013-1090-0

Toth, R. P., and Atkin, J. D. (2018). Dysfunction of optineurin in amyotrophic lateral sclerosis and glaucoma. *Front. Immunol.* 9, 1017. doi:10.3389/fimmu.2018.01017

Tumbarello, D. A., Manna, P. T., Allen, M., Bycroft, M., Arden, S. D., Kendrick-Jones, J., et al. (2015). The Autophagy receptor TAX1BP1 and the molecular motor myosin VI are required for clearance of *Salmonella typhimurium* by autophagy. *PLoS Pathog.* 11, e1005174. doi:10.1371/journal.ppat.1005174

Vallet, M., and Ralston, S. H. (2016). Biology and treatment of Paget's disease of bone. *J. Cell. Biochem.* 117, 289–299. doi:10.1002/jcb.25291

Vallet, M., and Ralston, S. H. (2016). Biology and treatment of Paget's disease of bone. *J. Cell. Biochem.* 117, 289–299. doi:10.1002/jcb.25291

Vallet, M., Soares, D. C., Wani, S., Sophocleous, A., Warner, J., Salter, D. M., et al. (2015). Targeted sequencing of the Paget's disease associated 14q32 locus identifies several missense coding variants in RIN3 that predispose to Paget's disease of bone. *Hum. Mol. Genet.* 24, 3286–3295. doi:10.1093/hmg/ddv068

Vallet, M., Sophocleous, A., Törnqvist, A. E., Azfer, A., Hof, R. v. t., Albagha, O. M., et al. (2021). Targeted inactivation of Rin3 increases trabecular bone mass by reducing bone resorption and favouring bone formation. *Calcif. Tissue Int.* 109, 92–102. doi:10.1007/s00223-021-00827-2

Visconti, M. R., Langston, A. L., Alonso, N., Goodman, K., Selby, P. L., Fraser, W. D., et al. (2010). Mutations of *SQSTM1* are associated with severity and clinical outcome in Paget disease of bone. *J. Bone Min. Res.* 25, 2368–2373. doi:10.1002/jbmr.132

Wang, Q. Y., Fu, S. J., Ding, N., Liu, S. Y., Chen, R., Wen, Z. X., et al. (2020). Clinical features, diagnosis and treatment of Paget's disease of bone in mainland China: A systematic review. *Rev. Endocr. Metab. Disord.* 21, 645–655. doi:10.1007/s11154-020-09544-x

Wang, W., Feng, W., Li, D., Liu, S., Gao, Y., Zhao, Z., et al. (2019). Fusion and hemagglutinin proteins of canine distemper virus promote osteoclast formation through NF-κB dependent and independent mechanisms. *Exp. Cell Res.* 378, 171–181. doi:10.1016/j.yexcr.2019.03.020

Wani, S., Daroszewska, A., Salter, D. M., van 't Hof, R. J., Ralston, S. H., and Albagha, O. M. E. (2022). The Paget's disease of bone risk gene PML is a negative regulator of osteoclast differentiation and bone resorption. *Dis. Model. Mech.* 15, 049318. doi:10.1242/dmm.049318

Watts, G. D., Wymer, J., Kovach, M. J., Mehta, S. G., Mumm, S., Darvish, D., et al. (2004). Inclusion body myopathy associated with Paget disease of bone and frontotemporal dementia is caused by mutant valosin-containing protein. *Nat. Genet.* 36, 377–381. doi:10.1038/ng1332

Wei, Z., Li, S., Tao, X., Zhu, G., Sun, Z., Wei, Z., et al. (2021). Mutations in profilin 1 cause early-onset Paget's disease of bone with giant cell tumors. *J. Bone Min. Res.* 36, 1088–1103. doi:10.1002/jbmr.4275

Werner, M. (2006). Giant cell tumour of bone: Morphological, biological and histogenetical aspects. *Int. Orthop.* 30, 484–489. doi:10.1007/s00264-006-0215-7

Whyte, M. P., and Hughes, A. E. (2002). Expansile skeletal hyperphosphatasia is caused by a 15-base pair tandem duplication in *TNFRSF11A* encoding RANK and is allelic to familial expansile osteolysis. *J. Bone Min. Res.* 17, 26–29. doi:10.1359/jbmr.2002.17.1.26

Whyte, M. P., Obrecht, S. E., Finnegan, P. M., Jones, J. L., Podgornik, M. N., McAlister, W. H., et al. (2002). Osteoprotegerin deficiency and juvenile Paget's disease. *N. Engl. J. Med.* 347, 175–184. doi:10.1056/NEJMoa013096

Whyte, M. P., Tau, C., McAlister, W. H., Zhang, X., Novack, D. V., Preliasco, V., et al. (2014). Juvenile Paget's disease with heterozygous duplication within TNFRSF11A encoding RANK. *Bone* 68, 153–161. doi:10.1016/j.bone.2014.07.019

Witzmann, F., Claeson, K. M., Hampe, O., Wieder, F., Hilger, A., Manke, I., et al. (2011). Paget disease of bone in a Jurassic dinosaur. *Curr. Biol.* 21, R647–R648. doi:10.1016/j.cub.2011.08.006

Wong, S. W., Huang, B. W., Hu, X., Ho-Kim, E., Kolb, J. P., Padilla, R. J., et al. (2020). Global deletion of Optineurin results in altered type I IFN signaling and abnormal bone remodeling in a model of Paget's disease. *Cell Death Differ.* 27, 71–84. doi:10.1038/s41418-019-0341-6

Wu, C. H., Fallini, C., Ticozzi, N., Keagle, P. J., Sapp, P. C., Piotrowska, K., et al. (2012). Mutations in the profilin 1 gene cause familial amyotrophic lateral sclerosis. *Nature* 488, 499–503. doi:10.1038/nature11280

Xue, P., Hu, X., Chang, E., Wang, L., Chen, M., Wu, T. H., et al. (2021). Deficiency of optineurin enhances osteoclast differentiation by attenuating the NRF2-mediated antioxidant response. *Exp. Mol. Med.* 53, 667–680. doi:10.1038/s12276-021-00596-w

Yagi, M., Miyamoto, T., Sawatani, Y., Iwamoto, K., Hosogane, N., Fujita, N., et al. (2005). DC-STAMP is essential for cell-cell fusion in osteoclasts and foreign body giant cells. *J. Exp. Med.* 202, 345–351. doi:10.1084/jem.20050645

Zach, F., Polzer, F., Mueller, A., and Gessner, A. (2018). p62/sequestosome 1 deficiency accelerates osteoclastogenesis *in vitro* and leads to Paget's disease-like bone phenotypes in mice. *J. Biol. Chem.* 293, 9530–9541. doi:10.1074/jbc.RA118.002449

Zaidi, A. H., and Manna, S. K. (2016). Profilin-PTEN interaction suppresses NF-κB activation via inhibition of IKK phosphorylation. *Biochem. J.* 473, 859–872. doi:10.1042/BJ20150624

Zhu, G., Wu, C. J., Zhao, Y., and Ashwell, J. D. (2007). Optineurin negatively regulates TNFalpha- induced NF-kappaB activation by competing with NEMO for ubiquitinated RIP. *Curr. Biol.* 17, 1438–1443. doi:10.1016/j.cub.2007.07.041

frontiers | Frontiers in Cell and Developmental Biology

TYPE Original Research
PUBLISHED 19 August 2022
DOI 10.3389/fcell.2022.920683

OPEN ACCESS

EDITED BY
Maria-Bernadette Madel,
Baylor College of Medicine,
United States

REVIEWED BY
David S. Gyori,
Semmelweis University, Hungary
Peng Chen,
Guangzhou University of Chinese Medicine, China
Koichi Matsuo,
Keio University School of Medicine, Japan
Stephan Blüml,
Medical University of Vienna, Austria

*CORRESPONDENCE
Kyung-Hyun Park-Min,
ParkminK@hss.edu

SPECIALTY SECTION
This article was submitted to Cellular Biochemistry,
a section of the journal
Frontiers in Cell and Developmental Biology

RECEIVED 14 April 2022
ACCEPTED 19 July 2022
PUBLISHED 19 August 2022

CITATION
Bae S, Oh B, Tsai J, Park PSU, Greenblatt MB, Giannopoulou EG and Park-Min K-H (2022), The crosstalk between MYC and mTORC1 during osteoclastogenesis. *Front. Cell Dev. Biol.* 10:920683. doi: 10.3389/fcell.2022.920683

The crosstalk between MYC and mTORC1 during osteoclastogenesis

Seyeon Bae[1,2], Brian Oh[1], Jefferson Tsai[1], Peter Sang Uk Park[1], Matthew Blake Greenblatt[3], Eugenia G. Giannopoulou[1,4] and Kyung-Hyun Park-Min[1,2,5]*

[1]Arthritis and Tissue Degeneration Program, David Z. Rosensweig Genomics Research Center, Hospital for Special Surgery, New York, NY, United States, [2]Department of Medicine, Weill Cornell Medical College, New York, NY, United States, [3]Department of Pathology, Weill Cornell Medical College, New York, NY, United States, [4]Biological Sciences Department, New York City College of Technology, City University of New York, Brooklyn, NY, United States, [5]BCMB Allied Program, Weill Cornell Graduate School of Medical Sciences, New York, NY, United States

Osteoclasts are bone-resorbing cells that undergo extensive changes in morphology throughout their differentiation. Altered osteoclast differentiation and activity lead to changes in pathological bone resorption. The mammalian target of rapamycin (mTOR) is a kinase, and aberrant mTOR complex 1 (mTORC1) signaling is associated with altered bone homeostasis. The activation of mTORC1 is biphasically regulated during osteoclastogenesis; however, the mechanism behind mTORC1-mediated regulation of osteoclastogenesis and bone resorption is incompletely understood. Here, we found that MYC coordinates the dynamic regulation of mTORC1 activation during osteoclastogenesis. MYC-deficiency blocked the early activation of mTORC1 and also reversed the decreased activity of mTORC1 at the late stage of osteoclastogenesis. The suppression of mTORC1 activity by rapamycin in mature osteoclasts enhances bone resorption activity despite the indispensable role of high mTORC1 activation in osteoclast formation in both mouse and human cells. Mechanistically, MYC induces Growth arrest and DNA damage-inducible protein (GADD34) expression and suppresses mTORC1 activity at the late phase of osteoclastogenesis. Taken together, our findings identify a MYC-GADD34 axis as an upstream regulator of dynamic mTORC1 activation in osteoclastogenesis and highlight the interplay between MYC and mTORC1 pathways in determining osteoclast activity.

KEYWORDS

MYC (c-myc), GADD34 (PPP1R15A), osteoclast (OC), mTORC1 (mechanistic target of rapamycin complex 1), bone resorption

Introduction

Osteoclasts are derived from myeloid lineage cells and regulate bone homeostasis by degrading bone (Teitelbaum, 2000; Ikeda and Takeshita, 2016). Bone resorption by osteoclasts is tightly regulated to maintain skeletal health, as alterations in the formation or activity of osteoclasts results in skeletal diseases, such as osteoporosis (Bi et al., 2017). Macrophage colony-stimulating factor (M-CSF) and receptor activator of nuclear factor kappa-B ligand (RANKL) are key cytokines contributing to osteoclast formation. M-CSF induces receptor activator of nuclear factor kappa-B (RANK) expression and in response to RANKL, those cells induce molecular and metabolic changes that drive osteoclast differentiation and function (Feng and Teitelbaum, 2013; Park-Min, 2019).

The mammalian target of rapamycin (mTOR) is a Serine/Threonine kinase. mTOR forms two distinct complexes, mTOR complex 1 (mTORC1) and mTORC2, which differentially regulate cellular programs. The mTORC1 pathway mainly regulates cell growth, metabolism, and protein synthesis, while mTORC2 controls cell survival (Saxton and Sabatini, 2017). The heterodimeric tuberous sclerosis complex (TSC) 1/2 complex negatively regulates mTORC1 activity by targeting its upstream Rheb GTPase, and the deletion of TSC1 or TSC2 leads to hyperactivation of mTORC1 (Zhang et al., 2003; Huang and Manning, 2008). Notably, the mTOR pathway play important roles in regulating skeletal development and homeostasis by affecting osteoblasts, osteoclasts, and chodrocytes (Chen and Long, 2018). The importance of mTORC1 signaling in osteoclast differentiation has been implicated by pharmacological and genetic modulation (Dai et al., 2017a; Zhang et al., 2017; Hiraiwa et al., 2019). Although mTORC1 activity is dynamically regulated during osteoclast differentiation, its role in osteoclasts remains controversial. Moreover, the mechanisms by which the mTOR pathway is regulated in osteoclasts remain unclear.

MYC is a transcription factor regulating cell proliferation, metabolism, and differentiation (Dang, 1999). The contribution of MYC to physiological and pathological bone loss has been previously highlighted (Bae et al., 2017). RANKL-inducible MYC drives osteoclast differentiation by reprogramming osteoclastogenic pathways and oxidative metabolism *via* direct regulation of nuclear factor of activated T cells, c1 (NFATc1) and estrogen receptor–related receptor α (ERRα), respectively. In addition to NFATc1 and ERRα-dependent pathways, multifaced roles of MYC can be supported by as-yet undefined mechanisms (Lorenzo, 2017). Given the importance of MYC in osteoclast biology, the precise mechanisms of MYC's action in osteoclasts need to be further clarified.

In this study, we identify MYC as an upstream regulator of mTORC1 signaling in osteoclastogenesis. mTORC1 activity is dynamically regulated during human and mouse osteoclast differentiation. Inactivation of mTORC1 in osteoclasts augments their bone-resorbing function, while prolonged activation of mTORC1 limits the bone-resorbing function of osteoclasts. MYC coordinates the dynamic regulation of mTORC1 by regulating GADD34. GADD34 is induced in a MYC-dependent manner and works as a negative regulator of mTORC1 during osteoclastogenesis. Our study highlights the importance of proper levels of mTORC1 activation in osteoclasts for the proper maintenance of healthy bone and suggests MYC/GADD34 axis as a potential target for mTORC1 regulation in bone diseases.

Materials and methods

Mice

Myeloid-specific MYC deficient mice ($MYC^{\Delta M}$) were obtained as described previously (Bae et al., 2017). Mice with osteoclast-specific deletion of TSC2 ($TSC2^{\Delta OC}$) were generated by crossing TSC2-floxed mice (Jackson Laboratory) with Cathepsin K-Cre mice (Nakamura et al., 2007), which were kindly provided by Dr. Matthew Greenblatt (Weill Cornell Medicine). Control WT mice consisted of littermate Cathepsin K-Cre mice for $TSC2^{\Delta OC}$ mice. All animals were maintained in a specific pathogen-free environment in the Weill Cornell Medicine College vivarium. All the experiments conformed to the ethical principles and guidelines approved by the Institutional and Animal Care and Use Committee of Weill Cornell Medical College.

Analysis of bone phenotype

μCT analysis (Bouxsein et al., 2010) and histomorphometry analysis was performed as described previously (Bae et al., 2017). Femurs were scanned using a μCT, with an isotropic voxel resolution of 6 μm (μCT35, Scanco, Brüttisellen, Switzerland; 55 kVp, 145 μA, 600 ms integration time). For analysis of femoral bone mass, the volume of interest (VOI) encompassed a 200-slice section in the metaphysis, proximal to the growth plate. To ensure the exclusion of primary spongiosa in the growth plate, VOIs began 55 slices proximal to the distal end of the growth plate. Trabecular bone parameters included bone volume fraction (BV/TV), trabecular thickness (Tb. Th), trabecular separation (Tb. Sp), and trabecular number (Tb. N). Three-dimensional reconstructions were generated by stacking thresholded 2D images from the contoured region. All samples were included in the analysis conducted in a blinded manner. After μCT analysis was done, femurs were decalcified with 10% buffered EDTA (Sigma-Aldrich) and embedded in paraffin. To assess osteoclast or osteoblast visualization on trabecular bone within the femur metaphysis, sections were stained with tartrate-resistant acid phosphatase (TRAP) and

methyl green or hematoxylin and eosin (Vector Laboratories, Burlingame, CA, United States). All measurements were performed using Osteometric software (Osteomeasure) according to standard procedures (Parfitt et al., 1987). Osteoclasts were identified as TRAP-positive cells that were multinucleated and adjacent to bone.

Reagents

Human macrophage colony-stimulating factor (M-CSF) and RANKL was purchased from Peprotech (Rocky Hill, NJ, United States). Rapamycin was obtained from Calbiochem. Antibodies were used for immunoblotting as follows: NFATc1 (Santa Cruz Biotechnology; sc-7294); α-tubulin (Sigma-Aldrich; T9026); phosphorylated p70S6K, p70S6K (Cell Signaling Technology; 9234, 2708); and GADD34 (Proteintech; 10449-1-AP). A mouse CTX-I and P1NP ELISA kits were purchased from Cloud-Clone (Wuhan, China).

Mouse osteoclast differentiation

Mouse bone marrow-derived macrophages (BMDMs) were prepared from bone marrow cells from 8-week-old mice as described previously (Bae et al., 2017). Non-adherent mouse bone marrow cells were cultured with α-MEM w/o nucleosides (Invitrogen) supplemented with 10% premium FBS (R&D systems), 1% L-glutamine (Invitrogen), and 1% penicillin/streptomycin (Invitrogen). For mouse osteoclast differentiation, mouse BMDMs were seeded on the 96-well plates at a density of 1×10^4 cells per well in triplicate with human M-CSF (20 ng/ml). Next day, cells were stimulated with human RANKL (50 ng/ml) and cultured for 3 days. Fresh medium with cytokines were replenished at day 2. Cells were fixed and stained for TRAP using the acid phosphatase leukocyte diagnostic kit (Sigma-Aldrich) as directed in the kit manual. Multinucleated (more than 3 nuclei) TRAP-positive osteoclasts were counted in triplicate wells.

Human osteoclast differentiation

Human CD14-postive cells were prepared from peripheral blood as described previously (Mun et al., 2021). Human CD14+ cells were cultured with α-MEM without nucleoside supplementation with 10% defined FBS (Cytiva) and 1% L-glutamine. For human osteoclast differentiation, human CD14-postive cells were plated on 96-well plates at a density of 1×10^5 cells per well in triplicate with human M-CSF (20 ng/ml) followed by human RANKL stimulation (40 ng/ml). Cells were cultured for 3 days.

Measurement of osteoclast activity

Mouse BMDMs or human CD14-positive cells were differentiated to mature osteoclasts as described above using Corning Osteo Assay Surface 96-well plates (Sigma-Aldrich). After rapamycin treatment for the indicated time points, cells were removed, and the remaining mineralized matrix and formed resorption pits were visualized with Toluidine Blue staining. The resorbed area was calculated as previously described (Fujii et al., 2021).

RNA sequencing and analysis

Total RNA was extracted using the RNeasy Mini Kit with DNase treatment (QIAGEN). RNA was processed and analyzed as described previously (Bae et al., 2017). Data from 2 biological replicates were used for bioinformatic analysis. The Gene Set Enrichment Analysis (GSEA) was used to analyze differentially expressed genes (https://www.gsea-msigdb.org/gsea/). NES (normalized enrichment score) is the primary static for examining gene set enrichment results (http://software.broadinstitue.org/doc/GSEAUserGuideTEXT.html#_Enrichment_Score_(ES).

Gene expression analysis

DNA-free RNA was obtained using the RNeasy Mini Kit with DNase treatment (QIAGEN), and 0.5 μg of total RNA was reverse transcribed using a First Strand cDNA Synthesis kit (Fermentas). Real-time quantitative PCR was performed with Fast SYBR Green Master Mix and a 7500 Fast Real-time PCR system (Applied Biosystems). Expression of the tested genes were normalized relative to the levels of *Hprt*. The primer sequences were as follows: murine *Ppp1r15a* (GADD34) Forward: 5′-GAC CCCTCCAACTCTCCTTC-3′ and Reverse: 5′-CTTCCTCAG CCTCAGCATTC-3′, *Hprt* Forward: 5′-TCCTCAGACCGC TTTTTGCC-3′ and Reverse: 5′-CTAATCACGACGCTGGGA CT-3′.

Immunoblotting analysis

Whole-cell extracts were electrophoretically separated on 7.5% SDS-PAGE, transferred to polyvinylide fluoride membranes (Millipore) and probed with specific antibodies.

RNA interference

Mouse BMDMs were transfected with 50 nmol of siRNA oligonucleotides (SMARTpool: ON-TARGETplus Ppp1r15a

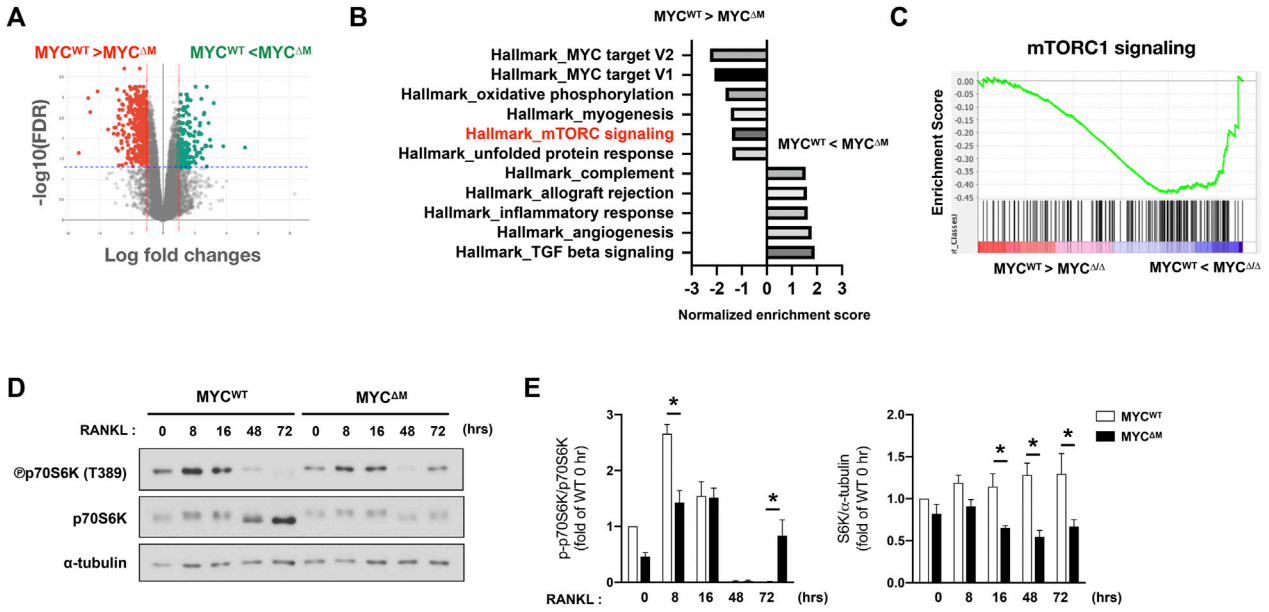

FIGURE 1
MYC regulates mTORC1 activity in osteoclastogenesis. **(A)** Mouse BMDMs from control (MYC^{WT}) mice and MYC-deficient ($MYC^{\Delta M}$) mice were stimulated with RANKL for 1 day. Volcano plot of differentially expressed genes (DEGs) in MYC-deficient cells relative to control cells after RANKL stimulation for 24 h from the RNA sequencing (RNA-seq) analysis (>1.5 fold). **(B,C)** Gene-set–enrichment analysis of DEGs with genes ranked on the basis of expression in $MYC^{\Delta M}$ relative to that in MYC^{WT}, showing the distribution of genes in the mTORC1 signaling gene set against the ranked list of the genes from the RNA-seq analysis. NES: normalized enrichment score, the primary statistic for examining gene set enrichment results. **(D)** Immunoblot of whole-cell lysates from control and MYC-deficient BMDMs after RANKL stimulation for the indicated time points with anti-phospho p70S6K, p70S6K, and α-tubulin antibodies. α-tubulin served as a loading control. Data are representative of four experiments. **(E)** Graph depicts the quantification of signal intensity of the phospho p70S6K and total p70S6K immunoblot using densitometry, normalized to WT control. Data are shown as mean ± SEM (n = 4). *p < 0.05 by one-way ANOVA with a *post hoc* Tukey test.

siRNA: L-047639-00-0005, ON-TARGETplus Non-targeting Pool: D-001810-10-20, Dharmacon) using the TransIT-TKO® transfection reagent (Mirus Bio) according to the manufacturer's instructions.

Statistical analysis

All statistical analyses were performed with GraphPad Prism 8 (GraphPad Software) using a two-tailed, paired or unpaired t test for two conditions or one-way ANOVA for multiple comparisons with a Tukey's *post-hoc* test. A p value of less than 0.05 was considered statistically significant.

Results

MYC is an upstream regulator of mammalian target of rapamycin complex 1 activation

We and others have established MYC as a key regulator of osteoclastogenesis (Battaglino et al., 2002; Bae et al., 2017). MYC expression is induced by RANKL, and MYC deficiency has been shown to suppress osteoclast formation and its bone-resorbing activity (Bae et al., 2017). To gain insight into the downstream pathways that are regulated by MYC at the early phases of osteoclastogenesis, we performed an unbiased transcriptomic analysis using RNA-seq to identify genes whose expression was affected by MYC in the early phases of the RANKL response. Bone marrow cells from control LysM-Cre (MYC^{wt}) and myeloid cell-specific MYC deficient ($MYC^{f/f}$ LysM-Cre, named $MYC^{\Delta M}$) mice were differentiated into BMDMs and then cultured with M-CSF and RANKL for 24 h. 1,332 differentially expressed genes (DEGs, 1.5 fold changes, FDR < 0.05) between MYC^{wt} and $MYC^{\Delta M}$ cells were detected; 454 genes were upregulated, and 888 genes were downregulated in MYC-deficient cells (Figure 1A). We performed gene set enrichment analysis (GSEA) (Mootha et al., 2003; Subramanian et al., 2005), broadly testing for the enrichment of well-defined gene sets from the comprehensive Molecular Signature Data Base v5.1 (www.broadinstitute.org) of DEGs. GSEA pathway analysis of DEGs revealed that MYC regulates genes related to mTORC1 signaling (Figures 1B,C). To check if mTORC1 signaling is affected by MYC deficiency, control and MYC-deficient BMDMs were stimulated with RANKL, and

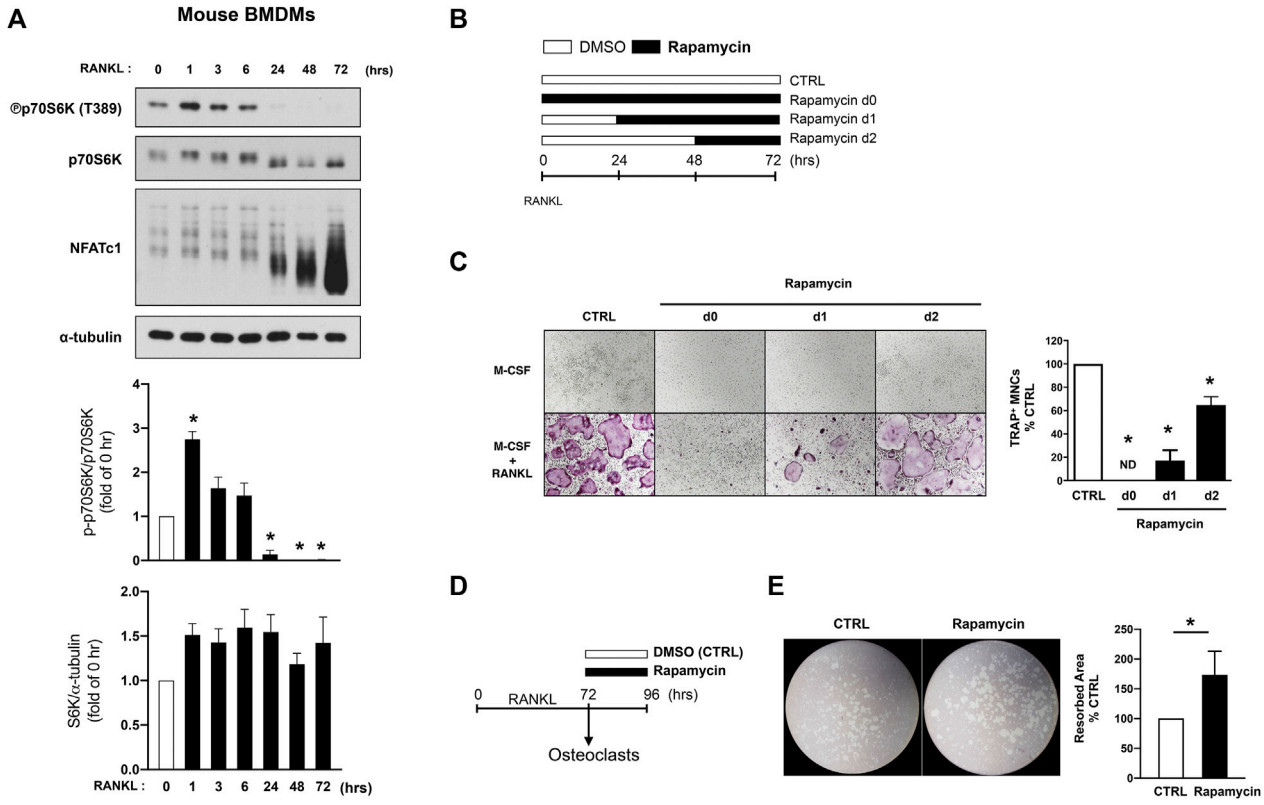

FIGURE 2
mTORC1 signaling has a biphasic effect on mouse osteoclastogenesis. **(A)** Immunoblot of whole-cell lysates from mouse BMDMs after RANKL stimulation for the indicated time points with anti-phospho p70S6K, p70S6K, NFATc1, and α-tubulin antibodies. α-tubulin served as a loading control. Graph depicts the quantification of signal intensity of the phospho p70S6K and total p70S6K immunoblot using densitometry, normalized to the control (n = 3). **(B)** A schematic diagram illustrating the experimental design in **(C)**. **(C)** Representative images show osteoclast differentiation after rapamycin treatment (100 nM) at different time points after RANKL stimulation. Graph depicts the number of TRAP-positive multinucleated cells (MNCs) counted in triplicate from three independent experiments. **(D)** A schematic diagram illustrating the experimental design in **(E)**. **(E)** Representative images show bone resorption activity of osteoclasts after rapamycin treatment for 24 h. Graph depicts the percentage of resorbed pit area per total area from six independent experiments. All data are shown as mean ± SEM. *$p < 0.05$ by one-way ANOVA with a *post hoc* Tukey test **(A,C)** or two-tailed, paired t test **(E)**. ND, not detected.

mTORC1 activity was examined. The activation of mTORC1 signaling can be determined by detecting the phosphorylation of its downstream targets, ribosomal protein S6 Kinase (S6K) and 4EBP1 (Ma and Blenis, 2009); phosphoS6K was used to detect mTORC1 activation in this study. We found that the levels of mTORC1 activity differed at early and late stages of osteoclastogenesis. mTORC1 was activated at the early phases of the RANKL response but was suppressed during the later phases of osteoclastogenesis (Figures 1D,E). Intriguingly, the biphasic regulation of mTORC1 activity was dependent on MYC (Figures 1D,E); the early activation of mTORC1 and suppression of mTORC1 at the later phase of osteoclastogenesis were attenuated by MYC deficiency. In addition, the expression of total p70S6K expression was also diminished in MYC-deficient cells (Figures 1D,E). Thus, our results suggest that MYC is required for both the early activation and late suppression of mTORC1 activity.

The level of mammalian target of rapamycin complex 1 activity affects osteoclast function

To further dissect the role of biphasic regulation of mTORC1 in osteoclastogenesis, we measured the regulation of mTORC1 activity in human and mouse cells. During mouse osteoclast differentiation, mTORC1 was activated 1 hour after RANKL stimulation and subsequently was suppressed below the baseline at 24 h after RANKL stimulation, as supported by a previous study (Hiraiwa et al., 2019) (Figure 2A). Given the transient activation of mTORC1 during osteoclastogenesis, we considered the possibility of a differential role of mTORC1 at different stages of osteoclastogenesis. To test this, we inhibited mTORC1 activation by rapamycin treatment, an inhibitor of mTORC1 (Li et al., 2014), at different time points after RANKL stimulation (Figure 2B). Consistent with the previous studies

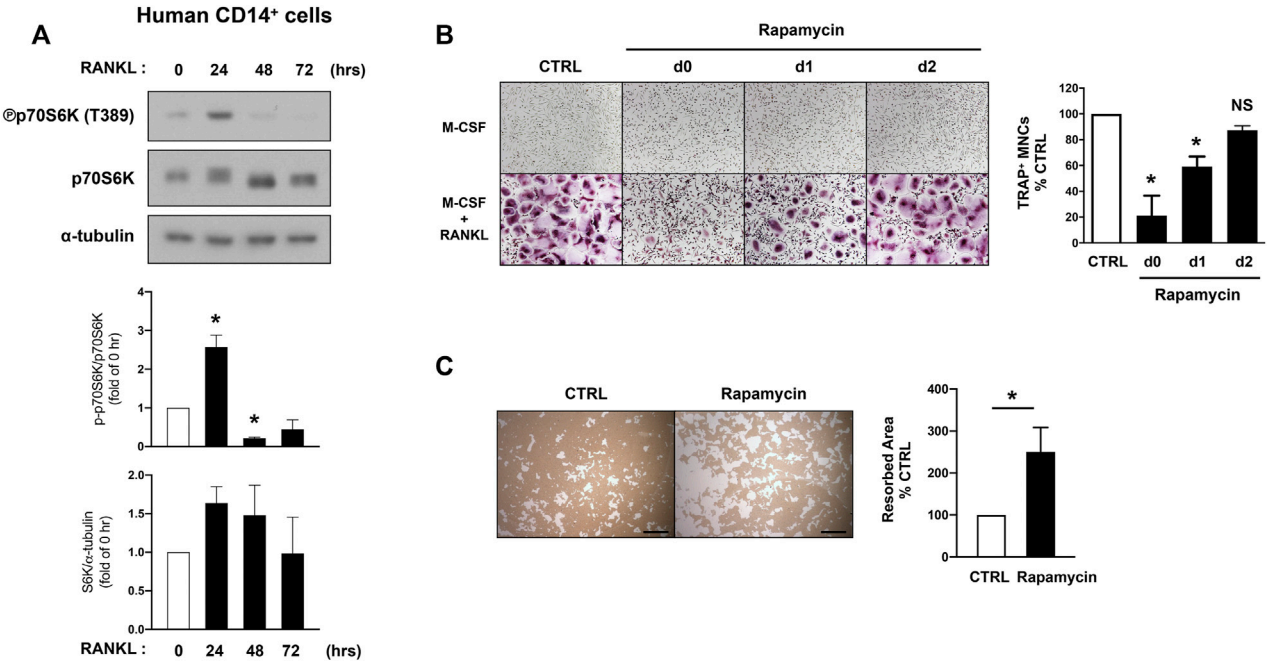

FIGURE 3
mTORC1 signaling has a biphasic effect on human osteoclastogenesis. **(A)** Immunoblot of whole-cell lysates from human CD14-positive cells after RANKL stimulation for the indicated time points with anti-phospho p70S6K, p70S6K, and α-tubulin antibodies. α-tubulin served as a loading control. Representative results from four independent donors are shown. Graph depicts the quantification of signal intensity of the phospho p70S6K and total p70S6K immunoblot using densitometry, normalized to the control (n = 4). **(B)** Representative images show human osteoclast differentiation after rapamycin treatment (100 nM) at different time points after RANKL stimulation. Graph depicts the number of TRAP-positive multinucleated cells (MNCs) counted in triplicate. Data are from four independent donors. **(C)** Representative images show bone resorption activity of human osteoclasts after rapamycin treatment for 48 h. Graph depicts the percentage of resorbed pit area per total area. Data are from four independent donors. Scale bar: 500 μm. All data are shown as mean ± SEM. *$p < 0.05$; NS, not significant by one-way ANOVA with a *post hoc* Tukey test **(A,B)** or two-tailed, paired t test **(C)**.

showing that mTORC1 activation is required for osteoclastogenesis (Glantschnig et al., 2003; Dai et al., 2017a), rapamycin treatment suppressed osteoclastogenesis (Figure 2C). While inhibition of mTORC1 by rapamycin treatment prior to RANKL stimulation nearly completely suppressed osteoclast formation, osteoclastogenesis was inhibited to a lesser extent when rapamycin was added at 2 days after RANKL stimulation (Figure 2C). We next tested if this suppressed mTORC1 activity is related to the bone-resorbing function of osteoclasts. Bone marrow-derived macrophages (BMDMs) were cultured with M-CSF and RANKL for 3 days to form mature osteoclasts, and mature osteoclasts then were treated with rapamycin or DMSO (Figure 2D). Notably, rapamycin-treated osteoclasts exhibited greater resorbing activity compared to vehicle-treated osteoclasts (Figure 2E). Rapamycin treatment on mature osteoclasts minimally affected TRAP-positive osteoclasts as displayed by TRAP-positive area, while significantly increasing resorbing area per TRAP-positive area (Supplementary Figure S1), suggesting that mTORC1 inactivation at the later stage of osteoclastogenesis may be required for the appropriate function of osteoclasts.

Hyperactive mTORC1 signaling is a clinical feature of patients with tuberous sclerosis complex (TSC) which is caused by inactivating pathogenic variants in either TSC1 or TSC2 genes, and sclerotic bone lesions have been frequently reported in TSC patients (Avila et al., 2010; Wu et al., 2017). However, the role of mTORC1 activity in human osteoclast differentiation has not been demonstrated yet. We examined how its activity is regulated in human osteoclastogenesis. Human CD14-postive cells were cultured with M-CSF and RANKL, and mTORC1 activity was examined by detecting the phosphorylation of S6K. Consistent with our observation in mouse cells, mTORC1 activity was dynamically regulated by RANKL stimulation; mTORC1 activity increased in response to RANKL at 24 h after stimulation, but its activity was decreased at the later phase of human osteoclastogenesis (Figure 3A). Consistent with the data observed in mouse cells (Figure 2), blocking mTORC1 activity by rapamycin treatment up to day one after RANKL stimulation suppressed osteoclast differentiation (Figure 3B). However, osteoclast differentiation was minimally affected when mTORC1 was inhibited at 2 days after RANKL stimulation (Figure 3B). After culturing human

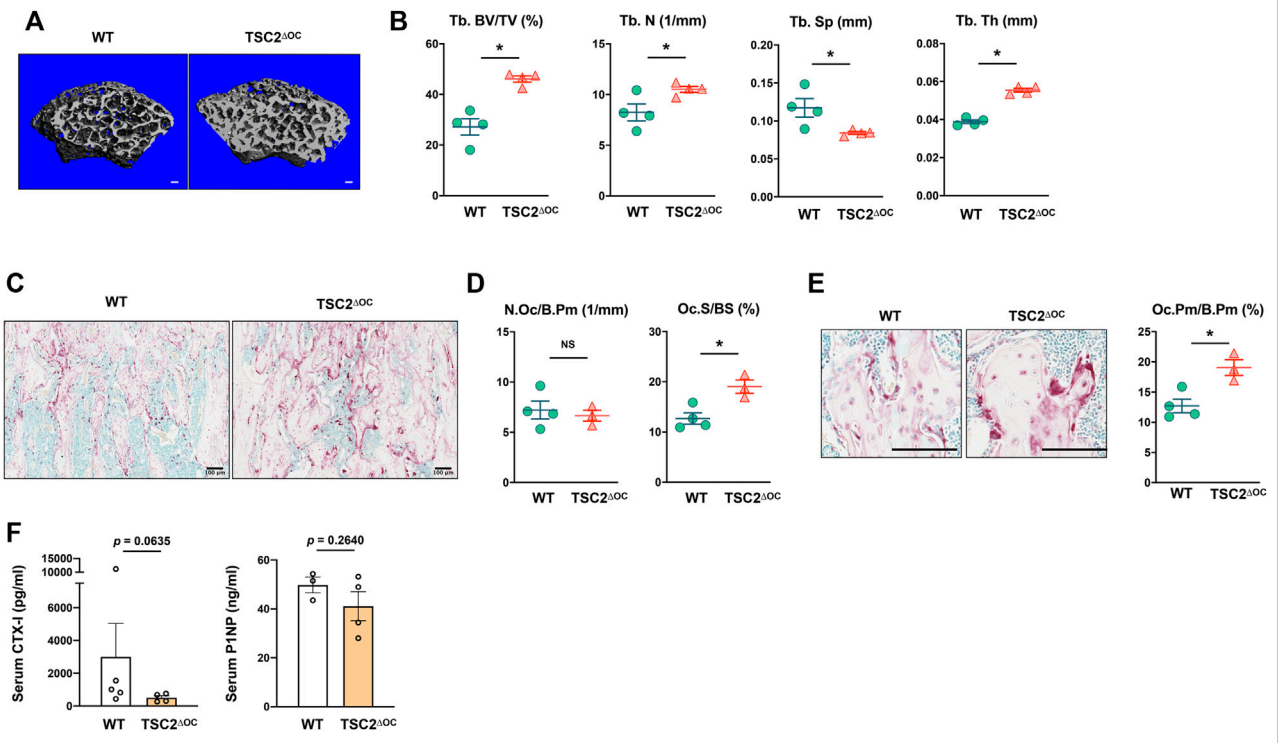

FIGURE 4
Hyperactivation of mTORC1 in osteoclasts impedes bone resorption. **(A)** Representative μCT reconstructed images of the trabecular architecture of the distal femurs from 8-week-old female TSC2-floxed Cathepsin K-Cre ($TSC2^{\Delta OC}$) and littermate control Cathepsin K-Cre (WT) mice. **(B)** μCT measurements for the indicated parameters of the trabecular bone in distal femurs. Bone volume/tissue volume ratio (BV/TV), trabecular numbers (Tb.N), trabecular thickness (Tb.Th), and trabecular space (Tb.Sp) were determined by μCT analysis. **(C)** Representative images showing the TRAP-positive, multinucleated osteoclasts (red) in the coronal sections of the distal femur. **(D)** Histomorphometric analysis of the trabecular bone. Number of osteoclasts per bone perimeter (N.Oc/B.Pm), osteoclast surface area per bone surface (Oc.S/BS). **(E)** Enlarged images from **(C)** showing the size of TRAP-positive, multinucleated osteoclasts (red). Graph depicts the size of osteoclasts. Osteoclast perimeter per bone perimeter (Oc.Pm/B.Pm). **(F)** The concentration of serum CTX-I and PINP measured by ELISA. All data are shown as mean ± SEM. *$p < 0.05$; NS, not significant by two-tailed, unpaired *t* test. Scale bar: 100 μm.

CD14-positive cells with M-CSF and RANKL to form mature osteoclasts, cells were treated with rapamycin or DMSO for 2 days. Furthermore, the suppression of mTORC1 in human mature osteoclasts by rapamycin treatment enhanced their bone-resorbing function (Figure 3C). Taken together, our results suggest that lower activity of mTORC1 at the later phases of osteoclastogenesis has a beneficial effect on the bone-resorbing function of osteoclasts.

Activation of mammalian target of rapamycin complex 1 in osteoclasts *in vivo* dysregulates bone homeostasis

To corroborate our observation showing mTORC1 activity inversely regulates the bone-resorbing function of osteoclast, we wished to force mTORC1 activation at the late phase of osteoclastogenesis *in vivo*. Given that TSC1 or TSC2 deficiency results in a hyperactive mTORC1 state (Inoki et al., 2002; Huang and Manning, 2008), we generated TSC2-floxed CtsK-Cre ($TSC2^{\Delta OC}$) mice by crossing TSC2-floxed mice with Cathepsin K-Cre mice and investigated their bone phenotype. Strikingly, $TSC2^{\Delta OC}$ mice exhibited a significantly higher trabecular bone mass compared to wild-type (WT) mice (Cathepsin K-Cre), along with significantly increased number and thickness of trabecular bone and decreased trabecular spacing (Figures 4A,B). Histomorphometric analysis of trabecular bone revealed that the number of osteoclasts was not changed in $TSC2^{\Delta OC}$ mice (Figures 4C,D). Similar to TSC1 deficient mice (Wu et al., 2017), $TSC2^{\Delta OC}$ mice had larger osteoclasts compared to those from WT mice (Figures 4D,E). There was no difference in the number of osteoblasts or the level of N-terminal propeptide of type I procollagen (P1NP), a serum bone formation marker, between $TSC2^{\Delta OC}$ mice and WT mice (Supplementary Figure S2; Figure 4F). Nonetheless, the level of CTX-I, a serum bone

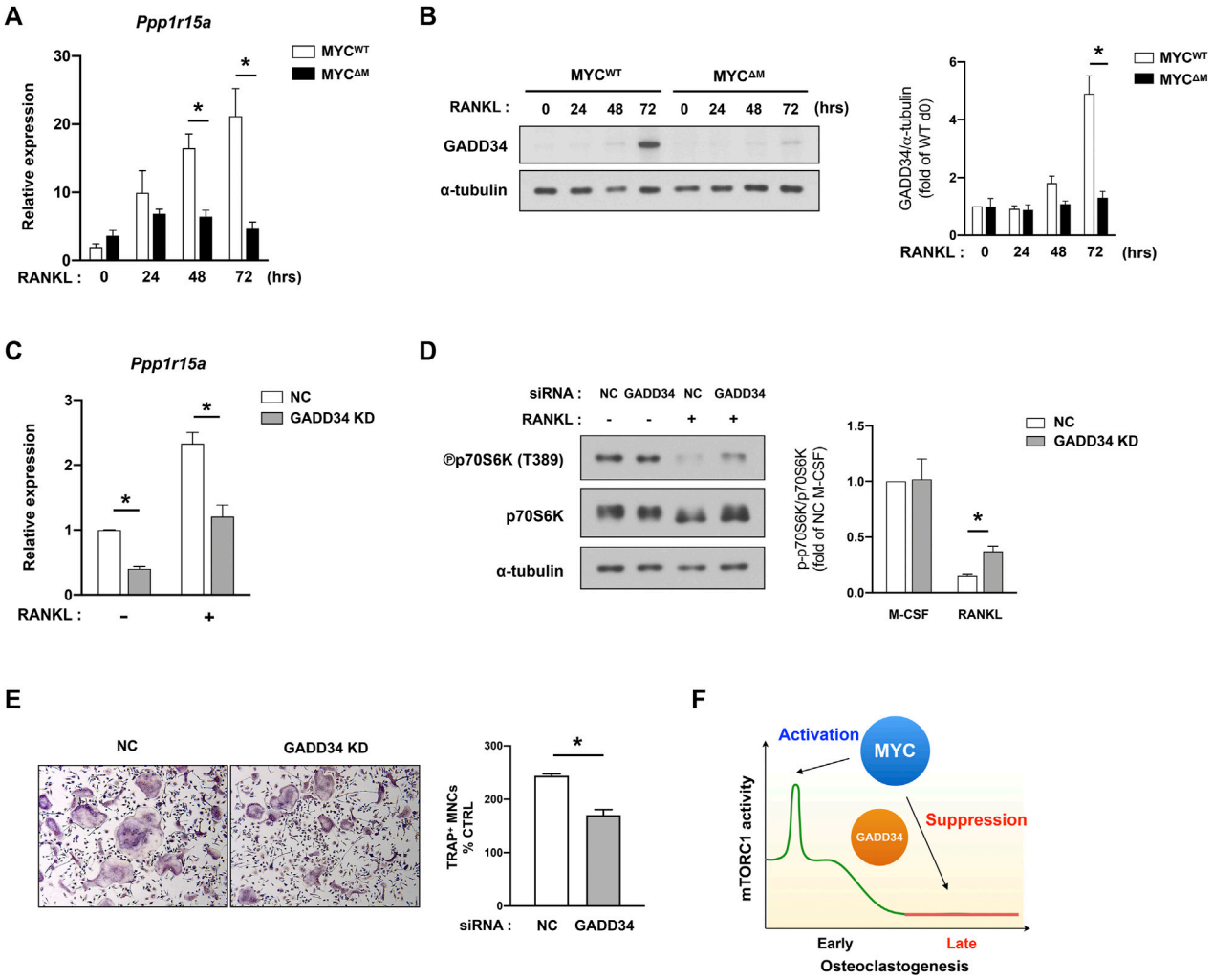

FIGURE 5
MYC/GADD34 axis inactivates mTORC1 in osteoclasts. **(A)** The mRNA expression of *Ppp1r15a* (encodes GADD34, relative to the *Hprt* housekeeping gene) in control (MYC^{WT}) and MYC-deficient ($MYC^{\Delta M}$) BMDMs after RANKL stimulation for the indicated time points (n = 4). **(B)** The protein expression of GADD34 determined by immunoblot using whole-cell lysates of control and MYC-deficient BMDMs after RANKL stimulation for the indicated time points. α-tubulin served as a loading control. Data are representative of three independent experiments. Graph depicts the quantification of signal intensity of the GADD34 immunoblot using densitometry and then normalized to WT control (n = 3). **(C–E)** Mouse BMDMs were transfected with siRNAs specific for GADD34. **(C)** The mRNA expression of *Ppp1r15a* (relative to the *Hprt* housekeeping gene) in negative-control (NC) or siRNAs specific for GADD34 transfected cells after RANKL stimulation for 3 days (n = 3). **(D)** Representative images for Immunoblot of whole-cell lysates with indicated antibodies. α-tubulin served as a loading control. Representative results from four independent experiments are shown. Graph depicts the quantification of signal intensity of the phospho p70S6K immunoblot using densitometry and taken as a ratio of phospho p70S6K over total p70S6K and then normalized to NC control (n = 4). **(E)** Osteoclastogenesis assay. BMDMs were cultured with M-CSF and RANKL for 3 days. Left, Representative images of TRAP-stained cells. Right, Quantification of TRAP positive multinucleated (more than three nuclei) cells (n = 3). **(F)** A diagram illustrating the dynamic regulation of mTORC1 activity by MYC. All data are shown as mean ± SEM. *$p < 0.05$ by one-way ANOVA with a *post hoc* Tukey test **(A–D)** or by two-tailed, paired t test **(E)**.

resorption marker, exhibited a decreasing trend in $TSC2^{\Delta OC}$ mice compared to WT mice (Figure 4F), indicating that osteoclasts from $TSC2^{\Delta OC}$ mice exhibited an attenuated resorbing function and caused increased bone mass. Taken together, using loss-of-function and gain-of function studies suggested that lower mTORC1 activity in mature osteoclasts is required for osteoclastic bone resorption.

The MYC/GADD34 axis negatively regulates mammalian target of rapamycin complex 1 in osteoclast differentiation

We wished to determine the mechanism of mTORC1 inactivation in the late phase of osteoclastogenesis by MYC. To search for the upstream regulator responsible for

repressing mTORC1, we screened known regulators of mTORC1, including Deptor (Varusai and Nguyen, 2018), Ddit4 (Foltyn et al., 2019), FOXOs (Lin et al., 2014), and BNIP3 (Li et al., 2007) on mTORC1 activation. However, none of these were able to rescue suppressed mTORC1 activity (data not shown).

To search for additional candidates, we referenced the RNA-seq analysis of MYC-deficient cells and found that the expression of genes associated with the unfolded protein response (UPR) were diminished in MYC-deficient cells (Figure 1); this was of particular interest given that the balance between the mTORC1 pathway and UPR tightly regulates protein synthesis (Walter and Ron, 2011). Growth arrest and DNA damage-inducible protein (GADD34, encoded by *Ppp1r15a*) is an important factor for the coordinate regulation of UPR. Moreover, in 293HEK cells and mouse embryonic fibroblasts, GADD34 leads to dephosphorylation of TSC2 and negatively regulates mTOR signaling (Watanabe et al., 2007; Uddin et al., 2011). Since GADD34 regulation in osteoclasts had not yet been investigated, we first tested GADD34 expression in osteoclastogenesis. Control and MYC deficient BMDMs were treated with RANKL, and the expression of GADD34 was measured. The transcription level of Gadd34 (*Ppp1r15a*) was increased in WT cells upon RANKL stimulation in a time-dependent manner, while MYC-deficient cells failed to induce its expression (Figure 5A). Concomitantly, RANKL-induced GADD34 protein expression was abrogated by MYC deficiency (Figure 5B), indicating MYC regulates the expression of GADD34 in osteoclastogenesis. To test if GADD34 plays a role in regulation of mTORC1 activity in osteoclasts, we knocked down the expression of GADD34 using nucleofecting siRNA oligos against *Ppp1r15a* and evaluated mTORC1 activity. *Ppp1r15a* mRNA expression was efficiently diminished in Gadd34-deficient cells compared to control cells (Figure 5C). GADD34 deficiency partially restored RANKL-induced mTORC1 inactivation (Figure 5D), suggesting that the MYC/GADD34 axis, in part, contributes to the suppression of mTORC1 in osteoclasts. GADD34 deficiency also suppressed osteoclastogenesis (Figure 5E). GADD34 deficiency showed a decreasing trend in osteoclastic bone resorption (Supplementary Figure S3). Taken together, our results suggest that GADD34 is a positive regulator of osteoclastogenesis and suppresses mTORC1 activity at the later stages of osteoclastogenesis.

Discussion

Both the mTOR pathway and MYC are critical modulators of osteoclastogenesis (Park-Min, 2019). However, the crosstalk between MYC and the mTOR pathway during osteoclastogenesis has never been studied previously. In this study, we show that MYC is an upstream regulator of mTOR pathway and modulates a biphasic activation of mTORC1 during osteoclastogenesis. It is well-documented that early activation of mTORC1 is required for osteoclast formation (Dai et al., 2017a; Zhang et al., 2017; Hiraiwa et al., 2019). However, we found that inactivation of mTORC1 in mature osteoclasts is important for the bone-resorbing function of osteoclasts. Accordingly, hyperactivation of mTORC1 in osteoclasts, by deleting TSC2 in mice, increased bone mass and suppressed osteoclast activity. MYC promoted mTORC1 activation at the early phases of osteoclastogenesis and suppressed mTORC1 activation at the later phases of osteoclastogenesis *via* induction of GADD34 (Figure 5F). Overall, our findings suggest that MYC regulates osteoclast differentiation and activity by tightly controlling mTORC1 activity.

MYC is a multifunctional helix-loop-helix leucine zipper transcription factor (Dang, 2012). Our previous report established the central role of MYC in osteoclasts and pathological bone loss. MYC is induced by RANKL stimulation (Bae et al., 2017). MYC is required for the induction of NFATc1 and plays a key role in oxidative phosphorylation in osteoclasts (Park-Min et al., 2014; Bae et al., 2017). This study further suggests that MYC is an upstream regulator of mTORC1 signaling in osteoclasts. Despite the importance of mTORC1 in skeletal development, the mechanism underlying the dynamic regulation of mTORC1 activity in osteoclasts remains unclear. Here, we show that MYC deficiency not only inhibited RANKL-induced mTORC1 activation and the expression of p70S6K at the early phases of osteoclastogenesis but also activated mTORC1 activation at the late phases of osteoclastogenesis. RANKL-mediated mTORC1 activation can be regulated by other signaling pathways. It has been shown that mTORC1 is activated by PI3K (The phosphoinositide 3 kinase)/Akt *via* inhibition of TSC1/2 (Shaw and Cantley, 2006). The PI3KAkt/mTOR pathway plays an important role in osteoclastogenesis (Moon et al., 2012) by several different mechanisms (Tiedemann et al., 2017; Yu et al., 2019). The mTOR-rictor-Akt circuit regulates osteoclast fusion and growth (Tiedemann et al., 2017). However, we did not detect any changes in the P13K/Akt pathway in MYC deficient cells (data not shown). In addition to the transcriptional control of osteoclast-specific genes by MYC, our study suggested that MYC may be involved in RANKL-induced protein synthesis in osteoclasts by regulating mTORC1 activity. Therefore, our results provide new insights into the role of MYC in osteoclastogenesis.

mTORC1 promotes anabolic functions including protein and lipid synthesis, and its activation is dependent on energy status and nutrient availability (Saxton and Sabatini, 2017). Aberrant mTORC1 signaling is associated with many human diseases, including cancer, diabetes, and neurological disorders (Inoki et al., 2005; Saxton and Sabatini, 2017).

mTORC1 activation is also important for bone remodeling by regulating osteoblasts (Riddle et al., 2014; Chen and Long, 2015; Dai et al., 2017b; Fitter et al., 2017; Martin et al., 2018) and osteoclasts (Dai et al., 2017a; Zhang et al., 2017; Huynh and Wan, 2018). During osteoclastogenesis, mTORC1 activation is biphasically regulated. However, the role of mTORC1 in osteoclasts is still controversial. Pharmacological studies established that mTOR signaling positively regulates osteoclastogenesis. However, recent genetic studies demonstrated that constitutive active mTOR signaling in TSC1 or TSC2 deficient cells suppresses osteoclastogenesis regardless of the stage of osteoclastogenesis (Wu et al., 2017; Zhang et al., 2017). We also found that prolonged mTORC1 activation in $TSC2^{\Delta OC}$ mice increases bone mass. Osteoclasts from $TSC2^{\Delta OC}$ mice were larger, although the number of osteoclasts in $TSC2^{\Delta OC}$ mice was comparable to that of the control mice. In addition, cathepsin K-expressing osteoclasts in $TSC2^{\Delta OC}$ mice were bigger and showed increased phospho-mTOR compared to osteoclasts in control mice (data not shown). These results implicate the broad but complicated effect of mTORC1 on osteoclast differentiation and activity.

The phenotype of osteoclasts in $TSC2^{\Delta OC}$ mice was similar to the phenotype of osteoclasts in $TSC1^{f/f}$-Ctsk-Cre mice (Wu et al., 2017). $TSC1^{f/f}$-Ctsk-Cre mice exhibited high bone mass and reduced bone resorption (Wu et al., 2017; Xu et al., 2018). However, inhibition of mTORC1 activation by raptor deficiency at the late phase of osteoclastogenesis using Cathepsin K-Cre also resulted in higher bone mass than in control mice (Dai et al., 2017a). Since either hyperactive or hypoactive mTORC1 at the late phase of osteoclastogenesis resulted in inhibition of osteoclast formation and increased bone mass, it is hard to draw a conclusion based on the genetic modification. Here, we show that rapamycin treatment in mature osteoclasts enhanced bone-resorbing activity, suggesting the importance of inactive mTOR signaling at the late phase of osteoclastogenesis for osteoclastic bone resorption. While several studies demonstrated that rapamycin administration increased bone mass (Chen et al., 2015; Luo et al., 2016; Bateman et al., 2019), other studies showed that bone marrow cells isolated from mice after two month-treatment with low doses of rapamycin exhibited increased osteoclastogenic activity and diminished bone mass (Rubert et al., 2015; Huynh and Wan, 2018). However, since rapamycin targets not only osteoclasts but also osteoblasts and other cells, the outcome of rapamycin administration *in vivo* could result from the coordinated interaction among various cell types. Nonetheless, these studies support that selectively modulating mTORC1 activity could be used to control osteoclast differentiation and function in pathological conditions. Given that dysregulation of mTORC1 is important for the proper regulation of osteoclastogenesis, further studies dissecting the role of mTORC1 in physiological bone remodeling will be required.

Our study is the first to show the regulation of GADD34 in osteoclastogenesis. GADD34 is an important component of the unfolded protein response (UPR) and is quickly induced in nutrient- or amino acid- deprived conditions (Novoa et al., 2001; Gambardella et al., 2020). Although cellular energy deficiencies usually lead to UPR (Bravo et al., 2013), we show that GADD34 is gradually induced by RANKL stimulation even in nutrient-rich media. Moreover, ATP formation is greatly increased during osteoclastogenesis (Nishikawa et al., 2015; Bae et al., 2017), and adenosine monophosphate-activated protein kinase (AMPK), a cellular energy censor, is suppressed in osteoclasts (Bae et al., 2017, unpublished observations), suggesting that osteoclast formation is accompanied by increased energy metabolism. However, a discrepancy between GADD34 mRNA and protein expression during osteoclastogenesis has been observed. GADD34 mRNA was induced at 24 h after RANKL stimulation, while GADD34 protein gradually increased from 2 days after RANKL stimulation. GADD34 protein is remarkably unstable due to proteasomal degradation at steady-state conditions (Brush and Shenolikar, 2008). Our data suggests that GADD34 protein is stabilized by an unknown mechanism at the later phase of osteoclastogenesis. Furthermore, we also show that, upon RANKL stimulation, GADD34 was not induced in MYC-deficient cells, suggesting that MYC positively regulates the expression of GADD34 or the stabilization of GADD34 proteins. In contrast to our observations, Amundson et al. (1998) showed that stress-induced GADD34 was attenuated by overexpression of v-MYC. Given that RANKL-induced GADD34 expression is dependent on MYC in osteoclasts in nutrient-sufficient conditions, further study is needed to identify how MYC regulates GADD34 in osteoclasts. Collectively, our data show that both MYC deficiency and GADD34 deficiency reversed suppressed mTORC1 activity at the late phase of osteoclastogenesis, suggesting the inhibitory role of the MYC/GADD34 axis in mTORC1 activation in osteoclasts. Considering that MYC is currently undruggable (Prochownik and Vogt, 2010) and that mTORC1 is difficult to productively target due to its complicated function in osteoclastogenesis, the MYC/GADD34 axis could be a potential druggable therapeutic target controlling the abnormal activity of osteoclasts.

Data availability statement

The RNA-seq data have been deposited in the Gene Expression Omnibus database with the accession code GEO: GSE202932.

Ethics statement

The animal study was reviewed and approved by Institutional and Animal Care and Use Committee of Weill Cornell Medical College.

Author contributions

SB conceptualized, designed, and performed most of the experiments, analyzed data, and wrote the manuscript. BO, JT, and PP analyzed data and bone phenotype. MG provided expertise and oversaw some animal experiments. EG performed bioinformatic analysis. K-HP-M conceptualized, designed, and oversaw the study and wrote the manuscript. All authors reviewed and provided input on the manuscript.

Funding

This work was supported by the National Institutes of Health 5R01 AR069562; 5R01 AR073156 (to K-HP-M) and by support for the Rosensweig Genomics Center from The Tow Foundation.

Conflict of interest

The authors declare that the research was conducted in the absence of any commercial or financial relationships that could be construed as a potential conflict of interest.

Publisher's note

All claims expressed in this article are solely those of the authors and do not necessarily represent those of their affiliated organizations, or those of the publisher, the editors and the reviewers. Any product that may be evaluated in this article, or claim that may be made by its manufacturer, is not guaranteed or endorsed by the publisher.

Supplementary material

The Supplementary Material for this article can be found online at: https://www.frontiersin.org/articles/10.3389/fcell.2022.920683/full#supplementary-material

References

Amundson, S. A., Zhan, Q., Penn, L. Z., and Fornace, A. J., JR. (1998). Myc suppresses induction of the growth arrest genes gadd34, gadd45, and gadd153 by DNA-damaging agents. *Oncogene* 17, 2149–2154. doi:10.1038/sj.onc.1202136

Avila, N. A., Dwyer, A. J., Rabel, A., Darling, T., Hong, C. H., and Moss, J. (2010). CT of sclerotic bone lesions: Imaging features differentiating tuberous sclerosis complex with lymphangioleiomyomatosis from sporadic lymphangioleiomymatosis. *Radiology* 254, 851–857. doi:10.1148/radiol.09090227

Bae, S., Lee, M. J., Mun, S. H., Giannopoulou, E. G., Yong-Gonzalez, V., Cross, J. R., et al. (2017). MYC-dependent oxidative metabolism regulates osteoclastogenesis via nuclear receptor ERRα. *J. Clin. Invest.* 127, 2555–2568. doi:10.1172/JCI89935

Bateman, J. F., Sampurno, L., Maurizi, A., Lamande, S. R., Sims, N. A., Cheng, T. L., et al. (2019). Effect of rapamycin on bone mass and strength in the α2(I)-G610C mouse model of osteogenesis imperfecta. *J. Cell. Mol. Med.* 23, 1735–1745. doi:10.1111/jcmm.14072

Battaglino, R., Kim, D., Fu, J., Vaage, B., Fu, X. Y., and Stashenko, P. (2002). c-myc is required for osteoclast differentiation. *J. Bone Min. Res.* 17, 763–773. doi:10.1359/jbmr.2002.17.5.763

Bi, H., Chen, X., Gao, S., Yu, X., Xiao, J., Zhang, B., et al. (2017). Key triggers of osteoclast-related diseases and available strategies for targeted therapies: A review. *Front. Med.* 4, 234. doi:10.3389/fmed.2017.00234

Bouxsein, M. L., Boyd, S. K., Christiansen, B. A., Guldberg, R. E., Jepsen, K. J., and Müller, R. (2010). Guidelines for assessment of bone microstructure in rodents using micro-computed tomography. *J. Bone Min. Res.* 25, 1468–1486. doi:10.1002/jbmr.141

Bravo, R., Parra, V., Gatica, D., Rodriguez, A. E., Torrealba, N., Paredes, F., et al. (2013). Endoplasmic reticulum and the unfolded protein response: Dynamics and metabolic integration. *Int. Rev. Cell Mol. Biol.* 301, 215–290. doi:10.1016/B978-0-12-407704-1.00005-1

Brush, M. H., and Shenolikar, S. (2008). Control of cellular GADD34 levels by the 26S proteasome. *Mol. Cell Biol.* 28, 6989–7000.

Chen, C., Akiyama, K., Wang, D., Xu, X., Li, B., Moshaverinia, A., et al. (2015). mTOR inhibition rescues osteopenia in mice with systemic sclerosis. *J. Exp. Med.* 212, 73–91. doi:10.1084/jem.20140643

Chen, J., and Long, F. (2018). mTOR signaling in skeletal development and disease. *Bone Res.* 6, 1. doi:10.1038/s41413-017-0004-5

Chen, J., and Long, F. (2015). mTORC1 signaling promotes osteoblast differentiation from preosteoblasts. *PLoS One* 10, e0130627. doi:10.1371/journal.pone.0130627

Dai, Q., Xie, F., Han, Y., Ma, X., Zhou, S., Jiang, L., et al. (2017a). Inactivation of regulatory-associated protein of mTOR (Raptor)/Mammalian target of rapamycin complex 1 (mTORC1) signaling in osteoclasts increases bone mass by inhibiting osteoclast differentiation in mice. *J. Biol. Chem.* 292, 196–204. doi:10.1074/jbc.M116.764761

Dai, Q., Xu, Z., Ma, X., Niu, N., Zhou, S., Xie, F., et al. (2017b). mTOR/Raptor signaling is critical for skeletogenesis in mice through the regulation of Runx2 expression. *Cell Death Differ.* 24, 1886–1899. doi:10.1038/cdd.2017.110

Dang, C. V. (2012). MYC on the path to cancer. *Cell* 149, 22–35. doi:10.1016/j.cell.2012.03.003

Dang, C. V. (1999). c-Myc target genes involved in cell growth, apoptosis, and metabolism. *Mol. Cell. Biol.* 19, 1–11. doi:10.1128/mcb.19.1.1

Feng, X., and Teitelbaum, S. L. (2013). Osteoclasts: New insights. *Bone Res.* 1, 11–26. doi:10.4248/BR201301003

Fitter, S., Matthews, M. P., Martin, S. K., Xie, J., Ooi, S. S., Walkley, C. R., et al. (2017). mTORC1 plays an important role in skeletal development by controlling preosteoblast differentiation. *Mol. Cell. Biol.* 37, e00668-16. doi:10.1128/MCB.00668-16

Foltyn, M., Luger, A. L., Lorenz, N. I., Sauer, B., Mittelbronn, M., Harter, P. N., et al. (2019). The physiological mTOR complex 1 inhibitor DDIT4 mediates therapy resistance in glioblastoma. *Br. J. Cancer* 120, 481–487. doi:10.1038/s41416-018-0368-3

Fujii, T., Murata, K., Mun, S. H., Bae, S., Lee, Y. J., Pannellini, T., et al. (2021). MEF2C regulates osteoclastogenesis and pathologic bone resorption via c-FOS. *Bone Res.* 9, 4.

Gambardella, G., Staiano, L., Moretti, M. N., De Cegli, R., Fagnocchi, L., Di Tullio, G., et al. (2020). GADD34 is a modulator of autophagy during starvation. *Sci. Adv.* 6, eabb0205. doi:10.1126/sciadv.abb0205

Glantschnig, H., Fisher, J. E., Wesolowski, G., Rodan, G. A., and Reszka, A. A. (2003). M-CSF, TNFalpha and RANK ligand promote osteoclast survival by signaling through mTOR/S6 kinase. *Cell Death Differ.* 10, 1165–1177. doi:10.1038/sj.cdd.4401285

Hiraiwa, M., Ozaki, K., Yamada, T., Iezaki, T., Park, G., Fukasawa, K., et al. (2019). mTORC1 activation in osteoclasts prevents bone loss in a mouse model of osteoporosis. *Front. Pharmacol.* 10, 684. doi:10.3389/fphar.2019.00684

Huang, J., and Manning, B. D. (2008). The TSC1-TSC2 complex: A molecular switchboard controlling cell growth. *Biochem. J.* 412, 179–190. doi:10.1042/BJ20080281

Huynh, H., and Wan, Y. (2018). mTORC1 impedes osteoclast differentiation via calcineurin and NFATc1. *Commun. Biol.* 1, 29. doi:10.1038/s42003-018-0028-4

Ikeda, K., and Takeshita, S. (2016). The role of osteoclast differentiation and function in skeletal homeostasis. *J. Biochem.* 159, 1–8. doi:10.1093/jb/mvv112

Inoki, K., Corradetti, M. N., and Guan, K. L. (2005). Dysregulation of the TSC-mTOR pathway in human disease. *Nat. Genet.* 37, 19–24. doi:10.1038/ng1494

Inoki, K., Li, Y., Zhu, T., Wu, J., and Guan, K. L. (2002). TSC2 is phosphorylated and inhibited by Akt and suppresses mTOR signalling. *Nat. Cell Biol.* 4, 648–657. doi:10.1038/ncb839

Li, J., Kim, S. G., and Blenis, J. (2014). Rapamycin: One drug, many effects. *Cell Metab.* 19, 373–379. doi:10.1016/j.cmet.2014.01.001

Li, Y., Wang, Y., Kim, E., Beemiller, P., Wang, C. Y., Swanson, J., et al. (2007). Bnip3 mediates the hypoxia-induced inhibition on mammalian target of rapamycin by interacting with Rheb. *J. Biol. Chem.* 282, 35803–35813. doi:10.1074/jbc.M705231200

Lin, A., Yao, J., Zhuang, L., Wang, D., Han, J., Lam, E. W., et al. (2014). The FoxO-BNIP3 axis exerts a unique regulation of mTORC1 and cell survival under energy stress. *Oncogene* 33, 3183–3194. doi:10.1038/onc.2013.273

Lorenzo, J. (2017). The many ways of osteoclast activation. *J. Clin. Invest.* 127, 2530–2532. doi:10.1172/JCI94606

Luo, D., Ren, H., Li, T., Lian, K., and Lin, D. (2016). Rapamycin reduces severity of senile osteoporosis by activating osteocyte autophagy. *Osteoporos. Int.* 27, 1093–1101. doi:10.1007/s00198-015-3325-5

Ma, X. M., and Blenis, J. (2009). Molecular mechanisms of mTOR-mediated translational control. *Nat. Rev. Mol. Cell Biol.* 10, 307–318. doi:10.1038/nrm2672

Martin, S. K., Fitter, S., El Khawanky, N., Grose, R. H., Walkley, C. R., Purton, L. E., et al. (2018). mTORC1 plays an important role in osteoblastic regulation of B-lymphopoiesis. *Sci. Rep.* 8, 14501. doi:10.1038/s41598-018-32858-5

Moon, J. B., Kim, J. H., Kim, K., Youn, B. U., Ko, A., Lee, S. Y., et al. (2012). Akt induces osteoclast differentiation through regulating the GSK3β/NFATc1 signaling cascade. *J. Immunol.* 188, 163–169. doi:10.4049/jimmunol.1101254

Mootha, V. K., Lindgren, C. M., Eriksson, K. F., Subramanian, A., Sihag, S., Lehar, J., et al. (2003). PGC-1alpha-responsive genes involved in oxidative phosphorylation are coordinately downregulated in human diabetes. *Nat. Genet.* 34, 267–273. doi:10.1038/ng1180

Mun, S. H., Bae, S., Zeng, S., Oh, B., Chai, C., Kim, M. J., et al. (2021). Augmenting MNK1/2 activation by c-FMS proteolysis promotes osteoclastogenesis and arthritic bone erosion. *Bone Res.* 9, 45. doi:10.1038/s41413-021-00162-0

Nakamura, T., Imai, Y., Matsumoto, T., Sato, S., Takeuchi, K., Igarashi, K., et al. (2007). Estrogen prevents bone loss via estrogen receptor alpha and induction of Fas ligand in osteoclasts. *Cell* 130, 811–823. doi:10.1016/j.cell.2007.07.025

Nishikawa, K., Iwamoto, Y., Kobayashi, Y., Katsuoka, F., Kawaguchi, S., Tsujita, T., et al. (2015). DNA methyltransferase 3a regulates osteoclast differentiation by coupling to an S-adenosylmethionine-producing metabolic pathway. *Nat. Med.* 21, 281–287. doi:10.1038/nm.3774

Novoa, I., Zeng, H., Harding, H. P., and Ron, D. (2001). Feedback inhibition of the unfolded protein response by GADD34-mediated dephosphorylation of eIF2alpha. *J. Cell Biol.* 153, 1011–1022. doi:10.1083/jcb.153.5.1011

Parfitt, A. M., Drezner, M. K., Glorieux, F. H., Kanis, J. A., Malluche, H., Meunier, P. J., et al. (1987). Bone histomorphometry: Standardization of nomenclature, symbols, and units. Report of the ASBMR histomorphometry nomenclature committee. *J. Bone Min. Res.* 2, 595–610. doi:10.1002/jbmr.5650020617

Park-Min, K. H. (2019). Metabolic reprogramming in osteoclasts. *Semin. Immunopathol.* 41, 565–572. doi:10.1007/s00281-019-00757-0

Park-Min, K. H., Lim, E., Lee, M. J., Park, S. H., Giannopoulou, E., Yarilina, A., et al. (2014). Inhibition of osteoclastogenesis and inflammatory bone resorption by targeting BET proteins and epigenetic regulation. *Nat. Commun.* 5, 5418. doi:10.1038/ncomms6418

Prochownik, E. V., and Vogt, P. K. (2010). Therapeutic targeting of myc. *Genes Cancer* 1, 650–659. doi:10.1177/1947601910377494

Riddle, R. C., Frey, J. L., Tomlinson, R. E., Ferron, M., Li, Y., Digirolamo, D. J., et al. (2014). Tsc2 is a molecular checkpoint controlling osteoblast development and glucose homeostasis. *Mol. Cell. Biol.* 34, 1850–1862. doi:10.1128/MCB.00075-14

Rubert, M., Montero, M., Guede, D., Caeiro, J. R., Martin-Fernandez, M., Diaz-Curiel, M., et al. (2015). Sirolimus and tacrolimus rather than cyclosporine A cause bone loss in healthy adult male rats. *Bone Rep.* 2, 74–81. doi:10.1016/j.bonr.2015.05.003

Saxton, R. A., and Sabatini, D. M. (2017). mTOR signaling in growth, metabolism, and disease. *Cell* 168, 960–976. doi:10.1016/j.cell.2017.02.004

Shaw, R. J., and Cantley, L. C. (2006). Ras, PI(3)K and mTOR signalling controls tumour cell growth. *Nature* 441, 424–430. doi:10.1038/nature04869

Subramanian, A., Tamayo, P., Mootha, V. K., Mukherjee, S., Ebert, B. L., Gillette, M. A., et al. (2005). Gene set enrichment analysis: A knowledge-based approach for interpreting genome-wide expression profiles. *Proc. Natl. Acad. Sci. U. S. A.* 102, 15545–15550. doi:10.1073/pnas.0506580102

Teitelbaum, S. L. (2000). Bone resorption by osteoclasts. *Science* 289, 1504–1508. doi:10.1126/science.289.5484.1504

Tiedemann, K., Le Nihouannen, D., Fong, J. E., Hussein, O., Barralet, J. E., and Komarova, S. V. (2017). Regulation of Osteoclast Growth and Fusion by mTOR/raptor and mTOR/rictor/Akt. *Front. Cell Dev. Biol.* 5, 54. doi:10.3389/fcell.2017.00054

Uddin, M. N., Ito, S., Nishio, N., Suganya, T., and Isobe, K. (2011). Gadd34 induces autophagy through the suppression of the mTOR pathway during starvation. *Biochem. Biophys. Res. Commun.* 407, 692–698. doi:10.1016/j.bbrc.2011.03.077

Varusai, T. M., and Nguyen, L. K. (2018). Dynamic modelling of the mTOR signalling network reveals complex emergent behaviours conferred by DEPTOR. *Sci. Rep.* 8, 643. doi:10.1038/s41598-017-18400-z

Walter, P., and Ron, D. (2011). The unfolded protein response: From stress pathway to homeostatic regulation. *Science* 334, 1081–1086. doi:10.1126/science.1209038

Watanabe, R., Tambe, Y., Inoue, H., Isono, T., Haneda, M., Isobe, K., et al. (2007). GADD34 inhibits mammalian target of rapamycin signaling via tuberous sclerosis complex and controls cell survival under bioenergetic stress. *Int. J. Mol. Med.* 19, 475–483. doi:10.3892/ijmm.19.3.475

Wu, H., Wu, Z., Li, P., Cong, Q., Chen, R., Xu, W., et al. (2017). Bone size and quality regulation: Concerted actions of mTOR in mesenchymal stromal cells and osteoclasts. *Stem Cell Rep.* 8, 1600–1616. doi:10.1016/j.stemcr.2017.04.005

Xu, S., Zhang, Y., Wang, J., Li, K., Tan, K., Liang, K., et al. (2018). TSC1 regulates osteoclast podosome organization and bone resorption through mTORC1 and Rac1/Cdc42. *Cell Death Differ.* 25, 1549–1566. doi:10.1038/s41418-017-0049-4

Yu, J., Adapala, N. S., Doherty, L., and Sanjay, A. (2019). Cbl-PI3K interaction regulates Cathepsin K secretion in osteoclasts. *Bone* 127, 376–385. doi:10.1016/j.bone.2019.07.009

Zhang, Y., Gao, X., Saucedo, L. J., Ru, B., Edgar, B. A., and Pan, D. (2003). Rheb is a direct target of the tuberous sclerosis tumour suppressor proteins. *Nat. Cell Biol.* 5, 578–581. doi:10.1038/ncb999

Zhang, Y., Xu, S., Li, K., Tan, K., Liang, K., Wang, J., et al. (2017). mTORC1 inhibits NF-κB/NFATc1 signaling and prevents osteoclast precursor differentiation, *in vitro* and in mice. *J. Bone Min. Res.* 32, 1829–1840. doi:10.1002/jbmr.3172

frontiers | Frontiers in Cell and Developmental Biology

TYPE Original Research
PUBLISHED 19 August 2022
DOI 10.3389/fcell.2022.921066

OPEN ACCESS

EDITED BY
Enrico Iaccino,
Magna Græcia University of Catanzaro, Italy

REVIEWED BY
David S. Gyori,
Semmelweis University, Hungary
Vasilios Panagopoulos,
University of Adelaide, Australia

*CORRESPONDENCE
Jack J. W. A. van Loon,
j.vanloon@amsterdamumc.nl

†These authors have contributed equally to this work

SPECIALTY SECTION
This article was submitted to Cellular Biochemistry, a section of the journal Frontiers in Cell and Developmental Biology

RECEIVED 15 April 2022
ACCEPTED 13 July 2022
PUBLISHED 19 August 2022

CITATION
Jansen IDC, van Velzen T, de Vries TJ, Szulcek R and van Loon JJWA (2022), Real-time quantification of osteoclastic resorptive activity by electric cell-substrate impedance sensing. *Front. Cell Dev. Biol.* 10:921066. doi: 10.3389/fcell.2022.921066

Real-time quantification of osteoclastic resorptive activity by electric cell-substrate impedance sensing

Ineke D.C. Jansen[1], Thijs van Velzen[1], Teun J. de Vries[1], Robert Szulcek[2,3,4†] and Jack J. W. A. van Loon[5,6,7,8*†]

[1]Department of Periodontology, Academic Centre for Dentistry Amsterdam (ACTA), University of Amsterdam and Vrije Universiteit Amsterdam, Amsterdam, Netherlands, [2]Department of Pulmonary Diseases, Amsterdam UMC, VU University Medical Center, Amsterdam Cardiovascular Sciences (ACS), Amsterdam, Netherlands, [3]Laboratory of in vitro Modeling Systems of Pulmonary and Thrombotic Diseases, Institute of Physiology, Charité—Universitätsmedizin Berlin, Corporate Member of Freie Universität Berlin and Humboldt-Universität zu Berlin, Berlin, Germany, [4]German Heart Center Berlin, Berlin, Germany, [5]Life Support and Physical Sciences Section (TEC-MMG), European Space Agency—European Space Research and Technology Centre (ESA-ESTEC), Noordwijk, Netherlands, [6]DESC (Dutch Experiment Support Center), Amsterdam University Medical Center Location VUmc, Amsterdam, Netherlands, [7]Department of Oral Cell Biology, Academic Centre for Dentistry Amsterdam (ACTA), University of Amsterdam and Vrije Universiteit Amsterdam, Amsterdam, Netherlands, [8]Department of Oral and Maxillofacial Surgery/Pathology, Amsterdam University Medical Center Amsterdam Bone Center (ABC), Amsterdam, Netherlands

In several diseases, bone resorption by osteoclasts is dysregulated. Thus far, no simple technique for real-time measurement of resorption is available. Here, we introduce an impedimetric bioassay for real-time monitoring of resorption by making use of the electrical insulating properties of the resorbable substrate calcium phosphate. Different chemical stimuli were applied to (pre)osteoclasts cultured on a layer of calcium phosphate in multi-well plates containing electrodes. By this, osteoclast activity can be measured continuously over days, and the effects of stimulating or inhibiting factors can be quantified. When cells were cultured in the presence of an inflammatory factor such as IL-1β, the resorptive activity started earlier. The measured decline in resistance was higher at culture day 5 than at cultures with M-CSF or M-CSF + RANKL (M-CSF norm. Resistance = 1, M-CSF + RANKL = 0.7, M-CSF + RANKL + IL-1β = 0.5). However, at day 11, this difference had nearly disappeared. Likewise, bisphosphonates were shown to inhibit osteoclastic activity. Our findings illustrate the importance of real-time monitoring; wherefore, this method has high potential not only for the study of osteoclast resorptive activity in the context of osteoclast function and diseases but also could find application in high-throughput drug-testing studies.

KEYWORDS

osteoclast, sensor, resorption, real-time quantification, bone, ECIS

1 Introduction

Osteoclasts are multinucleated cells uniquely equipped to resorb bone (Gothlin and Ericsson, 1976). They arise from mononuclear hematopoietic cells from the monocyte lineage (Boyle et al., 2003). These osteoclast precursor cells fuse to form multinucleated osteoclasts in the presence of macrophage colony-stimulating factor (M-CSF) and receptor activator of NF-κB ligand (RANKL) (Jansen et al., 2012).

Bone resorption can occur in distinct modes. Some osteoclasts resorb bone in a stationary way, leaving behind round resorption pits, whereas other osteoclasts resorb bone while moving over the bone surface by which they form resorption trenches (Merrild et al., 2015; Søe and Delaissé, 2017).

For the visualization of bone resorption, various staining methods can be used for instance; toluidine, Coomassie Brilliant Blue (CBB), and hematoxylin (Notoya et al., 1993; Vesprey and Yang, 2016; Cao et al., 2017). These dyes stain proteins including the bone matrix proteins that are exposed due to osteoclast activity and left in the resorption pit. However, all these staining methods that are used to visualize and semi-quantitatively evaluate bone resorption require the removal of osteoclasts. In addition, with these methods, it is not possible to quantify the absolute amount of resorption since only the resorbed area and not the depth of the resorption pit can be measured. Some researchers use advanced microscopy techniques, such as scanning electron microscopy, confocal microscopy, or infinite focus microscopy, for the calculation of resorption pit depth and osteoclast morphology (Chambers et al., 1984; Goldberg et al, 2012; Boyde and Jones, 1991; Winkler et al., 2010; Pascaretti-Grizon et al., 2011), but for all these methods, the cultures must be terminated and the resorbed area can only be measured at the end of the *in vitro* culture period and not real-time during the entire experiment. On-line measurements of resorption hold great potential to advance our knowledge on osteoclast kinetics in physiology and pathology. It could provide answers in mechanistic studies on the timing of resorption, the mode of action of various agents that are known or that are suspected of interfering with osteoclast activity, or the development of novel substrate materials, scaffolds, or coatings for tissue engineering and orthopedic interventions. In an attempt to visualize osteoclast activity in real-time, Alsharif et al., have used luminescent nanocrystals which were incorporated in the calcium phosphate coating and taken up by the osteoclasts during resorption, which could be quantified by confocal microscopy (Alsharif et al., 2013). The advantage of this optical measurement is that individual cells can be traced. However, this technology requires two steps before a signal is generated. It requires matrix resorption followed by nanocrystal internalization by the osteoclast. Both processes could be rate-limiting steps in the final measurement. Also, the raw data need to be processed and mathematically modeled to quantify the final activity.

Alternatively, Lo, Keese, and Giaever (Lo et al., 1993) showed that Electric Cell-substrate Impedance Sensing (ECIS) is a versatile tool to quantify cell behavior electrically (Giaever and Keese, 1991; Lo et al., 1993; Lo et al., 1995; Szulcek et al., 2015). ECIS is an easy-to-use, non-invasive real-time measurement system to quantify several cell biological processes, such as barrier integrity, cell adhesions, motility, and migration and responses to drugs and toxins in a single, automated measurement with a high temporal resolution of seconds (Szulcek et al., 2014). The ECIS principle to measure impedance (complex resistance to current flow) makes it an interesting method for measuring osteoclast resorptive activity. In the present study, ECIS was used as a novel method to monitor and quantify osteoclast resorptive activity during culturing. Wells containing measurement electrodes were coated with calcium phosphate, causing a constant resistance to the flowing current. During culturing with activated osteoclasts, the impedance was monitored at several time points as a function of resorptive activity.

The results of this study allow for more efficient and accurate research into the relation between osteoclasts and the on- and off-switches of resorptive activity. With the ECIS method, the resorptive activity can be measured continuously, which allows to deduce the exact time when resorption starts. Importantly, ECIS is much easier to handle than the staining methods and less time-consuming. This holds an enormous translational value when using models for enhanced osteoclast activity in diseases like osteoporosis, Paget's disease, or periodontitis, where the effect of medication on osteoclast activity can be monitored over time.

2 Materials and methods

2.1 Calcium phosphate coating

2.1.1 Pre-coating

To prepare calcium phosphate coatings (CAP), the procedure of Leeuwenburgh et al. (2001) was followed. A pre-coating was formed in a 96-well plate containing electrodes (Applied Biophysics, Troy, NY, USA) using a 5x concentrated tyrode solution. The solution (500 ml) contains 20 g NaCl, 0.5g KCl, 0.67 g $CaCl_2$*$2H_2O$, and 0.53 g $MgCl_2$*$6H_2O$. To lower the pH to 2, 10 Ll of 1 M HCl was added, followed by 0.18 g Na_2HPO_4*$2H_2O$ and small portions of $NaHCO_3$ (2.5 g in total). pH was maintained at 6.0 using 1 M HCl. The solution was sterilized using a 0.22-µm filter (Millipore, Amsterdam, Netherlands). 250 µL of this solution was added to every well, then the plate was sealed in a bag (stericlin, VPgroup, Feuchtwangen, DE), and placed in a 37°C incubation while gently shaking (150 rpm). The plate was incubated for 24 h and then washed three times with sterile demineralized water.

2.1.2 Crystalline layer of calcium phosphate

A calcium phosphate supersaturated solution (CPS) was used to induce crystal growth on the pre-coated well plate. The solution was prepared by adding 20 ml 1 M HCl to 500 ml demineralized water after which 0.18 g Na_2HPO_4*$2H_2O$, 4.0 g NaCl, 0.3 g $CaCl_2 2H_2O$, and 3.0 g TRIS were added. pH was corrected to 7.4 using 1 M HCl. The solution was sterilized using a filter (Millipore). In the 96-well plate, 250 ul of this solution was added to every pre-coated well (step 2.1.1). The plate was sealed in a bag (stericlin, VPgroup) and kept at 37°C for 48 h. CPS was removed, and the plate was washed with sterile demineralized water and dried overnight in a laminar flow cabinet.

2.1.3 Coated plate with HCl treatment

To investigate whether we can measure the gradual dissolvement of the CAP coating, HCl was added to the plate in an increasing concentration, and the resistance was measured in the ECIS machine for 130 min. HCl shifts the pH and thereby induces dissolution of the coating. The concentration series was 0.0025, 0.005, 0.0075, 0.01, 0.025, 0.05, 0.075, and 0.1N HCl. The series was added in triplicate, and the resistance was measured in the ECIS immediately after HCl addition.

2.2 Osteoclasts

2.2.1 Isolation and culturing of osteoclast precursors from mouse bone marrow

For the isolation of osteoclast precursors, the bone marrow of mice (C57BL/6) was used. Animal experiments were approved by the animal welfare committee of the VU University (DEC nr. ACTA 2014–2). Tibiae were dissected and transferred in a petri dish containing 3 ml α-MEM (Gibco, Paisley, United Kingdom) + 10% FCS (HyClone, Logan, UT) + 1% PSF (Sigma, St. Louis, MO, USA) + 100 µl heparin (170 IE/mL; Leo pharmaceutical products BV, Weesp, Netherlands). The tibiae were crunched in a mortar containing 5 mL of α-MEM + 10% FCS +1% PSF. To isolate bone marrow, the cell suspension was aspirated through a 21G needle, filtered through a 70-µm pore-size cell strainer (Greiner Bio-One, Monroe, NC), and collected in a 50-ml tube. A MUSE count and viability kit (MCH600103, Merck, Darmstadt, Germany) was used to determine the concentration of cells. The cell concentration was adjusted to $1.3*10^6$ cell/mL, and 10^5 cells were seeded per well. Osteoclasts were generated with 30 ng/mL M-CSF and 20 ng/mL RANKL (both from R&D Systems, Minneapolis, MI, USA) cultured for 11 days and refreshed twice, at days 3 and 7. To enhance the osteoclast resorptive activity, 10 ng/mL interleukin-1β (IL-1β; Sigma) or 10 ng/mL Tumor Necrosis Factor-α (TNF-α; R&D systems, Minneapolis, MI) was added directly to the culture medium in combination with M-CSF and RANKL, as mentioned above (Cao et al., 2016; Cao et al., 2017; Wang and He, 2020). To inhibit osteoclast activity, 20 ng/mL pamidronate (Sigma) was added to the cultures.

2.2.2 Isolation and culturing of osteoclast precursors from human blood

$CD14^+$ blood monocytes as osteoclast precursors were isolated from human peripheral blood mononuclear cells (PBMCs) (ten Harkel et al., 2015). Briefly, blood from a buffy coat (Sanquin, Amsterdam, Netherlands) was diluted with PBS containing 1% citrate (1:2) and spun down (800 g for 30 min, without brake) in lymphoprep (Elitech, Puteaux, France) gradient solution. The resulting interphase containing peripheral blood mononuclear cells (PBMCs) was collected and washed with 1% citrate in PBS before it was passed through a cell strainer (40 µm Greiner Bio-One Monroe, NC) to ensure the recovery of a pure mononuclear cell population. The cells were counted (Muse cell counter, Merck, Darmstadt, Germany), and the cell pellet was resuspended in 80 µL buffer (PBS containing 0.5% BSA and 2 mM EDTA) for 10^7 cells. Twenty µL of CD14-magnetic beads was added to this cell suspension (MACS microbeads, Miltenyi Biotech, Bergisch Gladbach, Germany). According to the manufacturer's instructions, the cells and CD14-beads were mixed and incubated for 15 min at 4°C. The LS column was placed in the magnetic field, rinsed, and subsequently, the cell suspension was applied to the column. Unlabeled cells will pass through. Then, the column is removed from the magnet and $CD14^+$ cells were flushed out and collected.

The isolated $CD14^+$ cells were plated on a calcium phosphate–coated ECIS 96-well plate at a density of 10^5 cells per well. Cells were cultured for 21 days in α-MEM (Gibco, Paisley, United Kingdom) supplemented with 10% FCS (HyClone, Logan, UT), 100 U/mL penicillin, 100 µg/ml streptomycin, and 250 ng/mL amphotericin B (Antibiotic Antimycotic solution, Sigma, St. Louis, MO) and for an additional 3 days with 25 ng/ml human recombinant M-CSF (R&D Systems, Minneapolis, MN) to induce differentiation. After these 3 days, the concentration of M-CSF was reduced to 10 ng/mL and combined with 2 ng/mL recombinant RANKL (R&D systems) till the end of the culture period. During culture, the cells were maintained at 37°C and 5% CO_2, and the culture medium was refreshed every 3–4 days for a period of 21 days. To enhance the osteoclast resorptive activity, 10 ng/mL interleukin-6 (IL-6; R&D) was added directly to the culture medium.

2.3 ECIS

The osteoclast precursors were cultured in a CAP coated 96-well plate containing electrodes (96W10idf PET, Applied Biophysics, Troy, USA), maintained at 37°C and 5% CO_2, and put in the ECIS (ECIS Z0 and 96W Array station, Applied Biophysics, NY, USA) where the resistance was measured at

64 kHz every 15 min. Data were registered using ECIS software. For detailed description and introductory videos, refer to (Szulcek et al., 2014). Representative data are shown at 64 kHz.

2.4 Osteoclast visualization

2.4.1 Tartrate resistance acidic phosphatase staining

When the mature osteoclasts were formed after 11 days for mouse cells and 21 days for human cells, the osteoclasts were visualized with TRAcP staining. The commercially available leukocyte acid phosphatase kit (Sigma-Aldrich, St Louis, MD, USA) was used following the manufacturer's instructions. In short, the wells were washed once with PBS and subsequently fixated with 4% formaldehyde in 0.1 M phosphate buffer (pH = 7.2) for 10 minutes at room temperature and subsequently washed once again with PBS and stained for TRAcP. The incubation time was 15 min for mouse cells and 60 min for human cells in the dark at room temperature. Subsequently, the nuclei were stained with 4′,6-diamidino-2-phenylindole (DAPI) and examined with an inverted fluorescence light microscope equipped with a digital camera (DM IL, Leica microsystems, GmbH, Wetzlar, Germany) using phase contrast for TRAcP staining and fluorescent light to visualize the nuclei.

2.4.2 Scanning electron microscopy

The area around the electrode lysed by osteoclasts was visualized with a scanning electron microscope (LS15 Zeiss, Oberkochen, Germany) at a magnification of ×2000. The bottom of the 96-well plates with electrodes was cut out with biopsy stans (Microtek, Mosta, Malta), dried in a vacuum oven (Vacutherm, Heraeus, Thermo Scientific, Waltham, MO, USA), and gold-sputtered for electron conductivity.

2.5 Statistical analysis

Data analysis was performed using GraphPad Prism 8 (GraphPad, San Diego, CA). One-way ANOVA was used to analyze differences between three or more groups at different time points. A paired t-test was used to analyze differences between two groups at different time points. The number of replicas was n = 6, unless indicated differently. Groups were considered significantly different when $p \leq 0.05$.

3 Results

3.1 Increasing concentrations of HCl result in gradual dissolving of the CAP coating

To assess whether an increase in conductivity was indeed the result of lysis of the CAP coating, an experiment was conducted with HCl-induced lysis of CAP (Figure 1). The dissolving of the CAP coating with gradually increasing concentrations of HCl started directly after addition to the culture well. After adding the HCl, the resistance was measured immediately in the ECIS. However, while placing the plates in the ECIS, some of the coatings – especially with the higher HCl concentration – already started to dissolve. This is the reason why the resistance was not the same for all the wells at t = 0. As such, 0.1, 0.075, 0.05, 0.025, and 0.01N HCl (Figure 1A) had already dissolved the CAP coating at the start of measurement, resulting in a lower normalized resistance. This gradually became less with a lower concentration where we could follow dissolution over time. The 0 and 0.0025N HCl started with high resistance, meaning that the CAP is not dissolved and decreases more slowly over time. Calculation of the area under the curve (Figure 1B) showed that significant differences exist between the two lowest concentrations (and 0.0025N HCl) and 0.025 and 0.075N HCl.

3.2 Osteoclasts resorb calcium phosphate on ECIS plates

Before correlating the presence of CAP-lysing osteoclasts and increased conductivity, it must be established that osteoclasts indeed lyse the CAP that was formed on the ECIS plates. Using SEM, we were able to show that osteoclasts are present on the CAP-coated ECIS plate. Osteoclasts were present in the CAP removed area, indicating that these osteoclasts were responsible for resorption. Cells were also visible on top of the CAP layer (Figure 2).

3.3 Stimulatory molecules contribute to more resorption of CAP

Preosteoclasts adhered normally to the CAP-coated ECIS plates (Figure 3). Without RANKL, no osteoclasts were formed. Only mononuclear cells were present, and the CAP coating was not lysed (Figure 3A). In cultures with M-CSF and RANKL, osteoclasts were formed, and the CAP coating was partly resorbed (Figure 3B). In Figure 4A a micrograph of the coated ECIS plate without cells and the CAP coating was not lysed. When the cells were cultured with M-CSF and RANKL, TRAcP-positive osteoclasts were formed and the coating was partly lysed, osteoclasts being present at the periphery of the lysed areas (Figure 4B,D). When one of the inflammatory cytokines such as IL-6 was added to the cultures in combination with M-CSF and RANKL, more TRAcP-positive osteoclasts were formed and more of the CAP area was resorbed (Figure 4C,E). In Figure 4F, the resorbed area of control and IL-6 is quantified. However, the percentage of the resorbed area in the triplicate wells is not significantly different (n = 3).

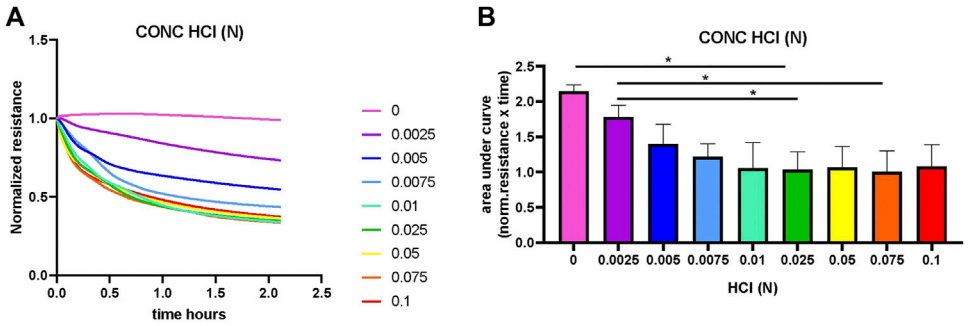

FIGURE 1
Dissolving of CAP by titration of HCl concentration. HCl was added in increasing concentrations to dissolve the calcium phosphate coating (CAP) on electrodes containing 96-well plates. Resistance was measured by ECIS at a frequency of 64 kHz for 2 hours. **(A)**. Overview of the normalized resistance for all HCL concentrations. In control with no HCl, CAP coating is not lysed and resistance not changed. The higher HCL concentrations had dissolved the CAP coating already at very early time points. **(B)**. Quantification of area under the curve shows significant differences (*p < 0.01 n = 3).

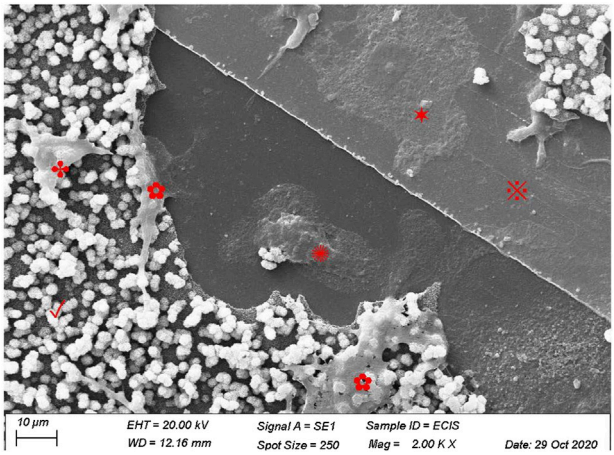

FIGURE 2
Human osteoclasts on CAP-coated ECIS plates. Human CD14+-cells were cultured for 21 days with M-CSF and RANKL and visualized by scanning electron microscopy. The image shows a partly intact CAP (✓) layer on the culture surface of ECIS wells. Some osteoclasts have lysed the CAP coating, exposing the electrode (※). Several osteoclasts were present on the bare multi-well plastic substrate (✺), on the electrode (✶), as well as osteoclasts that partially lysed CAP (✿), and an osteoclast still on top of the CAP coating (✣).

3.4 Stimulatory or non-stimulatory molecules contribute to a specific time-dependent resorption

The normalized resistance was measured at timepoint = 0 for cultures with only M-CSF, M-CSF and RANKL, M-CSF, and RANKL with either IL-1β, TNF-α, or Pamidronate (Figure 5). At t = 0, the normalized resistance is comparable for all cultures because no osteoclasts are formed yet and the coating is still intact (Figure 5A). As expected, when only M-CSF was added to the cultures the resistance stayed high in these cultures since no osteoclasts were formed, and the CAP coating was not lysed (Figure 5B). In the presence of M-CSF and RANKL with or without IL-1β, the resistance decreased to a comparatively low value on day 11, representing the endpoint measurement. Interestingly, real-time recording (Figure 5C) revealed that IL-1β induces osteoclast activity earlier in time (day 4 *vs.* day 5) and accelerates the lysis of calcium phosphate when compared to MR alone. Another unique pattern was observed when adding TNF-α, where a plateau of resistance was reached at a different level when compared to MR or MR + IL-1β (0.8 *vs.* 0.4; p < 0.05 n = 6). These real-time recordings show thus far unknown calcium

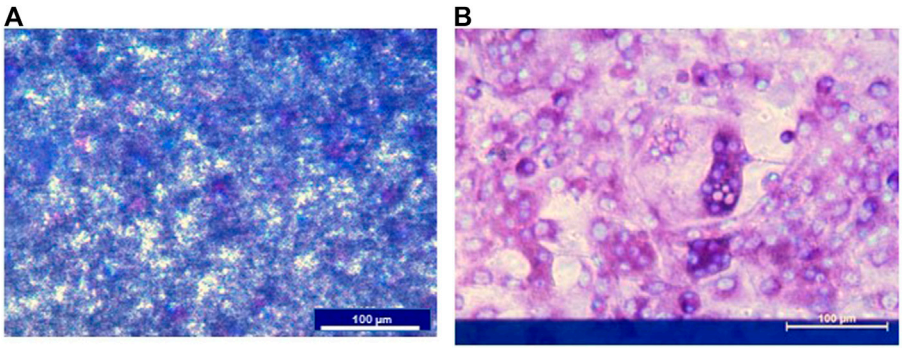

FIGURE 3
ECIS plate with CAP coating and mouse bone marrow cells cultured with M-CSF or M-CSF and RANKL. **(A)** Cells were cultured on an ECIS plate with CAP for 11 days with only M-CSF. No osteoclasts were formed, and the CAP coating is not lysed. Nuclei of the mononucleated cells were stained with DAPI (blue). **(B)**. When cultured for 11 days with M-CSF and RANKL multinucleated and TRAcP (purple), positive osteoclasts were formed. Nuclei stained with DAPI (blue). The blue horizontal bar in B is the ECIS plate electrode.

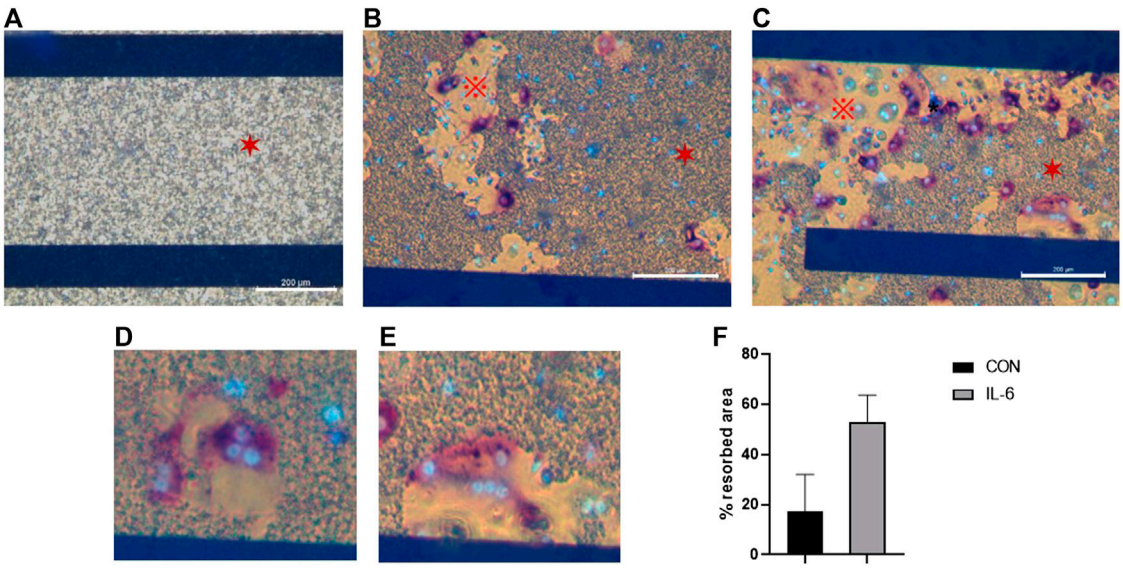

FIGURE 4
ECIS plate with CAP coating visualized with an inverted microscope. **(A)**. When no cells were present, the CAP coating (✶) is completely unaffected. **(B)**. Cells were cultured for 21 days with M-CSF and RANKL, and osteoclasts from human CD14+-cells were formed and able to dissolve the CAP coating. Osteoclasts were stained for TRAcP (purple) and nuclei with DAPI (blue). **(C)**. Osteoclasts were activated with IL-6 (i.e., M-CSF + RANKL + IL-6), resulting in higher dissolving activity. Osteoclasts were stained for TRAcP (purple) and nuclei with DAPI (blue). CAP coating (✶), dissolved area (※). **(D,E)** Higher magnification to illustrate that osteoclasts are located at the periphery of the CAP coating, where resorption takes place. **(F)** Percentage of the resorbed area in cultures with M-CSF + RANKL (=CON) and M-CSF + RANKL + IL-6 at day 21. Blue horizontal bars are the ECIS plate electrodes. Scale bar A-C = 200 µm.

phosphate lysis patterns that could be unique to the stimulus that was given and could provide novel mechanistic insights compared to endpoint quantifications. When osteoclast formation was inhibited with pamidronate, the resistance remained high, comparable with the culture with only M-CSF, due to lack of resorption (Figures 5B–D). Calculation of the area under the curve (Figure 5D) showed that significant differences exist between almost all incubations with IL-1β inducing the highest resorptive activity of mature osteoclasts. No differences are present in M and PAM since no active osteoclasts were present. All the differences between the other incubations were ever seen before with the classic endpoint staining.

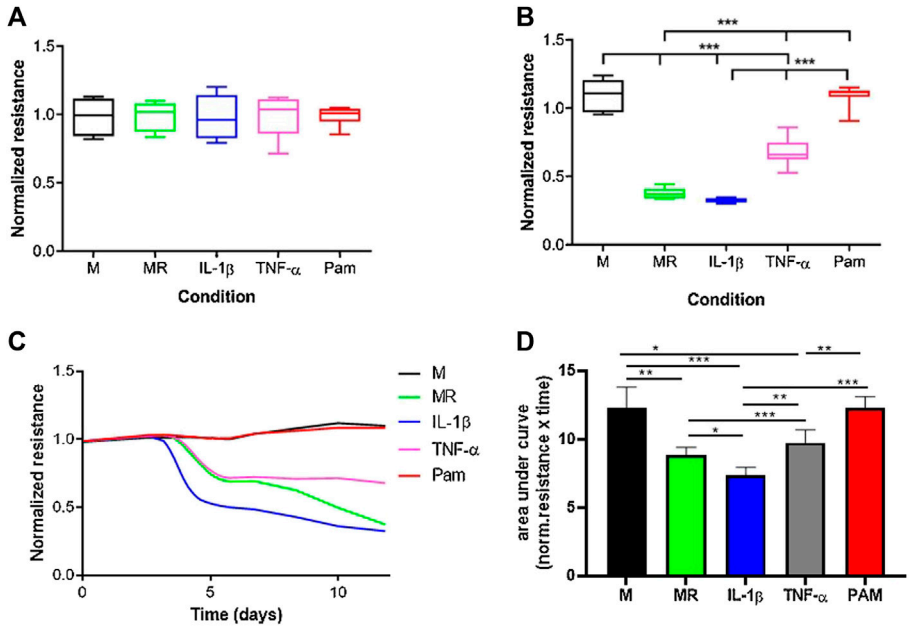

FIGURE 5
Real-time resorption quantification provides mechanistic insights into osteoclast formation and resorptive activity. M = medium with M-CSF, MR = medium with M-CSF and RANKL, IL = medium with M-CSF, RANKL and IL-1β, TNF-α = medium with M-CSF and RANKL and TNF-α, PAM = medium with M-CSF and RANKL and Pamidronate. Osteoclasts were generated from mouse bone marrow, and the resistance was measured for 11 days. **(A)**. No differences in resistance were found between the various conditions at timepoint zero since pre-osteoclasts were not differentiated into mature cells yet. **(B)**. After 11 days of culture, osteoclasts were formed and CAP coating was lysed, resulting in differences in resistance. Osteoclasts were formed in cultures with MR, IL-1β, and TNF-α, resulting in a lower resistance due to lysis of the CAP coating. In the cultures with only M or Pam, no active osteoclasts were present and no decline in resistance was recorded. (one -way ANOVA n = 6, ***$p < 0.05$). **(C)**. Overview of the resistance from day 0 to day 11. Typical for the lysis of CAP coating is the lag phase between days 0–4, where the resistance is not changed. Thus, no lysis has taken place because osteoclasts were not formed yet. From day 4, unique CAP lysis patterns emerge, likely due to differential activation of osteoclasts by MR supplemented with or without IL-1β or TNF-α, all leading to lower resistance. In the M and PAM cultures, no lysis occurred, likely due to the absence of osteoclasts, resulting in no change in resistance. **(D)**. Quantification of area under the curve shows significant differences (*$p < 0.01$, **$p < 0.001$, and ***$p < 0.0001$ n = 6) for most of the incubations. Only the incubations in which no osteoclasts were formed (M and PAM) show an equally high area under the curve. The incubation with IL-1β has the smallest area, which means that CAP lysis was the highest.

4 Discussion

In the present study, we show that ECIS can be used to accurately follow the onset and pattern of osteoclastic resorbing activity in real-time by measuring the electrical resistance of calcium phosphate–coated surfaces. We show that the decrease in resistance is due to CAP lysis by osteoclasts since addition of only M-CSF to the cultures or addition of an inhibitor of osteoclast activity, pamidronate, did not induce a decrease in resistance. On the other hand, when osteoclast activity was enhanced by adding IL-1β, a significant change in resistance, and thereby CAP resorption, was measured.

Continuous measurement of resistance by ECIS allows the analysis of the behavior of osteoclasts at any point during the culture and thereby provides a unique mechanistical look. Some significant differences were observed during this study that would not have been visible if only the end values of resistance were analyzed. An example of this is that when the cells were cultured with M-CSF and RANKL and IL-1β significantly, more CAP is lysed than when cultured with M-CSF and RANKL; the cells started resorption 1 day earlier; and the differences were no longer apparent at day 11. This means that IL-1β accelerated the initial lysis activity but not the total amount of the lysed substrate. Thus, the time point when the lysis is measured is important. In conventional methods, the cultures had to be stopped, probably at time points that are not always informative, for showing representative osteoclast activity. With the ECIS method, the cultures can continue and researchers can select time points with the relevant effect size based on real-time data.

The continuous measurement of the resorption is an important advantage and could be a great step forward in studying the direct effect of medication on bone degradation, such as bisphosphonates or cancer-inhibiting drugs with high-throughput screening methodologies, in the development of other biomimetic substrates or in co-culture studies. One might even speculate to use such coated surfaces as sensors to follow osteoclast or general

mineral resorption activity *in vivo*. One could also think of using the system for quantifying the production of a matrix shown by increasing impedance values.

In summary, this novel use of the ECIS technology makes it possible to measure osteoclast activity in an open and unbiased manner during culturing, revealing hitherto unknown profiles of resorptive activity. The ECIS method is a promising high-throughput technique to investigate the resorption activity of osteoclasts from patients suffering from, for example., Paget's disease fibrous dysplasia, osteoporosis, osteopetrosis, rheumatoid arthritis, or bone tumors with malfunctioning osteoclasts and analyze the effect of medication on osteoclast activity during culturing.

Data availability statement

The raw data supporting the conclusions of this article will be made available by the authors, without undue reservation.

Ethics statement

The animal study was reviewed and approved by VU University Amsterdam, NL: Animal Care DEC nr. ACTA 2014-2.

Author contributions

IJ and RS co-designed the experiments, performed the experiments, and co-wrote the manuscript. TV performed *in vitro* experiments and co-wrote the manuscript. TD contributed to the discussion and manuscript preparation. JV initiated the study and together with RS co-designed the experiments and supervised the study and edited the manuscript.

Funding

This work was partially supported by the Dutch CardioVascular Alliance (DCVA) (2012-08, 2014-11) awarded to the Phaedra and the RECONNECT consortium as well as the Impulse Grant 2018 awarded to the Phaedra IMPACT consortium. These Grants include collective funding from the Dutch Heart Foundation, the Dutch Federation of University Medical Centers, Netherlands Organization for Health Research and Development, and the Royal Netherlands Academy of Sciences.

Acknowledgments

We thank A. Werner for his help with the scanning electron microscope and Xue Manz for her help with the ECIS measurements.

Conflict of interest

The authors declare that the research was conducted in the absence of any commercial or financial relationships that could be construed as a potential conflict of interest.

Publisher's note

References

Alsharif, N. H., Al-Said, S. A. F., Birch, M. A., Horrocks, B. R., and Datta, H. K. (2013). Real-time activity bioassay of single osteoclasts using a silicon nanocrystal-impregnated artificial matrix. *Small* 9 (21), 3685–3692. doi:10.1002/smll.201203184

Boyde, A., and Jones, S. J. (1991). Pitfalls in pit measurement. *Calcif. Tissue Int.* 49 (2), 65–70. doi:10.1007/BF02565123

Boyle, W. J., Simonet, W. S., and Lacey, D. L. (2003). Osteoclast differentiation and activation. *Nature* 423 (6937), 337–342. doi:10.1038/nature01658

Cao, Y., Jansen, I. D., Sprangers, S., Stap, J., Leenen, P. J., Everts, V., et al. (2016). IL-1β differently stimulates proliferation and multinucleation of distinct mouse bone marrow osteoclast precursor subsets. *J. Leukoc. Biol.* 100 (3), 513–523. doi:10.1189/jlb.1A1215-543R

Cao, Y., Jansen, I. D. C., Sprangers, S., de Vries, T. J., and Everts, V. (2017). TNF-α has both stimulatory and inhibitory effects on mouse monocyte-derived osteoclastogenesis. *J. Cell. Physiol.* 232 (12), 3273–3285. doi:10.1002/jcp.26024

Chambers, T., Revell, P., Fuller, K., and Athanasou, N. (1984). Resorption of bone by isolated rabbit osteoclasts. *J. Cell Sci.* 66 (1), 383–399. doi:10.1242/jcs.66.1.383

Giaever, I., and Keese, C. R. (1991). Micromotion of mammalian cells measured electrically. *Proc. Natl. Acad. Sci. U. S. A.* 88 (17), 7896–7900. doi:10.1073/pnas.88.17.7896

Goldberg, S. R., Georgiou, J., Glogauer, M., and Grynpas, M. D. (2012). A 3D scanning confocal imaging method measures pit volume and captures the role of Rac in osteoclast function. *Bone* 51 (1), 145–152. doi:10.1016/j.bone.2012.04.018

Gothlin, G., and Ericsson, J. L. (1976). The osteoclast: Review of ultrastructure, origin, and structure-function relationship. *Clin. Orthop. Relat. Res.* 120, 201–231. doi:10.1097/00003086-197610000-00030

Jansen, I. D., Vermeer, J. A., Bloemen, V., Stap, J., and Everts, V. (2012). Osteoclast fusion and fission. *Calcif. Tissue Int.* 90 (6), 515–522. doi:10.1007/s00223-012-9600-y

Leeuwenburgh, S., Layrolle, P., Barrère, F., de Bruijn, J., Schoonman, J., van Blitterswijk, C. A., et al. (2001). Osteoclastic resorption of biomimetic calcium phosphate coatings *in vitro*. *J. Biomed. Mat. Res.* 56 (2), 208–215. doi:10.1002/1097-4636(200108)56:2<208::aid-jbm1085>3.0.co;2-r

Lo, C. M., Keese, C. R., and Giaever, I. (1995). Impedance analysis of MDCK cells measured by electric cell-substrate impedance sensing. *Biophys. J.* 69 (6), 2800–2807. doi:10.1016/S0006-3495(95)80153-0

Lo, C. M., Keese, C. R., and Giaever, I. (1993). Monitoring motion of confluent cells in tissue culture. *Exp. Cell Res.* 204 (1), 102–109. doi:10.1006/excr.1993.1014

Merrild, D. M., Pirapaharan, D. C., Andreasen, C. M., Kjærsgaard-Andersen, P., Møller, A. M., Ding, M., et al. (2015). Pit- and trench-forming osteoclasts: A distinction that matters. *Bone Res.* 3, 15032. doi:10.1038/boneres.2015.32

Notoya, K., Yoshida, K., Taketomi, S., Yamazaki, I., and Kumegawa, M. (1993). Inhibitory effect of ipriflavone on osteoclast-mediated bone resorption and new osteoclast formation in long-term cultures of mouse unfractionated bone cells. *Calcif. Tissue Int.* 53 (3), 206–209. doi:10.1007/BF01321839

Pascaretti-Grizon, F., Mabilleau, G., Basle, M. F., and Chappard, D. (2011). Measurement by vertical scanning profilometry of resorption volume and lacunae depth caused by osteoclasts on dentine slices. *J. Microsc.* 241 (2), 147–152. doi:10.1111/j.1365-2818.2010.03410.x

Søe, K., and Delaissé, J. M. (2017). Time-lapse reveals that osteoclasts can move across the bone surface while resorbing. *J. Cell Sci.* 130 (12), 2026–2035. doi:10.1242/jcs.202036

Szulcek, R., Bogaard, H. J., and van Nieuw Amerongen, G. P. (2014). Electric cell-substrate impedance sensing for the quantification of endothelial proliferation, barrier function, and motility. *J. Vis. Exp.* 85. doi:10.3791/51300

Szulcek, R., van Bezu, J., Boonstra, J., van Loon, J. J., and van Nieuw Amerongen, G. P. (2015). Transient intervals of hyper-gravity enhance endothelial barrier integrity: Impact of mechanical and gravitational forces measured electrically. *PLoS One* 10 (12), e0144269. doi:10.1371/journal.pone.0144269

ten Harkel, B., Schoenmaker, T., Picavet, D. I., Davison, N. L., de Vries, T. J., Everts, V., et al. (2015). The foreign body giant cell cannot resorb bone, but dissolves hydroxyapatite like osteoclasts. *PLoS One* 10 (10), e0139564. doi:10.1371/journal.pone.0139564

Vesprey, A., and Yang, W. (2016). Pit assay to measure the bone resorptive activity of bone marrow-derived osteoclasts. *Bio. Protoc.* 6 (12), e1836. doi:10.21769/BioProtoc.1836

Wang, T., and He, C. (2020). TNF-A and IL-6: The link between immune and bone system. *Curr. Drug Targets* 21 (3), 213–227. doi:10.2174/1389450120666190821161259

Winkler, T., Hoenig, E., Huber, G., Janssen, R., Fritsch, D., Gildenhaar, R., et al. (2010). Osteoclastic bioresorption of biomaterials: Two-and three-dimensional imaging and quantification. *Int. J. Artif. Organs* 33 (4), 198–203. doi:10.1177/039139881003300404

frontiers | Frontiers in Cell and Developmental Biology

TYPE Original Research
PUBLISHED 29 August 2022
DOI 10.3389/fcell.2022.966950

OPEN ACCESS

EDITED BY
Jesús Balsinde,
Instituto de Biología y Genética Molecular (CSIC), Spain

REVIEWED BY
Kieran F. Scott,
Western Sydney University, Penrith, Australia
David Balgoma,
University of Valladolid, Spain

*CORRESPONDENCE
Stefania Mariggiò,
stefania.mariggio@ibbc.cnr.it

†PRESENT ADDRESS
Maria Mangini,
Institute of Endocrinology and Experimental Oncology "G. Salvatore"-IEOS, Second Unit, National Research Council, Naples, Italy
Stefania Mariggiò, Institute of Biochemistry and Cell Biology, National Research Council, Naples, Italy

SPECIALTY SECTION
This article was submitted to Cellular Biochemistry, a section of the journal Frontiers in Cell and Developmental Biology

RECEIVED 11 June 2022
ACCEPTED 25 July 2022
PUBLISHED 29 August 2022

CITATION
Mangini M, D'Angelo R, Vinciguerra C, Payré C, Lambeau G, Balestrieri B, Charles JF and Mariggiò S (2022), Multimodal regulation of the osteoclastogenesis process by secreted group IIA phospholipase A_2. *Front. Cell Dev. Biol.* 10:966950. doi: 10.3389/fcell.2022.966950

Multimodal regulation of the osteoclastogenesis process by secreted group IIA phospholipase A_2

Maria Mangini[1†], Rosa D'Angelo[1], Caterina Vinciguerra[2], Christine Payré[3], Gérard Lambeau[3], Barbara Balestrieri[4], Julia F. Charles[5] and Stefania Mariggiò[1*†]

[1]Institute of Protein Biochemistry, National Research Council, Naples, Italy, [2]Institute of Biochemistry and Cell Biology, National Research Council, Naples, Italy, [3]Centre National de la Recherche Scientifique, Institut de Pharmacologie Moléculaire et Cellulaire, Université Côte d'Azur, Valbonne Sophia Antipolis, France, [4]Jeff and Penny Vinik Center for Translational Immunology Research, Department of Medicine, Division of Allergy and Clinical Immunology, Brigham and Women's Hospital, Harvard Medical School, Boston, MA, United States, [5]Departments of Orthopaedic Surgery and Medicine, Brigham and Women's Hospital, Harvard Medical School, Boston, MA, United States

Increasing evidence points to the involvement of group IIA secreted phospholipase A_2 (sPLA$_2$-IIA) in pathologies characterized by abnormal osteoclast bone-resorption activity. Here, the role of this moonlighting protein has been deepened in the osteoclastogenesis process driven by the RANKL cytokine in RAW264.7 macrophages and bone-marrow derived precursor cells from BALB/cJ mice. Inhibitors with distinct selectivity toward sPLA$_2$-IIA activities and recombinant sPLA$_2$-IIA (wild-type or catalytically inactive forms, full-length or partial protein sequences) were instrumental to dissect out sPLA$_2$-IIA function, in conjunction with reduction of sPLA$_2$-IIA expression using small-interfering-RNAs and precursor cells from *Pla2g2a* knock-out mice. The reported data indicate sPLA$_2$-IIA participation in murine osteoclast maturation, control of syncytium formation and resorbing activity, by mechanisms that may be both catalytically dependent and independent. Of note, these studies provide a more complete understanding of the still enigmatic osteoclast multinucleation process, a crucial step for bone-resorbing activity, uncovering the role of sPLA$_2$-IIA interaction with a still unidentified receptor to regulate osteoclast fusion through p38 SAPK activation. This could pave the way for the design of specific inhibitors of sPLA$_2$-IIA binding to interacting partners implicated in osteoclast syncytium formation.

KEYWORDS

group IIA secreted phospholipase A_2 (sPLA$_2$-IIA), p38 SAPK, osteoclastogenesis, osteoclast syncytia, LLKYK cyclic peptide

1 Introduction

Among the lipolytic enzymes, phospholipases A_2 (PLA_2) are acyl esterases, originally defined by their positional specificity to cleave the *sn-2* ester bond of glycerophospholipids, to release fatty acids and lysophospholipids (Dennis, 1994). Currently, more than 50 mammalian proteins are classified within the PLA_2 family, based on the homology with prototypical enzymes, even if they do not necessarily exert a PLA_2 activity (Murakami et al., 2020). Based on their structural relationships, PLA_2s are classified into secreted (Lambeau and Gelb, 2008), cytosolic (Kita et al., 2019), calcium-independent PLA_2s (Ramanadham et al., 2015), and within other groups that include platelet-activating factor acetylhydrolase (Kono and Arai, 2019), lysosomal PLA_2 (Shayman and Tesmer, 2019), PLA/acyltransferase (Hussain et al., 2017), α/β hydrolase (Thomas et al., 2014), and glycosylphosphatidylinositol-specific PLA_2 subfamilies (Murakami et al., 2020).

In mammals, PLA_2s participate in almost all biological processes, regulating pathophysiological functions related to membrane homeostasis, energy production and generation of body surface barriers, among others (Murakami, 2019). The peculiar tissue and cellular distribution of the different PLA_2s (Murakami et al., 2017), in conjunction with their substrate specificities toward the fatty acyl and/or headgroup moieties of the membrane phospholipids (Astudillo et al., 2019), and the availability of functional cofactors or regulatory proteins (Murakami et al., 2020), ensures a variety of distinct functions among these enzymes (Murakami, 2019). The recent advent of lipidomics, combined with studies of gene-manipulated mice or human diseases caused by mutations of PLA_2 enzymes, supported the definition of *in-vivo* functions of individual PLA_2s (Murakami et al., 2010; Murakami et al., 2015; Yamamoto et al., 2017; Kita et al., 2019; Murakami et al., 2019; Murakami et al., 2020; Sun et al., 2021).

The subfamily of secreted (s)PLA_2s comprises 12 mammalian proteins, namely IB, IIA, IIC (present in mice and rats, but pseudogene in humans; Tischfield et al., 1996), IID, IIE, IIF, III, V, X, XIIA, XIIB (catalytically inactive), and otoconin-95 (catalytically inactive structural protein in the inner ear; Lambeau and Gelb, 2008). Secreted PLA_2s are typically characterized by a low molecular mass (13–18 kDa), a conserved three-dimensional helical structure with high disulfide bond content, and a calcium-dependent enzymatic activity through the conserved His-Asp catalytic dyad (Lambeau and Gelb, 2008; Murakami et al., 2010; Murakami et al., 2020). The most studied member, $sPLA_2$-IIA, has a demonstrated primary function in host defense against invading pathogens (Doré and Boilard, 2019; Scott et al., 2021; Miki et al., 2022). As a secreted lipolytic enzyme, $sPLA_2$-IIA shows bactericidal activity through hydrolysis of Gram-positive membranes (Weinrauch et al., 1998), and anti-parasitic function through hydrolysis of oxidized phospholipids in the plasma lipoproteins of malaria patients, thus promoting *Plasmodium falciparum* killing effect (Dacheux et al., 2019; Dacheux et al., 2021). Secreted PLA_2-IIA is also referred as an inflammatory enzyme and amplifier of innate immune responses (Doré and Boilard, 2019; Doré et al., 2022). Indeed, by its hydrolysis of specific phospholipid substrates present in extracellular vesicles released by immune cells (Fourcade et al., 1995; Papadopoulos et al., 2020), or in extracellular mitochondria released by damaged organs or tissues, $sPLA_2$-IIA generates lysophospholipids and non-esterified fatty acids, among which are eicosanoid precursors (Murakami et al., 2020; Kudo et al., 2022).

Secreted PLA_2-IIA acts prevalently on extracellular lipids, and its membrane binding preference (phosphatidylglycerol > phosphatidylserine > phosphatidylcholine) suggests that it is almost inactive toward the intact plasma membrane of mammalian cells (Snitko et al., 1997; Koduri et al., 1998; Singer et al., 2002; Doré and Boilard, 2019). Loss of membrane asymmetry, due to glycerophospholipid scrambling, has been demonstrated during apoptosis (Atsumi et al., 1997), blood platelet activation (Suzuki et al., 2010), viral infection (Arganaraz et al., 2020; Snider et al., 2021), and the osteoclastogenesis of bone marrow-derived cells (Kang et al., 2020). This process can render the plasma membranes of mammalian cells susceptible to $sPLA_2$-IIA attack (Olson et al., 2010).

The $sPLA_2$-IIA cellular functions account for the enzymatic hydrolysis of glycerophospholipids, but can also occur in a catalysis-independent manner (Murakami et al., 2017; Doré and Boilard, 2019; Scott et al., 2021; Ivanusec et al., 2022). Several cellular and soluble receptors for $sPLA_2$-IIA have been characterized until now, starting from the cell surface M-type receptor for secreted phospholipases (Cupillard et al., 1999; Lambeau and Lazdunski, 1999), and these may be involved in the activation of downstream cellular signaling pathways with hydrolytic activity-independent mechanisms (Saegusa et al., 2008; Ivanusec et al., 2022). On the other hand, the $sPLA_2$-IIA protein is highly basic and can easily associate to the cell surface via heparin sulfated proteoglycans (Koduri et al., 1998; Murakami et al., 1999; Boilard et al., 2003; Boilard et al., 2006), and its interaction with the cellular membranes has been proposed to be sufficient to alter the lipid bilayer structure with consequent pathophysiological functions (Cirino et al., 1994; Lomonte et al., 1995).

Several studies have related $sPLA_2$-IIA to bone metabolism, mainly under pathological conditions. Abnormal osteoclast activity is the primary cause of the pathophysiology of Paget's disease of bone, for which pharmacological inhibition of osteoclast cell-to-cell fusion remains the best therapeutic strategy to mitigate bone loss and related fractures associated with this disorder (Coulthard

et al., 2011; Ferraz-de-Souza and Correa, 2013). De Brum-Fernandes and collaborators showed that $sPLA_2$-IIA is highly expressed in bones with high turnover, and in particular in Pagetic bone samples, and that $sPLA_2$-IIA inhibition abrogates osteoclast differentiation and function (Allard-Chamard et al., 2014b). Other groups found that $sPLA_2$-IIA inhibition prevents bone loss after ovariectomy in rats (Gregory et al., 2006), as well as bone erosion in rheumatoid arthritis (Bradley et al., 2005; Thwin et al., 2009). However, the precise role of $sPLA_2$-IIA in osteoclast formation and activity remained to be determined, as well as the role of its metabolites.

Here we provide evidence of a multimodal regulation of the osteoclastogenesis and of mature osteoclast activity by $sPLA_2$-IIA, using RAW264.7 murine macrophages as osteoclast precursors, or primary precursor cells from bone marrow of wild-type (wt) and *Pla2g2a*-knockout (ko) BALB/cJ mice. We also collected insights about the catalytically independent participation of $sPLA_2$-IIA in the selective regulation of osteoclast cell-to-cell fusion, through the activation of p38 SAPK-dependent pathways.

2 Materials and methods

2.1 Materials

Dulbecco's modified Eagle's medium (DMEM) supplemented with high glucose and GlutaMAX, Eagle's alpha-modified medium (α-MEM) supplemented with GlutaMAX, fetal bovine serum (cod. 10270), Hank's balanced salt solution supplemented without ($HBSS^-$) or with calcium and magnesium ($HBSS^{++}$), and phosphate-buffered saline (PBS) were from Gibco (Life Technologies Italia, Monza, Italy). Ammonium chloride (NH_4Cl), β-glycerophosphate, bovine serum albumin, Hoechst, L-glutamine, penicillin–streptomycin, pyrogallol, potassium bicarbonate ($KHCO_3$), saponin, silver nitrate, sodium azide, sodium deoxycholate, sodium dodecyl sulphate, sodium fluoride, sodium orthovanadate, Triton X-100, Tween-20, Mowiol 4–88, bromoenol lactone (BEL, cod. B1552), $cPLA_2α$ inhibitor ($cPLA_2α$–Inh., cod. 525143), SB203580 (cod. 559389), sPLA2-IIA Inhibitor I (Inhib-I, cod. 525145), KH064 (sPLA2 inhibitor, cod. S3319; or sPLA2-IIA inhibitor II, cod. 525146-M), LY311727 (cod. L6795), 2,4′-dibromoacetophenone (BPB, p-bromophenacyl bromide, cod. D38308), trifluoroacetic acid (TFA, cod. 91707) were from Sigma-Aldrich (St. Louis, MO, United States). Methyl arachidonyl fluorophosphonate (MAFP, cod. Ab141763) was from Abcam (Cambridge, UK). The purified recombinant mouse (mGIIA) and human $sPLA_2$-IIA (hGIIA), the human $sPLA_2$-IIA H48Q and mouse group V $sPLA_2$ (mGV) (Edwards et al., 2002; Ghomashchi et al., 2017), as well as the control and anti–mouse $sPLA_2$-IIA IgG fractions were produced as described (Nevalainen et al., 2005; Eerola et al., 2006). All $sPLA_2$ preparations had a purity higher than 99%, and were routinely checked for LPS contamination (Limulus amebocyte test, MP Biomedicals, Illkirch, France; or other sensitive assays), and discarded if the LPS concentration was above the detection limit of the assay (0.125 EU/mL). The synthetic cyclic peptides: FLSYK, WDIYR, LLKYK, with an amide bond between N- and C-terminus, were synthesized with a purity higher than 98.8% from Caslo ApS (Lyngby, Denmark). All other reagents were obtained at the highest purities available from Merck Life Science (Milano, Italy).

2.2 Animals

All the experiments with animals were performed at the Brigham and Women's Hospital, Harvard Medical School, Boston, MA, United States. The wild-type BALB/cJ mice were purchased from the Jackson Laboratory (Bar Harbor, ME, United States). The *Pla2g2a*-ko mice with a BALB/cJ genetic background were generated as previously described (Balestrieri et al., 2006), and backcrossed for 11 generations to a BALB/cJ background (Boilard et al., 2010). All the animal procedures were approved by the Institutional Animal Care and Use Committee for Brigham and Women's Hospital, and conformed to relevant guidelines and laws.

2.3 Cell culture

The RAW264.7 murine monocytes/macrophages (cod. TIB-71) were from American Type Culture Collection (ATCC, Manassas, VA, United States), and cultured in DMEM with 10% heat-inactivated (30 min at 55°C) fetal bovine serum, 2 mM L-glutamine, 100 U/mL penicillin and 100 μg/mL streptomycin. RAW264.7 cells were used between passages 10 and 30.

For transient interference, RAW264.7 cells were plated at 300,000 cells/well in 12-well plate in 1 mL growth medium without antibiotics. After 24 and 48 h, cells were double transfected with 125 pmol/well of small-interfering (si) RNAs against $sPLA_2$-IIA (si–$sPLA_2$-IIA) (murine group II $sPLA_2$ siRNA, sc-43818, from Santa Cruz Biotecnology, San Diego, CA, United States), or with non-targeting siRNAs (si–NT) (siGENOME non-targeting siRNA pool #2, cat. No. D-001206–14 from Dharmacon, Chicago, IL, United States), using Lipofectamine RNAiMAX reagent (Invitrogen, Carlsbad, CA, United States), according to the manufacturer instructions. One day after the second interference, cells were detached (with 600 μM EDTA in

PBS), and plated for the *in-vitro* osteoclastogenesis assays (as reported below), or for RNA extraction to determine the interference efficiency at 72 h of siRNA treatment.

2.4 Osteoclastogenesis assays

RAW264.7 cells were plated in differentiation medium (α-MEM without nucleosides supplemented with 10% heat-inactivated fetal bovine serum, 100 U/mL penicillin, and 100 μg/mL streptomycin) at a density of 1,250 cells/well in 96-well plates; at 5,000 cells/well on coverslips in 24-well plates for morphological analysis; or at 10,000 cells/well in 12-well plates for RNA extraction. Twenty-four hours later, and after every 48 h, the medium was replaced, and the cells were treated without or with 15–30 ng/mL 'Receptor activator of nuclear factor kappa-B ligand' (RANKL) (cod. 310–01 from Peprotech, London, UK), in the absence or presence of different agents diluted in the differentiation medium. The RANKL concentration used was adjusted according to batch-to-batch variability of the cytokine. The range of RANKL concentration specified in several figure/table legends implies that all the different treatments shown were analyzed under the same differentiation conditions of control samples. When differentiation was complete, cells were harvested in lysis buffer for RNA extraction or processed for the different assays (as reported below).

The *ex-vivo* osteoclastogenesis assays were carried out at the Brigham and Women's Hospital, according to published protocols (Charles et al., 2012; O'Brien et al., 2016). After euthanasia of mice, the femurs and tibias were removed and washed in 70% ethanol, and then with $HBSS^{-}$. The bone ends were excised, and the bone marrow flushed out. The extracted bone marrow cells were collected by centrifugation. Subsequently, the red blood cells were lysed by 2-min treatment with lysis solution (0.15 M NH_4Cl, 1 mM $KHCO_3$, in water), and the reaction was stopped by addition of fetal bovine serum and subsequent centrifugation. Total bone marrow cells (BMC) were plated at a density of 50,000 cells/well in 96-well plates to be differentiated for 4 days in differentiation medium for primary cells (α-MEM with nucleosides supplemented with 10% heat-inactivated fetal bovine serum, 100 U/mL penicillin, and 100 μg/mL streptomycin), containing 20 ng/mL M-CSF and 5 ng/mL RANKL, and then fixed for TRAP staining. In parallel, BMC were treated with 40 ng/mL M-CSF for 4 days in α-MEM with nucleosides supplemented with 10% heat-inactivated fetal bovine serum, 100 U/mL penicillin, and 100 μg/mL streptomycin, to expand the osteoclast precursor cells (OPC). After expansion, adherent OPC were detached using the Gibco cell dissociation buffer, and were plated at 10,000 cells/well in 96-well plates for TRAP staining and degradation assays (on Osteo Assay Surface), or at 40,000 cells/well in 24-well plates for immunofluorescence analysis, or at 60,000 cells/well in 12-well plates for RNA extraction. These cells were treated with 20 ng/mL M-CSF without or with 2.5 ng/mL RANKL in differentiation medium for primary cells, and the medium was replenished every other day. Differentiation was usually complete after 3–6 days. At the end, the cells were fixed with 4% (w/v) paraformaldehyde for TRAP staining and immunofluorescence analysis, or harvested in lysis buffer for RNA extraction (as reported below).

2.5 Ribonucleic acid extraction and real-time quantitative polymerase chain reaction

Total RNA was extracted using RNeasy isolation kits, cDNAs were obtained using QuantiTect Reverse Transcription kits, and real-time qPCR was performed with QuantiTect SYBR Green PCR kits, all according to the manufacturer instructions (all the kits were from Qiagen, Hilden, Germany). The primers used for real-time qPCR (LightCycler 480 Instrument II; Roche, Indianapolis, IN, United States) are listed in Supplementary Table S1. *β_2-Microglobulin* was used as housekeeping gene. The real-time qPCR program consisted of an initial step of 15 min at 95°C, and then 45 cycles, as follows: 94°C for 15 s, annealing temperature (see Supplementary Table S1) of each primer for 30 s, and 72°C for 30 s. The osteoclastogenesis marker mRNA levels, in cells subjected to pharmacological treatments, were quantified by real-time qPCR as fold of control levels, i.e., mRNA levels in cells treated with RANKL alone.

2.6 Measurement of $sPLA_2$ catalytic activity

The $sPLA_2$ enzymatic activity was determined using a commercially available colorimetric kit, $sPLA_2$ Assay kit from the Cayman Chemical Company (cod. 765001, Ann Arbor, MI, United States). Briefly, cells were scraped in assay buffer (25 mM Tris-HCl pH 7.5, 10 mM $CaCl_2$, 100 mM KCl, 0.3 mM Triton X-100) and lysed by sonication. The protein concentration was determined using the Bradford assay, and 250 μg total cell lysate was used to determine the catalytic activity, following the kit manufacturer instructions.

2.7 Immunofluorescence microscopy

After treatment with or without RANKL, cells were rinsed with $HBSS^{++}$ and fixed in 4% (w/v) paraformaldehyde (Electron Microscopy Sciences, Hatfield, PA, United States) for 10 min at room temperature, and then washed three times with $HBSS^{++}$.

Fixed cells were incubated for 1 h with blocking solution (50 mM NH_4Cl, 0.5% bovine serum albumin, 0.1% saponin, 0.02% sodium azide, in PBS), with 33 nM Alexa546-labeled phalloidin (Invitrogen) for filamentous actin visualization, and 2 μg/mL Hoechst for nucleus staining. Finally, the cells were washed three times with PBS plus 0.02% Tween-20, and the coverslips were mounted with Mowiol 4–88 and examined by confocal microscopy (LSM 510; Zeiss, Oberkochen, Germany). For the evaluation of osteoclast syncytium formation, the nuclei of multinucleated cells were counted in a blinded manner using a 63× objective, moving across the coverslip in the vertical and horizontal directions. No evident differences in cell numbers, due to cell toxicity or changes in proliferation rates, were observed for the differentiated cells treated in the absence or presence of the different treatments. As Inhib-I was purchased as trifluoroacetate (TFA) salt, the absence of cell toxicity induced by TFA was verified treating RAW264.7 cells with 50 μM TFA for up to 120 h (with 3 additions and medium changes every 48 h) in differentiation medium (in absence of RANKL), and analyzing annexin-V staining (Annexin V-FITC kit, from Milteny Biotech GmbH, Germany), and propidium iodide incorporation by FACS analysis.

2.8 TRAP staining and degradation assay

For TRAP staining, fixed cells were incubated with staining solution (1.5% sodium tartrate, 0.1% naphthol AS-MX phosphate, 1% N,N-dimethylformamide, 0.6% Fast Red LB Violet Salt in 0.1 M acetate buffer) for 15 min at 37°C. The reaction was stopped by washing cells three times with $HBSS^{++}$. Osteoclasts were quantified by counting TRAP-positive cells with three or more nuclei.

To measure resorptive function, osteoclasts were grown on Osteo Assay Surface plates from Corning (New York, United States) for 7 days. When differentiation was complete, the cells were removed (using 10% bleach) and the wells were stained with 5% silver nitrate for 1 h. The staining was stopped by addition of 1% pyrogallol. Images were taken with a Nikon TMS-F inverted microscope (Nikon Instruments Inc., Melville, NY, United States) at a final magnification of ×5 (BMC and OCP), or with EVOS XL Core microscope (Thermo Fisher Scientific, Waltham, MA United States) at a final magnification of ×2 (RAW264.7 derived osteoclasts), and the total resorbed areas were quantified using ImageJ (NIH).

2.9 Western blotting

Cell lysates were obtained by scraping cells into phospho-lysis buffer (50 mM Tris-HCl, pH 7.5, 300 mM NaCl, 1% sodium deoxycholate, 1% Triton X-100, 0.1% sodium dodecyl sulphate, 40 mM β-glycerophosphate, 50 mM sodium fluoride, 200 μM sodium orthovanadate, plus phosphatase and protease inhibitors from Roche). Following gentle homogenization by 20 passages through a 26-gauge needle, the lysates were centrifuged at 10,000× *g* for 5 min at 4°C, and the supernatants were collected.

Protein lysates were subjected to SDS-PAGE, and after electrophoresis, the proteins were transferred to a nitrocellulose membrane (PerkinElmer Life Science, Boston, MA, United States). For immunoblotting, the membranes were blocked with 5% non-fat dry milk in TBS (10 mM Tris-HCl, pH 7.4, 150 mM NaCl) plus 0.1% Tween-20 (T-TBS) for 30 min at room temperature, and incubated with primary antibodies (as listed below) in T-TBS plus 3% bovine serum albumin for 2 h at room temperature, or overnight at 4°C. The membranes were washed twice in T-TBS for 7 min, and then incubated with secondary antibodies conjugated to horseradish peroxidase (1:5,000) (Calbiochem, San Diego, CA, United States) in T-TBS with 5% non-fat milk for 30 min at room temperature. The membranes were then washed twice with T-TBS, and once with TBS for 5 min, and the signals were detected by ECL (Amersham Pharmacia, Piscataway, NJ, United States). The rabbit anti-phospho AKT (Ser473; D9E, cod. 4060), anti phospho-p44/42 MAPK (Thr202/Tyr204; Erk1/2, cod. 9101), anti-phospho p38 MAPK (Thr180/Tyr182; 3D7, cod. 9215), anti-p38 MAPK (cod. 9212), anti-phospho MAPKAPK-2 (T334; 27B7, cod. 3007), anti-MAPKAPK-2 (D1E11, cod. 12155), all used at dilution 1:1,000 were from Cell Signaling Technology (Danvers, MA, United States). The rabbit anti-AKT (B-1, cod. sc-5298, diluted 1:1,000), and anti-ERK1 (K-23, cod. sc-94, diluted 1:5,000) were from Santa Cruz Biotechnology.

2.10 Statistical analysis

Statistical analysis was performed with the GraphPad Prism software (GraphPad Software, Inc., La Jolla, CA, United States). Comparisons between groups were performed using Student's *t*-test and Analysis of Variance (ANOVA) with 95% confidence interval. p values < 0.05 were considered as statistically significant.

3 Results

3.1 Secreted PLA_2-IIA mRNA levels and enzymatic activity increase upon RANKL-induced murine osteoclastogenesis

The osteoclastogenesis process was assessed with the RAW264.7 monocyte/macrophage cell line (Collin-Osdoby and Osdoby, 2012; Mosca et al., 2021) and with primary osteoclast precursors from bone marrow of BALB/cJ mice (Charles et al., 2012; O'Brien et al., 2016). 'Receptor activator of nuclear factor kappa-B ligand' (RANKL) alone or in the

TABLE 1 Modulation of PLA_2 mRNA levels during murine osteoclastogenesis. RAW264.7 cells were treated without (w/o) or with 15–30 ng/mL RANKL for 72 h, while M-CSF–expanded OCP from wild-type (wt) and *Pla2g2a*-ko mice were treated with 20 ng/mL M-CSF alone (M-CSF) or with 2.5 ng/mL RANKL (M-CSF+RANKL) for 3–6 days, before RNA extraction.

	RAW264.7 cells		wt OCP		*Pla2g2a*-ko OCP	
PLA2 gene (protein)	**w/o**	**RANKL**	**M-CSF**	**M-CSF+ RANKL**	**M-CSF**	**M-CSF+ RANKL**
Pla2g1b (sPLA$_2$-IB)	1.00	0.68 ± 0.04*	1.00 ± 0.04	0.60 ± 0.03§§	1.44 ± 0.09§§	0.58 ± 0.03††
Pla2g2a (sPLA$_2$-IIA)	1.00	2.51 ± 0.21*	1.00 ± 0.06	1.98 ± 0.02§§§	–	–
Pla2g2c (sPLA$_2$-IIC)	1.00	4.27 ± 0.35*	–	–	–	–
Pla2g2d (sPLA$_2$-IID)[a]	–	–	–	–	–	–
Pla2g2e (sPLA$_2$-IIE)	1.00	3.95 ± 0.56*	1.00 ± 0.26	1.88 ± 0.15§§	3.25 ± 0.39§§	6.57 ± 0.83††
Pla2g2f (sPLA$_2$-IIF)[a]	–	–	–	–	–	–
Pla2g3 (sPLA$_2$-III)	1.00	0.82 ± 0.02*	1.00 ± 0.10	1.06 ± 0.11	1.16 ± 0.13	1.12 ± 0.16
Pla2g5 (sPLA$_2$-V)	1.00	2.62 ± 0.21*	1.00 ± 0.07	2.96 ± 0.28§§	2.42 ± 0.21§§§	4.89 ± 0.40††
Pla2g10 (sPLA$_2$-X)[b]	–	–	–	–	–	–
Pla2g12a (sPLA$_2$-XIIA)	1.00	1.08 ± 0.06	1.00 ± 0.02	0.99 ± 0.06	1.21 ± 0.18	0.87 ± 0.06
Pla2g12b (sPLA$_2$-XIIB)	1.00	0.86 ± 0.05	1.00 ± 0.11	0.99 ± 0.10	0.88 ± 0.12	0.74 ± 0.04
Pla2g4a (PLA$_2$-IVA, cPLA$_2$α)	1.00	0.61 ± 0.02***	1.00 ± 0.05	0.56 ± 0.08§	1.24 ± 0.14	0.50 ± 0.06†
Pla2g6 (PLA$_2$-VIA, iPLA$_2$β)	1.00	0.64 ± 0.02**	1.00 ± 0.08	1.59 ± 0.05§	0.95 ± 0.06	1.15 ± 0.17
Pla2g16 (PLA$_2$-XVI)[c]	1.00	0.91 ± 0.22	nd	nd	nd	nd

The transcripts were quantified by real-time qPCR, and normalized using *β2-microglobulin* expression, as the housekeeping gene. For RAW264.7 cells, PLA_2 mRNA, levels are shown as fold of cells treated without RANKL (w/o), and data are means ± SEM, of at least three independent experiments. For OCP, PLA_2 mRNA, levels are expressed as fold of wild-type OCP, treated only with M-CSF, and data are means ± SEM, of ten (sPLA$_2$-IIA, sPLA$_2$-V, sPLA$_2$-IIE) or five (other PLA$_2$s) age- and sex-matched mice for each genotype. *$p < 0.05$, **$p < 0.005$, ***$p < 0.001$ versus RAW264.7 cells treated without RANKL (w/o) (by paired Student's *t*-tests). $^{§}p < 0.05$, $^{§§}p < 0.005$, $^{§§§}p < 0.001$ versus wt OCP, treated with M-CSF alone; and $^{†}p < 0.05$, $^{††}p < 0.005$ versus ko OCP, treated with M-CSF alone; by one-way ANOVA). nd, not determined; –, undetectable, with primer efficiency verified with cDNA, of RAW264.7 cells treated for 1 h with 100 ng/mL lipopolysaccharide in DMEM, as reported in (Ao et al., 2010) ([a]), or with testis cDNA ([b]). *Pla2g16* transcription was analyzed in RAW264.7 cells treated with a single concentration of RANKL (15 ng/mL) ([c]).

TABLE 2 Secreted PLA_2 activity measured in cell lysates. RAW264.7 cells were treated without (w/o) or with 15 ng/mL RANKL for 72 h, in the absence or presence of 10 nM BPB. Phospholipase A_2 activity was analyzed in cell lysates (250 μg) in absence (–) or presence of the indicated PLA_2 inhibitors.

RAW264.7-cell treatment	**PLA_2 inhibitor**	**sPLA2 activity (nmoles/min/mL)**
w/o	–	0.40 ± 0.12**
	DMSO	0.43 ± 0.15§
	+10 μM LY311727	0.54 ± 0.17
RANKL	–	2.51 ± 0.42
	DMSO	2.32 ± 0.50
	+2 μM cPLA$_2$α–Inh.	3.24 ± 1.24§
	+1 μM BEL	2.33 ± 1.01
	+20 μM Inhib-I	1.38 ± 0.73§
	+40 μM KH064	0.09 ± 0.03§
	+100 nM BPB	0.05 ± 0.03§
	+10 μM LY311727	1.31 ± 0.34§
	+3 μg/assay ctrl IgGs	2.64 ± 0.02
	+3 μg/assay anti-mouse sPLA$_2$-IIA IgGs	2.08 ± 0.01††
RANKL + BPB	–	2.19 ± 0.44*

Data are means ± SEM, of at least three independent experiments. *$p < 0.05$, **$p < 0.005$ versus (–) untreated, $^{§}p < 0.05$ versus DMSO-treated, and $^{††}p < 0.005$ versus ctrl-IgG-treated RANKL-differentiated RAW264.7 cell lysates (paired Student's *t*-tests).

presence of 'macrophage colony-stimulating factor' (M-CSF) was used to induce osteoclast differentiation of RAW264.7 cells or bone marrow-derived precursors, respectively.

Transcriptional analysis of most PLA_2 family members, as assessed by real-time qPCR, indicated that the mRNA levels of $sPLA_2$-IIA, -IIC, -IIE, and -V increased upon RANKL-induced differentiation of RAW264.7 cells, while that of $sPLA_2$-IB, -III and of intracellular $cPLA_2\alpha$ (PLA_2-IVA) and $iPLA_2\beta$ (PLA_2-VIA) decreased (Table 1). Other $sPLA_2$s (-XIIA, -XIIB) and PLA_2-XVI showed almost unchanged mRNA levels, while $sPLA_2$-IID, -IIF, -X were not detectable (Table 1). These modulations were comparable to those observed within the osteoclastogenesis of bone marrow-derived M-CSF–expanded osteoclast precursors (OCP) from wt mice, with few exceptions: $sPLA_2$-IIC was not detectable in the primary system, $sPLA_2$-III was not modulated, and the $iPLA_2\beta$ levels increased during the osteoclastogenesis of wt OCP (Table 1; data from *Pla2g2a*-ko mice are commented in paragraph 3.3).

Phospholipase A_2 activity was assayed in cell extracts from undifferentiated or RANKL-treated RAW264.7 macrophages with a commercially available kit (see Section 2 for details), based on the use of the 1,2-dithio analog of diheptanoyl phosphatidylcholine, which serves as a substrate for most PLA_2s (Hendrickson et al., 1983; Reynolds et al., 1992). A 6-fold increase in PLA_2 activity was measured in osteoclasts compared to undifferentiated cells (Table 2). This activity was not blocked by inhibitors of intracellular PLA_2s, like the $cPLA_2\alpha$ specific inhibitor ($cPLA_2\alpha$–Inh.; San Pietro et al., 2009; Seno et al., 2000); or the $iPLA_2\beta$ irreversible inhibitor (BEL; Ackermann et al., 1995; Zizza et al., 2012). Instead, various inhibitors of $sPLA_2$s were efficient. Indeed, Inhib-I (Church et al., 2001; Zizza et al., 2012) reduced by 40%, while KH064 (Hansford et al., 2003; Kim et al., 2020) and the potent and covalent inhibitor of $sPLA_2$-IIA and other $sPLA_2$s (BPB; Kim et al., 2020; Marchi-Salvador et al., 2009) almost abolished the measured activity of RANKL lysates (Table 2). Moreover, a significant inhibition was seen with 10 μM LY311727, a quite specific inhibitor of $sPLA_2$-IIA versus other mouse and human $sPLA_2$s (Singer et al., 2002; Kim et al., 2020), which showed an apparent IC_{50} of 6.8 μM, and by a specific anti-mouse $sPLA_2$-IIA IgG fraction (Eerola et al., 2006) (Table 2, Supplementary Figure S1).

The monitored catalytic activity, together with the expression profile in the above settings, was suggestive of a $sPLA_2$ role in RANKL-induced differentiation of murine precursor cells, reasonably that of $sPLA_2$-IIA.

3.2 Secreted PLA_2s mediate the murine osteoclastogenesis

In addition to $sPLA_2$s (Bradley et al., 2005; Gregory et al., 2006; Allard-Chamard et al., 2014b), cytosolic PLA_2s were reported to participate in the osteoclastogenesis process (Bonventre, 2004; Kim et al., 2010; Allard-Chamard et al., 2014a). Therefore, inhibitors targeting the three major types of PLA_2s were used to unveil their role (if any) in the osteoclastogenesis process of RAW264.7 macrophages. Real-time qPCR analysis of the osteoclastogenesis markers showed that the $sPLA_2$ inhibitor (Inhib-I) was efficient to reduce the RANKL-induced transcription of all the analyzed markers (*Nfatc1*, *Cathepsin-k*, *Mmp-9*, *Trap* and *Ctr*) by at least 50%, and was the only treatment able to significantly impair the osteoclast syncytium formation (Supplementary Figures S2, S3). Specific $cPLA_2\alpha$ inhibition, by $cPLA_2\alpha$–Inh., reduced by 40% only *Nfatc1* mRNA levels, while $iPLA_2\beta$ blockage with BEL reduced *Nfatc1* and *Trap* mRNA levels by 35% and 45%, respectively, in RANKL-differentiated cells (Supplementary Figure S2). Instead, the active site directed, irreversible inhibitor of both $cPLA_2\alpha$ and $iPLA_2\beta$ (MAFP; Balsinde and Dennis, 1996; Lio et al., 1996), was not able to inhibit the RANKL-induced transcription of any marker nor the osteoclast fusion (Supplementary Figures S2, S3).

Although long-term treatment of cells with pharmacological inhibitors has to be taken with extreme caution, these data supported the hypothesis of $sPLA_2$ involvement, seemingly $sPLA_2$-IIA, in the regulation of the osteoclastogenesis of RAW264.7 macrophages. Instead, intracellular PLA_2s did not seem to play a relevant role, as their inhibitors mainly reduced RANKL-induced transcription of *Nfatc1*, while the other marker mRNA levels and the osteoclast-syncytium formation were almost comparable to that of cells treated with RANKL alone. The absence of any effect by the less specific inhibitor MAFP could be consequent to the blockade of both positive and negative pathways regulated by distinct PLA_2 isoforms.

3.3 Secreted PLA_2-IIA plays a role in murine osteoclast differentiation and activity

The involvement of $sPLA_2$-IIA was deepened using cells with reduced or abolished $sPLA_2$-IIA expression. RAW264.7 macrophages were transfected with specific small interfering (si)RNAs that significantly decreased by 50% the $sPLA_2$-IIA mRNA expression (Figure 1A). This treatment did not affect the mRNA levels of intracellular PLA_2s, $sPLA_2$-IIC and -IIE, but slightly reduced that of $sPLA_2$-V (Supplementary Table S2). The RANKL-induced differentiation of siRNA transfected cells showed a significantly reduced transcription, by about 40%, of the main osteoclastogenesis markers (*Nfatc1*, *Cathepsin-k*, *Mmp-9*, *Trap* and *Ctr*), upon $sPLA_2$-IIA interference (Figures 1B–F). The osteoclast-syncytium formation was also impaired by $sPLA_2$-IIA interference, with lower numbers of osteoclasts with more than 10 nuclei, compared to cells interfered with the no-targeting siRNAs (Figures 1G,H).

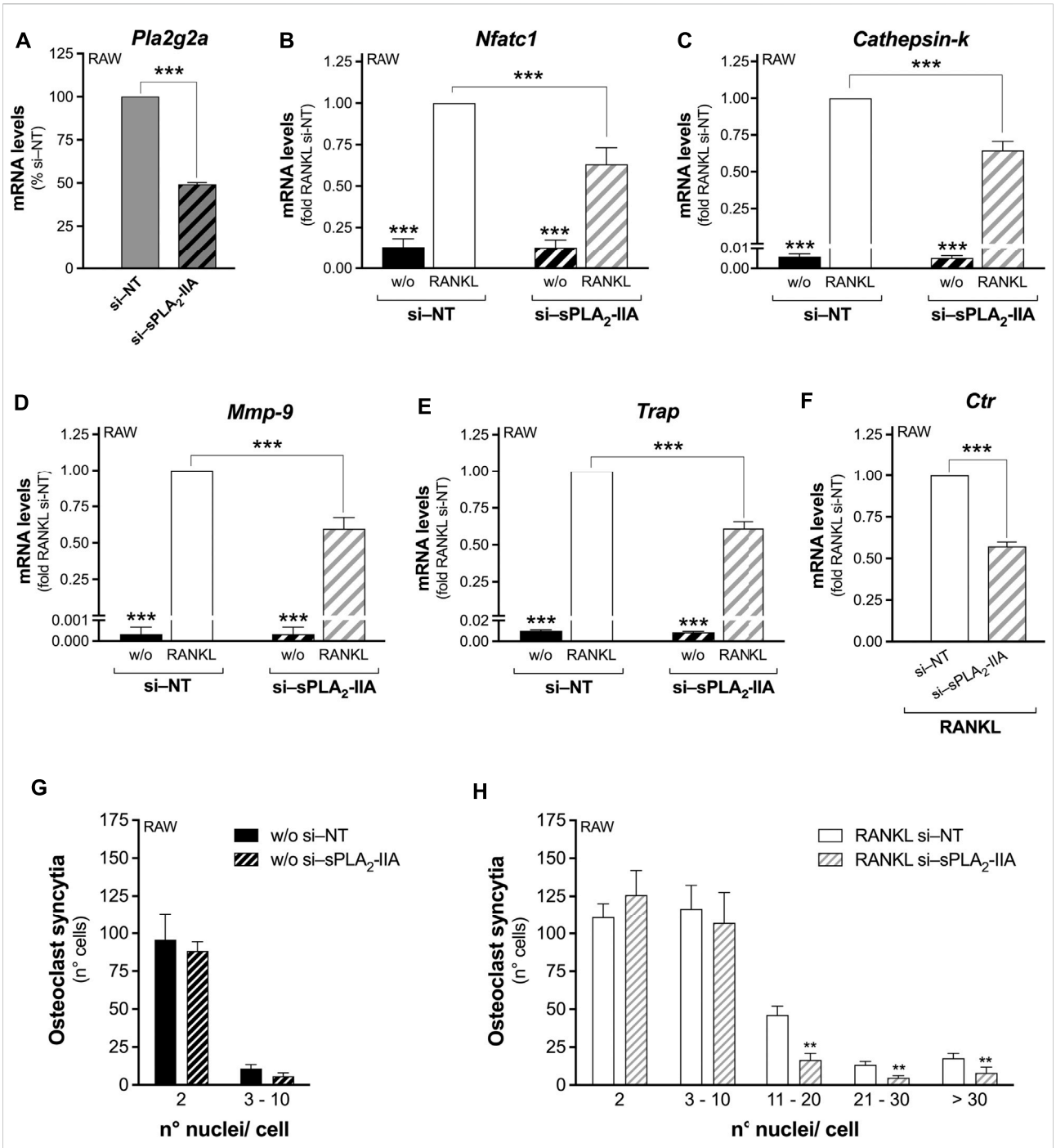

FIGURE 1
Secreted PLA_2-IIA interference in RAW264.7 precursor cells inhibits RANKL-induced osteoclast differentiation. RAW264.7 cells were interfered for 72 h with no-targeting (si–NT) or $sPLA_2$-IIA specific (si–$sPLA_2$-IIA) siRNAs, and subsequently treated in the absence (w/o) or presence of 15–30 ng/mL RANKL for the following 48 h. **(A)** *Pla2g2a* mRNA levels of 72-h interfered RAW264.7 cells were quantified by real-time qPCR, and normalized using *β2-microglobulin* expression, as the housekeeping gene. Data are means ± SEM from six independent experiments. ***$p < 0.005$, paired Student's *t*-test. **(B–F)** After 48 h of RANKL treatment, the differentiation markers were quantified by real-time qPCR, and normalized using *β2-microglobulin* expression, as the housekeeping gene. The mRNA levels of *Ctr* were undetectable in undifferentiated cells. Data are expressed as fold of RANKL-differentiated si–NT cells (RANKL si–NT), and are shown as means ± SEM of three independent experiments. ***$p < 0.005$ versus RANKL si–NT (one-way ANOVA or paired Student's *t*-tests). **(G,H)** Osteoclast syncytium formation was determined as number of nuclei/cell, by fluorescence microscopy. Data are means ± SEM of three independent experiments performed in duplicates. **$p < 0.01$ versus correspondent RANKL si–NT (paired Student's *t*-tests).

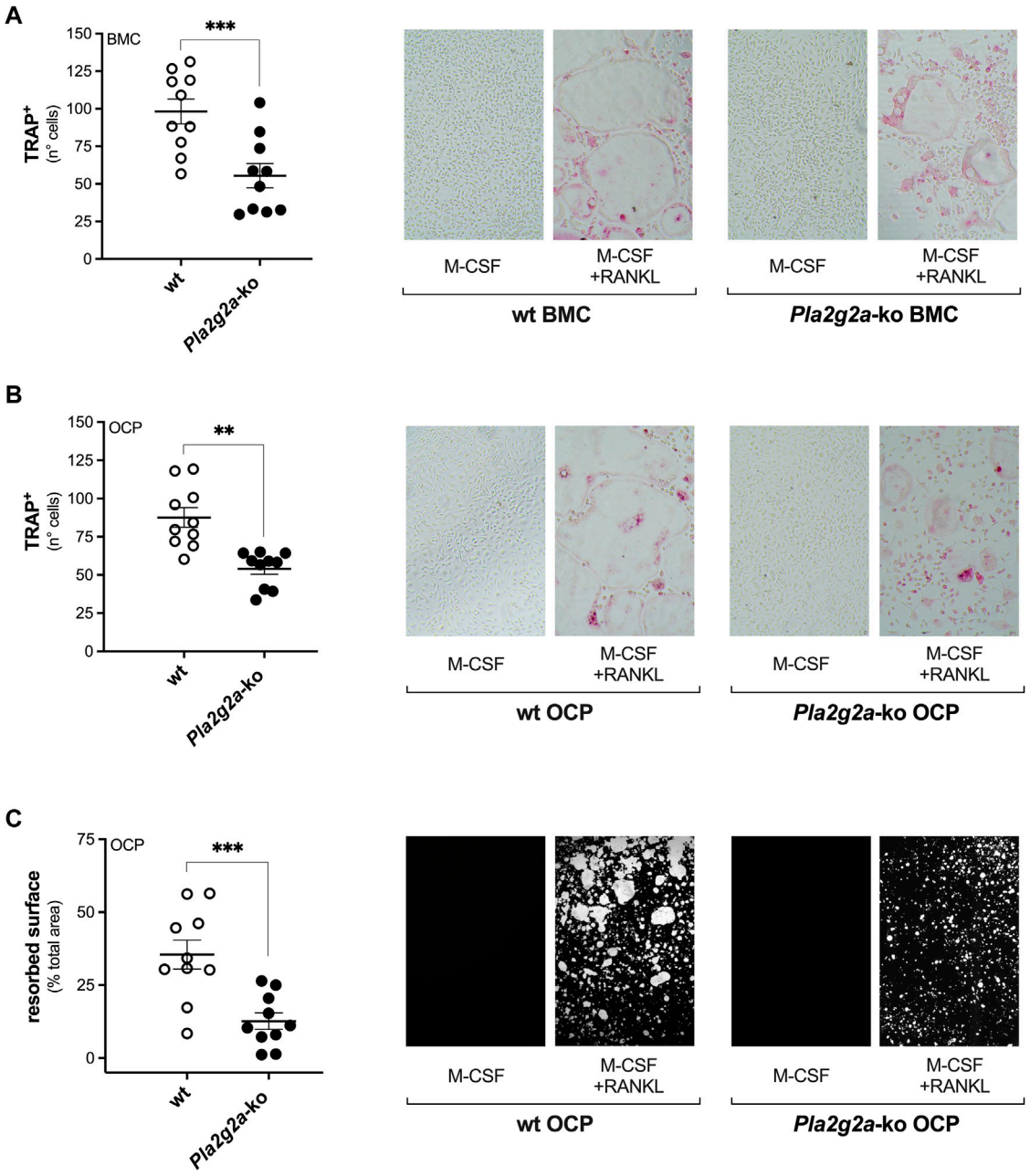

FIGURE 2
Osteoclast precursor cells derived from bone marrows of *Pla2g2a*-ko mice show reduced *ex-vivo* osteoclast differentiation and activity. **(A)** Freshly isolated total bone marrow cells (BMC) were differentiated with 20 ng/mL M-CSF and 5 ng/mL RANKL for 4 days, then fixed and stained for TRAP. **(B,C)** BMC were expanded with 40 ng/mL M-CSF for 4 days, and the obtained osteoclast precursor cells (OCP) were differentiated with 20 ng/mL M-CSF and 2.5 ng/mL RANKL for further 3–6 days. Then, OCP were fixed and stained for TRAP **(B)**, or their degrading activity was evaluated on Osteo Assay Surface plates **(C)**. Data are means ± SEM of ten age- and sex-matched mice for each genotype, analyzed in triplicates **(A,B)**, or duplicates **(C)**. On the right of each graph are representative images of TRAP staining **(A,B)**, and of Osteo Assay Surface plates analyzed for the degrading activity **(C)**, acquired with Nikon TMS-F inverted microscope, at a final magnification of ×5. $^{**}p < 0.01$; $^{***}p < 0.005$ versus wt (unpaired Student's *t*-tests).

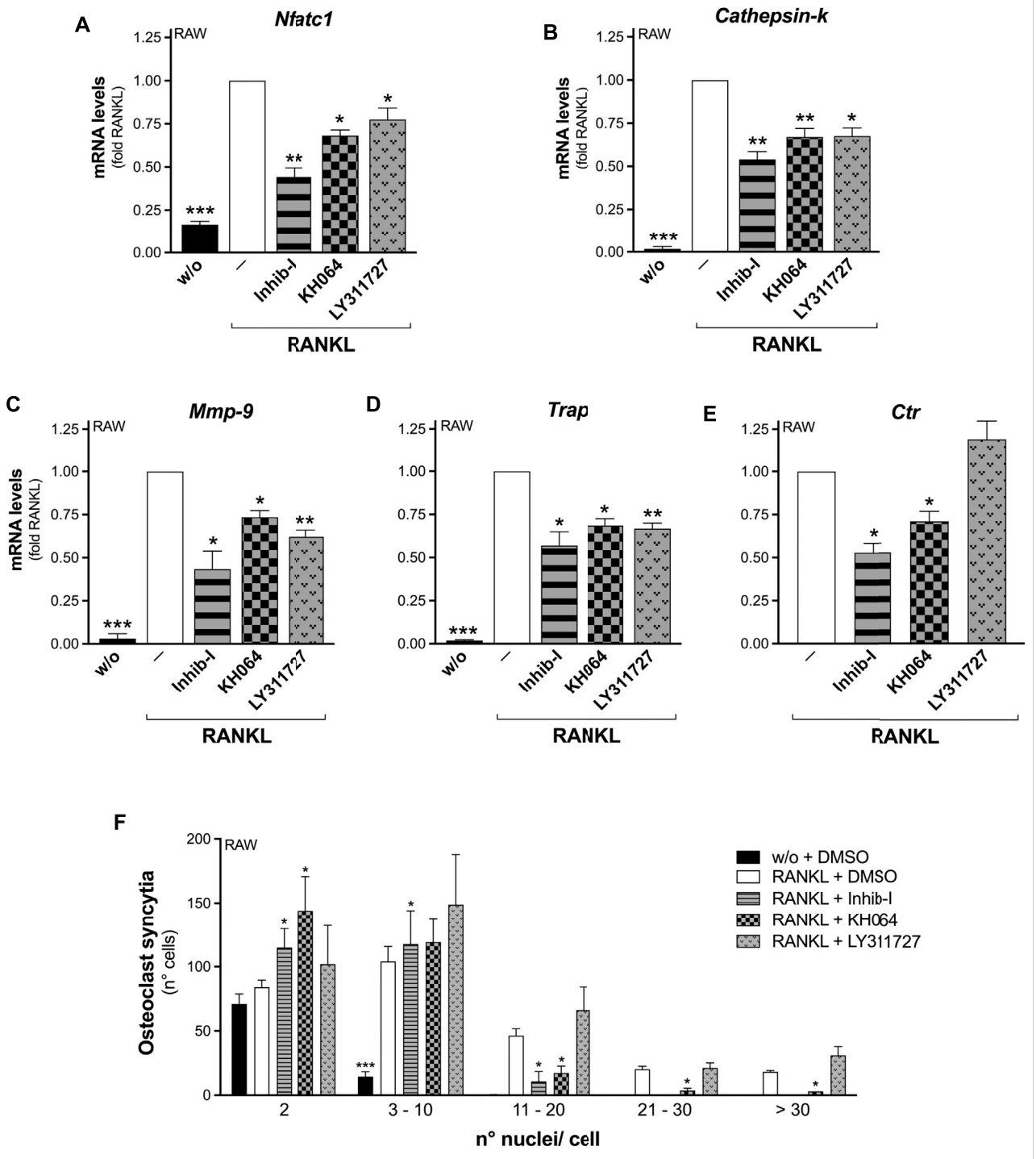

FIGURE 3
Bifunctional inhibitors of $sPLA_2$-IIA impair RANKL-induced osteoclastogenesis of RAW264.7 macrophages. **(A–E)** RAW264.7 cells were treated without (w/o) or with 30 ng/mL RANKL for 72 h, in presence of the indicated $sPLA_2$-IIA inhibitors (20 μM Inhib-I, 40 μM KH064, 30 μM LY311727) or with DMSO as carrier (–). The differentiation markers were quantified by real-time qPCR, and normalized using *β2-microglobulin* expression, as the housekeeping gene. Data are expressed as fold of RANKL, and are means ± SEM of three independent experiments. **(F)** RAW264.7 cells were treated without (w/o) or with 15–30 ng/mL RANKL for 72–96 h, in presence of the above indicated $sPLA_2$-IIA inhibitors or with DMSO as carrier. Osteoclast syncytium formation was determined as number of nuclei/cell, by fluorescence microscopy. Data are means ± SE of three independent experiments. *$p < 0.05$; **$p < 0.01$; ***$p < 0.005$ versus correspondent RANKL (paired Student's *t*-tests).

Furthermore, *ex-vivo* osteoclast differentiation was carried out with primary osteoclast precursors obtained from bone marrow of wt and *Pla2g2a*-ko BALB/cJ mice (Balestrieri et al., 2006; Boilard et al., 2010). The PLA_2 expression profile in M-CSF–expanded OCP from *Pla2g2a*-ko mice was similar to the wt counterpart, with the exception of *Pla2g1b*, *Pla2g2e* and *Pla2g5* that were expressed at higher levels, and the obvious lack of *Pla2g2a* (Table 1). Osteoclasts obtained from total bone marrow cells (BMC) or M-CSF–expanded OCP of *Pla2g2a*-ko mice, were less numerous (evaluated as TRAP-positive cells), and with lower degrading activity, compared to differentiated precursors from wt mice (Figure 2). In accordance with the RANKL-induced differentiation of $sPLA_2$-IIA–interfered RAW264.7 macrophages, the differentiation of OCP from *Pla2g2a*-ko mice showed highly reduced marker transcription, and inhibition of osteoclast fusion, with lower numbers of osteoclasts containing more than 10 nuclei, compared to wt osteoclasts (Supplementary Figure S4).

Altogether, both pharmacological and molecular tools indicated the prevalent role of $sPLA_2$-IIA in RANKL-induced differentiation of RAW264.7 macrophages. The impaired maturation, fusion and activity of osteoclasts derived from *Pla2g2a*-ko bone-marrow precursors paralleled the data obtained with the $sPLA_2$-IIA–interfered RAW264.7 cell line, despite the increased transcription of *Pla2g2e* and *Pla2g5* in the *Pla2g2a*-ko OCP.

3.4 Pharmacological blockade of $sPLA_2$-IIA impairs murine osteoclastogenesis

The crystal structures of $sPLA_2$-IIA in complex with KH064 and LY311727 showed that these competitive inhibitors bind to the active site of $sPLA_2$-IIA and also perturbate the binding surface at the entrance of the cavity (Lee et al., 2013). Therefore, these small molecules are able to block not only the $sPLA_2$-IIA enzymatic activity, but also its possible interaction with binding partners. This was shown to be the case for methyl-indoxam, another active site $sPLA_2$ inhibitor, which perturbates the interaction of various mouse $sPLA_2$s to PLA_2R1, shifting the affinity for this latter by up to 300-fold (Boilard et al., 2006).

Differentiation assays carried out in the presence of the small molecule KH064 showed that it acted similarly to the peptide Inhib-I, impairing RANKL-induced osteoclastogenesis. Indeed, both inhibitors significantly reduced the RANKL-stimulated transcription of all five osteoclastogenesis markers monitored, either with RAW264.7-macrophage precursors (Figures 3A–E), and with wt OCP (Supplementary Figures S5A–E). In addition, both inhibitors impaired osteoclast cell-to-cell fusion, as indicated by the decreased number of osteoclasts with more than 10 nuclei among RANKL-differentiated RAW264.7 cells (Figure 3F), and with more than 3 nuclei with wt OPC (Supplementary Figures S5F,G). As further confirmation, a significantly reduced formation of TRAP-positive cells from wt OCP was obtained in the presence of both KH064 and Inhib-I (Supplementary Figure S6). Strikingly, all these inhibitory effects were not seen differentiating *Pla2g2a*-ko OCP (Supplementary Figures S5, S6).

The LY311727 inhibitor was also capable to inhibit the osteoclastogenesis of RAW264.7 cells, but less potently, as it reduced RANKL-triggered *Nfatc1*, *Cathepsin-k*, *Mmp-9*, and *Trap* transcription, but not that of *Ctr*, nor the osteoclast-syncytium formation (Figure 3).

The results obtained with two structurally different inhibitors of $sPLA_2$-IIA, namely Inhib-I and KH064, further support the involvement of this protein in the different steps of the murine osteoclastogenesis process, from the transcriptional remodeling of key genes to the osteoclast fusion. The absence of any effect with *Pla2g2a*-ko OPC confirmed the specificity of these inhibitors toward $sPLA_2$-IIA, at least under our assay conditions.

3.5 Secreted PLA_2-IIA regulates the osteoclastogenesis of RAW264.7 macrophages by two distinct mechanisms

The results shown so far provide the rationale to analyze in more detail the mechanism by which $sPLA_2$-IIA regulates the osteoclastogenesis process. To this end, we took advantage of purified recombinant $sPLA_2$-IIA of murine and human origin, including a H48Q catalytic site mutant which has less than 5% of wt activity (Edwards et al., 2002). The active site and catalytic mechanism of these two $sPLA_2$-IIA orthologs are conserved and both enzymes share the same interfacial kinetic properties and substrate specificities (Cupillard et al., 1999; Valentin et al., 1999; Valentin et al., 2000; Singer et al., 2002). However, they have a rather low identity at the protein level (69%), especially on the protein surface, with a number of different amino acids that likely explain their different binding properties to proteins including PLA_2R1 and Factor Xa (Cupillard et al., 1999; Mounier et al., 2000). Experimental evidence indicated that the 70–74 region of human $sPLA_2$-IIA is relevant for $sPLA_2$-IIA binding to membranes or putative signaling partners (Tseng et al., 1996). In addition, peptides derived from this $sPLA_2$-IIA primary sequence were reported to competitively antagonize the $sPLA_2$-IIA binding activity, and consequent $sPLA_2$-IIA cellular functions, in a species-specific mode (Church et al., 2001).

The addition of recombinant mouse $sPLA_2$-IIA (mGIIA) significantly reinforced the RANKL-induced transcription of all the differentiation markers analyzed, by more than 1.5-fold, during the differentiation of RAW264.7 macrophages (Figure 4). Even if with lower potency, the human enzyme (hGIIA) also increased the transcription of *Nfatc1*, *Cathepsin-k*, *Trap* and *Ctr*. Conversely, the catalytically inactive mutant

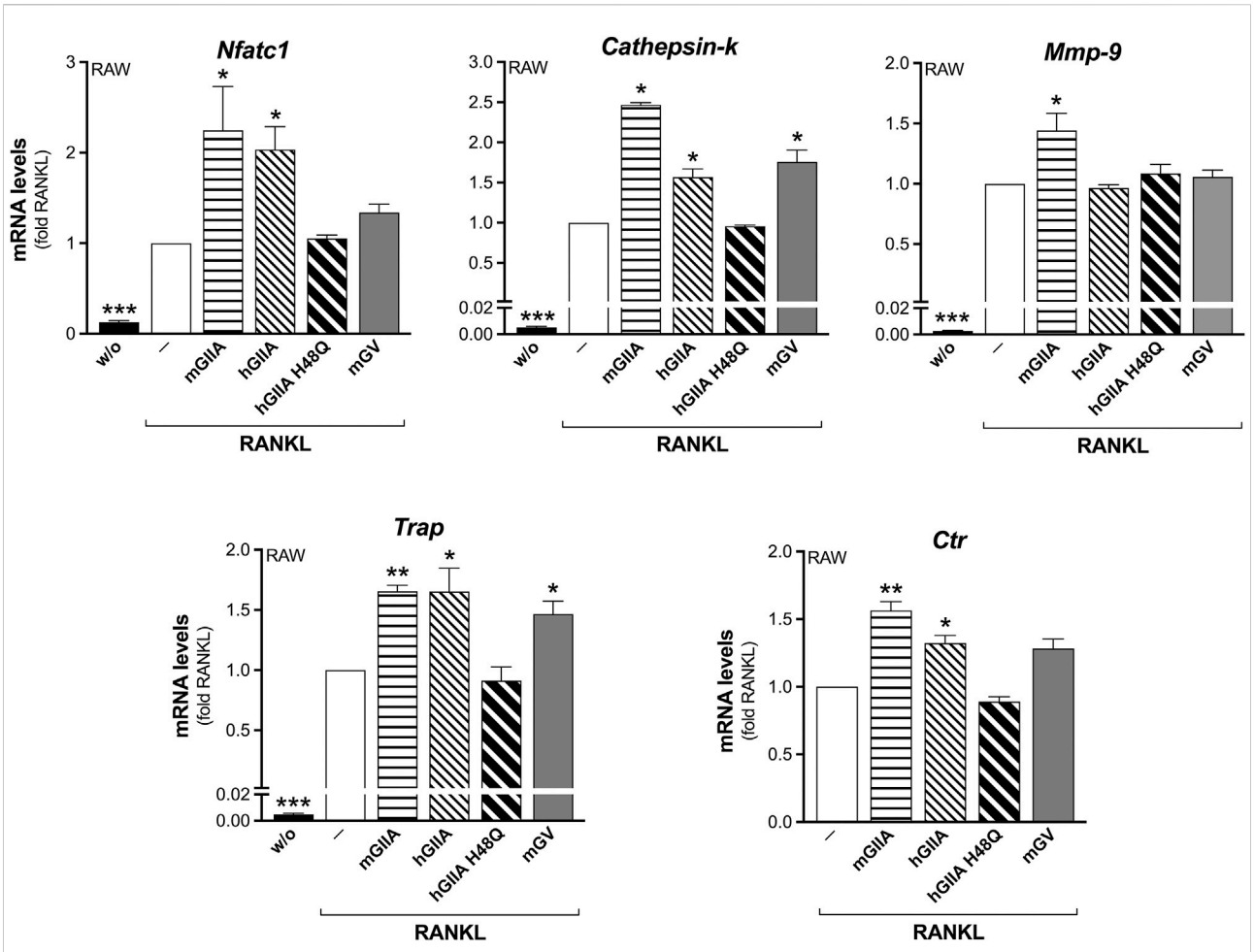

FIGURE 4
Murine recombinant sPLA$_2$-IIA stimulates RANKL-induced osteoclastogenesis of RAW264.7 macrophages. RAW264.7 cells were treated without (w/o) or with 15 ng/mL RANKL for 72 h, in presence of the indicated recombinant proteins: 30 nM murine sPLA$_2$-IIA (mGIIA), 30 nM human sPLA$_2$-IIA (hGIIA), 30 nM human sPLA$_2$-IIA H48Q (hGIIA H48Q), 100 nM murine sPLA$_2$-V (mGV); or with PBS (–) as carrier. The differentiation markers were quantified by real-time qPCR, and normalized using *β2-microglobulin* expression, as the housekeeping gene. Data are expressed as fold of RANKL, and are means ± SEM of three independent experiments. *$p < 0.05$; **$p < 0.01$; ***$p < 0.005$ versus RANKL (paired Student's *t*-tests).

H48Q (hGIIA H48Q) was without any effect (Figure 4). In parallel, the mouse sPLA$_2$-V (mGV) was found to stimulate only the transcription of *Cathepsin-k* and *Trap*, but at a higher concentration of 100 nM (Figure 4). The *Mmp-9* transcription was stimulated only by mGIIA, and not by the human enzymes (active and mutated), nor by mGV (Figure 4). Finally, the RANKL-induced osteoclast syncytium formation was modulated only by mGIIA, with a significantly increased number of osteoclasts with more than 10 nuclei (Figure 5).

Three cyclic pentapeptides were synthesized based on the FLSYK sequence of human sPLA$_2$-IIA (^{70}FLSYK^{74}; Church et al., 2001; Tseng et al., 1996), and the corresponding one in *C. durissus terrificus venom* sPLA$_2$-IIA (^{70}WDIYR^{74}; Church et al., 2001; Tseng et al., 1996), and in mouse sPLA$_2$-IIA (^{84}LLKYK^{89}) (Figure 6A). The LLKYK murine peptide, but not that from other species, was able to reduce the RANKL-induced *Mmp-9* transcription and cell-to-cell fusion, leaving unaffected the *Nfatc1* and *Ctr* transcription (Figures 6B–E). As the fusion step is crucial for the osteoclast activity, the effect of these peptides on the degrading activity was analyzed. The murine cyclic pentapeptide, LLKYK, was able to reduce by more than 50% the resorbing activity of mature osteoclasts on hydroxyapatite-coated plates, while the human FLSYK was ineffective (Figure 7).

In addition to the above experiments with the H48Q mutant, the role of mouse sPLA$_2$-IIA enzymatic activity in osteoclastogenesis was confirmed by the use of BPB. This alkylating agent covalently binds to the histidine residue of the active site, but preserves the sPLA$_2$-IIA surface properties and sPLA$_2$-IIA binding properties to cells (Lee et al., 2013). Figure 6 shows that BPB treatment of RAW264.7 macrophages led to a clear inhibition of transcription for various RANKL-

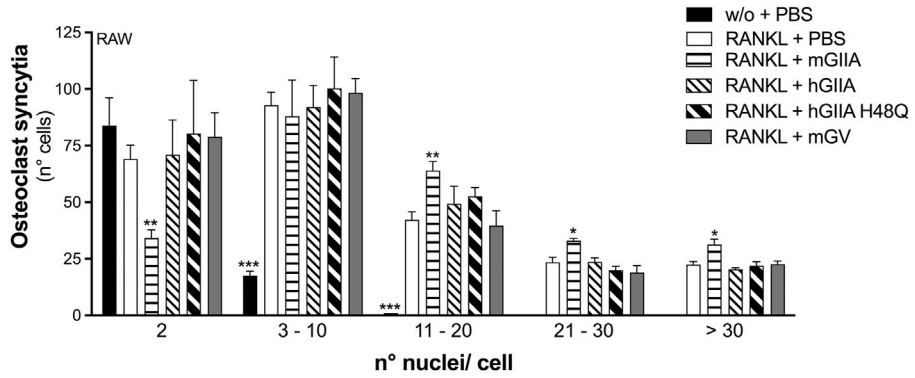

FIGURE 5
Murine recombinant $sPLA_2$-IIA stimulates RANKL-induced osteoclast fusion of RAW264.7 macrophages. RAW264.7 cells were treated without (w/o) or with 15 ng/mL RANKL for 72 h, in presence of the indicated recombinant proteins: 30 nM murine $sPLA_2$-IIA (mGIIA), 30 nM human $sPLA_2$-IIA (hGIIA), 30 nM human $sPLA_2$-IIA H48Q (hGIIA H48Q), 100 nM murine $sPLA_2$-V (mGV); or with PBS as carrier. Osteoclast syncytium formation was determined as number of nuclei/cell, by fluorescence microscopy. Data are means ± SE of three independent experiments. *$p < 0.05$; **$p < 0.01$; ***$p < 0.005$ versus correspondent RANKL (paired Student's *t*-tests).

induced markers of the osteoclastogenesis, with reduction of *Nfatc1*, *Mmp-9* and *Ctr* levels by 40%, 30%, and 60%, respectively. In addition, *Cathepsin-k* and *Trap* transcription were significantly reduced by about 50% in RANKL-treated cells, and the osteoclast fusion process was not inhibited at all (Supplementary Figure S7).

Altogether, these results were indicative of the sole requirement of $sPLA_2$-IIA catalytic activity for RANKL-induced marker transcription, with the exception of *Mmp-9*. Instead, $sPLA_2$-IIA regulation of the osteoclast fusion occurred independently of its enzymatic activity, and was specific for mouse recombinant $sPLA_2$-IIA.

3.6 Secreted PLA_2-IIA regulates osteoclast fusion through p38 SAPK activation

The syncytium formation constitutes a crucial step for the osteoclast bone resorbing activity (Soe, 2020), and the unveiled catalysis-independent regulation of this process by $sPLA_2$-IIA pushed toward the definition of the signaling pathways involved. Evaluation of RANKL downstream effectors in RAW264.7 macrophages, by Western blot analysis, displayed a significant activation of p38 SAPK and of one of its downstream substrates (MAPKAPK-2), while the phosphorylation levels of ERK1/2 MAPKs and AKT did not significantly differed from that of undifferentiated cells (Figure 8). Cell treatment with the different $sPLA_2$-IIA inhibitors revealed that Inhib-I and KH064 counteracted the RANKL-induced phosphorylation of p38 SAPK and of MAPKAPK-2, while BPB and LY311727 were without effect (Figure 8).

The osteoclastogenesis of RAW264.7 macrophages in the presence of p38 inhibition by SB203580, showed a foreseen blunted RANKL-induced phosphorylation of MAPKAPK-2 (Figure 8), but also a selectively impaired osteoclast fusion (Figure 9). Consistently, *ex-vivo* differentiation of M-CSF–expanded OPC, both wt and *Pla2g2a*-ko, upon SB203580 treatment produced significantly less TRAP-positive cells, maintaining unaffected the rate of the osteoclastogenesis marker transcription (Supplementary Figure S8).

These results suggested that p38 SAPK, a kinase part of the RANKL-triggered signaling (Park et al., 2017), mediated the osteoclast fusion but not the osteoclastogenesis marker transcription. In addition, p38 SAPK seemed to be downstream of the $sPLA_2$-IIA catalysis-independent modulation of the osteoclastogenesis, selectively required for a fully functional osteoclast multinucleation.

4 Discussion

The findings here summarized prove the $sPLA_2$-IIA multimodal regulation of RANKL-induced differentiation of murine osteoclast precursor cells. Whereas the osteoclastogenesis marker transcription requires $sPLA_2$ hydrolytic activity, $sPLA_2$-IIA participation in the osteoclast fusion and degrading activity occurs in a catalysis-independent manner and leads to the increased activation of p38 SAPK, presumably through the interaction with a still unidentified receptor.

This experimental evidence arises from *in-vitro* osteoclastogenesis assays performed with the well-validated and simplified model, based on the use of RAW264.7 macrophages as osteoclast precursor cells (Cuetara et al., 2006). The results obtained with this Abelson leukemia virus-transformed cell line, established from a BALB/c mouse strain (BAB/14; Raschke et al., 1978), were validated in *ex-vivo*

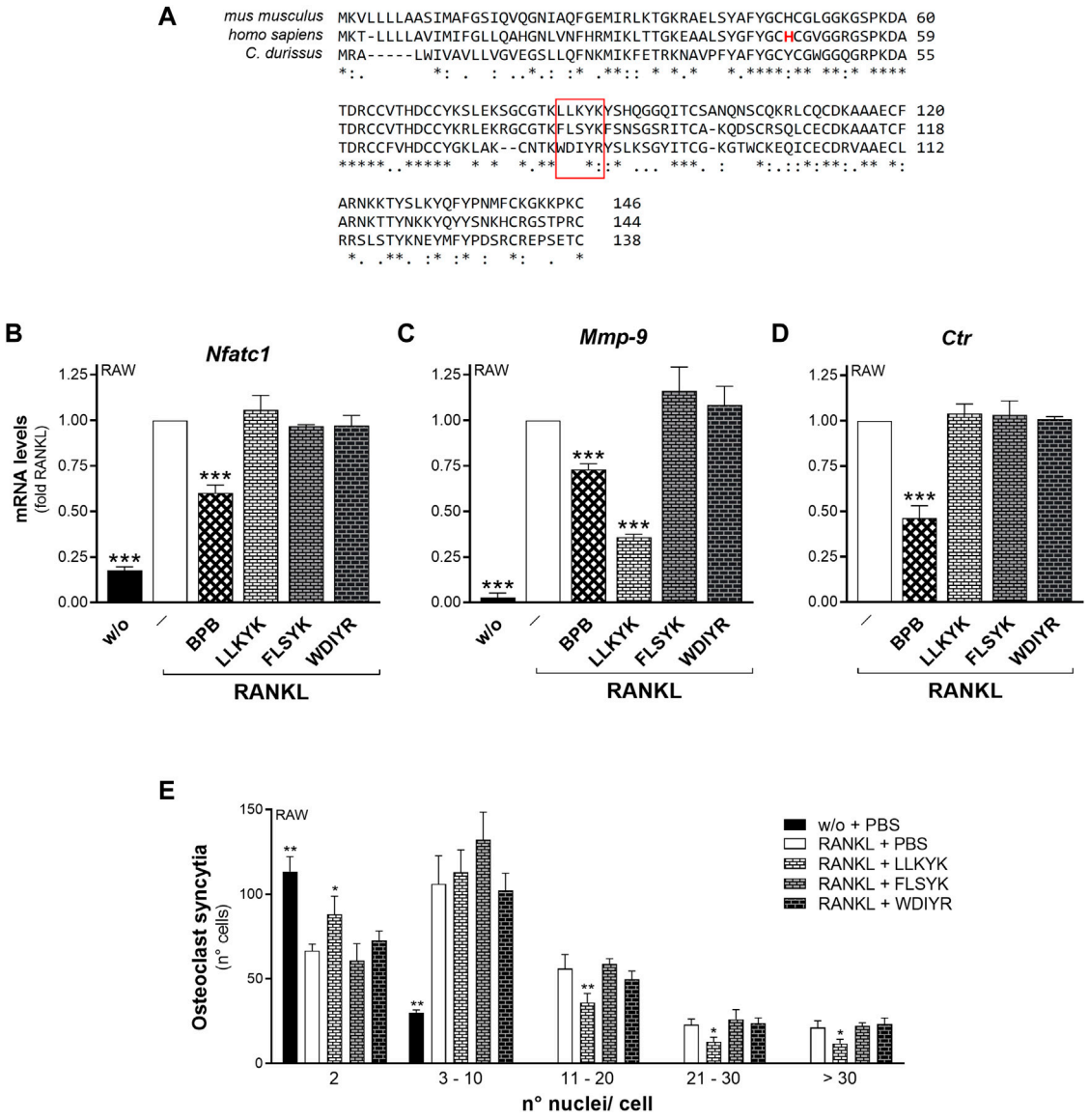

FIGURE 6
The LLKYK cyclic peptide inhibits RANKL-induced *Mmp-9* transcription and osteoclast fusion of RAW264.7 macrophages. **(A)** Alignment of sPLA$_2$-IIA sequences from *mus musculus* (UniProtKB - P31482), *homo sapiens* (UniProtKB - P14555), and *C. durissus* (UniProtKB - P24027). Consensus symbols indicate residue conservation, as calculated with the Clustal Omega program. The pentapeptide sequences are boxed in red, and the catalytic histidine residue in the human sPLA$_2$-IIA sequence is shown in red-letter code. **(B–D)** RAW264.7 cells were treated without (w/o) or with 15–30 ng/mL RANKL for 72 h, in presence of the carriers (–), or 10 nM BPB, or 250 μM of the indicated peptides (LLKYK from the murine sPLA$_2$-IIA sequence, FLSYK from that of human sPLA$_2$-IIA, WDIYR from that of *C. durissus*). The differentiation markers were quantified by real-time qPCR analysis, and normalized using *β2-microglobulin* expression, as the housekeeping gene. Data are expressed as fold of RANKL, and are means ± SEM of at least three independent experiments. **(E)** RAW264.7 cells were treated without (w/o) or with of 15 ng/mL RANKL for 72 h, in presence of the indicated peptides (250 μM), or with PBS as carrier. Osteoclast syncytium formation was determined as number of nuclei/cell, by fluorescence microscopy. Data are means ± SE of six independent experiments. *$p < 0.05$; **$p < 0.01$; ***$p < 0.005$ versus correspondent RANKL (paired Student's *t*-tests).

osteoclastogenesis assays with primary precursor cells from BALB/cJ mice. Within these model systems, the transcriptional remodeling induced by RANKL results in increased sPLA$_2$-IIA, -IIE, and -V mRNA levels, suggesting their involvement in the differentiation process or in mature osteoclast activity. These sPLA$_2$s are all located in the distal part of the mouse chromosome 4 and lie within the so-called sPLA$_2$ gene cluster (Valentin et al., 2000). The RANKL-triggered

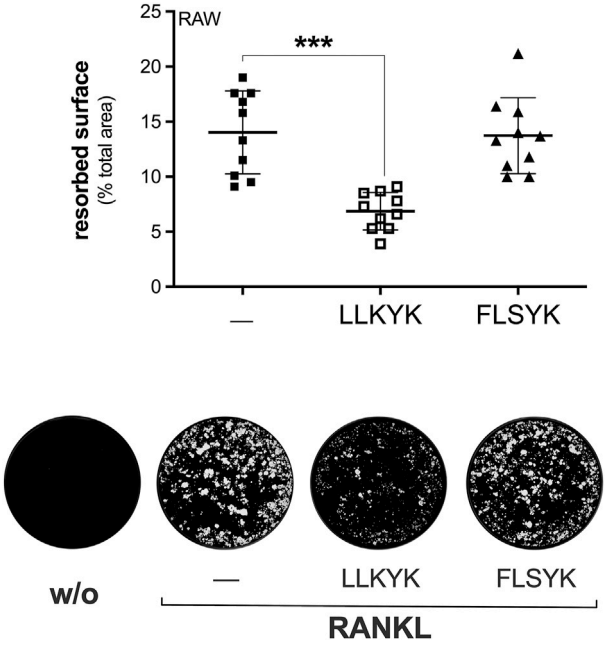

FIGURE 7
The LLKYK cyclic peptide inhibits RANKL-induced osteoclast resorbing activity of RAW264.7 macrophages. RAW264.7 cells plated on Osteo Assay Surface plates were treated without (w/o) or with 15 ng/mL RANKL for 7 days, in presence of PBS (–) or 250 μM of the indicated cyclic pentapeptides (LLKYK from murine $sPLA_2$-IIA sequence, and FLSYK from that of human $sPLA_2$-IIA). Below are shown representative images of the degrading activity, acquired with the EVOS XL Core microscope at a final magnification of ×2. Data are means ± SEM of three independent experiments performed in triplicates. ***$p < 0.005$, paired Student's *t*-test.

transcription of $sPLA_2$-IIA could be consequent to an increased NF-κB activity, as this transcription factor is downstream the RANKL-activated signaling (Park et al., 2017), and has been reported to mediate the $sPLA_2$-IIA transcription under inflammatory conditions. Indeed, cytokines such as TNF-α and IL-1β that are upregulated during inflammatory processes were shown to promote $sPLA_2$-IIA expression in different cellular lineages, through the involvement of the transcription factor NF-κB (Vadas et al., 1991; Couturier et al., 1999; Beck et al., 2003). Though unable to detect $sPLA_2$-IIA protein expression, with RAW264.7-cell lysates we succeeded in monitoring a PLA_2 enzymatic activity that increased upon RANKL-induced differentiation, and that was impaired by inhibitors and a blocking antibody specific for $sPLA_2$-IIA. This observation, together with the reported evidence of $sPLA_2$-IIA involvement in pathologies of the bone system, led us to investigate the role of this enzyme in the osteoclastogenesis process.

The unique genetic background of inbred BALB/cJ mice allowed the production of a *Pla2g2a* knock out from 129Sv mice (Balestrieri et al., 2006; Boilard et al., 2010). Indeed, a number of mouse strains generally used for research purposes (C57BL/6, 129Sv, A/J, C58/J, P/J, and B10. RIII) are naturally knock out for *Pla2g2a*, due to a frameshift mutation in the gene (Kennedy et al., 1995; MacPhee et al., 1995). Here, both *Pla2g2a*-ko primary cells and $sPLA_2$-IIA–interfered RAW264.7 macrophages were instrumental to unveil $sPLA_2$-IIA role in both osteoclast maturation and fusion. In addition, the use of inhibitors selective for the different $sPLA_2$-IIA activities dissected the underlying mechanisms of action.

The first open question that remains to be answered is how $sPLA_2$-IIA could regulate osteoclast maturation via its enzymatic activity in a cell-autonomous context. The preferential cellular substrates for this enzyme are prevalently distributed in the inner (cytosolic) leaflet of normal plasma membranes (as phosphatidylserine, phosphatidylethanolamine or phosphatidylglycerol), and are thus not accessible in resting cells, also because the required conditions for $sPLA_2$-IIA hydrolysis are not met in the cytosol (Bezzine et al., 2002; Singer et al., 2002). Of note, phosphatidylserine externalization has been reported to occur in pre-osteoclasts obtained from mouse bone marrow-derived cells, and was shown to be crucial for their M-CSF/RANKL-induced multinucleation (Kang et al., 2020). Interestingly, we observed an increased transcription of TMEM16F, a lipid scramblase and major contributor to the process of phosphatidylserine exposure (Pedemonte and Galietta, 2014), during the first 24 h of RANKL-induced differentiation of RAW264.7 macrophages (data not shown). A hallmark of TMEM16 scramblases is their lack of specificity, as phosphatidylinositol transbilayer movement across proteoliposomes reconstituted with purified fungal *Nectria haematococca* TMEM16 has been reported (Wang et al., 2018). Among the metabolites mediating $sPLA_2$-IIA cellular effects, the lysophosphatidylinositol could be a reasonable candidate, as several studies have already highlighted its involvement in the osteoclastogenesis process (Whyte et al., 2009; Mosca et al., 2021). In particular, we have recently showed that lysophosphatidylinositol stimulates the osteoclast maturation of RAW264.7 macrophages, with increased transcription of *Nfatc1, Cathepsin-k, Trap, and Ctr*, without any effect on the osteoclast syncytium formation, through GPR55-mediated signal transduction (Mosca et al., 2021). This is consistent with the requirement of $sPLA_2$-IIA catalytic activity exclusively for the regulation of the osteoclastogenesis marker transcription in our assay conditions. Indeed, both murine and human recombinant $sPLA_2$-IIA increased the RANKL-induced transcription of *Nfatc1, Cathepsin-k, Trap, and Ctr*, but not the catalytically inactive $sPLA_2$-IIA H48Q mutant. In addition, treatment of RAW264.7 macrophages with the alkylating agent BPB, which halts the $sPLA_2$-IIA enzymatic activity without changing the overall conformation of the protein surface (Lee et al., 2013), induced a significant reduction of the osteoclastogenesis marker transcription, without affecting the osteoclast fusion. Although this inhibitor is a general alkylating agent and its administration to intact cells cannot guarantee for a $sPLA_2$-IIA specific targeting (Scott et al., 2021), we verified that under BPB treatment the $sPLA_2$-IIA enzymatic activity is

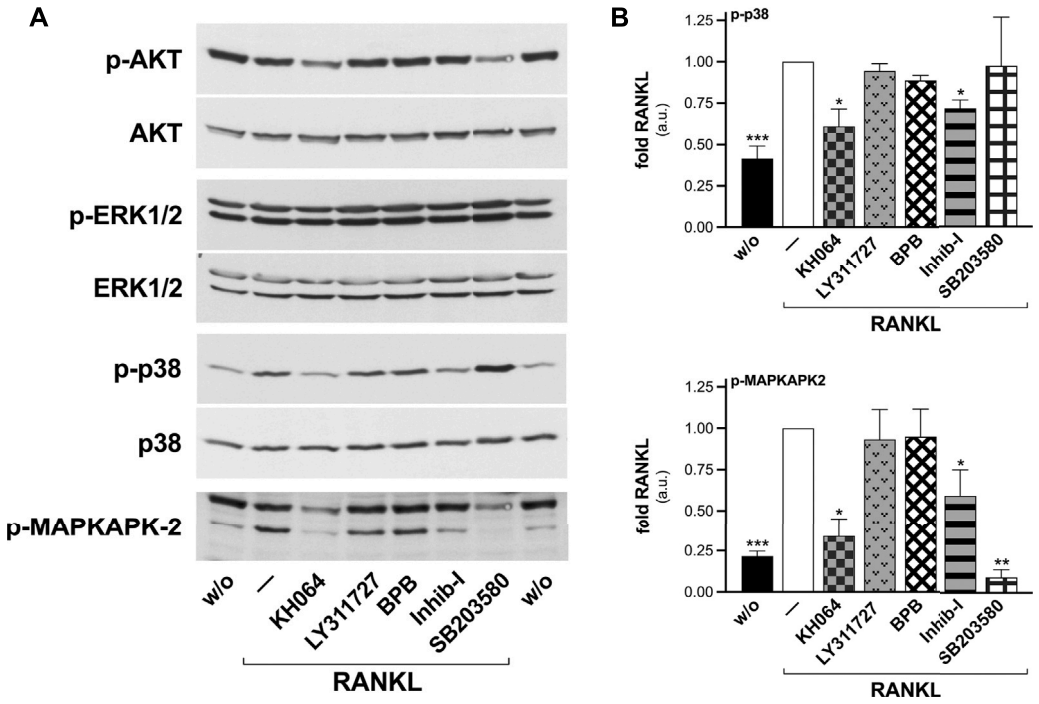

FIGURE 8
KH064 and Inhib-I counteract the RANKL-induced activation of p38 SAPK in differentiated RAW264.7 macrophages. RAW264.7 cells were treated without (w/o) or with 15–30 ng/mL RANKL for 72–96 h, in presence of the indicated sPLA2-IIA inhibitors (40 μM KH064, 30 μM LY311727, 10 nM BPB, 20 μM Inhib-I, 25 μM SB203580), or with DMSO as carrier (–). **(A)** Western blotting of phosphorylated (p-AKT, p-ERK1/2, p-p38, p-MAPKAPK-2), and total AKT, ERK1/2, and p38 are shown, from an experiment representative of at least three independents. **(B)** Densitometric analysis by arbitrary units (a.u.) of p38 (top) and 50-kDa MAPKAPK-2 (bottom) phosphorylation levels, normalized for the correspondent protein levels. Data are expressed as fold of cells treated with RANKL, and are means ± SE of at least three independent experiments. *$p < 0.05$; **$p < 0.01$; ***$p < 0.005$ versus RANKL (paired Student's *t*-tests).

significantly impaired in RANKL-differentiated RAW264.7 macrophages (Table 2). However, off-target effects cannot be completely ruled out.

Substantial progress has been made recently in the identification of the molecular machinery involved in osteoclast fusion, but the role of the lipid components in osteoclast syncytium formation is still under investigation. In different cell-to-cell fusion models, changes in membrane lipid composition have been shown to have relevant roles through the involvement of phospholipase activity (Chernomordik and Kozlov, 2008). For instance, in sperm fertilization of oocytes, changes in the acyl-chain composition of the main membrane glycerophospholipids may depend on another secreted phospholipase A_2: sPLA$_2$-X (Escoffier et al., 2010). Inhibition of osteoclast functions by sPLA$_2$-IIA blockade has been reported by different groups, both *in vitro* and in animal models. In Pagetic bone samples, sPLA$_2$-IIA was shown to be expressed at high levels and to stimulate the osteoclast differentiation and function by a mechanism that may be independent of its enzymatic activity (Allard-Chamard et al., 2014b). Consistently, under our assay conditions, sPLA$_2$-IIA regulation of osteoclast cell-to-cell fusion seems to occur independently of its enzymatic activity. Indeed, not only two specific sPLA$_2$-IIA inhibitors (Inhib-I and KH064), but mostly the cyclic pentapetide (LLKYK) derived from the murine sPLA$_2$-IIA primary sequence, were able to impair the RANKL-induced syncytium formation and the osteoclast functional activity. Of note, the LLKYK peptide was not able to affect the osteoclastogenesis marker transcription, which seems to depend exclusively on sPLA$_2$-IIA catalytic activity, with the exception of *Mmp-9* transcription that is regulated by sPLA$_2$-IIA through multiple mechanisms. Differently from KH064, LY311727 did not affect the osteoclast fusion event. An explanation for the different behavior of these two sPLA$_2$-IIA inhibitors in regulating the osteoclast fusion could reside in their peculiar ability to perturbate sPLA$_2$-IIA interaction with a putative binding partner (Boilard et al., 2006), or their different cell-membrane permeability (Mounier et al., 2004; Jemel et al., 2011). Indeed, the sPLA$_2$-IIA exhibits compartmentalization, not only for the enzymatic activity primarily occurring in the extracellular environment with a requirement of millimolar calcium concentrations. Even if the binding with a PLA$_2$ receptor on the cell surface can occur,

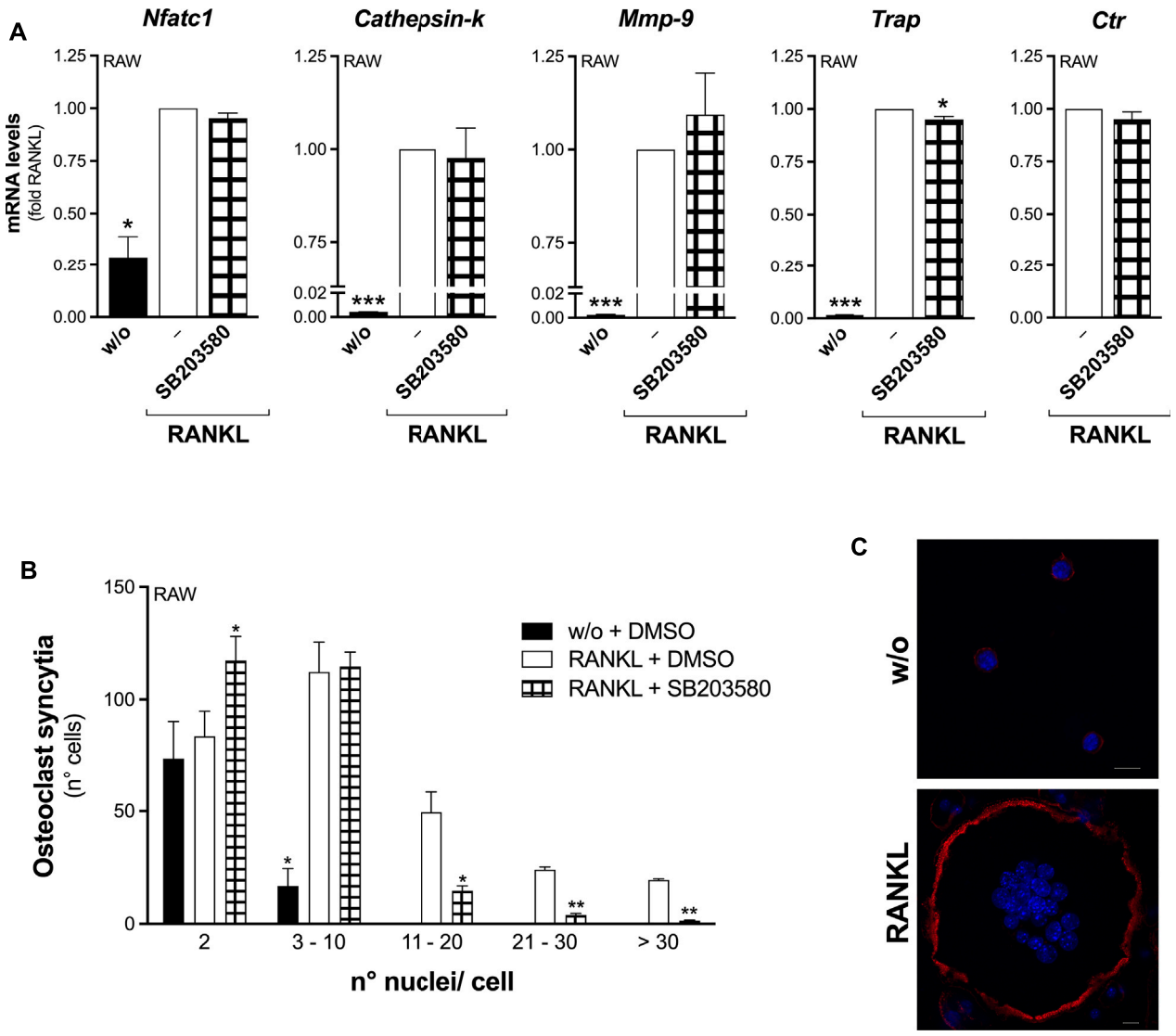

FIGURE 9
The p38 SAPK inhibitor selectively reduces RANKL-induced osteoclast fusion of RAW264.7 macrophages. **(A)** RAW264.7 cells were treated without (w/o) or with 15–30 ng/mL RANKL for 72 h, in presence of 25 μM SB203580 or with DMSO as carrier (–). The differentiation markers were quantified by real-time qPCR, and normalized using *β2-microglobulin* expression, as the housekeeping gene. Data are expressed as fold of RANKL, and are means ± SEM of three independent experiments. **(B)** Osteoclast syncytium formation was determined as number of nuclei/cell, by fluorescence microscopy. Data are means ± SE of three independent experiments. *$p < 0.05$; **$p < 0.01$; ***$p < 0.005$ versus correspondent RANKL (paired Student's *t*-tests). **(C)** Representative confocal images of RAW264.7 cells treated without (w/o) or with RANKL for 72 h, fixed and stained for confocal imaging. Phalloidin staining allows visualization of filamentous actin (red), while Hoechst staining reveals cell nuclei (blue, see Section 2 for details). Scale bars, 10 μm.

several other sPLA$_2$-IIA interactions occur upon its internalization (Scott et al., 2021).

Studies over the last decade have revealed that dysregulated lipid metabolism is one of the fundamental metabolic alterations that enable cancer cell survival and sustain rapid tumor growth and cell proliferation (Kroemer and Pouyssegur, 2008). The expression of several sPLA$_2$s is altered in various cancer cells, and in the neighboring stromal and immune cells at primary or metastatic tumor sites (Cummings, 2007; Murakami et al., 2011; Brglez et al., 2014; Sukocheva et al., 2019; Scott et al., 2021). Once secreted, sPLA$_2$s can have both autocrine and paracrine roles, to induce metabolic and signaling changes in a tumor (Kamphorst et al., 2013). The expression of sPLA$_2$-IIA is increased in the serum and tumors of patients with prostate, esophageal and lung cancers, and it is associated with poorer patient survival. Thus, the elevated levels of sPLA$_2$-IIA in the plasma of these cancer patients has led to

the suggestion of a biomarker role for sPLA$_2$-IIA (Kupert et al., 2011). However, it remains unclear whether increased serum sPLA$_2$-IIA levels are cancer-specific or whether they reflect inflammatory reactions during malignancy (Kupert et al., 2011). Of note, bone metastases are a common complication of epithelial cancers, of which breast, prostate and lung carcinomas are the most common (Kan et al., 2016). Serum levels of sPLA$_2$-IIA can also rise from 100-fold to 1,000-fold during acute inflammatory disorders, such as sepsis, acute pancreatitis, peritonitis and chronic rheumatoid arthritis (Triggiani et al., 2005). Intriguingly, inflammatory pathologies such as rheumatoid arthritis and spondyloarthritides have also been associated with localized bone resorption and generalized osteoporosis (Szentpetery et al., 2017).

Many of the observed effects of sPLA$_2$-IIA on biological systems, particularly in pathological settings characterized by persistent aberrant expression of this protein, may be attributed to direct or indirect perturbation of intracellular cell signaling pathways mediated by protein-protein interactions (Scott et al., 2021). Among the potential candidates, the M-type receptor PLA$_2$R1 is able to bind murine sPLA$_2$-IIA at low nanomolar concentrations, even if with an affinity 6–10-fold lower compared to sPLA$_2$-IB (Cupillard et al., 1999; Rouault et al., 2007). In the lung, the proposed role for PLA$_2$R1 is the clearance of PLA$_2$-IB from the bronchoalveolar fluid by endocytosis and lysosomal degradation in airway smooth muscle cells (Tamaru et al., 2013). Otherwise, PLA$_2$-IB binding to PLA$_2$R1 may promote downstream signaling pathways, with activation of stress kinases and key enzymes part of the phospholipid and sphingolipid metabolism, able to generate pro-inflammatory bioactive lipid derivatives (Mandal et al., 2001). Furthermore, the highly basic nature of sPLA$_2$-IIA allows its interaction with the negatively-charged heparan sulfates found at the cell surface (Murakami et al., 1999; Boilard et al., 2003), and with components of the coagulation cascade such as Factors Va and Xa (Mounier et al., 2000). The sPLA$_2$-IIA interfacial binding site has been reported to be relevant for vimentin binding at the surface of apoptotic human T cells (Boilard et al., 2003). Instead, the arginine residues 74 and 100 in the human sPLA$_2$-IIA sequence are crucial for the interaction with integrins $\alpha_V\beta_3$ and $\alpha_4\beta_1$ that leads to integrin activation and monocytic cell proliferation (Takada and Fujita, 2017). Intriguingly, several of these sPLA$_2$-IIA binding partners are not only main components of the osteoclast adhesion zone, but play a crucial role in the activation of osteoclasts to resorb the bone, as it is the case for vimentin and integrins ($\alpha_V\beta_3$, $\alpha_V\beta_5$, and $\alpha_2\beta_1$, among others) (Marchisio et al., 1984; Karanth et al., 2021).

More work will be necessary to dissect out each of the many regulatory pathways responsible for sPLA$_2$-IIA actions during the osteoclast fusion and to identify the putative sPLA$_2$-IIA receptor involved. These studies could pave the way for therapeutic application of sPLA$_2$-IIA inhibitors. An ideal blocker would be required to selectively inhibit sPLA$_2$-IIA binding to the specific receptor implicated in the osteoclast fusion. This will probably guarantee a tissue and cellular specific action. Several PLA$_2$ inhibitors, including sPLA$_2$ blockers, have been evaluated in clinical trials for the treatment of osteoarthritis, rheumatoid arthritis, atherosclerosis, sepsis and atopic dermatitis, among others, but none has reached the market (Nikolaou et al., 2019). The main limitation seems to be a lack of selectivity among the different human sPLA$_2$s upon systemic administration, also as a consequence of a lack of a comprehensive knowledge on cellular functions connected with each sPLA$_2$ subtype. Despite the fact that the rational design of selective inhibitors for the enzymatic activity of the different PLA$_2$s is a challenging issue, due to the highly conserved catalytic domain within this family of enzymes (Lambeau and Gelb, 2008; Oslund et al., 2008; Burke and Dennis, 2009; Cao et al., 2013), selective targeting of sPLA$_2$ ligand function has higher potentialities. This expectation could be fulfilled by monoclonal antibodies specifically raised against each enzyme (Pothlichet et al., 2020). Such sPLA$_2$-interaction inhibitors could be proposed as alternatives to the bisphosphonates (Center et al., 2020; D'Oronzo et al., 2021), the actual treatment of choice for several osteoclast disorders, since bisphosphonates are contraindicated in older patients with kidney impairment or cardiac disease (Dos Santos Ferreira et al., 2017; Rogers et al., 2020; de Roij van Zuijdewijn et al., 2021).

Data availability statement

The raw data supporting the conclusions of this article will be made available by the authors, without undue reservation.

Ethics statement

The animal study was reviewed and approved by Institutional Animal Care and Use Committee for Brigham and Women's Hospital.

Author contributions

MM, RD'A, and CV performed experiments and contributed to data analysis. BB, JC designed experiments with the primary cell cultures, performed the data analysis, interpreted the data and contributed to writing of the manuscript. GL and CP produced the recombinant sPLA$_2$-IIA proteins and antibodies; GL interpreted the data and contributed to writing of the manuscript. SM designed and

performed experiments, analyzed and interpreted the data, conducted the project, and wrote the manuscript. All authors reviewed the manuscript.

Funding

This work was supported by the P.O.R. FESR Campania SATIN and PRIN project 2012CK5RPF_05 (to SM); and by the Agence Nationale de la Recherche (ANR-20-CE14-0024-01) and the Fondation de la Recherche Médicale (DEQ20180339193) (to GL). MM was supported by the Young Researcher Mobility Program of Fondazione Berlucchi and by the University of Campania "Luigi Vanvitelli" for her visit of the JC and BB laboratories at the Brigham and Women's Hospital-Harvard Medical School (Boston, MA, United States).

Acknowledgments

We thank all colleagues who kindly provided reagents.

Conflict of interest

The authors declare that the research was conducted in the absence of any commercial or financial relationships that could be construed as a potential conflict of interest.

Publisher's note

All claims expressed in this article are solely those of the authors and do not necessarily represent those of their affiliated organizations, or those of the publisher, the editors and the reviewers. Any product that may be evaluated in this article, or claim that may be made by its manufacturer, is not guaranteed or endorsed by the publisher.

Supplementary material

The Supplementary Material for this article can be found online at: https://www.frontiersin.org/articles/10.3389/fcell.2022.966950/full#supplementary-material

References

Ackermann, E. J., Conde-Frieboes, K., and Dennis, E. A. (1995). Inhibition of macrophage Ca^{2+}-independent phospholipase A_2 by bromoenol lactone and trifluoromethyl ketones. *J. Biol. Chem.* 270 (1), 445–450. doi:10.1074/jbc.270.1.445

Allard-Chamard, H., Dufort, P., Haroun, S., and de Brum-Fernandes, A. J. (2014a). Cytosolic phospholipase A_2 and eicosanoids modulate life, death and function of human osteoclasts *in vitro*. *Prostagl. Leukot. Essent. Fat. Acids* 90 (4), 117–123. doi:10.1016/j.plefa.2013.12.009

Allard-Chamard, H., Haroun, S., and de Brum-Fernandes, A. J. (2014b). Secreted phospholipase A_2 type II is present in Paget's disease of bone and modulates osteoclastogenesis, apoptosis and bone resorption of human osteoclasts independently of its catalytic activity *in vitro*. *Prostagl. Leukot. Essent. Fat. Acids* 90 (2-3), 39–45. doi:10.1016/j.plefa.2013.12.007

Ao, C., Huo, Y., Qi, L., Xiong, Z., Xue, L., and Qi, Y. (2010). Pioglitazone suppresses the lipopolysaccharide-induced production of inflammatory factors in mouse macrophages by inactivating NF-kappaB. *Cell Biol. Int.* 34 (7), 723–730. doi:10.1042/CBI20090005

Arganaraz, G. A., Palmeira, J. D. F., and Arganaraz, E. R. (2020). Phosphatidylserine inside out: A possible underlying mechanism in the inflammation and coagulation abnormalities of COVID-19. *Cell Commun. Signal.* 18 (1), 190. doi:10.1186/s12964-020-00687-7

Astudillo, A. M., Balboa, M. A., and Balsinde, J. (2019). Selectivity of phospholipid hydrolysis by phospholipase A_2 enzymes in activated cells leading to polyunsaturated fatty acid mobilization. *Biochim. Biophys. Acta. Mol. Cell Biol. Lipids* 1864 (6), 772–783. doi:10.1016/j.bbalip.2018.07.002

Atsumi, G., Murakami, M., Tajima, M., Shimbara, S., Hara, N., and Kudo, I. (1997). The perturbed membrane of cells undergoing apoptosis is susceptible to type II secretory phospholipase A_2 to liberate arachidonic acid. *Biochim. Biophys. Acta* 1349 (1), 43–54. doi:10.1016/s0005-2760(97)00082-9

Balestrieri, B., Hsu, V. W., Gilbert, H., Leslie, C. C., Han, W. K., Bonventre, J. V., et al. (2006). Group V secretory phospholipase A_2 translocates to the phagosome after zymosan stimulation of mouse peritoneal macrophages and regulates phagocytosis. *J. Biol. Chem.* 281 (10), 6691–6698. doi:10.1074/jbc.M508314200

Balsinde, J., and Dennis, E. A. (1996). Distinct roles in signal transduction for each of the phospholipase A_2 enzymes present in P388D1 macrophages. *J. Biol. Chem.* 271 (12), 6758–6765. doi:10.1074/jbc.271.12.6758

Beck, S., Lambeau, G., Scholz-Pedretti, K., Gelb, M. H., Janssen, M. J., Edwards, S. H., et al. (2003). Potentiation of tumor necrosis factor α-induced secreted phospholipase A_2 (sPLA$_2$)-IIA expression in mesangial cells by an autocrine loop involving sPLA$_2$ and peroxisome proliferator-activated receptor α activation. *J. Biol. Chem.* 278 (32), 29799–29812. doi:10.1074/jbc.M211763200

Berrie, C. P., Iurisci, C., Piccolo, E., Bagnati, R., and Corda, D. (2007). Analysis of phosphoinositides and their aqueous metabolites. *Methods Enzymol.* 434, 187–232. doi:10.1016/S0076-6879(07)34011-1

Bezzine, S., Bollinger, J. G., Singer, A. G., Veatch, S. L., Keller, S. L., and Gelb, M. H. (2002). On the binding preference of human groups IIA and X phospholipases A_2 for membranes with anionic phospholipids. *J. Biol. Chem.* 277 (50), 48523–48534. doi:10.1074/jbc.M203137200

Boilard, E., Bourgoin, S. G., Bernatchez, C., Poubelle, P. E., and Surette, M. E. (2003). Interaction of low molecular weight group IIA phospholipase A_2 with apoptotic human T cells: Role of heparan sulfate proteoglycans. *FASEB J.* 17 (9), 1068–1080. doi:10.1096/fj.02-0938com

Boilard, E., Lai, Y., Larabee, K., Balestrieri, B., Ghomashchi, F., Fujioka, D., et al. (2010). A novel anti-inflammatory role for secretory phospholipase A_2 in immune complex-mediated arthritis. *EMBO Mol. Med.* 2 (5), 172–187. doi:10.1002/emmm.201000072

Boilard, E., Rouault, M., Surrel, F., Le Calvez, C., Bezzine, S., Singer, A., et al. (2006). Secreted phospholipase A_2 inhibitors are also potent blockers of binding to the M-type receptor. *Biochemistry* 45 (44), 13203–13218. doi:10.1021/bi061376d

Bonventre, J. (2004). Cytosolic phospholipase A_2α reigns supreme in arthritis and bone resorption. *Trends Immunol.* 25 (3), 116–119. doi:10.1016/j.it.2004.01.006

Bradley, J. D., Dmitrienko, A. A., Kivitz, A. J., Gluck, O. S., Weaver, A. L., Wiesenhutter, C., et al. (2005). A randomized, double-blinded, placebo-controlled clinical trial of LY333013, a selective inhibitor of group II secretory phospholipase A_2, in the treatment of rheumatoid arthritis. *J. Rheumatol.* 32 (3), 417–423.

Brglez, V., Lambeau, G., and Petan, T. (2014). Secreted phospholipases A_2 in cancer: Diverse mechanisms of action. *Biochimie* 107 Pt, 114–123. doi:10.1016/j.biochi.2014.09.023

Burke, J. E., and Dennis, E. A. (2009). Phospholipase A_2 biochemistry. *Cardiovasc. Drugs Ther.* 23 (1), 49–59. doi:10.1007/s10557-008-6132-9

Cao, J., Burke, J. E., and Dennis, E. A. (2013). Using hydrogen/deuterium exchange mass spectrometry to define the specific interactions of the

phospholipase A_2 superfamily with lipid substrates, inhibitors, and membranes. *J. Biol. Chem.* 288 (3), 1806–1813. doi:10.1074/jbc.R112.421909

Center, J. R., Lyles, K. W., and Bliuc, D. (2020). Bisphosphonates and lifespan. *Bone* 141, 115566. doi:10.1016/j.bone.2020.115566

Charles, J. F., Hsu, L. Y., Niemi, E. C., Weiss, A., Aliprantis, A. O., and Nakamura, M. C. (2012). Inflammatory arthritis increases mouse osteoclast precursors with myeloid suppressor function. *J. Clin. Invest.* 122 (12), 4592–4605. doi:10.1172/JCI60920

Chernomordik, L. V., and Kozlov, M. M. (2008). Mechanics of membrane fusion. *Nat. Struct. Mol. Biol.* 15 (7), 675–683. doi:10.1038/nsmb.1455

Church, W. B., Inglis, A. S., Tseng, A., Duell, R., Lei, P. W., Bryant, K. J., et al. (2001). A novel approach to the design of inhibitors of human secreted phospholipase A_2 based on native peptide inhibition. *J. Biol. Chem.* 276 (35), 33156–33164. doi:10.1074/jbc.M101272200

Cirino, G., Cicala, C., and Sorrentino, L. (1994). Human recombinant platelet phospholipase A_2 exacerbates poly-L-arginine induced rat paw edema. *Inflammation* 18 (1), 59–66. doi:10.1007/BF01534598

Collin-Osdoby, P., and Osdoby, P. (2012). RANKL-mediated osteoclast formation from murine RAW 264.7 cells. *Methods Mol. Biol.* 816, 187–202. doi:10.1007/978-1-61779-415-5_13

Coulthard, L. G., Costello, J., Robinson, B., Shiels, I. A., Taylor, S. M., and Woodruff, T. M. (2011). Comparative efficacy of a secretory phospholipase A_2 inhibitor with conventional anti-inflammatory agents in a rat model of antigen-induced arthritis. *Arthritis Res. Ther.* 13 (2), R42. doi:10.1186/ar3278

Couturier, C., Brouillet, A., Couriaud, C., Koumanov, K., Bereziat, G., and Andreani, M. (1999). Interleukin 1β induces type II-secreted phospholipase A_2 gene in vascular smooth muscle cells by a nuclear factor κB and peroxisome proliferator-activated receptor-mediated process. *J. Biol. Chem.* 274 (33), 23085–23093. doi:10.1074/jbc.274.33.23085

Cuetara, B. L., Crotti, T. N., O'Donoghue, A. J., and McHugh, K. P. (2006). Cloning and characterization of osteoclast precursors from the RAW264.7 cell line. *Vitro Cell. Dev. Biol. Anim.* 42 (7), 182–188. doi:10.1290/0510075.1

Cummings, B. S. (2007). Phospholipase A_2 as targets for anti-cancer drugs. *Biochem. Pharmacol.* 74 (7), 949–959. doi:10.1016/j.bcp.2007.04.021

Cupillard, L., Mulherkar, R., Gomez, N., Kadam, S., Valentin, E., Lazdunski, M., et al. (1999). Both group IB and group IIA secreted phospholipases A_2 are natural ligands of the mouse 180-kDa M-type receptor. *J. Biol. Chem.* 274 (11), 7043–7051. doi:10.1074/jbc.274.11.7043

D'Oronzo, S., Wood, S., and Brown, J. E. (2021). The use of bisphosphonates to treat skeletal complications in solid tumours. *Bone* 147, 115907. doi:10.1016/j.bone.2021.115907

Dacheux, M., Chaouch, S., Joy, A., Labat, A., Payre, C., Petit-Paitel, A., et al. (2021). Role of human group IIA secreted phospholipase A_2 in malaria pathophysiology: Insights from a transgenic mouse model. *Biochimie* 189, 120–136. doi:10.1016/j.biochi.2021.06.009

Dacheux, M., Sinou, V., Payre, C., Jeammet, L., Parzy, D., Grellier, P., et al. (2019). Antimalarial activity of human group IIA secreted phospholipase A_2 in relation to enzymatic hydrolysis of oxidized lipoproteins. *Infect. Immun.* 87 (11), e00556-19. doi:10.1128/IAI.00556-19

de Roij van Zuijdewijn, C., van Dorp, W., Florquin, S., Roelofs, J., and Verburgh, K. (2021). Bisphosphonate nephropathy: A case series and review of the literature. *Br. J. Clin. Pharmacol.* 87 (9), 3485–3491. doi:10.1111/bcp.14780

Dennis, E. A. (1994). Diversity of group types, regulation, and function of phospholipase A_2. *J. Biol. Chem.* 269 (18), 13057–13060. doi:10.1016/s0021-9258(17)36794-7

Doré, E., and Boilard, E. (2019). Roles of secreted phospholipase A_2 group IIA in inflammation and host defense. *Biochim. Biophys. Acta. Mol. Cell Biol. Lipids* 1864 (6), 789–802. doi:10.1016/j.bbalip.2018.08.017

Doré, E., Joly-Beauparlant, C., Morozumi, S., Mathieu, A., Levesque, T., Allaeys, I., et al. (2022). The interaction of secreted phospholipase A_2-IIA with the microbiota alters its lipidome and promotes inflammation. *JCI Insight* 7 (2), e152638. doi:10.1172/jci.insight.152638

Dos Santos Ferreira, D., Jesus de Oliveira Pinto, B. L., Kumar, V., Cardoso, V. N., Fernandes, S. O., Souza, C. M., et al. (2017). Evaluation of antitumor activity and cardiac toxicity of a bone-targeted pH-sensitive liposomal formulation in a bone metastasis tumor model in mice. *Nanomedicine* 13 (5), 1693–1701. doi:10.1016/j.nano.2017.03.005

Edwards, S. H., Thompson, D., Baker, S. F., Wood, S. P., and Wilton, D. C. (2002). The crystal structure of the H48Q active site mutant of human group IIA secreted phospholipase A_2 at 1.5 A resolution provides an insight into the catalytic mechanism. *Biochemistry* 41 (52), 15468–15476. doi:10.1021/bi020485z

Eerola, L. I., Surrel, F., Nevalainen, T. J., Gelb, M. H., Lambeau, G., and Laine, V. J. (2006). Analysis of expression of secreted phospholipases A_2 in mouse tissues at protein and mRNA levels. *Biochim. Biophys. Acta* 1761 (7), 745–756. doi:10.1016/j.bbalip.2006.04.002

Escoffier, J., Jemel, I., Tanemoto, A., Taketomi, Y., Payre, C., Coatrieux, C., et al. (2010). Group X phospholipase A_2 is released during sperm acrosome reaction and controls fertility outcome in mice. *J. Clin. Invest.* 120 (5), 1415–1428. doi:10.1172/JCI40494

Ferraz-de-Souza, B., and Correa, P. H. (2013). Diagnosis and treatment of paget's disease of bone: A mini-review. *Arq. Bras. Endocrinol. Metabol.* 57 (8), 577–582. doi:10.1590/s0004-27302013000800001

Fourcade, O., Simon, M. F., Viode, C., Rugani, N., Leballe, F., Ragab, A., et al. (1995). Secretory phospholipase A_2 generates the novel lipid mediator lysophosphatidic acid in membrane microvesicles shed from activated cells. *Cell* 80 (6), 919–927. doi:10.1016/0092-8674(95)90295-3

Ghomashchi, F., Brglez, V., Payre, C., Jeammet, L., Bezzine, S., Gelb, M. H., et al. (2017). Preparation of the full set of recombinant mouse- and human-secreted phospholipases A_2. *Methods Enzymol.* 583, 35–69. doi:10.1016/bs.mie.2016.10.034

Gregory, L. S., Kelly, W. L., Reid, R. C., Fairlie, D. P., and Forwood, M. R. (2006). Inhibitors of cyclo-oxygenase-2 and secretory phospholipase A_2 preserve bone architecture following ovariectomy in adult rats. *Bone* 39 (1), 134–142. doi:10.1016/j.bone.2005.12.017

Hansford, K. A., Reid, R. C., Clark, C. I., Tyndall, J. D., Whitehouse, M. W., Guthrie, T., et al. (2003). D-Tyrosine as a chiral precusor to potent inhibitors of human nonpancreatic secretory phospholipase A_2 (IIa) with antiinflammatory activity. *Chembiochem* 4 (2-3), 181–185. doi:10.1002/cbic.200390029

Hendrickson, H. S., Hendrickson, E. K., and Dybvig, R. H. (1983). Chiral synthesis of a dithiolester analog of phosphatidylcholine as a substrate for the assay of phospholipase A_2. *J. Lipid Res.* 24 (11), 1532–1537. doi:10.1016/s0022-2275(20)37877-9

Hussain, Z., Uyama, T., Tsuboi, K., and Ueda, N. (2017). Mammalian enzymes responsible for the biosynthesis of N-acylethanolamines. *Biochim. Biophys. Acta. Mol. Cell Biol. Lipids* 1862 (12), 1546–1561. doi:10.1016/j.bbalip.2017.08.006

Ivanusec, A., Sribar, J., and Krizaj, I. (2022). Secreted phospholipases A_2 - not just enzymes: Revisited. *Int. J. Biol. Sci.* 18 (2), 873–888. doi:10.7150/ijbs.68093

Jemel, I., Ii, H., Oslund, R. C., Payre, C., Dabert-Gay, A. S., Douguet, D., et al. (2011). Group X secreted phospholipase A_2 proenzyme is matured by a furin-like proprotein convertase and releases arachidonic acid inside of human HEK293 cells. *J. Biol. Chem.* 286 (42), 36509–36521. doi:10.1074/jbc.M111.268540

Kamphorst, J. J., Cross, J. R., Fan, J., de Stanchina, E., Mathew, R., White, E. P., et al. (2013). Hypoxic and Ras-transformed cells support growth by scavenging unsaturated fatty acids from lysophospholipids. *Proc. Natl. Acad. Sci. U. S. A.* 110 (22), 8882–8887. doi:10.1073/pnas.1307237110

Kan, C., Vargas, G., Pape, F. L., and Clezardin, P. (2016). Cancer cell colonisation in the bone microenvironment. *Int. J. Mol. Sci.* 17 (10), E1674. doi:10.3390/ijms17101674

Kang, J. H., Ko, H. M., Han, G. D., Lee, S. Y., Moon, J. S., Kim, M. S., et al. (2020). Dual role of phosphatidylserine and its receptors in osteoclastogenesis. *Cell Death Dis.* 11 (7), 497. doi:10.1038/s41419-020-2712-9

Karanth, D. S., Martin, M. L., and Holliday, L. S. (2021). Plasma membrane receptors involved in the binding and response of osteoclasts to noncellular components of the bone. *Int. J. Mol. Sci.* 22 (18), 10097. doi:10.3390/ijms221810097

Kennedy, B. P., Payette, P., Mudgett, J., Vadas, P., Pruzanski, W., Kwan, M., et al. (1995). A natural disruption of the secretory group II phospholipase A_2 gene in inbred mouse strains. *J. Biol. Chem.* 270 (38), 22378–22385. doi:10.1074/jbc.270.38.22378

Kim, R. R., Chen, Z., Mann, T. J., Bastard, K., K, F. S., and Church, W. B. (2020). Structural and functional aspects of targeting the secreted human group IIA phospholipase A_2. *Molecules* 25 (19), E4459. doi:10.3390/molecules25194459

Kim, Y. S., Min, K. S., Lee, H. D., Oh, H. W., and Kim, E. C. (2010). Effect of cytosolic phospholipase A_2 on proinflammatory cytokine-induced bone resorptive genes including receptor activator of nuclear factor kappa B ligand in human dental pulp cells. *J. Endod.* 36 (4), 636–641. doi:10.1016/j.joen.2009.12.009

Kita, Y., Shindou, H., and Shimizu, T. (2019). Cytosolic phospholipase A_2 and lysophospholipid acyltransferases. *Biochim. Biophys. Acta. Mol. Cell Biol. Lipids* 1864 (6), 838–845. doi:10.1016/j.bbalip.2018.08.006

Koduri, R. S., Baker, S. F., Snitko, Y., Han, S. K., Cho, W., Wilton, D. C., et al. (1998). Action of human group IIa secreted phospholipase A_2 on cell membranes. Vesicle but not heparinoid binding determines rate of fatty acid release by exogenously added enzyme. *J. Biol. Chem.* 273 (48), 32142–32153. doi:10.1074/jbc.273.48.32142

Kono, N., and Arai, H. (2019). Platelet-activating factor acetylhydrolases: An overview and update. *Biochim. Biophys. Acta. Mol. Cell Biol. Lipids* 1864 (6), 922–931. doi:10.1016/j.bbalip.2018.07.006

Kroemer, G., and Pouyssegur, J. (2008). Tumor cell metabolism: cancer's achilles' heel. *Cancer Cell* 13 (6), 472–482. doi:10.1016/j.ccr.2008.05.005

Kudo, K., Miki, Y., Carreras, J., Nakayama, S., Nakamoto, Y., Ito, M., et al. (2022). Secreted phospholipase A_2 modifies extracellular vesicles and accelerates B cell lymphoma. *Cell Metab.* 34 (4), 615–633.e8. e618. doi:10.1016/j.cmet.2022.02.011

Kupert, E., Anderson, M., Liu, Y., Succop, P., Levin, L., Wang, J., et al. (2011). Plasma secretory phospholipase A_2-IIa as a potential biomarker for lung cancer in patients with solitary pulmonary nodules. *BMC Cancer* 11, 513. doi:10.1186/1471-2407-11-513

Lambeau, G., and Gelb, M. H. (2008). Biochemistry and physiology of mammalian secreted phospholipases A_2. *Annu. Rev. Biochem.* 77, 495–520. doi:10.1146/annurev.biochem.76.062405.154007

Lambeau, G., and Lazdunski, M. (1999). Receptors for a growing family of secreted phospholipases A_2. *Trends Pharmacol. Sci.* 20 (4), 162–170. doi:10.1016/s0165-6147(99)01300-0

Lee, L. K., Bryant, K. J., Bouveret, R., Lei, P. W., Duff, A. P., Harrop, S. J., et al. (2013). Selective inhibition of human group IIA-secreted phospholipase A_2 (hGIIA) signaling reveals arachidonic acid metabolism is associated with colocalization of hGIIA to vimentin in rheumatoid synoviocytes. *J. Biol. Chem.* 288 (21), 15269–15279. doi:10.1074/jbc.M112.397893

Lio, Y. C., Reynolds, L. J., Balsinde, J., and Dennis, E. A. (1996). Irreversible inhibition of Ca^{2+}-independent phospholipase A_2 by methyl arachidonyl fluorophosphonate. *Biochim. Biophys. Acta* 1302 (1), 55–60. doi:10.1016/0005-2760(96)00002-1

Lomonte, B., Tarkowski, A., and Hanson, L. A. (1995). Phospholipase A_2 and inflammation. *Mol. Med. Today* 1 (1), 9. doi:10.1016/1357-4310(95)80011-5

MacPhee, M., Chepenik, K. P., Liddell, R. A., Nelson, K. K., Siracusa, L. D., and Buchberg, A. M. (1995). The secretory phospholipase A_2 gene is a candidate for the *Mom1* locus, a major modifier of Apc^{Min}-induced intestinal neoplasia. *Cell* 81 (6), 957–966. doi:10.1016/0092-8674(95)90015-2

Mandal, A. K., Zhang, Z., Chou, J. Y., and Mukherjee, A. B. (2001). Pancreatic phospholipase A_2 via its receptor regulates expression of key enzymes of phospholipid and sphingolipid metabolism. *FASEB J.* 15 (10), 1834–1836. doi:10.1096/fj.00-0831fje

Marchi-Salvador, D. P., Fernandes, C. A., Silveira, L. B., Soares, A. M., and Fontes, M. R. (2009). Crystal structure of a phospholipase A_2 homolog complexed with p-bromophenacyl bromide reveals important structural changes associated with the inhibition of myotoxic activity. *Biochim. Biophys. Acta* 1794 (11), 1583–1590. doi:10.1016/j.bbapap.2009.07.005

Marchisio, P. C., Cirillo, D., Naldini, L., Primavera, M. V., Teti, A., and Zambonin-Zallone, A. (1984). Cell-substratum interaction of cultured avian osteoclasts is mediated by specific adhesion structures. *J. Cell Biol.* 99 (5), 1696–1705. doi:10.1083/jcb.99.5.1696

Miki, Y., Taketomi, Y., Kidoguchi, Y., Yamamoto, K., Muramatsu, K., Nishito, Y., et al. (2022). Group IIA secreted phospholipase A_2 controls skin carcinogenesis and psoriasis by shaping the gut microbiota. *JCI Insight* 7 (2), e152611. doi:10.1172/jci.insight.152611

Mosca, M. G., Mangini, M., Cioffi, S., Barba, P., and Mariggiò, S. (2021). Peptide targeting of lysophosphatidylinositol-sensing GPR55 for osteoclastogenesis tuning. *Cell Commun. Signal.* 19 (1), 48. doi:10.1186/s12964-021-00727-w

Mounier, C. M., Ghomashchi, F., Lindsay, M. R., James, S., Singer, A. G., Parton, R. G., et al. (2004). Arachidonic acid release from mammalian cells transfected with human groups IIA and X secreted phospholipase A_2 occurs predominantly during the secretory process and with the involvement of cytosolic phospholipase A_2-α. *J. Biol. Chem.* 279 (24), 25024–25038. doi:10.1074/jbc.M313019200

Mounier, C. M., Luchetta, P., Lecut, C., Koduri, R. S., Faure, G., Lambeau, G., et al. (2000). Basic residues of human group IIA phospholipase A_2 are important for binding to factor Xa and prothrombinase inhibition comparison with other mammalian secreted phospholipases A_2. *Eur. J. Biochem.* 267 (16), 4960–4969. doi:10.1046/j.1432-1327.2000.01523.x

Murakami, M., Kambe, T., Shimbara, S., Yamamoto, S., Kuwata, H., and Kudo, I. (1999). Functional association of type IIA secretory phospholipase A_2 with the glycosylphosphatidylinositol-anchored heparan sulfate proteoglycan in the cyclooxygenase-2-mediated delayed prostanoid-biosynthetic pathway. *J. Biol. Chem.* 274 (42), 29927–29936. doi:10.1074/jbc.274.42.29927

Murakami, M., Miki, Y., Sato, H., Murase, R., Taketomi, Y., and Yamamoto, K. (2019). Group IID, IIE, IIF and III secreted phospholipase A_2s. *Biochim. Biophys. Acta. Mol. Cell Biol. Lipids* 1864 (6), 803–818. doi:10.1016/j.bbalip.2018.08.014

Murakami, M., Nakatani, Y., Atsumi, G. I., Inoue, K., and Kudo, I. (2017). Regulatory functions of phospholipase A_2. *Crit. Rev. Immunol.* 37 (2-6), 127–195. doi:10.1615/CritRevImmunol.v37.i2-6.20

Murakami, M. (2019). Novel functions of phospholipase A_2s: Overview. *Biochim. Biophys. Acta. Mol. Cell Biol. Lipids* 1864 (6), 763–765. doi:10.1016/j.bbalip.2019.02.005

Murakami, M., Sato, H., Miki, Y., Yamamoto, K., and Taketomi, Y. (2015). A new era of secreted phospholipase A_2. *J. Lipid Res.* 56 (7), 1248–1261. doi:10.1194/jlr.R058123

Murakami, M., Sato, H., and Taketomi, Y. (2020). Updating phospholipase A_2 biology. *Biomolecules* 10 (10), E1457. doi:10.3390/biom10101457

Murakami, M., Taketomi, Y., Girard, C., Yamamoto, K., and Lambeau, G. (2010). Emerging roles of secreted phospholipase A_2 enzymes: Lessons from transgenic and knockout mice. *Biochimie* 92 (6), 561–582. doi:10.1016/j.biochi.2010.03.015

Murakami, M., Taketomi, Y., Sato, H., and Yamamoto, K. (2011). Secreted phospholipase A_2 revisited. *J. Biochem.* 150 (3), 233–255. doi:10.1093/jb/mvr088

Nevalainen, T. J., Eerola, L. I., Rintala, E., Laine, V. J., Lambeau, G., and Gelb, M. H. (2005). Time-resolved fluoroimmunoassays of the complete set of secreted phospholipases A_2 in human serum. *Biochim. Biophys. Acta* 1733 (2-3), 210–223. doi:10.1016/j.bbalip.2004.12.012

Nikolaou, A., Kokotou, M. G., Vasilakaki, S., and Kokotos, G. (2019). Small-molecule inhibitors as potential therapeutics and as tools to understand the role of phospholipases A_2. *Biochim. Biophys. Acta. Mol. Cell Biol. Lipids* 1864 (6), 941–956. doi:10.1016/j.bbalip.2018.08.009

O'Brien, W., Fissel, B. M., Maeda, Y., Yan, J., Ge, X., Gravallese, E. M., et al. (2016). RANK-independent osteoclast formation and bone erosion in inflammatory arthritis. *Arthritis Rheumatol.* 68 (12), 2889–2900. doi:10.1002/art.39837

Olson, E. D., Nelson, J., Griffith, K., Nguyen, T., Streeter, M., Wilson-Ashworth, H. A., et al. (2010). Kinetic evaluation of cell membrane hydrolysis during apoptosis by human isoforms of secretory phospholipase A_2. *J. Biol. Chem.* 285 (14), 10993–11002. doi:10.1074/jbc.M109.070797

Oslund, R. C., Cermak, N., and Gelb, M. H. (2008). Highly specific and broadly potent inhibitors of mammalian secreted phospholipases A_2. *J. Med. Chem.* 51 (15), 4708–4714. doi:10.1021/jm800422v

Papadopoulos, S., Kazepidou, E., Antonelou, M. H., Leondaritis, G., Tsapinou, A., Koulouras, V. P., et al. (2020). Secretory phospholipase A_2-IIA protein and mRNA pools in extracellular vesicles of bronchoalveolar lavage fluid from patients with early acute respiratory distress syndrome: A new perception in the dissemination of inflammation? *Pharm. (Basel)* 13 (11), E415. doi:10.3390/ph13110415

Park, J. H., Lee, N. K., and Lee, S. Y. (2017). Current understanding of RANK signaling in osteoclast differentiation and maturation. *Mol. Cells* 40 (10), 706–713. doi:10.14348/molcells.2017.0225

Pedemonte, N., and Galietta, L. J. (2014). Structure and function of TMEM16 proteins (anoctamins). *Physiol. Rev.* 94 (2), 419–459. doi:10.1152/physrev.00039.2011

Pothlichet, J., Rose, T., Bugault, F., Jeammet, L., Meola, A., Haouz, A., et al. (2020). PLA2G1B is involved in CD4 anergy and CD4 lymphopenia in HIV-infected patients. *J. Clin. Invest.* 130 (6), 2872–2887. doi:10.1172/JCI131842

Ramanadham, S., Ali, T., Ashley, J. W., Bone, R. N., Hancock, W. D., and Lei, X. (2015). Calcium-independent phospholipases A_2 and their roles in biological processes and diseases. *J. Lipid Res.* 56 (9), 1643–1668. doi:10.1194/jlr.R058701

Raschke, W. C., Baird, S., Ralph, P., and Nakoinz, I. (1978). Functional macrophage cell lines transformed by Abelson leukemia virus. *Cell* 15 (1), 261–267. doi:10.1016/0092-8674(78)90101-0

Reynolds, L. J., Hughes, L. L., and Dennis, E. A. (1992). Analysis of human synovial fluid phospholipase A_2 on short chain phosphatidylcholine-mixed micelles: Development of a spectrophotometric assay suitable for a microtiterplate reader. *Anal. Biochem.* 204 (1), 190–197. doi:10.1016/0003-2697(92)90160-9

Rogers, M. J., Monkkonen, J., and Munoz, M. A. (2020). Molecular mechanisms of action of bisphosphonates and new insights into their effects outside the skeleton. *Bone* 139, 115493. doi:10.1016/j.bone.2020.115493

Rouault, M., Le Calvez, C., Boilard, E., Surrel, F., Singer, A., Ghomashchi, F., et al. (2007). Recombinant production and properties of binding of the full set of mouse secreted phospholipases A_2 to the mouse M-type receptor. *Biochemistry* 46 (6), 1647–1662. doi:10.1021/bi062119b

Saegusa, J., Akakura, N., Wu, C. Y., Hoogland, C., Ma, Z., Lam, K. S., et al. (2008). Pro-inflammatory secretory phospholipase A_2 type IIA binds to integrins αvβ3 and α4β1 and induces proliferation of monocytic cells in an integrin-dependent manner. *J. Biol. Chem.* 283 (38), 26107–26115. doi:10.1074/jbc.M804835200

San Pietro, E., Capestrano, M., Polishchuk, E. V., DiPentima, A., Trucco, A., Zizza, P., et al. (2009). Group IV phospholipase $A_2\alpha$ controls the formation of inter-cisternal continuities involved in intra-Golgi transport. *PLoS Biol.* 7 (9), e1000194. doi:10.1371/journal.pbio.1000194

Scott, K. F., Mann, T. J., Fatima, S., Sajinovic, M., Razdan, A., Kim, R. R., et al. (2021). Human group IIA phospholipase A_2–Three decades on from its discovery. *Molecules* 26 (23), 7267. doi:10.3390/molecules26237267

Seno, K., Okuno, T., Nishi, K., Murakami, Y., Watanabe, F., Matsuura, T., et al. (2000). Pyrrolidine inhibitors of human cytosolic phospholipase A_2. *J. Med. Chem.* 43 (6), 1041–1044. doi:10.1021/jm9905155

Shayman, J. A., and Tesmer, J. J. G. (2019). Lysosomal phospholipase A_2. *Biochim. Biophys. Acta. Mol. Cell Biol. Lipids* 1864 (6), 932–940. doi:10.1016/j.bbalip.2018.07.012

Singer, A. G., Ghomashchi, F., Le Calvez, C., Bollinger, J., Bezzine, S., Rouault, M., et al. (2002). Interfacial kinetic and binding properties of the complete set of human and mouse groups I, II, V, X, and XII secreted phospholipases A_2. *J. Biol. Chem.* 277 (50), 48535–48549. doi:10.1074/jbc.M205855200

Snider, J. M., You, J. K., Wang, X., Snider, A. J., Hallmark, B., Zec, M. M., et al. (2021). Group IIA secreted phospholipase A_2 is associated with the pathobiology leading to COVID-19 mortality. *J. Clin. Invest.* 131 (19), e149236. doi:10.1172/JCI149236

Snitko, Y., Koduri, R. S., Han, S. K., Othman, R., Baker, S. F., Molini, B. J., et al. (1997). Mapping the interfacial binding surface of human secretory group IIa phospholipase A_2. *Biochemistry* 36 (47), 14325–14333. doi:10.1021/bi971200z

Soe, K. (2020). Osteoclast fusion: Physiological regulation of multinucleation through heterogeneity-potential implications for drug sensitivity. *Int. J. Mol. Sci.* 21 (20), E7717. doi:10.3390/ijms21207717

Sukocheva, O., Menschikowski, M., Hagelgans, A., Yarla, N. S., Siegert, G., Reddanna, P., et al. (2019). Current insights into functions of phospholipase A_2 receptor in normal and cancer cells: More questions than answers. *Semin. Cancer Biol.* 56, 116–127. doi:10.1016/j.semcancer.2017.11.002

Sun, G. Y., Geng, X., Teng, T., Yang, B., Appenteng, M. K., Greenlief, C. M., et al. (2021). Dynamic role of phospholipases A_2 in health and diseases in the central nervous system. *Cells* 10 (11), 2963. doi:10.3390/cells10112963

Suzuki, J., Umeda, M., Sims, P. J., and Nagata, S. (2010). Calcium-dependent phospholipid scrambling by TMEM16F. *Nature* 468 (7325), 834–838. doi:10.1038/nature09583

Szentpetery, A., Horvath, A., Gulyas, K., Petho, Z., Bhattoa, H. P., Szanto, S., et al. (2017). Effects of targeted therapies on the bone in arthritides. *Autoimmun. Rev.* 16 (3), 313–320. doi:10.1016/j.autrev.2017.01.014

Takada, Y., and Fujita, M. (2017). Secreted phospholipase A_2 type IIA ($sPLA_2$-IIA) activates integrins in an allosteric manner. *Adv. Exp. Med. Biol.* 925, 103–115. doi:10.1007/5584_2016_95

Tamaru, S., Mishina, H., Watanabe, Y., Watanabe, K., Fujioka, D., Takahashi, S., et al. (2013). Deficiency of phospholipase A_2 receptor exacerbates ovalbumin-induced lung inflammation. *J. Immunol.* 191 (3), 1021–1028. doi:10.4049/jimmunol.1300738

Thomas, G., Brown, A. L., and Brown, J. M. (2014). *In vivo* metabolite profiling as a means to identify uncharacterized lipase function: Recent success stories within the alpha beta hydrolase domain (ABHD) enzyme family. *Biochim. Biophys. Acta* 1841 (8), 1097–1101. doi:10.1016/j.bbalip.2014.01.004

Thwin, M. M., Douni, E., Arjunan, P., Kollias, G., Kumar, P. V., and Gopalakrishnakone, P. (2009). Suppressive effect of secretory phospholipase A_2 inhibitory peptide on interleukin-1β-induced matrix metalloproteinase production in rheumatoid synovial fibroblasts, and its antiarthritic activity in hTNFtg mice. *Arthritis Res. Ther.* 11 (5), R138. doi:10.1186/ar2810

Tischfield, J. A., Xia, Y. R., Shih, D. M., Klisak, I., Chen, J., Engle, S. J., et al. (1996). Low-molecular-weight, calcium-dependent phospholipase A_2 genes are linked and map to homologous chromosome regions in mouse and human. *Genomics* 32 (3), 328–333. doi:10.1006/geno.1996.0126

Triggiani, M., Granata, F., Giannattasio, G., and Marone, G. (2005). Secretory phospholipases A_2 in inflammatory and allergic diseases: Not just enzymes. *J. Allergy Clin. Immunol.* 116 (5), 1000–1006. doi:10.1016/j.jaci.2005.08.011

Tseng, A., Inglis, A. S., and Scott, K. F. (1996). Native peptide inhibition. Specific inhibition of type II phospholipases A_2 by synthetic peptides derived from the primary sequence. *J. Biol. Chem.* 271 (39), 23992–23998. doi:10.1074/jbc.271.39.23992

Vadas, P., Pruzanski, W., Stefanski, E., Ellies, L. G., Aubin, J. E., Sos, A., et al. (1991). Extracellular phospholipase A_2 secretion is a common effector pathway of interleukin-1 and tumour necrosis factor action. *Immunol. Lett.* 28 (3), 187–193. doi:10.1016/0165-2478(91)90002-r

Valentin, E., Ghomashchi, F., Gelb, M. H., Lazdunski, M., and Lambeau, G. (1999). On the diversity of secreted phospholipases A_2. Cloning, tissue distribution, and functional expression of two novel mouse group II enzymes. *J. Biol. Chem.* 274 (44), 31195–31202. doi:10.1074/jbc.274.44.31195

Valentin, E., Singer, A. G., Ghomashchi, F., Lazdunski, M., Gelb, M. H., and Lambeau, G. (2000). Cloning and recombinant expression of human group IIF-secreted phospholipase A_2. *Biochem. Biophys. Res. Commun.* 279 (1), 223–228. doi:10.1006/bbrc.2000.3908

Wang, L., Iwasaki, Y., Andra, K. K., Pandey, K., Menon, A. K., and Butikofer, P. (2018). Scrambling of natural and fluorescently tagged phosphatidylinositol by reconstituted G protein-coupled receptor and TMEM16 scramblases. *J. Biol. Chem.* 293 (47), 18318–18327. doi:10.1074/jbc.RA118.004213

Weinrauch, Y., Abad, C., Liang, N. S., Lowry, S. F., and Weiss, J. (1998). Mobilization of potent plasma bactericidal activity during systemic bacterial challenge. Role of group IIA phospholipase A_2. *J. Clin. Invest.* 102 (3), 633–638. doi:10.1172/JCI3121

Whyte, L. S., Ryberg, E., Sims, N. A., Ridge, S. A., Mackie, K., Greasley, P. J., et al. (2009). The putative cannabinoid receptor GPR55 affects osteoclast function *in vitro* and bone mass *in vivo*. *Proc. Natl. Acad. Sci. U. S. A.* 106 (38), 16511–16516. doi:10.1073/pnas.0902743106

Yamamoto, K., Miki, Y., Sato, H., Murase, R., Taketomi, Y., and Murakami, M. (2017). Secreted phospholipase A_2 specificity on natural membrane phospholipids. *Methods Enzymol.* 583, 101–117. doi:10.1016/bs.mie.2016.09.007

Zizza, P., Iurisci, C., Bonazzi, M., Cossart, P., Leslie, C. C., Corda, D., et al. (2012). Phospholipase A_2IVα regulates phagocytosis independent of its enzymatic activity. *J. Biol. Chem.* 287 (20), 16849–16859. doi:10.1074/jbc.M111.309419

Frontiers in
Cell and Developmental Biology

Explores the fundamental biological processes of life, covering intracellular and extracellular dynamics.

The world's most cited developmental biology journal, advancing our understanding of the fundamental processes of life. It explores a wide spectrum of cell and developmental biology, covering intracellular and extracellular dynamics.

Discover the latest Research Topics

See more →

Frontiers

Avenue du Tribunal-Fédéral 34
1005 Lausanne, Switzerland
frontiersin.org

Contact us

+41 (0)21 510 17 00
frontiersin.org/about/contact